ANALYSIS OF HAMILTONIAN BOUNDARY VALUE PROBLEMS AND SYMPLECTIC INTEGRATION

A thesis presented in partial fulfilment of the
requirements for the degree of

Doctor of Philosophy
in
Mathematics

at Massey University, Manawatū,
New Zealand.

Christian Offen

2020

Contents

List of Tables

List of Figures

Abstract

Ordinary differential equations (ODEs) and partial differential equations (PDEs) arise in most scientific disciplines that make use of mathematical techniques. As exact solutions are in general not computable, numerical methods are used to obtain approximate solutions. In order to draw valid conclusions from numerical computations, it is crucial to understand which qualitative aspects numerical solutions have in common with the exact solution. Symplecticity is a subtle notion that is related to a rich family of geometric properties of Hamiltonian systems. While the effects of preserving symplecticity under discretisation on long-term behaviour of motions is classically well known, in this thesis

(a) the role of symplecticity for the bifurcation behaviour of solutions to Hamiltonian boundary value problems is explained. In parameter dependent systems at a bifurcation point the solution set to a boundary value problem changes qualitatively. Bifurcation problems are systematically translated into the framework of classical catastrophe theory. It is proved that existing classification results in catastrophe theory apply to persistent bifurcations of Hamiltonian boundary value problems. Further results for symmetric settings are derived.

(b) It is proved that to preserve generic bifurcations under discretisation it is necessary and sufficient to preserve the symplectic structure of the problem.

(c) The catastrophe theory framework for Hamiltonian ODEs is extended to PDEs with variational structure. Recognition equations for A-series singularities for functionals on Banach spaces are derived and used in a numerical example to locate high-codimensional bifurcations.

(d) The potential of symplectic integration for infinite-dimensional Lie-Poisson systems (Burgers' equation, KdV, fluid equations, ...) using Clebsch variables is analysed. It is shown that the advantages of symplectic integration can outweigh the disadvantages of integrating over a larger phase space introduced by a Clebsch representation.

(e) Finally, the preservation of variational structure of symmetric solutions in multisymplectic PDEs by multisymplectic integrators on the example of (phase-rotating) travelling waves in the nonlinear wave equation is discussed.

Acknowledgements

First and foremost, I would like to thank my supervisor Distinguished Professor Robert McLachlan. Thank you for your excellent guidance, your open-door policy, our countless, fruitful discussions as well as our non-academical conversations and your enthusiasm. You have helped me grow as a person and researcher with academical advice and with your encouragement to go to conferences and do research visits.

Next, I would like to thank the Marsden Fund of the Royal Society Te Apārangi and the School of Fundamental Sciences of Massey University for funding my PhD studies as well as the New Zealand Mathematical Society and the Isaac Newton Institute for Mathematical Sciences of the University of Cambridge (UK), for support and hospitality during the programme Geometry, compatibility and structure preservation in computational differential equations (July to December 2019).

Moreover, I would like to thank my collaborators and co-authors Dr Lisa Kreusser and Ben Tapley. It has been a productive time as well as a great pleasure to work with you here at Massey University and at the University of Cambridge. I am indebted to Professor Carola Schönlieb for inviting me to the Department of Applied Mathematics and Theoretical Physics, University of Cambridge. Another big thanks goes to Professor Elena Celledoni and Professor Brynjulf Owren. Your research visit here in 2018 at Massey University and meeting you at conferences has been very inspiring and I enjoyed our discussions. Thank you also for inviting me to the scientific semester at the Isaac Newton Institute which fit perfectly to my research project and broadened my horizons in many ways.

Moreover, I would like to thank Professor Reinout Quispel. It has been great to visit you at La Trobe University (Australia) in 2017 and it has been a pleasure to meet you at various conferences and at the Isaac Newton Institute. Thanks for interesting discussions and our collaboration. Next, I would like to thank Professor Klas Modin as well as his PhD student Milo Viviani. Your research visit here in 2018 has been very stimulating.

Thanks also to Professor Bernd Krauskopf and Professor Hinke Osinga for inviting me to a research visit of the Applied Dynamical Systems research group at the University of Auckland in 2017 and for our discussions of my research project in its early

stages. Moreover, I would like to thank Professor Peter Donelan for providing some insights into Singularity Theory at an early stage of my research project during a visit of the University of Wellington in 2017. Furthermore, I would like to thank Dr David Ham for inviting me to an inspiring research visit of the Imperial College London in 2019 and Professor Ari Stern and his PhD student Mary Barker for valuable advice on some numerical aspects of this work and ideas for future research.

Another thanks goes to Professor Thom ter Elst for proofreading parts of my collaborative paper on bifurcations in PDEs (Chapter 11). Thanks also to Professor Chris Budd, Professor Peter Hydon and Dr Mats Vermeeren for discussions on multisymplecticity during my time at the Isaac Newton Institute and at the conference SciCADE 2019.

Finally, I would like to thank my parents, colleagues, and friends for always supporting me and bringing happiness to my life.

Chapter 1

Introduction

1.1 The idea of bifurcation analysis and symplecticity

Hamiltonian systems occur as mathematical models that describe a wide range of physical systems ranging from classical mechanical systems describing the movement of planets, particles, electrons in electrodynamics fields or molecular dynamics to hydrodynamical systems. Moreover, they can be utilised, for instance, when drawing samples from statistical distributions numerically using Hamiltonian Monte Carlo methods. Mathematical models often contain parameters. Depending on the values of the parameters, a Hamiltonian boundary value problem might have a unique solution, no solution, or many solutions. As parameters are varied, the set of solutions can undergo qualitative changes, called *bifurcations*. In the simplest example, two solutions can merge and annihilate as a parameter is varied. For instance, the Bratu problem, that we will introduce as an example later, describes a combustion process which admits two time-invariant heat distributions for parameter values $\mu \lesssim 3.51$. As the parameter value is increased, the heat distributions become more and more similar to each other until they coincide at $\mu \approx 3.51$. If the parameter value is increased beyond this critical value then no invariant heat distribution exists. The situation is illustrated in the *bifurcation diagram* plotted in Figure 1.1. The singular point at which the solutions merge is called a *bifurcation point*.

When more parameters are present then solutions to boundary value problems can interact in more complicated ways. Of particular relevance are those phenomena which are stable and cannot be destroyed by introducing small perturbations since we expect these to occur in models describing real world phenomena. When trying to understand a mathematical model with parameters, then locating bifurcation points is important because at these highly singular points the model behaviour changes qualitatively. However, as mathematical models consisting of ordinary or partial differential

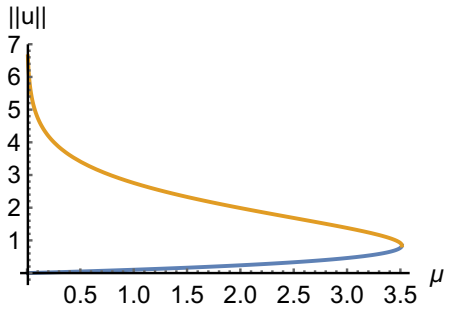

Figure 1.1: Two branches of solutions to the Bratu problem merge and annihilate in a fold bifurcation at the parameter value $\mu \approx 3.51$.

equations typically exceed the complexity of differential equations for which exact solutions can be obtained, solutions need to be computed numerically using an integration scheme which discretises the model equation.

A structure present in Hamiltonian systems is *symplecticity*. It is well known that if the model equations are Hamiltonian systems then preserving the symplectic structure of the system under discretisation leads to excellent behaviour of the numerical solution in long-term simulations. Advantages include excellent energy conservation properties of the numerical solution, preservation of the topology of the phase portrait like the absence of artificial attractors or the preservation of statistical quantities as well as chaotic and non-chaotic behaviour. Indeed, the numerical solutions behave like exact solutions of a nearby Hamiltonian system which is advantageous when analysing the numerical solution and explains why the numerical solution shares so many geometric properties with the exact solution.

Whether preserving symplectic structure when computing bifurcation diagrams for boundary value problems is relevant or not is not clear a priori since the classical results refer to long-term integrations. In contrast, in typical boundary value problems for Hamiltonian systems the problem is posed on a time-interval of fixed length. In this thesis we show that there are bifurcation phenomena which are related to the symplecticity of the problem. Indeed, we will translate Hamiltonian boundary value problems systematically into critical point problems: solutions to boundary value problems correspond to critical points $x \in U$ of parameter dependent functions $S_\mu \colon U \to \mathbb{R}$ defined on an open neighbourhood U in $\mathbb{R}^n$ with parameters μ. More precisely, we will show that families of Hamiltonian boundary value problems up to symplectomorphisms correspond to smooth function families up to stably right-equivalence (with notions to be made precise later).

The bifurcation behaviour of critical points is classified in classical catastrophe theory. We will show that the classification covers persistent bifurcations of Hamiltonian

boundary value problems. We will prove that symplectic integration schemes preserve all persistent bifurcations exactly while non-symplectic discretisation schemes destroy certain persistent bifurcations. This means when bifurcation diagrams are computed using a non-symplectic integrator on a Hamiltonian boundary value problem then incorrect bifurcations can show up or bifurcation points can disappear.

1.2 Motivational example

Before providing a review of the relevant notions and a more rigorous and general treatment, we give a motivational example which will sketch the relation between bifurcations of solutions to Hamiltonian boundary value problems and the bifurcation of critical points of parameter dependent functions. It illustrates some key ideas and was the starting point of the research findings presented in this work.

Let p, q be the standard coordinates of $\mathbb{R}^2$ with the standard symplectic structure $\omega = \mathrm{d}p \wedge \mathrm{d}q$. We consider the two-parameter family of Hamiltonian systems defined by

$$H_\mu \colon \mathbb{R}^2 \to \mathbb{R}, \quad H_\mu(p,q) = p^2 + \mu_1 q + \mu_2 q^2 + q^4.$$

For $\mu \in \mathbb{R}^2$ the time-τ-flow map $\phi_\mu \colon \mathbb{R}^2 \to \mathbb{R}^2$ of the Hamiltonian vector field X_H assigns to initial values $(p(0), q(0))$ the solution of Hamilton's equations

$$\begin{cases} \dot{q}(t) &= \frac{\partial H_\mu}{\partial p}(p(t), q(t)) \\ \dot{p}(t) &= -\frac{\partial H_\mu}{\partial q}(p(t), q(t)) \end{cases} \tag{1.2.1}$$

at time τ. Each map ϕ_μ is symplectic. Let us consider the Dirichlet boundary value problem

$$q(0) = q^* \qquad q(\tau) = Q^* \tag{1.2.2}$$

for $q^*, Q^* \in \mathbb{R}$. In other words, we look for orbits of the Hamiltonian flow which start on the line $\mathbb{R} \times \{q^*\}$ in the phase space $\mathbb{R}^2$ and end on the line $\mathbb{R} \times \{Q^*\}$ at time τ. Since solutions to initial value problems are unique, we can specify a solution to (1.2.1) and (1.2.2) by the value $p(0)$. This means we seek solutions $p(0)$ to the equation

$$(q \circ \phi_\mu)(p(0), q^*) = Q^*. \tag{1.2.3}$$

Figure 1.2 shows a bifurcation diagram, i.e. a plot of solutions $p(0)$ of (1.2.3) over the μ-plane for the integration time $\tau = 4$ and the boundary values $q^* = 0.2 = Q^*$. The plot shows a *cusp bifurcation*. Compared with the fold bifurcation displayed in Figure 1.1 it requires two parameters to occur. Depending on the parameter values μ_1,

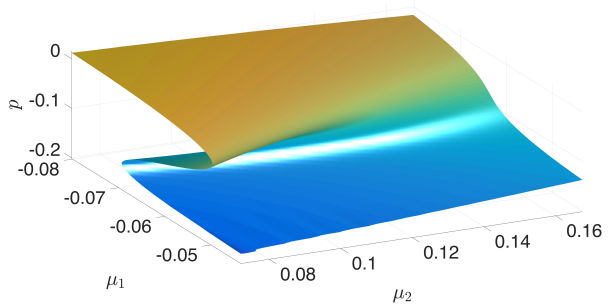

Figure 1.2: A plot of solutions p to the Hamiltonian boundary value problem (1.2.3) over the parameter space for $\tau = 4$, $q^* = 0.2 = Q^*$ shows a cusp bifurcation. Depending on the parameter values μ_1, μ_2 the problem has 3 or 2 solutions or 1 solution. To obtain the plot the Hamiltonian flow was approximated using the symplectic Störmer–Verlet scheme, which will be introduced in Example 3.3.2, with time step size 0.1.

μ_2 the problem has 3 or 2 solutions or 1 solution in the considered range of parameters. The cusp bifurcation is one of the seven elementary catastrophes classified by Thom (1973). The bifurcation persists under small perturbations, i.e. a small perturbation of the Hamiltonian or the boundary condition results in a bifurcation diagram which qualitatively looks like the bifurcation diagram of the unperturbed system shown in Figure 1.2. This means that the above bifurcation is a *persistent* phenomenon in Dirichlet problems for families of Hamiltonian systems with two parameters. (Notions will be made more precise in the following chapters.)

The occurrence of bifurcations from Thom's list of classical catastrophes (Table 1.1) is related to the symplecticity of the maps ϕ_μ. Indeed, it is an instance of the fact that many boundary value problems for symplectic maps are governed by catastrophe theory which we will explain in the following chapters. Let us sketch the connection here for Dirichlet problems for symplectic maps on $\mathbb{R}^{2n}$. Let $\phi_\mu \colon (\mathbb{R}^{2n}, \omega) \to (\mathbb{R}^{2n}, \omega)$ denote a family of symplectic maps. We equip $(\mathbb{R}^{2n}, \omega)$ with Darboux coordinates $p_1, \dots, p_n, q^1, \dots, q^n$ such that $\omega = \sum_{j=1}^n \mathrm{d}p_j \wedge \mathrm{d}q^j$. Let $\pi_1, \pi_2 \colon \mathbb{R}^{2n} \times \mathbb{R}^{2n} \to \mathbb{R}^{2n}$ denote the projection to the first or second factor of the cross product $\mathbb{R}^{2n} \times \mathbb{R}^{2n}$, respectively. We equip $\mathbb{R}^{2n} \times \mathbb{R}^{2n}$ with the symplectic form $\omega \oplus (-\omega) := \pi_1^*\omega - \pi_2^*\omega$ and obtain coordinates $p_1, \dots p_n, q^1, \dots, q^n, P_1, \dots P_n, Q^1, \dots, Q^n$ on $\mathbb{R}^{2n} \times \mathbb{R}^{2n}$ by pulling back the coordinates $p_1, \dots, p_n, q^1, \dots, q^n$ from $\mathbb{R}^{2n}$ with π_1 and π_2. The graphs of the symplectic maps can be embedded as Lagrangian submanifolds:

$$\Gamma_\mu = \{(p, q, \phi_\mu(p, q)) \,|\, (p, q) \in \mathbb{R}^{2n}\} \subset (\mathbb{R}^{2n} \times \mathbb{R}^{2n}, \omega \oplus (-\omega)).$$

ADE class	name	germ	miniversal unfolding
A_2	fold	x^3	$x^3+\mu_1 x$
A_3	cusp	x^4	$x^4+\mu_2 x^2+\mu_1 x$
A_4	swallowtail	x^5	$x^5+\mu_3 x^3+\mu_2 x^2+\mu_1 x$
A_5	butterfly	x^6	$x^6+\mu_4 x^4+\mu_3 x^3+\mu_2 x^2+\mu_1 x$
D_4^+	hyperbolic umbilic	x^3+xy^2	$x^3+xy^2+\mu_3(x^2-y^2)+\mu_2 y+\mu_1 x$
D_4^-	elliptic umbilic	x^3-xy^2	$x^3-xy^2+\mu_3(x^2+y^2)+\mu_2 y+\mu_1 x$
D_5	parabolic umbilic	x^2y+y^4	$x^2y+y^4+\mu_4 x^2+\mu_3 y^2+\mu_2 y+\mu_1 x$

Table 1.1: Thom's seven elementary catastrophes (Lu, 1976, p.89), (Gilmore, 1993, p.66). The table shows all stable singularities for parameter families with at most 4 parameters up to right-left equivalence. Plotting the critical points x such that $\nabla_x F_\mu(x)=0$ of a function family (miniversal unfolding) F_μ over the parameter space we obtain bifurcation diagrams. Up to reparametrisation and parameter-dependent changes of coordinates the fold looks like Figure 1.1 and the cusp looks like Figure 1.2.

The 1-form

$$\alpha=\sum_{j=1}^{n}((q^*-q_j)\mathrm{d}p_j-(Q^*-Q_j)\mathrm{d}P_j)$$

on $\mathbb{R}^{2n}\times\mathbb{R}^{2n}$ is a primitive of $\omega\oplus(-\omega)$ and, therefore, closed on the simply connected submanifolds Γ_μ for each μ. Thus, there exists a family of primitives $S_\mu\colon\Gamma_\mu\to\mathbb{R}$ with $\mathrm{d}S_\mu=\iota_\mu^*\alpha$, where $\iota_\mu\colon\Gamma_\mu\hookrightarrow\mathbb{R}^{2n}\times\mathbb{R}^{2n}$ is the natural inclusion. Where p_j,P_j $(1\le j\le n)$ constitutes a local coordinate system on Γ_μ, i.e. where $\det\left(\frac{\partial(p_j\circ\phi_\mu)}{\partial q^i}\right)_{i,j}\neq 0$, the problem

$$(q\circ\phi_\mu)(p,q^*)=Q^*$$

is equivalent to $\iota_\mu^*\alpha=0$ or

$$\mathrm{d}S_\mu=0.$$

We can conclude that the bifurcations in the boundary value problem (1.2.2) for families of symplectic maps ϕ_μ behave like the *gradient zero problem* or *critical points problem*. Therefore, bifurcations of solutions are classified in *catastrophe theory*. If no more than four parameters are present and the bifurcation cannot be destroyed by introducing small perturbation terms then the problem must be equivalent to one of Thom's list of classical catastrophes (Table 1.1).

1.3 Further results of the dissertation

Next to the classification and the consideration of how symplectic integrators preserve persistent bifurcations, we will use the catastrophe framework to analyse how typical

boundary conditions such as Dirichlet boundary conditions can affect which bifurcations occur. Indeed, we will prove that Dirichlet boundary conditions prohibit some of the bifurcations which persistently occur in the full problem class of Hamiltonian boundary value problems. Moreover, we will see that extra structure can cause more bifurcations to occur as persistent phenomena than just the ones in Thom's list (Table 1.1). For instance, we will prove that in completely integrable systems a novel pitchfork bifurcation occurs as a persistent phenomena. Moreover, if the Hamiltonian and the boundary conditions are invariant under a symmetry action then the symmetry is inherited by the corresponding critical points problem. This will constitute Part II of the thesis, whereas Part I consists of a review of relevant notions and concepts.

In Part III we will consider three generalisations of the concept of Hamiltonian ODEs to the PDE setting. First we will interpret Hamiltonian structure as the existence of a variational principle. Using this viewpoint we can transfer catastrophe classification results to a broad class of partial differential equations. In particular, we will develop detection formulas for A-series bifurcations and show in a numerical experiment how to locate high-codimensional bifurcations computationally.

As a second generalisation we consider infinite-dimensional Lie–Poisson systems. These cover important PDEs such as Burgers' equation, the Korteweg–de Vries equation (KdV), the Camassa-Holm equation and Euler's fluid equations. Using Clebsch variables, we will, on the example of Burgers' equation and related equations, lift the Lie–Poisson system to a Hamiltonian system defined on an infinite-dimensional symplectic space, where, after discretisation, symplectic integration methods can be applied. We will show that the advantages of symplectic integration can outweigh the disadvantage of calculating on a larger phase space.

As a third generalisation of Hamiltonian ODEs to the PDE setting, we consider multi-symplectic systems. Here we analyse how integration schemes which preserve multi-symplectic structure can preserve structure that governs symmetric solutions such as travelling waves in the nonlinear wave equation.

Part I

Review of relevant concepts

The following part of the thesis provides some introductory notes to the mathematical concepts that are relevant to this thesis. In Chapter 2 we recall some elementary notions in symplectic geometry and Hamiltonian systems and give first examples. In particular, we introduce the notion of complete integrability and symmetries briefly, as they will be relevant later on.

We proceed in Chapter 3 with basic notions in numerical analysis and introduce (partitioned) Runge–Kutta methods. In particular, we recall the implicit and explicit midpoint rule as well as the Störmer–Verlet scheme, which will be used in our numerical simulations. Moreover, we recall the notion of symplectic integrators which is essential to understand the implications of the main results of this thesis for numerical computations.

Chapter 4 continues the review of concepts by recalling the scientific terminology used when describing boundary value problems as well as by presenting some ideas of solution strategies and discretisation schemes. In particular, we recall shooting methods, finite difference schemes, and Galerkin's method. Moreover, we present numerical continuation methods, which will be employed especially in Chapter 11 to compute bifurcation diagrams.

We conclude the review with an introduction to some notions and concepts in singularity theory and catastrophe theory in Chapter 5. We will give the reader an idea of the mathematical meaning of the classification seen in Table 1.1 as well as provide more illustrations of the elementary catastrophes. Moreover, we contrast the classification of the bifurcation behaviour of critical points of a scalar-valued function with the behaviour of roots of a function between spaces of the same dimension.

Throughout this work we will denote the end of a definition, example, observation, or remark by $\triangle$. The end of a proof is denoted by $\square$.

Chapter 2

Symplectic geometry and Hamiltonian mechanics

The notions of *symplecticity* and *Hamiltonian systems* are of central importance for the analysis done in this work. We will, therefore, review a selection of elementary notions in symplectic geometry and Hamiltonian mechanics. References are Libermann and Marle, 1987; McDuff and Salamon, 2017. An introductory reference is Haro, 1998. Here, we will simultaneously pursue a coordinate independent as well as a classical approach to define required notions to obtain some flexibility in the presentation of arguments later. Several alternative (equivalent) ways of introducing symplectic structures are presented in V. I. Arnold, Khukhro, et al., 2007, Ch. 1.3. Some familiarity with basic notions in differential geometry is assumed. For an introduction see, for instance, Warner, 1983. We will remain in the setting of finite dimensional manifolds to avoid the technicalities of infinite dimensional manifolds Kriegl and Michor, 1997. A development of the theory of symplectic geometry and Hamiltonian systems on infinite dimensional *linear* spaces can be found in Marsden and Ratiu, 1999b.

2.1 Preliminary definitions, examples, and observations

Definition 2.1.1 (Symplectic map on $\mathbb{R}^{2n}$)**.** Let

$$J = \begin{pmatrix} 0 & I_n \\ -I_n & 0 \end{pmatrix}$$

be a matrix in $\mathbb{R}^{2n\times 2n}$, where I_n denotes an n-dimensional identity matrix. A diffeomorphism $\phi\colon \mathbb{R}^{2n} \to \mathbb{R}^{2n}$ is *symplectic (with respect to the symplectic structure J)* if

$$\mathrm{D}\phi^\top(z) J \mathrm{D}\phi(z) = J$$

for all $z \in \mathbb{R}^{2n}$, where $\mathrm{D}\phi(z)$ denotes the Jacobian matrix of the map ϕ at z and $\mathrm{D}\phi^\top(z)$ its transpose. △

The notion can be generalised as follows to allow for a coordinate free treatment.

Definition 2.1.2 (symplectic manifold)**.** A smooth manifold M equipped with a closed, nondegenerate differential 2-form ω is called a *symplectic manifold*. △

Definition 2.1.3 (symplectic map / symplectomorphism)**.** A diffeomorphism $\phi\colon M \to M'$ between two symplectic manifolds (M, ω) and (M', ω') is called a *symplectic map* or *symplectomorphism* if $\phi^*\omega' = \omega$, where ϕ^* denotes the pullback of the map ϕ. In other words, for all $m \in M$ and all vectors v, w in the tangent space T_mM at m

$$\omega'_{\phi(m)}(\mathrm{d}\phi_m(v), \mathrm{d}\phi_m(w)) = \omega_m(v, w).$$

Here $\mathrm{d}\phi_m(v) = \phi_*(v)$ denotes the differential of ϕ at the point m evaluated at the tangent vector v, i.e. the pushforward of v by ϕ. △

The theory of Riemannian geometry, in which manifolds are equipped with a metric, differs from the theory of symplectic geometry. One striking difference is that locally all symplectic manifolds of the same dimension are symplectomorphic and a standard form can be provided.

Theorem 2.1.1 (Theorem of Darboux)**.** *Let (M, ω) be a symplectic manifold. For each $m \in M$ there exists an open neighbourhood $U \subset M$ around m and local coordinates $p_1, \ldots, p_n, q^1, \ldots, q^n$ defined on U such that*

$$\omega = \sum_{j=1}^{n} \mathrm{d}p_j \wedge \mathrm{d}q^j.$$

In other words, any two symplectic manifolds M, M' are locally symplectomorphic, i.e. around any two points $p \in M$ and $p' \in M$ there exist open neighbourhoods U, U' and a symplectomorphism $\phi\colon U \to U'$.

Remark 2.1.1. The coordinate system $p_1, \ldots, p_n, q^1, \ldots, q^n$ are referred to as *Darboux-coordinates*. To prove the theorem, one can first prove a linear version, i.e. prove that skew-symmetric, nondegenerate bilinear forms on $\mathbb{R}^{2n}$ (*linear symplectic forms*) can, after a linear coordinate transformation, be represented by the matrix

$$J = \begin{pmatrix} 0 & I \\ -I & 0 \end{pmatrix}.$$

Darboux's theorem can then be proved for manifolds using a *Moser-type argument* connecting two given symplectic forms ω_0 and ω_1 on a sufficiently small neighbourhood

by a smooth family ω_t of symplectic forms and constructing a smooth family ψ_t of diffeomorphisms such that $\psi_t^*\omega_t = \omega_0$. A proof can be found in Libermann and Marle, 1987. △

Remark 2.1.2. From Darboux's theorem it follows that the dimension of every symplectic manifold M is even. Let us remark on a few global properties of symplectic manifolds. Let $\dim(M) = 2n$. It is easy to verify in Darboux coordinates that the n-th exterior power ω^n is nondegenerate. Thus, ω^n is a volume form and M is orientable. It follows that symplectic maps on M are orientation and volume preserving. However, if $n \geq 1$ then the group of symplectic maps is smaller then the group of volume preserving maps (see e.g. Gromov's non-squeezing theorem (McDuff and Salamon, 2017, Ch.12)). Orientable surfaces ($n = 1$) admit symplectic structures: we can use their volume forms as symplectic structures. However, not every even dimensional, orientable manifold admits a symplectic structure: spheres of dimension $2n$ with $n \geq 2$ are counterexamples as can be deduced from their algebraic topological structure.[1] △

Remark 2.1.3. In the setting of Darboux's theorem the vector fields of the coordinate functions $\frac{\partial}{\partial p_1}, \ldots, \frac{\partial}{\partial p_n}, \frac{\partial}{\partial q^1}, \ldots, \frac{\partial}{\partial q^n}$ constitute a local frame for the tangent bundle $TM \to M$ over M. We have

$$\omega\left(\frac{\partial}{\partial p_i}, \frac{\partial}{\partial q^j}\right) = \begin{cases} 1, & j = i \\ 0, & j \neq i \end{cases}, \quad \omega\left(\frac{\partial}{\partial q^i}, \frac{\partial}{\partial q^j}\right) = 0, \quad \omega\left(\frac{\partial}{\partial p_j}, \frac{\partial}{\partial p_i}\right) = 0.$$

Thus, in the considered local frame the symplectic form ω corresponds to the nondegenerate, skew-symmetric bilinear form that is represented by the matrix

$$J = \begin{pmatrix} 0 & I \\ -I & 0 \end{pmatrix},$$

where I denotes an identity matrix of size $n \times n$. Moreover, the condition $\phi^*\omega = \omega$ for a map on M to be symplectic translates to

$$\mathrm{D}\phi^\top J \mathrm{D}\phi = J.$$

We have, thus, recovered Definition 2.1.1. △

Example 2.1.1 (Cotangent bundle). An important example of a symplectic manifold is the cotangent bundle. Let us describe its canonical symplectic structure in detail. Consider a smooth manifold X. The cotangent bundle $\pi\colon T^*X \to X$ admits a symplectic

[1] A $2n$-dimensional sphere S^{2n} with $n \geq 2$ is a compact manifold without boundary. Therefore, its volume form μ cannot have a primitive (by Stokes's theorem) and the cohomology class $[\mu]$ must be nontrivial. However, the cohomology class $[\omega^n] = [\omega \wedge \ldots \wedge \omega] = [\omega] \cup \ldots \cup [\omega]$ for any 2-form ω is trivial because the second cohomology class of S^{2n} is zero. Here $\cup$ denotes the cup-product. Thus, ω^n cannot be a volume form and ω cannot be a symplectic form.

structure which can be defined canonically[2] as follows: define the 1-form λ on T^*X by

$$\lambda_\alpha(v) = \alpha(\mathrm{d}\pi|_\alpha(v)) \quad \text{for all } \alpha \in T^*X, v \in T_\alpha T^*X.$$

The 1-form λ is called the *Liouvillian-1-form*. The symplectic structure on T^*X is given as $\omega = \mathrm{d}\lambda$. Indeed, the 2-form ω is closed since $\mathrm{d}^2 = 0$, as required. Let us give a description of ω in local coordinates to show non-degeneracy as well as for reference later. For all $\alpha \in T^*X$ we find local coordinates $x_1, \dots, x_n$ for X centred at $\pi(\alpha)$. Define coordinates $p_1, \dots, p_n, q^1, \dots, q^n$ on T^*X by

$$q^i = x^i \circ \pi \quad \text{and } p_i \text{ as the linear extension of } p_i(\gamma) = \gamma\left(\frac{\partial}{\partial x^i}\right) \text{ for } 1 \leq i \leq n.$$

For $\alpha \in T^*X$ we calculate

$$\begin{aligned}
\lambda_\alpha\left(\frac{\partial}{\partial q^i}\Big|_\alpha\right) &= \alpha\left(\mathrm{d}\pi|_\alpha\left(\frac{\partial}{\partial q^i}\Big|_\alpha\right)\right) \\
&= \sum_{j=1}^n \alpha\left(\frac{\partial}{\partial x^j}\Big|_{\pi(\alpha)}\right) \mathrm{d}x^j|_{\pi(\alpha)}\left(\mathrm{d}\pi|_\alpha\left(\frac{\partial}{\partial q^i}\Big|_\alpha\right)\right) \\
&= \sum_{j=1}^n \alpha\left(\frac{\partial}{\partial x^j}\Big|_{\pi(\alpha)}\right) \mathrm{d}\underbrace{(x^j \circ \pi)}_{=q^j}|_\alpha\left(\frac{\partial}{\partial q^i}\Big|_\alpha\right) \\
&= \sum_{j=1}^n \alpha\left(\frac{\partial}{\partial x^j}\Big|_{\pi(\alpha)}\right) \cdot \delta_{ij} \\
&= \alpha\left(\frac{\partial}{\partial x^i}\Big|_{\pi(\alpha)}\right) \\
&= p_i(\alpha)
\end{aligned}$$

where δ is the Kronecker delta with $\delta_{ij} = 1$ if $i = j$ and 0 otherwise. Similarly,

$$\lambda_\alpha\left(\frac{\partial}{\partial p^i}\Big|_\alpha\right) = \sum_{j=1}^n \alpha\left(\frac{\partial}{\partial x^j}\Big|_{\pi(\alpha)}\right) \mathrm{d}\underbrace{(x^j \circ \pi)}_{=q^j}|_\alpha\left(\frac{\partial}{\partial p^i}\Big|_\alpha\right) = 0.$$

Therefore,

$$\lambda = \sum_{i=1}^n \left(\lambda\left(\frac{\partial}{\partial q^i}\right)\mathrm{d}q^i + \lambda\left(\frac{\partial}{\partial p^i}\right)\mathrm{d}p_i\right) = \sum_{i=1}^n p_i \mathrm{d}q^i.$$

We obtain

$$\omega = \sum_{i=1}^n \mathrm{d}p_i \wedge \mathrm{d}q^i \tag{2.1.1}$$

[2] In a coordinate independent way

which is nondegenerate since $\omega^n = \omega \wedge \ldots \wedge \omega$ is a volume form. △

Different notions exist for submanifolds of symplectic manifolds to describe how the symplectic structure degenerates when restricted to a submanifold. Of central importance for this work is the notion of *Lagrangian* submanifolds, defined below, on which ω fully degenerates. A framework which we will develop to describe bifurcations of solutions to certain boundary value problems will involve the intersection of such manifolds in an ambient symplectic manifold.

Definition 2.1.4 (isotropic, Lagrangian, symplectic, coisotropic submanifold)**.** Let (M, ω) be a symplectic manifold of dimension $2n$. Consider an inclusion $\iota\colon L \hookrightarrow M$ of a submanifold L into M. If $\iota^*\omega = 0$, i.e.

$$\forall m \in L \; \forall v, w \in T_m L : \omega_m(v, w) = 0,$$

then L is called *isotropic*. If L is isotropic and $\dim L = n$ then L is called *Lagrangian*. If $(L, \iota^*\omega)$ constitutes a symplectic manifold then L is called *symplectic*. If

$$T_m L^{\perp_\omega} := \{v \in T_m M : \omega(v, w) = 0 \text{ for all } w \in T_m L\} \subseteq T_m L$$

then L is called *coisotropic*. △

Remark 2.1.4. A Lagrangian submanifold L of a symplectic manifold M is maximally isotropic as well as minimally coisotropic. △

The following calculus result is handy when working with cotangent bundles.

Proposition 2.1.2. *Consider the cotangent bundle $\pi\colon T^*X \to X$ over a smooth manifold X with the canonical symplectic structure $\omega = \mathrm{d}\lambda$ defined in Example 2.1.1. If $\beta\colon X \to T^*X$ is a 1-form on X then*

$$\beta^*\lambda = \beta.$$

Here β on the left hand side of the assertion is to be interpreted as a map $\beta\colon X \to T^*X$ and on the right hand side as a 1-form on X.

Proof. Let $x \in X$ and $w \in T^*_x X$. We have

$$\begin{aligned}\beta^*\lambda_x(w) &= \lambda_{\beta(x(w))}(\mathrm{d}\beta|_x(w)) = \beta(x)(\mathrm{d}\pi|_{\beta(x)}(\mathrm{d}\beta|_x(w))) \\ &= \beta(x)(\mathrm{d}(\underbrace{\pi \circ \beta}_{=\mathrm{id}\colon X \to X})_x(w))) = \beta_x(w).\end{aligned}$$

□

Corollary 2.1.3. *Since pullback and an application of the differential operator d commute it follows that $\beta(X)$ is a Lagrangian manifold of $(T^*X, \mathrm{d}\lambda)$ if and only if the 1-form β is closed.*

Example 2.1.2. Of importance to this project is the following relation of symplectic maps with Lagrangian submanifolds: consider the symplectic manifold (M, ω) with local Darboux coordinates $(p, q) = (p_1, \dots, p_n, q^1, \dots, q^n)$ and $(\widetilde{M}, \tilde{\omega})$ with local Darboux coordinates $(P, Q) = (P_1, \dots, P_n, Q^1, \dots, Q^n)$. Define the projections $\pi\colon M \times \widetilde{M} \to M$ and $\tilde{\pi}\colon M \times \widetilde{M} \to \widetilde{M}$. The manifold $(M \times \widetilde{M}, \omega_\times)$ with $\omega_\times = \pi^*\omega - \tilde{\pi}^*\tilde{\omega}$ is a symplectic manifold with local Darboux coordinates (p, Q, q, P). Here, we do not differentiate between a coordinate function q^j, p_j, Q^j, P_j and its pullback with the appropriate projection to simplify notation. The graph L of a symplectic map $\phi\colon M \to \widetilde{M}$ is a Lagrangian submanifold of $(M \times \widetilde{M}, \omega_\times)$ because

$$(\mathrm{id}_M, \phi)^*(\omega_\times) = \omega - \phi^*\omega = 0.$$

Conversely, the above calculation shows that a Lagrangian submanifold of $M \times \widetilde{M}$ defines a symplectic map wherever it can be written as a graph over M, i.e. parametrized by the coordinates p, q. △

In the following chapter we will relate boundary value problems for symplectic maps to the problem of finding critical points of a smooth function. To construct these functions we will need the classical tool of *generating functions*.

Definition 2.1.5 (generating functions)**.** We continue in the setting of Example 2.1.2. However, we drop the requirement that L is the graph of a symplectic map. Consider the following locally defined differential one-forms on $(M \times \widetilde{M}, \omega_\times)$.

$$\theta_1 = \sum_{j=1}^{n} q^j \mathrm{d}p_j - Q^j \mathrm{d}P_j \qquad \theta_2 = \sum_{j=1}^{n} q^j \mathrm{d}p_j + P_j \mathrm{d}Q^j,$$
$$\theta_3 = \sum_{j=1}^{n} -p_j \mathrm{d}q^j - Q^j \mathrm{d}P_j \qquad \theta_4 = \sum_{j=1}^{n} -p_j \mathrm{d}q^j + P_j \mathrm{d}Q^j.$$

The one-forms fulfil $\mathrm{d}\theta_j = -\omega_\times$ such that each θ_j is closed on Lagrangian submanifolds L of $M \times \widetilde{M}$ and therefore, by the Poincaré Lemma, admits a local primitive $S_j\colon \tilde{L} \to \mathbb{R}$, where $\tilde{L} \subset L$. The function S_j is called a *generating function of type j for L*. If L is the graph of a symplectic map ϕ then we also say *generating function of type j for ϕ*. △

We can express the generating functions introduced in Definition 2.1.5 in local coordinates: wherever $(p, P) = (p_1, \dots, p_n, P_1, \dots, P_n)$ constitutes a local coordinate system on L we can express S_1 as a map in (p, P). We write $S_1 = S_1(p, P)$ and

consider

$$\sum_{j=1}^{n} \frac{\partial S_1}{\partial p_j} \mathrm{d}p_j + \frac{\partial S_1}{\partial P_j} \mathrm{d}P_j = \mathrm{d}S_1 = \theta_1 = \sum_{j=1}^{n} q^j \mathrm{d}p_j - Q^j \mathrm{d}P_j. \tag{2.1.2}$$

The differential 1-forms $\mathrm{d}p_j$, $\mathrm{d}q^j$, $\mathrm{d}P_j$, $\mathrm{d}Q^j$ constitute a local frame for the cotangent bundle over $M \times \widetilde{M}$ and provide at each point $(m, \tilde{m})$ a basis for $T^*_{(m,\tilde{m})}(M \times \widetilde{M})$. Therefore, comparing coefficients in (2.1.2) we can conclude that L can be recovered locally as

$$\left\{ (p,q,P,Q) \middle| q^j = \frac{\partial S_1}{\partial p_j}(p,P), -Q^j = \frac{\partial S_1}{\partial P_j}(p,P) \right\}. \tag{2.1.3}$$

On the other hand, a map S_1 of (p,P) generates a Lagrangian submanifold via (2.1.3). Analogously, if (p,Q) constitutes local coordinates on L then we can express $S_2 = S_2(p,Q)$ and recover L locally as

$$\left\{ (p,q,P,Q) \middle| q^j = \frac{\partial S_2}{\partial p_j}(p,Q), P_j = \frac{\partial S_2}{\partial Q_j}(p,Q) \right\}.$$

If (q,P) constitutes local coordinates on L then we can express $S_3 = S_3(q,P)$ and recover L locally as

$$\left\{ (p,q,P,Q) \middle| -p_j = \frac{\partial S_3}{\partial q^j}(q,P), -Q^j = \frac{\partial S_3}{\partial P_j}(q,P) \right\}.$$

If (q,Q) constitutes local coordinates on L then we can express $S_4 = S_4(q,Q)$ and recover L locally as

$$\left\{ (p,q,P,Q) \middle| -p_j = \frac{\partial S_4}{\partial q^j}(q,Q), P_j = \frac{\partial S_4}{\partial Q^j}(q,Q) \right\}.$$

The collection of generating functions defined in Definition 2.1.5 is by no means complete but there are other primitives θ of $-\omega_\times$ inducing truly different generating functions. An example is $\theta = \sum_{j=1}^{n}(p_j - P_j)\mathrm{d}q^j + (Q^j - q^j)\mathrm{d}P_j$.

Let us now recover the notions of classical Hamiltonian mechanics in the presented setting.

Definition 2.1.6 (Hamiltonian system)**.** A symplectic manifold (M,ω) equipped with a smooth map $H\colon M \to \mathbb{R}$ is called a *Hamiltonian system.* △

Definition 2.1.7 (Hamiltonian vector field)**.** Let (M,ω,H) be a Hamiltonian system. Since the 2-form ω is nondegenerate, there exists a unique vector field X_H on M such that

$$\mathrm{d}H = -\omega(X_H, .).$$

The vector field X_H is called *Hamiltonian vector field for* (M,ω,H). △

In a frame induced by Darboux coordinates $p^1, \dots, p^n, q_1, \dots, q_n$ the Hamiltonian vector field with respect to the system (M, ω, H) is given as

$$X_H = \sum_{j=1}^{n} \frac{\partial H}{\partial p_j} \frac{\partial}{\partial q^j} - \frac{\partial H}{\partial q_j} \frac{\partial}{\partial p^j} \tag{2.1.4}$$

and its flow lines $\gamma \colon I \to M$, where $I \subset \mathbb{R}$ is an open neighbourhood of 0, fulfil the first order ordinary differential equation

$$\frac{\mathrm{d}}{\mathrm{d}t}(q^j \circ \gamma)(t) = \frac{\partial H}{\partial p_j}(\gamma(t)) \quad \text{and} \quad \frac{\mathrm{d}}{\mathrm{d}t}(p_j \circ \gamma)(t) = -\frac{\partial H}{\partial q_j}(\gamma(t))$$

for $j \in \{1, \dots, n\}$. Abbreviating $q^j \circ \gamma$ with q^j and $p_j \circ \gamma$ with p_j the differential equation reads

$$\dot{q}^j = \frac{\partial H}{\partial p_j}(p, q) \quad \text{and} \quad \dot{p}_j = -\frac{\partial H}{\partial q_j}(p, q) \quad \text{for all } j \in \{1, \dots, n\}, \tag{2.1.5}$$

where $\dot{q}^j$ and $\dot{p}_j$ denote time derivatives. Using the local coordinate $z = (p, q)$ the differential equation reads

$$\dot{z} = J^{-1} \nabla H(z), \tag{2.1.6}$$

Definition 2.1.8 (Hamilton's equations, motions and flow)**.** If X_H is a Hamiltonian vector field then the flow equation

$$\frac{\mathrm{d}}{\mathrm{d}t}\gamma(t) = X_H(\gamma(t))$$

as well as its expression in Darboux coordinates (2.1.5) or (2.1.6) are called *Hamilton's equations*. The flow lines of a Hamiltonian vector field X_H are called *motions of the system* and the flow map for X_H is called a *Hamiltonian flow*. △

Hamilton's equations are form invariant under symplectic changes of coordinates. Moreover, only symplectic transformation leave Hamilton's equations invariant for all Hamiltonians. Indeed, this is the historical motivation to consider symplectic transformations. The statements are made precise in the following proposition.

Proposition 2.1.4 (symplectic change of coordinates)**.** *Let (M, ω, H) be a Hamiltonian system and let ϕ be a symplectic map. Define $\tilde{H} = H \circ \phi^{-1}$. The Hamiltonian vector fields $X_{\tilde{H}}$ and X_H are ϕ-related, i.e. for all $z \in M$*

$$X_{\tilde{H}}(\phi(z)) = \phi_*(X_H(z)) = \mathrm{d}\phi|_z(X_H(z)).$$

Therefore, under a symplectic change of coordinates Hamilton's equations $\frac{\mathrm{d}}{\mathrm{d}t}\gamma(t) = X_H(\gamma(t))$ translate to $\frac{\mathrm{d}}{\mathrm{d}t}\tilde{\gamma}(t) = X_{\tilde{H}}(\tilde{\gamma}(t))$, where $\tilde{\gamma} = \phi \circ \gamma$, i.e. Hamilton's equations

are left form invariant. Moreover, symplectic maps are exactly the diffeomorphisms which leave Hamilton's equations form invariant for all Hamiltonians.

Proof. Let $\tilde{z} = \phi(z)$. We have

$$\begin{aligned}-\omega_{\tilde{z}}(X_{\tilde{H}}(\tilde{z}),\cdot) &= \mathrm{d}(H\circ\phi^{-1})|_{\tilde{z}} = \mathrm{d}H|_z \circ \mathrm{d}\phi^{-1}|_{\tilde{z}} = -\omega_z(X_H(z), \mathrm{d}\phi^{-1}|_{\tilde{z}}(\cdot)) \\ &= -\omega_z(\mathrm{d}\phi^{-1}|_{\tilde{z}}(\mathrm{d}\phi|_z(X_H(z))), \mathrm{d}\phi^{-1}|_{\tilde{z}}(\cdot)) = -(\phi^{-1})^*(\omega_{\tilde{z}})(\mathrm{d}\phi|_z(X_H(z)),\cdot)\end{aligned}$$

Notice that to each $v \in T_zM$ there exists H such that $X_H(z) = v$. Now $X_{\tilde{H}}(\tilde{z}) = \phi_*(X_H(z))$ for all Hamiltonians H and $z \in M$ if and and only if the last expression of the calculation above coincides with $-\omega_z(\mathrm{d}\phi|_z(X_H(z)),\cdot)$ for all H and z. That is true if and only if $(\phi^{-1})^*(\omega_{\tilde{z}}) = \omega_z$. □

Remark 2.1.5. The proof of Proposition 2.1.4 can be done in local coordinates as follows.

$$\begin{aligned}\dot{\tilde{z}} &= \mathrm{D}\phi(z)\dot{z} = \mathrm{D}\phi(z)J^{-1}\nabla H(z) = \mathrm{D}\phi(z)J^{-1}\nabla(\tilde{H}\circ\phi)(\phi^{-1}(\tilde{z})) \\ &= \underbrace{\mathrm{D}\phi(z)}_{\overset{(*)}{=} J^{-1}\mathrm{D}\phi(z)J} J^{-1}\mathrm{D}\phi^{-1}(\phi(z))\nabla\tilde{H}(\tilde{z}) \overset{(*)}{=} J^{-1}\nabla\tilde{H}(\tilde{z}).\end{aligned}$$

The equations $(*)$ hold for all H and z if and only if ϕ is symplectic. This means Hamilton's equations are form invariant exactly under symplectic changes of coordinates. △

Example 2.1.3. The movement of a particle of unit mass in a gravitational field $V\colon \mathbb{R}^n \to \mathbb{R}$ can be described by Newton's law of motion as $\ddot{x} = -\nabla V(x)$, where $x(t) \in \mathbb{R}^n$ describes the position of the particle at time t. Setting $q = x$ and $p = \dot{x}$ the equations of motion arise as Hamilton's equations on $\mathbb{R}^{2n}$ equipped with the standard symplectic structure for the Hamiltonian

$$H(p,q) = \frac{1}{2}\langle p,p\rangle + V(q),$$

where $\langle,\rangle$ denotes the Euclidean scalar product in $\mathbb{R}^n$. △

2.2 Conservation laws for Hamiltonian systems

Proposition 2.2.1. *Let (M,ω,H) be a Hamiltonian system. The Hamiltonian H is a constant of motion, i.e. for any flow line $\gamma\colon I \to \mathbb{R}$ of the Hamiltonian vector field X_H we have $H\circ\gamma = H$.*

Proof. For all $\tau \in I$

$$\left.\frac{\mathrm{d}}{\mathrm{d}t}\right|_\tau (H\circ\gamma)(t) = \mathrm{d}H|_{\gamma(\tau)}(\dot{\gamma}(\tau)) = -\omega_{\gamma(\tau)}(X_H(\gamma(\tau)),\dot{\gamma}(\tau)) = -\omega_{\gamma(\tau)}(\dot{\gamma}(\tau),\dot{\gamma}(\tau)) = 0.$$

□

Quantities that are constant along motions are also called *integrals of motion.*

Proposition 2.2.2. *At each time τ the Hamiltonian flow ϕ_τ of a Hamiltonian system (M, ω, H) defines a symplectic map.*[3]

Proof. Using the definition of the Lie-derivative and the properties of a flow map

$$\frac{\mathrm{d}}{\mathrm{d}t}\bigg|_{t=\tau} \phi_t^*\omega = \frac{\mathrm{d}}{\mathrm{d}t}\bigg|_{t=0} (\phi_\tau^* \circ \phi_t^*)\omega = \phi_\tau^* \left(\frac{\mathrm{d}}{\mathrm{d}t}\bigg|_{t=0} \phi_t^*\omega \right) = \phi_\tau^* \mathcal{L}_{X_H}\omega.$$

Using Cartan's formula for the Lie derivative it follows that

$$\mathcal{L}_{X_H}\omega = \iota_{X_H} \underbrace{\mathrm{d}\omega}_{=0} + \mathrm{d}\underbrace{\iota_{X_H}\omega}_{=-\mathrm{d}H} = 0,$$

where $\iota_{X_H}\alpha$ denotes the contraction of a differential form α with the vector field X_H. As $\phi_0 = \mathrm{id}$ we conclude $\phi_\tau^*\omega = \omega$. □

Remark 2.2.1. Alternatively, Proposition 2.2.2 can be proved in local coordinates: expressing the flow ϕ_t and the Hamiltonian H in local Darboux coordinates $z = (p, q)$ we obtain

$$\frac{\mathrm{d}}{\mathrm{d}t}\phi_t(z) = J^{-1}\nabla H(\phi_t(z)).$$

Differentiation w.r.t. z yields

$$\frac{\mathrm{d}}{\mathrm{d}t}\mathrm{D}\phi_t(z) = J^{-1}\mathrm{Hess}(H)(\phi_t(z))\mathrm{D}\phi_t(z),$$

where $\mathrm{D}\phi_t(z)$ denotes the Jacobi-matrix of the flow map ϕ_t at z and $\mathrm{Hess}(H)(\phi_t(z))$ the Hessian matrix of H at $\phi_t(z)$. We have

$$\begin{aligned}
\frac{\mathrm{d}}{\mathrm{d}t}(\mathrm{D}\phi_t(z)^\top J \mathrm{D}\phi_t(z)) &= (J^{-1}\mathrm{Hess}(H)(\phi_t(z))\mathrm{D}\phi_t(z))^\top J \mathrm{D}\phi_t(z) \\
&\quad + \mathrm{D}\phi_t(z)^\top \underbrace{JJ^{-1}}_{=\mathrm{Id}} \mathrm{Hess}(H)(\phi_t(z))\mathrm{D}\phi_t(z) \\
&= \mathrm{D}\phi_t(z)^\top \mathrm{Hess}(H)(\phi_t(z)) \underbrace{J^{-T}J}_{=-\mathrm{Id}} \mathrm{D}\phi_t(z) \\
&\quad + \mathrm{D}\phi_t(z)^\top \mathrm{Hess}(H)(\phi_t(z))\mathrm{D}\phi_t(z) \\
&= 0
\end{aligned}$$

[3] If the vector field X_H is not complete, this statement holds locally.

Let I be the identity matrix of dimension $\dim(M)$. Together with

$$\mathrm{D}\phi_0(z)^\top J \mathrm{D}\phi_0(z) = IJI = J$$

the above calculation shows that the flow map is symplectic. △

Remark 2.2.2. The symplecticity of Hamiltonian flows corresponds to the conservation of a certain quadratic quantity. In the setting of Remark 2.2.1, solutions to the augmented system

$$\begin{aligned} \dot{z} &= J^{-1}\nabla H(z) \\ \dot{v}_1 &= J^{-1}\mathrm{Hess}\, H(z) v_1 \\ \dot{v}_2 &= J^{-1}\mathrm{Hess}\, H(z) v_2. \end{aligned} \tag{2.2.1}$$

with initial data $(z(0), v_1(0), v_2(0))$ are given as

$$z(t) = \phi_t(z(0)), \qquad v_1(t) = \mathrm{D}\phi_t(z(0))v_1(0), \qquad v_2(t) = \mathrm{D}\phi_t(z(0))v_2(0).$$

As can be deduced from the calculation in Remark 2.2.1, symplecticity of the flow map of $\dot{z} = J^{-1}\nabla H(z)$ is equivalent to the conservation of the quadratic quantity

$$Q(z, v_1, v_2) = v_1^\top J v_2$$

by the flow of the augmented system (2.2.1). △

Definition 2.2.1 (Poisson bracket)**.** For two smooth functions $f, g\colon M \to \mathbb{R}$ on a symplectic manifold (M, ω) we define the *Poisson bracket* $\{f, g\}\colon M \to \mathbb{R}$ of f and g by

$$\{f, g\} := \omega(X_f, X_g)$$

where X_f and X_g denote Hamiltonian vector fields with respect to f and g. △

In the following, the evaluation of a vector field X at the (germ of a locally defined) function f is denoted by $X(f)$. This corresponds to the Lie derivative of f along the vector field X, i.e. $\mathcal{L}_X(f)$. The following properties of the Poisson bracket can be computed directly from the definition.

Lemma 2.2.3. *We have*

$$\{f, g\} = \omega(X_f, X_g) = -\mathrm{d}f(X_g) = -X_g(f).$$

Lemma 2.2.4. *We have*

$$[X_f, X_g] = X_{\{f,g\}}.$$

Proof. Let Y be a vector field.

$$\begin{aligned}
-\omega(X_{\{f,g\}}, Y) &= \mathrm{d}\{f,g\}(Y) \\
&= (\mathrm{d}\omega(X_f, X_g))(Y) \\
&= -(\mathrm{d}\iota_{X_f}\iota_{X_g}\omega)(Y) - (\iota_{X_f}\underbrace{\mathrm{d}(\iota_{X_g}\omega)}_{=-\mathrm{d}^2 g=0})(Y) \\
&= -\left(\mathrm{d}\circ\iota_{X_f} + \iota_{X_f}\circ\mathrm{d}\right)(\iota_{X_g}\omega)\,(Y) \\
\text{(Cartan's formula)} &= -\mathcal{L}_{X_f}\left(\iota_{X_g}\omega\right)(Y) \\
\text{(Lie derivative of 1-form)} &= -\mathcal{L}_{X_f}\left((\iota_{X_g}\omega)(Y)\right) + (\iota_{X_g}\omega)(\mathcal{L}_{X_f}(Y)) \\
&= -\mathcal{L}_{X_f}\left(\omega(X_g, Y)\right) + \omega(X_g, \mathcal{L}_{X_f}(Y)) \\
\text{(Leibniz rule to first term)} &= -\underbrace{\mathcal{L}_{X_f}(\omega)}_{=0}(X_g, Y) - \omega(\mathcal{L}_{X_f}(X_g), Y) \\
&= -\omega([X_f, X_g], Y).
\end{aligned}$$

The claim follows by the nondegeneracy of ω. □

Lemma 2.2.5. *The Poisson bracket fulfils the Jacobi-identity,*

$$\{f,\{g,h\}\} + \{g,\{h,f\}\} + \{h,\{f,g\}\} = 0.$$

Proposition 2.2.6. *The Poisson bracket is skew-symmetric and bilinear over $\mathbb{R}$ and fulfils the Jacobi identity. Therefore, the Poisson bracket is a Lie bracket on the space $\mathcal{C}^\infty(M)$ of smooth functions $M \to \mathbb{R}$. Moreover, since $[X_f, X_g] = X_{\{f,g\}}$ the map $f \mapsto X_f$ defines a Lie-algebra homomorphism $(\mathcal{C}^\infty(M), \{\cdot,\cdot\}) \to (\Gamma(TM), [.,.])$. Here $\Gamma(TM)$ denotes the vector fields on M (sections of the tangent bundle) and $[\cdot,\cdot]$ the commutator of vector fields.*

Remark 2.2.3. Using (2.1.4) we can express the Poisson bracket locally in Darboux coordinates as

$$\{f,g\} = \sum_{j=1}^{n} \frac{\partial g}{\partial q_j}\frac{\partial f}{\partial p^j} - \frac{\partial g}{\partial p_j}\frac{\partial f}{\partial q^j}.$$

△

Remark 2.2.4. Sign conventions for ω, X_H or $\{\cdot,\cdot\}$ as well as the ordering of the coordinates p ,q or q, p are not consistent in the literature (Hall, 2013; Bates and Weinstein, 1997; Golubitsky, I. Stewart, and Marsden, 1987; Brugnano, Iavernaro, and Trigiante, 2012; Libermann and Marle, 1987). Notice that in other sign conventions $f \mapsto X_f$ can be an anti-homomorphism in contrast to Proposition 2.2.6. △

Proposition 2.2.7. *Let (M, ω, H) be a Hamiltonian system with Hamiltonian vector field X_H and flow map ϕ_t. Let $f\colon M \to \mathbb{R}$ be a smooth function. The function f is an integral of motion if and only if $\{H, f\} = 0$*

Proof. We have

$$\frac{\mathrm{d}}{\mathrm{d}t} f \circ \phi_t = (\mathrm{d}f \circ \phi_t)(X_H \circ \phi_t) = \{H, f\} \circ \phi_t.$$

□

Definition 2.2.2 (Poisson commuting)**.** Functions f, g with $\{f, g\} = 0$ are said to *Poisson commute.* △

Later in this work we will investigate boundary value problems in Hamiltonian systems. For these problems not only symplectic structure will play a role: sometimes a Hamiltonian system has more integrals of motion than the Hamiltonian which can have an effect on how solutions to boundary value problems behave as parameters are varied. Let us introduce the notion of *complete integrability.* These are systems which have a maximal set of Poisson commuting integrals.

Definition 2.2.3 (Completely (Liouville) integrable system)**.** Let (M, ω, H) be a Hamiltonian system with $\dim M = 2n$. If there exist n pairwise Poisson commuting integrals of motion $f_1, \ldots, f_n$ such that the differentials $\mathrm{d}f_1, \ldots, \mathrm{d}f_n$ are linearly independent on a dense open subset M_0 of M then (M, ω, H) is a *completely (Liouville) integrable system.* △

Example 2.2.1. Any Hamiltonian system with $n = 1$ is a completely integrable system if the complement of $\{x \in M : \mathrm{d}H_x = 0\}$ is open and dense since the Hamiltonian itself is a conserved quantity. Moreover, sums of completely integrable systems are completely integrable: consider two completely integrable systems (M, ω, H), (M', ω', H') and the projections $\pi\colon M \times M' \to M$ and $\pi'\colon M \times M' \to M'$. Then the system $(M \times M', \pi^*\omega + \pi'^*\omega', H \circ \pi + H' \circ \pi')$ is completely integrable. △

A motion in a completely integrable system will remain in a common level set of $f_1, \ldots, f_n$. Moreover, a motion is either entirely contained in M_0 or in its complement $M \setminus M_0$.[4] The non-empty level sets of $f|_{M_0} = (f_1, \ldots, f_n)|_{M_0}\colon M_0 \to \mathbb{R}$ are Lagrangian submanifolds of M_0 of dimension n. These are invariant under the flow of $X_{f_1}, \ldots, X_{f_n}$ and form integral submanifolds of the (integrable) foliation spanned by the vector fields $X_{f_1}, \ldots, X_{f_n}$ on M_0. The flow of X_H is a linear combination of $X_{f_1}, \ldots, X_{f_n}$ with coefficients that are constant on each level set. Let N denote a connected component of a non-empty level set of $f|_{M_0}$ and assume that $X_{f_1}|_N, \ldots, X_{f_n}|_N$ are complete vector fields. We are now prepared to make assertions about global properties of the

[4] One can verify that non-degeneracy of $\mathrm{d}f_1 \wedge \ldots \wedge \mathrm{d}f_n$ is preserved along motions.

Hamiltonian system. Indeed, the following theorem says that in the compact case N is isomorphic to a torus or otherwise isomorphic to the cross product of a torus with a suitable Euclidean space. Moreover, motions on N are affine linear in suitable coordinates.

Theorem 2.2.8 (angle-coordinates)**.** *In the setting described above, there exists an integer $0 \leq k \leq n$ and a diffeomorphism $\Psi\colon \mathbb{R}^k/\mathbb{Z}^k \times \mathbb{R}^{n-k} \xrightarrow{\sim} N$. The universal covering $\mathbb{R}^n \to \mathbb{R}^k/\mathbb{Z}^k \times \mathbb{R}^{n-k} =: \mathbb{T}$ induces coordinates on $\mathbb{T}$. Composing the coordinate functions with Ψ^{-1} we obtain global coordinates $x^1, \ldots, x^n$ on N. The diffeomorphism Ψ can be chosen such that the Hamiltonian flow ϕ_t on N is an affine linear map $\phi_t(x) = x + tv$ for a fixed $v \in \mathbb{R}^n$.*

The diffeomorphism is constructed using the linear action of $\mathbb{R}^n$ on N induced by the commuting Hamiltonian flows $\phi^{X_{f_1}}, \ldots, \phi^{X_{f_n}}$:

$$\big((t_1, \ldots, t_n), y\big) \mapsto (\phi_{t_1}^{X_{f_1}} \circ \ldots \circ \phi_{t_n}^{X_{f_n}})(y)$$

The space $\mathbb{T}$ is constructed by quotienting out the isotropy group of the above action with respect to some point on N. Moreover, using the constants of motions $f_1, \ldots, f_n$ we can extend the coordinate system $x^1, \ldots, x^n$ of N to a coordinate system of a neighbourhood of N as made more precise by the following

Theorem 2.2.9 (action-angle-coordinates)**.** *Assume that N is compact. There exists an open neighbourhood $U \subset M_0$ of N such that $f|_U\colon U \to f(U)$ is a trivial fibre bundle with a symplectic trivialisation $\phi\colon U \to (\mathbb{R}^n/\mathbb{Z}^n) \times f(U)$. The symplectic structure on $(\mathbb{R}^n/\mathbb{Z}^n) \times f(U) \subset \mathbb{R}^{2n}$ is induced by the standard symplectic structure on $\mathbb{R}^{2n}$.*

Remark 2.2.5. The coordinates in the above theorems are called *action-angle coordinates* and the level sets $f|_U^{-1}(a)$ are called *Liouville tori*. The coordinates $x^1, \ldots, x^n$ can be interpreted as angle-coordinates. The term *action* refers to the values of the constants of motion $f_1, \ldots, f_n$. For proofs of the above theorems see, e.g., V. I. Arnold, 1989. △

Example 2.2.2. Consider the Hamiltonian $H(p, q) = \tilde{H}(q)$ on $(\mathbb{R}^{2n}, \omega)$ with the standard symplectic structure. Hamilton's equations in the notation of (2.1.5) read

$$\dot{q} = 0, \qquad \dot{p} = -\nabla \tilde{H}(q).$$

The coordinate functions $q_1, \ldots, q_n$ are n functionally independent, Poisson commuting constants of motion, i.e. $\mathrm{d}q_1, \ldots, \mathrm{d}q_n$ are linearly independent at each point in $\mathbb{R}^{2n}$. The

motion to the initial value (q_0, p_0) is described by the linear map

$$t \mapsto \begin{pmatrix} p_0 \\ q_0 \end{pmatrix} + t \begin{pmatrix} -\nabla \tilde{H}(q_0) \\ 0 \end{pmatrix}. \qquad \triangle$$

Example 2.2.3. Consider the frictionless mathematical pendulum (mass $m = 1$, massless incompressible rod of length 1, gravitational acceleration $g = 1$) whose deflection angle q is described by the differential equation $\ddot{q} + \sin(q) = 0$. A first order formulation is given by Hamilton's equations for the Hamiltonian system

$$H(p, q) = \frac{1}{2}p^2 - \cos(q) \tag{2.2.2}$$

on the symplectic manifold $M := \mathbb{R} \times \mathbb{R}/(2\pi\mathbb{Z})$ where the symplectic structure and the coordinates p, q are induced by the standard structures on the covering manifold $\mathbb{R}^2$. Define $M_0 := (\mathbb{R} \times \mathbb{R}/(2\pi\mathbb{Z})) \setminus \{(0, 0), (0, \pi)\}$. The system is completely integrable since the Hamiltonian H is a constant of motion, $\mathrm{d}H \neq 0$ for $(p, q) \in M_0$ and X_H is a complete vector field. A phase portrait, i.e. a plot of level sets of H, is displayed in Figure 2.1. The points $(0, 0), (0, \pi)$ are equilibria since $\mathrm{d}H|_{M \setminus M_0}$ vanishes. The invariant set $H^{-1}(1)$ is the union of two *homoclinic orbits* joining the saddle equilibrium $(0, \pi)$ with itself. However, the motions on $H^{-1}(1) \setminus \{(0, \pi)\}$ do not reach $(0, \pi)$ in finite time.

Moreover, $H^{-1}(1)$ separates the phase space M into three connected components corresponding to three different ways the pendulum can behave: the level sets lying in the compact component which contains the point $(p, q) = (0, 0)$ correspond to oscillations of the pendulum back and forth or calmly hanging down at $(p, q) = (0, 0)$. The orbits in the component containing $(p, q) = (p, 0)$ with $p > \sqrt{2}$ and the component containing $(p, q) = (p, 0)$ with $p < -\sqrt{2}$ correspond to a rotation of the pendulum. The movements on the separatrix described by the mathematical model are of a rather theoretical nature: at the saddle equilibrium $(0, \pi)$ the mathematical pendulum stands on its rod and a movement starting on any other points of the separatrix approaches the state $(0, \pi)$ while becoming arbitrarily slow. $\triangle$

In general, the motions in completely integrable systems cannot leave their Liouville tori and are called *quasi-periodic motions*. In case of compact Liouville tori the motions are periodic if and only if there exists a nontrivial $\mathbb{Z}$-linear combination of $v_1, \ldots, v_n$ to zero, where v comes from the *angle-coordinate-theorem* Theorem 2.2.9. The angles v can be thought of as belonging to the Liouville torus since each motion $x + tv$ running on the torus has the same v. The case where $v_1, \ldots, v_n$ are not $\mathbb{Z}$-linearly dependent is called the *non-resonant* case.

It is of interest what happens to the Liouville tori if the Hamiltonian system is

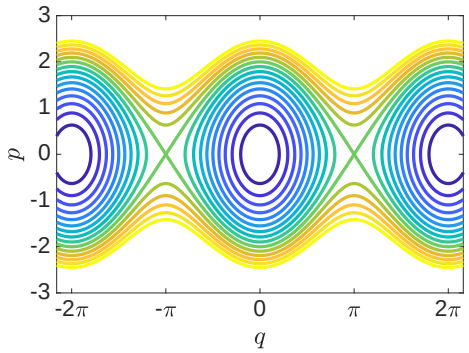

Figure 2.1: Level sets of the Hamiltonian $H(p,q) = \frac{1}{2}p^2 - \cos(q)$ for the mathematical pendulum

perturbed slightly such that complete integrability is destroyed. This question is answered by *perturbation theory for integrable systems* or *KAM-theory*, where *KAM* stands for Kolmogorov, Arnold and Moser. An introduction can be found in V. I. Arnold, Khukhro, et al., 2007. Roughly speaking, under non-degeneracy conditions most non-resonant tori deform and persist for sufficiently small perturbations but get destroyed when the perturbation becomes too large. Destroyed tori are being replaced by a set in the phase space where motion (in many cases) becomes chaotic. How much perturbation a torus can resist depends on how irrational the frequency vector v is. A typical condition that allows statements about persistence is the Diophantine condition: there exist $\alpha, \beta > 0$ such that

$$|\sum_{j=1}^{n} k_j v_j| \geq \beta \|k\|^{-\alpha} \tag{2.2.3}$$

for all $k \in \mathbb{Z}^k \setminus \{0\}$ (V. I. Arnold, Khukhro, et al., 2007, Ch.6).

Example 2.2.4. Returning to the mathematical pendulum from Example 2.2.3, we introduce a small time periodic forcing term in the vertical direction

$$\ddot{q} = -\sin(q) - \epsilon \sin(t) \tag{2.2.4}$$

with $\epsilon \in \mathbb{R}$. It has the time dependent Hamiltonian

$$\tilde{H}(t,p,q) = \frac{1}{2}p^2 - \cos(q) + \epsilon \sin(t) q. \tag{2.2.5}$$

To obtain an *autonomous*, i.e. a time-independent Hamiltonian H, we interpret t as a second component of the q-variable and introduce its conjugate momentum as a second

component of the p-variable. We obtain

$$\begin{aligned} H &: \mathbb{R}^3 \times \mathbb{R}/2\pi\mathbb{Z} \to \mathbb{R} \\ (p,q) = (p_1,p_2,q_1,q_2) &\mapsto \frac{1}{2}p_1^2 + p_2 - \cos(q_1) + \epsilon \sin(q_2)q_1. \end{aligned} \tag{2.2.6}$$

Notice that we have lifted the variable q_1, which corresponds to q in (2.2.4) and (2.2.5), from $\mathbb{R}/2\pi\mathbb{Z}$ to $\mathbb{R}$. On the contrary, we consider q_2, which corresponds to the time variable t in (2.2.4) and (2.2.5), as a variable on $\mathbb{R}/2\pi\mathbb{Z}$ rather than on $\mathbb{R}$, where the time variable was originally defined. This setting takes into account that the forcing is 2π-periodic and will turn out to be convenient in the analysis.

Hamilton's equations are

$$\begin{aligned} \dot{q}_1 &= p_1 \\ \dot{q}_2 &= 1 \\ \dot{p}_1 &= -\sin(q_1) - \epsilon \sin(q_2) \\ \dot{p}_2 &= -\epsilon \cos(q_2)q_1. \end{aligned}$$

Now we can analyse the four-dimensional phase portrait. If $\epsilon = 0$ then we obtain a completely integrable Hamiltonian system with integrals H and p_2. The invariant manifolds coincide with the Cartesian product of (periodic continuations of) the invariant manifolds of the free mathematical pendulum with the q_2-circle $\mathbb{R}/2\pi\mathbb{Z}$. However, increasing ϵ, the regular movements get more and more destroyed. Since $\dot{q}_2 = 1$ every orbit is transversal to the (*Poincaré-*) section $q_2 = 0$ and returns to the section every 2π time units. To obtain an illustration of the phase space movement, we plot the intersection points of a motion with the section $q_2 = 0$ for 10000 periods of the forcing term. This corresponds to the image of 10000 iterates of a so called *Poincaré map*. A projection of the image to the q_1, p_1-plane is displayed in Figure 2.2. The figure shows several orbits, i.e. iterates for various initialisations. The solid lines show the phase plot of the unperturbed system, for orientation. One can see that orbits near the separatrix of the unperturbed system have dissolved. Other periodic orbits have broken up into periodic islands surrounded by chaotic regions.

The plot in Figure 2.2 was obtained numerically. Hamilton's equation were solved using the symplectic *Störmer–Verlet scheme* which will be introduced in Example 3.3.2. Indeed, symplectic methods capture important qualitative features of Hamiltonian systems as will be made more precise in Section 3.5. △

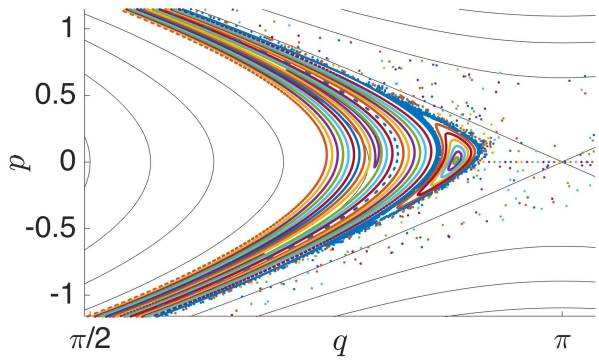

Figure 2.2: Subset of the phase portrait of the perturbed system $\tilde{H}(t,q,p) = \frac{1}{2}p^2 - \cos(q) + \epsilon\sin(t)q$ with $\epsilon = 0.02$. The underlying dynamics have been calculated for 1000 periods of the forcing term using the Störmer–Verlet scheme (Example 3.3.2) with 30 steps per period. The plot shows every 30th calculated point. For orientation, the thin black solid lines show the phase plot of the unperturbed system.

2.3 Symplectic symmetries

Symmetries are an important concept in Hamiltonian dynamics as they help to understand the motion of the system and allow for reductions to smaller dimensional systems. Let us briefly introduce the notions required in the following chapters. For a more extensive study consult, for instance, Marsden, Misiolek, et al., 2007.

2.3.1 Continuous symmetries

A *Lie group* G is a smooth manifold which has the structure of a group. Consider a *Lie group action* of G on a smooth manifold M, i.e. a group homomorphism

$$\sigma\colon G \mapsto \mathrm{Diff}(M), \quad g \mapsto (m \mapsto g.m)$$

such that the map

$$G \times M \mapsto M, \quad (g,m) \mapsto g.m$$

is smooth. Here $\mathrm{Diff}(M)$ denotes the group of diffeomorphisms on M. If (M,ω) is a symplectic manifold and $\sigma(G) \subset \mathrm{Diff}(M)$ is a subgroup of the symplectomorphisms on M then the group action is called *symplectic*.

Notice that symplectic group actions $\sigma\colon G \mapsto \mathrm{Sp}(M)$ leave the symplectic form ω of M invariant. Thus, if a Hamiltonian H of a Hamiltonian system (M,ω,H) is invariant under all symplectomorphisms $\sigma(g)$ for $g \in G$ then the equations of motions are invariant such that motions are mapped to motions under $\sigma(g)$ for every $g \in G$. We refer to symplectic group actions leaving H invariant as *continuous symmetries of*

the Hamiltonian system.

Under mild assumptions on the group action there is a deep relation between conserved quantities and continuous symmetries of Hamiltonian systems, explained by the famous *Noether theorem*: in the abelian case, to a k-dimensional symplectic group action one can construct a k-dimensional conserved integral of motion. (Under non-degeneracy conditions the integrals are independent.) See Hairer, Lubich, and Wanner, 2013, Ch. VI for details. On the other hand, the ideas presented in the paragraph preceding the angle-coordinates theorem (Theorem 2.2.8) can be made precise and it can be shown that flow maps of conserved quantities give rise to symplectic group actions.

2.3.2 Time reversal symmetry

Let us introduce a non-continuous symmetry, which frequently appears in Hamiltonian systems: the *time reversal symmetry*. For this, we need the concept of related vector fields which has already been mentioned in Proposition 2.1.4.

Definition 2.3.1 (related vector fields)**.** Let M and N be smooth manifolds and $\rho\colon M \to N$ a smooth map. Two vector fields $X \in \Gamma(TM)$, $Y \in \Gamma(TM)$ are called *ρ-related* if

$$\rho_* X = \rho^* Y,$$

where $\rho_* X$ denotes the push-forward of X and $\rho^* Y$ the pull-back of Y. In other words $\mathrm{d}\rho \circ X = Y \circ \rho$. △

Example 2.3.1. Recall from Proposition 2.1.4 that the Hamiltonian vector fields X_H and $X_{H\circ\phi^{-1}}$ are ϕ-related if ϕ is symplectic. △

Definition 2.3.2 (reversible vector field)**.** Let M be a smooth manifold and $\rho\colon M \to M$ be a diffeomorphism with $\rho^2 = -\mathrm{id}$. A vector field $X \in \Gamma(TM)$ is called *ρ-reversible* if and only if X is ρ-related to $-X$. △

Proposition 2.3.1. *Let ϕ_t denote the flow map of a ρ-reversible vector field $X \in \Gamma(TM)$ on a smooth manifold M at time t. Then*

$$\rho \circ \phi_t = \phi_{-t} \circ \rho.$$

Proof. The claimed equality holds for $t = 0$ and differentiating $\rho \circ \phi_t$ as well as $\phi_{-t} \circ \rho$ with respect to t shows that both maps are flow maps of $-X$. Therefore the claim follows by the uniqueness property of flow maps. □

Definition 2.3.3 (time-reversal Hamiltonian system)**.** A Hamiltonian system with a ρ-reversible Hamiltonian vector field is called a *time-reversal Hamiltonian system.* △

In time-reversal Hamiltonian systems the motions remain invariant if one applies ρ to the phase space and inverts time.

Example 2.3.2. The Hamiltonian system $(\mathbb{R}^{2n}, \omega, H)$ for the standard symplectic structure with mechanical Hamiltonian

$$H(p,q) = \frac{1}{2}\langle p, p\rangle - V(q)$$

is a time-reversal Hamiltonian system. The map ρ is given as $\rho(p,q) = (-p,q)$. The motions of H remain invariant if time as well as all momenta p are reversed. The unperturbed pendulum is a concrete example of a mechanical Hamiltonian system (see Figure 2.1). △

Chapter 3

Numerical integration and structure preserving methods

Let us follow Hairer, Lubich, and Wanner, 2013 to define and characterize numerical schemes to solve ordinary differential equations (ODEs) that take into account geometric structures and conserved quantities of the flow. For a general introduction to ODE theory and numerical approaches we refer to Atkinson, Han, and D. E. Stewart, 2011.

3.1 Basic notions of numerical methods

Consider the following non-autonomous system of first order ordinary differential equations

$$\dot{y} = f(t, y) \tag{3.1.1}$$

where f is defined near a point $(t_0, y_0) \in \mathbb{R} \times \mathbb{R}^n$.

Definition 3.1.1 (one-step method)**.** A *numerical-one-step method* assigns a map $\Phi_h \colon y_0 \mapsto y_1$ to a sufficiently regular ODE (3.1.1), a start-time t_0 and all sufficiently small parameters $h > 0$. The map Φ_h is called a *one-step map*. △

If defined, we say that the sequence $\{y_{j+1} = \Phi_h(y_j)\}_{j=1}^N$ with $h = \frac{\tau}{N}$ *approximates* a solution of the initial value problem (3.1.1) with $y(t_0) = y_0$ on the interval $[t_0, t_0 + \tau]$ at the time steps $\{t_0 + jh\}_{j=1}^N$ (regardless of how good the approximation is).

So called *multi-step methods* are implicitly defined by relating all elements (but a finite number of start values) of an approximating sequence with a finite number of previous elements. Formally, these methods are equivalent to one-step methods acting on higher dimensional spaces.

Definition 3.1.2 (order of a method)**.** A method is of *order* p if $p \in \mathbb{N}$ is the largest

integer such that for all $n \in \mathbb{N}$ and all analytic $f\colon \mathbb{R} \times \mathbb{R}^n \to \mathbb{R}^n$ in (3.1.1)

$$y_1 - y(t_0 + h) = \mathcal{O}(h^{p+1}) \quad \text{as } h \to 0. \tag{3.1.2}$$

Here y denotes the solution to the initial value problem (3.1.1) with $y(t_0) = y_0$. The above term is called *local error*. If $p > 0$ then the method is called *consistent*. △

Remark 3.1.1. To define the order of a method with respect to the class of analytic functions f is convenient because by the Cauchy–Kowalevski theorem (see, for instance, Teschl, 2012, §4) solutions are unique and analytic such that (3.1.2) is defined. It is interesting to note that defining the order of a method only for the class of scalar $f\colon \mathbb{R} \to \mathbb{R}$ leads to a different order theory, not just for exotic methods but even for classical classes of integrators like *Runge–Kutta methods* (see definition below), as remarked in Butcher, 2009. △

Remark 3.1.2. By definition, the order of convergence of a numerical method is defined asymptotically as $h \to 0$ and does not *per se* contain information on how the method behaves for large or moderate time-steps. Depending on the conditioning of the ODE, one might be forced to choose the step-size h very small to enjoy convergence properties. △

Remark 3.1.3 (adaptive methods). An ODE can be differently conditioned in different parts of the phase space. While in some parts small step-sizes are required to keep the accuracy of the method within a certain tolerance, in other parts choosing larger steps can be admissible and boost efficiency. It can, therefore, be advantageous to vary the step-size h during the integration process dynamically. Such methods are called *adaptive* and can be significantly more efficient (Ilie, Söderlind, and Corless, 2008). Adapting the time steps dynamically can be interpreted as solving a modified system with a non-adaptive method (Hairer, Lubich, and Wanner, 2013, Ch. VIII.2). However, in general the modified system will *not* inherit geometric structures from the initial problem. For some approaches to introduce adaptive time-stepping while preserving a Hamiltonian structure of a system see Hairer, Lubich, and Wanner, 2013, Ch. VIII. △

3.2 Runge–Kutta methods

An important class of one-step-methods are *Runge–Kutta methods*. Consider the following scheme of real numbers, called *Butcher tableau*,

$$\begin{array}{c|c} c & A \\ \hline & b^\top \end{array}, \tag{3.2.1}$$

where $A \in \mathbb{R}^{s\times s}$ is a real matrix and $b, c \in \mathbb{R}^s$ are real column vectors.

Definition 3.2.1 (Runge–Kutta method)**.** Let c_i in (3.2.1) correspond to the i^{th} row sum of A, i.e. $c_i = \sum_{j=1}^{s} a_{ij}$ for $i = 1, \dots, s$. The *s-stage Runge–Kutta method* corresponding to the Butcher tableau (3.2.1) and to the step-size h is a numerical one-step method. Applied to the ODE (3.1.1) it is defined as the map $y_0 \mapsto \Phi_h(y_0) = y_1$, where

$$y_1 = y_0 + h\sum_{i=1}^{s} b_i k_i \qquad \text{with } k_i = f\left(t_0 + c_i h, y_0 + h\sum_{j=1}^{s} a_{ij}k_j\right), \quad i = 1, \dots, s. \tag{3.2.2}$$

The values k_i are called *stages*. △

Remark 3.2.1. If the matrix A is a lower triangular matrix then (3.2.2) provides explicit formulas for $\Phi_h(y_0)$. In that case the method is called *explicit*. Otherwise the method is called *implicit* and the calculation of y_1 in (3.2.2) requires the solution of a system of equations. Therefore, the above scheme (3.2.2) will not induce a well defined map $y_0 \mapsto y_1$ for all Butcher tableaux, step-sizes h and general ODEs (3.1.1). We will consider only those Runge–Kutta methods, which induce a well defined map at least for the class of linear, invertible functions $f\colon y \mapsto f(y)$ in (3.1.1). Given such a method, the existence and locally uniqueness of the map $y_0 \mapsto y_1$ for more general regular ODEs can be obtained by the implicit function theorem for sufficiently small parameters h. △

Remark 3.2.2 (B-series). Computing the formal Taylor series of the local error $y_1 - y(y_0 + h)$ around $h = 0$ for a general Runge–Kutta method applied to (3.1.1) with $y(t_0) = y_0$ one can find conditions on the components $A = (a_{ij}), b = (b_i), c = (c_i)$ of the Butcher tableaux for the method to be of order p. For $p \leq 3$ these are given by

$$\begin{array}{l} \sum_{i=1}^{s} b_i = 1 \\ \sum_{i=1}^{s} b_i = 1, \quad \sum_{i=1}^{s} b_i c_i = \frac{1}{2} \\ \sum_{i=1}^{s} b_i = 1, \quad \sum_{i=1}^{s} b_i c_i = \frac{1}{2}, \quad \sum_{i=1}^{s} b_i c_i^2 = \frac{1}{3}, \quad b^\top A c = \frac{1}{6} \end{array}$$

for order 1, 2 and 3 respectively (see Hairer, Lubich, and Wanner, 2013, p. 25). However, to construct Runge–Kutta methods of high order it is necessary to allow a quickly growing number of stages s to make sure that the equations representing the order conditions are solvable. If one limits the number of stages s and/or requires the method to be explicit, then limits for the order p, so called *order barriers*, can be derived (Butcher, 2009). To compute series expansions of solutions $y(t_0 + h)$ to (3.1.1) and of Runge–Kutta methods applied to (3.1.1) in the step-size h (so called *B-series*) in order to obtain order conditions for higher order Runge–Kutta methods, it is convenient to use a clever notation making use of rooted trees. J.C. Butcher obtained a formal power

series expansion of Runge–Kutta methods and could write down a general expression for order conditions. See Butcher, 2010 for a review. An introduction to B-series and trees including some historical remarks can be found in McLachlan, Modin, Munthe-Kaas, et al., 2017 as well as in Hairer, Lubich, and Wanner, 2013, Ch. III. △

Below we present the scheme as well as the Butcher tableau of some Runge–Kutta methods of low order from Hairer, Lubich, and Wanner, 2013, Ch. II.1.1.

3.2.1 Order $p = 1$.

- Explicit Euler method.

$$y_1 = y_0 + hf(t_0, y_0), \qquad \begin{array}{c|c} 0 & 0 \\ \hline & 1 \end{array}$$

- Implicit Euler method.

$$y_1 = y_0 + hf(t_0 + h, y_1), \qquad \begin{array}{c|c} 1 & 1 \\ \hline & 1 \end{array}$$

3.2.2 Order $p = 2$.

- Implicit trapezoidal rule.

$$y_1 = y_0 + \frac{h}{2}\big(f(t_0, y_0) + f(t_0 + h, y_1)\big), \qquad \begin{array}{c|cc} 0 & 0 & 0 \\ 1 & 1/2 & 1/2 \\ \hline & 1/2 & 1/2 \end{array}$$

- Implicit midpoint rule.

$$y_1 = y_0 + hf\left(t_0 + \frac{1}{2}h, \frac{y_0 + y_1}{2}\right), \qquad \begin{array}{c|c} 1/2 & 1/2 \\ \hline & 1 \end{array}$$

- Heun's method.

$$y_1 = y_0 + \frac{1}{2}h\big(f(t_0, y_0) + f(t_0 + h, y_0 + hf(t_0, y_0))\big), \qquad \begin{array}{c|cc} 0 & 0 & 0 \\ 1 & 1 & 0 \\ \hline & 1/2 & 1/2 \end{array}$$

- Explicit midpoint method.

$$y_1 = y_0 + hf\left(t_0 + \frac{1}{2}h, y_0 + \frac{1}{2}hf(t_0, y_0)\right),$$

0	0	0
1/2	1/2	0
	0	1

3.2.3 Order $p = 4$.

Examples of a Runge–Kutta methods of order 4 are the methods *RK4* given by the Butcher tableau

0				
1/2	1/2			
1/2	0	1/2		
1	0	0	1	
	1/6	1/3	1/3	1/6

and the 3/8-rule

0				
1/3	1/3			
2/3	−1/3	1		
1	1	−1	1	
	1/8	3/8	3/8	1/8.

Notice that both methods are explicit such that the one-step maps are cheap to evaluate numerically.

3.3 Partitioned methods

In the following we concentrate on autonomous first order differential equations. Recall that any time-dependent system (3.1.1) can be replaced by an autonomous system by adding the differential equation $\dot{t} = 1$ to the set of ODEs and the initial condition $t(0) = t_0$ if an initial value problem is considered. See the perturbed mathematical pendulum (Example 2.2.4), for instance.

It can be useful to treat different variables in initial value problems with different numerical methods. Consider the following differential equations in partitioned form

$$\dot{y} = f(y, z), \quad \dot{z} = g(y, z). \tag{3.3.1}$$

In (3.3.1) the vector valued functions y and z are allowed to be of different dimension.

Definition 3.3.1 (partitioned Runge–Kutta method)**.** Consider the two tableaux

$$\begin{array}{c|c} c & A \\ \hline & b^\top \end{array} \qquad \begin{array}{c|c} \hat{c} & \hat{A} \\ \hline & \hat{b}^\top \end{array}$$

each corresponding to s-stage Runge–Kutta methods. A *partitioned Runge–Kutta method* for (3.3.1) is given by $(y_0, z_0) \mapsto (y_1, z_1)$ where

$$y_1 = y_0 + h\sum_{i=1}^{s} b_i k_i, \qquad z_1 = z_0 + h\sum_{i=1}^{s} \hat{b}_i l_i$$

$$k_i = f\left(y_0 + h\sum_{j=1}^{s} a_{ij}k_j, z_0 + h\sum_{j=1}^{s} \hat{a}_{ij}l_j\right), \quad l_i = g\left(y_0 + h\sum_{j=1}^{s} a_{ij}k_j, z_0 + h\sum_{j=1}^{s} \hat{a}_{ij}l_j\right).$$

△

Example 3.3.1 (Symplectic Euler method). The *symplectic*[1] Euler method or *semi-implicit Euler method* is represented by the Butcher tableaux

$$\begin{array}{c|c} 1 & 1 \\ \hline & 1 \end{array} \qquad \begin{array}{c|c} 1 & 0 \\ \hline & 1 \end{array}.$$

This corresponds to the scheme

$$\begin{aligned} y_1 &= y_0 + hf(y_1, z_0) \\ z_1 &= z_0 + hg(y_1, z_0). \end{aligned} \tag{3.3.2}$$

Here the y-variable is treated with the implicit Euler scheme while the z-variable is treated with the explicit Euler method. △

Example 3.3.2 (Störmer–Verlet scheme). Another example is the second order accurate *Störmer–Verlet* scheme, which we will frequently employ in our numerical simulations. It is given by the Butcher tableaux

$$\begin{array}{c|cc} 0 & 0 & 0 \\ 1 & 1/2 & 1/2 \\ \hline & 1/2 & 1/2 \end{array} \qquad \begin{array}{c|cc} 1/2 & 1/2 & 0 \\ 1/2 & 1/2 & 0 \\ \hline & 1/2 & 1/2 \end{array}.$$

Notice that the above scheme becomes explicit if f does not depend on y and g does

[1] The name will be explained in the following.

not depend on z. In that case we obtain

$$\begin{aligned} y_1 &= y_0 + hf\left(z_0 + \frac{1}{2}hg(y_0)\right) \\ z_1 &= z_0 + \frac{1}{2}h\left(g(y_0) + g(y_1)\right). \end{aligned}$$

The term $z_0 + \frac{1}{2}hg(y_0)$ can be interpreted as a first order approximation of $z_{1/2}$ using the explicit Euler method. For reference, we give the formulas of the 2nd order symplectic Störmer–Verlet numerical integration scheme for Hamilton's equations (2.1.5). The method reads

$$\begin{aligned} p_{n+1/2} &= p_n - \frac{h}{2}\nabla_q H(p_{n+1/2}, q_n) \\ q_{n+1} &= q_n + \frac{h}{2}\big(\nabla_p H(p_{n+1/2}, q_n) + \nabla_p H(p_{n+1/2}, q_{n+1})\big) \\ p_{n+1} &= p_{n+1/2} - \frac{h}{2}\nabla_q H(p_{n+1/2}, q_{n+1}). \end{aligned}$$

The scheme is explicit if the coordinate expression of the Hamiltonian function H separates the variables q and p, i.e. if H is of the form

$$H(p, q) = K(p) + V(q).$$

This is the case for mechanical Hamiltonians, for instance. If H separates q and p then the Störmer–Verlet integration scheme is commonly referred to as *Leapfrog method* (Hairer, Lubich, and Wanner, 2013, p. I.3.1).

△

3.4 Adjoint and symmetric methods

Definition 3.4.1 (adjoint method and symmetric method)**.** If Φ_h is a numerical one step method, then $\Phi_h^* := \Phi_{-h}^{-1}$ is called the *adjoint method* to Φ_h. If $\Phi_h^* = \Phi_h$ then the method is called *symmetric*. △

Example 3.4.1. The implicit Euler method is the adjoint method to the explicit Euler method. The trapezoidal rule and the midpoint rule are symmetric. △

Remark 3.4.1. The flow map ϕ_τ at time τ of a vector field fulfils $\phi_\tau^{-1} = \phi_{-\tau}$. Symmetric numerical methods preserve a discrete version of this property. △

3.5 Symplectic integrators

Hamiltonian flows are symplectic (see Chapter 2). Let us introduce numerical methods which preserve this property.

3.5.1 Definitions and examples

Definition 3.5.1 (symplectic numerical method)**.** A numerical (one-step) method assigns to Hamilton's equations for a Hamiltonian system locally defined one-step maps Φ_h. If for all smooth Hamiltonians H there exists $h_0 > 0$ such that for all $0 < h < h_0$ the map Φ_h is symplectic then the numerical method is called *symplectic*. △

Remark 3.5.1. Often the restriction to positive h in Definition 3.5.1 can be lifted and the condition $0 < h < h_0$ be replaced by $|h| < h_0$. Using the latter condition in the definition of a symplectic method, a method is symplectic if and only if its adjoint method is symplectic. △

Example 3.5.1. The symplectic Euler method applied to a Hamiltonian system in the standard form (2.1.5) reads

$$\begin{aligned} q_1 &= q_0 + h\nabla_p H(p_0, q_1) \\ p_1 &= p_0 - h\nabla_q H(p_0, q_1). \end{aligned}$$

The adjoint scheme is given by

$$\begin{aligned} q_1 &= q_0 + h\nabla_p H(p_1, q_0) \\ p_1 &= p_0 - h\nabla_q H(p_1, q_0). \end{aligned}$$

In the formula above the indices are used as in (3.3.2) and do *not* denote vector components. It can be calculated that the Jacobian matrix of the map $\Phi_h \colon (p_0, q_0)^\top \mapsto (p_1, q_1)^\top$ is symplectic (Hairer, Lubich, and Wanner, 2013, Thm. 3.3) for h in a small neighbourhood of 0. It follows that the symplectic Euler method and its adjoint method are symplectic numerical methods. △

Example 3.5.2. Applied to the first order formulation $\dot{q} = p$, $\dot{p} = -\nabla V(q)$ of the second order problem $\ddot{x} = -\nabla V(x)$ the Störmer–Verlet scheme coincides with $\Phi_{h/2} \circ \Phi^*_{h/2}$ where $\Phi_{h/2}$ is the symplectic Euler scheme. Thus, the Störmer–Verlet scheme is symplectic on this problem class. It is also symplectic–but implicit–on general Hamiltonian systems. See Hairer, Lubich, and Wanner, 2003, pp. 412–414 for four different proofs. △

3.6 Further approaches and variational integrators

If a symplectic method is implicit, the equations that occur need to be solved up to round-off error to preserve symplecticity. See Tan, 2005 for an analysis of symplectic Runge–Kutta methods (which are all implicit) combined with fixed point iterations or Newton iterations. In Geiser, Lüskow, and Schneider, 2015 an approach is presented to efficiently tackle non-separable Hamiltonian systems. A class of semi-implicit integrators is introduced which are symplectic only on separable Hamiltonian systems but still perform well on non-separable Hamiltonian systems.

There is a variety of approaches to construct and analyse symplectic integrators. Conditions on the coefficients of general Runge–Kutta methods and partitioned Runge–Kutta methods can be derived (Hairer, Lubich, and Wanner, 2013, Ch. VI.4). Moreover, the composition of symplectic methods leads to new symplectic methods. For a construction of symplectic method bases on the Hamilton–Jacobi equation see Hairer, Lubich, and Wanner, 2013, Ch. VI.5.

Another approach is to discretise Hamilton's principle. In the continuous formulation the principle states that a motion $(q(t), \dot{q}(t))$ of a Hamiltonian system is a critical point of the action integral

$$\mathcal{S}(q) = \int_{t_0}^{t_1} L(q(t), \dot{q}(t))\mathrm{d}t$$

among all curves q with $q(t_0) = q_0$ and $q(t_1) = q_1$ for given q_0 and q_1. Here, L is called the *Lagrangian* of the problem. Using an approximation of the integral $L_h(q_n, q_{n+1}) \approx \int_{t_n}^{t_{n+1}} L(q(t), \dot{q}(t))\mathrm{d}t$ as a generating function leads to a symplectic map $(q_n, p_n) \mapsto (q_{n+1}, p_{n+1})$ which can be used as a one-step map. See Hairer, Lubich, and Wanner, 2013, Ch. VI.6 and references therein for an analysis and examples.

3.7 Preservation of Hamiltonian structure – energy conservation

While symplectic integrators preserve the symplectic structure of a Hamiltonian system exactly, the numerical flow does not leave the Hamiltonian invariant. However, as will be made precise in the following, there exists a modified Hamiltonian which is preserved exponentially well on exponentially long time intervals. The numerical flow looks like the exact flow of a slightly perturbed Hamiltonian system and the numerical solution appears to have the correct structural properties.

Theorem 3.7.1. *Consider a Hamiltonian system with analytic Hamiltonian* $H : D \to$

$\mathbb{R}$ with $D \subset \mathbb{R}^{2n}$. Apply a symplectic integrator Φ_h of order p with step-size h to Hamilton's equations. Consider a numerical solution $y_0, y_1, \ldots$ that remains in a compact set $K \subset D$. Expanding $\Phi_h(y)$ in h we obtain

$$\Phi_h(y) = y + hJ^{-1}\nabla H(y) + h^2 d_2(y) + h^3 d_3(y) + \ldots.$$

Assume that all d_j are analytic and do not grow too fast in j, i.e. there exists $M \in \mathbb{R}$ such that $\|d_j(y)\| \leq M^j$ for all $y \in K$. Then there exists a formal power series

$$\tilde{H}(y) = H(y) + h^p \tilde{H}_{p+1}(y) + h^{p+1}\tilde{H}_{p+2}(y) + \ldots$$

and $h_0 \in \mathbb{R}$ and $N(h) \in \mathbb{Z}$ such that

$$\tilde{H}_{\leq N(h)}(y_n) = \tilde{H}_{\leq N(h)}(y_0) + \mathcal{O}\left(e^{-\frac{h_0}{2h}}\right) \tag{3.7.1}$$

$$H(y_n) = H(y_0) + \mathcal{O}\left(h^p\right) \tag{3.7.2}$$

for all $n \in \mathbb{N}$ with $nh \leq e^{\frac{h_0}{2h}}$ (exponentially long) for a constant $h_0 \in \mathbb{R}$. Here $\tilde{H}_{\leq N(h)}$ denotes the truncation after the Nth summand of the formal power series $\tilde{H}$ and $N(h)$ is the largest integer satisfying $hN(h) \leq h_0$.

The assumptions formulated in Theorem 3.7.1 on the method Φ_h are fulfilled for all introduced symplectic methods. The formal power series $\tilde{H}$ can be obtained using a technique called *backward error analysis*. However, the series does in general not converge for h in an open neighbourhood of 0. Therefore, to obtain (3.7.1) one has to work with a truncated series and introduce an error term which is exponentially small in h^{-1}. Decreasing h the truncation error in the Hamiltonian $\tilde{H}$ decreases exponentially (see (3.7.1)), while the truncation index $N(h)$ only grows like h^{-1}. Moreover, in the sense of formal power series in h, the symplectic map Φ_h is the flow of the *modified equation* $\dot{y} = J^{-1}\nabla\tilde{H}(y)$ such that we can refer to $\tilde{H}$ as a Hamiltonian rather than just a modified conserved quantity. See chapter IX in Hairer, Lubich, and Wanner, 2013 for a proof of Theorem 3.7.1 and further details.

The excellent energy[2] preservation property of the symplectic Störmer–Verlet scheme is illustrated in Figure 3.1. While the energy error $H(q,p) - H(q_0,p_0)$ oscillates and remains bounded for the 2nd order accurate symplectic integrator (hinting at the existence of a modified conserved quantity), the energy error for the non-symplectic explicit midpoint rule, which is of the same order, grows linearly on the simulated time interval when applied to the Hamiltonian $H(q,p) = \frac{1}{2}p^2 - \cos(q)$ of the free pendulum (2.2.2) with step-size 0.1. We can see a clear advantage of the symplectic method for long-term

[2]Here, *energy* refers to the Hamiltonian. In many applications in physics the Hamiltonian represents the energy of the system.

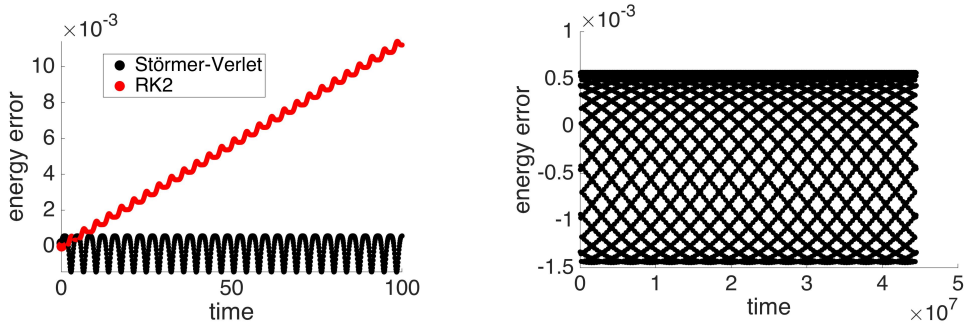

Figure 3.1: The figure to the left shows the energy error of the symplectic Störmer–Verlet scheme and the non-symplectic explicit midpoint rule (RK2) applied to the Hamiltonian system of the free pendulum $H(q,p) = \frac{1}{2}p^2 - \cos(q)$ from (2.2.2). The initial values $(q_0, p_0) = (1, 1)$ and the step-size $h = 0.1$ were used to obtain the plots. The plot to the right shows the long time behaviour of the energy error for the Störmer–Verlet scheme. Here, only every 10^5th point is plotted.

simulations.

Chapter 4

Boundary value problems

Boundary value problems for differential equations are systems of differential equations together with specified values of a sought solution and its derivative at specific points. Unfortunately, there are no theorems similar to the Picard-Lindelöf theorem for initial value problems for ODEs available to clarify in a general setting under which conditions a solution to a boundary value problem exists or is unique. However, many different classes of problems have been analysed, see e.g. Bernfeld and Lakshmikantham, 1974; Bailey, 1968. Indeed, in the following chapters non-uniqueness of solutions to boundary value problems is an essential part of our investigations: we will analyse how the topology of solution sets to boundary value problems changes as parameters in the problem are varied (bifurcations), link bifurcation behaviour to the intrinsic structure of the boundary value problem and point out implications for numerical computations.

4.1 Typical boundary conditions

Before presenting numerical approximation schemes for boundary value problems, let us review some typical boundary conditions.

4.1.1 Boundary value problems for ordinary differential equation

For $F\colon \mathbb{R} \times \mathbb{R}^n \times \mathbb{R}^n \to \mathbb{R}^n$ consider the ordinary differential equation (ODE)

$$\dot{y} = F(t, y, \dot{y}) \tag{4.1.1}$$

and the boundary condition

$$g(y(a), y(b)) = 0. \tag{4.1.2}$$

The equations (4.1.1) and (4.1.2) constitute a boundary value problem, where $y\colon [a, b] \to \mathbb{R}^n$ is sought. The ODE (4.1.1) together with the boundary condition (4.1.2) constitute

a *boundary value problem*. Typically, (4.1.2) consists of n independent equations. If

$$g(y(a), y(b)) = y(a) - y_0$$

for some $y_0 \in \mathbb{R}^n$ then the problem is called an *initial value problem (IVP)*. If the expression $g(y(a), y(b))$ genuinely depends on $y(a)$ and $y(b)$ then the problem is called a *2 point boundary value problem*. If $g(y(a), y(b))$ is of the form

$$g(y(a), y(b)) = \begin{pmatrix} g^a(y(a)) \\ g^b(y(b)) \end{pmatrix}$$

then the boundary condition is called *separated*. If $n = 2m$ and

$$g(y(a), y(b)) = \begin{pmatrix} y^1(a) \\ \vdots \\ y^m(a) \\ y^1(b) \\ \vdots \\ y^m(b) \end{pmatrix} - \begin{pmatrix} y_0^a \\ \\ \\ y_0^b \\ \\ \end{pmatrix}$$

for $y_0^a, y_0^b \in \mathbb{R}^m$ then the problem is called a *Dirichlet problem*. Furthermore, a Dirichlet problem is *homogeneous* if $y_0^a = 0 = y_0^b$. A Dirichlet problem arises, for example, when formulating the problem

$$\ddot{u} = f(t, u, \dot{u}) \quad u(a) = u^a,\ u(b) = u^b$$

with $u^a, u^b \in \mathbb{R}^m$ and $f\colon \mathbb{R} \times \mathbb{R}^m \times \mathbb{R}^m \to \mathbb{R}$ as a 1st order system of ODEs. The problem

$$\ddot{u} = f(t, u, \dot{u}) \quad \dot{u}(a) = u^a,\ \dot{u}(b) = u^b$$

is called a *Neumann problem* and $u^a, u^b \in \mathbb{R}^m$ are called the *Neumann data* of the problem. Combining Dirichlet and Neumann boundary conditions component wise in a linear way to

$$u^j(a) + \alpha_a^j \dot{u}^j(a) = \beta_a^j,\ u^j(b) + \alpha_b^j \dot{u}^j(b) = \beta_b^j, \quad 1 \leq j \leq m$$

with $\alpha^a, \beta^a, \alpha^b, \beta^b \in \mathbb{R}^m$ we obtain *Robin boundary conditions*. The problem

$$\ddot{u} = f(t, u, \dot{u}) \quad u(a) = u^a,\ \dot{u}(a) = \dot{u}^a$$

is called a *Cauchy problem*. Its 1st order formulation is an IVP.

4.1.2 Boundary value problems for partial differential equation

The above definitions are also used in the setting of partial differential equations (PDEs). For $F\colon \Omega \times \mathbb{R}^M \to \mathbb{R}$ with a domain $\Omega \subset \mathbb{R}^k$ and $M \in \mathbb{N}$ we consider the PDE

$$F\left(x, u, \{u_{x_{i_1}}\}_{i_1}, \{u_{x_{i_1 i_2}}\}_{i_1 i_2}, \dots, \{u_{x_{i_1 i_2 \dots i_l}}\}_{(i_j)_j}\right) = 0. \tag{4.1.3}$$

Equation (4.1.3) depends on $x \in \Omega$ (space-time) and the l-jet of u. The PDE is to be solved for $u\colon \Omega \to \mathbb{R}$. Assume that $\partial\Omega$ is sufficiently regular, e.g. piecewise smooth. A typical boundary condition has the form

$$G\left(u, \{u_{x_{i_1}}\}_{i_1}, \{u_{x_{i_1 i_2}}\}_{i_1 i_2}, \dots, \{u_{x_{i_1 i_2 \dots i_l}}\}_{(i_j)_j}\right) = 0 \quad \text{on } \partial\Omega.$$

If we specify $u|_{\partial\Omega}$ then we obtain a *Dirichlet problem*. Specifying the normal derivative u_n along $\partial\Omega$ we obtain a *Neumann problem*. A condition of the form

$$g_1 u + g_2 u_n = g$$

for given $g_1, g_2, g\colon \partial\Omega \to \mathbb{R}$ is called a *Robin condition*.

The mentioned boundary conditions appear, for example, when modelling the temperature of material/fluids using the heat equation. Dirichlet boundary conditions model a heat distribution on the surface $\partial\Omega$ that is constant in time while homogeneous Neumann conditions $u_n|_{\partial\Omega}$ correspond to an insulated vessel (no heat transfer through the surface $\partial\Omega$). Robin boundary conditions refer to convection heating or cooling of the material in the region bounded by Ω (Larsson and Thomée, 2003).

4.2 Shooting or marching methods

There are different strategies available for solving boundary value problems for differential equations. One of them is called a *shooting method* or *marching method*.

Consider the two-point boundary value problem

$$\begin{pmatrix} \dot{q} \\ \dot{p} \end{pmatrix} = F \begin{pmatrix} q \\ p \end{pmatrix}, \qquad q(t_a) = q_a,\, q(t_b) = q_b \tag{4.2.1}$$

for a map F that is locally Lipschitz-continuous on a sufficiently large domain in $\mathbb{R}^{2n}$, where the curves q and p are sought. Let $\big(q(\,\cdot\,; p_a), p(\,\cdot\,; p_a)\big)\colon [t_a, t_b] \to \mathbb{R}^{2n}$ denote the solution to the initial value problem

$$\begin{pmatrix} \dot{q}(t; p_a) \\ \dot{p}(t; p_a) \end{pmatrix} = F \begin{pmatrix} q(t; p_a) \\ p(t; p_a) \end{pmatrix}, \qquad q(t_a; p_a) = q_a, \quad p(t_a; p_a) = p_a. \tag{4.2.2}$$

The problem (4.2.1) can now be translated into the task of finding all $p_a \in \mathbb{R}^n$ such that $q(t_b; p_a) = q_b$ because solutions to initial value problems are unique. This explains the name *shooting or marching method*: using an initial guess p_a the evaluation of $q(t_b; p_a)$ corresponds to shooting or marching to the endpoint at time t_b. The value $q(t_b; p_a)$ can then be compared to q_b in order to improve the next guess for p_a. This may be repeated until the distance $\|q(t_b; p_a) - q_b\|$ is below a given tolerance or until the updates of p_a in each step become smaller then a specified value. In computations, a solution to (4.2.2) for a given p_a can be approximated using an ode solver that is efficient and accurate for the problem F. The equation $q(t_b; p_a) - q_b = 0$ can then be solved using another numerical method as, for example, Newton's method, fix-point iterations or, in the one-dimensional case, using a bisection type algorithm.

Whether a solution is found using this approach and which solution is approximated highly depends on the initial guess. In the one-dimensional case one can evaluate $p_a \mapsto q(t_b; p_a) - q_b$ (with low accuracy) on a grid to obtain good initial guesses (change of sign) for a bisection type algorithm. In this way we can find all solutions p_a in a given interval provided that the grid is fine enough and F is sufficiently regular. Another idea to obtain good initial guesses for $q(t_b; p_a) - q_b = 0$ is to use the solutions of a nearby problem or a series of problems converging to the original problem (4.2.1). This is particularly helpful if the original problem is a small perturbation of a well-behaved problem or if a whole series of problems has to be solved anyway. This idea is known as *continuation* and has the nice side effect that one can see how a solution evolves with the perturbation parameter. Some refinements of this approach will be presented in Section 4.5.

Shooting methods are not constrained to problems which are strictly of the form (4.2.2). To illustrate this, consider, for instance, the following problem which contains first derivatives

$$q(t_a) = q_a, \quad \alpha q(t_b) + \beta \dot{q}(t_b) = \gamma$$

with $\alpha, \beta, \gamma \in \mathbb{R}^n$ and assume that solutions $\big(q(\cdot; p_a), q(\cdot; p_a)\big)$ to the initial value problem (4.2.2) can be obtained numerically to sufficient accuracy. The problem reduces to finding the roots p_a of

$$\alpha q(t_b; p_a) + \beta(\pi_q \circ F)(q(t_b; p_a), p(t_b; p_a)) - \gamma = 0,$$

where π_q denotes the projection to the q-components. Again, a root-finding algorithm can be used to obtain solutions.

Stability issues can occur when shooting methods are applied over long time-intervals. If so, it can be useful to subdivide the time-interval $[a, b]$ into sub-intervals $t_a = t_0 < t_1 < \ldots < t_N = t_b$. The values of the solution at the time steps t_i are

sought. The condition that all pieces fit together continuously and that the start and endpoints fulfil the initial boundary condition is considered as a (high-dimensional) boundary value problem. The advantage is that the numerical integration only needs to take place over each sub-interval rather than the full interval. Such integrations can be done in parallel. The technique is called *multiple shooting*. Details can be found, for instance, in Gander and Vandewalle, 2007.

4.3 Finite difference methods

In Chapter 3 we reviewed Runge–Kutta methods to solve initial value problems for ODEs. Let us present another method to discretise differential equations which is also applicable for PDEs.

We illustrate the idea of *finite difference schemes* on the *Bratu problem*: for a domain $\Omega \subset \mathbb{R}^n$ with topological boundary $\partial\Omega$ let us consider the following elliptic PDE with Dirichlet boundary condition

$$\Delta u + \mu e^u = 0, \quad u|_{\partial\Omega} = 0 \tag{4.3.1}$$

where $\mu \in \mathbb{R}$ is a parameter and Δ denotes the Laplace operator. The problem is known as the n-dimensional Bratu problem. It appears in models describing chemical reactions (combustion model, chemical reactor theory) and the expansion of the universe (Chandrasekhar model). An analytical solution is available for $n = 1$. See Mohsen, 2014 for a survey on different approaches to solve this problem numerically and for references to applications.

Consider the square $\Omega = [0,1] \times [0,1]$ in the x,y-plane. We introduce the grid $\{(x_i, y_j)\}_{i=0,\dots,N+1, j=0,\dots,M+1}$ with uniform spacing $\Delta x = \frac{1}{N+1}$ in the x-direction and uniform spacing $\Delta y = \frac{1}{M+1}$ in the y direction. There are $N \cdot M$ interior grid points $\{(x_i, y_j)\}_{i=1,\dots,N, j=1,\dots,M}$ which are not determined by the boundary condition and must be calculated.

The central difference formula $\frac{f(x+h/2)-f(x-h/2)}{h}$ is a 2nd order approximation in h of the derivative $f'(x)$ for a regular map f. Applying this formula again to $f'(x+h/2)$ and $f'(x-h/2)$ we obtain the 2nd order accurate approximation

$$f''(x) \approx \frac{f(x+h) - 2f(x) + f(x-h)}{h^2}. \tag{4.3.2}$$

We denote an approximation to $u(x_i, y_i)$ for a solution u of (4.3.1) by $u_{i,j}$. Using (4.3.2) to approximate the partial derivatives $\frac{\partial^2}{\partial x^2}$ and $\frac{\partial^2}{\partial y^2}$ we obtain

$$\frac{u_{i+1,j} - 2u_{i,j} + u_{i-1,j}}{\Delta x^2} + \frac{u_{i,j+1} - 2u_{i,j} + u_{i,j-1}}{\Delta y^2} = -\mu e^{u_{i,j}}$$

for all interior grid points $1 \leq i \leq N$ and $1 \leq j \leq M$, whereas

$$u_{0,j} = u_{i,0} = u_{i,N+1} = u_{N+1,j} = 0$$

for all $0 \leq i \leq N+1$ and $0 \leq j \leq M+1$ are determined by the Dirichlet boundary condition. Let $U = \{u_{i,j}\}_{i=1,\dots,N,j=1,\dots,M}$ denote the matrix of approximated values over interior grid points. The discretised version of (4.3.1) is second order accurate in Δx and Δy. In matrix form it reads

$$\frac{1}{\Delta x^2} T_N U + \frac{1}{\Delta y^2} U T_M + \mu e^U = 0. \tag{4.3.3}$$

Here $e^U = (e^{u_{i,j}})_{i,j}$ denotes a point-wise exponential of the elements of U and T_N and T_M are tridiagonal Toeplitz matrices of the form

$$\begin{pmatrix} -2 & 1 & & & \\ 1 & -2 & 1 & & \\ & \ddots & \ddots & \ddots & \\ & & 1 & -2 & 1 \\ & & & 1 & -2 \end{pmatrix}$$

where T_N is $N \times N$-dimensional and T_M is of dimension $M \times M$. Equation (4.3.3) can now be solved using, e.g., the MATLAB built-in function `fsolve`. If one would like to use an iteration scheme which requires the Jacobian of (4.3.3), as, for example, Newton's method, it is helpful to rewrite the system using the Kronecker product $\otimes$ as follows

$$\left(I_M \otimes \frac{1}{\Delta x^2} T_N + \frac{1}{\Delta y^2} T_M^\top \otimes I_N \right) \overline{u} = e^{\overline{u}}$$

such that a Jacobian matrix can easily be obtained. Here I_M and I_N are identity matrices of dimension M and N, respectively. The vector $\overline{u}$ denotes a vectorisation of the matrix $U = \{u_{i,j}\}_{i=1,\dots,N,j=1,\dots,M}$ in which all columns $u_{\cdot,j}$ of U are stacked on top of each other, i.e.

$$\overline{u}^\top = \left(u_{\cdot,1}^\top, \quad u_{\cdot,2}^\top, \quad \dots, \quad u_{\cdot,N-1}^\top, \quad u_{\cdot,N}^\top \right).$$

When implementing the required matrices, using a data type for sparse systems is recommended. In each Newton step a *Sylvester equation* needs to be solved. More information on equations of Sylvester type can be found in Bhatia and Rosenthal, 1997 and references therein. As suggested in Mohsen, 2014, initial guesses for iterative solvers can be obtained as

$$u_{i,j} = a \sin(\pi x_i) \sin(\pi y_i), \qquad a \in \mathbb{R}. \tag{4.3.4}$$

In case $h = \Delta x = \Delta y$ we obtain the following set of difference equations, known as the *five-point stencil*,

$$\frac{u_{i-1,j} + u_{i,j-1} - 4u_{i,j} + u_{i,j+1} + u_{i+1,j}}{h^2} + \mu e^{u_{i,j}} = 0$$

for all $i, j \in \{1, \ldots, N\}$ together with the boundary condition

$$u_{0,j} = u_{i,0} = u_{i,N+1} = u_{N+1,j} = 0$$

for all $0 \leq i, j \leq N + 1$. Thus, another way of writing (4.3.3) is

$$\frac{1}{h^2}\begin{pmatrix} T & I & & & \\ I & T & I & & \\ & \ddots & \ddots & \ddots & \\ & & I & T & I \\ & & & I & T \end{pmatrix}\begin{pmatrix} u_{\cdot,1} \\ u_{\cdot,2} \\ \vdots \\ u_{\cdot,N-1} \\ u_{\cdot,N} \end{pmatrix} + \mu \begin{pmatrix} e^{u_{\cdot,1}} \\ e^{u_{\cdot,2}} \\ \vdots \\ e^{u_{\cdot,N-1}} \\ e^{u_{\cdot,N}} \end{pmatrix} = 0. \tag{4.3.5}$$

Here I denotes an $N \times N$-dimensional identity matrix. The matrix T is an $N \times N$-dimensional, tridiagonal Toeplitz matrix of the form

$$T = \begin{pmatrix} -4 & 1 & & & \\ 1 & -4 & 1 & & \\ & \ddots & \ddots & \ddots & \\ & & 1 & -4 & 1 \\ & & & 1 & -4 \end{pmatrix}$$

Since the matrix in (4.3.5) is very sparse it is recommended to use appropriate data types when implementing (4.3.5). Moreover, the Kronecker product can be used to generate the matrix structure. Again, the above equation may be solved using `fsolve` or using Newton iterations. Notice that a Jacobian matrix of (4.3.5) is easily obtained and can improve (or is required) for the iteration methods. Using different values for the parameter a in the initial guess (4.3.4) we find two solutions for $\mu = 0.1$. Their plots are displayed in Figure 4.1.

In the example of a full finite difference discretisation of the Bratu problem, we have considered grids with uniform spacings. However, finite-difference methods can be used with non-uniform grids as well. Adaptive finite difference methods have successfully been applied to various problems. See, for instance, Oberman and Zwiers, 2016 and references therein.

Remark 4.3.1. Using shooting methods to solve a boundary value problem it is important to be able to solve initial value problems efficiently. In terms of computational

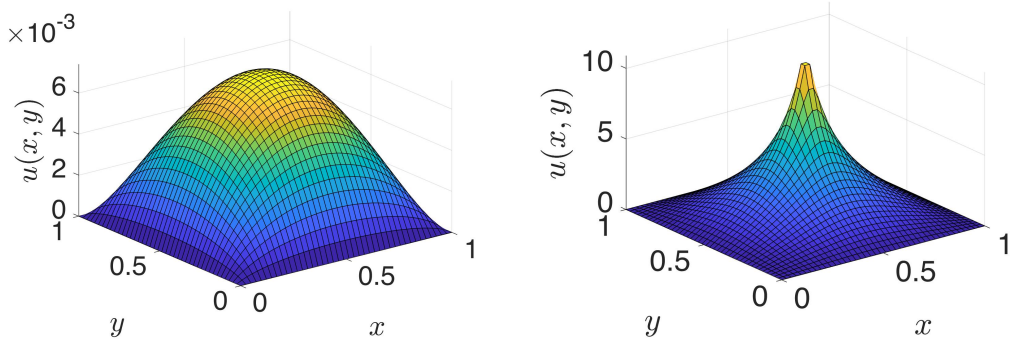

Figure 4.1: Plot of a high- and low energy solutions to the Bratu problem for the parameter value $\mu = 0.1$ using 6400 interior grid points.

costs, this can favour explicit methods for time-stepping. When applying the 5-point stencil to the Bratu problem, we have used a full discretisation scheme which couples each grid point to all of its neighbours. It is impossible to solve the obtained equations sequentially but all equations need to be solved at once which makes the scheme implicit. However, in full discretisation schemes the cost-difference between explicit and implicit vanishes because iterative methods are used to solve the required system of equations and reasonable initial guesses are available. △

4.4 Finite element methods

Another popular method to solve PDEs are *finite element methods* which belong to the family of *Galerkin methods*. Let us explain the mechanism for the linear PDE $Lu = f$ for scalar-valued functions f and linear differential operators L on a domain Ω. The PDE is viewed in an appropriate Hilbert space together with a sequence of finite dimensional subspaces that converge in an appropriate way to the original Hilbert space. On each subspace we choose the solution u, for which the error term $Lu - f$ is orthogonal to the subspace and, therefore, minimal: for a finite basis $\{\phi_j\}$ consider the ansatz $u = \sum_j c_j \phi_j$ leading to $Lu = \sum_j c_j L\phi_j$. One can determine the coefficients $\{c_i\}$ using the equations $\langle \phi_j, Lu - f \rangle = 0$, where $\langle ., . \rangle$ denotes the scalar product of the Hilbert space. In the classical approach, the boundary conditions are incorporated in the Hilbert space. In the following, we will elaborate on these ideas. See Brenner and Scott, 2008; Renardy and Rogers, 2004b for references.

4.4.1 Weak formulations and existence and uniqueness properties

For a discussion of existence and uniqueness properties for different types of PDEs we refer to Renardy and Rogers, 2004b of which we will give a short review. The *Riesz*

representation theorem relates a Hilbert space $(H, \langle\cdot,\cdot\rangle)$ with its dual space H^*, i.e. the space of all linear functionals on H which are bounded with respect to the operator norm.

Theorem 4.4.1 (Riesz representation theorem)**.** *Let $(H, \langle .,.\rangle)$ be a Hilbert space and H^* its dual space. For $l \in H^*$ there exists a unique $u \in H$ such that $\langle u, v\rangle = l(v)$ for all $v \in H$.*

Proof. See, for instance, Renardy and Rogers, 2004a, Thm. 6.52 or Lax, 2002, Thm. 4, §6.3. □

The *Lax-Milgram theorem* can be interpreted as a generalisation of Theorem 4.4.1.

Theorem 4.4.2 (Lax-Milgram theorem)**.** *Let $(H, \langle .,.\rangle)$ be a Hilbert space and H^* its dual space. Consider a bilinear form $B\colon H \times H \to \mathbb{R}$ with*

$$|B(u,v)| \leq c_1\|u\|_H\|v\|_H \quad \forall u, v \in H \quad \textit{(bounded)}$$
$$B(u,u) \geq c_2\|u\|_H^2 \quad \forall u \in H \quad \textit{(coercive)}.$$

Here $\|.\|_H$ denotes the norm on H induced by the scalar product. For any $l \in H^*$ there exists a unique solution $u \in H$ to

$$B(u,v) = l(v) \quad \forall v \in H.$$

Proof. See, for instance, Renardy and Rogers, 2004a, §9.2.2 or Lax, 2002, Thm. 6, §6.3. □

For the formulation of PDEs, *Sobolev spaces*, especially those which are Hilbert spaces, are popular: let Ω be an open subset of the Euclidean space $\mathbb{R}^n$. For $k \geq 1$ we can define the Sobolev spaces

$$H^k(\Omega) = \left\{ u \in L^2(\Omega) : D^\alpha u \in L^2(\Omega) \text{ for all } \alpha \in \mathbb{N}_0^n \text{ with } \sum_{j=1}^n \alpha_j \leq k \right\}$$

where $D^\alpha u = \frac{\partial^{|\alpha|} u}{\partial x_1^{\alpha_1} \ldots \partial x_n^{\alpha_n}}$ denotes the weak αth partial derivative. Equipped with the inner product

$$\langle u, v\rangle = \sum_{|\alpha| \leq k} \langle D^\alpha u, D^\alpha v\rangle_{L^2(\Omega)}$$

$H^k(\Omega)$ is a Hilbert space. The induced norm is denoted by $\|.\|_{H^k(\Omega)}$. We denote the closure of smooth functions with compact support $\mathcal{C}_0^\infty(\Omega)$ in $H^k(\Omega)$ by $H_0^k(\Omega)$. The space $H_0^k(\Omega)$ is a sub-Hilbert space of $H^k(\Omega)$.

Theorem 4.4.3 (Poincaré inequality)**.** *Let the domain Ω be contained in a strip $-a < x_1 < a < \infty$ for some $a \in \mathbb{R}^+$. There exists a constant C depending on k and a such that*

$$\|u\|^2_{H^k(\Omega)} \leq C \sum_{|\alpha|=k} \|D^\alpha u\|^2_{L^2(\Omega)}.$$

Proof. See Renardy and Rogers, 2004a, Thm. 7.32. □

Corollary 4.4.4. *For bounded domains Ω the symmetric, bilinear form*

$$\langle u, v\rangle_{H^1_0(\Omega)} = \int_\Omega \langle \nabla u, \nabla v\rangle \mathrm{d}x$$

is an inner product on $H^1_0(\Omega)$ which induces a norm that is equivalent to $\|\cdot\|_{H^1(\Omega)}$.

Example 4.4.1 (Poisson equation). On a bounded domain Ω consider the Poisson equation with Dirichlet boundary conditions

$$-\Delta u = f, \qquad u_{|\partial\Omega} = 0$$

with $f \in L^2(\Omega)$. The weak formulation is given as

$$\langle u, v\rangle_{H^1_0(\Omega)} = \int_\Omega f v \,\mathrm{d}x, \quad \forall v \in \mathcal{C}^\infty_0(\Omega)$$

where $u \in H^1_0(\Omega)$ is sought. Corollary 4.4.4 together with the Riesz representation theorem (Theorem 4.4.1) guarantees existence and uniqueness of a solution $u \in H^1_0(\Omega)$. △

Remark 4.4.1. Under further assumptions on the regularity of Ω or the right hand side f in Example 4.4.1, stronger statements about the regularity of u can be obtained. A typical tool for this is the *Sobolev embedding theorem*, see, for instance, Renardy and Rogers, 2004a, §7.2.3, and properties of the Dirichlet Laplacian operator $-\Delta$ (see, for instance, Friedman, 1969). △

On a space-time domain $\Omega \times (0, T)$ parabolic equations, like

$$\frac{\partial u}{\partial t} + Au = f$$

with

$$Au := -\mathrm{div}(\alpha \nabla u) + \langle \beta, \nabla u\rangle_{\mathbb{R}^n} + \gamma u$$

and with appropriate conditions on $\alpha, \gamma \colon \Omega \to \mathbb{R}$, $\beta \colon \Omega \to \mathbb{R}^n$ together with a boundary condition of the form $u(., 0) = \eta$ can be treated in the framework of *abstract ODEs* $u \colon [0, T] \to D(A) \subset L^2(\Omega)$, where $D(A)$ denotes the domain of the operator A. See Renardy and Rogers, 2004b, Ch.11 for details.

4.4.2 Galerkin's method

As motivated in the last Section 4.4.1, let H be a Hilbert space and consider a problem of the form

$$B(u, \phi) = l(\phi) \quad \forall \phi \in H \tag{4.4.1}$$

where $l \in H^*$. Let B be bounded and coercive such that there exists a unique solution $u \in H$ by the Lax-Milgram theorem (Theorem 4.4.2). Consider be a sequence of finite dimensional subspaces $(H_k)_{k\in\mathbb{N}}$ of H which approximate H. More precisely, we impose the condition

$$\lim_{k\to\infty} \inf_{\phi\in H_k} \|u - \phi\|_H = 0,$$

where u denotes the unique solution to the problem (4.4.1). For each $k \in \mathbb{N}$

$$B(u_k, \phi) = l(\phi) \quad \forall \phi \in H_k$$

has a unique solution $u_k \in H_k$ (again by the Lax-Milgram theorem). If $\{\Phi_i\}_{i=1}^{\dim H_k}$ is a basis of H_k then the ansatz $u_h = \sum_{i=1}^{\dim H_k} c_i \Phi_i$ leads to the following linear system of equations

$$Kc = b, \tag{4.4.2}$$

where $K = (B(\Phi_i, \Phi_j))_{i=1}^{\dim H_k}$, $b = (l(\Phi_i))_{i=1}^{\dim H_k}$ and $c = (c_i)_{i=1}^{\dim H_k}$. The matrix K is called the *stiffness matrix*. By Céa's Lemma (Brenner and Scott, 2008, Thm. 2.8.1), u_k converges to the solution u as $k \to \infty$.

Example 4.4.2. Consider the 1-dimensional equation $-u_{xx} + u = f$ with Dirichlet boundary conditions on the real interval $\Omega = (0, 1)$. Integration by parts leads to the weak Dirichlet problem $\langle u_x, \phi\rangle_{H^1(\Omega)} = \langle f, \phi\rangle_{L^2(\Omega)}$ for all $\phi \in H_0^1(\Omega)$. By the discussion in Section 4.4.1, there exists a unique solution in $H_0^1(\Omega)$ provided that $f \in L^2(\Omega)$. $\triangle$

As a sequence of approximating subspaces to $H_0^1(\Omega)$ we consider one dimensional finite element spaces for Dirichlet boundary conditions: consider an equidistant grid $\{x_j\}_{j=0}^{N+1}$ with $N \in \mathbb{N}$ interior grid points. The finite element space is given by continuous maps of $\overline{\Omega} = [0, 1]$ that are affine linear between grid points and fulfil the boundary condition, i.e.

$$S_N^0 = \{u \in C^0(\overline{\Omega}) : \forall 1 \le i \le N+1\, \exists s_i, t_i \in \mathbb{R} : u_{|[x_{i-1},x_i]}(x) = s_i x + t_i, u(0) = 0 = u(1)\},$$

A basis is given by the hat-functions $\Phi_1, \dots, \Phi_N \in S_N^0$ with

$$\Phi_i(x_j) = \begin{cases} 1 & \text{if } i = j \\ 0 & \text{if } i \neq j. \end{cases}$$

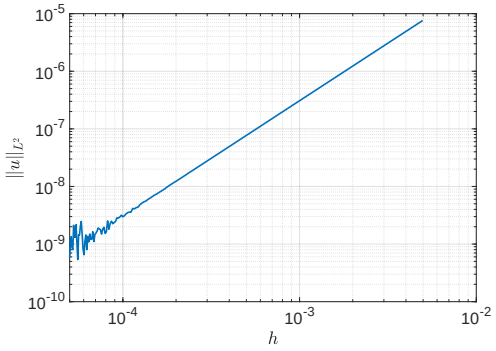

Figure 4.2: Comparison of analytic solution and numerical solution of the Dirichlet problem $-u_{xx} + u = x^2 - x - 2$ obtained using the standard FEM. The error is plotted in the discrete L^2-norm against the grid spacing h.

Let $h = \frac{1}{N+1}$ denote the spacing between grid points. An application of the Galerkin scheme leads to the linear system of equations $Kc = b$ from (4.4.2) with

$$K = \frac{1}{h}\begin{pmatrix} 2 & -1 & & & \\ -1 & 2 & -1 & & \\ & \ddots & \ddots & \ddots & \\ & & -1 & 2 & -1 \\ & & & -1 & 2 \end{pmatrix} + \frac{h}{6}\begin{pmatrix} 4 & 1 & & & \\ 1 & 4 & 1 & & \\ & \ddots & \ddots & \ddots & \\ & & 1 & 4 & 1 \\ & & & 1 & 4 \end{pmatrix}$$

and

$$b = \frac{h}{6}\begin{pmatrix} 4 & 1 & & & \\ 1 & 4 & 1 & & \\ & \ddots & \ddots & \ddots & \\ & & 1 & 4 & 1 \\ & & & 1 & 4 \end{pmatrix}\begin{pmatrix} f(x_1) \\ f(x_2) \\ \dots \\ f(x_{N-1}) \\ f(x_N) \end{pmatrix}$$

If $f(x) = x^2 - x - 2$ then the unique solution in $H_0^1(\Omega)$ is given as $u(x) = x(x-1)$. The numerical solution is compared to the analytical solution in Figure 4.2. We can see second order convergence until round-off errors start occurring below $h = 10^{-4}$.

Indeed, there exists general theory predicting second order convergence making use of the regularity of Ω and its boundary $\partial\Omega$ as well as the $H^2(\Omega)$-regularity of the solution. For general solutions in $H^1(\Omega)$ linear convergence is guaranteed. Higher order schemes can be derived using finite element spaces with better interpolation properties. This can be done by generalising S_N to piecewise polynomial functions of a given order.

Finite element methods allow a high flexibility to model differential equations and boundary conditions on a huge variety of shapes and spaces. Depending on the shapes,

the approximating spaces and their bases can be chosen to respect this structure, leading to good convergence properties and sparse matrices in (4.4.2). We refer again to Brenner and Scott, 2008 for more information and rigorous derivation of error estimates. For two-dimensional problems a typical choice of finite elements is the space spanned by pyramids with respect to a sufficiently regular triangulation of the space: for each point (x_i, y_i) in the space grid defined by the nodes of the triangles we consider a function $\Phi_{i,j}$ that is 1 at (x_i, y_i) and 0 at all other grid points. The function $\Phi_{i,j}$ is required to be affine linear over each triangle. The construction of the system (4.4.2) by hand can take a while for complicated shapes. Such processes have been automated for many different kind of finite elements, user-defined domains and meshes in highly developed toolboxes as, e.g., the *Partial Differential Equation Toolbox* for MATLAB (The MathWorks, 2019) or C++/Python based software *Dolphin* (Logg and Wells, 2010), *Fenics* (Alnaes et al., 2015), and *Firedrake* (Rathgeber et al., 2016). An overview of different finite elements in use is given in the *Periodic Table of the Finite Elements* (D. N. Arnold and Logg, 2014).

4.5 Continuation methods

In this work, we will consider boundary value problems with parameters for which we will compute *bifurcation diagrams* numerically. These are diagrams showing how branches of solutions to boundary value problems continue and possibly interact with other solution branches as parameters are varied, like in Figure 4.3 to which we will refer frequently. In the following we will review some methods to continue solutions along a parameter. The technique is of interest in order to understand the solution set of a problem and to identify tipping points or bifurcation points, i.e. parameter values at which the structure of the solution set changes abruptly. Numerical continuation has been an active research area (Abbott, 1978; Bathe and Dvorkin, 1983; Crisfield, 1981; Krauskopf, Osinga, and Galán-Vioque, 2007; Rheinboldt, 1981; Riks, 1972; Wagner and Wriggers, 1988; Wriggers and Simo, 1990). Dynamical systems software packages like *AUTO* (Doedel, Champneys, Fairgrieve, et al., 2000; Doedel, Govaerts, and Y. A. Kuznetsov, 2003), *CONTENT* (Govaerts, Y. A. Kuznetsov, and Sijnave, 1998) and *MATCONT* (Dhooge, Govaerts, and Y. A. Kuznetsov, 2003; Dhooge, Govaerts, Y. A. Kuznetsov, et al., 2003) are available for the continuation process of solutions and the detection of bifurcations. While these are mostly tailored to be used on ODEs, there are packages for PDEs as well, as, for instance, the MATLAB package *pde2path* (Uecker, Wetzel, and Rademacher, 2014).

Consider a continuously Fréchet differentiable function $G\colon X\times\mathbb{R}^m \to X$, where X is a Banach space, e.g. $X = L^2(\mathbb{R})$ equipped with the L^2-norm. By the implicit function

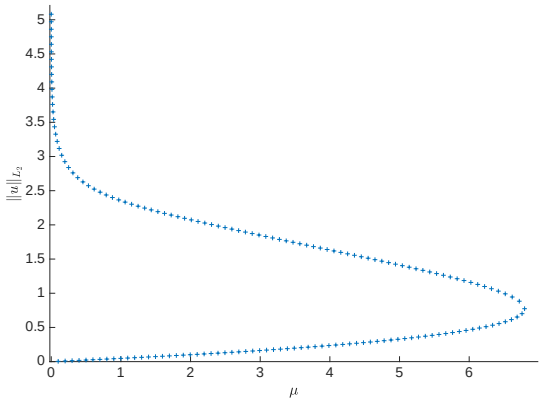

Figure 4.3: Application of pseudo-arclength continuation to the 2-dimensional Bratu problem (4.3.1). The discrete, 2-dimensional L_2-norm is plotted against the parameter value μ. The step size for the Euler predictor step is $\Delta s = 0.1$ and 100 inner grid points were used in the computations. The starting guess is the constant zero solution at $\mu = 0$.

theorem for Banach spaces (Kielhöfer, 2012), we can locally parametrise solutions u of

$$G(u, \lambda) = 0 \tag{4.5.1}$$

as $u(\lambda)$ where the Fréchet derivative $G_u = \frac{\partial G}{\partial u}$ is a Banach space isomorphism $X \to X$. A simple approach to numerically calculate $u(\lambda)$ for λ near λ_{old} is to use a solution u_{old} to the parameter λ_{old} as an initial guess for an iterative method applied to (4.5.1).

Let us follow Krauskopf, Osinga, and Galán-Vioque, 2007, §1 on how this idea can be enhanced. Also see Keller, 1976.

4.5.1 Euler–Newton continuation

Differentiating $G(u(\lambda), \lambda) = 0$ with respect to λ, we obtain the linear equation

$$G_u u_\lambda + G_\lambda = 0. \tag{4.5.2}$$

We can evaluate the above equation at a known solution $(u_{\text{old}}, \lambda_{\text{old}})$ and then solve for $u_\lambda(\lambda_{\text{old}})$. An Euler-step forward

$$u^0 = u_{\text{old}} + u_\lambda(\lambda_{\text{old}}) \cdot (\lambda_{\text{new}} - \lambda_{\text{old}}) \tag{4.5.3}$$

provides us with a start value for Newton's method to solve for u_{new} in

$$G(u_{\text{new}}, \lambda_{\text{new}}) = 0. \tag{4.5.4}$$

Fixing step-sizes for $\lambda_{\text{new}} - \lambda_{\text{old}}$ one can continue a solution along the parameter λ. In computations, notice that an LU-decomposition of G_u in (4.5.2) is available from the last iterate of Newton's method of the previous step. What happens when G_u in (4.5.2) becomes singular? For instance, in Figure 4.3 we see two solution branches annihilating. The phenomenon is referred to as a *fold bifurcation*. The meeting point $(u_{\text{fold}}, \lambda_{\text{fold}})$ is called a *limit point* or *fold point*. At the fold point the linear map $G_u(u_{\text{fold}}, \lambda_{\text{fold}})$ fails to be an isomorphism. The implicit function theorem does not apply, and the solution branch cannot be continued in the positive parameter direction λ. Even if the algorithm does not reach the singular point $(u_{\text{fold}}, \lambda_{\text{fold}})$ exactly, a continuation in the positive λ direction will eventually lead to a prediction step with $\lambda_{\text{new}} > \lambda_{\text{fold}}$ such that (4.5.4) does not have a solution.

4.5.2 Pseudo-arclength continuation

To resolve fold bifurcations as in Figure 4.3 correctly, we present the *pseudo-arclength continuation method* first introduced by Keller (Keller, 1976). It is implemented in the software package AUTO (Doedel, Champneys, Fairgrieve, et al., 2000; Doedel, Govaerts, and Y. A. Kuznetsov, 2003). The idea is to parametrise a solution branch (u, λ) along an approximation s of its arclength and apply Euler–Newton continuation to a system consisting of the problem $G(u(s), \lambda(s)) = 0$ and a condition forcing that the parametrisation approximates arclength: let $(X, \langle , \rangle)$ be a Hilbert space and the parameter space be 1-dimensional. Denote a solution of $G(u(s), \lambda(s)) = 0$ by $(u_0, \lambda_0) = (u(s_0), \lambda(s_0))$ and a direction vector, i.e. a tangent vector to the solution branch at (u_0, λ_0) by $(\dot{u}_0, \dot{\lambda}_0)$.

We normalise the system $G(u(s), \lambda(s)) = 0$ using a condition $N(u(s), \lambda(s), s)$ which approximates the arclength between a point $(u(s), \lambda(s))$ on the solution branch in $X \times \mathbb{R}$ to the reference point (u_0, λ_0). For computational reasons, the following approximation is useful: the direction vector $(\dot{u}_0, \dot{\lambda}_0)$ is the unit normal vector of a hyperplane in $X \times \mathbb{R}$. The pseudo arclength condition $N(u_1, \lambda_1, s_1) = 0$ with $s_1 = s + \Delta s$ says that the new point (u_1, λ_1) lies a distance Δs from the hyperplane. We obtain the system

$$\begin{aligned} G(u_1, \lambda_1) &= 0 \\ N(u_1, \lambda_1, s_1) &= 0, \end{aligned} \tag{4.5.5}$$

where

$$N(u,\lambda,s) = \left\langle \begin{pmatrix} \dot{u}_0 \\ \dot{\lambda}_0 \end{pmatrix}, \begin{pmatrix} u-u_0 \\ \lambda-\lambda_0 \end{pmatrix} \right\rangle_{X\times\mathbb{R}} - (s-s_0)^2. \tag{4.5.6}$$

The system (4.5.5) can be solved using an iterative solver, like, for instance, Newton's method. As an initial guess we can take the predictor $(u_0,\lambda_0)+\Delta s(\dot{u}_0,\dot{\lambda}_0)$. The Jacobi matrix in Newton's scheme

$$\begin{pmatrix} G_u & G_\lambda \\ N_u & N_\lambda \end{pmatrix} \tag{4.5.7}$$

is regular on a neighbourhood of the solution branch wherever a solution $(u(s),\lambda(s))$ for a fixed s is isolated. This covers regular points, where $G_u(u(s),\lambda(s))$ is an isomorphism, as well as fold points, see Keller, 1976, Thm. 3.3. After the Newton scheme has converged, the decomposition of the matrix (4.5.7) from the last iteration of the Newton scheme can be used to solve for the new direction vector $(\dot{u}_1,\dot{\lambda}_1)$ by solving

$$\begin{pmatrix} G_u(u_1,\lambda_1) & G_\lambda(u_1,\lambda_1) \\ N_u(u_1,\lambda_1) & N_\lambda(u_1,\lambda_1) \end{pmatrix} \begin{pmatrix} \underline{\dot{u}}_1 \\ \underline{\dot{\lambda}}_1 \end{pmatrix} = \begin{pmatrix} 0 \\ 1 \end{pmatrix} \tag{4.5.8}$$

for $(\underline{\dot{u}}_1,\underline{\dot{\lambda}}_1)$ and normalising. The calculation (4.5.8) can be justified by differentiating the system $(G(u(s),\lambda(s)),N(u(s),\lambda(s),s))=0$ with respect to the parameter s. The special structure of (4.5.7) can be exploited in computations. Under the assumption that G_u is non-singular and admits a cheap LU decomposition, a *bordered LU decomposition* is efficient. Though G_u becomes singular exactly at a fold point, the algorithm works in practice (Krauskopf, Osinga, and Galán-Vioque, 2007, §1.2.4).

The pseudo-arclength condition can be enforced in different ways. Another approach, presented in Bolstad and Keller, 1986, is to calculate a predictor (u^0,λ^0) in the space $X\times\mathbb{R}$ of length Δs and then find a point on the solution branch (u_1,λ_1) such that the line connecting (u^0,λ^0) with (u_1,λ_1) and the tangent at the previous point (u_0,λ_0) are perpendicular. We are describing this approach below for the case where G_u is assumed to be non-singular. In numerical examples this algorithm performs well also around fold points, where G_u becomes singular (Figure 4.3).

Deriving $G(u(s),\lambda(s))=0$ with respect to s gives

$$G_u\dot{u} + G_\lambda\dot{\lambda} = 0, \tag{4.5.9}$$

where a dot above a symbol denotes differentiation with respect to the parameter s. Solutions $(\dot{u}_0,\dot{\lambda}_0)$ at $(u_0,\lambda_0)=(u(s_0),\lambda(s_0))$ to the above equation form a line tangent

to the solution branch at (u_0, λ_0) in $X \times \mathbb{R}$. There are two solutions with norm 1, i.e.

$$\left\langle \begin{pmatrix} u_0 \\ \lambda_0 \end{pmatrix}, \begin{pmatrix} u_0 \\ \lambda_0 \end{pmatrix} \right\rangle_{X\times\mathbb{R}} = \|\dot{u}_0\|_X^2 + \dot{\lambda}_0^2 = 1, \tag{4.5.10}$$

where $\|\dot{u}_0\|_X$ denotes the norm in X. The two solutions of equation (4.5.9) at (u_0, λ_0) and (4.5.10) can be computed as follows: let ϕ denote the solution to the linear equation

$$G_u(u_0, \lambda_0)\phi = -G_\lambda(u_0, \lambda_0)$$

(assuming that G_u is an isomorphism). Then

$$\dot{\lambda}_0 = \pm(1 + \|\phi\|_X^2)^{-\frac{1}{2}}, \qquad \dot{u}_0 = \dot{\lambda}_0\phi.$$

Let (u_{-1}, λ_{-1}) denote the solution that is followed by (u_0, λ_0). We choose a sign for $\dot{\lambda}_0$ such that we do not run backwards when making an Euler step using $(\dot{u}_0, \dot{\lambda}_0)$: the vector $\begin{pmatrix} \dot{u}_0 \\ \dot{\lambda}_0 \end{pmatrix}$ is a unit normal vector to a hyperplane at (u_0, λ_0) separating $X \times \mathbb{R}$ into two parts. We require the vector $\begin{pmatrix} u_0 - u_{-1} \\ \lambda_0 - \lambda_{-1} \end{pmatrix}$ to lie in the part of $X \times \mathbb{R}$ into which the normal vector is pointing, i.e.

$$\left\langle \begin{pmatrix} \dot{u}_0 \\ \dot{\lambda}_0 \end{pmatrix}, \begin{pmatrix} u_0 - u_{-1} \\ \lambda_0 - \lambda_{-1} \end{pmatrix} \right\rangle_{X\times\mathbb{R}} > 0. \tag{4.5.11}$$

To a given step size $\Delta s > 0$ we make an Euler step

$$u^0 = u_0 + \Delta s\dot{u}_0, \qquad \lambda^0 = \lambda_0 + \Delta s\dot{\lambda}_0.$$

to obtain a predictor u^0. Let $s_1 = s_0 + \Delta s$. To regularise the problem

$$G(u(s_1), \lambda(s_1)) = 0 \tag{4.5.12}$$

we add the condition that the new solution $(u(s_1), \lambda(s_1))$ is the projection of the predictor (u^0, λ^0) to the solution branch along the normal vector $(\dot{u}_0, \dot{\lambda}_0)$ to the mentioned hyperplane, i.e. we require

$$N(u(s_1), \lambda(s_1)) = \left\langle \begin{pmatrix} \dot{u}_0 \\ \dot{\lambda}_0 \end{pmatrix}, \begin{pmatrix} u(s_1) - u^0 \\ \lambda(s_1) - \lambda^0 \end{pmatrix} \right\rangle_{X\times\mathbb{R}} = 0. \tag{4.5.13}$$

Finally, the system consisting of (4.5.12) and (4.5.13) can be solved using Newton iterations with the start value (u^0, λ^0).

An application of the continuation method to the Bratu problem leads to the plot displayed in Figure 4.3. The scheme captures this bifurcation without problems.

We refer to Chang, Chien, and Jeng, 2005 for a discussion on how to trace solution surfaces or manifolds and detect bifurcations, where the parameter λ is two or higher dimensional. In actual computations the problem (4.5.1) will be a discretisation of a continuous problem. Since the condition of the problem might change with the parameter λ, it can be helpful to vary the grid that has been used to obtain the discretisation. See e.g. Brandt, 1977; Bolstad and Keller, 1986 and references therein for possible approaches.

Chapter 5

Singularity theory and catastrophe theory

Let us briefly introduce the notions and classification results from classical catastrophe theory or singularity theory as used in this work. For a more complete and very detailed discussion we refer to Du Plessis and Wall, 1995. An introduction can be found in V. I. Arnold, Gusein-Zade, and Varchenko, 1985; Demazure, 2000.

The idea of catastrophe theory is to classify all smooth, real valued functions $F\colon U \to \mathbb{R}$ for U a neighbourhood of a point in $\mathbb{R}^n$ (without loss of generality $0 \in \mathbb{R}^n$) up to changes of coordinates. Representatives can then be ordered by degeneracy, i.e. how many parameters are needed to be introduced such that the singularity F cannot be removed by small perturbations. This leads to Table 1.1 when no more than four parameters are allowed. The classification captures the different ways in which critical points of smooth functions can bifurcate as parameters are varied.

To contrast a problem of the form $\nabla_x F_\mu(x) = 0$, where $F_\mu\colon U \to \mathbb{R}$, $U \subset \mathbb{R}^n$ open and non-empty, and μ a parameter, with a problem of the form $G_\mu(x) = 0$, where $G_\mu\colon U \to \mathbb{R}^n$, we first start in a general setting for functions between two arbitrary manifolds before entering the catastrophe setting.

In the following we will restrict ourselves to the smooth, real category. A treatment of the holomorphic case can be found in V. I. Arnold, Goryunov, et al., 1998; V. I. Arnold, Goryunov, et al., 1993. Our definitions follow Du Plessis and Wall, 1995, §1 and Wassermann, 1974.

5.1 Equivalence relations for germs and stability

The space of smooth functions $\mathcal{C}^\infty(N, P)$ between two smooth manifolds N and P is equipped with the Whitney $\mathcal{C}^\infty$-topology (Golubitsky and Guillemin, 1973). When we say that a statement $\mathcal{P}$ holds for a function $F \in \mathcal{C}^\infty(N, P)$ and is persistent or generic

under sufficiently small perturbations of F, then this means that there exists an open neighbourhood $\mathcal{U}$ of F with respect to the Whitney $\mathcal{C}^\infty$-topology such that $\mathcal{P}$ holds for all functions $G \in \mathcal{U}$. Moreover, stability notions refer to this topology.

For local considerations, it is convenient to use the notion of *function germs* which we borrow from sheaf theory.

Definition 5.1.1 (function germ)**.** Let N, P be smooth manifolds, $x \in N$, $y \in P$ and $x \in U, \tilde{U} \subset N$ open neighbourhoods. Two functions $F\colon U \to P$, $\tilde{F}\colon \tilde{U} \to P$ with $F(x) = y = \tilde{F}(x)$ are equivalent if there exists an open neighbourhood W of x such that the restrictions $F|_W$ and $\tilde{F}|_W$ coincide. The equivalence class $\hat{F}$ of F is called the *germ* of F. △

We will write $F\colon (N, x) \to (P, y)$ to denote the germ of a function in $\mathcal{C}^\infty(N, P)$ mapping the localisation point $x \in N$ to $y \in P$.

Definition 5.1.2 (right equivalence)**.** Two smooth functions $F, G \in \mathcal{C}^\infty(N, P)$ are *right-equivalent* if there exists a diffeomorphism $R\colon N \to N$ such that $F = G \circ R$. Two smooth germs $\hat{F}, \hat{G}\colon (N, x) \to (P, y)$ are *right-equivalent* if there is an open neighbourhood U of x and an open neighbourhood V of y such that for representatives $F, G \in \mathcal{C}^\infty(U, V)$ of $\hat{F}$ and $\hat{G}$ there exist a local diffeomorphism $R\colon U \to U$ with $R(x) = x$ such that $F = G \circ R$ on an open neighbourhood of x. △

Definition 5.1.3 (right-left equivalence)**.** Two smooth functions $F, G \in \mathcal{C}^\infty(N, P)$ are *right-left equivalent* if there exist diffeomorphisms $R\colon N \to N$ and $L\colon P \to P$ such that $F = L \circ G \circ R$. Two smooth germs $\hat{F}, \hat{G}\colon (N, x) \to (P, y)$ are *right-left equivalent* if there exist open neighbourhoods U of x and V of y as well as representatives $F, G \in \mathcal{C}^\infty(U, V)$ of $\hat{F}$ and $\hat{G}$ and local diffeomorphisms $R\colon U \to U$ and $L\colon V \to V$ with $R(x) = x$ and $L(y) = y$ such that $F = L \circ G \circ R$ on a neighbourhood of x. △

Definition 5.1.4 (stable functions)**.** A function $F \in \mathcal{C}^\infty(N, P)$ is *$\mathcal{C}^\infty$-stable with respect to right-(left) equivalence* if there exists an open neighbourhood $\mathcal{W} \subset \mathcal{C}^\infty(N, P)$ of F such that any $G \in \mathcal{W}$ is right-(left) equivalent to F. △

Definition 5.1.5 (stable function germ)**.** A germ $\hat{F}\colon (N, x) \to (P, y)$ is *$\mathcal{C}^\infty$-stable with respect to right-left equivalence* if for every representative $F \in \mathcal{C}^\infty(U, V)$ of $\hat{F}$ there exists a relatively compact open neighbourhood U' of x in U and an open neighbourhood $\mathcal{W} \subset \mathcal{C}^\infty(U, V)$ of F such that for all $G \in \mathcal{W}$ there exist a smooth embedding $R\colon U \to U'$ with $x \in R(U)$, an open neighbourhood $V' \subset V$ of $F(R(U'))$, and a smooth embedding $L\colon V' \to V$ such that $G|_{U'} = L \circ F \circ R$. In case P has linear structure and $L\colon V' \to V$ can be chosen to be a translation then $\hat{F}\colon (N, x) \to (P, y)$ is *$\mathcal{C}^\infty$-stable with respect to right equivalence.* △

5.2 Density of Morse functions and Whitney's classification of planar maps

Definition 5.2.1 (critical point)**.** Let $F \in \mathcal{C}^\infty(N, P)$. A point $a \in N$ is a *critical point* of F if the differential $\mathrm{d}F|_a \colon T_aN \to T_{F(a)}P$ is not surjective. △

Definition 5.2.2 (Morse point)**.** Let $f \in \mathcal{C}^\infty(N, \mathbb{R})$. A critical point $a \in N$ is a *Morse point* if in local coordinates around $a \in N$ the Hessian form of f at a is nondegenerate. △

Definition 5.2.3 (Morse function)**.** A function is a *Morse function* if all its critical points (there might be none) are Morse points. △

Remark 5.2.1. Notice that the notion of a critical point is also well-defined for germs and for right-(left) equivalence classes of germs at the point where the germ is localised. Since Morse points are required to be critical points, the definition is independent of the choice of local coordinates. △

Theorem 5.2.1 (Morse lemma)**.** *Let f be the germ of a Morse function $\hat{f} \in \mathcal{C}^\infty(N, \mathbb{R})$ at a critical point p. Assume that the Hessian matrix of f at p has k positive and $n-k$ negative eigenvalues. There exist local coordinates $y_1, \ldots, y_n$ on N centred at p such that f is of the form*

$$f(y_1, \ldots, y_n) = f(p) + y_1^2 + \ldots + y_k^2 - y_{k+1}^2 - \ldots - y_n^2.$$

Proof. See, for instance, Milnor, 1969, Lemma 2.2. The statement also follows from Theorem 5.3.2 below. □

Theorem 5.2.2 (Morse functions are dense)**.** *The set $\mathcal{U}$ of $\mathcal{C}^\infty$-right stable maps in $\mathcal{C}^\infty(\mathbb{R}^n, \mathbb{R})$ is open and dense. For $f \in \mathcal{U}$ all critical points are Morse points and the values of f at critical points are pairwise distinct (Demazure, 2000, p. 4.11.3).*

More interesting singularities occur persistently if the dimension of the target space is increased or if the function is parameter dependent. To illustrate this point, we report a classification results by Whitney for smooth maps $\mathbb{R}^2 \to \mathbb{R}^2$.

Theorem 5.2.3. *Let $F \in \mathcal{C}^\infty(\mathbb{R}^2, \mathbb{R}^2)$ be a right-left-stable function. The critical points of f constitute a 1-dimensional (possibly empty) submanifold $C \subset \mathbb{R}^2$. For each critical point $p \in C$ the germ of $y \mapsto f(p+y)$ at $y = 0$ is right-left-equivalent to the germ at 0 of either*

- *(fold)*

$$\begin{pmatrix} x \\ y \end{pmatrix} \mapsto \begin{pmatrix} x \\ y^2 \end{pmatrix}$$

- *(cusp)*

$$\begin{pmatrix} x \\ y \end{pmatrix} \mapsto \begin{pmatrix} x \\ y^3 - xy \end{pmatrix}$$

(Demazure, 2000, §4.8).

Remark 5.2.2. The fact that the stable functions form a dense set is true for $\mathcal{C}^\infty(\mathbb{R}^n, \mathbb{R})$ but is *not* true for general function spaces $\mathcal{C}^\infty(\mathbb{R}^n, \mathbb{R}^m)$: indeed, there are *bad dimensions* (n, m) where there exist open, non-empty subsets $\mathcal{W}$ in which no element constitutes a stable function. Therefore, in classification results of functions up to right-(left) equivalence moduli (extra variables) occur in normal forms (V. I. Arnold, Gusein-Zade, and Varchenko, 1985, Chapter 3, Remark 2 or Du Plessis and Wall, 1995, §8.2). Moreover, as we will see at the end of this section, we will encounter moduli in the setting of scalar-valued function germs as well when we consider parameter dependent function germs. △

5.3 Unfoldings and the splitting theorem

We now explain a setting for parameter dependent function germs

$$F\colon (N \times \mathbb{R}^d, (x, 0)) \to (\mathbb{R}, y), \qquad (x, \mu) \mapsto F(x; \mu)$$

following the dissertation of Wassermann, 1974. Also see Wall, 1981, §3. We will introduce an equivalence relation that respects the fibration. In contrast to the notion introduced in Definition 5.1.2, diffeomorphisms are not allowed to act arbitrarily on a neighbourhood of $(x, 0) \in N \times \mathbb{R}^d$ but are required to be fibred. Therefore, the considered equivalence relation is finer and we can expect more classes of persistent singularities then in the setting considered in Theorem 5.2.2, where the only stable singularities are locally quadratic. Intuitively, while the germ at $x = 0$ of the function f given by $f(x) = x^3$ is unstable, i.e. it does *not* satisfy Definition 5.1.5, the singularity x^3 of the germ at $(x, \mu) = (0, 0)$ of the parameter dependent function $F(x; \mu) = x^3 + \mu x$ is not removable under small fibred perturbations. In other words, if G is a small fibred perturbation of F then G is equivalent to the original F under the action of a fibred change of coordinates from the right plus a translation from the left.

Definition 5.3.1 (unfolding)**.** A function germ $F\colon (N \times \mathbb{R}^d, (x, 0)) \to (\mathbb{R}, y)$ is called an *unfolding* of the function germ $f\colon (N, x) \to (\mathbb{R}, y)$, where $f(z) = F(z; 0)$. △

When classifying local singularities of functions, the function value at a singular point is not important, neither is the choice of coordinates centred at a point where the function is singular. Choosing local coordinates on N centred at x and an affine-linear

coordinate on $\mathbb{R}$ centred at y it suffices to consider unfoldings $(\mathbb{R}^n \times \mathbb{R}^d, 0) \to (\mathbb{R}, 0)$. Let us show how to compare two unfoldings of the same germ.

Definition 5.3.2 (right-morphism between unfoldings)**.** Denote the projection $\mathbb{R}^n \times \mathbb{R}^d \to \mathbb{R}^d$ by π_d and the projection $\mathbb{R}^n \times \mathbb{R}^r \to \mathbb{R}^r$ by π_r. The inclusion of $\mathbb{R}^n$ into $\mathbb{R}^n \times \mathbb{R}^d$ or $\mathbb{R}^n \times \mathbb{R}^r$ is denoted by $\mathrm{id} \times 0$. Let $F\colon (\mathbb{R}^n \times \mathbb{R}^d, 0) \to (\mathbb{R}, 0)$ and $G\colon (\mathbb{R}^n \times \mathbb{R}^r, 0) \to (\mathbb{R}, 0)$ be unfoldings of the same germ. A *right-morphism* from G to F consists of a germ $\Phi\colon (\mathbb{R}^n \times \mathbb{R}^r, 0) \to (\mathbb{R}^n \times \mathbb{R}^d, 0)$ and a germ $\alpha\colon (\mathbb{R}^r, 0) \to (\mathbb{R}, 0)$ such that

(1) $\Phi \circ (\mathrm{id} \times 0) = \mathrm{id} \times 0$, i.e. a representative of Φ maps $(x, 0) \in \mathbb{R}^n \times \mathbb{R}^r$ to $(x, 0) \in \mathbb{R}^n \times \mathbb{R}^d$ whenever defined,

(2) there exist a germ $\psi\colon (\mathbb{R}^r, 0) \to (\mathbb{R}^d, 0)$ such that $\pi_d \circ \Phi = \psi \circ \pi_r$, i.e. the map Φ maps fibres to fibres,

(3) $G(x; s) = F(\Phi(x; s)) + \alpha(s)$.

The situation is illustrated in the following diagram:

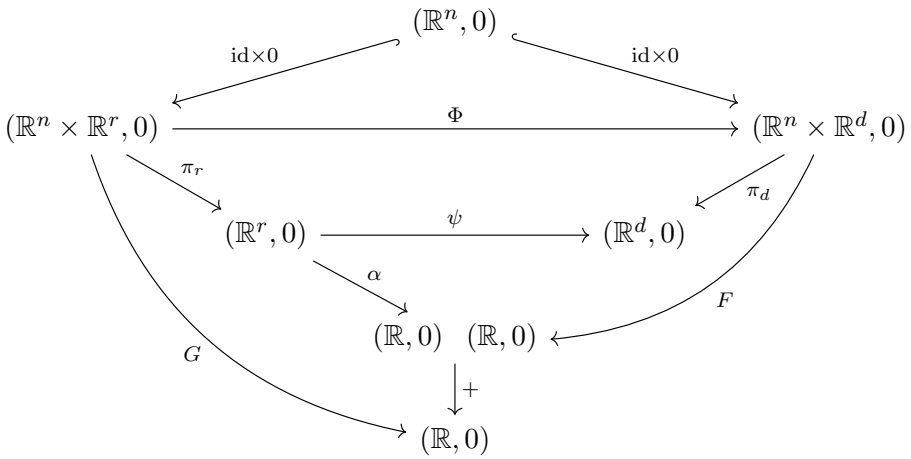

△

Definition 5.3.3 (right-left morphism between unfoldings)**.** In the right-left category, the translation of F with an element α in Definition 5.3.2 is replaced by a general transformation acting from the left, i.e. condition (3) reads

$$G(x; s) = \lambda(F(\Phi(x; s)); s),$$

where $\lambda\colon (\mathbb{R} \times \mathbb{R}^d, 0) \to (\mathbb{R}, 0)$ such that a representative maps $(t, 0) \in \mathbb{R} \times \mathbb{R}^d$ to $t \in \mathbb{R}$ whenever defined (Wassermann, 1974, §3). △

Remark 5.3.1. With an appropriate definition of compositions of morphisms the unfoldings of a fixed germ can be given the structure of a category in which the unfoldings are the objects (Wassermann, 1974, §3 or Wall, 1981). This justifies our nomenclature. △

More general notions which also apply to parameter dependent non-scalar-valued germs or different equivalence classes can be found in Du Plessis and Wall, 1995; Wall, 1981. The scalar-valued setting with right (-left) equivalence is the one considered in classical catastrophe theory.

An important concept is the notion of *versality*. Intuitively, a versal unfolding of a germ contains all possible fibred perturbations which leave the germ invariant.

Definition 5.3.4 ((mini-)versal unfolding)**.** If $F\colon (\mathbb{R}^n \times \mathbb{R}^d, 0) \to (\mathbb{R}, 0)$ is an unfolding of $f\colon (\mathbb{R}^n, 0) \to (\mathbb{R}, 0)$ such that for any other unfolding $G\colon (\mathbb{R}^n \times \mathbb{R}^r, 0) \to (\mathbb{R}, 0)$ of f there exist a morphism from G to F then F is called a *versal unfolding of* f. If the unfolding dimension d is minimal such that a versal unfolding of f exist then F is called a *miniversal unfolding of* f. △

Versal unfoldings are *topologically* $\mathcal{C}^\infty$*-stable*, i.e. a small perturbation G of a versal unfolding F is *equivalent as an unfolding* to F. Developing a precise topological notion of stability and equivalence of unfoldings is rather technical. One problem is that admissible small perturbations will not leave the reference germ and its localisation point invariant. In his dissertation, Wassermann (1974) develops a notion of equivalence and six topological notions of stability and shows that all of them are equivalent to versality of unfoldings. The reader can also find a treatment in Du Plessis and Wall, 1995.

Let us show how to construct a miniversal unfolding to a given germ. The set of germs at 0 of functions $\mathbb{R}^n \to \mathbb{R}$ forms a local ring. Its unique maximal ideal is denoted by $\mathfrak{m}(n)$ and consists of the germs of functions that map 0 to 0. It is generated by the coordinate functions of $\mathbb{R}^n$. We will show the technique for the right category. See, for instance, Wassermann, 1974 for the left-right category.

Definition 5.3.5 (local algebra, multiplicity)**.** Let $f\colon (\mathbb{R}^n, 0) \to (\mathbb{R}, 0)$ be a germ with critical point at 0. The *local algebra* of f at 0 is defined as the quotient

$$Q_f = \mathfrak{m}(n)/I_{\nabla f},$$

where $I_{\nabla f}$ denotes the ideal in $\mathfrak{m}(n)$ generated by the partial derivatives $\left(\frac{\partial f}{\partial x_i}\right)_{1\leq i\leq n}$ of f. The real dimension $\mu(f) = \dim_{\mathbb{R}}(Q_f)$ of the $\mathbb{R}$-module Q_f is called the *multiplicity* of the critical point of f. △

Example 5.3.1. The germ f of $x \mapsto x^3$ has $\mu(f) = 1$ at 0 and $g(x, y) = xy^2$ has $\mu(g) = \infty$. △

Theorem 5.3.1 (miniversal unfolding)**.** *A* miniversal unfolding *for the right-category of a germ $f \in \mathfrak{m}(n)$ with $\mu(f) < \infty$ is given by*

$$F(x; s) = f(x) + \sum_{j=1}^{\mu(f)} s_j \phi_j(x),$$

where $\phi_1, \ldots, \phi_{\mu(f)}$ is an $\mathbb{R}$-basis of the local algebra Q_f.

Remark 5.3.2. In V. I. Arnold, Gusein-Zade, and Varchenko, 1985 miniversal unfolding as well as the local algebra is defined with respect to the ring of germs at 0 rather than with respect to $\mathfrak{m}(n)$ as in Wassermann, 1974; Lu, 1976. Arnold refers to miniversal unfolding as per Definition 5.3.4 as *truncated miniversal unfolding* and his definition of μ differs from the one presented here by the constant 1. △

Locally around critical points, a parameter dependent function can be split into a degenerate, parameter dependent part and a nondegenerate quadratic part using fibred changes of coordinates. This is made precise by the following theorem.

Theorem 5.3.2 (Splitting theorem, (Weinstein, 1971a))**.** *Let $F\colon (\mathbb{R}^n \times \mathbb{R}^d, 0) \to (\mathbb{R}, 0)$ be an unfolding of a germ $f\colon (\mathbb{R}^n, 0) \to (\mathbb{R}, 0)$, where f has a critical point at 0. There exists*

- *$k \geq 0$ and an unfolding $G\colon (\mathbb{R}^k \times \mathbb{R}^d, 0) \to (\mathbb{R}, 0)$ with critical point at 0 and $\frac{\partial^2 G}{\partial x_i x_j}(0) = 0$ for all $1 \leq i, j \leq k$,*
- *a nondegenerate quadratic form $Q\colon (\mathbb{R}^{n-k}, 0) \to (\mathbb{R}, 0)$,*
- *and the germ of a local diffeomorphism $\Phi\colon (\mathbb{R}^n \times \mathbb{R}^d, 0) \to (\mathbb{R}^k \times \mathbb{R}^d \times \mathbb{R}^{n-k}, 0)$ with $\pi_d \circ \Phi = \pi_d$*

such that

$$F(\Phi(x_1, \ldots, x_n, s_1, \ldots, s_d)) = G(x_1, \ldots, x_k; s_1, \ldots, s_d) + Q(x_{k+1}, \ldots, x_n).$$

Moreover, Q is defined uniquely up to right-equivalence and G is determined up to composition from the right with local diffeomorphism germs $\Psi\colon (\mathbb{R}^k \times \mathbb{R}^d, 0) \to (\mathbb{R}^k \times \mathbb{R}^d, 0)$ with $\pi_d \circ \Psi = \pi_d$.

Remark 5.3.3. The nondegenerate quadratic form Q in Theorem 5.3.2 is of the form

$$Q(x_{k+1}, \ldots, x_n) = x_{k+1}^2 + \ldots + x_{k+l}^2 - x_{k+l+1}^2 - \ldots - x_n^2,$$

where l is the number of positive eigenvalues of the Hessian matrix of $x \mapsto F(x; 0)$. △

Corollary 5.3.3. *The special case $k = 0$, $d = 0$ recovers the Morse lemma (Theorem 5.2.1).*

Remark 5.3.4. A non-fibred version ($d = 0$) of the statement is called *splitting lemma* or *parametric Morse lemma*. Here, the word *parametric* does *not* refer to parameters in the function but refers to the proof idea in which the Morse lemma is applied parameterwise. A proof can be found in Bröcker, 1975, §14.12, Wassermann, 1974, Lemma 5.12, or V. I. Arnold, Gusein-Zade, and Varchenko, 1985, §6.2. △

In view of Theorem 5.3.2 it makes sense to consider function germs only up to an addition of nondegenerate quadratic forms. For this we introduce the notion of *stably equivalence*.

Definition 5.3.6 (stably equivalence)**.** Two function germs $F\colon (\mathbb{R}^n, 0) \to (\mathbb{R}, 0)$ and $\tilde{F}\colon (\mathbb{R}^{\tilde{n}}, 0) \to (\mathbb{R}, 0)$ are *stably right-(left) equivalent* if there exist nondegenerate quadratic forms $Q\colon (\mathbb{R}^m, 0) \to \mathbb{R}$ and $\tilde{Q}\colon (\mathbb{R}^{\tilde{m}}, 0) \to \mathbb{R}$ with $n + m = \tilde{n} + \tilde{m}$ such that $F + Q$ and $\tilde{F} + \tilde{Q}$ are right-(left) equivalent. △

We can formulate another corollary to Theorem 5.3.2 which uses the uniqueness properties.

Corollary 5.3.4. *Two function germs $F, \tilde{F}\colon (\mathbb{R}^n, 0) \to (\mathbb{R}, 0)$ are right-(left) equivalent if and only if they are stably right-(left) equivalent.*

5.4 Classification results

Function germs up to stably equivalence have been classified by Mather, Thom, Arnold V. I. and others, see, for instance, V. I. Arnold, Goryunov, et al., 1998; V. I. Arnold, Goryunov, et al., 1993. Table 1.1 form the motivational example shows Thom's classical list of seven elementary catastrophes including their miniversal unfoldings. It is a complete list of function germs f for which 0 is a critical point, $f(0) = 0$ and the multiplicity μ is at most 4 up to stably right-left equivalence. The miniversal unfoldings constitute representatives of all topologically stable function families with at most four parameters. If we consider stably right-equivalence instead then an additional cusp singularity $-x^4$ and an additional butterfly singularity $-x^6$ occur. See Figures 5.1 and 5.2 for illustrations or Offen, 2019a; Offen, 2019c for animations. An elementary reference with an extensive analysis of singularities of low multiplicity is Gilmore, 1993.

Up to the barrier $\mu(f) \leq 4$, normal forms can be written down without a continuous parameter, i.e. the normal forms are isolated. However, allowing higher degeneracies there can be continuous families of germs where each germ has the same level of degeneracy but all family members are inequivalent. This forces the introduction of continuous

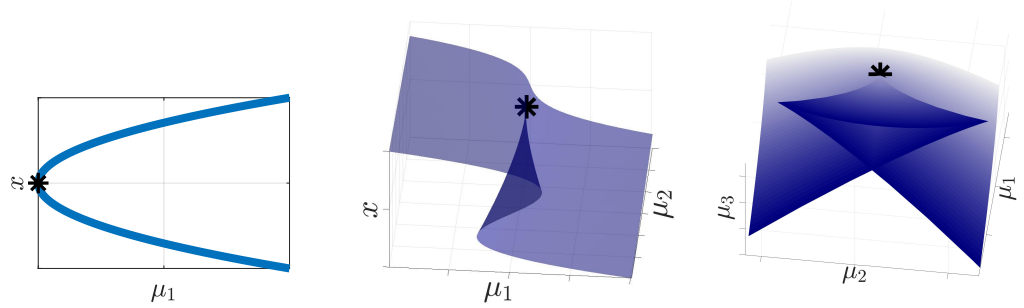

Figure 5.1: The diagrams show the critical points of the miniversal unfoldings of the fold (A_2), cusp (A_3) and the swallowtail singularity (A_4) (from left to right). The most singular points are marked by $*$. The bifurcation diagram for the swallowtail shows the parameter values for degenerate critical points. Each point in the sheet corresponds to a fold singularity, an intersection of sheets means that two fold singularities happen at the same parameter value but at different points x in the phase space, points on the two edges correspond to cusp points. The point where the two edges join with the intersection line is a swallowtail point marked by $*$. See Offen, 2019a for an animation of the cusp and swallowtail singularity.

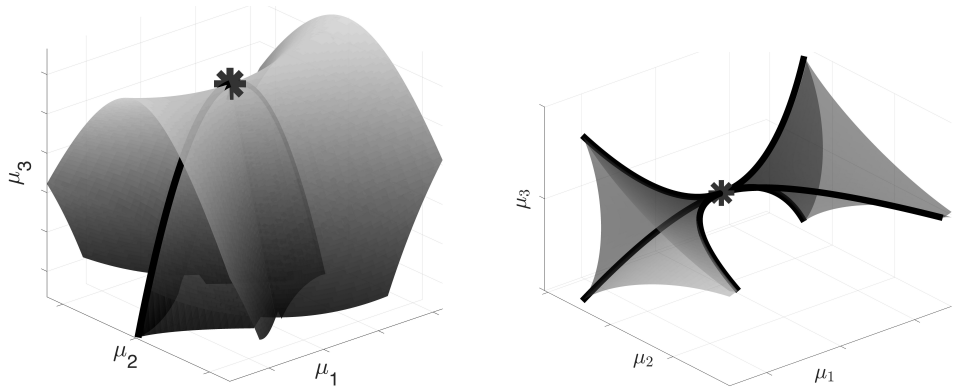

Figure 5.2: The plots show those configurations of the parameters μ_1, μ_2, μ_3 for which the problem $\nabla_x F(x; s) = 0$ becomes singular, where F is the miniversal unfolding of a hyperbolic umbilic (D_4^+) or elliptic umbilic (D_4^-) singularity. Imagine moving around the parameter μ and watching the solutions bifurcating in the phase space. As μ crosses a sheet two solutions annihilate (fold - A_2). For μ in the intersection of two sheets there are two simultaneous fold singularities at different positions in the phase space. Crossing an edge three solutions merge into one (or vice versa). Points contained in an edge correspond to cusp singularities. The marked points denote the most degenerate points, i.e. the location of the umbilic singularities. In the hyperbolic umbilic bifurcation to the left, moving the parameter μ upwards along the μ_3 axis through the singular point four solutions annihilate. At the most singular point a sheet of folds touches a line of cusp singularities. The elliptic umbilic to the right can be thought of as three lines of cusps touching tangentially. Animations can be found in Offen, 2019c.

ADE class	$A_k^{\pm}$	$D_k^{\pm}$, $k \geq 4$	$E_6^{\pm}$	E_7	E_8
germ	$\pm x^{k+1}$	$x^2y \pm y^{k-1}$	$x^3 \pm y^4$	$x^3 + xy^3$	$x^3 + y^5$,

Table 5.1: The table shows all real simple singularities up to right-equivalence. The positive and negative germs for A_k^+ and A_k^- are equivalent if k is even or $k = 1$. (V. I. Arnold, Gusein-Zade, and Varchenko, 1985, §17.1)

ADE class	germ	condition on parameter
$P_8 = T_{3,3,3}$	$x^3 + ax^2z \pm xz^2 + y^2z$	$a^2 \neq 4$, if $+$
$X_9 = T_{2,4,4}$	$\pm x^4 \pm y^4 + ax^2y^2$	$a^2 \neq 4$, if $++$ or $--$
$J_{10} = T_{2,3,6}$	$x^3 + ax^2y^2 \pm xy^4$	$a^2 \neq 4$, if $+$
$J_{10+k} = T_{2,3,6+k}$	$x^3 + x^2y^2 + ay^{6+k}$	$a \neq 0, k > 0$
$X_{9+k} = T_{2,4,4+k}$	$\pm x^4 \pm x^2y^2 + ay^{4+k}$	$a \neq 0, k > 0$
$Y_{r,s} = T_{2,r,s}$	$\pm x^2y^2 \pm x^r + ay^s$	$a \neq 0, r, s > 4$
$\tilde{Y}_r = \tilde{T}_{2,r,r}$	$\pm(x^2 + y^2)^2 + ax^r$	$a \neq 0, r > 4$
$P_{8+k} = T_{3,3,3+k}$	$x^3 \pm x^2z + y^2z + az^{k+3}$	$a \neq 0, k > 0$
$R_{l,m} = T_{3,l,m}$	$x(x^2 + yz) \pm y^l \pm az^m$	$a \neq 0, m \geq l > 4$
$\tilde{R}_m = \tilde{T}_{3,m,m}$	$x(\pm x^2 + y^2 + z^2) + ay^m$	$a \neq 0, m > 4$
$T_{p,q,r}$	$\pm x^p \pm y^q \pm z^r + axyz$	$a \neq 0, \frac{1}{p} + \frac{1}{q} + \frac{1}{r} < 1$
$\tilde{T}_{p,m} = \tilde{T}_{p,m,m}$	$x(y^2 + z^2) \pm x^p + ay^m$	$a \neq 0, \frac{1}{p} + 2\frac{1}{m} < 1$

Table 5.2: The table shows unimodal singularities up to right-equivalence. The given list plus 14 exceptional families constitute all unimodal singularities. The parameter a is continuous while k, l, m, p, q, r, s are natural numbers. (V. I. Arnold, Gusein-Zade, and Varchenko, 1985, §17.1)

parameters[1] in the normal form. The minimal count of such parameters is called the *modality of the germ*. For a definition of modality in terms of geometric properties of a germ see V. I. Arnold, Gusein-Zade, and Varchenko, 1985, p. 184.

Arnold extended Thom's classification (Table 1.1), sorted the singularities into series, and provided a link to the classification of simple Lie groups. His nomenclature is known as ADE-classification due to the relation of the simple (i.e. modality 0) singularities with the Coxeter groups A_k, D_k, E_6, E_7, E_8. Subscripts to the letters indicate the multiplicity of the singularity: for instance, A_k has multiplicity $k-1$. Table 5.1 shows a classification of all simple singularities up to stably right equivalence. In particular, the list contains Thom classical catastrophes (Table 1.1). Table 5.2 presents a classification of unimodal singularities for stably right equivalence.

Some singularities can be obtained from higher degenerate singularities by a small perturbation. For instance, perturbing the singularity x^{k+1} to $x^{k+1} + \epsilon x^k$ for $\epsilon > 0$

[1] Modality is not to be confused with the number of parameters in a miniversal unfolding. The first example of a germ with modality greater than zero is P_8 in Table 5.2.

arbitrarily small we obtain a singularity $x^{k+1}+\epsilon x^k$ which is equivalent to the singularity x^k. An arrangement of the singularities in a hierarchy can be found in V. I. Arnold, Gusein-Zade, and Varchenko, 1985, §17.

Remark 5.4.1 (codimension of a germ). Next to modality and multiplicity, there is the notion of *codimension* of a germ, which coincides with the multiplicity of a germ if the singularity is simple, i.e. of modality zero. △

Part II

Bifurcations of solutions to Hamiltonian boundary value problems and their preservation under discretisation

A bifurcation is a qualitative change in a family of solutions to an equation produced by varying parameters. In contrast to local bifurcations of dynamical systems that are often related to a change in the number or stability of equilibria, bifurcations of boundary value problems are global in nature and may not be related to any obvious change in dynamical behaviour.

In Chapter 6 we develop a framework to study bifurcations of solutions of boundary-value problems for symplectic maps using the language of (finite dimensional) catastrophe theory. Catastrophe theory is a well-developed framework which studies the bifurcations of critical points of functions. Our approach offers an alternative to the analysis of critical points in infinite dimensional function spaces, typically used in the study of bifurcation of variational problems, and opens the way to the detection of more exotic bifurcations than the simple folds and cusps that are often found in examples. In Chapter 7 the framework is used to study popular boundary conditions, integrable systems and systems with symmetries.

The chapter is followed by Chapter 8 in which we analyse the effects of conformal symplectic symmetries on Hamiltonian boundary value problems within the new framework. Chapter 9 will explain the implications of the obtained results for numerical computations. We will show that certain generic codimension 3 bifurcations are preserved under discretisation if and only if a symplectic integrator is used. The chapters 6-9 present the development of the framework with a focus on its application with some justifications and proofs postponed to Chapter 10 in which a careful analysis focusing on pure aspects of the framework is undertaken.

While Part II focuses on a setting which applies to ODEs arising in finite dimensional Hamiltonian systems, the subsequent Part III covers aspects for PDEs, infinite dimensional Hamiltonian systems (Lie–Poisson systems) and multi-symplecticity.

Chapter 6

Hamiltonian boundary value problems and catastrophe theory

Chapter 6 and 7 are an adaption of McLachlan and Offen, 2018a.

We develop a novel framework to analyse bifurcations of solutions to Hamiltonian boundary value problems, or, more generally, to boundary value problems of symplectic maps. We associate certain such problems with a geometric picture involving the intersection of Lagrangian submanifolds, and hence with critical points of suitable generating functions. Singularities can then be understood using classical catastrophe theory.

6.1 Example of a Hamiltonian boundary value problem– The Bratu problem

To motivate the notion of *Hamiltonian boundary value problems*, we return to the Bratu problem from Sections 4.3 and 4.5. A reaction–diffusion model for combustion processes is given by the PDE

$$u_t = u_{xx} + \mu e^u, \qquad u(t,0) = 0 = u(t,1) \tag{6.1.1}$$

with parameter $\mu > 0$. Finding steady-state solutions $x \mapsto u(x)$ of (6.1.1), i.e. solving the Dirichlet problem

$$u_{xx} + \mu e^u = 0, \quad u(0) = 0 = u(1) \tag{6.1.2}$$

and analysing their bifurcation behaviour is known as the Bratu problem (Mohsen, 2014). For positive μ smaller than a critical parameter value $\mu^* \approx 3.51$ there are two solutions. As μ is increased the solutions approach each other, merge at $\mu = \mu^*$ and annihilate each other. We say that the solutions undergo a fold bifurcation (see

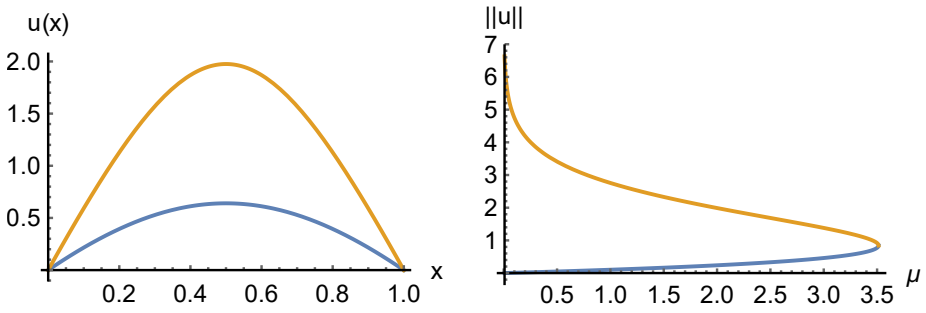

Figure 6.1: Left plot: solutions to the Bratu problem (6.1.2) for $\mu = 3$. Right plot: bifurcation diagram of the Bratu problem (6.1.2) showing a fold bifurcation at $\mu \approx 3.51$.

Figure 6.1). A Hamiltonian formulation of (6.1.2) is given as the first order system

$$\begin{aligned} \dot{q} &= \quad \nabla_p H(p,q) = p \\ \dot{p} &= -\nabla_q H(p,q) = -\mu e^q \end{aligned} \tag{6.1.3}$$

together with the boundary condition $q(0) = 0 = q(1)$ for the Hamiltonian

$$H(p,q) = \frac{1}{2}p^2 + \mu e^q \tag{6.1.4}$$

defined on $T^*\mathbb{R} \cong \mathbb{R}^2$.

The boundary value problem is visualised in Figure 6.2. A Hamiltonian motion, i.e. a solution curve to (6.1.3), solves the boundary value problem $q(0) = 0 = q(1)$ if it starts on the line $\Lambda = \{(p,q) = (p,0) \,|\, p \in \mathbb{R}\}$ and returns to Λ after time 1. For $0 < \mu < \mu^*$ two such solutions are illustrated as black curves starting at $\times$ and ending at o. This is an example of a *Hamiltonian boundary value problem* or *Lagrangian boundary value problem* which we define in the following section.

6.2 Definition and examples for Hamiltonian and Lagrangian boundary value problems

Definition 6.2.1 (Lagrangian boundary value problem for a symplectic map)**.** Consider a symplectic map $\phi\colon (M,\omega) \to (M',\omega')$ and projections $\pi\colon M \times M' \to M$ and $\pi'\colon M \times M \to M'$. Define the symplectic form $\omega \oplus (-\omega') := \pi^*\omega - \pi'^*\omega'$ on the manifold $M \times M'$, where * denotes the pull-back operation. The graph Γ of ϕ constitutes a Lagrangian submanifold in the symplectic manifold $(M \times M', \omega \oplus (-\omega'))$. If Π is another Lagrangian submanifold in $(M \times M', \omega \oplus (-\omega'))$, then (ϕ, Π) is called a *Lagrangian boundary value problem (for ϕ)*. Its solution is the intersection of Γ with Π. △

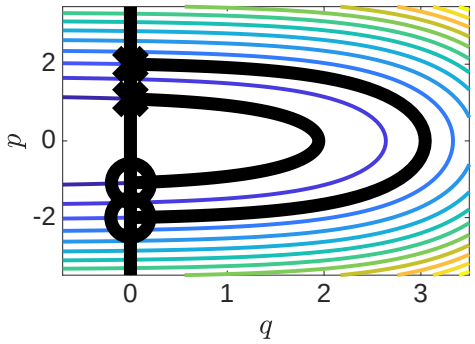

Figure 6.2: Illustration of the Bratu problem (6.1.2) regarded as a boundary value problem for the Hamiltonian system. The plot shows a contour plot of the Hamiltonian $H(p,q) = \frac{1}{2}p^2 + \mu e^q$ from (6.1.4) for a typical parameter value $\mu \in (0, \mu^*)$. All motions follow the contour lines clockwise. The boundary condition $q(0) = 0 = q(1)$ is visualised as the straight line Λ defined by $q = 0$ in the phase space $\mathbb{R}^2$. A solution to the boundary value problem is a motion which starts on the line Λ and ends on Λ after time 1. The plot depicts two motions initialised at the crosses $\times$ which reach the line $q = 0$ after time $t = 1$ and are, therefore, solutions to the boundary value problem.

Most commonly symplectic maps arise as flow maps to Hamiltonian systems.

Definition 6.2.2 (Hamiltonian boundary value problem)**.** If in a Lagrangian boundary value problem for ϕ the map ϕ arises as the flow map of a Hamiltonian system, then the boundary value problem is called a *Hamiltonian boundary value problem.* △

In our investigations (with the exception of symmetry considerations later) it is irrelevant whether the symplectic map belonging to a Lagrangian boundary value problem has the structure of a Hamiltonian flow map. Therefore, the notion of Lagrangian boundary value problems and Hamiltonian boundary value problems can be regarded as synonyms for now.

Remark 6.2.1. Lagrangian boundary value problems (ϕ, Π) with $\Gamma = \operatorname{graph}\phi$ can be localized near a solution $z \in \Pi \cap \Gamma$: shrink M to an open neighbourhood of $\pi(z)$, M' to an open neighbourhood of $\pi'(z)$ and restrict ω, ω' and ϕ accordingly. △

Example 6.2.1. If $(M, \omega) = (M', \omega')$, then the periodic boundary value problem $\phi(z) = z$ is a Lagrangian boundary value problem where $\Pi = \{(m, m) \mid m \in M\}$ is the diagonal. △

Example 6.2.2. Classical Dirichlet, Neumann and Robin boundary value problems for second order ordinary differential equations on $\mathbb{R}^n$ of the form $\ddot{u}(t) = \nabla_u G(t, u(t))$ can be regarded as Lagrangian boundary value problems for the flow map of the Hamiltonian system $(\mathbb{R}^{2n}, \omega = \sum \mathrm{d}p_j \wedge \mathrm{d}q^j, H)$ with the (possibly time-dependent) Hamiltonian

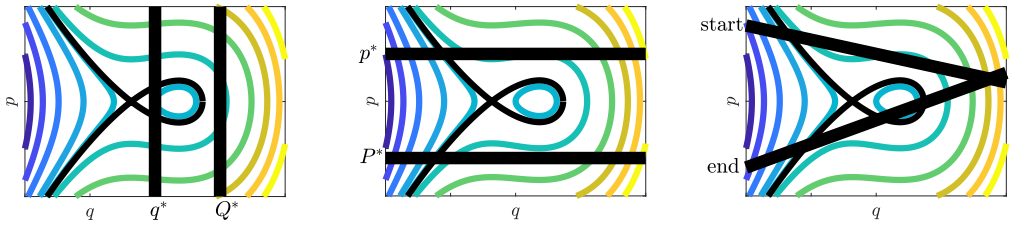

Figure 6.3: The plots show illustrations of Dirichlet, Neumann and Robin boundary conditions as described in Example 6.2.2 in a phase portrait of a time independent Hamiltonian system.

$H(t,p,q) = \frac{1}{2}\|p\|^2 - G(t,q)$ as illustrated in Figure 6.3 for $n = 1$: a motion is a solution to

- the Dirichlet problem $u(t_0) = q^*$, $u(t_1) = Q^*$ if the motion $(p(t), q(t)) = (\dot{u}(t), u(t))$ starts on the submanifold $\mathbb{R}^n \times q^*$ at time t_0 and ends on the submanifold $\mathbb{R}^n \times Q^*$ at time t_1,
- the Neumann problem $\dot{u}(t_0) = p^*$, $\dot{u}(t_1) = P^*$ if the motion $(p(t), q(t)) = (\dot{u}(t), u(t))$ starts on $p^* \times \mathbb{R}^n$ and ends on $P^* \times \mathbb{R}^n$, or
- the Robin problem $u^j(t_0) + \alpha_0^j \dot{u}^j(t_0) = \beta_0^j$, $u^j(t_1) + \alpha_1^j \dot{u}^j(t_1) = \beta_1^j$, $j = 1, \dots, n$ if the motion $(p(t), q(t)) = (\dot{u}(t), u(t))$ starts on the submanifold $\{(p,q) \,|\, q^j + \alpha_0^j p_j = \beta_0^j\}$ and ends on the submanifold $\{(p,q) \,|\, q^j + \alpha_1^j p_j = \beta_1^j\}$ for constant coefficients α_k^j, β_k^j.

We have $\Pi = \mathbb{R}^n \times \{q^*\} \times \mathbb{R}^n \times \{Q^*\}$ for the Dirichlet problem, $\Pi = \{p^*\} \times \mathbb{R}^n \times \{P^*\} \times \mathbb{R}^n$ for the Neumann problem and $\Pi = \{(p,q,P,Q) \,|\, q^j + \alpha_0^j p^j = \beta_0^j,\ Q^j + \alpha_1^j P^j = \beta_1^j\}$ for the Robin problem. △

Example 6.2.3 (Non-example). Let $\omega = \sum_{j=1}^n \mathrm{d}p_j \wedge \mathrm{d}q^j$ be the standard symplectic form on $\mathbb{R}^{2n}$. Consider a symplectic map $\phi \colon \mathbb{R}^{2n} \to \mathbb{R}^{2n}$. The boundary condition $\phi(p,q) = (q,p)$ does *not* yield a Lagrangian boundary value problem since $\Pi = \{(p,q,q,p) \,|\, (p,q) \in \mathbb{R}^{2n}\}$ is not Lagrangian in $(\mathbb{R}^{2n} \times \mathbb{R}^{2n}, \omega \oplus -\omega)$. △

Example 6.2.4 (Linear boundary conditions).

$$A \begin{pmatrix} p \\ q \\ P \\ Q \end{pmatrix} = \begin{pmatrix} \alpha \\ \beta \end{pmatrix}$$

with $A \in \mathbb{R}^{2n\times 4n}$ of maximal rank and $\alpha, \beta \in \mathbb{R}^n$ constitute Lagrangian submanifolds if and only if $V^\top JV = 0$ where the columns of $V \in \mathbb{R}^{4n\times 2n}$ span the kernel of A and J represents the symplectic form $\omega \oplus (-\omega)$ on $\mathbb{R}^{2n} \times \mathbb{R}^{2n}$, i.e.

$$J = \begin{pmatrix} 0 & I_n & 0 & 0 \\ -I_n & 0 & 0 & 0 \\ 0 & 0 & 0 & -I_n \\ 0 & 0 & I_n & 0 \end{pmatrix}.$$

Here $I_n \in \mathbb{R}^{n\times n}$ denotes the identity matrix. If $n = 1$, then

$$q + p = \alpha, \quad Q + P = \beta$$

corresponds to

$$A = \begin{pmatrix} 1 & 1 & 0 & 0 \\ 0 & 0 & 1 & 1 \end{pmatrix}, \quad V = \begin{pmatrix} 1 & 1 \\ -1 & -1 \\ 1 & -1 \\ -1 & 1 \end{pmatrix}$$

and constitutes a Lagrangian boundary condition. On the other hand,

$$q - p - Q + P = \alpha, \quad q + p + Q + P = \beta$$

correspond to

$$A = \begin{pmatrix} -1 & 1 & 1 & -1 \\ 1 & 1 & 1 & 1 \end{pmatrix}, \quad V = \begin{pmatrix} 1 & 0 \\ 0 & 1 \\ 0 & -1 \\ -1 & 0 \end{pmatrix}$$

and does *not* constitute a Lagrangian boundary condition. △

A map ϕ can be symplectic with respect to several non-equivalent[1] symplectic structures. The question whether a boundary value problem for such a map is Lagrangian depends on the considered symplectic structure as the following Example 6.2.5 illustrates. We present a map ϕ which is symplectic with respect to the standard symplectic structure ω and commutes with a non-symplectic map Ψ. The map ϕ is, therefore, symplectic with respect to the pulled-back structure $(\Psi^{-1})^*\omega$ as well. However, as Ψ is not symplectic with respect to ω, the symplectic structures ω and $(\Psi^{-1})^*\omega$ are not equivalent and there are submanifolds which are Lagrangian with respect to ω but not with respect to $(\Psi^{-1})^*\omega$. Using such a submanifold as a boundary condition gives rise to a problem which is Lagrangian with respect to only one of the symplectic structures.

[1] The sets of Lagrangian manifolds do not coincide.

Example 6.2.5. Consider $\mathbb{R}^4$ with coordinates p_1, q^1, p_2, q^2 and with the standard symplectic form

$$\omega = \mathrm{d}p_1 \wedge \mathrm{d}q^1 + \mathrm{d}p_2 \wedge \mathrm{d}q^2.$$

The map describing the motion of two independent harmonic oscillators

$$(P_1, Q^1, P_2, Q^2) = \phi_t(p_1, q^1, p_2, q^2)$$

with

$$\begin{pmatrix} P_1 \\ Q^1 \\ P_2 \\ Q^2 \end{pmatrix} = \begin{pmatrix} \cos t & -\sin t & & \\ \sin t & \cos t & & \\ & & \cos t & -\sin t \\ & & \sin t & \cos t \end{pmatrix} \begin{pmatrix} p_1 \\ q^1 \\ p_2 \\ q^2 \end{pmatrix}$$

is symplectic with respect to ω and its graph $\Gamma \subset (\mathbb{R}^4 \times \mathbb{R}^4, \omega \oplus (-\omega))$ is Lagrangian. Here we consider the ordering p_1, q^1, p_2, q^2 of coordinates on $\mathbb{R}^4$ and the induced ordering on $\mathbb{R}^4 \times \mathbb{R}^4$ rather than gathering the ps and qs to give the map of the system of harmonic oscillators a simple form. Consider the embedding

$$\iota \colon \mathbb{R}^4 \to \mathbb{R}^4 \times \mathbb{R}^4, \quad \iota(p_1, q^1, p_2, q^2) = \begin{pmatrix} 2p_1, & q^1, & p_2, & q^2, & 2p_2, & q^2, & p_1, & q^1 \end{pmatrix}^\top,$$

where $^\top$ denotes transposition. We have

$$\iota^*(\omega \oplus -\omega) = \mathrm{d}p_1 \wedge \mathrm{d}q^1 - \mathrm{d}p_2 \wedge \mathrm{d}q^2$$

such that $\Pi = \iota(\mathbb{R}^4)$ is *not* Lagrangian with respect to ω. Consider the diffeomorphism $\Psi \colon \mathbb{R}^4 \to \mathbb{R}^4$ defined by

$$(P_1, Q^1, P_2, Q^2) = \Psi(p_1, q^1, p_2, q^2)$$

with

$$\begin{pmatrix} P_1 \\ Q^1 \\ P_2 \\ Q^2 \end{pmatrix} = \begin{pmatrix} 2 & & & \\ & 2 & & \\ & & 1 & \\ & & & 1 \end{pmatrix} \begin{pmatrix} p_1 \\ q^1 \\ p_2 \\ q^2 \end{pmatrix}.$$

Define the symplectic structure

$$\tilde{\omega} = (\Psi^{-1})^* \omega = \frac{1}{2} \mathrm{d}p_1 \wedge \mathrm{d}q^1 + \mathrm{d}p_2 \wedge \mathrm{d}q^2.$$

We have $\Psi^{-1} \circ \phi_t \circ \Psi = \phi_t$ such that $\phi_t^* \tilde{\omega} = \tilde{\omega}$. Therefore, ϕ_t is symplectic with respect to $\tilde{\omega}$ and its graph $\Gamma \subset (\mathbb{R}^4 \times \mathbb{R}^4, \tilde{\omega} \oplus (-\tilde{\omega}))$ is Lagrangian. Moreover, $\iota^*(\tilde{\omega} \oplus$

$(-\tilde{\omega})) = 0$ such that $\Pi = \iota(\mathbb{R}^4)$ is Lagrangian with respect to $\tilde{\omega}$. It follows that (ϕ_t, Π) is a Lagrangian boundary value problem if ϕ_t is considered as a symplectic map $\phi_t \colon (\mathbb{R}^4, \tilde{\omega}) \to (\mathbb{R}^4, \tilde{\omega})$ but not if ϕ_t is considered as a symplectic map $\phi_t \colon (\mathbb{R}^4, \omega) \to (\mathbb{R}^4, \omega)$. △

6.3 Lagrangian boundary value problems and catastrophe theory

Let us identify Lagrangian boundary value problems if the problems are locally symplectomorphic when considered as a local intersection problem of Lagrangian submanifolds. As we are interested in bifurcation behaviour, we allow the boundary value problems to depend on parameters: this means the symplectic map as well as the boundary condition is allowed to be parameter dependent.

Definition 6.3.1 (equivalent Lagrangian boundary value problems for symplectic maps)**.** Consider smooth families of symplectic maps $\phi_\mu \colon M \to M'$ and $\tilde{\phi}_\mu \colon \widetilde{M} \to \widetilde{M'}$ with (multi-dimensional) parameter μ and families of Lagrangian boundary value problems (ϕ_μ, Π_μ) and $(\tilde{\phi}_\mu, \tilde{\Pi}_\mu)$. Let $z^* \in M$, $\tilde{z}^* \in \widetilde{M}$ and μ^* a parameter value. The boundary value problem (ϕ_μ, Π_μ) is equivalent at z^* to the problem $(\tilde{\phi}_\mu, \tilde{\Pi}_\mu)$ at $\tilde{z}^*$ if after a reparametrisation of the families of boundary value problems, where the reparametrisation fixes μ^*, and after shrinking $M \times M'$ around $(z^*, \phi_{\mu^*}(z^*))$ and $\widetilde{M} \times \widetilde{M'}$ around $(\tilde{z}^*, \tilde{\phi}_{\mu^*}(\tilde{z}^*))$ there exists a family of symplectomorphisms $\Phi_\mu \colon M \times M' \to \widetilde{M} \times \widetilde{M'}$ such that

$$\Phi_\mu(\Gamma_\mu) = \tilde{\Gamma}_\mu, \quad \Phi_\mu(\Pi_\mu) = \tilde{\Pi}_\mu, \quad \Phi_{\mu^*}((z^*, \phi_*(z^*))) = (\tilde{z}^*, \tilde{\phi}_*(\tilde{z}^*)).$$

Here Γ_μ is the graph of ϕ and $\tilde{\Gamma}_\mu$ is the graph of $\tilde{\phi}$. △

The idea behind Definition 6.3.1 is that both considered families of Lagrangian boundary value problems show qualitatively the same bifurcation behaviour. Indeed, we will use the ideas sketched in Section 1.2 to relate families of Lagrangian boundary value problems to smooth families of locally defined maps which can be understood using catastrophe theory. The following theorem constitutes the main result of Part II of this work. It says that the equivalence relation from Definition 6.3.1 matches the equivalence relation considered in catastrophe theory. It justifies translating notions, techniques, and classification results of catastrophe theory to the setting of Lagrangian boundary value problems. This has far reaching consequences for the analysis of bifurcations as well as the computation of bifurcation diagrams.

Theorem 6.3.1. *Consider two families of Lagrangian boundary value problems* $\mathfrak{L} = (\phi_\mu, \Pi_\mu)$ *in* M *and* $\tilde{\mathfrak{L}} = (\tilde{\phi}_\mu, \tilde{\Pi}_\mu)$ *in* $\widetilde{M}$*. Let* μ^* *be a parameter value and let* z^* *lie in the domain of* ϕ_{μ^*} *and* $\tilde{z}^*$ *in the domain of* $\tilde{\phi}_{\mu^*}$*. The families* $\mathfrak{L}$ *and* $\tilde{\mathfrak{L}}$ *localised at*

(μ^*, z^*) or $(\mu^*, \tilde{z}^*)$, respectively, are equivalent if and only if $\dim M = \dim \widetilde{M}$ *and the corresponding function families $h = (h_\mu)$ and $\tilde{h} = (\tilde{h}_\mu)$ are stably right equivalent in the sense of catastrophe theory.*

Roughly speaking, stably right equivalent in the sense of catastrophe theory allows

- the action of fibre-wise, i.e. μ-dependent, right-diffeomorphisms
- a μ-dependent translation
- diffeomorphic changes of the parameter μ
- the direct addition and subtraction of nondegenerate quadratic forms that have been isolated as in the splitting theorem (Theorem 5.3.2).

Corollary 6.3.2. *If $\mathfrak{L}$ and $\tilde{\mathfrak{L}}$ as in Theorem 6.3.1 are equivalent, then the germs at 0 of h_{μ^*} and $\tilde{h}_{\mu^*}$ are stably right equivalent.*

Remark 6.3.1 (Identification of Lagrangian boundary value problems across dimensions). Since the right equivalence classes of the associated function families to Lagrangian boundary value problems fully encode the bifurcation behaviour, it is reasonable to identify Lagrangian boundary value problems if and only if their associated families are stably right equivalent even when the dimensions of the problems differ. Moreover, problems can be identified even when their parameter spaces differ. This takes into account that some parameters can enter trivially after a suitable reparametrisation. For this, two Lagrangian boundary value problems $(\phi_\mu, \Pi_\mu)_{\mu\in I}$ and $(\tilde{\phi}_{\tilde{\mu}}, \tilde{\Pi}_{\tilde{\mu}})_{\tilde{\mu}\in\tilde{I}}$ are identified if there exist extensions of the parameter spaces such that $(\phi_\mu, \Pi_\mu)_{(\mu,\mu')\in I\times\mathbb{R}^l}$ and $(\tilde{\phi}_{\tilde{\mu}}, \tilde{\Pi}_{\tilde{\mu}})_{(\tilde{\mu},\tilde{\mu}')\in\tilde{I}\times\mathbb{R}^{\tilde{l}}}$ are equivalent in the sense of Definition 6.3.1. Similarly, two families of maps $(h_\mu)_{\mu\in I}$ and $(\tilde{h}_{\tilde{\mu}})_{\tilde{\mu}\in\tilde{I}}$ are identified if there exist extensions of the parameter spaces such that $(h_\mu)_{(\mu,\mu')\in I\times\mathbb{R}^l}$ and $(\tilde{h}_{\tilde{\mu}})_{(\tilde{\mu},\tilde{\mu}')\in\tilde{I}\times\mathbb{R}^{\tilde{l}}}$ are stably equivalent. △

In the following we will show how to associate the aforementioned smooth families of maps, give examples and draw first conclusions. The justification that the stably equivalence class of the maps are well-defined, i.e. independent of all choices made in the association process, is postponed to Chapter 10.

Remark 6.3.2. The presented framework allows a translation of boundary value problems which make use of *global* structure of the phase space, like Dirichlet problems, into *local* problems involving intersections of Lagrangian submanifolds. △

6.3.1 Comparison with some classical approaches

Before explaining the association process of function families to families of Lagrangian boundary value problems, we briefly compare our approach with classical approaches.

The process of associating a function to an intersection problem of Lagrangian submanifolds of a (fixed) cotangent bundle is classically known as *morsification of Lagrangian intersections* (Eliashberg and Gromov, 1998, p.33). In our work, Lagrangian submanifolds are not arbitrary but motivated by the setting of boundary value problems which leads to extra structure of the problem. Moreover, a bundle structure is not naturally present in our setting but is introduced as an auxiliary structure. This makes an analysis of the ambiguity introduced by the choice of a cotangent bundle structure necessary and the use of appropriate notions of equivalence from catastrophe theory.

Our approach allows the restriction to local phenomena which simplifies the treatment considerably. In contrast, the treatment of global Lagrangian intersection problems crucially involves the topology of the manifolds. Let us refer at this point to Arnold's conjecture, which (in a special case which has been proved) asserts a lower bound for the number of fixed points of Hamiltonian diffeomorphisms. The statement can be interpreted as a lower bound for the number of intersection points of a Lagrangian submanifold and a Hamiltonian-isotopic Lagrangian submanifold (Fukaya, 2010). Generalisations of Arnold's conjecture can be found in Oh, 1995; Ciriza and Pejsachowicz, 2000; Polterovich, 2001.

Weinstein (1973) develops a similar geometric picture which he uses to address global existence questions about solutions to boundary value problems. The focus is on fixed boundary value problems in Hamiltonian systems with regular (i.e., non-singular and non-bifurcating) manifolds as solutions. In contrast to Weinstein, 1973, the solutions considered here are typically isolated and we consider families of boundary value problems and local bifurcations of their solutions. In addition, in Weinstein, 1973 a fixed energy-time relation is imposed.

The geometric picture of intersecting Lagrangian submanifolds here and in Weinstein, 1973 is to be contrasted with studies that involve Lagrangian intersections in the phase space. In this work a pair of Lagrangian submanifolds represents a boundary value problem. The manifolds are submanifolds of the product of the phase space with itself. In contrast, Lagrangian submanifolds of phase spaces often represent objects of dynamical interest (e.g. invariant manifolds) and their intersections provide information about the dynamics; see e.g. Haro, 2000; Lochak, Marco, and Sauzin, 2003; Lomelí, Meiss, and Ramírez-Ros, 2008b.

There is another approach to the study of bifurcations of boundary value problems, which we mention briefly to contrast with the setting here. It is often used for PDEs and we will turn to this approach in Part III.

Many weak formulations of PDEs arise as variations of functionals such that critical points of functionals correspond to weak solutions of the PDE. For a family of smooth functions $f_\mu\colon \mathbb{R} \to \mathbb{R}$ and an open, bounded domain $\Omega \subset \mathbb{R}^d$ we consider the following

PDE with Dirichlet boundary conditions

$$\begin{cases} \Delta u &= f'_\mu(u) \\ u|_{\partial\Omega} &= 0. \end{cases} \tag{6.3.1}$$

An example is the Bratu problem, where $f_\mu(u) = -\mu e^u$ (see Section 6.1). The weak formulation of (6.3.1) is given as

$$\forall v \in E: \quad \int_\Omega \big(\langle \nabla u(x), \nabla v(x)\rangle + f'_\mu(u(x))v(x)\big)\,\mathrm{d}x = 0, \tag{6.3.2}$$

where $u \in E$ is sought. Here $x = (x_1, \ldots, x_d)$ are coordinates on $\mathbb{R}^d$, $\langle ., . \rangle$ denotes the Euclidean inner product on $\mathbb{R}^d$ and E is an appropriate Banach space which incorporates Dirichlet boundary conditions. We may take $E = H^1_0(\Omega) \cap H^k(\Omega)$ with $k > \frac{d}{2} + 1$, where H^k, H^1_0 are Sobolev spaces (see Section 4.4.1) or impose growth conditions on f_μ if we want to use a larger space E. The equation (6.3.2) can be written as

$$\forall v \in E : DS|_u(v) = 0,$$

where D denotes the Fréchet derivative and $S_\mu \colon E \to \mathbb{R}$ is the parameter dependent functional

$$S_\mu(u) = \int_\Omega \left(\frac{1}{2}\langle \nabla u, \nabla u\rangle + f_\mu(u)\right) \mathrm{d}x.$$

Bifurcation points (μ^*, u^*) of solutions to (6.3.2) thus correspond to degenerate zeros of the Fréchet derivative of S.

There exist general statements about basic bifurcations in the *critical points of a functional problem*, typically under technical assumptions which allow Lyapunov-Schmidt reductions to finite dimensional problems (Kielhöfer, 2012; Portaluri and Waterstraat, 2014). Note that even in the case $d = 1$, i.e. boundary value problems for ODEs, this approach uses the setting of functional analysis whereas ours is purely finite dimensional throughout.

6.3.2 Lagrangian intersections and catastrophe theory

Definition 6.3.2 (local intersection problem)**.** Let $\mu^* \in \mathbb{R}^p$ and let I be an open neighbourhood of μ^*. Consider two smooth families $(\Lambda_\mu)_{\mu\in I}$ and $(\Gamma_\mu)_{\mu\in I}$ of submanifolds of a manifold M. Let $z^* \in \Lambda_{\mu^*} \cap \Gamma_{\mu^*}$. The collection $\mathfrak{L} = \big((\Lambda_\mu)_{\mu\in I}, (\Gamma_\mu)_{\mu\in I}, (\mu^*, z^*)\big)$ is called a *local intersection problem in* M. If (M, ω) is a symplectic manifold and the families $(\Lambda_\mu)_{\mu\in I}$ and $(\Gamma_\mu)_{\mu\in I}$ consist of Lagrangian submanifolds, then $\mathfrak{L}$ is called a *local Lagrangian intersection problem in* (M, ω). △

Remark 6.3.3 (Notation). If $\iota\colon N \to M$ is an embedding of a submanifold N into an ambient manifold M and $f\colon M \to X$ is a map, then we denote the pullback $\iota^* f\colon N \to X$ by $f|_N$. △

The following lemma asserts that two families of Lagrangian submanifolds can locally be mapped symplectomorphically to graphical Lagrangian families.

Lemma 6.3.3. *Let $\left((\Lambda_\mu)_{\mu\in\tilde{I}}, (\Gamma_\mu)_{\mu\in\tilde{I}}, (\mu^*, z^*)\right)$ be a local Lagrangian intersection problem in (T^*N, ω). There exists an open neighbourhood $V \subset T^*N$ of z^*, a symplectomorphism Ψ defined on $T^*(\pi(V))$ fixing z^* and an open neighbourhood $I \subset \tilde{I} \subset \mathbb{R}^p$ of μ^* such that for all $\mu \in I$ the Lagrangian submanifolds $\Psi(\Lambda_\mu \cap V)$ and $\Psi(\Gamma_\mu \cap V)$ are graphical in $T^*(\pi(V))$, i.e. $\pi|_{\Psi(\Gamma_\mu\cap V)}$ and $\pi|_{\Psi(\Lambda_\mu\cap V)}$ are injective immersions.*

Proof. The proof idea is to linearise the problem in local Darboux coordinates and construct a linear transformation which makes the linearised problem graphical and, therefore, makes the original problem locally graphical.

Let us shrink N (and $\Lambda_\mu, \Gamma_\mu \subset T^*N$ accordingly) to a coordinate neighbourhood of $\pi(z^*) \in N$ with coordinates $x^1, \dots, x^n$. We consider Darboux coordinates $p_1, \dots, p_n, q^1, \dots, q^n$ on T^*N centred at z^*, more precisely, the coordinate functions are given by

$$\begin{aligned} q^i &\colon T^*N \to \mathbb{R}, \quad q^i = x^i \circ \pi \\ p_i &\colon T^*N \to \mathbb{R}, \quad \gamma \mapsto \gamma\left(\frac{\partial}{\partial x^i}\Big|_{\pi(\gamma)}\right) - z^*\left(\frac{\partial}{\partial x^i}\Big|_{\pi(z^*)}\right) \end{aligned}$$

for $i \in \{1, \dots, n\}$. The coordinates are Darboux coordinates for the canonical symplectic structure of cotangent bundles (see Example 2.1.1). Let $n_1 = \dim(T_{z^*}\Lambda_{\mu^*} \cap T_{z^*}\Gamma_{\mu^*})$ and $n_2 = n - n_1$. Consider the symplectic basis $\frac{\partial}{\partial p_1}\Big|_{z^*}, \dots, \frac{\partial}{\partial p_n}\Big|_{z^*}, \frac{\partial}{\partial q^1}\Big|_{z^*}, \dots, \frac{\partial}{\partial q^n}\Big|_{z^*}$ on $T_{z^*}T^*N$. In Lorand and Weinstein, 2015 all pairs of coisotropic linear subspaces of finite dimensional vector spaces are classified. Using this classification result, there exists a linear symplectic map on $T_{z^*}T^*N$ represented by a matrix M_0 mapping $T_{z^*}\Lambda_{\mu^*}$ to the Lagrangian subspace spanned by the columns of A_0 and $T_{z^*}\Gamma_{\mu^*}$ to the space spanned by the columns of B_0 where

$$A_0 = \begin{pmatrix} 0_{n_1\times n_1} & 0_{n_1\times n_2} \\ 0_{n_2\times n_1} & 0_{n_2\times n_2} \\ \mathrm{Id}_{n_1} & 0_{n_1\times n_2} \\ 0_{n_2\times n_1} & \mathrm{Id}_{n_2} \end{pmatrix} \quad \text{and} \quad B_0 = \begin{pmatrix} 0_{n_1\times n_1} & 0_{n_1\times n_2} \\ 0_{n_2\times n_1} & \mathrm{Id}_{n_2} \\ \mathrm{Id}_{n_1} & 0_{n_1\times n_2} \\ 0_{n_2\times n_1} & 0_{n_2\times n_2} \end{pmatrix}.$$

Here Id_k denotes the k-dimensional identity matrix and $0_{k\times l}$ the zero matrix in

$\mathbb{R}^{k\times l}$. Using the linear, symplectic transformation represented by the matrix

$$M = \begin{pmatrix} \mathrm{Id}_n & 0_{n\times n} \\ \mathrm{Id}_n & \mathrm{Id}_n \end{pmatrix}$$

A_0 and B_0 are mapped to matrices of the form $\begin{pmatrix} * \\ \mathrm{Id}_n \end{pmatrix}$. Their columns span Lagrangian subspaces which are graphs over span $\left\{ \frac{\partial}{\partial q^j}\Big|_{z^*} \right\}_{1\le j\le n}$. Using the coordinate system $p_1,\dots,p_n,q^1,\dots,q^n$, the matrix $M\cdot M_0$ defines a symplectic map Ψ on T^*N. By construction, $\Psi(z^*) = z^*$ and for all μ near μ^* the Lagrangian manifolds $\Psi(\Lambda_\mu)$ and $\Psi(\Gamma_\mu)$ are locally around z^* graphs over the zero-section in T^*N. □

Let us recall the notion of a catastrophe set in catastrophe theory.

Definition 6.3.3 (catastrophe set of a singularity)**.** Let N be a smooth manifold and let $h = (h_\mu)_{\mu\in I}$ be a family of smooth maps $h_\mu\colon N\to\mathbb{R}$. The set

$$\{(\mu,x)\in I\times N \mid \nabla h_\mu(x) = 0\}$$

is called the *catastrophe set of the family* h. △

We may use a similar definition in the setting of local Lagrangian intersection problems.

Definition 6.3.4 (catastrophe set of intersection problems)**.** Consider the local intersection problem $\mathfrak{L} = \big((\Lambda_\mu)_{\mu\in I},(\Gamma_\mu)_{\mu\in I},(\mu^*,z^*)\big)$ in (T^*N,ω) such that $\pi|_{\Lambda_\mu}$ and $\pi|_{\Gamma_\mu}$ are injective immersions for all $\mu\in I$. The set

$$\{(\mu,\pi(z)) \mid \mu\in I,\, z\in\Lambda_\mu\cap\Gamma_\mu\}$$

is called the *catastrophe set of the local intersection problem* $\mathfrak{L}$. △

The following theorem asserts that the intersection of two families of Lagrangian submanifolds locally behaves like the gradient-zero problem for a smooth family of local maps on N.

Theorem 6.3.4 (Singularity-Lagrangian linkage theorem)**.** *Consider the local intersection problem* $\mathfrak{L} = \big((\Lambda_\mu)_{\mu\in\tilde I},(\Gamma_\mu)_{\mu\in\tilde I},(\mu^*,z^*)\big)$ *in* (T^*N,ω)*. There exists*

- *an open neighbourhood* $\underline{V}\subset\mathbb{R}^{\dim N}$ *of the origin and a smooth family* $(h_\mu)_{\mu\in I}$ *of smooth maps* $h_\mu\colon\underline{V}\to\mathbb{R}$ *with* $h_{\mu^*}(0) = 0$,

- *an open neighbourhood $V \subset T^*N$ of z^* and a symplectomorphism Ψ on $T^*(\pi(V))$ fixing z^* and mapping $\mathfrak{L}$ to a local Lagrangian intersection problem*

$$\big((\Psi(\Lambda_\mu \cap V))_{\mu\in I}, (\Psi(\Gamma_\mu \cap V))_{\mu\in I}, (\mu^*, z^*)\big)$$

in $T^*\pi(V)$ with the same catastrophe set as $(h_\mu)_{\mu\in I}$.

In other words, up to a local symplectomorphism to each local Lagrangian intersection problem there exists a family of maps with the same catastrophe set.

Proof. By Lemma 6.3.3 there exists an open neighbourhood $V \subset T^*N$ of z^*, a symplectomorphism Ψ defined on $T^*(\pi(V))$ fixing z^* and an open neighbourhood $I \subset \tilde{I} \subset \mathbb{R}^p$ of μ^* such that for all $\mu \in I$ the maps $\pi|_{\Psi(\Gamma_\mu\cap V)}$ and $\pi|_{\Psi(\Lambda_\mu\cap V)}$ are injective immersions. Let $U = \pi(V)$ and denote $\Psi(\Gamma_\mu \cap V)$ and $\Psi(\Lambda_\mu \cap V)$ again by Γ_μ and Λ_μ. There exist 1-forms $\alpha_\mu, \beta_\mu \colon U \to T^*U$ such that $\alpha_\mu(U) = \Gamma_\mu$ and $\beta_\mu(U) = \Lambda_\mu$.

The 1-forms α_μ and β_μ are closed since Γ_μ and Λ_μ are Lagrangian submanifolds (Corollary 2.1.3). Shrinking U to a simply connected domain around $\pi(z^*)$ denoted again by U and the manifolds Γ_μ and Λ_μ to their intersections with $\pi^{-1}(U)$, the 1-forms are exact. We find $f_\mu, g_\mu \colon U \to \mathbb{R}$ such that $\mathrm{d}f_\mu = \alpha_\mu$, $\mathrm{d}g_\mu = \beta_\mu$, $f_{\mu^*}(\pi(z^*)) = 0 = g_{\mu^*}(\pi(z^*))$ and f_μ and g_μ depend smoothly on μ . Thus, for all $x \in U$ we have $\alpha_\mu(x) = \beta_\mu(x) \in \Gamma_\mu \cap \Lambda_\mu$ if and only if $\mathrm{d}(f_\mu - g_\mu)|_x = 0$. Expressing $f_\mu - g_\mu$ in local coordinates centred at $\pi(z^*)$ we obtain h_μ. □

Remark 6.3.4. We will justify in Chapter 10 that the presented translation procedure in Lemma 6.3.3 and in the linkage Theorem 6.3.4 of local Lagrangian intersection problems $\mathfrak{L}$ to families $h = (h_\mu)_{\mu\in I}$ of local functions determines h up to stably right equivalence in the sense of catastrophe theory. Though the ambient symplectic manifold T^*N has the structure of the cotangent bundle, the equivalence class of h actually does not depend on the bundle structure of T^*N but only on its symplectic structure (otherwise using Lemma 6.3.3 would cause ambiguity). △

Remark 6.3.5. An equivalence relation that is coarser than right equivalence is *right-left equivalence*. In addition to right equivalences on h, an additional action from the left, i.e. on the target space $\mathbb{R}$, by a family of local diffeomorphisms is allowed. Since associated function families to Lagrangian boundary value problems are well-defined up to right equivalence, they are also well-defined up to right-left equivalence. However, right-left equivalence of associated function families does not imply equivalence of the Lagrangian boundary value problems as the relation is strictly coarser than right equivalence. In particular, for right-left equivalence the ordering of $(\Lambda_\mu)_{\mu\in I}$ and $(\Gamma_\mu)_{\mu\in I}$ is irrelevant. △

We can translate the notions *versal* and *miniversal* from catastrophe theory to the setting of Lagrangian intersection problems. Roughly speaking, a parametrised

family of maps is *versal* if the family covers all small perturbations. Introducing a new unfolding parameter does not destroy or lead to new effects. Versal families do not possess any symmetries affecting the bifurcation behaviour which can be destroyed by a small symmetry-breaking perturbation. This means the bifurcation diagrams of a slightly perturbed problem qualitatively looks the same as the bifurcation diagram of the original problem. See Section 5.3 for details.

Definition 6.3.5 (versal Lagrangian intersection problem)**.** A local Lagrangian intersection problem is called *(mini-)versal* if and only if its associated family of function h given by Theorem 6.3.4 is (mini-)versal in the sense of catastrophe theory for right equivalence. △

Function germs up to stably equivalence are classified in catastrophe theory. In particular, this induces a classification of versal local Lagrangian intersection problems via the Singularity-Lagrangian linkage theorem (Theorem 6.3.4). This fact may be summarised as follows.

Corollary 6.3.5. *Versal local Lagrangian intersection problems are governed by catastrophe theory.*

Moreover, the proof of the Singularity-Lagrangian linkage Theorem 6.3.4 tells us under which conditions we leave the setting of catastrophe theory.

Proposition 6.3.6. *Consider an intersection problem $\Lambda_\mu \cap \Gamma_\mu$ of two graphical families of submanifolds $(\Lambda_\mu)_\mu \subset T^*N$ and $(\Gamma_\mu)_\mu \subset T^*N$ where at least one of the families varies through arbitrary, i.e. not necessarily Lagrangian, submanifolds of dimension n, where $2n$ is the dimension of the ambient space. The intersection problem corresponds to the problem $\eta_\mu = 0$ with a family of 1-forms η_μ on N.*

Proof. Since the families of submanifolds are graphical, each Λ_μ and Γ_μ are the images of N under 1-forms β_μ or α_μ, respectively. With $\eta_\mu := \alpha_\mu - \beta_\mu$ the intersection problem corresponds to the problem $\eta_\mu = 0$. Now we construct an example showing that any family of 1-forms $(\eta_\mu)_\mu$ can occur even if one of the families, say $(\Gamma_\mu)_\mu$, is special (e.g. Lagrangian). Since the manifolds Γ_μ are graphical, there exist 1-forms α_μ such that $\alpha_\mu(N) = \Gamma_\mu$. Set $\Lambda_\mu = (\eta_\mu + \alpha_\mu)(N)$. Now $z \in \Gamma_\mu \cap \Lambda_\mu$ if and only if $\eta_\mu(\pi(z)) = 0$. □

Remark 6.3.6. The construction of the family of 1-forms η in the proof of Proposition 6.3.6 is canonical: since the construction of η does not involve any choices, the family η is uniquely determined by the intersection problem. Notice that in contrast to the setting of the Singularity-Lagrangian linkage theorem (Theorem 6.3.4), we have restricted our attention to the special case of graphical families in cotangent bundles.

Moreover, a coordinate representation induces ambiguity: if we choose local coordinates $x^1, \ldots, x^n$ on N, then we can write each η_μ as

$$\eta_\mu = \sum_{j=1}^{n} (\eta_\mu)_j \mathrm{d}x^j, \quad \text{with} \quad (\eta_\mu)_j = \eta_\mu \left(\frac{\partial}{\partial x^j} \right)$$

and assign the smooth, parameter-dependent function

$$H_\mu = \Big((\eta_\mu)_1, \quad \ldots, \quad , (\eta_\mu)_n \Big)^\top$$

to the considered graphical intersection problem $\Lambda_\mu \cap \Gamma_\mu$. Roots of H_μ correspond to solutions of the intersection problem. Since this involves a choice of local coordinates, the family H is defined up to an action $\psi \mapsto \mathrm{D}\psi^{-T} \circ \psi \cdot H_\mu \circ \psi$ by diffeomorphisms on each element H_μ of the family. In particular, H is well-defined up to right-left equivalence and fits into the setting of *zeros-of-a-function problems*. Compared to catastrophe theory, the functions H_μ do not necessarily arise as gradients of scalar-valued maps. In particular, this needs to be considered when working with perturbations: the zeros-of-a-function problem $H_\mu = 0$ can be perturbed by any function family $G_\mu \colon \mathbb{R}^m \to \mathbb{R}^k$ to $H_\mu + \epsilon G_\mu$ for ϵ sufficiently small (even if H_μ happens to arise as a gradient). In contrast, perturbations of a catastrophe problem $\nabla h_\mu = 0$ respect the gradient structure, i.e. $\nabla h_\mu = 0$ is perturbed to $\nabla(h_\mu + \epsilon g_\mu) = 0$ for a scalar-valued function family g_μ. References with classification results are Du Plessis and Wall, 1995; Wall, 1971. Also see Chapter 5. △

Proposition 6.3.7. *A degenerate subcase of Proposition 6.3.6 is that the family Γ_μ is Lagrangian and versal while Λ_μ is constant and not Lagrangian. This corresponds to the problem $\mathrm{d}f_\mu = \beta$, where β is not closed (see Corollary 2.1.3). Although the parameter μ enters in the same way as in the gradient-zero problem, the bifurcations are* not *generally governed by catastrophe theory.*

Proof. If h_μ is the truncated miniversal unfolding of the hyperbolic umbilic singularity D_4^+, i.e.

$$h_\mu(x, y) = x^3 + xy^2 + \mu_3(x^2 + y^2) + \mu_2 y + \mu_1 x$$

then the bifurcation behaviour of $\mathrm{d}h_\mu(x, y) = \epsilon \cdot x\mathrm{d}y$ changes qualitatively if $\epsilon > 0$, i.e. the bifurcation diagram of the perturbed system is not fibrewise diffeomorphic to the diagram of the miniversal unfolding of D_4^+. This can be deduced from the fact that only for $\epsilon = 0$ there exists a path in the μ-space such that four solutions merge to one solution while in the perturbed system this bifurcation breaks up into two fold bifurcations. This means that D_4 together with its unfolding is not a normal form in this problem class, so catastrophe theory does not cover this case. (We will analyse in

detail how D-series singularities break in Chapter 9). □

We can formulate a reverse direction of the Singularity-Lagrangian linkage Theorem 6.3.4.

Proposition 6.3.8. *For each gradient-zero-problem there exists a local Lagrangian intersection problem with the same catastrophe set.*

Proof. Let $I = \mathbb{R}^p$ and $h_\mu \colon \mathbb{R}^n \to \mathbb{R}$ be a smooth family of smooth maps. Let Γ_μ be the image of the 1-form $\mathrm{d}h_\mu$ and Λ_μ be the zero section in $T^*\mathbb{R}^n$. The intersection $\{(\mu, z) \in \Gamma_\mu \cap \Lambda_\mu\}$ is a catastrophe set of the family h_μ. □

6.4 Application of the Lagrangian intersection framework to Lagrangian boundary value problems

6.4.1 Translation procedure for Lagrangian boundary value problems

Interpreting Lagrangian boundary value problems for symplectic maps (Definition 6.2.1) as local Lagrangian intersection problems (Definition 6.3.2) and using the Singularity-Lagrangian linkage Theorem 6.3.4 we can associate smooth families of maps to Lagrangian boundary value problems for symplectic maps. Critical points of the maps correspond to solutions of the boundary value problem. Below we summarize the translation steps.

- Symplectic maps and Lagrangian boundary conditions constitute Lagrangian submanifolds in a product manifold.
- Locally around a point of interest the product manifold is identified with a neighbourhood of the zero section in a cotangent bundle. The identification can be obtained by choosing Darboux coordinates.
- After shrinking the involved manifolds and the parameter space and after applying a symplectic transformation all involved Lagrangian submanifolds are graphical.
- The Lagrangian submanifolds can be written as images of exact 1-forms that admit local primitives which can be chosen to depend smoothly on the parameter. The primitives related to the boundary conditions can be subtracted from the primitives related to the symplectic maps.
- We obtain a smooth family of functions whose critical points correspond to solutions of the boundary value problem.

(The motivational example from Section 1.2 shows a slightly different viewpoint where the 1-forms are defined on the Lagrangian graph $\Gamma_\mu \subset \mathbb{R}^2 \times \mathbb{R}^2$ and the primitive α of the symplectic form $\omega_\times$ is chosen in view of the Dirichlet boundary value problem.)

6.4.2 Application of catastrophe theory to Lagrangian boundary value problems

Definition 6.4.1 ((mini-)versal family of symplectic maps)**.** A smooth family $(\phi_\mu)_{\mu\in I}$ of symplectic maps $\phi_\mu\colon (M,\omega) \to (M',\omega')$ is *(mini-)versal at* $(\mu^*, z^*) \in I \times M$ if there exists an open neighbourhood $(\mu^*, z^*) \in \tilde{I} \times \widetilde{M} \subset I \times M$ such that the smooth family $(h_\mu)_{\mu\in\tilde{I}}$ generating[2] the symplectic maps $(\phi_\mu|_{\widetilde{M}})_{\mu\in\tilde{I}}$ constitutes a (mini-)versal unfolding of the germ of h_{μ^*} at the point corresponding to $(\mu^*, z^*, \phi_{\mu^*}(z^*))$. △

Now we can use Corollary 6.3.5 and Propositions 6.3.6 and 6.3.7 to obtain the following statements.

Proposition 6.4.1. *Let $\phi_\mu\colon (M,\omega) \to (M',\omega')$ be a versal family of symplectic maps with graph $\Gamma_\mu \subset (M \times M', \omega \oplus -\omega')$ at (μ^*, z^*). Consider a boundary value problem for ϕ_μ of the form $\Gamma_\mu \cap \Lambda_\mu$ where the boundary conditions are represented by a family of submanifolds $\Lambda_\mu \subset M \times M'$.*

- *If the family of submanifolds $(\Lambda_\mu)_\mu$ is constant and Lagrangian, then locally around (μ^*, z^*) the intersection $\{(\mu, z) \in \Gamma_\mu \cap \Lambda_\mu\}$ corresponds to a catastrophe set in catastrophe theory.*
- *If the family $(\Lambda_\mu)_\mu$ varies through arbitrary $2n$-dimensional submanifolds, then locally around (μ^*, z^*) the intersection $\{(\mu, z) \in \Gamma_\mu \cap \Lambda_\mu\}$ can be understood as a zeros-of-a-function problem / equilibria-of-vector-fields problem.*
- *If the family $(\Lambda_\mu)_\mu$ is a constant non-Lagrangian submanifold of dimension $2n$, then the intersection $\{(\mu, z) \in \Gamma_\mu \cap \Lambda_\mu\}$ is, generally speaking, not governed by catastrophe theory.*

[2] In the sense of generating functions; see Definition 2.1.5 or A. C. d. Silva, 2008.

Chapter 7

Obstructions for bifurcations by boundary conditions, the effects of symmetry, and Liouville integrability

Chapter 6 and 7 are an adaption of McLachlan and Offen, 2018a.

We will use the framework introduced in Chapter 6 to study the following three cases.

- Some common boundary conditions, such as Dirichlet- and Neumann boundary conditions for second-order systems, restrict the possible types of bifurcations that can occur. For example, in generic planar systems only the A-series beginning with folds and cusps can occur.
- Completely integrable systems, such as planar Hamiltonian systems, can exhibit a novel *periodic pitchfork bifurcation*.
- Systems with Hamiltonian symmetries or reversing symmetries can exhibit restricted bifurcations associated with the symmetry.

7.1 Obstructions for bifurcations in low dimensions

In the motivational example we considered a Dirichlet problem for the flow map of a planar Hamiltonian system (Section 1.2) and found a cusp bifurcation (Figure 1.2). By the ADE-series classification (see Section 5.4 or V. I. Arnold, Goryunov, et al., 1998, p. 33), the cusp bifurcation belongs to the A-series. The general classification

provides some motivation to introduce more parameters in the planar Hamiltonian and chase up more complicated bifurcations. Clearly, if we restrict to planar systems, we cannot find bifurcations whose germs have normal forms with more than two variables because the number of variables used for the normal forms in the ADE classification tables is minimal. However, the normal forms of D or E series bifurcations only use two variables. Do they occur in planar Dirichlet problems?

In the following we will prove that, no matter how many parameters we introduce, only A series bifurcations are possible in the planar Dirichlet problem. Indeed, we would need an at least four-dimensional system to find D or E series bifurcations. This is also true for Dirichlet problems for arbitrary symplectic maps which do not necessarily arise as Hamiltonian flows. The reason why we have to double the dimension can be seen from the geometric picture that we develop in this section.

The geometric idea is the following: by Proposition 6.3.8 each type of local Lagrangian intersection can be achieved with two families of Lagrangian submanifolds $(\Gamma_\mu)_{\mu\in I}, (\Lambda_\mu)_{\mu\in I}$. However, if the boundary condition Λ_μ is constant in μ and if $(\Gamma_\mu)_{\mu\in I}$ is a Lagrangian embedding of *graphs* of symplectic maps, then this restricts the way Γ_μ and Λ_μ can intersect. Depending on how Λ_μ lies in its ambient manifold, the manifolds Γ_μ and Λ_μ cannot touch in a way that the intersection of their tangent spaces at the intersection point is of maximal dimension. This prohibits certain bifurcations.

Going through the construction of associated families to local Lagrangian intersection problems presented in the proof of the Singularity-Lagrangian linkage theorem (Theorem 6.3.4) yields the following observation.

Proposition 7.1.1. *Let $\big((\Lambda_\mu)_{\mu\in I}, (\Gamma_\mu)_{\mu\in I}, (\mu^*, z^*)\big)$ be a local Lagrangian intersection problem. If m is the dimension of the intersection of the tangent spaces $T_{z^*}\Lambda_{\mu^*}$ and $T_{z^*}\Gamma_{\mu^*}$ then only those singularities can occur at (μ^*, z^*) which can be obtained in the gradient-zero-problem $\nabla g_\mu = 0$ for a family of smooth maps $g_\mu\colon \mathbb{R}^k \to \mathbb{R}$ with $k \leq m$.*

Remark 7.1.1. If $m = 0$, then the above proposition states that there is no singularity at (μ^*, z^*). △

Let us analyse Dirichlet/Neumann problems and periodic boundary conditions.

Proposition 7.1.2. *Let $q^*, p^*, Q^*, P^* \in \mathbb{R}^{2n}$. In the Dirichlet problem*

$$q = q^*, \quad \phi_\mu^Q(p, q) = Q^* \tag{7.1.1}$$

as well as in the Neumann problem

$$p = p^*, \quad \phi_\mu^P(p, q) = P^* \tag{7.1.2}$$

for a smooth family of symplectic maps $\phi_\mu\colon \mathbb{R}^{2n} \to \mathbb{R}^{2n}$ only those singularities occur

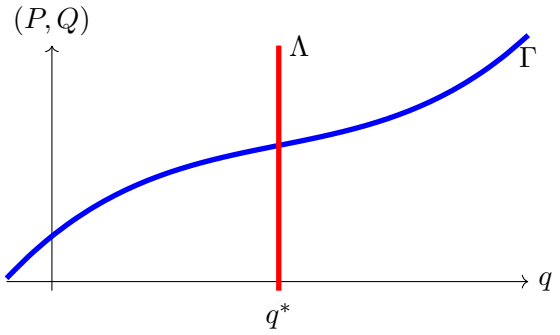

Figure 7.1: Illustration of the geometric situation in Proposition 7.1.2. The manifold Λ is the graph of a local diffeomorphism and, therefore, cannot be tangential to the Dirichlet boundary condition Γ.

which can be obtained in the gradient-zero-problem $\nabla g_\mu = 0$ *for a smooth family of smooth maps* $g_\mu \colon \mathbb{R}^k \to \mathbb{R}$ *with* $k \leq n$.

Before proving Proposition 7.1.2, we formulate two corollaries. In a generic setting, Proposition 7.1.2 allows us to use the ADE-classification (see Section 5.4 or V. I. Arnold, Goryunov, et al., 1998, p. 33) to obtain statements about which singularities can occur.

Corollary 7.1.3. *In Dirichlet and Neumann problems for versal families of symplectic maps on* $M = T^*\mathbb{R}$ *only A-series bifurcations occur persistently under small perturbations within the class of Lagrangian Dirichlet or Neumann problems.*

Corollary 7.1.4. *In Dirichlet and Neumann problems for versal families of symplectic maps on* $M = T^*\mathbb{R}^2$ *with at most 7 parameters only singularities of modality 0 (simple singularities) occur persistently under small perturbations within the class of Lagrangian Dirichlet or Neumann problems.*

Proof of Proposition 7.1.2. The geometric idea behind the proof is illustrated in Figure 7.1. Let us suppress the index μ in the following. Consider the inclusion map

$$\iota \colon (M, \omega) \hookrightarrow (M \times M, \omega \oplus -\omega), \quad \iota(z) = (z, \phi(z)).$$

We have $\iota(M) = \Gamma$ and the push-forward map $\mathrm{d}\iota \colon TM \to T\Gamma$ is a bundle diffeomorphism. Using the frame $\frac{\partial}{\partial p_1}, \ldots, \frac{\partial}{\partial p_n}, \frac{\partial}{\partial q^1}, \ldots, \frac{\partial}{\partial q^n}$ for the tangent bundle $TM \to M$ and the frame $\frac{\partial}{\partial p_1}, \ldots, \frac{\partial}{\partial p_n}, \frac{\partial}{\partial q^1}, \ldots, \frac{\partial}{\partial q^n}, \frac{\partial}{\partial P_1}, \ldots, \frac{\partial}{\partial P_n}, \frac{\partial}{\partial Q^1}, \ldots, \frac{\partial}{\partial Q^n}$ on the tangent bundle $T(M \times M) \to M \times M$ we can express $\mathrm{d}\iota$ by the matrix

$$\mathrm{D}\iota = \begin{pmatrix} \mathrm{Id}_n & 0 \\ 0 & \mathrm{Id}_n \\ \mathrm{D}_p\phi^P & \mathrm{D}_q\phi^P \\ \mathrm{D}_p\phi^Q & \mathrm{D}_q\phi^Q \end{pmatrix}. \tag{7.1.3}$$

At each z the columns $\gamma_1, \ldots, \gamma_{2n}$ of $\mathrm{D}\iota(z)$ span the space $T_{(z,z)}\Gamma \subset T_{(z,z)}(M \times M)$. Consider the Dirichlet problem defined by $\Lambda = \mathbb{R}^n \times \{q^*\} \times \mathbb{R}^n \times \{Q^*\}$. The tangent spaces of $\Lambda \subset M \times M$ are spanned by the columns $\lambda_1, \ldots, \lambda_{2n}$ of the matrix

$$\begin{pmatrix} \mathrm{Id}_n & 0 \\ 0 & 0 \\ 0 & \mathrm{Id}_n \\ 0 & 0 \end{pmatrix}.$$

Therefore, at an intersection point $(z, z) \in \Gamma \cap \Lambda$ the intersection of the tangent spaces $T_{(z,z)}\Gamma \cap T_{(z,z)}\Lambda \subset T_{(z,z)}(M \times M)$ is an isotropic linear subspace. Let $v \in T_{(z,z)}\Gamma \cap T_{(z,z)}\Lambda$. We have

$$\sum_{j=1}^{2n} a_j\gamma_j = v = \sum_{j=1}^{2n} b_j\lambda_j$$

for some coefficients $a_j, b_j \in \mathbb{R}$. From the structure of the matrices $\mathrm{D}\iota(z)$ and the matrix for $T_{(z,z)}\Lambda$ we see that $a_j = 0$ for $n \leq j \leq 2n$. Therefore, $\dim(T_{(z,z)}\Gamma \cap T_{(z,z)}\Lambda) \leq n$. We conclude that only those singularities can occur which in catastrophe theory admit a description with at most n variables. Swapping the roles of q and p shows the statement for Neumann problems. □

Remark 7.1.2. The statement of Proposition 7.1.2 will be re-obtained in a slightly generalised form in the following chapter as Proposition 8.2.2 in a coordinate-free framework. △

Periodic boundary conditions, on the other hand, do not impose restrictions, as the following proposition shows.

Proposition 7.1.5. *In periodic boundary value problems $\phi_\mu(p, q) = (p, q)$ for smooth families of symplectic maps in $2n$ variables all singularity bifurcations which admit descriptions in at most $2n$ variables occur.*

Proof. Let h be any smooth parameter-dependent scalar-valued function in $2n$ variables $t_1, \ldots, t_{2n}$. By Theorem 5.3.2 h is stably right equivalent (as specified in Theorem 5.3.2) to a function of the form

$$h_\mu(t_1, \ldots, t_{2n}) = \tilde{h}_\mu(t_1, \ldots, t_r) + t_{r+1}^2 + \ldots + t_{r+l}^2 - t_{r+l+1}^2 \ldots - t_{2n}^2,$$

with $r \leq 2n$, $0 \leq l \leq 2n - r$. The map $\tilde{h}_\mu(t_1, \ldots, t_r)$ is fully reduced at $(\mu, t) = (0, 0)$, i.e. $\tilde{h}_0(0) = 0$, $\nabla \tilde{h}_0(0) = 0$ and the Hessian matrix $\operatorname{Hess} \tilde{h}_0(0) = 0$ vanishes.

Due to the structure of h_μ, the matrix $\frac{\partial^2 g_\mu}{\partial p \partial Q}$ of mixed derivatives of the map

$$g_\mu(p, Q) = h_\mu(p, Q) + \sum_{j=1}^{n} p^j Q_j$$

is the identity matrix at $(\mu, p, Q) = (0, 0, 0)$. Now we use g_μ as a generating function to obtain symplectic maps $(Q, P) = \phi_\mu(p, q)$: by the implicit function theorem, the system of equations $q = \nabla_p g_\mu(p, Q)$ is solvable for Q defining a smooth function $Q_\mu(p, q)$ with $Q_\mu(0, 0) = 0$ near $(\mu, p, Q) = (0, 0, 0)$. Defining $P_\mu(p, q) = \nabla_Q g(p, Q_\mu(p, q))$ we obtain a map $\phi_\mu(p, q) = (P_\mu(p, q), Q_\mu(p, q))$ locally around $(q, p) = (0, 0)$. The map ϕ_μ is symplectic with respect to $\omega = \sum_{j=1}^{n} \mathrm{d}p_j \wedge \mathrm{d}q^j$ because g_μ is a generating function of type 2 (see Definition 2.1.5).

In the following $\mathbb{R}^{2n}$ is equipped with coordinates (p, Q) and $T^*\mathbb{R}^{2n}$ has coordinates (p, q, P, Q) where (p, Q) are coordinates for the zero-section. Locally around $(\mu, p, Q) = (0, 0, 0)$ the image of $\mathrm{d}g_\mu \colon \mathbb{R}^{2n} \to T^*\mathbb{R}^{2n}$ given as

$$\{(p, q, P, Q) \,|\, q = \nabla_p g_\mu(p, Q),\ P = \nabla_Q g_\mu(p, Q)\}$$

coincides with the graph $\Gamma_\mu \subset T^*\mathbb{R}^n \times T^*\mathbb{R}^n \cong T^*\mathbb{R}^{2n}$ of the symplectic map $\phi_\mu \colon T^*\mathbb{R}^n \to T^*\mathbb{R}^n$ given as

$$\Gamma_\mu = \{(p, q, P, Q) \,|\, (P, Q) = \phi_\mu(q, p)\}.$$

Defining $f(p, Q) = \sum_{j=1}^{n} p^j Q_j$ the image of $\mathrm{d}f \colon \mathbb{R}^{2n} \to T^*\mathbb{R}^{2n}$ given as

$$\Lambda = \{(p, q, P, Q) \,|\, q = Q,\ p = P\}$$

corresponds to periodic boundary conditions. Since $\mathrm{d}g_\mu - \mathrm{d}f = \mathrm{d}h_\mu$, the periodic boundary value problem for ϕ_μ shows the same bifurcation behaviour as h_μ. □

Example 7.1.1. Applying the construction of the proof of Proposition 7.1.5 to the miniversal deformation of the hyperbolic umbilic singularity D_4^+ (see Table 1.1 and Figure 5.2), i.e. to

$$h_\mu(t_1, t_2) = t_1^3 + t_1 t_2^2 + \mu_3(t_1^2 - t_2^2) + \mu_2 t_2 + \mu_1 t_1,$$

we obtain the generating function

$$g_\mu(p, Q) = p^3 + pQ^2 + \mu_3(p^2 - Q^2) + \mu_2 Q + \mu_1 p + pQ$$

and the symplectic map $\phi_\mu(p,q) = \big(P_\mu(p,q), Q_\mu(p,q)\big)$ with

$$P_\mu(p,q) = (p-\mu_3)\left(-1+2\sqrt{-3p^2-2p\mu_3+q-\mu_1+\frac{1}{4}}\right)+\mu_2+q$$
$$Q_\mu(p,q) = -\frac{1}{2}+\sqrt{-3p^2-2p\mu_3+q-\mu_1+\frac{1}{4}}.$$

The map ϕ_μ is well-defined near $(\mu_1,\mu_2,\mu_3,p,q) = (0,0,0,0,0)$ and has a fixed point if and only if $\nabla h_\mu(p,Q) = 0$. △

If we do not restrict the dimension of the phase space, then we can obtain each singularity that occurs in the gradient-zero-problem for a family $h_\mu\colon \mathbb{R}^n \to \mathbb{R}$ in Dirichlet and Neumann problems. Indeed, for any type of a Lagrangian boundary value problem and any gradient-zero singularity we can construct a family of symplectic maps defined on a sufficiently high-dimensional space such that the boundary value problem undergoes the same bifurcation as the gradient-zero-problem: each Lagrangian boundary condition locally has a generating function. We formulate the following proposition for the generating function suitable for Neumann problems. Analogous statements hold for Dirichlet problems with p and q as well as P and Q swapped.

Proposition 7.1.6. *Let $h_\mu\colon \mathbb{R}^n \to \mathbb{R}$, $q \mapsto h_\mu(q)$ be a family of smooth maps locally defined around $(\mu,q) = (0,0)$ and let $B_\mu\colon \mathbb{R}^n \times \mathbb{R}^n \to \mathbb{R}$, $(q,Q) \mapsto B_\mu(q,Q)$ be a smooth family locally defined around $(\mu,q,Q) = (0,0,0)$. There exists a family of symplectic maps $\phi_\mu\colon \mathbb{R}^{2n} \to \mathbb{R}^{2n}$, $(p,q) \mapsto \phi_\mu(p,q)$ locally defined around $(\mu,p,q) = (0,0,0)$ such that the boundary value problem*

$$\phi_\mu^P(\nabla_q B_\mu(q,Q),q) = -\nabla_Q B_\mu(q,Q)$$

locally around the origin shows the same bifurcation behaviour as the gradient-zero problem $\nabla h_\mu(q) = 0$.

Remark 7.1.3. For the Neumann problem (7.1.2) we can use

$$B_\mu(q,Q) = \langle q,p^*\rangle - \langle Q,P^*\rangle$$

in the above statement. Here $\langle .,. \rangle$ denotes the scalar product on $\mathbb{R}^n$. △

Proof of Proposition 7.1.6. Define

$$g_\mu(q,Q) = h_\mu(q) + c\sum_{j=1}^{n}(Q_j+q_j)^2 + B_\mu(q,Q),$$

where $c \in \mathbb{R}$ is a constant such that $\frac{\partial^2 B_\mu}{\partial q \partial Q} + 2cI_n$ is invertible near $(\mu,q,Q) = (0,0,0)$.

Since $\frac{\partial^2 g_\mu}{\partial q \partial Q}$ is invertible, the system of equations $p = \nabla_q g_\mu(q, Q)$ locally defines $Q_\mu(p, q)$ by the implicit function theorem. We obtain the required family of symplectic maps as

$$\phi_\mu(p, q) = \big(-\nabla_Q g_\mu(q, Q_\mu(p, q)), Q_\mu(p, q)\big).$$

□

We may formulate a corollary analogous to Proposition 6.3.8 for boundary value problems:

Corollary 7.1.7. *For each (versal) gradient-zero problem there exists a (versal) family of symplectic maps such that the boundary value problem shows the same bifurcation behaviour as the gradient-zero problem.*

Remark 7.1.4. The above Corollary 7.1.7 holds with or without the parenthesized word "versal". Let us emphasise at this point that the translation procedure of Lagrangian boundary value problems to gradient-zero problems (Lemma 6.3.3, Theorem 6.3.4, and Propositions 6.3.6 and 6.3.8) is obtained without a restriction to a versal setting. Versality is needed to link results to the known ADE classification of singularities in catastrophe theory as in Corollary 6.3.5 and Proposition 6.4.1. However, Propositions 7.1.1, 7.1.2 and 7.1.5, dealing with restrictions on which bifurcations can occur, hold for general systems. The implications for versal settings are formulated in Corollaries 7.1.3 and 7.1.4. △

7.2 Effects of complete integrability - Periodic pitchfork bifurcations

In the previous section we have seen that Dirichlet and Neumann type problems for symplectic maps allow fewer types of bifurcation than one might naively expect from the ADE-classification results. In this section they will surprise us with more bifurcations than expected: in applications, symplectic maps often arise as time-τ-maps of Hamiltonian flows. Those arising in completely integrable Hamiltonian systems (see Definition 2.2.3) form an important subclass. Families of Hamiltonian diffeomorphisms in completely integrable systems show more bifurcations than expected from the ADE-classification in certain very common boundary value problems like homogeneous Dirichlet problems. We will present a numerical example first and then develop a general model to explain the *periodic pitchfork bifurcation*. It provides a nontrivial example for the effects of extra structure on bifurcation behaviour.

7.2.1 Numerical example.

Planar Hamiltonian systems are completely integrable. Let us consider the Hamiltonian

$$H(x, y) = y^2 + 0.01y^3 + x^3 + \mu x$$

on the symplectic vector space $(\mathbb{R}^2, \mathrm{d}x \wedge \mathrm{d}y)$. The term $0.01y^3$ is included to break global time-reversal symmetry. This will help us to distinguish effects of complete integrability from effects of time-reversal symmetry, which we will analyse separately in Section 7.3.1. Figure 7.2 shows the bifurcation diagram for the 2-point boundary value problem

$$x(0) = 1, \quad x(1) = 1 \tag{7.2.1}$$

for the time-1-map of the Hamiltonian flow. We see a *pitchfork bifurcation*. It is persistent under small perturbations of the Hamiltonian, i.e. repeating the experiment with a slightly perturbed Hamiltonian leads to the same observations. This is surprising since according to Thom's list of elementary catastrophes (Table 1.1) only fold bifurcations are expected to be persistent when only one parameter is present.[1] There is also no obvious $\mathbb{Z}/2\mathbb{Z}$ symmetry present in the system. However, using our catastrophe theory framework, this pitchfork bifurcation can be realised as a standard $\mathbb{Z}/2\mathbb{Z}$-symmetric pitchfork bifurcation but only in a very subtle way as we will see in Section 7.2.3.

Figure 7.3 shows the motions of the Hamiltonian system which fulfil the boundary condition (7.2.1). The marker $*$ is used to indicate the start point of the motion and o is used for the end point. The black solid line indicates the boundary condition $G = \{1\} \times \mathbb{R}$ in the phase space. At $\mu = -53.306$ there are three solutions to the boundary value problem. The two solution from the outer branches of the pitchfork in Figure 7.2 come from a periodic orbit with period 1 crossing G twice. The solution from the inner branch corresponds to another periodic orbit with period slightly smaller than 1. Increasing μ, all three solutions merge to an orbit of period 1 tangential to G. Increasing μ further to $\mu = -20$, there exists one solution of the boundary value problem which comes from an orbit with period slightly greater than 1.

Since the bifurcation does not occur in Thom's list (Table 1.1), the family of Hamiltonian diffeomorphisms cannot be versal at the pitchfork point $(\mu^*, (x^*, y^*))$, i.e. the family does not cover all possible perturbations within the class of symplectic maps because all symplectic maps of the family are planar Hamiltonian diffeomorphisms. Indeed, the bifurcation is persistent under small perturbations of the Hamiltonian because periodic orbits occur persistently as 1-parameter families in planar Hamiltonian systems and these can become tangential to the boundary condition. In contrast, it is

[1] This experiment was performed before the author started working on a theoretical framework. Therefore, for the author the surprise came with some delay.

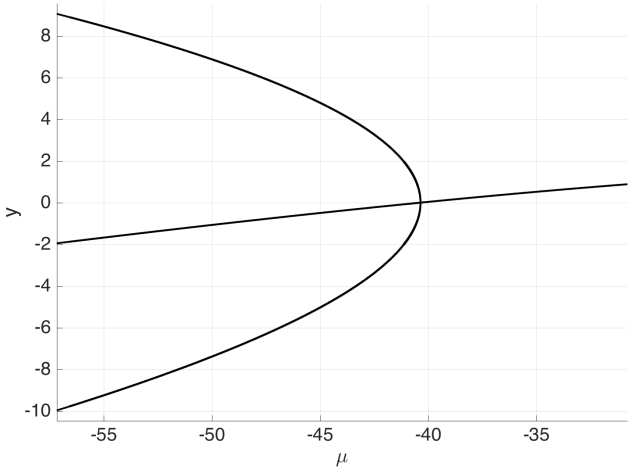

Figure 7.2: The diagram shows a pitchfork bifurcation in the 2-point-boundary value problem $x(0) = 1 = x(1)$ for the time-1-map of the Hamiltonian $H(x, y) = y^2 + x^3 + \mu x + 0.01y^3$. The flow map is obtained numerically using the (symplectic) Störmer–Verlet method (Example 3.3.2). The boundary value problem is solved using a shooting method.

a degenerate situation for a symplectic map to have a 1-parameter family of invariant sets diffeomorphic to S^1.

Motivated by the mechanism causing the phenomenon, we will call the bifurcation *periodic pitchfork bifurcation*. As we will see in the next section, the bifurcation is not just a planar phenomenon but generalises to completely integrable systems of arbitrary dimensions.

7.2.2 Model for periodic pitchforks in completely integrable systems

We generalise the observations from the numerical example to higher dimensions and to a more general class of boundary conditions.

Definition 7.2.1 ((symmetrically) separated Lagrangian boundary conditions)**.** Consider a family of symplectic maps $\phi_\mu \colon X \to X$ and let G_μ, $\tilde{G}_\mu$ be a family of Lagrangian submanifolds in X. The boundary condition

$$z \in G_\mu \quad \text{and} \quad \phi_\mu(z) \in \tilde{G}_\mu.$$

is called a *separated Lagrangian boundary condition*. If $G_\mu = \tilde{G}_\mu$ for all μ, then the boundary condition is called a *symmetrically separated Lagrangian boundary condition*. △

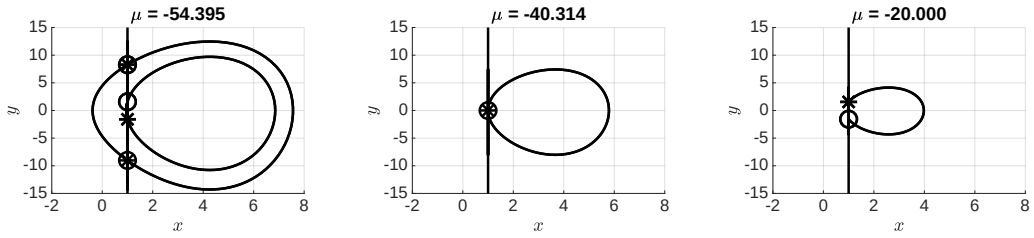

Figure 7.3: The diagram shows the orbits corresponding to the solution branches in Figure 7.2 for different values of μ specified above the plots. It illustrates the mechanism of the periodic pitchfork bifurcation for planar systems. The orbits are computed using the symplectic Störmer–Verlet method. The marker $*$ denotes the start point of the orbit and o the end point.

Example 7.2.1. The Dirichlet boundary condition (7.2.1) used in the numerical example (Section 7.2.1) is symmetrically separated in the sense of Definition 7.2.1. The corresponding manifold G_μ is given as the line $G = \{1\} \times \mathbb{R} \subset (\mathbb{R}^2, \mathrm{d}x \wedge \mathrm{d}y)$. More generally, Dirichlet conditions are symmetrically separated boundary conditions if and only if the start- and endpoint coincide. △

Remark 7.2.1. Submanifolds G, $\tilde{G}$ of a symplectic manifold (X, ω) are both Lagrangian if and only if the product $G \times \tilde{G} \subset (X \times X, \omega \oplus -\omega)$ is Lagrangian. Therefore, separated Lagrangian boundary conditions are Lagrangian boundary conditions. △

Definition 7.2.2 (pitchfork bifurcation)**.** The set

$$\{(\mu, x) \,|\, \nabla_x F(\mu, x) = 0\},$$

is a catastrophe set of a pitchfork bifurcation if F is equivalent to $f(\mu, x) = x^4 + \mu x^2$ or $f(\mu, x) = -x^4 + \mu x^2$ as right-unfoldings. △

Roughly speaking, a pitchfork bifurcation has a catastrophe set looking qualitatively like Figure 7.2. See Wassermann, 1974; Lu, 1976 for equivalences of unfoldings. Notice that f is not a versal unfolding of the map germ x^4 in the usual, unrestricted catastrophe theory framework since the universal unfolding of the cusp $x^4 + \mu_2 x^2 + \mu_1 x$ is not equivalent to the unfolding f from Definition 7.2.2. This is the reason why the pitchfork bifurcation is not a persistent phenomenon in gradient-zero-problems. However, in the presence of a $\mathbb{Z}/2\mathbb{Z}$-symmetry, it becomes persistent under small symmetric perturbations (Poston and I. Stewart, 1978, p.352), (Wassermann, 1988, p.486). In V. I. Arnold (1978) it occurs as the singularity B_2. Indeed, in Section 7.2.3 we will show that a hidden $\mathbb{Z}/2\mathbb{Z}$-symmetry related to the complete integrability and the symmetry of the boundary condition is present.

Theorem 7.2.1 (pitchfork bifurcations in completely integrable systems)**.** *Consider a one-parameter family of $2n$-dimensional completely integrable Hamiltonian systems with time-τ-flow maps ϕ_μ and symmetrically separated boundary conditions for ϕ_μ defined by Lagrangian manifolds G_μ. Assume that for $\mu = 0$ a compact, resonant Liouville torus T (common level set of the integrals of motion) with period τ intersects G_0 in an isolated point p such that $T_pT \cap T_pG$ is one-dimensional. Then either the catastrophe set of the boundary value problem shows a pitchfork bifurcation at $(\mu, z) = (0, p)$ or the problem is degenerate.*

Proof. Scaling the Hamiltonian H_μ, we can assume that $\tau = 1$. In a neighbourhood of T and $\mu = 0$, there exist action angle coordinates $(\theta_\mu, I_\mu) = (\theta_{\mu_1}, \dots, \theta_{\mu_n}, I_\mu^1, \dots, I_\mu^n)$ such that $\theta_\mu(p) = 0$, $I_\mu(p) = 0$ and $I_\mu^1, \dots, I_\mu^n$ are constants of motion (Theorem 2.2.9). Viewing the systems in these coordinates, we do not need to keep track of the initial μ-dependence and denote the coordinates as (θ, I). Let us refer to the θ-component of the symplectic map ϕ_μ as ϕ_μ^θ. It suffices to consider a constant Lagrangian family $G_\mu = G$. Assume that the submanifold G can (locally) be parametrised with θ. Since G is Lagrangian, there exists a scalar-valued function g with $g(0) = 0$ such that $G = \{(\theta, \nabla g(\theta)) \,|\, \theta \in (\mathbb{R}/2\pi\mathbb{Z})^n\}$. The intersection of the tangent space T_pT and T_pG is one-dimensional such that the Hessian matrix of g at p has exactly one vanishing eigenvalue. By the splitting theorem (Section 5.3), locally around $\theta = 0$ there exists a change in the θ-coordinates fixing 0 such that

$$g(\theta) = h(\theta_1) + q(\theta_2, \dots, \theta_n), \quad \text{with} \quad h(0) = h'(0) = h''(0) = 0$$

and $q(\theta_2, \dots, \theta_n) = \sum_{j=2}^n \epsilon_j \theta_j^2$ is a nondegenerate quadratic map with $\epsilon_j \in \{-1, 1\}$. Define $\mathrm{Sgns} := \mathrm{diag}(\epsilon_1, \dots, \epsilon_n)$ for later.

A motion starting at an intersection point $(\theta, I) = (\theta, \nabla g(\theta))$ of a Liouville torus with G is a solution to the boundary value problem if and only if the endpoint $(\phi_\mu^\theta(\theta, I), I)$ of the motion also lies on G. Therefore, (θ, I) solves the boundary value problem if and only if $I = \nabla g(\theta)$ and θ fulfils

$$0 = b_\mu(\theta) := \nabla g \left(\phi_\mu^\theta(\theta, \nabla g(\theta))\right) - \nabla g(\theta).$$

By the assumptions on the intersection of T and G

- the Liouville torus T intersects with G in $(\theta, I) = (0, 0)$, i.e. $\nabla g(0) = 0$.
- The intersection of T and G is tangential such that $h(0) = h'(0) = h''(0) = 0$ as obtained by the splitting theorem.
- All motions on the Liouville torus T are periodic with period 1, i.e. $\phi_0^\theta(\theta, 0) = \theta$ such that the Jacobian $\mathrm{D}_\theta\phi_0(\theta, 0)$ is the identity matrix.

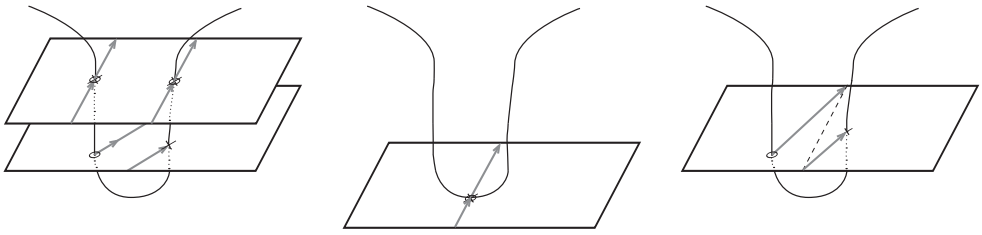

Figure 7.4: Illustration of the mechanism in a four-dimensional phase space before, at and after passing through the bifurcation point. Opposite edges of the parallelograms are identified. They represent Liouville tori. The line intersecting the Liouville tori represents the manifold G_μ. Gray arrows represent motions of the system starting and ending at an intersection point of a Liouville torus with G_μ within time $\tau = 1$.

The situation is illustrated in the schematic picture in the middle of Figure 7.4. Locally around $\theta = 0$, the first component of b_μ is given as

$$b_\mu^1(\theta) = h'\left(\phi_\mu^{\theta_1}(\theta, \nabla_\theta g(\theta))\right) - h'(\theta_1).$$

Using the statements formulated in the bullet point list, a Taylor series expansion of $b_\mu^1(\theta)$ around $\mu = 0$, $\theta = 0$ has no constant term and the coefficients of μ, $\theta_1, \ldots, \theta_n$ and θ_1^2 vanish. The other coefficients are non-zero under non-degeneracy assumptions on the problem. Moreover, for the remaining components $b_\mu^{2,\ldots,n}(\theta)$ the Jacobian $D_{\theta_2,\ldots,\theta_n} b_0^{2,\ldots,n}(0) = \mathrm{Sgns} \cdot D_{I_2,\ldots,I_n} \phi_0^{\theta_2,\ldots,\theta_n}(0,0)$ has full rank (again by non-degeneracy). By the implicit function theorem, locally around $(\mu, \theta) = (0,0)$ there exist functions $\theta_j(\mu, \theta_1)$ with $\theta_j(0,0) = 0$ $(j \geq 2)$ such that

$$b_\mu^{2,\ldots,n}(\theta_1, \theta_2(\mu,\theta_1), \ldots, \theta_n(\mu,\theta_1)) = 0.$$

Moreover, using $\left.\frac{\partial b^j}{\partial \theta_1}\right|_{(\mu,\theta)=(0,0)} = 0$ and $\left.\frac{\partial b^j}{\partial \theta_i}\right|_{(\mu,\theta)=(0,0)} \neq 0$ for $i, j \geq 2$, we conclude $\frac{\partial \theta_j(0,\theta_1)}{\partial \theta_1}(0) = 0$. Therefore, in the Taylor series expansion of

$$b_\mu^1(\theta_1, \theta_2(\mu,\theta_1), \ldots, \theta_n(\mu,\theta_1))$$

around $\mu = 0$ and $\theta = 0$ there is (still) no constant term and the coefficients of μ, θ_1 and θ_1^2 vanish. Thus, there is a pitchfork bifurcation at $(\mu, \theta, I) = (0,0,0)$ unless the problem is degenerate. □

We conclude that the pitchfork bifurcation occurs generically in symmetrically separated 1-parameter boundary value problems in completely integrable Hamiltonian systems. The mechanism of the bifurcation in the phase space is illustrated in Figure 7.4.

Remark 7.2.2. The map h in the proof of Theorem 7.2.1 is a map germ $(\mathbb{R}, 0) \to (\mathbb{R}, 0)$

with

$$h(0) = h'(0) = h''(0) = 0$$

and, under non-degeneracy assumptions, $h'''(0) \neq 0$. This means that h has a singularity of type A_2 (fold). A fold singularity is a persistent phenomenon in one-parameter families of smooth maps.

Allowing more parameters and arbitrarily high-dimensional phase spaces, we can achieve any local Lagrangian intersection problem as an intersection of G_μ and T. When k parameters are present, then any versal family of smooth maps with k parameters can occur as h and lead to new persistent bifurcations. Thus, an analysis analogous to the proof of Theorem 7.2.1 can be carried out for the other normal forms from Arnold's ADE-classification. The type of singularity corresponds to the type of contact of the boundary condition and the Liouville torus at the bifurcation point. Recall that we have identified Lagrangian intersections up to local symplectomorphisms with catastrophes up to stably right equivalence. Thus, one could attempt to classify all bifurcations of this mechanism by the type of Lagrangian contact. △

7.2.3 Symmetry based explanation of the periodic pitchfork

Let us view the periodic pitchfork bifurcation as an effect of symmetry present in completely integrable systems. Indeed, we will show how complete integrability leads to a local $\mathbb{Z}/2\mathbb{Z}$ mirror symmetry in the generating function for the Hamiltonian diffeomorphism related to the system. Thus, the periodic pitchfork is related to the bifurcation B_2 in Arnold's list for the $\mathbb{Z}/2\mathbb{Z}$-symmetric gradient-zero problem (V. I. Arnold, 1978). Other references for the gradient-zero-problem with symmetry are Wassermann, 1988 and Poston and I. Stewart, 1978, Ch.14 §15. The following can be regarded as an alternative proof of Theorem 7.2.1.

Consider a one-parameter family of completely integrable Hamiltonian systems of fixed dimension $2n$ with Hamiltonians H_μ. Consider symmetrically separated Lagrangian boundary conditions. Suppressing the μ-dependence of the action angle coordinates, the equations of motions read

$$\begin{aligned} \dot{I} &= 0 \\ \dot{\alpha} &= \nabla_I H_\mu(I). \end{aligned}$$

The time-1-map of the flow maps (I, α) to (K, β) with

$$\begin{aligned} K &= I \\ \beta &= \nabla_I H_\mu(I) + \alpha. \end{aligned} \tag{7.2.2}$$

Let us assume that $\nabla_I H_0(0) = 0$ and Hess $H_0(0)$ is nondegenerate. Locally near $I = 0$ and $\mu = 0$ there exists F_μ such that $F_0(0) = 0$ and $\xi = \nabla_I H_\mu(F(\xi))$. For (μ, ξ) near $(0, 0)$ we have

$$\mathrm{Id} = \mathrm{Hess}\, H_\mu(F_\mu(\xi))\mathrm{D}F_\mu(\xi)$$

such that the Jacobian $\mathrm{D}F_\mu(\xi)$ is symmetric and F_μ has a primitive denoted by $\mathcal{H}_\mu$. The function $S_\mu(\alpha, \beta) = \mathcal{H}_\mu(\beta - \alpha)$ is a generating function (Definition 2.1.5) of the time-1-map in (7.2.2).

Assume that locally near $(I, \alpha) = (0, 0)$, the boundary condition can be expressed as $I = \tilde{g}_\mu(\alpha)$, $K = \tilde{g}_\mu(\beta)$. Since the boundary condition is Lagrangian, there exists a local map g with $g(0) = 0$ such that $\nabla g(\alpha) = \tilde{g}(\alpha)$. Assume that there exists a local change of coordinates in the α variables fixing 0 such that g is of the form

$$g(\alpha) = \alpha_1^3 + q(\alpha_2, \ldots, \alpha_n).$$

(Recall from the proof of Theorem 7.2.1 that this holds generically at a 1-dimensional touch of the boundary condition with an invariant submanifold.) The change of variables in α can be extended to a symplectic change of variables (I, α) in the phase space fixing $(I, \alpha) = (0, 0)$. The equations of motion keep their structure and we denote the new coordinates and maps by the same symbols as before. The boundary condition can be obtained from the generating function $B(\alpha, \beta) = \alpha_1^3 - \beta_1^3 + q(\alpha_2, \ldots, \alpha_n) - q(\beta_2, \ldots, \beta_n)$. Solutions to the boundary value problem correspond to critical points of

$$G_\mu(\alpha, \beta) = B(\alpha, \beta) - \mathcal{H}_\mu(\beta - \alpha) = \alpha_1^3 - \beta_1^3 - \mathcal{H}_\mu(\beta - \alpha) + q(\alpha_2, \ldots, \alpha_n) - q(\beta_2, \ldots, \beta_n).$$

Notice that G_μ is invariant under the transformation $(\alpha_1, \beta_1) \mapsto (-\beta_1, -\alpha_1)$. Now, following V. I. Arnold (1978), bifurcations on the fixed-point set of the transformation correspond to $\mathbb{Z}/2\mathbb{Z}$ bifurcations. Under the given assumptions, the bifurcation B_2 occurs at $(I, \alpha) = (0, 0)$. □

7.3 Effects of symmetry

The previous Section 7.2 shows that extra structure (complete integrability) in Lagrangian boundary value problems can lead to the occurrence of extra bifurcations which are not generic in the gradient-zero-problem. Clearly, if in the Singularity-Lagrangian linkage theorem (Theorem 6.3.4) the generating functions f_μ of symplectic maps and the generating functions g_μ of the boundary conditions obey the same symmetry relation, then the bifurcations of the boundary value problem will be governed by the gradient-zero-problem for scalar-valued maps obeying that symmetry. In the following we will analyse how symmetries of Hamiltonian systems, (or, more generally,

of families of symplectic maps and their boundary conditions), translate to symmetries of generating functions and are, therefore, relevant for the prediction and explanation of bifurcation behaviour.

7.3.1 Classical time reversal symmetry

In view of the importance of classical Hamiltonian mechanics, we first show a numerical example illustrating the mechanism of a pitchfork bifurcation which is related to *time reversal symmetry* (see Section 2.3.2) of the system, and then explain the general impact of time reversibility on mechanical systems in their standard form. In Section 7.3.2 we present a more general treatment of symmetries and reversal symmetries.

Numerical example

Consider the time-reversal Hamiltonian system (Definition 2.3.3)

$$H(x, y) = \cos(y^2) + \mu x^2 + x^3.$$

on $(\mathbb{R}^2, \mathrm{d}x \wedge \mathrm{d}y)$. We consider the Dirichlet boundary value problem $\phi^X(1, y) = 1$ where ϕ is the time-0.1-map of the Hamiltonian flow and ϕ^X its x-component. In other words, a motion of the Hamiltonian system solves the boundary value problem if and only if it starts and ends after time $\tau = 0.1$ on the line $\{1\} \times \mathbb{R}$ in the phase space. The described boundary condition is Lagrangian, symmetrically separated (Definition 7.2.1) and $\mathbb{Z}/2\mathbb{Z}$-symmetric with respect to the x-axis. Using the Störmer–Verlet method to integrate Hamilton's equations we obtain a bifurcation diagram showing a pitchfork bifurcation (Figure 7.5). The motions involved in the bifurcation are plotted in Figure 7.6 for two different values of the parameter μ. We see that one of the orbits constitutes two solutions to the boundary value problem making use of the time reversal symmetry of the system. This orbit merges with another orbit that solves the boundary condition exactly where both orbits become tangential to the boundary condition. At this point the relation $\frac{\partial H_\mu}{\partial y}(1, y) = 0$ is necessarily fulfilled.

Indeed, the $\mathbb{Z}/2\mathbb{Z}$ symmetry of the Hamiltonian induces a time reversal symmetry (see Section 2.3.2) of the flow which the boundary condition respects such that the bifurcations of the system are governed by the gradient-zero-problem with symmetry. Let us describe the symmetry in a more general setting using generating functions (see Definition 2.1.5).

Mechanical Hamiltonians

Let $(x, y) = (x^1, \ldots, x^n, y_1, \ldots, y_n)$ be symplectic coordinates and $H_\mu(x, y)$ a family of Hamiltonian functions such that $H_\mu(x, y) = H_\mu(x, -y)$. For example, mechanical

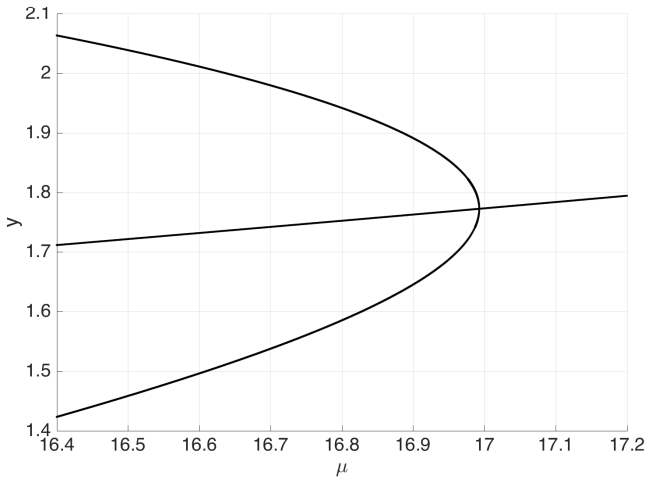

Figure 7.5: Bifurcation diagram for a time-reversal Hamiltonian and boundary condition $x(0) = 1 = x(0.1)$. The Hamiltonian flow is obtained using the symplectic Störmer–Verlet method with step size 0.0005.

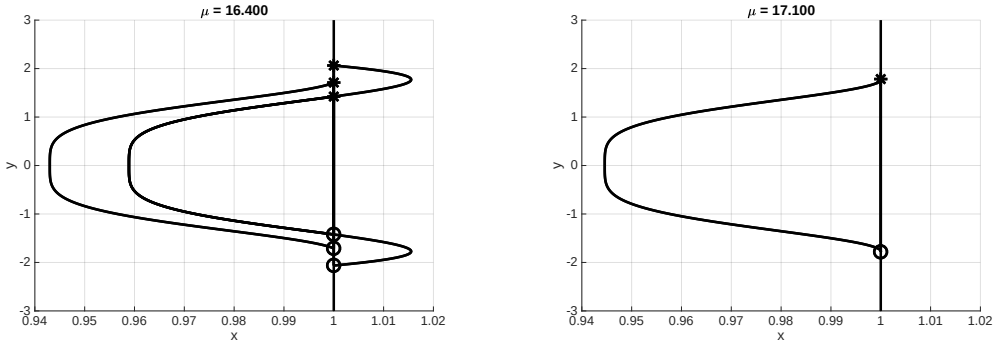

Figure 7.6: Motions involved in the pitchfork bifurcation shown in Figure 7.5. The motions obey the time-reversal symmetry of the system.

Hamiltonians $H_\mu(x,y) = \frac{1}{2}\langle y,y\rangle - V(x)$, where $\langle .,. \rangle$ is the Euclidean scalar product and V a scalar-valued map, fulfil this condition. Denote the time-τ-map of the Hamiltonian system H_μ by ϕ_μ and define $X_\mu = x \circ \phi_\mu$ and $Y_\mu = y \circ \phi_\mu$. By the symmetry of H_μ, the Hamiltonian system is time reversal symmetric such that

$$\phi_\mu\big(X_\mu(a,b), -Y_\mu(a,b)\big) = (a,-b) \tag{7.3.1}$$

for all points (a,b) in the phase space. Assume $\det\left(\frac{\partial Y_\mu}{\partial x}\right)_{i,j} \neq 0$ such that y, Y_μ constitutes a coordinate system. There exist generating functions $S_\mu(y,Y)$ such that

$$\begin{pmatrix} x \\ -X_\mu \end{pmatrix} = \nabla S_\mu(y, Y_\mu).$$

Let $\xi(y,Y) = (-Y,-y)$. By (7.3.1) the following holds:

$$\nabla S_\mu = \begin{pmatrix} x \\ -X_\mu \end{pmatrix} = \begin{pmatrix} X_\mu \circ \xi \\ -x \circ \xi \end{pmatrix} = \nabla(S_\mu \circ \xi).$$

The time reversal symmetry of the problem corresponds to an invariance of the generating function S. Now, if a boundary condition for ϕ_μ can be represented by a generating function $B_\mu(y,Y)$ of the same type as S_μ such that $\nabla B_\mu = \nabla(B_\mu \circ \xi)$, then the gradient-zero-problem for $S_\mu - B_\mu$ will be governed by singularity theory for maps with the symmetry ξ.

If, for instance, the boundary conditions are symmetrically separated with Lagrangian manifold G_μ in the phase space and if y constitutes a coordinate system for G_μ (as in the numerical example), then $G_\mu = \{(y, \nabla b_\mu(y))\}_y$ for some scalar-valued map b_μ. We can choose $B_\mu(y,Y) = b_\mu(y) - b_\mu(Y)$. Then $\nabla B_\mu = \nabla(B_\mu \circ \xi)$. In the numerical example we have $G_\mu = \{1\} \times \mathbb{R}$, $b_\mu(y) = y$ and $B_\mu(y,Y) = y - Y$.

We conclude that extra symmetry in Lagrangian boundary value problems can allow the persistent occurrence of bifurcations, which are non-persistent in the class of Lagrangian boundary value problems, if the symplectic map and the boundary conditions obey the same symmetry relation. The problem reduces to the gradient-zero-problem with symmetry. In the following Section 7.3.2 we provide a more general treatment of symmetries and reversing symmetries on bifurcation problems.

7.3.2 General treatment of symmetries and reversing symmetries

The following setting is convenient when describing the interaction of generating functions and symmetries. Let U be a finite dimensional vector space and U^* its dual vector

space. On the direct sum $V = U \oplus U^*$ we consider the symplectic form

$$\omega\big((u,u^*),(v,v^*)\big) = u^*(v) - v^*(u).$$

Denote a copy of the symplectic vector space (V,ω) by $(\underline{V} = \underline{U} \oplus \underline{U}^*, \underline{\omega})$. Consider the symplectic space $\big(V \oplus \underline{V}, \omega \oplus (-\underline{\omega})\big)$ with symplectic form

$$\omega \oplus (-\underline{\omega}) = \mathcal{P}^*\omega - \underline{\mathcal{P}}^*\underline{\omega},$$

where $\mathcal{P}\colon V \oplus \underline{V} \to V$ and $\underline{\mathcal{P}}\colon V \oplus \underline{V} \to \underline{V}$ denote the natural projections. In applications, the splitting $U \oplus \underline{U}^*$ occurs naturally: in Hamiltonian mechanics, U models a configuration space and $\underline{U}^*$ the space of momenta.

For the following considerations it is sufficient to consider locally defined, symplectic maps ϕ which map 0 to 0 in the space $V = U \oplus U^*$ as we can locally trivialize symplectic manifolds M around each $z \in M$ and $\phi(z) \in M$ using centred Darboux coordinates. In the following we will describe the effects of ordinary and reversing symmetries on generating functions and, thus, on the local bifurcation behaviour of Lagrangian boundary value problems. In order to avoid cumbersome notation and repeating remarks that domains of definition might shrink, we neglect to incorporate in our notation that maps are defined only on neighbourhoods of 0 of the corresponding spaces.

Consider a symplectic map $\phi\colon V \to \underline{V}$ mapping 0 to 0 and a diffeomorphism $\Psi\colon V \to V$. Let Ψ^1 denote the U-component of the map Ψ and Ψ^2 the U^*-component, i.e. $\Psi(v) = (\Psi^1(v), \Psi^2(v)) \in U \oplus U^*$. Moreover, assume there exists a generating function $S\colon U \oplus \underline{U} \to \mathbb{R}$ defined around 0 such that for all $(u,\underline{u}) \in U \oplus \underline{U}$ the following Lagrangian submanifolds of $(V \oplus \underline{V}, \omega \oplus (-\omega))$ coincide:

$$\Gamma = \{(v,\phi(v)) | v \in V\} = \{\big(u, \mathrm{D}_u S(u,\underline{u}), \underline{u}, -\mathrm{D}_{\underline{u}} S(u,\underline{u})\big) \,|\, (u,\underline{u}) \in U \oplus \underline{U}\}.$$

Ordinary symmetry

Proposition 7.3.1. *The relation*

$$\Psi^{-1} \circ \phi \circ \Psi = \phi \tag{7.3.2}$$

is equivalent to $\forall (u,\underline{u}) \in U \oplus \underline{U}$:

$$\begin{aligned} \mathrm{D}_u S\Big(\Psi^1(u, \mathrm{D}_u S(u,\underline{u})), \Psi^1(\underline{u}, -\mathrm{D}_{\underline{u}} S(u,\underline{u}))\Big) &= \Psi^2\Big(u, \mathrm{D}_u S(u,\underline{u})\Big) \\ -\mathrm{D}_{\underline{u}} S\Big(\Psi^1(u, \mathrm{D}_u S(u,\underline{u})), \Psi^1(\underline{u}, -\mathrm{D}_{\underline{u}} S(u,\underline{u}))\Big) &= \Psi^2\Big(\underline{u}, -\mathrm{D}_{\underline{u}} S(u,\underline{u})\Big) \end{aligned} \tag{7.3.3}$$

Remark 7.3.1. If Ψ is additionally symplectic, then Ψ is referred to as an *ordinary symmetry* for ϕ. If, for instance, the map ϕ is given as a Hamiltonian diffeomorphism

and Ψ is a symplectic map on the phase space leaving the Hamiltonian invariant, then Ψ as well as Ψ^{-1} are ordinary symmetries for ϕ. △

Proof of Proposition 7.3.1. The relation $\phi \circ \Psi = \Psi \circ \phi$ is equivalent to $(\Psi \times \Psi)(\Gamma) = \Gamma$, where $(\Psi \times \Psi)\colon V \oplus \underline{V} \to V \oplus \underline{V}$, $(\Psi \times \Psi)(v, \underline{v}) = (\Psi(v), \Psi(\underline{v}))$ denotes the diagonal action. The relation $(\Psi \times \Psi)(\Gamma) = \Gamma$ is equivalent to (7.3.3). □

The following proposition analyses the effects of symmetries on the phase space $U \oplus U^*$ which restrict to the Lagrangian submanifold U. Examples are spatial symmetries of mechanical systems.

Proposition 7.3.2. *Let $h\colon U \to U$ be a diffeomorphism. The symplectic map $\Psi = (\Psi^1, \Psi^2)\colon U \oplus U^* \to U \oplus U^*$ defined by*

$$\Psi^1(u, u^*) = h(u) \quad \Psi^2(u, u^*) = u^* \circ \mathrm{D}h^{-1}(u) \tag{7.3.4}$$

is an ordinary symmetry for ϕ if and only if S is invariant under h, i.e.

$$S \circ (h \times h) = S,$$

holds true (up to a constant), where $(h \times h)(u, \underline{u}) = (h(u), h(\underline{u})) \in U \oplus \underline{U}$ denotes the diagonal action.

Remark 7.3.2. The symplectic map Ψ defined in (7.3.4) corresponds to the cotangent lifted action of h (see Marsden and Ratiu, 1999a, §6.3, for instance). The reader might be familiar with its representation in Darboux coordinates p, q of the cotangent bundle: $q \mapsto h(q), p \mapsto \mathrm{D}h(q)^{-t}p$. △

Proof of Proposition 7.3.2. The relation $S \circ (h \times h) = S$ (up to a constant) is equivalent to

$$\mathrm{D}(S(h(u), h(\underline{u}))) = \mathrm{D}S(u, \underline{u}) \quad \forall (u, \underline{u}) \in U \oplus \underline{U},$$

which is equivalent to $\forall (u, \underline{u}) \in U \oplus \underline{U}$:

$$\begin{aligned} (\mathrm{D}_u S)(h(u), h(\underline{u})) &= \quad \mathrm{D}_u S(u, \underline{u}) \circ \mathrm{D}h^{-1}(u) \\ -(\mathrm{D}_{\underline{u}} S)(h(u), h(\underline{u})) &= -\mathrm{D}_{\underline{u}} S(u, \underline{u}) \circ \mathrm{D}h^{-1}(\underline{u}), \end{aligned}$$

which is equivalent to (7.3.3) with Ψ defined as in (7.3.4). The claim follows by Proposition 7.3.1. □

Analogously to Lemma 6.3.3, after a symplectic change of coordinates in $V \oplus \underline{V}$, we can assume that boundary conditions as well as the graph Γ of a symplectic map ϕ are both graphical over $U \oplus \underline{U}$, where the projection $V \oplus \underline{V} \to U \oplus \underline{U}$ is given as

$\big((u,u^*),(\underline{u},\underline{u}^*)\big) = (u,\underline{u})$. We state the following proposition which gives a criterion for when Ψ is a symmetry for separated, Lagrangian boundary conditions.

Proposition 7.3.3. *Let $B(u,\underline{u}) = b(u) - \underline{b}(\underline{u})$ for local maps $b\colon U \to \mathbb{R}$, $\underline{b}\colon \underline{U} \to \mathbb{R}$. Consider*

$$G = \{(u, \mathrm{D}b(u)) \,|\, u \in U\}, \quad \underline{G} = \{(\underline{u}, \mathrm{D}\underline{b}(\underline{u})) \,|\, \underline{u} \in \underline{U}\}, \quad \Lambda := G \times \underline{G} \subset V \oplus \underline{V}$$

The relations (7.3.3) stated with B instead of S are fulfilled if and only if

$$\Psi(G) = G \quad \Psi(\underline{G}) = \underline{G}. \tag{7.3.5}$$

Proof. Notice that Λ is generated by B, i.e.

$$\Lambda = G \times G = \{(u, \mathrm{D}_u B(u,\underline{u}), \underline{u}, -\mathrm{D}_{\underline{u}} B(u,\underline{u}) \,|\, (u,\underline{u}) \in U \oplus \underline{U}\}.$$

The relation (7.3.5) holds true if and only if the submanifold Λ is invariant under the diagonal action $\Psi \times \Psi$ if and only if (7.3.3) stated with B instead of S holds true. □

Corollary 7.3.4. *If Ψ as in (7.3.4) is an ordinary symmetry for a family of symplectic maps and a family of separated Lagrangian boundary conditions invariant under Ψ is given, then the Lagrangian boundary value problem behaves like the gradient-zero problem $\tilde{S}(u,\underline{u}) = 0$ with symmetry $\tilde{S} \circ (h \times h) = \tilde{S}$. Using the notation of the propositions, $\tilde{S} = S - B$.*

Examples

- Spatial symmetries of mechanical systems on U with phase space $U \oplus U^*$ can be phrased as maps $h\colon U \to U$. A symplectic map Ψ defined as in (7.3.4) is an ordinary symmetry for the Hamiltonian diffeomorphism ϕ. The generating function S of ϕ fulfils $S \circ (h \times h) = S$.
  - Let $h(u) = -u$, $\Psi(u,u^*) = (-u,-u^*)$. It follows that S fulfils the $\mathbb{Z}/2\mathbb{Z}$ symmetry relation $S(-u,-\underline{u}) = S(u,\underline{u})$.
  - For $\lambda \in \mathbb{R} \setminus \{0\}$ let $h_\lambda(u) = \lambda u$, $\Psi_\lambda(u,u^*) = (\lambda u, \lambda^{-1}u^*)$. Then $S(\lambda u, \lambda \underline{u}) = S(u,\underline{u})$, i.e. S is homogeneous (of degree 1).
- Consider the Dirichlet problem $u = 0$, $\underline{u} = 0$ for a symplectic map with generating function $S\colon U^* \oplus \underline{U}^* \to \mathbb{R}$ invariant under the cotangent lifted action of a linear, spatial symmetry $A\colon U \to U$. The problem behaves like the gradient-zero problem for S with diagonal symmetry $A^\top$, i.e. $S \circ (A^\top \times A^\top) = S$. Here $A^\top$ denotes the transpose of the linear map A. Notice that the structure of the boundary

condition forces us to use $(u^*, \underline{u}^*)$ as coordinates for the generating function. Therefore, in contrast to Proposition 7.3.2, the diagonal right action on S is by $A^\top$ rather than by A.

- In case of k independent, Poisson commuting integrals of motions, there exist symplectic coordinates such that the Hamiltonian $H\colon U \oplus U^* \to \mathbb{R}$ does not depend on $u^1, \dots, u^k$. This means for each $\lambda \in \mathbb{R}^k$ the translation

$$h(u^1, \dots, u^k, u^{k+1}, \dots, u^n) = h(u^1 + \lambda_1, \dots, u^k + \lambda_k, u^{k+1}, \dots, u^n)$$

gives rise to an ordinary symmetry for the Hamiltonian diffeomorphism. Its generating function $S\colon U \oplus \underline{U} \to \mathbb{R}$ depends on the following $2n-k$ variables: $u_1 - \underline{u}_1, \dots, u_k - \underline{u}_k, u_{k+1}, \underline{u}_{k+1}, \dots, u_n, \underline{u}_n$. Notice that periodic boundary conditions

$$\underline{u} - u = 0, \quad \underline{u}^* - u^* = 0$$

share this symmetry property. This recovers the fact that solutions to periodic boundary value problems for Hamiltonian diffeomorphisms with k integrals of motion are k-dimensional manifolds. In planar Hamiltonian systems, for instance, solutions to periodic boundary value problems are not isolated but given by periodic orbits of the correct frequency.

Reversal symmetry

Proposition 7.3.5. *The relation*

$$\Psi^{-1} \circ \phi \circ \Psi = \phi^{-1} \tag{7.3.6}$$

is equivalent to $\forall (u, \underline{u}) \in U \oplus \underline{U}$:

$$\begin{aligned} \mathrm{D}_u S\Big(\Psi^1(\underline{u}, -\mathrm{D}_{\underline{u}} S(u, \underline{u})), \Psi^1(u, \mathrm{D}_u S(u, \underline{u}))\Big) &= \Psi^2\Big(\underline{u}, -\mathrm{D}_{\underline{u}} S(u, \underline{u})\Big) \\ -\mathrm{D}_{\underline{u}} S\Big(\Psi^1(\underline{u}, -\mathrm{D}_{\underline{u}} S(u, \underline{u})), \Psi^1(u, \mathrm{D}_u S(u, \underline{u}))\Big) &= \Psi^2\Big(u, \mathrm{D}_u S(u, \underline{u})\Big). \end{aligned} \tag{7.3.7}$$

Remark 7.3.3. If in addition Ψ is anti-symplectic, i.e. $\Psi^*\omega = -\omega$, then Ψ is referred to as a *reversal symmetry* for ϕ. For example, this situation arises if ϕ is given as a Hamiltonian diffeomorphism and Ψ is a anti-symplectic map on the phase space leaving the Hamiltonian invariant. Inverting (7.3.6), it follows that Ψ is a reversal symmetry for ϕ if and only if Ψ^{-1} is a reversal symmetry. △

Proof of Proposition 7.3.5. The relation $\phi \circ \Psi = \Psi \circ \phi^{-1}$ is equivalent to $(\Psi \underline{\times} \Psi)(\Gamma) = \Gamma$, where $(\Psi \underline{\times} \Psi)(v, \underline{v}) = (\Psi(\underline{v}), \Psi(v))$ denotes the reversal action. The invariance of Γ is

equivalent to (7.3.7). □

The following proposition analyses the effects of reversal symmetries on the phase space $V = U \oplus U^*$ which restrict to the Lagrangian submanifold U. Examples are spatial reversal symmetries.

Proposition 7.3.6. *Let $h\colon U \to U$ be a diffeomorphism. The anti-symplectic map $\Psi = (\Psi^1, \Psi^2)\colon U \oplus U^* \to U \oplus U^*$ defined by*

$$\Psi^1(u, u^*) = h(u) \quad \Psi^2(u, u^*) = -u^* \circ \mathrm{D}h^{-1}(u). \tag{7.3.8}$$

is a reversal symmetry for ϕ if and only if S is invariant under h, i.e.

$$S \circ (h \underline{\times} h) = S,$$

holds true (up to a constant), where $(h \underline{\times} h)(u, \underline{u}) = (h(\underline{u}), h(u)) \in U \oplus \underline{U}$ denotes the reversal action.

Proof. The relation $S \circ (h \underline{\times} h) = S$ (up to a constant) is equivalent to

$$\mathrm{D}(S(h(\underline{u}), h(u))) = \mathrm{D}S(u, \underline{u}) \quad \forall (u, \underline{u}) \in U \oplus \underline{U},$$

which is equivalent to $\forall (u, \underline{u}) \in U \oplus \underline{U}$:

$$\begin{aligned}(\mathrm{D}_{\underline{u}} S)(h(\underline{u}), h(u)) \circ \mathrm{D}h(u) &= \mathrm{D}_u S(u, \underline{u}) \\ (\mathrm{D}_u S)(h(\underline{u}), h(u)) \circ \mathrm{D}h(\underline{u}) &= \mathrm{D}_{\underline{u}} S(u, \underline{u})\end{aligned}$$

which is equivalent to (7.3.7) with Ψ defined as in (7.3.8). The claim follows by Proposition 7.3.5. □

The next proposition gives a criterion when an anti-symplectic map Ψ is a reversal symmetry for separated, Lagrangian boundary conditions. The statement holds, however, for all diffeomorphisms $\Psi\colon V \to V$.

Proposition 7.3.7. *Let $B(u, \underline{u}) = b(u) - \underline{b}(\underline{u})$ for local maps $b\colon U \to \mathbb{R}$, $\underline{b}\colon \underline{U} \to \mathbb{R}$. Consider*

$$G = \{(u, \mathrm{D}b(u)) \,|\, u \in U\}, \quad \underline{G} = \{(\underline{u}, \mathrm{D}\underline{b}(\underline{u})) \,|\, \underline{u} \in \underline{U}\}, \quad \Lambda := G \times \underline{G} \subset V \oplus \underline{V}$$

The relations (7.3.7) stated with B instead of S are fulfilled if and only if

$$\Psi(G) = \underline{G} \quad \Psi(\underline{G}) = G. \tag{7.3.9}$$

Remark 7.3.4. In contrast to Proposition 7.3.3, the manifolds G and $\underline{G}$ get swapped by the diffeomorphism Ψ. △

Proof of Proposition 7.3.7. Notice that Λ is generated by B, i.e.

$$\Lambda = G \times G = \{(u, \mathrm{D}_u B(u, \underline{u}), \underline{u}, -\mathrm{D}_{\underline{u}} B(u, \underline{u}) \,|\, (u, \underline{u}) \in U \oplus \underline{U}\}.$$

The relation (7.3.9) holds true if and only if the submanifold Λ is invariant under the reversal action $\Psi \underline{\times} \Psi$ if and only if (7.3.7) stated with B instead of S holds true. □

Corollary 7.3.8. *If Ψ as in (7.3.8) is a reversal symmetry for a family of symplectic maps and a family of separated Lagrangian boundary conditions invariant under Ψ in the sense of (7.3.9) is given, then the local Lagrangian boundary value problem behaves like the gradient-zero problem $\tilde{S}(u, \underline{u}) = 0$ with symmetry $\tilde{S} \circ (h \underline{\times} h) = \tilde{S}$. In the setting of the propositions, $\tilde{S} = S - B$.*

Examples

- Let $h(u) = u$ such that $\Psi(u, u^*) = (u, -u^*)$. Then $S(u, \underline{u}) = S(\underline{u}, u)$.
- Let $h(u) = -u$ such that $\Psi(u, u^*) = (-u, u^*)$. Then $S(u, \underline{u}) = S(-\underline{u}, -u)$. This recovers the results of Section 7.3.1.
- For $\lambda \in \mathbb{R} \setminus \{0\}$ let $h_\lambda(u) = \lambda u$, so $\Psi_\lambda(u, u^*) = (\lambda u, -\lambda^{-1} u^*)$. Then $S(\lambda \underline{u}, \lambda u) = S(u, \underline{u})$. In particular, $S(\underline{u}, u) = S(u, \underline{u})$. The map S is homogeneous and symmetric.

Let us relate these findings to the *periodic* pitchfork described in Sections 7.2.2 and 7.2.3. Recall from the examples of ordinary symmetries that integrals of motions lead to translation symmetries. In completely integrable systems in action angle coordinates, the generating function $S \colon U \oplus \underline{U} \to \mathbb{R}$ of the Hamiltonian flow only depends on the difference $u - \underline{u}$ of the angles. In particular, S is invariant under the transformation $(u_1, \underline{u}_1) \mapsto (-\underline{u}_1, -u_1)$.

Recall from Section 7.2.3 that under the assumption that a periodic orbit touches the boundary condition and gives rise to a solution of the boundary value problem, there exists a symplectic change of coordinates on $U \oplus U^*$ such that the symmetrically separated boundary condition is invariant under $(u_1, \underline{u}_1) \mapsto (-\underline{u}_1, -u_1)$ as well, locally around the touch point. The bifurcation behaviour corresponds to the gradient-zero-problem with a $\mathbb{Z}/2\mathbb{Z}$ symmetry. In a one-parameter family of systems with a $\mathbb{Z}/2\mathbb{Z}$ symmetry a pitchfork bifurcation is a generic phenomenon, i.e. pitchfork bifurcations persist under small perturbations that respect the symmetry.

While the $\mathbb{Z}/2\mathbb{Z}$ symmetry in completely integrable systems appears rather hidden and becomes visible using action angle coordinates, the $\mathbb{Z}/2\mathbb{Z}$ symmetry in time-reversal systems is more apparent and again picked up by symmetrically separated Dirichlet boundary conditions since these share the phase space symmetry as explained in Section 7.3.1. Again, a pitchfork bifurcation becomes a generic phenomenon in one-parameter families of problems.

7.4 Summary of Chapters 6 and 7

In Chapters 6 and 7 we have shown that Lagrangian boundary value problems for symplectic maps can be regarded as local intersection problems of Lagrangian submanifolds. This, in turn, corresponds to finding critical points of a smooth function (given as the difference of generating functions) and gives a *finite dimensional* approach to bifurcation theory for Hamiltonian boundary value problems. This allows us to

- link generic problems to Thom's seven elementary catastrophes and to Arnold's ADE-classification, a framework known as catastrophe theory,
- explain how certain, typical boundary conditions can prohibit bifurcations,
- analyse how extra structure for symplectic maps can lead to extra bifurcations.

An instance of our analysis of how boundary conditions can prohibit bifurcations is the following result: in Dirichlet problems for $2n$-dimensional systems only those bifurcations can occur which can be obtained in critical points of smooth function problems in at most n variables. This means, for example, that in Dirichlet problems for planar symplectic maps only A-series type bifurcations can occur persistently. In contrast, using periodic boundary conditions D-series singularities are also possible. Moreover, extra structure for symplectic maps can lead to extra bifurcations. In symmetrically separated boundary value problems for flows of completely integrable Hamiltonian systems, we describe a pitchfork-type bifurcation, which we call the periodic pitchfork bifurcation. In this novel bifurcation, two complete periodic solutions bifurcate from a path of partial periodic orbits.

Lagrangian boundary value problems for symplectic maps correspond to gradient-zero-problems with symmetry if the symplectic map and the boundary values are governed by the same symmetry relation. Here, additional bifurcations can occur which make use of the symmetry of the system. Propositions 7.3.3 and 7.3.7 describe when separated Lagrangian boundary conditions fulfil a given symmetry. For instance, in one parameter families of time-reversal, symmetric Hamiltonian systems a time-reversal pitchfork can occur persistently.

For structurally simple symmetries, which split into separated actions on two Lagrangian subspaces (e.g. spatial symmetries), the Propositions 7.3.2 and 7.3.6 reveal which symmetry is induced in the corresponding gradient-zero-problem. In contrast, for arbitrary group actions we do not have a characterization of which symmetries induce a correspondence between boundary value problems and critical points of symmetric functions.

The framework presented here raises the possibility of discovering exotic bifurcations in examples from physics, and also of discovering further new phenomena induced in specific classes of equations. In the next chapter we will extend our investigations to *conformal symplectic symmetries* which will, in particular, allow us to analyse singularities that occur in *conjugate loci*.

Chapter 8

Conformal symplectic symmetries and conjugate loci

Chapter 8 is an adaption of McLachlan and Offen, 2018b.

We continue our investigations into the effects of boundary conditions and symmetries for bifurcations of solutions of boundary-value problems for symplectic maps arising as Hamiltonian diffeomorphisms. The framework of Chapters 6 and 7 is used to prove the existence of obstructions arising from conformal symplectic symmetries on the bifurcation behaviour of solutions to Hamiltonian boundary value problems.

Consider the action $g \mapsto \chi_g$ of a Lie group G on a symplectic manifold (M, ω), where χ_g is a diffeomorphism on M. While for a symplectic Lie group action χ_g is required to leave ω invariant, i.e. $\chi_g^*\omega = \omega$, in case of a conformal symplectic action χ_g preserves ω only up to a g dependent constant $c(g)$, i.e. $\chi_g^*\omega = c(g) \cdot \omega$, where c depends smoothly on g. A *conformal symplectic symmetry* of a Hamiltonian system is a conformal symplectic Lie group action which leaves the Hamiltonian invariant up to a constant depending on the acting group element. Examples include Hamiltonian systems with scaling symmetries. The central example of this chapter are Hamiltonian systems on cotangent bundles whose motions correspond to geodesics on their base manifold. We will investigate the effects of the symmetries in the light of our catastrophe theory framework. Under non-degeneracy conditions, a group action by conformal symplectic symmetries has the effect that the flow map cannot degenerate in a direction which is tangential to the action. This imposes restrictions on which singularities can occur in boundary value problems. Our results generalise classical results about conjugate loci on Riemannian manifolds to Hamiltonian boundary value problems with conformal symplectic symmetries.

8.1 Introduction

In the most frequently studied situation of a group acting on a symplectic manifold, the group acts by symplectic or Hamiltonian actions and leaves a Hamiltonian flow invariant. In another case, the group acts by Hamiltonian actions but the flow is conformal symplectic (McLachlan and Perlmutter, 2001). In contrast, in this chapter we consider conformal symplectic actions on Hamiltonian flows and their effects on bifurcations in boundary value problems. As an example of a Hamiltonian boundary value problem let us consider the conjugate points problem for geodesics on Riemannian manifolds: recall that geodesics are locally length minimising. Roughly speaking, two points q and Q are *conjugate* if a geodesic starting at q stops to be length minimising when reaching Q. More precisely, we have the following definition.

Definition 8.1.1 (conjugate points, conjugate locus)**.** Two points q and Q on a Riemannian manifold connected by a geodesic γ are called *conjugate points* if there exists a nontrivial Jacobi vector field along γ vanishing at q and Q. In other words, there exists a nontrivial vector field along γ which arises as a variational vector field for variations through geodesics fixing q and Q (Flaherty and Carmo, 1992, Ch.5). The set of all points conjugate to q is called the *conjugate locus to* q. △

Remark 8.1.1. As an alternative to Definition 8.1.1 one can define q and Q to be conjugate if Q is the image of a critical point of the geodesic exponential map at q (Wall, 1977). △

Example 8.1.1 (conjugate locus on 2-dimensional Gaussian). The left plot of Figure 8.1 shows the graph of a (slightly perturbed) 2-dimensional Gaussian and the conjugate locus to the point q marked as $*$ in the plot. There are three geodesics connecting q with a point Q in between the solid black lines where $Q_1 > 0$ while there is a unique geodesic if Q is outside that region. Keeping q fixed and varying Q two of the geodesics merge in a fold bifurcation as Q crosses one of the solid black lines. If Q crosses the meeting point of the lines of folds all connecting geodesics merge into one. The meeting point corresponds to a cusp singularity. △

Example 8.1.2 (Conjugate locus on ellipsoid). Other examples of conjugate points are antipodal points on a sphere. Let us fix the point $q = (q^1, q^2, q^3) = (-\frac{1}{\pi}, 0, 0)$ on a 2-sphere in $\mathbb{R}^3$ of circumference 2. Its only conjugate point is the antipodal point $Q = (\frac{1}{\pi}, 0, 0)$. Perturbing the sphere to an ellipsoid the conjugate locus consists of four cusps connected by lines of fold singularities as visualised in the plot to the right of Figure 8.1, unless q happens to be an umbilic point of the ellipsoid. This is known as the last geometric statement of Jacobi (Itoh and Kiyohara, 2004). △

Later, we will extend the conjugate locus examples 8.1.1 and 8.1.2 and consider bifurcations of conjugate points (*conjugate points problems*) in which not only the

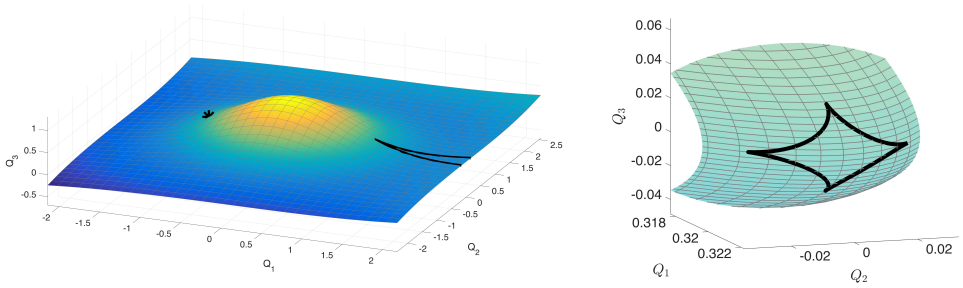

Figure 8.1: Conjugate loci on a perturbed graph of a 2-dimensional Gaussian and on an ellipsoid. See Examples 8.1.1 and 8.1.2.

endpoint Q can vary but also the start point q. Here we expect higher degenerate singularities to occur.

In general, on a Riemannian manifold (N, g) geodesic motions can be interpreted as motions of a Hamiltonian system defined on the cotangent bundle $\pi\colon T^*N \to N$: for the Hamiltonian

$$H(\alpha) = \frac{1}{2}\alpha\left(g^{-1}(\alpha)\right), \quad \alpha \in T^*N \tag{8.1.1}$$

motions correspond to velocity vector fields of geodesics under the bundle isomorphism g between the tangent bundle TN and the cotangent bundle T^*N. (A formulation in local coordinates will be given in Section 9.3.4, where we will focus on computational aspects.) If Φ is the associated Hamiltonian flow at time 1, then the problem of connecting two points $q, Q \in N$ by a geodesic can be formulated as the following boundary value problem for Φ: find $\alpha \in T^*N$ such that

$$\pi(\alpha) = q, \quad (\pi \circ \Phi)(\alpha) = Q. \tag{8.1.2}$$

The Hamiltonian formulation reveals symplectic structure hidden in the geodesic problem: the above problem (8.1.2) is a boundary value problem for a symplectic map. Indeed, the symplectic structure has an effect on the kind of bifurcations which can occur in boundary value problems and whether the singularities persist under small perturbations. Moreover, the Hamiltonian H (8.1.1) has a conformal symplectic symmetry under which Φ is invariant. In contrast to boundary value problems for arbitrary symplectic maps, the Dirichlet-type form of the boundary condition and the symmetry properties turn out to impose restrictions on which of these singularities actually can occur.

The remainder of the chapter is structured as follows. In Section 8.2 we fix notation and provide a coordinate-free framework which is convenient for the analysis of separated Lagrangian boundary value problems which include, in particular, our

Examples 8.1.1 and 8.1.2.

In Section 8.3 the framework is used to prove the main result of this chapter: if a Hamiltonian is invariant under a conformal symplectic action of a k-dimensional Lie group, then the degree of degeneracy of a singularity in a separated Lagrangian boundary value problem cannot exceed $n-k$, where $2n$ is the phase space dimension, if the action is tangential to the boundary condition and under non-degeneracy conditions on the group action and the Hamiltonian vector field. This extends the result of Proposition 7.1.2 that separated Lagrangian boundary value problems can only degenerate up to dimension n, which is the lowest upper bound that one can achieve in the general setting without symmetries. The new result applies in particular to homogeneous Hamiltonians such as (8.1.1). This means that, under nondegeneracy assumptions, we expect only the A-series singularities to occur persistently in conjugate points problems on Riemannian surfaces not matter how many parameters enter in the metric. In contrast, Proposition 7.1.2 does not exclude D- or E-series singularities. This provides an alternative approach to the conjugate points problem on Riemannian manifolds and recovers classical results about conjugate loci (Wall, 1977; Weinstein, 1970).

8.2 Definitions, notation, and framework

Let us fix our notation for *separated (Lagrangian) boundary value problems.*

Definition 8.2.1 (Separated (Lagrangian) boundary value problem)**.** Let (M,ω) and (M',ω') be two symplectic manifolds with $\dim M = 2n = \dim M'$. Consider a symplectic map $\phi\colon M \to M'$ and n-dimensional submanifolds $\Lambda \subset M$ and $\Lambda' \subset M'$. The collection (ϕ,Λ,Λ') is called a *separated boundary value problem.* Its solution is given as

$$\{z \in \Lambda \mid \phi(z) \in \Lambda'\} = \phi^{-1}(\Lambda') \cap \Lambda.$$

If $\Lambda \subset M$ and $\Lambda' \subset M'$ are Lagrangian submanifolds, then (ϕ,Λ,Λ') is called a *separated Lagrangian boundary value problem.* △

Remark 8.2.1. Let (M,ω) and (M',ω') be $2n$-dimensional symplectic manifolds and $\Lambda \subset M$ and $\Lambda' \subset M'$ be n-dimensional submanifolds. The submanifold $\Pi = \Lambda \times \Lambda' \subset (M \times M', \omega \oplus -\omega')$ is Lagrangian if and only if Λ and Λ' are Lagrangian submanifolds. Therefore, the separated boundary value problems which are Lagrangian boundary value problems (Definition 6.2.1) are exactly the separated Lagrangian boundary value problems. △

Example 8.2.1. The classical Dirichlet, Neumann and Robin boundary value problems considered in Example 6.2.2 constitute separated Lagrangian boundary value problems

if regarded as boundary value problems for a Hamiltonian flow map (Figure 6.3). Periodic boundary conditions, however, constitute Lagrangian boundary value problems which cannot be regarded as separated boundary value problems. This leads to a different bifurcation behaviour as seen in Chapter 7. △

Observation 8.2.1 (Local coordinate description). All separated Lagrangian boundary value problems are locally equivalent: by Darboux-Weinstein's theorem neighbourhoods of Lagrangian submanifolds are locally symplectomorphic to neighbourhoods of the zero section of the cotangent bundle over the submanifolds Weinstein, 1971b, Corollary 6.2. Therefore, a separated Lagrangian boundary value problem $(\phi, \Lambda, \Lambda')$ for $\phi\colon (M,\omega) \to (M',\omega')$ is locally given as

$$x = x^*, \quad \phi^X(x,y) = X^*, \tag{8.2.1}$$

with $x^*, X^* \in \mathbb{R}^{2n}$ and with local Darboux coordinates $(x,y) = (x^1, \dots x^n, y_1, \dots y_n)$ for M and $(X,Y) = (X^1, \dots X^n, Y_1, \dots Y_n)$ for M'. In (8.2.1) the symbol ϕ^X is a shorthand for $X \circ \phi$. In particular, Dirichlet, Neumann and Robin boundary conditions can be treated on the same footing in the bifurcation context. In contrast, periodic boundary conditions are not separated. This manifests in the different bifurcation behaviour described in Propositions 7.1.2 and 7.1.5. △

Let us consider the separated Lagrangian boundary value problem (8.2.1) on the phase space $M = M' = \mathbb{R}^{2n}$ with the standard symplectic form $\sum_{j=1}^n \mathrm{d}x^j \wedge \mathrm{d}y_j$. Introducing a multi-dimensional parameter μ in the map ϕ or in the boundary condition, the bifurcation diagram of (8.2.1) can be viewed as

$$\{(\mu, y) \,|\, h_\mu(y) = 0\} \tag{8.2.2}$$

with

$$h_\mu(y) = \phi^X_{(\mu)}(x^*, y) - X^*_\mu. \tag{8.2.3}$$

We easily re-obtain Proposition 7.1.2 (in a slightly more general form).

Proposition 8.2.1. *If the dimension of the kernel of the Jacobian matrix of the map* (8.2.3) *at a parameter value μ and a value y is m, then the degeneracy of the singularity of the corresponding critical-points-of-a-function problem at (μ, y) is m.*

For further analysis it will be handy to have a coordinate free version of observation 8.2.1 and Proposition 8.2.1 available. Given $\phi\colon (M,\omega) \to (M',\omega')$, consider a separated Lagrangian boundary value problem $(\phi, \Lambda, \Lambda')$. Localising the problem, if necessary, there is an integrable distribution $\mathcal{D}$ on M' such that Λ' is a leaf of $\mathcal{D}$ and the projection $M' \to M'/\mathcal{D}$, $z' \mapsto [z']$ is a submersion.[1] Consider a composition of the

[1] An example where $M'/\mathcal{D}$ does *not* inherit a smooth manifold structure via the projection map is

restricted map $\phi_{|\Lambda}$ with the projection to the leaf space $M'/\mathcal{D}$, i.e.

$$\left[\phi_{|\Lambda}\right] : \Lambda \to M'/\mathcal{D}.$$

The solution of the separated Lagrangian boundary value problem corresponds to the preimage of $[\Lambda'] \in M'/\mathcal{D}$ under the above map. Now we can reformulate Proposition 8.2.1 as follows.

Proposition 8.2.2. *In the considered setting, if $z \in \Lambda$ is a solution, i.e. $\phi(z) \in \Lambda'$, then the dimension of the kernel of the map*

$$\mathrm{d}\left[\phi_{|\Lambda}\right]\big|_z : T_z\Lambda \to T_{[z']}\left(M'/\mathcal{D}\right) \tag{8.2.4}$$

coincides with the degeneracy of the singularity of the corresponding critical-points-of-a-function problem.

Remark 8.2.2. For determining the kernel of (8.2.4) we can weaken the condition that Λ' is a leaf of $\mathcal{D}$ to the requirement that $\mathcal{D}_{z'} = T_{z'}\Lambda'$. △

8.3 Obstructions for singularities in systems with conformal symplectic symmetry

By Proposition 8.2.2, the geometric structure of separated Lagrangian boundary value problems forbids bifurcations whose fully reduced representatives of the corresponding critical-points problems need more variables than half the dimension of the phase space. It turns out that in systems with a (nontrivial) conformal symplectic, k-dimensional group action leaving the boundary condition and the motions invariant up to time-rescaling even stronger restrictions apply. Indeed, if the Hamiltonian vector field is not tangential to the boundary condition, then in $2n$-dimensional systems only singularities of degeneracy at most $n - k$ occur in separated Lagrangian boundary value problems. Moreover, the requirement that the boundary condition is invariant can be weakened to the condition that the action is tangential to the boundary condition.

The new result applies to homogeneous Hamiltonian systems and we will show that this provides an alternative viewpoint for bifurcations of geodesics and recovers classical results about multiplicities of conjugate points along geodesics.

the foliation of a torus $M' = \mathbb{R}^2/\mathbb{Z}$ by dense orbits $t \mapsto (\alpha, 1)t$ for irrational α. Shrinking M' resolves the problem.

8.3.1 Conformal symplectic symmetric Hamiltonian systems

Definition 8.3.1 (Conformal symplectic map)**.** Let (M, ω) and (M', ω') be two symplectic manifolds. A map $\chi\colon M \to M'$ is called a *conformal symplectic map* if

$$\chi^*\omega' = \theta \cdot \omega \tag{8.3.1}$$

for some $\theta \in \mathbb{R}$. △

Example 8.3.1. Let N be a smooth manifold. The cotangent bundle $M = T^*N$ with the projection map $\pi\colon M \to N$ can be equipped with the symplectic structure $\omega = -\mathrm{d}\lambda$, where λ denotes the Liouvillian-1-form on M which is canonically defined by

$$\lambda_\alpha(v) = \alpha(\mathrm{d}\pi|_\alpha(v)) \quad \text{for all } \alpha \in M,\, v \in T_\alpha M. \tag{8.3.2}$$

To $\theta \in \mathbb{R}$ consider $\chi\colon M \to M$ with $\chi(\alpha) = \theta \cdot \alpha$, where $\cdot$ denotes the usual scalar multiplication of 1-forms with real numbers. The map χ is a conformal symplectic map with $\chi^*\omega = \theta \cdot \omega$ because for each $\beta \in M$ and $w \in T_\beta M$ we have

$$(\chi^*\lambda)|_\beta(w) = \lambda|_{\theta\cdot\beta}(\mathrm{d}\chi(w)) \overset{(8.3.2)}{=} (\theta \cdot \beta)(\mathrm{d}(\pi \circ \chi)(w)) = (\theta \cdot \beta)(\mathrm{d}\pi(w)) = (\theta \cdot \lambda)|_\beta(w),$$

where we have used that χ preserves the fibres of the cotangent bundle. △

Remark 8.3.1 (Sign convention). Notice that the symplectic structure $\omega = -\mathrm{d}\lambda$ of the cotangent bundle in Example 8.3.1 and the symplectic structure $\omega = \mathrm{d}\lambda$ in Example 2.1.1 differ by a sign. In this chapter, we will use the symplectic structure $\omega = -\mathrm{d}\lambda$ from Example 8.3.1 for the cotangent bundle. For consistency, we consider Hamiltonian vector fields X_H to a Hamiltonian H defined on a symplectic manifold (M, ω) as defined by the relation $\mathrm{d}H = \iota_{X_H}\omega = \omega(X_H, \cdot)$ rather than $\mathrm{d}H = -\iota_{X_H}\omega$, where $\iota_{X_H}\omega$ denotes the contraction of the 2-form ω by the vector field X_H. The different sign convention does not have any effect on the qualitative statements in this chapter. △

Remark 8.3.2. Dropping the condition that the factor θ in (8.3.1) of Definition 8.3.1 is constant does not yield a generalisation of the notion of conformal symplecticity as the following calculation shows. Let (M, ω) and (M', ω') be symplectic manifolds with $\dim M > 2$. If a map $\chi\colon M \to M'$ fulfils $\chi^*\omega' = \theta \cdot \omega$ for a smooth map $\theta\colon M \to \mathbb{R}$, then θ is constant, i.e. χ is a conformal symplectic map: since ω is closed,

$$0 = \chi^*(\mathrm{d}\omega') = \mathrm{d}\chi^*(\omega') = \mathrm{d}(\theta \cdot \omega) = \mathrm{d}\theta \wedge \omega + \theta \wedge \mathrm{d}\omega = \mathrm{d}\theta \wedge \omega.$$

By non-degeneracy of ω and $\dim M > 2$ it follows that θ is constant. Therefore, χ is a conformal symplectic map (Kobayashi, 1972). △

Before formulating the main theorem of this section, we prove the following lemma.

Lemma 8.3.1 (Conformal symplectic transformations of Hamiltonians)**.** *Let (M, ω, H) and (M', ω', H') be two Hamiltonian systems with flow maps ϕ_t and ϕ'_t, respectively. Consider a conformal symplectic diffeomorphism $\chi\colon M \to M'$ with $\chi^*\omega' = \theta \cdot \omega$ for $\theta \in \mathbb{R}$. If $H' \circ \chi = \eta \cdot H$ for $\eta \in \mathbb{R}$, then*

$$\chi \circ \phi_{(\eta/\theta)\cdot t} = \phi'_t \circ \chi$$

(wherever defined).

Proof. Since χ is a diffeomorphism and ω' is nondegenerate, $\chi^*\omega' = \theta \cdot \omega$ is nondegenerate such that $\theta \neq 0$. In particular, the time-scaling factor η/θ in the assertion is well-defined. Define Hamiltonian vector fields X_H and $X'_{H'}$ by

$$\mathrm{d}H = \iota_{X_H}\omega, \qquad \mathrm{d}H' = \iota_{X'_{H'}}\omega',$$

where $\iota_X\omega$ denotes the contraction of the 2-form ω with a vector field X. We calculate

$$\begin{aligned}\theta \cdot \iota_{\chi^*(X'_{H'})}\omega &= \iota_{\chi^*(X'_{H'})}(\chi^*\omega') = \chi^*\big(\iota_{X'_{H'}}\omega'\big)\\ &= \chi^*\mathrm{d}H' = \mathrm{d}(H' \circ \chi) = \eta \cdot \mathrm{d}H = \eta \cdot \iota_{X_H}\omega.\end{aligned}$$

Since $\theta \neq 0$ we have

$$\iota_{\chi^*(X'_{H'})}\omega = \frac{\eta}{\theta}\iota_{X_H}\omega = \iota_{(\eta/\theta)X_H}\omega = \iota_{X_{(\eta/\theta)\cdot H}}\omega.$$

By non-degeneracy of the symplectic form ω it follows that the vector fields $X_{(\eta/\theta)\cdot H}$ and $\chi^*X'_{H'}$ coincide. Notice further that if $\dot\gamma(t) = X_H(\gamma(t))$, then

$$\frac{\mathrm{d}}{\mathrm{d}t}\big(\gamma(\alpha t)\big) = \alpha\dot\gamma(\alpha t) = \alpha X_H(\gamma(\alpha t)) = X_{\alpha H}(\gamma(\alpha t))$$

for $\alpha \in \mathbb{R}$, i.e. $t \mapsto \gamma(\alpha t)$ is a flow line of the Hamiltonian vector field corresponding to the Hamiltonian αH. We can conclude that the following statements are equivalent.

- The curve $t \mapsto \gamma(t) \in M$ is a flow line of X_H through $\gamma(0)$ at $t = 0$.
- The curve $t \mapsto \gamma((\eta/\theta) \cdot t) \in M$ is a flow line of $X_{(\eta/\theta)\cdot H} = \chi^*X'_{H'}$ through $\gamma(0)$ at $t = 0$.
- The curve $t \mapsto (\chi \circ \gamma)((\eta/\theta) \cdot t) \in M'$ is a flow line of $X'_{H'}$ through $\chi(\gamma(0))$ at $t = 0$.

Thus

$$\chi \circ \phi_{(\eta/\theta)\cdot t} = \phi'_t \circ \chi.$$

□

Example 8.3.2. Consider the Hamiltonian

$$H(\alpha) = \frac{1}{2}\alpha(g^{-1}(\alpha)), \quad \alpha \in T^*N$$

from (8.1.1) on the cotangent bundle $(M = T^*N, \omega)$ over a smooth Riemannian manifold (N, g). The multiplicative Lie group of positive real numbers $\mathbb{R}^+ = (0, \infty)$ acts on M by the conformal symplectic diffeomorphisms $\chi_\theta \colon M \to M$, $\chi_\theta(\alpha) = \theta \cdot \alpha$ analysed in Example 8.3.1. We have $H \circ \chi_\theta = \theta^2 \cdot H$ such that for the Hamiltonian flow ϕ_t

$$\chi_\theta \circ \phi_{\theta \cdot t} = \phi_t \circ \chi_\theta \tag{8.3.3}$$

by Lemma 8.3.1. The motions of the Hamiltonian system (M, ω, H) correspond to the velocity vector fields of the geodesics on N under the bundle isomorphism between TN and T^*N defined by g. Therefore (8.3.3) corresponds to the fact that a geodesic γ' starting at $q \in N$ with initial velocity $\dot\gamma'(0) = \theta \cdot v \in T_qN$ reaches the same point $\gamma'(t) \in N$ after time t as a geodesic γ starting at $q \in N$ with initial velocity $\dot\gamma(0) = v \in T_qN$ after time $\theta \cdot t$ and the end velocities fulfil $\theta \cdot \dot\gamma'(t) = \dot\gamma(\theta \cdot t)$. △

8.3.2 Singularity obstructions for conformal symplectic Hamiltonian boundary value problems

Consider a Hamiltonian system $(\widetilde{M}, \omega, H)$ with Hamiltonian flow map denoted by ϕ_t and two Lagrangian submanifolds $\Lambda, \Lambda' \subset \widetilde{M}$. Denote the time-1-map ϕ_1 by ϕ and assume that there exists $z \in \Lambda$ with $z' = \phi(z) \in \Lambda'$. Consider the separated Lagrangian boundary value problem $(\phi, \Lambda, \Lambda')$ localised around $z \in M \subset \widetilde{M}$, $z' \in M' \subset \widetilde{M}$, where M, M' are open subsets of $\widetilde{M}$.

The following theorem shows that if H is invariant up to scaling under a conformal symplectic action of a k-dimensional Lie group acting tangentially to Λ at z and $X_H(z') \notin T_{z'}\Lambda'$, then the degeneracy of the singularity at z is at most $\frac{1}{2}\dim M - k$. This refines the statement of the Propositions 8.2.1 and 8.2.2 and applies, for instance, everywhere away from $y = 0$ to the Dirichlet-type problem (8.2.1) if H is homogeneous in y.

Theorem 8.3.2 (Singularity obstructions for conformal symplectic Hamiltonian boundary value problems)**.** *Consider a separated Lagrangian boundary value problem $(\phi, \Lambda, \Lambda')$ localised at a solution $z \in \Lambda \subset (M, \omega)$, $z' = \phi(z) \in \Lambda' \subset (M', \omega)$ in an ambient Hamiltonian system $(\widetilde{M}, \omega, H)$ with flow map ϕ_t denoting $\phi_1 = \phi$. Consider a Lie group G with action $g \mapsto \chi_g$ on $M \cup M'$ defined locally on a neighbourhood U of the neutral element $e \in G$ and the neighbourhood $\mathfrak{U} = \exp^{-1}(U)$ of 0 in the Lie algebra of G. Assume that there exist smooth maps $\theta, \eta \colon \mathfrak{U} \to \mathbb{R}$ such that for all $V \in \mathfrak{U}$*

1. *the action is conformal symplectic,* $\chi_{\exp(V)}^* \omega = \theta(V) \cdot \omega$,
2. *the Hamiltonian is invariant under the action up to scaling,* $H \circ \chi_{\exp(V)} = \eta(V) \cdot H$,
3. *the time scaling factor for the flow map is not stationary at* $s = 0$, *i.e.*

$$\frac{\mathrm{d}}{\mathrm{d}s}\bigg|_{s=0} \left(\frac{\eta(sV)}{\theta(sV)} \right) \neq 0, \tag{8.3.4}$$

4. *the group acts tangentially to* Λ *at* z, *i.e.* $V_z^\# \in T_z\Lambda$, *where* $V^\#$ *is the fundamental vector field corresponding to* V,
5. *and the Hamiltonian vector field is not tangential to* Λ' *at* z', *i.e.* $X_H(z') \notin T_{z'}\Lambda'$.

Then the degeneracy of a singularity of the Lagrangian boundary value problem at z *is at most* $\frac{1}{2} \dim M - \dim G$.

We prepare the proof of Theorem 8.3.2 by discussing the assumptions.

Remark 8.3.3. The assumptions of the theorem imply that $\theta(V) \neq 0$ for all $V \in \mathfrak{U}$ and

$$\theta(0) = 1 = \eta(0). \tag{8.3.5}$$

The quotient $\eta(sV)/\theta(sV)$ is the time-scaling factor appearing in Lemma 8.3.1. Applied to the setting of the theorem, the lemma says

$$\chi_{\exp(sV)} \circ \phi_{\eta(sV)/\theta(sV) \cdot t} = \phi_t \circ \chi_{\exp(sV)}. \tag{8.3.6}$$

△

Remark 8.3.4. Let $\dim M = 2n$ and $\dim G = k$. The non-stationary assumption (8.3.4) can be interpreted as a non-degeneracy assumption on the action. It implies that the intersections of the isotropy groups near z and z' with U are trivial and that the group orbits of G constitute a k-dimensional foliation around z and z'. In particular, $k \leq \frac{1}{2} \dim M$ due to the tangency condition. △

Remark 8.3.5. The non-stationary assumption (8.3.4) ensures that the time-scaling in (8.3.6) depends on s to linear order. This means that the assumptions do *not* apply to symplectic group actions leaving H invariant. △

Proof of Theorem 8.3.2. Step 1. We construct an integrable distribution $\mathcal{D}$ over M' with leaves consisting of orbit families and with $\mathcal{D}_{z'} = T_{z'}\Lambda'$.

Let $2n = \dim M'$ and $k = \dim G$. By Remark 8.3.4 we have $k \leq n$ and the orbits of the group action provide a k-dimensional foliation O of M' (shrinking M' around z' if necessary). There exists an $n - k$-dimensional manifold N containing z' which is

transversal to each orbit O_a with $a \in N$ such that $T_{z'}N \oplus T_{z'}O_{z'} = T_{z'}\Lambda'$. The collection of orbits $L_{z'} = \bigcup_{a\in N} O_a$ defines an n-dimensional submanifold of M'. By construction $T_{z'}L_{z'} = T_{z'}\Lambda'$.

We extend $L_{z'}$ to a foliation of M' as follows: shrinking M', if necessary, the projection map $\pi\colon M' \to M'/O$ to the $2n-k$-dimensional space of leaves is a submersion and $\pi(L_{z'})$ is a smooth, $n-k$-dimensional submanifold of M'/O (thought of as N). Shrinking M', if necessary, we find a foliation $\mathcal{L}$ of M'/O with leaf $\mathcal{L}_{\pi(z')} = \pi(L_{z'})$. The preimages of the leaves of $\mathcal{L}$ under π^{-1} form the desired foliation of M' and give rise to an integrable distribution $\mathcal{D}$.

Step 2. We show that the kernel of the map

$$\mathrm{d}\left[\phi_{|\Lambda}\right]\big|_z : T_z\Lambda \to T_{[z']}\left(M'/\mathcal{D}\right)$$

is at most $n-k$-dimensional such that the claim follows by Proposition 8.2.2. Let $V \in \mathfrak{U}$ with fundamental vector field $V^\#$. By assumption $V_z^\# \in T_z\Lambda$. We calculate

$$\begin{aligned}
\mathrm{d}\left[\phi_{|\Lambda}\right]\big|_z\left(V_z^\#\right) &= \frac{\mathrm{d}}{\mathrm{d}s}\Big|_{s=0}\left[\left(\phi_1 \circ \chi_{\exp(sV)}\right)(z)\right] \\
&\overset{(8.3.6)}{=} \frac{\mathrm{d}}{\mathrm{d}s}\Big|_{s=0}\left[\left(\chi_{\exp(sV)} \circ \phi_{\eta(sV)/\theta(sV)\cdot 1}\right)(z)\right] \\
&\overset{(*)}{=} \frac{\mathrm{d}}{\mathrm{d}s}\Big|_{s=0}\left[\left(\phi_{\eta(sV)/\theta(sV)\cdot 1}\right)(z)\right] \\
&= \left[\frac{\mathrm{d}}{\mathrm{d}s}\Big|_{s=0}\left(\frac{\eta(sV)}{\theta(sV)}\right)\cdot X_H\left(\phi_{\eta(0)/\theta(0)}(z)\right)\right] \\
&\overset{(8.3.5)}{=} \left[\underbrace{\frac{\mathrm{d}}{\mathrm{d}s}\Big|_{s=0}\left(\frac{\eta(sV)}{\theta(sV)}\right)}_{\neq 0 \text{ by } (8.3.4)}\cdot \underbrace{X_H(z')}_{\notin \mathcal{D}_{z'}=T_{z'}\Lambda'}\right] \\
&\neq 0.
\end{aligned}$$

The equality $(*)$ is due to the invariance of the distribution $\mathcal{D}$ under the group action. Since the Lie-algebra $\mathfrak{U}$ is k-dimensional and the fundamental vector fields $V^\#$ are independent at z we can conclude that the kernel of $\mathrm{d}\left[\phi_{|\Lambda}\right]\big|_z$ is at most $n-k$-dimensional. □

Theorem 8.3.2 applies to Hamiltonian systems where the Hamiltonian is homogeneous in the direction of Λ and Λ'.

Consider the cotangent bundle over a smooth manifold with symplectic coordinates $(x,y) = (x^1,\dots,x^n,y_1,\dots,y_n)$ and a homogeneous Hamiltonian in the y-coordinates. Then Theorem 8.3.2 applies to the Dirichlet-type problem (8.2.1) leading to the following proposition.

Proposition 8.3.3 (Singularity obstruction for separated Lagrangian boundary value problem in homogeneous Hamiltonian systems)**.** *Let* $(\mathbb{R}^{2n}, \sum \mathrm{d}x^j \wedge \mathrm{d}y_j, H)$ *be a Hamiltonian system with* $H(x, \lambda y) = \lambda^p H(x, y)$ *with* $p \neq 1$ *and* $\nabla_y H(x, y) \neq 0$ *for all* $y \neq 0$*. Then*

$$\dim \ker D_y \phi^X \leq n - 1,$$

at points which are not mapped to the $\{y = 0\}$*-subspace by the Hamiltonian time-1-map* ϕ*.*

Remark 8.3.6. The condition $H(x, y) \neq 0$ for $y \neq 0$ implies $\nabla_y H(x, y) \neq 0$ for $y \neq 0$ for homogeneous Hamiltonians in y. △

Proof of Proposition 8.3.3. We consider the positive real numbers $\mathbb{R}^+$ as a multiplicative Lie group with action $\chi_r(x, y) = (x, ry)$, $\theta(r) = r$ and $\eta(r) = r^p$. The action preserves the fibres $\{x\} \times \mathbb{R}^n$ of the cotangent bundle $T^*\mathbb{R}^n \cong \mathbb{R}^{2n}$. The assumption $p \geq 2$ implies that the time-scaling factor $\eta(r)/\theta(r) = r^{p-1}$ is not stationary at the neutral element 1 (in the sense of the non-stationary assumption (8.3.4)). Due to $\nabla_y H(x, y) \neq 0$ for $y \neq 0$ the Hamiltonian vector field X_H is not tangent to any fibre $\{x\} \times \mathbb{R}^n$ unless $y = 0$. Now the assertion follows by Theorem 8.3.2. □

Instead of referring to Theorem 8.3.2, we can also carry out the proof of Proposition 8.3.3 directly in local coordinates. It corresponds to choosing the vertical polarisation

$$\mathcal{D} = \operatorname{span}\left\{\frac{\partial}{\partial y_1}, \ldots, \frac{\partial}{\partial y_n}\right\},$$

in the theorem's proof.

Direct proof of Proposition 8.3.3. Let $(a, b) \in \mathbb{R}^n \times \mathbb{R}^n \cong \mathbb{R}^{2n}$ with $b \neq 0$. The map $y \mapsto \phi^X(a, y)$ has an n-dimensional domain space. We prove the claim by showing that $b \in \mathbb{R}^n \cong T_b\mathbb{R}^n$ is not an element of the kernel $\ker D_y \phi^X(a, b)$; the assertion then follows

by Proposition 8.2.1.

$$\begin{aligned}
\mathrm{D}\phi^X(a,b)\begin{pmatrix}0\\ b\end{pmatrix} &= \lim_{\epsilon\to 0}\frac{1}{\epsilon}\left((x\circ\phi_1)(a,(1+\epsilon)b)-(x\circ\phi_1)(a,b)\right)\\
&\overset{(*)}{=} \lim_{\epsilon\to 0}\frac{1}{\epsilon}\left((x\circ\phi_{(1+\epsilon)^{p-1}})(a,b)-(x\circ\phi_1)(a,b)\right)\\
&= \left.\frac{\mathrm{d}}{\mathrm{d}t}\right|_{t=1}(x\circ\phi_{t^{p-1}})(a,b)\\
&= (p-1)\mathrm{d}x(X_H(\phi_1(a,b)))\\
&= (p-1)\mathrm{d}x(X_H((x\circ\phi)(a,b),(y\circ\phi)(a,b)))\\
&= (p-1)\nabla_y H((x\circ\phi)(a,b),(y\circ\phi)(a,b))\\
&\neq 0,
\end{aligned}$$

where we have used Lemma 8.3.1 to obtain the equality $(*)$. □

Example 8.3.3. Proposition 8.3.3 applies to Hamiltonian systems with Hamiltonians of the form

$$H(x,y)=\frac{1}{2}y^\top A(x)y \quad \text{with} \quad A(x)\in \mathrm{GL}(n,\mathbb{R}) \text{ for all } x, \tag{8.3.7}$$

where $\mathrm{GL}(n,\mathbb{R})$ denotes the group of invertible matrices. (The restriction to invertible matrices forces $\nabla_y H(x,y)=0 \implies y=0$ as required in Proposition 8.3.3.) △

Remark 8.3.7. Recall that by the Darboux-Weinstein theorem Weinstein, 1971b, Thm. 7.1 polarisations transversal to a Lagrangian submanifold Λ give rise to symplectomorphisms from local neighbourhoods of Λ to neighbourhoods of the zero section in the cotangent bundle $T^*\Lambda$ such that the polarisation is carried to the vertical polarisation in $T^*\Lambda$. The canonical coordinates on the cotangent bundle $T^*\Lambda$ can be used to induce local symplectic coordinates on neighbourhoods of the submanifold Λ in the ambient symplectic manifold. This shows that the statement of Proposition 8.3.3 applies to Hamiltonians which are homogeneous in the direction of any polarisation tangential to the boundary condition. △

Example 8.3.4. To linearly independent $a^{(s)}=(a_1^{(s)},\dots,a_n^{(s)})\in\mathbb{R}^n$ with $1\le s\le k\le n$ consider the action of $(\mathbb{R}^+)^k=(0,\infty)^k$ on $(\mathbb{R}^{2n},\sum \mathrm{d}x^j\wedge\mathrm{d}y_j,H)$ by the conformal symplectic transformations $\chi_\lambda^{(s)}$ with

$$\begin{aligned}
x^j &\mapsto \lambda^{a_j^{(s)}}x^j\\
y_j &\mapsto \lambda^{c-a_j^{(s)}}y_j.
\end{aligned}$$

Assume that $H\circ\chi_\lambda^{(s)}=\lambda^p\cdot H$ for all $s\le k$. Without loss of generality, $c=1$. Assume that $p\neq 1$. Since scaling symmetries commute, the Lie group action is well-defined.

Moreover, the action fulfils the non-stationary assumption (8.3.4) since $p \neq 1$ and the $a^{(s)}$ are linearly independent.

If H is a polynomial and separated, i.e. its Hessian is of block-diagonal form, then H is of the form

$$H(x,y) = \sum_{b=1}^{m_1} \alpha_b \prod_{j=1}^{l_b^{(1)}} x^{\sigma_b^{(1)}(j)} + \sum_{b=1}^{m_2} \beta^b \prod_{j=1}^{l_b^{(2)}} y_{\sigma_b^{(2)}(j)}$$

with $m_1, m_2 \in \mathbb{N}_0$, $l_b^{(1)}, l_b^{(2)} \in \mathbb{N}_{>0}$, $\{\alpha_b\}_1^{m_1}, \{\beta_b\}_1^{m_2} \subset \mathbb{R} \setminus \{0\}$ and maps

$$\sigma_{b_\tau}^{(\tau)} \colon \{1, \dots, l_{b_\tau}^{(\tau)}\} \to \{1, \dots, n\} \quad \text{for } 1 \leq b_\tau \leq m_\tau,\ \tau \in \{1,2\}$$

such that for all $1 \leq s \leq k$

$$\forall 1 \leq b \leq m_1 : \sum_{j=1}^{l_b^{(1)}} a^{(s)}_{\sigma_b^{(1)}(j)} = p \quad \text{and} \quad \forall 1 \leq b \leq m_2 : \sum_{j=1}^{l_b^{(2)}} (1 - a^{(s)}_{\sigma_b^{(2)}(j)}) = p.$$

Let Λ be a Lagrangian submanifold which is tangent to the vector field

$$\sum_{j=1}^{n} a_j^{(s)} x^j \frac{\partial}{\partial x^j} + (1 - a_j^{(s)}) y_j \frac{\partial}{\partial y_j}$$

at z for all $s \leq k$ and let Λ' be any Lagrangian manifold transversal to the Hamiltonian vector field X_H. By Theorem 8.3.2, the maximal degeneracy of a singularity occurring in the Lagrangian boundary value problem $(\phi, \Lambda, \Lambda')$ for the time-1-map ϕ of the Hamiltonian flow at z is $n - k$. △

The following reformulation of Theorem 8.3.2 can be handy when considering conformal actions which naturally decompose into a conformal and a symplectic action.

Corollary 8.3.4. *Let $(\phi, \Lambda, \Lambda')$ be a separated Lagrangian boundary value problem localised around a solution $z \in \Lambda \subset (M, \omega)$, $z' = \phi(z) \in \Lambda' \subset (M', \omega')$ in an ambient Hamiltonian system $(\widetilde{M}, \omega, H)$ with time-1-map ϕ such that $X_H(z') \notin T_{z'}\Lambda'$. Let G be a Lie group acting conformally on M and M' by $g \mapsto \chi_g$ and symplectically by $g \mapsto \Psi_g$, where the actions are defined locally around a neighbourhood U of the neutral element $e \in G$ and the neighbourhood $\mathfrak{U} = \exp^{-1}(U)$ of 0 in the Lie algebra of G. Moreover, assume that for all $V \in \mathfrak{U}$ the fundamental vector fields $V^\#$ and $V^{\#\#}$ corresponding to the infinitesimal actions with V fulfil*

$$V_z^\# + V_z^{\#\#} \in T_z\Lambda.$$

Define $\theta \colon \mathfrak{U} \to \mathbb{R}$ by $\chi^*_{\exp(V)}\omega = \theta(V) \cdot \omega$ and assume there exists $\eta \colon \mathfrak{U} \to \mathbb{R}$ fulfilling

the non-stationary assumption (8.3.4) *such that for all* $V \in \mathfrak{U}$

$$H \circ \chi_{\exp(V)} \circ \Psi_{\exp(V)} = \eta(V) \cdot H.$$

Then the degeneracy of a singularity of the Lagrangian boundary value problem at z *is at most* $\frac{1}{2}\dim M - \dim G$.

Example 8.3.5. The scaling symmetries in Example 8.3.4 naturally decompose into symplectic scaling transformations $\Psi_\lambda^{(a)}$ with

$$x^j \mapsto \lambda^{a_j} x^j$$
$$y_j \mapsto \lambda^{-a_j} y_j$$

and the conformal symplectic transformation $\chi_\lambda(x, y) = (x, \lambda y)$ considered in Example 8.3.1. △

8.3.3 Geodesic bifurcations

Application of Theorem 8.3.2

Let us use the results obtained in Section 8.3.2 to analyse which singularities occur in conjugate loci on smooth Riemannian manifolds. As mentioned in the introductory example in Section 8.1, the motions of the Hamiltonian system $(T^*N, -\mathrm{d}\lambda, H)$ with

$$H(\alpha) = \frac{1}{2}\alpha\left(g^{-1}(\alpha)\right) \tag{8.3.8}$$

correspond to the velocity vector fields of geodesics on the smooth Riemannian manifold (N, g). Finding a geodesic which connects two points $x, X \in N$ corresponds to solving the boundary value problem

$$\pi(\alpha) = x, \quad (\pi \circ \Phi)(\alpha) = X, \tag{8.3.9}$$

where Φ is the time-1-map of the Hamiltonian flow on T^*N. Together with the observations in Example 8.3.2 and Theorem 8.3.2 reproves the following classical fact Flaherty and Carmo, 1992, Ch.5.

Proposition 8.3.5. *The dimension of the kernel of the geodesic exponential map on a Riemannian manifold is strictly less than the dimension of the manifold.*

As well as applying Theorem 8.3.2 directly to conclude Proposition 8.3.5, one can also use Proposition 8.3.3 because H takes the form (8.3.7) when expressed in canonical coordinates where A is the matrix representation of g^{-1} in the corresponding frame. Recall that if γ is a geodesic starting at time $t = 0$ at x with $\dot\gamma(0) = y$, then x and

$\gamma(1)$ are conjugate points if and only if the kernel of the exponential map evaluated at $y \in T_xN$ is nontrivial. The dimension of the kernel corresponds to the multiplicity of the conjugate points. Thus, Proposition 8.3.5 implies the following statement.

Proposition 8.3.6. *The multiplicity of conjugate points on an n-dimensional Riemannian manifold N cannot exceed $n-1$. In other words, at points in a conjugate locus with respect to some fixed point in N the degeneracy of a singularity is at most $n-1$.*

Remark 8.3.8. The space of Jacobi fields along a geodesic γ vanishing at $\gamma(0)$ corresponds to the space $T_{\gamma(0)}N$ via $J \mapsto \frac{\nabla}{\mathrm{d}t}J(0)$, where $\frac{\nabla}{\mathrm{d}t}$ denotes the covariant derivative along γ with respect to the Levi–Civita connection on (N, g). Classically, Proposition 8.3.6 is proved by noting that the Jacobi field $t \mapsto t\dot{\gamma}(t)$ along the curve γ does not vanish at $\gamma(1)$ Flaherty and Carmo, 1992, Ch.5. △

In the Examples 8.1.1 and 8.1.2 we saw isolated cusp singularities connected by lines of fold singularities in the conjugate locus of a 2-dimensional Gaussian and in the conjugate locus of a 2-dimensional ellipsoid embedded in $\mathbb{R}^3$ (Figure 8.1). The singularities persist under small perturbations of the metric or the reference point. The occurrence of fold and cusp singularities as generic singularities in conjugate loci on surfaces is not a coincidence. Consider the conjugate locus to a fixed-point x on an n-dimensional Riemannian manifold (N, g). The Hamiltonian boundary value problem (8.3.9) has n parameters given by the position of the endpoint X. Assuming that considering the position of the endpoint X as parameters of the boundary value problem (8.3.9) yields a versal unfolding of the corresponding critical-points-of-a-function problem and that no other obstructions than the one described by Theorem 8.3.2 apply (cf. Janeczko and Mostowski, 1995, p. 362), those singularities occur persistently, i.e. unremovably under small perturbations of the metric or the reference point, which occur as persistent singularities in the critical-points problem for families with n parameters in at most $n-1$ variables. By the classification results of catastrophe theory (see Section 5.4) this means that in conjugate loci on Riemannian surfaces fold (A_2) and cusp (A_3) singularities occur generically. Cusp singularities occur at isolated points and fold singularities in 1-parameter families.

If we allow the reference point x to vary as well on the manifold, then even more singularities can become generic phenomena because the corresponding Hamiltonian boundary value problem has $2n$ parameters, namely the reference point x and the endpoint X. However, the degeneracy of the singularities is still bounded by $n-1$. Again, assuming that considering x and X as parameters of the corresponding Hamiltonian boundary value problem (8.3.9) yields a versal unfolding of the problem, those singularities occur persistently which also occur persistently in the critical-points problem for families with $2n$ parameters in at most $n-1$ variables. On a Riemannian

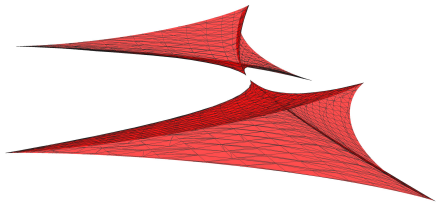

Figure 8.2: Elliptic umbilic bifurcation D_4^- in the conjugate-points-problem on a perturbed 3-dimensional ellipsoid embedded in $\mathbb{R}^4$. Three lines of cusps merge to an elliptic umbilic singularity. To capture this bifurcation numerically, preserving the symplectic structure of the problem when discretising is essential as will be explained in Chapter 9.

surface these are fold (A_2), cusp (A_3), swallowtail (A_4) and butterfly (A_5) singularities, where the singularities A_j occur generically in $5-j$-parameter families.

This recovers results from Waters, 2017 where the creation and annihilation of cusps in the conjugate locus on a surface is analysed by studying Jacobi's equations.

Further remarks on bifurcations in the conjugate points problem

There is a variety of aspects to the conjugate points problem on a Riemannian manifold. Fixing the reference point, the exponential map can be viewed as a Lagrangian map (Janeczko and Mostowski, 1995) for which singularities are classified (V. I. Arnold, Gusein-Zade, and Varchenko, 2012, Part III). Moreover, under non-degeneracy assumptions the conjugate locus of an exponential map with respect to a fixed reference point can locally be identified with families of skew-symmetric matrices (Weinstein, 1970). Illustrative and related to the presented viewpoint is a paper by Waters (2017) which includes an analysis of how the conjugate locus as a whole can bifurcate as the reference point moves on a surface. A functional analytic approach to the geodesic bifurcation problem (in an extended sense) can be found in Piccione, Portaluri, and Tausk, 2004. Calculating geodesics on submanifolds of the Euclidean space is often motivated by the task of finding distance minimising curves between two points. Several methods are presented in Baek, Deopurkar, and Redfield, 2007. An approach using geodesics as homotopy curves can be found in Thielhelm, Vais, and Wolter, 2015.

Moreover, we will examine implications of the symplectic structure in the problem for numerical computations in Chapter 9: a correctly captured elliptic umbilic bifurcation (D_4^-) in the conjugate locus of a perturbed 3-dimensional ellipsoid can be seen in Figure 8.2. Three lines of cusp bifurcations (A_3) merge in an elliptic umbilic point. If the symplectic structure was ignored in the discretisation of the problem, the lines of cusps would fail to merge and no elliptic umbilic point would be visible. Details will be discussed in Example 9.3.3.

Chapter 9

Bifurcation-preserving discretisations for Hamiltonian boundary value problems

Chapter 9 is an adaption of McLachlan and Offen, 2019; McLachlan and Offen, 2020b.

In this chapter we study numerical aspects of the theory presented so far. In particular, we show that symplectic integrators preserve all stable bifurcations of Hamiltonian boundary value problems and that nonsymplectic integrators do not. We provide a universal description of how umbilic bifurcations break when nonysmplectic integrators are used. Moreover, we show how extra structure induced by separated boundary value problems, including classical Dirichlet problems, can be exploited to numerically locate bifurcations. As seen in Chapter 8, geodesics connecting two points are an example of a Hamiltonian boundary value problem with separated boundary conditions. We introduce the jet-RATTLE method, a symplectic integrator that easily computes geodesics and their bifurcations. Finally, we study numerical aspects of the periodic pitchfork bifurcation discovered in Section 7.2, a codimension-1 bifurcation arising in Liouville integrable Hamiltonian systems. It is not preserved by either symplectic or nonsymplectic integrators, but in some circumstances symplecticity greatly reduces the error.

9.1 Motivation and introduction

Symplectic integrators can be excellent for Hamiltonian initial value problems. Reasons for this include their preservation of invariant sets like tori, good energy behaviour, nonexistence of attractors, and good behaviour of statistical properties. These all refer to *long-time* behaviour. They are directly connected to the dynamical behaviour of

symplectic maps $\varphi\colon M \to M$ on the phase space under iteration. Boundary value problems, in contrast, are posed for fixed (and often quite short) times. Symplecticity manifests as a symplectic map $\varphi\colon M \to M$ which is not iterated. Is there any point, therefore, for a symplectic integrator to be used on a Hamiltonian boundary value problem? In this chapter we show that symplectic integrators preserve bifurcations of Hamiltonian boundary value problems and that nonsymplectic integrators do not.

To draw valid conclusions from numerical results one has to make sure that the bifurcations in the boundary value problem for the exact flow are still present after discretisation. This is important for two reasons: bifurcations of high codimension act as *organising centres* (see Gilmore, 1993, Part I, Ch.7) in the bifurcation diagram. A high codimensional bifurcation determines which lower codimensional bifurcations occur in a neighbourhood of the singular point. It is, therefore, desirable to capture these correctly. Furthermore, bifurcation diagrams are typically computed using *continuation methods* (see Section 4.5): higher codimensional bifurcations can only be detected correctly if they are not broken in the discretised boundary value problem. This means, preservation of the bifurcation behaviour is a goal in its own right but also crucial for computations.

Relevant to this chapter are A-series bifurcations and D-series bifurcations as presented in Thom's list of classical catastrophes and Arnold's extension (see Tables 1.1 and 5.1). A-series bifurcations can be modelled as the qualitative change of the solution set to $\nabla g_\mu(x) = 0$ with $g_\mu(x) = x^{n+1} + \sum_{j=1}^{n-1} \mu_j x^j$ as the parameter μ is varied. They are denoted by A_n and the first instances are called *fold* ($n = 2$), *cusp* ($n = 3$), *swallowtail* ($n = 4$). The first two D-series bifurcations are given by $g_\mu(x, y) = x^3 \pm xy^2 + \mu_3(x^2 + y^2) + \mu_2 y + \mu_1 x$. They are denoted by $D_4^\pm$ and are called *hyperbolic umbilic bifurcation* (D_4^+) and *elliptic umbilic bifurcation* D_4^-. The bifurcations A_2, A_3, A_4, D_4^+, D_4^- are (in an appropriate equivalence relation) the only bifurcations which occur in generic Hamiltonian boundary value problems with up to three parameters as seen in previous chapters.

Symplecticity in Hamiltonian boundary value problems does not seem to have been addressed in the literature, even in very detailed numerical studies like Beyn and Thümmler, 2007; Galan-Vioque, Almaraz, and Macías, 2014. The AUTO software (Doedel, Champneys, Dercole, et al., 2007) is based on Gauss collocation, which is symplectic when the equations are presented in canonical variables. The two-point boundary-value codes MIRKDC (Enright and Muir, 1996), TWPBVP (Cash, Hollevoet, et al., 2013) and TWPBVPL (Bashir-Ali, Cash, and H. H. M. Silva, 1998; Cash and Mazziay, 2006) are based on non-symplectic Runge–Kutta methods. MATLAB's `bvp4c` uses 3-stage Lobatto IIIA (Kierzenka and Shampine, 2001), which is not symplectic. Note that symplectic integration sometimes requires the use of implicit methods. For

initial value problems, these are typically computationally more expensive than explicit methods. However, for boundary value problems solved in the context of parameter continuation, this distinction largely disappears as excellent initial approximations are available. Other approaches like Grass and Uecker, 2017; Uecker, 2016 use the code TOM (Mazzia, Sestini, and Trigiante, 2006; Mazzia, Sestini, and Trigiante, 2009; Mazzia and Trigiante, 2004). Moreover, Hamiltonian boundary value methods, designed to preserve Hamiltonians up to any fixed polynomial order, can be used where energy conservation is essential (Amodio, Brugnano, and Iavernaro, 2015; Brugnano, Iavernaro, and Trigiante, 2015).

The remainder of the chapter is structured as follows.

- In Section 9.2 we analyse how bifurcations of the gradient-zero problem break if perturbed with a map which does not admit a primitive. This models the effect of using a non-symplectic integrator to solve Lagrangian boundary value problems in Hamiltonian systems.
- In Section 9.3 we analyse separated Lagrangian boundary conditions which include classical Dirichlet-, Neumann- and Robin- boundary conditions.
  - We describe structure present in data which is computed when numerically solving separated Lagrangian boundary value problems. This can be helpful to locate bifurcations. As an example, a D-series bifurcation in a Hénon-Heiles type Hamiltonian system is computed numerically.
  - We explain the role of symplecticity in the computation of conjugate loci and illustrate how the RATTLE method can be used in this context.
- In Section 9.4 we describe how periodic pitchfork bifurcations introduced in Section 7.2 in completely integrable Hamiltonian systems can be captured numerically. This involves
  - a description of the bifurcation mechanism of the exponentially small broken pitchfork bifurcation in the numerical flow of a planar Hamiltonian system,
  - the development of a nontrivial, analytical 4-dimensional model system with a periodic pitchfork bifurcation and numerical experiments showing that the bifurcation in the numerical flow is broken up to the order of the integrator,
  - theoretical considerations showing that the pitchfork bifurcation is captured exponentially well by a symplectic integrator in important cases of completey integrable systems like planar systems or systems with affine-linear integrals of motion. In general completely integrable systems, however, the bifurcation is captured up to the order of the integrator used to discretise Hamilton's equations.

9.2 Broken gradient-zero bifurcations

In applications symplectic maps arise as flow maps of Hamiltonian systems (Hamiltonian diffeomorphisms). These can be discretised using different numerical integrators.

Definition 9.2.1 (symplectic integrator)**.** A symplectic integrator assigns to a time-step-size $h > 0$ (discretisation parameter) and a Hamiltonian system a symplectic map which approximates the time-h-map of the Hamiltonian flow of the system. △

Remark 9.2.1. For a finite sequence of positive time-step-sizes $h_1, \dots, h_N$ summing to τ the composition of all time-h_j-map approximations obtained by a symplectic integrator yields an approximation to the Hamiltonian-time-τ-map, which is a symplectic map. △

Remark 9.2.2 (non-symplectic integrator). When using the term non-symplectic integrator (applied to a Hamiltonian system) we require the obtained approximations of Hamiltonian-time-τ-maps to constitute nowhere symplectic maps on the phase space. This excludes non-generic examples where an approximation happens to be symplectic on some open subsets of the phase space. △

Recall that two map-families are (right-left) equivalent if they coincide up to suitable reparametrisation and parameter dependent changes of variables in the domain and target space. Consider a family of Hamiltonian Lagrangian boundary value problems and consider an approximation of the Hamiltonian-time-τ-map by an integrator. If the family of maps corresponding to the discretised problems by the procedure described in Section 6.4 is equivalent to the family of maps for the exact problem, then we say *the integrator preserves the bifurcation of the problem.* This means the computed bifurcation diagram qualitatively looks the same as the exact bifurcation diagram.

Proposition 9.2.1. *A symplectic integrator with any fixed (but not necessarily uniform) step-size, applied to any autonomous or nonautonomous Hamiltonian Lagrangian boundary value problem, preserves stable bifurcations of any codimension for sufficiently small maximal step-sizes.*

Proof. A Hamiltonian diffeomorphism which is slightly perturbed by a symplectic integrator is a symplectic map near the exact flow map. Therefore, an application of a symplectic integrator introduces a small perturbation of the Hamiltonian boundary value problem within the class of Lagrangian boundary value problems for symplectic maps. The considered bifurcations are stable under such perturbations. □

Proposition 9.2.1 implies that using a symplectic integrator to solve Hamilton's equations in order to solve a Lagrangian boundary value problem we obtain a bifurcation diagram which is qualitatively correct even when computing with low accuracy and not preserving energy.

In contrast, nonsymplectic integrators do not preserve all bifurcations, even for arbitrary small step-sizes. However, they do preserve the simplest class of A-series bifurcations, i.e. folds, cusps, swallowtails, butterflies, ...

Proposition 9.2.2. *A symplectic or non-symplectic integrator with any fixed (but not necessarily uniform) step-size, applied to any autonomous or nonautonomous Hamiltonian Lagrangian boundary value problem, preserves bifurcations of stable A-series singularities for sufficiently small maximal step-sizes. However, each non-symplectic integrator breaks the bifurcations of all stable D-series singularities for any positive maximal step-size.*[1]

Remark 9.2.3. For the fold bifurcation in the Bratu problem (see Figure 6.1) the proposition says that any integrator with fixed step-size will capture the bifurcation correctly, i.e. the bifurcation diagram of the discretised system will qualitatively look the same as Figure 6.1. △

Proof of Proposition 9.2.2. As explained in Chapter 6, solutions to Hamiltonian boundary value problems locally correspond to the roots of an $\mathbb{R}^{2n}$-valued function F defined on an open subset of $\mathbb{R}^{2n}$ with F arising as the gradient of a scalar-valued map. A small perturbation of the symplectic flow map corresponds to a small perturbation $\tilde{F}$ of F. The map $\tilde{F}$ has gradient structure if and only if the perturbation of the map is symplectic. This is because the primitives of F and $\tilde{F}$ correspond to the difference of a generating function for the symplectic flow and a generating function for the Lagrangian boundary condition. The existence of the primitives is equivalent to the symplecticity of the flow and the Lagrangian nature of the boundary condition. As the boundary condition is not perturbed, whether the perturbed flow map is a symplectic map is equivalent to whether $\tilde{F}$ admits a primitive.

A-series bifurcations are stable in the roots-of-a-function problem and are, therefore, persistent under any small perturbation of F. This is not true for D-series bifurcations: there is no versal unfolding of the roots-of-a-function type singularity ∇g corresponding to the singularity $D^{\pm}_{k+2}$ $(k \geq 2)$ represented by $g(x, y) = x^2 y \pm y^{k+1}$ by exact maps as we will see from Lemma 9.2.3. Indeed, in Proposition 9.2.4 we will prove that D-series bifurcations either decompose into A-series bifurcations or vanish. □

Before formulating and proving Lemma 9.2.3 and, thus, completing the proof of Proposition 9.2.2, let us take a closer look at the first two D-series bifurcations. Denote the unfolding of the hyperbolic umbilic singularity D^{+}_{4} with parameter μ by

$$g_\mu(x, y) = x^3 + xy^2 + \mu_3(x^2 + y^2) + \mu_2 y + \mu_1 x.$$

[1] More generally, a generic singularity $g(x^1, \ldots, x^n)$ of the exact flow is broken in the numerical flow of a non-symplectic integrator if and only if for a versal unfolding $(g_\mu)_\mu$ of g the family $(\nabla g_\mu(x^1, \ldots, x^n))_\mu$ does not constitute a versal roots-of-a-function-type unfolding.

As the bifurcation diagram to the problem $\nabla g_\mu(x,y) = 0$ is too high-dimensional to visualise, the left plot in Figure 9.1 shows the corresponding level bifurcation set, i.e. the set of points in the parameter space at which a bifurcation occurs, which is given as

$$\{\mu \in \mathbb{R}^3 \,|\, \exists (x,y) \in \mathbb{R}^2 : \nabla g_\mu(x,y) = 0,\ \det \operatorname{Hess} g_\mu(x,y) = 0\}. \tag{9.2.1}$$

The plot to the right of Figure 9.1 shows a perturbed version of the hyperbolic umbilic bifurcation, which is the set

$$\{\mu \in \mathbb{R}^3 \,|\, \exists (x,y) \in \mathbb{R}^2 : \nabla g_\mu(x,y) + f_\epsilon(x,y) = 0,\ \det \mathrm{D}(\nabla g_\mu + f_\epsilon)(x,y) = 0\} \tag{9.2.2}$$

for $\epsilon \neq 0$ near 0 and a smooth family of maps $f_\epsilon \colon \mathbb{R}^2 \to \mathbb{R}^2$ with $f_0 = 0$ such that $f_\epsilon \neq \nabla h_\epsilon$ for any $h_\epsilon \colon \mathbb{R}^2 \to \mathbb{R}$ unless $\epsilon = 0$. Here $\mathrm{D}(\nabla g_\mu + f_\epsilon)(x,y)$ denotes the Jacobian matrix of the map $(x,y) \mapsto (\nabla g_\mu + f_\epsilon)(x,y)$.

Each point in the sheets corresponds to a fold singularity (A_2) and points on edges to cusp singularities (A_3). At parameter values where the sheets self-intersect there are two simultaneous fold singularities in the phase space. In the unperturbed system two lines of simultaneous folds merge with a line of cusps to a hyperbolic umbilic point Gilmore, 1993, p. I.5. In the perturbed picture the line of cusps decomposes into three segments and two swallowtail points (A_4) occur where two lines of cusps merge with a line of simultaneous folds. Notice that there are no swallowtail points in the unperturbed level bifurcation set.

Figure 9.2 shows a level bifurcation set of an elliptic umbilic singularity (D_4^-) and a perturbed version of the gradient-zero problem with a map that does not admit a primitive. Here we use the universal unfolding

$$g_\mu(x,y) = x^3 - xy^2 + \mu_3(x^2+y^2) + \mu_2 y + \mu_1 x.$$

We see that in the perturbed picture the lines of cusps fail to merge such that there is no elliptic umbilic point but only folds and cusp bifurcations.

In the remainder of this section we will prove

- a general formula useful to analyse how D-series bifurcations deconstruct under perturbations which do not respect the gradient structure modelling a non-symplectic discretisation (Lemma 9.2.3),
- that the situations displayed in Figures 9.1 and 9.2 are universal, i.e. all general roots-of-a-function type perturbations have the same described effects (Propositions 9.2.6 and 9.2.7)
- and that non-gradient-like perturbations decompose D-series singularities into A-series singularities (Proposition 9.2.4).

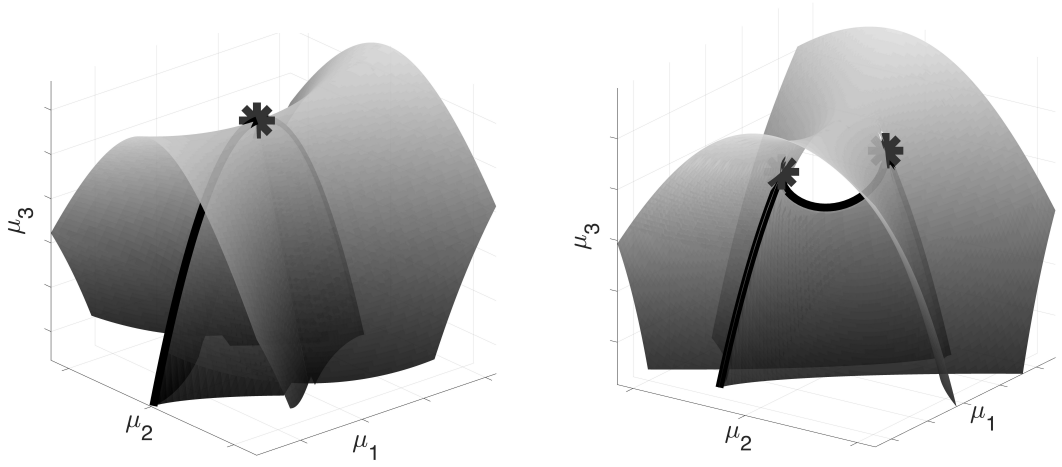

Figure 9.1: The plots show those configurations of the parameters μ_1, μ_2, μ_3 for which the problem $\nabla g_\mu(x, y) = 0$ or $(\nabla g_\mu + f_\epsilon)(x, y) = 0$ becomes singular. Imagine moving around the parameter μ and watching the solutions bifurcating in the phase space. As μ crosses a sheet two solutions merge and vanish or are born (fold - A_2). For μ in the intersection of two sheets there are two simultaneous fold singularities at different positions in the phase space. Crossing an edge three solutions merge into one (or vice versa). Points contained in an edge correspond to cusp singularities. At the marked point in the left plot of the unperturbed problem there is a hyperbolic umbilic singularity. Moving the parameter μ upwards along the μ_3 axis through the singular point four solutions merge and annihilate. In the perturbed version to the right the hyperbolic umbilic point decomposes into two swallowtail points. While the left plot illustrates the behaviour of a symplectic integrator which will correctly show a hyperbolic umbilic bifurcation D_4^+, the right plot illustrates the behaviour of a non-symplectic integrator which will incorrectly show two nearby swallowtail bifurcations (A_4). For a rotating animation see Offen, 2019c.

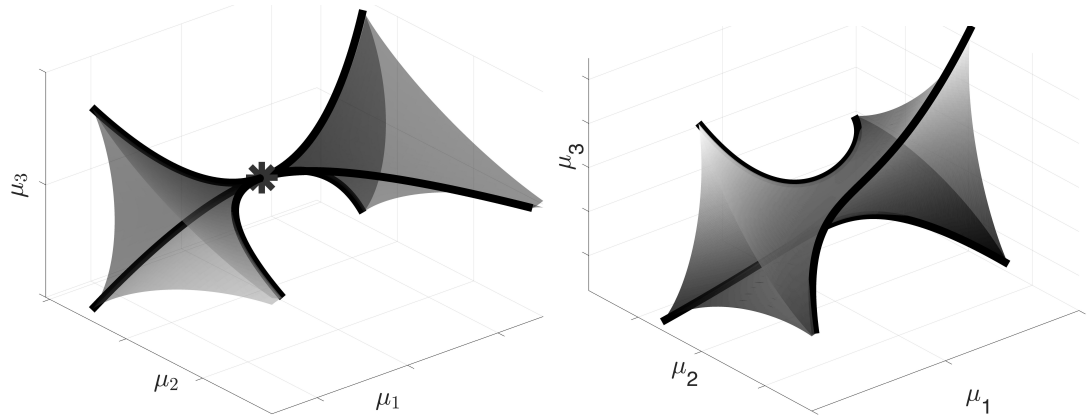

Figure 9.2: An exact (left) and a perturbed (right) version of the bifurcation level set of an elliptic umbilic singularity D_4^-. The elliptic umbilic point marked by an asterisk in the left plot is not present in the right plot where three lines of cusps fail to merge. The left figure illustrates a bifurcation diagram obtained by a symplectic integrator correctly showing a D_4^- singularity, the plot to the right illustrates using a non-symplectic integrator incorrectly showing no elliptic umbilic point. For a rotating animation see Offen, 2019b.

For this we will use the algebraic framework developed by Mather and presented, e.g. in the second lecture on C^∞ stability and classification by Wall (1971). The following lemma analyses how D-series singularities unfold in the roots-of-a-function problem and completes the proof of Proposition 9.2.2.

Lemma 9.2.3. *Consider the D-series singularity $D_{k+2}^{\pm}$ ($k \geq 2$) defined by the germ $g(x,y) = x^2y \pm y^{k+1}$. A universal unfolding of ∇g in the free module of rank 2 over the ring $\mathbb{R}[[x,y]]$ of formal power series in the variables x and y is given as*

$$f_\mu(x,y) = \begin{pmatrix} 2xy \\ x^2 \pm (k+1)y^k \end{pmatrix} + \mu_1 \begin{pmatrix} 1 \\ 0 \end{pmatrix} + \mu_2 \begin{pmatrix} 0 \\ 1 \end{pmatrix} + \mu_3 \begin{pmatrix} x \\ 0 \end{pmatrix} + \mu_4 \begin{pmatrix} y \\ 0 \end{pmatrix} + \sum_{j=1}^{k-2} \mu_j \begin{pmatrix} 0 \\ y^j \end{pmatrix}.$$

Proof. Wall (1971, p.187) describes a process developed by Mather to obtain universal unfoldings of topological singularities in the module $\mathcal{M}\mathbb{R}[[x,y]]^2$, where $\mathcal{M}$ is the maximal ideal of the local ring $\mathbb{R}[[x,y]]$. Let us imitate this procedure in the bigger module $\mathbb{R}[[x,y]]^2$ to unfold the singularity

$$f(x,y) = \nabla g(x,y) = \begin{pmatrix} 2xy \\ x^2 \pm (k+1)y^k \end{pmatrix}.$$

We obtain relations r_1 and r_2 as the components of f. Let I be the ideal in $\mathbb{R}[[x,y]]$

generated by the components

$$r_1 = 2xy \quad \text{and} \quad r_2 = x^2 \pm (k+1)y^k$$

of f and let $\partial_1 r$ and $\partial_2 r$ be the first and second vector of the Hessian matrix of f, i.e.

$$\partial_1 r = \begin{pmatrix} \frac{\partial r_1}{\partial x} \\ \frac{\partial r_2}{\partial x} \end{pmatrix} = 2\begin{pmatrix} y \\ x \end{pmatrix}, \quad \partial_2 r = \begin{pmatrix} \frac{\partial r_1}{\partial y} \\ \frac{\partial r_2}{\partial y} \end{pmatrix} = \begin{pmatrix} 2x \\ \pm k(k+1)y^{k-1} \end{pmatrix}.$$

Let L be the submodule generated by $I\mathbb{R}[[x,y]]^2$, $\partial_1 r$ and $\partial_2 r$ in $\mathbb{R}[[x,y]]^2$ (rather than in $\mathcal{M}\mathbb{R}[[x,y]]^2$ as in Wall, 1971, p. 187). To understand the quotient

$$Q = \mathbb{R}[[x,y]]^2 / L$$

of the $\mathbb{R}[[x,y]]$-modules $\mathbb{R}[[x,y]]^2$ and L we notice that in the quotient Q

$$\left[\begin{pmatrix} xy \\ 0 \end{pmatrix}\right] = \left[\begin{pmatrix} 0 \\ 0 \end{pmatrix}\right] = \left[\begin{pmatrix} 0 \\ xy \end{pmatrix}\right]$$

due to relation r_1. Using this, $k \geq 2$ and the relations r_2, $\partial_1 r$ and $\partial_2 r$ it follows that

$$\begin{aligned}
\left[\begin{pmatrix} x^2 \\ 0 \end{pmatrix}\right] &= \frac{1}{2}x\left[\begin{pmatrix} 2x \\ 0 \end{pmatrix}\right] = \frac{1}{2}x\left[\begin{pmatrix} 0 \\ \mp k(k+1)y^{k-1} \end{pmatrix}\right] = \mp\frac{1}{2}k(k+1)y^{k-2}\left[\begin{pmatrix} 0 \\ xy \end{pmatrix}\right] = \left[\begin{pmatrix} 0 \\ 0 \end{pmatrix}\right] \\
\left[\begin{pmatrix} y^2 \\ 0 \end{pmatrix}\right] &= y\left[\begin{pmatrix} y \\ 0 \end{pmatrix}\right] = y\left[\begin{pmatrix} 0 \\ -x \end{pmatrix}\right] = -\left[\begin{pmatrix} 0 \\ xy \end{pmatrix}\right] = \left[\begin{pmatrix} 0 \\ 0 \end{pmatrix}\right] \\
\left[\begin{pmatrix} 0 \\ x^2 \end{pmatrix}\right] &= x\left[\begin{pmatrix} 0 \\ x \end{pmatrix}\right] = x\left[\begin{pmatrix} -y \\ 0 \end{pmatrix}\right] = -\left[\begin{pmatrix} xy \\ 0 \end{pmatrix}\right] = \left[\begin{pmatrix} 0 \\ 0 \end{pmatrix}\right] \\
\left[\begin{pmatrix} 0 \\ y^k \end{pmatrix}\right] &= \pm\frac{1}{k+1}\left[\begin{pmatrix} 0 \\ \pm(k+1)y^k \end{pmatrix}\right] = \pm\frac{1}{k+1}\left[\begin{pmatrix} 0 \\ \mp x^2 \end{pmatrix}\right] = \left[\begin{pmatrix} 0 \\ 0 \end{pmatrix}\right].
\end{aligned}$$

Therefore, any element in Q is of the form

$$\left[\begin{pmatrix} c + \alpha x + \beta y \\ d + \gamma x + \sum_{j=1}^{k-1} \delta_j y^j \end{pmatrix}\right]$$

for $c, \alpha, \beta, d, \gamma, \delta_j \in \mathbb{R}$. Due to $\partial_1 r$ and $\partial_2 r$ we can assume without loss of generality that γ and δ_{k-1} vanish. We obtain

$$Q = \operatorname{span}_{\mathbb{R}}\left\{\left[\begin{pmatrix} 1 \\ 0 \end{pmatrix}\right], \left[\begin{pmatrix} 0 \\ 1 \end{pmatrix}\right], \left[\begin{pmatrix} x \\ 0 \end{pmatrix}\right], \left[\begin{pmatrix} y \\ 0 \end{pmatrix}\right], \left[\begin{pmatrix} 0 \\ y \end{pmatrix}\right], \left[\begin{pmatrix} 0 \\ y^2 \end{pmatrix}\right], \ldots, \left[\begin{pmatrix} 0 \\ y^{k-2} \end{pmatrix}\right]\right\}.$$

Here $\operatorname{span}_{\mathbb{R}}\{.,\ldots,.\}$ denotes the space of all linear combinations of the elements listed between the brackets using coefficients in $\mathbb{R}$. Since the set of all calculated spanning elements is linearly independent in Q, we can use their representatives to unfold f universally in $\mathbb{R}[[x,y]]$. □

Remark 9.2.4. The roots-of-a-function type singularity ∇g which corresponds to the singularity $D^{\pm}_{k+2}$ $(k \geq 2)$ represented by the map germ $g(x,y) = x^2 y \pm y^{k+1}$ is classified as $B_{2,k}$ for D^{+}_{k+2} and as $B'_{2,k}$ for D^{-}_{k+2} in Du Plessis and Wall, 1995, p. 268. If k is odd, then the classes D^{+}_{k+2} and D^{-}_{k+2} as well as $B_{2,k}$ and $B'_{2,k}$ coincide. The hyperbolic umbilic D^{+}_{4} corresponds to $B_{2,2}$, the elliptic umbilic D^{-}_{4} to $B'_{2,2}$ and the parabolic umbilic D_5 to $B_{3,2}$. △

Remark 9.2.5. In Mather's work and in Wall's lecture notes Wall, 1971, p. 198 the B series is denoted by I, II, IV. In particular, the singularity $B_{2,2}$ is denoted as $I_{2,2}$, $B'_{2,2}$ as $II_{2,2}$ and $B_{3,2}$ as $I_{2,3}$. △

Proposition 9.2.4. *A non-symplectic integrator with any fixed (but not necessarily uniform) step-size, applied to any autonomous or nonautonomous generic Hamiltonian Lagrangian boundary value problem decomposes D-series singularities into A-series singularities for any positive maximal step-size.*

Proof. Let g_μ be a smooth family of maps with a D-series singularity. To prove the assertion, we need to show that in any general roots-of-a-function type perturbation of the problem $\nabla g_\mu = 0$ around the singular point only A-series singularities occur.

By singularity theory, the family g_μ is stably right-left equivalent to an unfolding of the D-series bifurcation defined by the germ

$$g(x,y) = x^2 y \pm y^{k+1} \quad (k \geq 2).$$

By Lemma 9.2.3, a general perturbation of the problem $\nabla g_\mu = 0$ will, after a further change of variables, be of the form

$$f_{\mu,\tilde{\mu}}(x,y) = \nabla(g_\mu + h_{\mu,\tilde{\mu}})(x,y) + \begin{pmatrix} y \\ 0 \end{pmatrix}.$$

Since the Jacobian matrix $\mathrm{D} f_{\mu,\tilde{\mu}}(x,y)$ cannot vanish, only those singularities can occur which require a rank-drop of at most 1. These are exactly the A-series singularities. □

To analyse the breaking of hyperbolic and elliptic umbilic singularities D^{+}_{4} and D^{-}_{4} it is convenient to formulate the following special case of Lemma 9.2.3.

Lemma 9.2.5. *Consider the germ defined by $g(x,y) = x^2y \pm y^3$. A universal unfolding of ∇g in $\mathbb{R}[[x,y]]^2$ is given by*

$$f_\mu(x,y) = \begin{pmatrix} 2xy \\ x^2 \pm 3y^2 \end{pmatrix} + \mu_1 \begin{pmatrix} 1 \\ 0 \end{pmatrix} + \mu_2 \begin{pmatrix} 0 \\ 1 \end{pmatrix} + \mu_3 \begin{pmatrix} \mp x \\ y \end{pmatrix} + \mu_4 \begin{pmatrix} y \\ 0 \end{pmatrix}.$$

Proof. If $k = 2$ in the proof of Lemma 9.2.3, then

$$\partial_2 r = \begin{pmatrix} 2x \\ \pm 6y \end{pmatrix}.$$

Therefore

$$\left[\begin{pmatrix} x \\ 0 \end{pmatrix}\right] = \frac{1}{4}\left[\begin{pmatrix} x \\ 0 \end{pmatrix}\right] + \frac{3}{4}\left[\begin{pmatrix} x \\ 0 \end{pmatrix}\right] = \frac{1}{4}\left[\begin{pmatrix} 0 \\ \mp 3y \end{pmatrix}\right] + \frac{3}{4}\left[\begin{pmatrix} x \\ 0 \end{pmatrix}\right] = \mp\frac{3}{4}\left[\begin{pmatrix} \mp x \\ y \end{pmatrix}\right].$$

Thus,

$$Q = \operatorname{span}_{\mathbb{R}}\left\{\left[\begin{pmatrix} 1 \\ 0 \end{pmatrix}\right], \left[\begin{pmatrix} 0 \\ 1 \end{pmatrix}\right], \left[\begin{pmatrix} x \\ 0 \end{pmatrix}\right], \left[\begin{pmatrix} y \\ 0 \end{pmatrix}\right]\right\}$$

obtained by Lemma 9.2.3 can be rewritten to

$$Q = \operatorname{span}_{\mathbb{R}}\left\{\left[\begin{pmatrix} 1 \\ 0 \end{pmatrix}\right], \left[\begin{pmatrix} 0 \\ 1 \end{pmatrix}\right], \left[\begin{pmatrix} \mp x \\ y \end{pmatrix}\right], \left[\begin{pmatrix} y \\ 0 \end{pmatrix}\right]\right\}.$$

We obtain the asserted unfolding. □

The lemmas provide the tools needed to analyse how D-series bifurcations decompose if perturbed within the roots-of-a-function problem. This models the effect of using a non-symplectic integrator to resolve a D-series bifurcation in a Hamiltonian boundary value problem. The following proposition shows that the situation shown in Figure 9.1 for the hyperbolic umbilic D_4^+ is universal.

Proposition 9.2.6. *A hyperbolic umbilic singularity D_4^+ in the critical-points problem $\nabla g_\mu = 0$ for a smooth family of real valued maps g_μ decomposes into two swallowtail points A_4 under a small, general perturbation, i.e. a perturbation that does not respect the gradient structure.*

Proof. By singularity theory, the family g_μ is stably right-left equivalent to the universal unfolding

$$g_\mu(x,y) = y^3 + x^2y + \mu_3(y^2 - x^2) + \mu_2 y + \mu_1 x$$

(see Table 1.1) of the singularity D_4^+. Comparing ∇g_μ with the unfolding obtained in Lemma 9.2.5 we see that ∇g_μ constitutes an unfolding of ∇g in $\mathbb{R}[[x,y]]^2$ which can be

made universal by adding the term $\mu_4 \begin{pmatrix} y \\ 0 \end{pmatrix}$. This gives

$$f_\mu(x,y) = \begin{pmatrix} 2xy \\ x^2+3y^2 \end{pmatrix} + \mu_1 \begin{pmatrix} 1 \\ 0 \end{pmatrix} + \mu_2 \begin{pmatrix} 0 \\ 1 \end{pmatrix} + 2\mu_3 \begin{pmatrix} -x \\ y \end{pmatrix} + \mu_4 \begin{pmatrix} y \\ 0 \end{pmatrix}.$$

Let us fix $\mu_4 \neq 0$. Only A-series bifurcations are possible because the Jacobian Df_μ cannot vanish. A-series bifurcations are determined by their codimension. We have

$$\det Df_\mu(x,y) = -4\left(x + \frac{\mu_4}{4}\right)^2 + 12\left(y - \frac{\mu_3}{3}\right)^2 + \frac{1}{4}\mu_4^2 - \frac{16}{3}\mu_3^2.$$

At values x, y, μ_3 with $\det Df_\mu(x,y) = 0$ bifurcations occur with parameters μ_1, μ_2 uniquely determined by $f_\mu(x,y) = 0$. If $\mu_3 \notin \{-\frac{\sqrt{3}}{8}\mu_4, \frac{\sqrt{3}}{8}\mu_4\}$, then we see codimension-2 bifurcations, i.e. cusp bifurcations, with cusp points lying on hyperbolas. For $\mu_3 \in \{-\frac{\sqrt{3}}{8}\mu_4, \frac{\sqrt{3}}{8}\mu_4\}$ the cusps merge to codimension-3 bifurcations, i.e. swallowtail bifurcations with swallowtail points at $(x,y) = (-\frac{1}{4}\mu_4, \pm\frac{\sqrt{3}}{24}\mu_4)$. □

An alternative, simpler but less general calculation for D_4^+ can be found in Appendix A. The following proposition shows that the situation shown in Figure 9.2 for the elliptic umbilic D_4^- is universal.

Proposition 9.2.7. *If a generic smooth family of maps $\nabla g_\mu = 0$ for real valued maps g_μ has an elliptic umbilic singularity, then a small, general perturbation in the module $\mathbb{R}[[x,y]]^2$ will decompose the singularity into three separated lines of cusps.*

Proof. By singularity theory, the family g_μ is stably right-left equivalent to

$$g_\mu(x,y) = y^3 - x^2y + \mu_3(x^2+y^2) + \mu_2 y + \mu_1 x$$

(see Table 1.1). By Lemma 9.2.3 the family ∇g_μ constitutes a unfolding of ∇g in $\mathbb{R}[[x,y]]^2$ which can be made universal by adding the term $\mu_4 \begin{pmatrix} y \\ 0 \end{pmatrix}$. This gives

$$f_\mu(x,y) = \begin{pmatrix} -2xy \\ 3y^2 - x^2 \end{pmatrix} + \mu_1 \begin{pmatrix} 1 \\ 0 \end{pmatrix} + \mu_2 \begin{pmatrix} 0 \\ 1 \end{pmatrix} + 2\mu_3 \begin{pmatrix} x \\ y \end{pmatrix} + \mu_4 \begin{pmatrix} y \\ 0 \end{pmatrix}.$$

We have

$$\det \mathrm{D} f_\mu(x,y) = -4\left(x - \frac{\mu_4}{4}\right)^2 - 12\left(y - \frac{\mu_3}{3}\right)^2 + \frac{16}{3}\mu_3^2 + \frac{1}{4}\mu_4^2. \tag{9.2.3}$$

At any μ_3, μ_4, x, y with $\det \mathrm{D} f_\mu(x,y) = 0$ a bifurcation takes place with parameters μ_1, μ_2 uniquely determined by $f_\mu(x,y) = 0$. Inspecting (9.2.3) we see that the

codimension-2 cusp bifurcations, which occur for $\mu_4 = 0$, survive a perturbation but cannot merge to a higher codimensional bifurcation if $\mu_4 \neq 0$. □

Singularities that are stable in the gradient-zero-problem but unstable in the roots-of-a-function problem decompose under small perturbations into singularities which are stable in the roots-of-a-function problem. The process can remove high-codimensional singularities and can make singularities occur which do not exist in the exact problem. This illustrates that the roots-of-a-function problem is different to the gradient zero problem and demonstrates the importance of the preservation of symplectic structure when computing bifurcation diagrams for Hamiltonian boundary value problems.

9.3 Separated Lagrangian problems

Given the significance of Dirichlet-, Neumann-, Robin- boundary value problems in applications, we continue our analysis of the bifurcation behaviour in separated Lagrangian boundary value problems and provide a numerical example in which we locate a D-series bifurcation in a Hénon-Heiles-type system.

9.3.1 Analysis of structures induced by separated Lagrangian boundary conditions

For reference, we recall from Section 8.2 that any separated Lagrangian boundary value problem $(\phi\colon (M,\omega) \to (M',\omega'), \Lambda, \Lambda')$ is locally given as

$$x = x^*, \quad \phi^X(x,y) = X^*. \tag{9.3.1}$$

Here $(x,y) = (x^1,\dots x^n, y_1,\dots y_n)$ for M, $(X,Y) = (X^1,\dots X^n, Y_1,\dots Y_n)$ are local Darboux coordinates for M' and $x^*, X^* \in \mathbb{R}^{2n}$. In (9.3.1) the symbol ϕ^X is a shorthand for $X \circ \phi$. Introducing a parameter μ in the map ϕ or in the boundary condition, the bifurcation diagram can be viewed as

$$\{(\mu,y) \,|\, h_\mu(y) = 0\} \tag{9.3.2}$$

with

$$h_\mu(y) = \phi^X_\mu(x^*,y) - X^*_\mu. \tag{9.3.3}$$

In particular the Jacobian matrix $\mathrm{D}h_\mu(y)$ coincides with $\mathrm{D}_y\phi^X_\mu(x^*,y)$.

Corollary 9.3.1. *If $n = 2$, then the Jacobian matrix $\mathrm{D}_y\phi^X_\mu$ vanishes at a D-series bifurcation.*

Remark 9.3.1. As (9.3.1) constitutes a separated Lagrangian boundary value problem, the problem is locally equivalent to a gradient-zero problem $\nabla g_\mu(z) = 0$ in n variables (Proposition 7.1.2). In contrast to h_μ, the maps ∇g_μ arise as gradients of smooth maps such that the bifurcation behaviour is governed by catastrophe theory. Indeed, the bifurcations which occur as generic bifurcations in gradient-zero problems $\nabla g_\mu(z) = 0$ with smooth families of maps g_μ in n variables occur as stable bifurcations in separated Lagrangian boundary value problems with $2n$-dimensional phase spaces.

The gradient structure is not visible in (9.3.3). Naively, it appears like the problem $h_\mu(y) = 0$ should behave like a general roots-of-a-function-type problem for maps in n variables. However, we know that it behaves like the gradient-zero-problem, so where has the gradient structure gone? The map ϕ_μ^X is a component of the map ϕ_μ which is symplectic. However, symplecticity of the Jacobian matrix $\mathrm{D}\phi(x, y)$ does *not* force any extra structure on the submatrix $D_y\phi^X(x, y)$ at points (x, y) in the phase space. Indeed, the extra structure hides away in the following detail: for $n > 1$ those small perturbations $\tilde{h}(y) = h_\mu(y) + \xi_\mu(y)$ of h_μ which are required to break gradient-zero bifurcations leading to a roots-of-a-function-type behaviour do *not* come from *small* perturbations of ϕ through symplectic maps.

In other words, for a fixed parameter μ^* it is impossible to obtain a versal roots-of-a-function-type unfolding of h_{μ^*} by varying ϕ through symplectic maps to produce an unfolding h_μ via (9.3.3). △

9.3.2 Numerical example. Hénon-Heiles Hamiltonian system

In the following we consider a Hénon-Heiles system, which is a Hamiltonian system originally derived to model galactic dynamics and is known to exhibit chaotic behaviour (Hénon, 1983; Tabor, 1989). Consider the Hamiltonian

$$H(x, y) = \frac{1}{2}\|y\|^2 + \frac{1}{2}\|x\|^2 - 10\left(x_1^2 x_2 - \frac{x_2^3}{3}\right) \tag{9.3.4}$$

on the phase space $\mathbb{R}^2 \times \mathbb{R}^2$. In (9.3.4) the norm $\|.\|$ denotes the Euclidean norm on $\mathbb{R}^2$. We obtain a symplectic map ϕ by integrating Hamilton's equations

$$\dot{x} = \nabla_y H(x, y), \quad \dot{y} = -\nabla_x H(x, y)$$

up to time $\tau = 1$ using the 2nd order symplectic Störmer–Verlet scheme with 10 time-steps. We consider the Dirichlet-type problem

$$x = x^*, \quad \phi^X(x, y) = X^*. \tag{9.3.5}$$

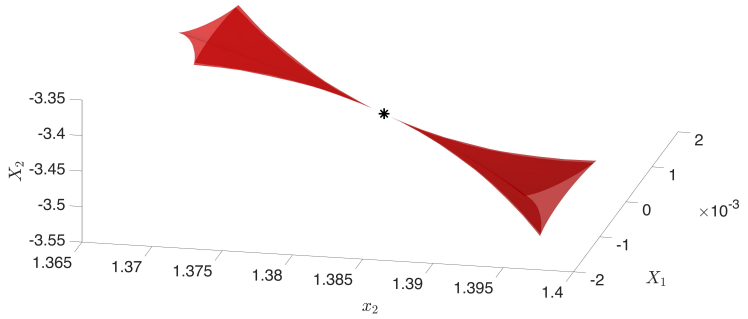

Figure 9.3: Elliptic umbilic D_4^- in the problem (9.3.5) for the numerical time-1-map of the Hénon-Heiles system (9.3.4) where the boundary values are parameters and $x_1^* = 0$ is fixed to reduce dimensionality. The numerical flow was obtained using the 2nd order symplectic Störmer–Verlet scheme (see Example 3.3.2) with 10 time-steps. The asterisk denotes the calculated position of the elliptic umbilic singularity. Derivatives were obtained using automatic differentiation.

This time we let x^* and X^* be the parameters of the problem. The (high-dimensional) bifurcation diagram can be thought of as the graph of ϕ plotted over the parameter space $(x^*, X^*) = (x, X)$. To reduce dimensionality we fix the parameter $x_1^* = 0$ leaving the parameters x_2, X_1, X_2 free. The level bifurcation set, i.e. the set of points in the parameter space at which a bifurcation occurs in a chosen subset U of the phase space, is given as

$$\{(x_2, \phi^X(0, x_2, y_1, y_2)) \mid \det D_y \phi^X(0, x_2, y_1, y_2) = 0, (0, x_2, y_1, y_2) \in U\}.$$

Figure 9.3 shows the level bifurcation set of the problem near an elliptic umbilic singularity D_4^-. Derivatives of the symplectic approximation to ϕ were obtained using automatic differentiation. The D-series bifurcation was found numerically by solving $D_y\phi(0, x_2, y_1, y_2) = 0$ as justified in Corollary 9.3.1. We see that the elliptic umbilic bifurcation is preserved.

9.3.3 Breaking of an elliptic umbilic bifurcation using a non-symplectic integrator

Let us compare the capturing of an elliptic umbilic bifurcation D_4^- by the second order accurate symplectic Störmer–Verlet method to a non-symplectic method of the same order of accuracy. For this we consider the Dirichlet problem for the Hénon-Heiles-type Hamiltonian system described in Section 9.3.2. In contrast to the numerical experiment described in Section 9.3.2, we reduce the number of time-steps from $N = 10$ to $N = 5$

and perturb the Hamiltonian from (9.3.4) with the extra term $0.01y_2 \sin(y_1)$ to

$$H(x,y) = \frac{1}{2}\|y\|^2 + \frac{1}{2}\|x\|^2 - 10\left(x_1^2 x_2 - \frac{x_2^3}{3}\right) + 0.01y_2 \sin(y_1).$$

This is done to make the break more obvious. In the considered boundary value problem

$$(x^1, x^2) = (0, (x^*)^2), \quad (\phi^{X^1}, \phi^{X^2}) = ((X^*)^1, (X^*)^2),$$

where $\phi^X = (\phi^{X^1}, \phi^{X^2})$ are the x-components of the Hamiltonian flow map at time 1 and $(x^*)^2$, $(X^*)^1$, $(X^*)^2$ the parameters of the problem, the level bifurcation set is locally given by

$$\mathcal{B} = \{(x^2, \phi^X(0, x^2, y_1, y_2)) \mid \det D_y\phi^X(0, x^2, y_1, y_2) = 0, (0, x^2, y_1, y_2) \in U\}, \quad (9.3.6)$$

for a subset $U \subset \mathbb{R}^4$ of the phase space. The level bifurcation set $\mathcal{B}$ can be obtained from

$$B = \{(x^2, y_1, y_2) \mid \det D_y\phi^X(0, x^2, y_1, y_2) = 0, (0, x^2, y_1, y_2) \in U\}. \quad (9.3.7)$$

using ϕ^X. Figures 9.4 and 9.5 show plots of the sets B (to the left) and $\mathcal{B}$ (to the right). For Figure 9.4 the flow ϕ was approximated with the symplectic Störmer–Verlet method (see Example 3.3.2). We see an elliptic umbilic bifurcation, where three lines of cusps merge in one singular point marked by an asterisk. Its position in the phase portrait of the numerical flow can be calculated as a root of $(x^2, y_1, y_2) \mapsto D_y\phi^X(0, x^2, y_1, y_2)$. For Figure 9.5 the flow ϕ was approximated with the explicit midpoint rule (RK2 – see Section 3.2.2), which is a second-order non-symplectic Runge–Kutta method. While the sheets in the plot for B still approach a singular point they cannot reach it and connect smoothly rather than in a singular point. In the level bifurcation set this has the effect that we do not obtain an elliptic umbilic bifurcation but three lines of cusp bifurcations which fail to merge in an umbilic point.

The computations were first done to high accuracy such that the bifurcation diagrams obtained by the Störmer–Verlet method and by RK2 were close. Then, to see which parts of the low-accuracy bifurcation diagrams correspond to each other, the step sizes were increased gradually and the movement of the singular point where the matrix $D_y\phi^X(0, x^2, y_1, y_2)$ is near the zero matrix was tracked in both simulations.

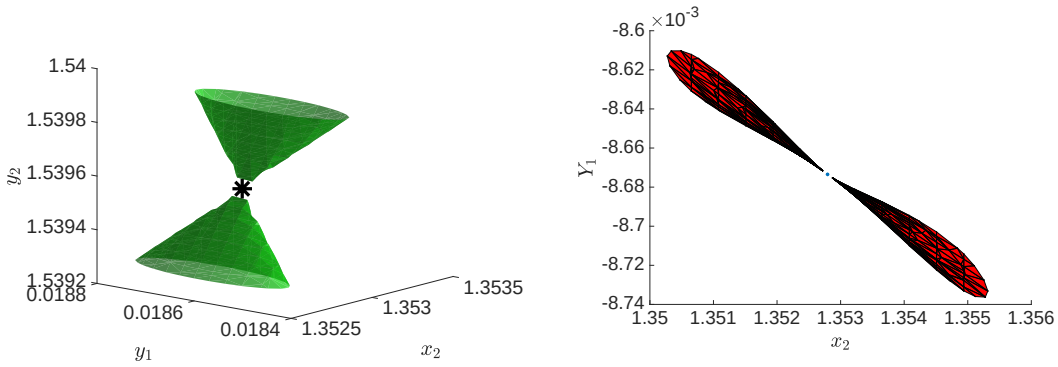

Figure 9.4: Resolving an elliptic umbilic bifurcation D_4^- with the symplectic Störmer–Verlet method. The plot to the left shows the set B defined in (9.3.6) and the plot to the right shows the level bifurcation set $\mathcal{B}$ defined in (9.3.7).

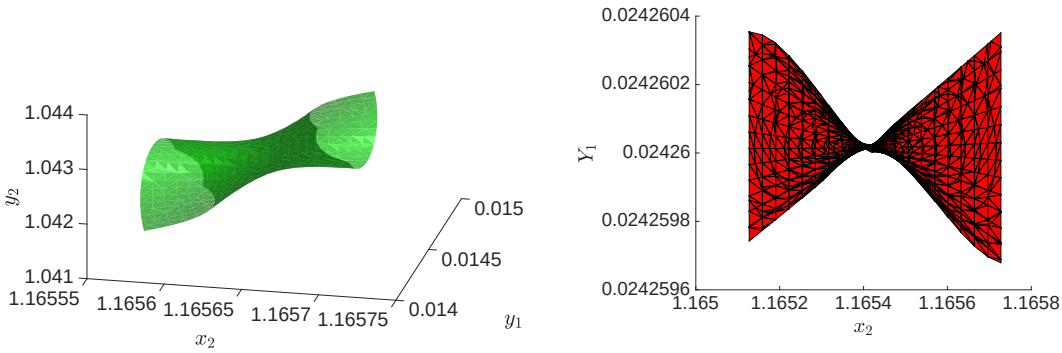

Figure 9.5: Resolving an elliptic umbilic bifurcation D_4^- with the non-symplectic second order Runge–Kutta method. The plot to the left shows the set B (9.3.6) and the plot to the right shows the level bifurcation set $\mathcal{B}$ (9.3.7). The set was rotated around the Y_2 axis by 0.0271rad in order to allow for a convenient rescaling of the axes. Instead of an elliptic umbilic bifurcation there are three lines of cusp bifurcations which fail to merge.

9.3.4 Computation of conjugate loci

Symplectic structure in the geodesic conjugate points problem

Let us return to the analysis of singularities in conjugate loci which we started in Chapter 8 and consider computational aspects. Let (N, g) be an n-dimensional Riemannian manifold with cotangent bundle T^*N which is equipped with local Darboux coordinates $q^1, \dots, q^n, p_1, \dots, p_n$. Define the Hamiltonian

$$H(q,p) = \frac{1}{2} \sum_{i,j=1}^{n} g^{ij}(q) p_i p_j, \tag{9.3.8}$$

where g^{ij} is the (i,j)-entry of the inverse of the matrix representation of the Riemannian metric g in the coordinate frame $\frac{\partial}{\partial q_1}, \dots, \frac{\partial}{\partial q_n}$. The Hamiltonian motions correspond to solutions of the geodesic equation

$$\ddot{\gamma}^k = -\Gamma^k_{ij} \circ \gamma \cdot \dot{\gamma}^i \dot{\gamma}^j,$$

where $\gamma^j = q^j \circ \gamma$ denote the components of γ and

$$\Gamma^k_{ij} = \frac{1}{2} \sum_{l=1}^{n} g^{kl} \left(\frac{\partial g_{jl}}{\partial q_i} + \frac{\partial g_{li}}{\partial q_j} - \frac{\partial g_{ij}}{\partial q_l} \right)$$

the Christoffel symbols with respect to the Levi-Civita connection.

The Hamiltonian formulation reveals the symplectic structure in the problem of connecting two points by a geodesic as the start and endpoints move apart. On a surface this structure is not relevant because the maximal multiplicity of conjugate points is 1 by Proposition 8.3.6. Therefore, only singularities whose degeneracy is 1 can occur. For a generic setting this means that a small, possibly non-symplectic perturbation of the problem will only move such singularities slightly but would not change their type or remove them (Proposition 9.2.2). However, if the Riemannian manifold is at least 3-dimensional one has to capture the symplectic structure in order to be able to find unbroken D-series bifurcations as explained in Section 9.2. This requires using symplectic integrators.

Structure preserving discretisation – jet-RATTLE method

The Hamiltonian (9.3.8) is not separable so symplectic integration requires the use of an implicit method. In the popular 2nd order symplectic Störmer–Verlet scheme, for instance, $\dim N$-dimensional equations have to be solved in each time-step causing high computational costs. In applications (N, g) is often given as a low codimensional submanifold of a Euclidean space where g is the induced metric; a fact which can be

exploited. Indeed, on a codimension-k submanifold the symplectic RATTLE method only requires a k-dimensional system of equations to be solved in each time-step. This is particularly efficient for hypersurfaces where $k = 1$. A derivation of the general RATTLE method can be found in Hairer, Lubich, and Wanner, 2013, Ch. VII 1.4. For our purposes it is advisable to have a derivative of the RATTLE-approximation of the geodesic exponential map available. This can be achieved using automatic differentiation. Moreover, in what follows we present a 1-jet version of the RATTLE method for geodesics on hypersurfaces.

Using RATTLE to compute geodesics of the hypersurface $f^{-1}(0)$ requires only the value and first derivative of f; the metric tensor and Christoffel symbols are not needed. Jet-RATTLE, needed to reliably detect conjugate points, also requires the second derivative of f.

Let (N, g) be a hypersurface of $\mathbb{R}^n$ defined by the equation $f(q) = 0$ for $f\colon \mathbb{R}^n \to \mathbb{R}$ such that $\nabla f(q) \neq 0$ for all $q \in \mathbb{R}^n$. Here g refers to the induced Riemannian metric on the hypersurface N. In order to compute geodesics on (N, g) with respect to the Levi-Civita connection, we apply the RATTLE method to the Hamiltonian

$$H(q, p) = \frac{1}{2}\langle p, p\rangle$$

defined on the cotangent bundle over $T^*\mathbb{R}^n$. Here $(q, p) = (q^1, \ldots, q^n, p_1, \ldots, p_n)$ are Darboux coordinates. In the above formula $\langle ., . \rangle$ denotes the Euclidean scalar product. For a fixed time-step $h > 0$ the RATTLE method gives rise to a map on T^*N which is symplectic with respect to the symplectic structure on cotangent bundles (assuming convergence of the implicit scheme). See Leimkuhler and Skeel, 1994.

The formulas for the time-h-map Ψ_h calculating the two n-dimensional vectors (q_{m+1}, p_{m+1}) from the initial values (q_m, p_m) read:

$$0 = f\left(q_m + h\left(p_m - \frac{h}{2}\nabla f(q_m)\cdot\lambda\right)\right) \tag{9.3.9}$$

$$p_{m+\frac{1}{2}} = p_m - \frac{h}{2}\nabla f(q_m)\cdot\lambda \tag{9.3.10}$$

$$q_{m+1} = q_m + h p_{m+\frac{1}{2}} \tag{9.3.11}$$

$$n = \frac{\nabla f(q_{m+1})}{\|\nabla f(q_{m+1})\|} \tag{9.3.12}$$

$$p_{m+1} = p_{m+\frac{1}{2}} - \left\langle n, p_{m+\frac{1}{2}}\right\rangle n \tag{9.3.13}$$

After the 1-dimensional equation (9.3.9) is solved for $\lambda \in \mathbb{R}$ the remaining equations can be evaluated explicitly.

Remark 9.3.2. The formulas (9.3.12, 9.3.13) describe a projection of $p_{m+\frac{1}{2}}$ to the tangent space at q_{m+1}. The effect is wiped out by (9.3.9, 9.3.10, 9.3.11) of the following step, i.e. the value for q_{m+2} does not depend on whether we set p_{m+1} according to (9.3.13) or simply $p_{m+1} = p_{m+\frac{1}{2}}$. If the formulas are iterated, then the projection step (9.3.12, 9.3.13) is only needed in the last step of the iteration (unless one is interested in the intermediate values for p). Indeed, in the examples presented in this chapter not only the intermediate p-values but also the final momentum is irrelevant. This means for the calculation of conjugate loci one can simply use

$$\begin{aligned} 0 &= f\left(q_m + h\left(p_m - \frac{h}{2}\nabla f(q_m)\cdot\lambda\right)\right)\\ p_{m+1} &= p_m - \frac{h}{2}\nabla f(q_m)\cdot\lambda\\ q_{m+1} &= q_m + hp_{m+1}. \end{aligned}$$ △

The derivative $D\Psi_h$ of the time-h-map (including the projection step) can be obtained by evaluating the following formulas. We interpret the vectors q_m, p_m and the gradient vectors $\nabla f(q_m)$, $\nabla_q\lambda$, etc. as column vectors such that, for instance, $\nabla f(q_m)(\nabla_q\lambda)^\top$ denotes a dyadic product. The symbol I refers to an m-dimensional identity matrix.

$$\begin{aligned} \nabla_q\lambda &= \frac{-\lambda\mathrm{Hess}\, f(q_m)n + \frac{2}{h^2}n}{\langle n, \nabla f(q_m)\rangle}\\ \nabla_p\lambda &= \frac{2n}{h\langle n, \nabla f(q_m)\rangle}\\ D_q\left(p_{m+\frac{1}{2}}\right) &= -\frac{h}{2}\left(\mathrm{Hess}\, f(q_m)\lambda + \nabla f(q_m)(\nabla_q\lambda)^\top\right)\\ D_p\left(p_{m+\frac{1}{2}}\right) &= I - \frac{h}{2}\nabla f(q_m)\nabla_p\lambda^\top\\ D_q(q_{m+1}) &= I + hD_q\left(p_{m+\frac{1}{2}}\right)\\ m &= \frac{\nabla f(q_m)}{\|\nabla f(q_m)\|}\\ D_p(q_{m+1}) &= hD_p\left(p_{m+\frac{1}{2}}\right)\\ D_q(n) &= \frac{1}{\|\nabla f(q_{m+1})\|}\left(\mathrm{Hess}\, f(q_{m+1})D_q(q_{m+1}) - nn^\top\mathrm{Hess}\, f(q_{m+1})D_q(q_{m+1})\right)\\ D_p(n) &= \frac{1}{\|\nabla f(q_{m+1})\|}\left(\mathrm{Hess}\, f(q_{m+1})D_p(q_{m+1}) - nn^\top\mathrm{Hess}\, f(q_{m+1})D_p(q_{m+1})\right)\\ D_q(p_{m+1}) &= D_q\left(p_{m+\frac{1}{2}}\right) - \langle n, p_{m+\frac{1}{2}}\rangle D_q(n) - np_{m+\frac{1}{2}}^\top D_q(n) - nn^\top D_q\left(p_{m+\frac{1}{2}}\right)\\ D_p(p_{m+1}) &= D_p\left(p_{m+\frac{1}{2}}\right) - \langle n, p_{m+\frac{1}{2}}\rangle D_p(n) - np_{m+\frac{1}{2}}^\top D_p(n) - nn^\top D_p\left(p_{m+\frac{1}{2}}\right) \end{aligned}$$

When the time-h-map Ψ_h is iterated M-times to obtain the numerical time-Mh-map Φ, the derivatives can be updated as follows

$$\begin{aligned} V^{(0)} &= I \\ V^{(m)} &= D\Psi_h(q_{m-1}, p_{m-1})V^{(m-1)}, \quad m = 1, \dots, M. \end{aligned}$$

We obtain the derivatives as $D\Phi(q_0, p_0) = V^{(M)}$. We refer to this 1-jet version of the RATTLE method applied to a hypersurface as *jet-RATTLE*.

Numerical examples using the jet-RATTLE method

Example 9.3.1. Let us add some computational details to Proposition 8.3.6 from Chapter 8. Figure 9.6 shows the conjugate locus on the graph of the perturbed 2-dimensional Gaussian

$$0 = f(q_1, q_2, q_3) = h(q_1, q_2) - q_3 = \exp(-q_1^2 - 0.9q_2^2) + 0.01q_1^3 + 0.011q_2^3 - q_3$$

to the point $q^* = (-1, 0, h(-1, 0))$, i.e. the points which are conjugate to q^*. Here subscripts denote components. For numerical computations notice that the conjugate locus is the level bifurcation set of the Dirichlet problem for the geodesic equations on the graph of h, where the (Q_1, Q_2)-coordinate of the end point are the parameters of the problem. We can discretise the 1-jet of the geodesic exponential map by applying the jet-RATTLE method to $f(q) = 0$. Let us refer to the Q_1 and Q_2-component of the numerical flow as $\Phi^{Q_{1,2}}$.

The matrix

$$A = \begin{pmatrix} 1 & 0 \\ 0 & 1 \\ \frac{\partial f}{\partial q_1}(q^*) & \frac{\partial f}{\partial q_2}(q^*) \end{pmatrix}$$

maps $\mathbb{R}^2$ to the tangent space of the graph of h at q^*. The level bifurcation set is obtained by calculating the zero-level set of

$$\begin{pmatrix} p_1 \\ p_2 \end{pmatrix} \mapsto \det D_{p_1,p_2} \Phi^{Q_{1,2}} \left(q^*, A \begin{pmatrix} p_1 \\ p_2 \end{pmatrix} \right) \cdot A$$

and mapping the set to the graph of h using Φ. The bifurcation behaviour persists and is also present in the unperturbed setting, where $h(q_1, q_2) = \exp(-q_1^2 - q_2^2)$. △

Example 9.3.2. Revisiting Example 8.1.2, the plot to the left of Figure 9.7 shows the conjugate locus on the perturbed 2-dimensional ellipsoid

$$(0.98q_1^2 + 0.97q_2^2 + 1.02q_3^2) - 1/\pi^2 + 0.1(-q_1^3 - 1.2q_2^3 + 0.7q_3^3) = 0$$

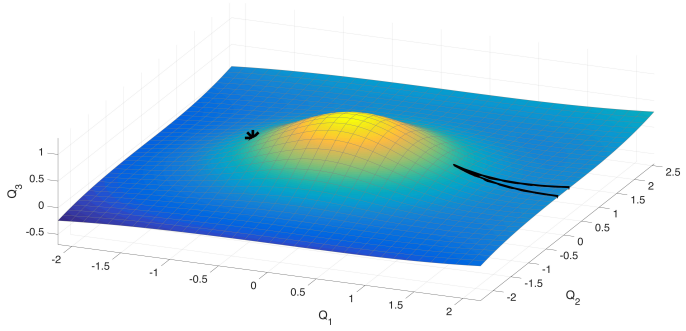

Figure 9.6: Conjugate locus to $q^*(-1, 0, h(-1, 0))$ on the graph of a perturbed 2-dimensional Gaussian. The conjugate locus contains a cusp singularity.

to $q^* = (q_1^*, q_2^*, q_3^*) = (-0.316472, 0, 0)$ projected along Q_1 to the Q_2/Q_3 plane. Notice that Q_2, Q_3 constitute a coordinate system in the considered regime near the approximate antipodal point of q^*. We see a formation of cusps. On an unperturbed ellipsoid we see four cusp bifurcations as shown in the right hand side plot of Figure 9.7 unless q^* is an umbilic point of the ellipsoid, in which case the formation collapses to a point. △

Example 9.3.3. The plot in the centre and to the right of Figure 9.8 shows a subset of the conjugate locus to $(q_1^*, q_2^*, q_3^*, q_4^*) = (-0.355367, 0, 0, 0)$ on the perturbed 3-dimensional ellipsoid

$$f(q) = 0.98q_1^2 + 0.95q_2^2 + 1.05q_3^2 + 1.03q_4^2 - \frac{1}{\pi^2} + 0.5(q_1^3 + 1.1q_2^3 + 0.9q_3^3 + 1.05q_4^3) = 0.$$

The functions Q_2, Q_3, Q_4 constitute a coordinate system in the considered regime. The variables Q_2, Q_3, Q_4 act as three parameters in the corresponding boundary value problem such that we can find bifurcations of codimension 3. Indeed, the conjugate locus contains an elliptic umbilic singularity where three lines of cusps merge. The plot to the left shows the position of the singularities in the tangent space at q^* in spherical coordinates: the coordinates p_1, p_2, p_3, p_4 can be obtained by first mapping

$$(r, \theta, \phi) \mapsto \rho = (\rho_1, \rho_2, \rho_3) = (r \sin\theta \cos\phi, r \sin\theta \sin\phi, r \cos\theta),$$

and then mapping $\rho \mapsto A\rho$, where A is a 4×3-dimensional matrix whose columns are an orthonormal basis of the kernel of $p \mapsto \nabla f(q^*)p$ near $\begin{pmatrix} 0_{1\times 3} \\ \mathrm{Id}_3 \end{pmatrix}$. The plot in the centre and to the right can be obtained from the plot to the left by calculating the p variables and applying the exponential map at q^*. We see that the elliptic umbilic bifurcation is preserved. △

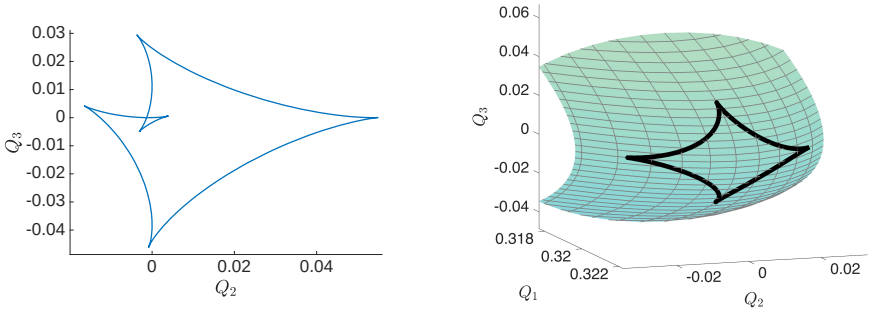

Figure 9.7: Conjugate locus on a perturbed ellipsoid (left) and on an unperturbed ellipsoid (right). We see formations of cusps connected by lines of fold singularities.

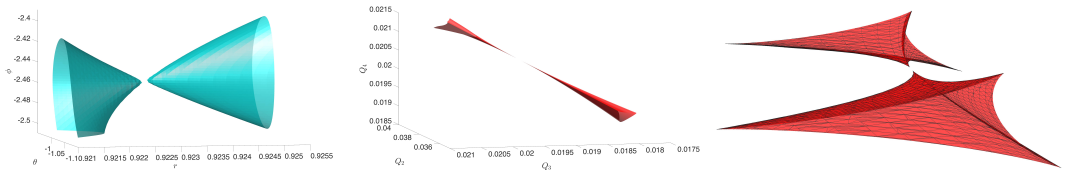

Figure 9.8: Degeneracy of the geodesic exponential map near an approximately antipodal point on a perturbed 3-dimensional ellipsoid. The plot to the left shows the position of the singularities in a parametrisation of the phase space, the plot in the centre the level bifurcation set (which is the conjugate locus) in the Q_1, Q_2, Q_3 coordinates showing an elliptic umbilic bifurcation. The right plot is obtained from the middle plot by rotation allowing for a convenient rescaling of the axes.

9.4 Preservation of periodic pitchfork bifurcations

As proved in Section 7.2, a periodic pitchfork bifurcation (see Figure 7.2) is a persistent phenomenon in 1-parameter families of boundary value problems in completely integrable Hamiltonian systems with symmetrically separated Lagrangian boundary conditions.

In the following, we will analyse how symplectic integrators can be useful to capture periodic pitchfork bifurcations. We will

- show numerical examples comparing non-symplectic and symplectic methods in generic planar systems and describe the mechanism of the bifurcation in the numerical phase space obtained by a symplectic method in planar systems (Section 9.4.1),
- construct an analytic example of a periodic pitchfork bifurcation in a nontrivial, 4-dimensional completely integrable system and run a numerical experiment how it is captured when using a symplectic integrator (Section 9.4.2),
- run further numerical experiments on how periodic pitchfork bifurcations are captured in higher-dimensional systems with affine-linear symmetries (Section 9.4.3), and
- give theoretical reasoning for the observed behaviour and explain general underlying principles (Section 9.4.4).

9.4.1 Periodic pitchfork in planar Hamiltonian systems - quality of preservation and numerical phase plots for a symplectic integrator

Consider a μ-parameter family of Hamiltonian systems with phase space $T^*\mathbb{R}$ equipped with the symplectic structure $\mathrm{d}q \wedge \mathrm{d}p$ and Hamiltonians

$$H_\mu(q,p) = p^2 + 0.1p^3 - 0.01\cos(p) + q^3 - 0.01q^2 + \mu q. \tag{9.4.1}$$

Let Q_μ denote the q component of the Hamiltonian flow to H_μ at time $\tau = 1.7$. We consider the Dirichlet-type boundary value problem

$$Q_\mu(0.2, p) = 0.2.$$

A motion starting at the line $q = 0.2$ in the phase space is a solution to the boundary value problem if and only if it returns to the line after time $\tau = 1.7$. Figure 9.9 shows how a pitchfork bifurcation in a Dirichlet problem for a generic, 1-parameter family

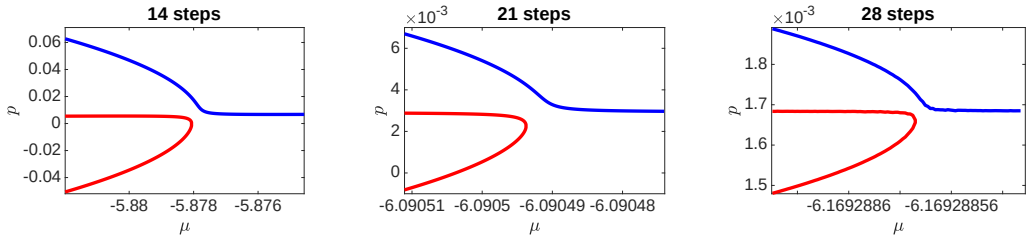

Figure 9.9: Plot of bifurcation diagrams of Hamiltonian boundary value problem solved with the symplectic Störmer–Verlet method using 14 steps, 21 steps and 28 steps. Notice the different scaling of the axes.

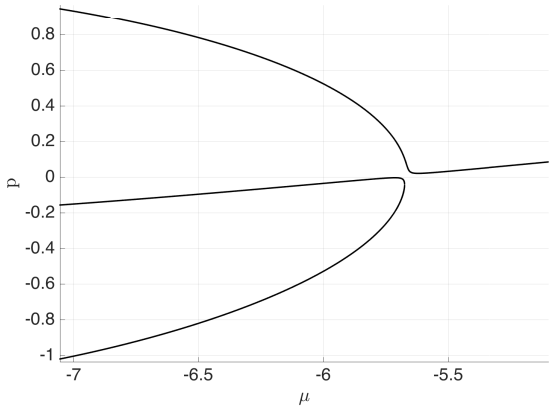

Figure 9.10: Plot of bifurcation diagrams of Hamiltonian boundary value problem solved with the symplectic Störmer–Verlet method using 11 steps.

of planar Hamiltonian systems is captured by the symplectic Störmer–Verlet method with 14, 21 and 28 steps. Notice the different scaling of the axes in the plots. We see that only few time-steps are needed to capture the bifurcation very well. The strong improvement of the shape of the pitchfork by doubling the number of steps indicates a convergence to the correct shape which is better than polynomial. Indeed, exponential convergence will be proved in Theorem 9.4.2.

For the matter of visualisation of the mechanism in the phase space, we reduce the number of time-steps to 11. The bifurcation diagram is displayed in Figure 9.10. For small parameter values there are three solutions. As μ increases two of them merge in a fold bifurcation.

Figure 9.11 illustrates the mechanism of the broken pitchfork bifurcation in the phase space. A solution to the boundary value problem is represented by 11 points (number of time-steps) in the phase space. In the plots the initial point is marked

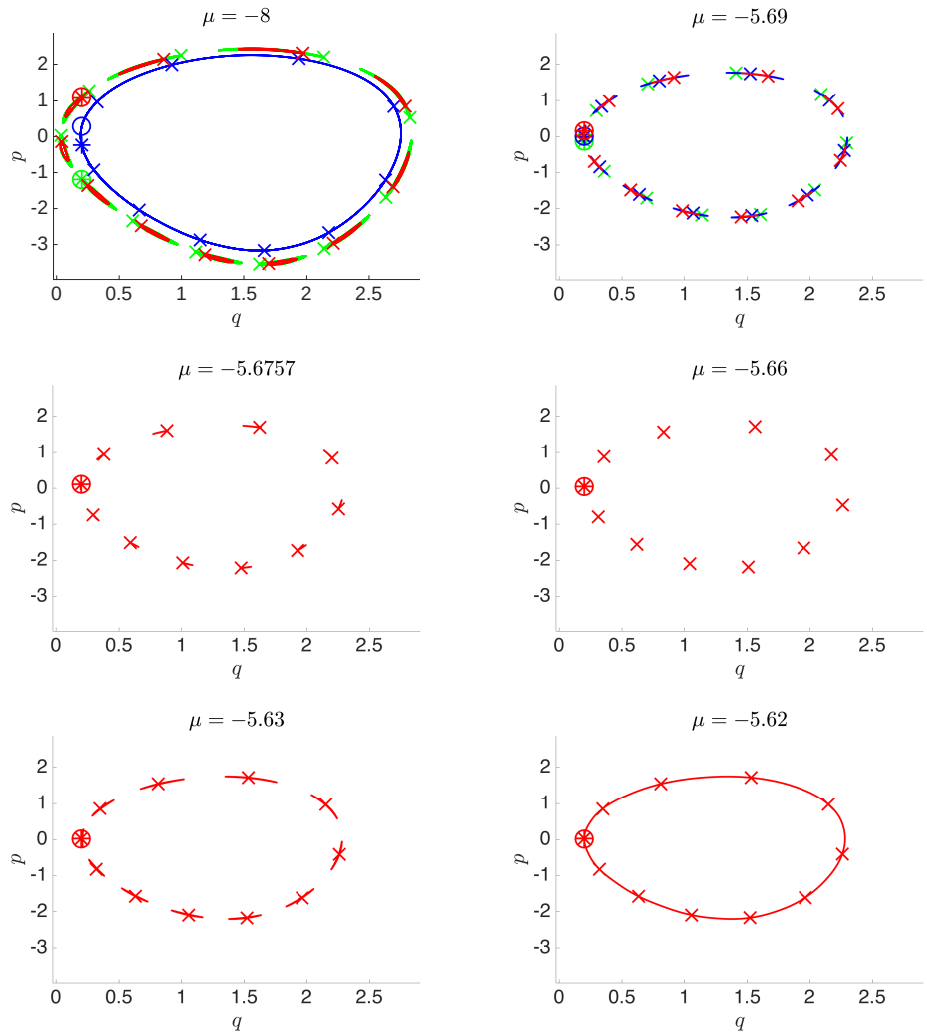

Figure 9.11: Plot of invariant sets and orbits of the numerical flow involved in the slightly broken periodic pitchfork bifurcation of Figure 9.10. Two solutions (green and blue) merge and annihilate in a fold bifurcations while another solution (red) persists. The persistent solution becomes 11-periodic shortly after the other solutions undergo a fold bifurcation. If the pitchfork bifurcation was preserved exactly, all three solutions would merge through an 11-periodic orbit into one solution.

by $*$, the end point by o and the other points by $\times$. As required by the boundary condition, the q-coordinate of the initial- and end point is 0.2. The 11 points belong to an invariant set which can be computed by iterating the discrete flow map ϕ_h with time-step $h = \tau/11$. The solutions corresponding to the outer branches of the broken pitchfork bifurcation constitute nearly periodic orbits of ϕ_h. Their invariant sets consist of 11 KAM-islands. The inner branch corresponds to a non-periodic solution belonging to a connected invariant set. As the parameter μ increases, the invariant set of the inner branch breaks up into 11 islands which merge with the invariant set of one of the nearly periodic solutions from the outer branches. We see a fold bifurcation in the bifurcation diagram of the numerical flow. The remaining outer branch is continued as μ increases. It becomes a periodic orbit shortly after the fold bifurcation, and then loses periodicity again. This mechanism can be compared to the mechanism of the exact periodic pitchfork bifurcation which we explained in Section 7.2 and illustrated in Figure 7.3. In the exact bifurcation the outer branches correspond to the same periodic orbit in the phase space and the pitchfork bifurcation takes place exactly when the orbit corresponding to the inner branch becomes a periodic orbit of period τ that is tangential to the boundary condition.

Let us compare the preservation of periodic pitchfork bifurcations using a symplectic integrator (Figures 9.9 and 9.10) with a non-symplectic integrator of the same order of accuracy. To understand what is happening in the latter case we compute a larger part of the bifurcation diagram using the non-symplectic second order explicit midpoint rule (RK2 – see Section 3.2.2). The upper and middle branch of the pitchfork bifurcation do not exist in the numerical bifurcation diagram until we use more than 25 steps (Figure 9.12). With 200 steps the bifurcation is recognisable and with 400 steps we obtain a diagram comparable with the 14-steps Störmer–Verlet calculation in Figure 9.9. As the computational costs per step are similar if the Hamiltonian is separated, we conclude that the symplectic Störmer–Verlet method performs significantly better than the non-symplectic method RK2.

Figure 9.13 shows how the 4th order accurate, time-reversal symmetric, 3-stage Lobatto IIIA method captures the pitchfork bifurcation. The scheme is not symplectic but conjugate symplectic up to order 6 (Hairer and Zbinden, 2012).

The symmetry properties of the method do not play a role as the considered Hamiltonian system is not time-reversal symmetric. Comparing Figure 9.9 with 9.13 we see that the Störmer–Verlet scheme slightly beats the Lobatto IIIA method in terms of how well it preserves the shape of the periodic pitchfork bifurcation although it is of lower order. Figure 9.14 shows the bifurcation diagram if the Hamiltonian boundary value problems are solved with MATLAB's build-in codes `bvp4c` and `bvp5c` (MATLAB R2016b). These are multi-purpose codes which are designed to solve general two-point

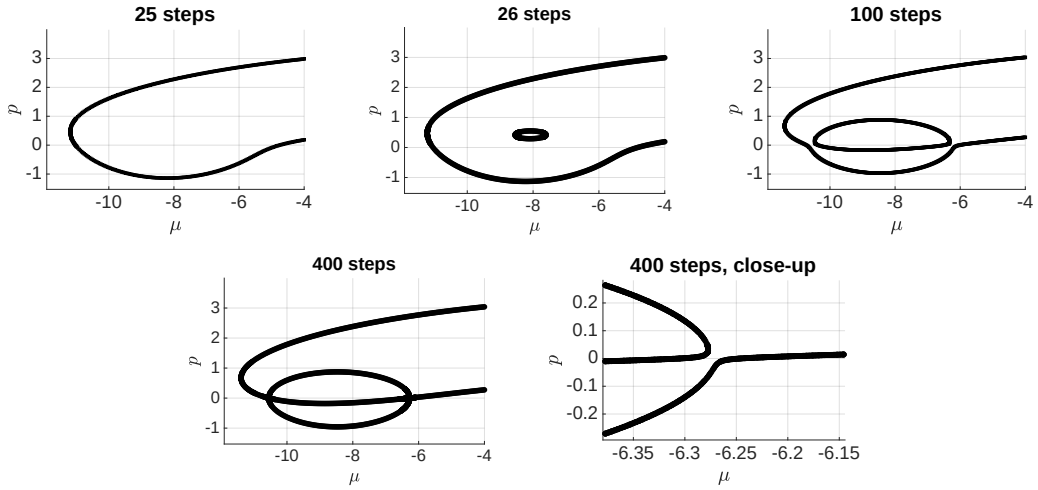

Figure 9.12: Plot of bifurcation diagrams of Hamiltonian boundary value problem solved with RK2 and different number of integration steps.

boundary value problems for ODEs. The code `bvp4c` is based on the 4th-order, 3-stage Lobatto IIIA method while `bvp5c` uses the 4-stage Lobatto IIIA formula. Both codes re-mesh the time-grid if the solution does not meet tolerance criteria. The methods require an initial guess for a solution of the boundary value problem defined on a user supplied initial mesh (Kierzenka and Shampine, 2001).

In our experiment we do the following (primitive) continuation method: we use initial guesses from the Lobatto IIIA experiment (Figure 9.13) at $\mu = -6.5$, let `bvp4c` or `bvp5c` solve the boundary value problem and use the solution as a new initial guess for the boundary value problem at the next μ -value. The process is repeated for each branch. We leave the error tolerances at their default values. Allowing the methods to use up to 10^5 mesh points in time, the codes run without issuing warnings. As μ varies, the codes adapt the time-meshes and we do not obtain consistent bifurcation diagrams. This is because the resulting diagram shows for each μ a snapshot of a bifurcation diagram of a different parameter-family of numerical flows. This illustrates that a μ-dependent re-meshing strategy for the time-grid destroys the bifurcation diagram.

Figure 9.15 shows that using a fixed, non-uniform mesh destroys the excellent behaviour of symplectic methods for capturing the periodic pitchfork bifurcation that we saw in Figure 9.9. This is in contrast to the bifurcations analysed in Section 9.2, where using a non-uniform mesh does *not* change the behaviour of the integrator qualitatively. The mesh used in the numerical example is the image of a uniform grid on the interval $[0, 1]$ under the map $t \mapsto \tau \frac{\exp(5t)\sin(2.6t)}{\exp(5)\sin(2.6)}$ with 226 and 905 grid points. Here, all step-sizes are smaller than in a uniform grid with 100 or 400 grid points, respectively. With a fixed, non-uniform mesh the Störmer–Verlet scheme still generates a symplectic flow

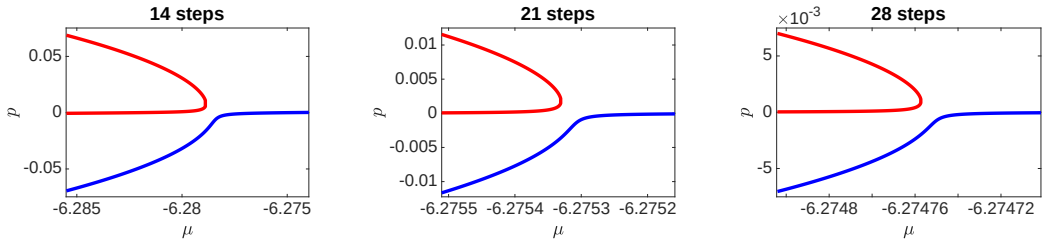

Figure 9.13: Bifurcation diagrams for Hamilton's equations to (9.4.1) solved with the 4th order Lobatto IIIA method and different number of time steps. The implicit equations arising in the method were solved up to round-off errors using Newton iterations. The scheme is conjugate symplectic up to order 6 and preserves the periodic pitchfork bifurcation only slightly worse than the symplectic 2nd order Störmer–Verlet scheme in Figure 9.9.

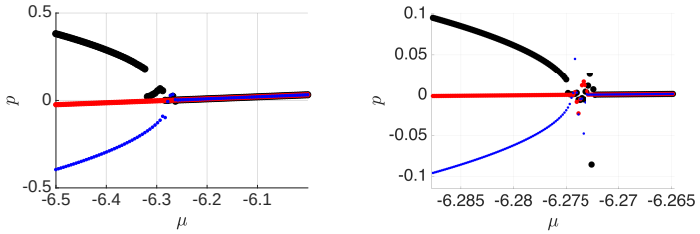

Figure 9.14: Bifurcation diagrams for Hamilton's equations to (9.4.1) solved with MATLAB's bvp4c (left) and bvp5c (right), which use a re-meshing strategy destroying the bifurcation diagram.

map. However, it loses its energy conservation properties and behaves similar to RK2 (Figure 9.12) when computing the bifurcation diagram of a periodic pitchfork. This will be explained in more detail later (Remark 9.5.1).

9.4.2 Construction of a periodic pitchfork in a nontrivial 4-dimensional Hamiltonian system

Let us construct a nontrivial, 4-dimensional completely integrable Hamiltonian system with a periodic pitchfork bifurcation that is not removable under small perturbations within the class of symmetrically separated Lagrangian boundary value problems for completely integrable Hamiltonian systems.

The circle S^1 can be viewed as the quotient space $\mathbb{R}/[0, 2\pi]$. Local coordinates on S^1 can be obtained as the inverse of suitable restrictions of the projection map $\mathbb{R} \to \mathbb{R}/[0, 2\pi] = S^1$. In this way, we obtain everywhere local coordinates (q_1, q_2) for the torus $S^1 \times S^1$. Let us denote a copy of the torus $S^1 \times S^1$ by $\overline{S}^1 \times \overline{S}^1$ and its coordinates obtained as local inverses of the projection $\mathbb{R} \to \mathbb{R}/[0, 2\pi]$ by $(\overline{q}_1, \overline{q}_2)$. Let

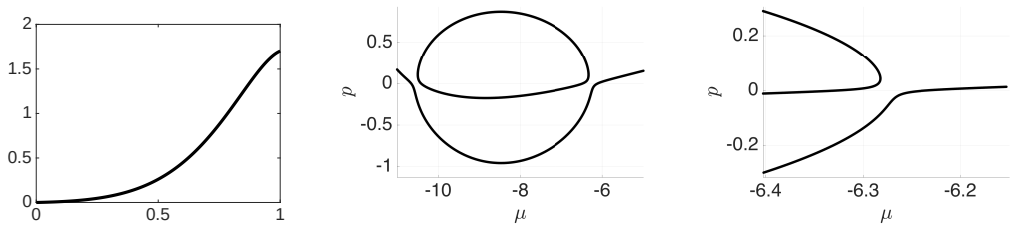

Figure 9.15: Bifurcation diagrams for Hamilton's equations to (9.4.1) solved with the Störmer–Verlet method using a non-uniform mesh for the time-integration. The mesh is obtained by mapping a uniform mesh on the interval $[0, 1]$ with the function whose graph is plotted to the left. The diagram in the centre corresponds to 226 mesh-points (finer than a uniform mesh with 100 points) and the diagram to the right corresponds to 905 mesh points (finer than a uniform mesh with 400 points). Here the Störmer–Verlet method behaves similar to RK2 (see Figure 9.12) and much worse than with a uniform grid (Figure 9.9).

ϵ, κ be non-zero values in the real, open interval $(-1, 1)$. The map

$$\Big(q_1, q_2\Big) \mapsto \Big(q_1 + \epsilon\cos(q_2), q_2 + \kappa\cos(q_1)\Big) \tag{9.4.2}$$

gives rise to a diffeomorphism $h\colon S^1 \times S^1 \to \overline{S}^1 \times \overline{S}^1$. Its cotangent lifted map Ψ is given as

$$\Psi\colon T^*(S^1 \times S^1) \to T^*(\overline{S}^1 \times \overline{S}^1), \quad \Big(q, p\Big) \mapsto \Big(h(q), Dh(q)^{-T}p\Big)\,. \tag{9.4.3}$$

Here $Dh(q)^{-T}$ denotes the inverse of the transpose of the Jacobian matrix of h at the point q. On the cotangent bundle of $\overline{S}^1 \times \overline{S}^1$ we consider the following family of Hamiltonians

$$\overline{H}_\mu(\overline{q}, \overline{p}) = \overline{p}_1^3 + \mu\overline{p}_1 + \overline{p}_2^2. \tag{9.4.4}$$

Using the canonical symplectic form $-\mathrm{d}\overline{\lambda}$ on the cotangent bundle $T^*(\overline{S}^1 \times \overline{S}^1)$, we obtain a family of completely integrable Hamiltonian systems. The two independent integrals of motions are given as the coordinate functions $\overline{p}_1, \overline{p}_2$. From Hamilton's equations we see that a motion is periodic at $\mu = 0$ if $\overline{p}_1(0)^2/\overline{p}_2(0)$ is rational with initial condition $(\overline{q}, \overline{p}) = (\overline{q}_1(0), \overline{q}_2(0), \overline{p}_1(0), \overline{p}_2(0))$. In particular, motions on the Liouville torus

$$\overline{T} = \left\{(\overline{q}_1, \overline{q}_2, \overline{p}_1, \overline{p}_2) = \left(\overline{q}_1, \overline{q}_2, 1, \frac{3}{2}\right) \;\middle|\; (\overline{q}_1, \overline{q}_2) \in \overline{S}^1 \times \overline{S}^1\right\}$$

are periodic for $\mu = 0$ and their period is $\tau = 2\pi/3$. Now consider the family of Hamiltonian systems $(T^*(S^1 \times S^1), -\mathrm{d}\lambda, H_\mu)$ with Hamiltonians $H_\mu = \overline{H}_\mu \circ \Psi$. The map Ψ is symplectic such that a curve γ is a motion in $(T^*(S^1 \times S^1), -\mathrm{d}\lambda, H_\mu)$ if and only

if $\Psi \circ \gamma$ is a motion in $(T^*(\overline{S}^1 \times \overline{S}^1), -\mathrm{d}\overline{\lambda}, \overline{H}_\mu)$. The preimage $T = \Psi^{-1}(\overline{T})$ is a Liouville torus with orbits of the same period $\tau = 2\pi/3$. The point $z = (\pi/2, 0, 1 - 3\kappa/2, 3/2)$ is an isolated point in the intersection of T with the Lagrangian submanifold

$$B = \left\{ (q_1, q_2, p_1, p_2) = \left(q_1, q_2, 1 - \frac{3}{2}\kappa, \frac{3}{2} \right) \,\middle|\, q_1, q_2 \in S^1 \right\}.$$

Moreover, the tangent spaces of T at z and of B at z intersect in a 1-dimensional subspace which can be verified by a consideration of their images under the symplectomorphism Ψ. Since the parameter μ enters in a generic way, the lemma below follows by Theorem 7.2.1.

Lemma 9.4.1. *For $\epsilon, \kappa \in (-1, 1) \setminus \{0\}$ there exists a periodic pitchfork bifurcation at $\mu = 0$ at the point $z = (\pi/2, 0, 1 - 3/2\kappa, 3/2)$ in the symmetrically separated Lagrangian boundary value problem*

$$P_\mu \left(q_1, q_2, 1 - \frac{3}{2}\kappa, \frac{3}{2} \right) = \begin{pmatrix} 1 - \frac{3}{2}\kappa \\ \frac{3}{2} \end{pmatrix}$$

for the family of time-$2\pi/3$-maps (Q_μ, P_μ) of the completely integrable Hamiltonian system $(T^*(S^1 \times S^1), -\mathrm{d}\lambda, H_\mu)$, where $-\mathrm{d}\lambda$ is the canonical symplectic form for cotangent bundles and $H_\mu = \overline{H}_\mu \circ \Psi$ is defined by (9.4.2), (9.4.3), (9.4.4).

Figure 9.16 shows the bifurcation diagrams of the numerical flow for the boundary value problem described in Lemma 9.4.1 for $\epsilon = \kappa = 0.1$. Hamilton's equations are solved over the time interval $[0, 2\pi/3]$ using the symplectic 2nd order Störmer–Verlet method with 20, 40 and 80 time-steps. The results indicate that the periodic pitchfork bifurcation of the exact flow is only captured up to the accuracy of the integrator. The integrals $\overline{q}_1 = q_1 + 0.1\cos(q_2)$ and $\overline{q}_2 = q_2 + 0.1\cos(q_1)$ are nonlinear functions of (q, p) and are *not* preserved.

9.4.3 Affine linear symmetries and the Störmer–Verlet method

The Störmer–Verlet method preserves linear invariants Hairer, Lubich, and Wanner, 2013, Thm. IV 1.5 and quadratic invariants of the form $Q(q, p) = q^\top A p$ for a fixed matrix A Hairer, Lubich, and Wanner, 2013, Thm. IV 2.3. Let us see how a periodic pitchfork bifurcation is captured in two numerical examples of completely integrable Hamiltonian systems with simple symmetries / invariants.

Example 9.4.1 (Cyclic variable). If a variable does not occur in the expression of a Hamiltonian, then its conjugate momentum is a conserved quantity. The conserved quantity can be treated as a parameter for the system such that Hamilton's equations can be solved on a space whose dimension is reduced by two where the cyclic variable

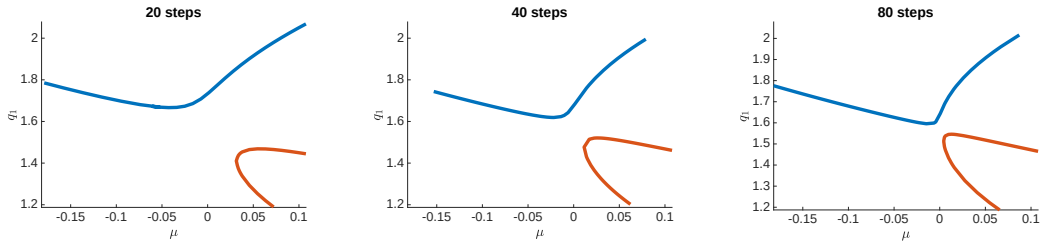

Figure 9.16: Plot of bifurcation diagrams for the boundary value problem given in Lemma 9.4.1 projected along the q_2-axis. The symplectic 2nd order Störmer–Verlet method is used. The shape of the periodic pitchfork bifurcation is only captured as by the accuracy of the method. The integrals $\overline{q}_1 = q_1 + 0.1\cos(q_2)$ and $\overline{q}_2 = q_2 + 0.1\cos(q_1)$ are nonlinear functions of (q, p) and are *not* preserved.

and its conjugate momentum do not appear as dynamical variables. The evolution in the cyclic variable can then be integrated separately. If the phase space dimension is $2n$ and the Hamiltonian has $n-1$ cyclic variables, then we can obtain the same behaviour as for planar Hamiltonian systems by applying the symplectic integrator to the reduced planar system. However, even if we apply the Störmer–Verlet method to the non-reduced system, the conjugate momenta are preserved as these are affine linear integrals of motions. The integrals correspond to translation symmetries in the cyclic variables.

We consider the family of Hamiltonian systems defined by

$$H_\mu(q_1, q_2, p_1, p_2) = q_1^3 + \mu q_1 + p_1 p_2 + p_1^2 + \frac{1}{10}(p_1^3 + p_2^3) \tag{9.4.5}$$

on the phase space $\mathbb{R}^4$ with the standard symplectic structure. The variable q_2 is cyclic. Let us consider the symmetric Dirichlet boundary value problem

$$q(0) = \begin{pmatrix} 0.2 \\ 0.1 \end{pmatrix} = q(5). \tag{9.4.6}$$

Using the symplectic, 2nd order Störmer–Verlet method to calculate the numerical flow, we find a pitchfork bifurcation. Introducing the cyclic variable into the Hamiltonian by adding the term $0.01q_2$ breaks the pitchfork bifurcation. This confirms that the pitchfork bifurcation is due to the completely integrable structure (see Figure 9.17).

We reduce the number of time steps in our calculation to analyse how the pitchfork bifurcation breaks. Figure 9.18 shows that there is a clearly visible break when 14 steps are used. If 15 steps are used, however, the break can only be spotted in a close-up. The p_1-axis is scaled approximately by a factor 10 and the p_2-axis and μ-axis by 1000. Since the number of steps is only increased by 1, corresponding to an increase

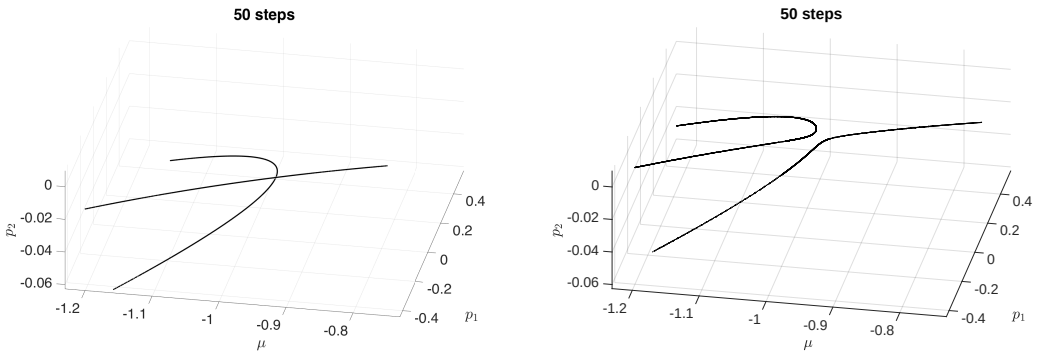

Figure 9.17: The plot to the left shows a periodic pitchfork bifurcation in the 4-dimensional Hamiltonian system (9.4.5) with a cyclic variable for the boundary value problem (9.4.6). The plot to the right shows how the pitchfork breaks if the former cyclic variable is introduced in the Hamiltonian. This confirms that the appearance of the pitchfork is due to the complete integrable structure. For both plots the Störmer–Verlet method with 50 time-steps was used.

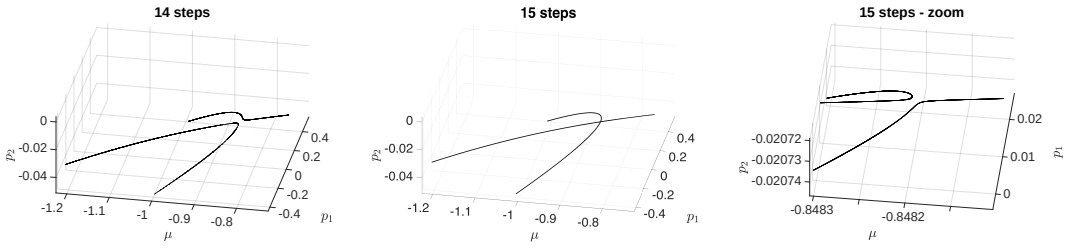

Figure 9.18: The plots show how the periodic pitchfork bifurcation shown in the left hand side plot of Figure 9.17 breaks as we reduce the number of time-steps in the Störmer–Verlet scheme. While the break is clearly visible when 14 steps are used, it can only be spotted in a close-up when 15 steps are used.

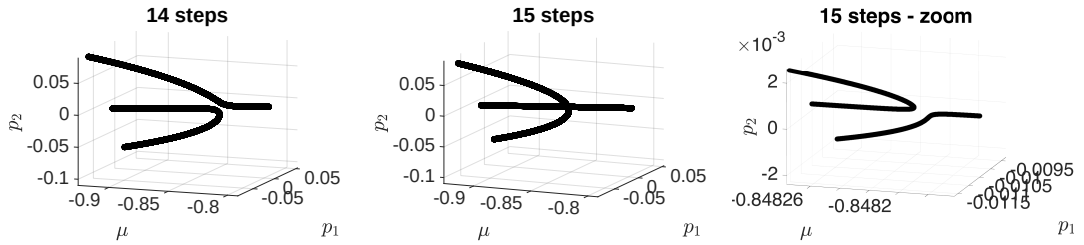

Figure 9.19: The plots show how a periodic pitchfork bifurcation is captured if one of the integrals is a linear map. While the break is clearly visible when 14 steps are used, it can only be spotted in a close-up when 15 steps are used. This is in analogy to the cyclic-variable case (Figure 9.18) but different to the case of more complicated integrals (Figure 9.16).

by approximately 7%, this indicates a capturing to higher than polynomial order as we will justify in Theorem 9.4.2. △

Example 9.4.2 (Linear conservation law / linear symmetry). Let us apply a linear, symplectic change of coordinates to the Hamiltonian boundary value problem (9.4.5) with (9.4.6) in the cyclic-variable example and test the behaviour of the Störmer–Verlet method. If $A \in \mathrm{Gl}(n, \mathbb{R})$ is a linear transformation of $\mathbb{R}^n$, then

$$\begin{pmatrix} \tilde{q} \\ \tilde{p} \end{pmatrix} = \Psi(q, p) = \begin{pmatrix} Aq \\ A^{-T} p \end{pmatrix} \tag{9.4.7}$$

is a symplectic transformation on $T^*\mathbb{R}^n$. We consider

$$A = \begin{pmatrix} -1 & 2 \\ 3 & 1 \end{pmatrix}.$$

and apply the transformation defined by Ψ to the Hamiltonian boundary value problem (9.4.5) - (9.4.6) considered in Example 9.4.1. In the transformed system $H \circ \Psi^{-1}$ and $q_2 \circ \Psi^{-1}$ are integrals of motions.

Figure 9.19 shows the analogous situation to Figure 9.18 in the new coordinates. We see that a linear change of coordinates does not have any effect on how well the bifurcation is captured. This is to be contrasted to the integrable system presented in Section 9.4.2 whose quantities are not affine-linear in the variables used to integrate the Hamiltonian flow and the bifurcation is captured only up to the accuracy of the integrator (Figure 9.16). △

9.4.4 Theoretical consideration of the effects of symplectic structure preserving discretisation in completely integrable systems

To which extent the completely integrable structure of a system is present in the numerical flow determines how well a pitchfork bifurcation is captured. This is made precise in the following theorem.

Theorem 9.4.2 (preservation of periodic pitchfork bifurcation)**.** *Consider a smooth 1-parameter family of Hamiltonian boundary value problems for $2n$-dimensional completely integrable Hamiltonian systems with symmetrically separated Lagrangian boundary conditions and a generic periodic pitchfork bifurcation. Consider a discretisation of the Hamiltonian flows by a symplectic integrator with order of accuracy k and constant step-size h. In a generic setting for sufficiently small h the family of numerical flows has a bifurcation that is close to a pitchfork bifurcation*

- *to exponential order in h^{-1} if all n integrals are preserved exponentially well (e.g. in the planar case)*
- *to order k otherwise.*

Remark 9.4.1. Recall from Theorem 7.2.1 that a periodic pitchfork bifurcation occurs at an intersection point z of the boundary condition Λ with a Liouville torus $\mathcal{T}$ invariant under the Hamiltonian flow, such that the intersection of the tangent spaces $T_z\mathcal{T}$ and $T_z\Lambda$ is 1-dimensional. The torus $\mathcal{T}$ is required to consist of periodic orbits of a given period τ. It is, therefore, highly resonant and immediately destroyed when the Hamiltonian flow is perturbed, even when the perturbation is symplectic. Thus, results obtained by KAM-theory about the exponentially long persistence of invariant Liouville tori under symplectic discretisation (see Hairer, Lubich, and Wanner, 2013, Ch. X5.2) do not apply in this setting as non-resonance conditions are not fulfilled. This is why symplectic integrators can break the structure significant for pitchfork bifurcations in a general setting as we saw in Figure 9.16. △

Proof of Theorem 9.4.2. Recall from Section 7.2.3 that the completely integrable structure and the structure of the boundary conditions induce a $\mathbb{Z}/2\mathbb{Z}$-symmetry in the associated function of the problem family. The singular point of a pitchfork bifurcation is unfolded under the presence of a $\mathbb{Z}/2\mathbb{Z}$-symmetry to a pitchfork bifurcation. The corresponding critical-points-of-a-function problem is defined by the family $(x^4+\mu_2x^2)_{\mu_2}$, i.e. the generating function of the problem family is stably right-left equivalent to the family $(x^4+\mu_2x^2)_{\mu_2}$, where μ_2 is the family parameter. Unfolding of x^4 without the $\mathbb{Z}/2\mathbb{Z}$-symmetry leads, however, to the normal form of a cusp bifurcation which is defined by the family $(x^4+\mu_2x^2+\mu_1x)_{\mu_1,\mu_2}$. The effect of the symmetry breaking parameter μ_1 is illustrated in Figure 9.20: the bifurcation, which is present for $\mu_1=0$,

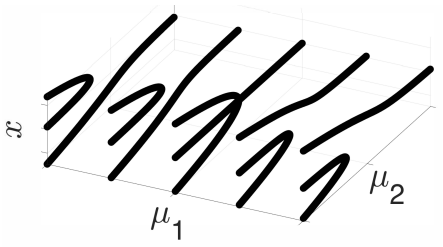

Figure 9.20: The figure shows the critical point set of the model cusp $x^4 + \mu_2 x^2 + \mu_1 x$ over the μ_1/μ_2-parameter space for selected values of μ_1. For $\mu_1 = 0$ we see a pitchfork bifurcation.

breaks if $\mu_1 \neq 0$. Approximating the Hamiltonian flow with an integrator introduces the discretisation parameter h as an additional parameter to the problem family. The discretisation does not respect the completely integrable structure which corresponds to a $\mathbb{Z}/2\mathbb{Z}$-structure of the generating function.

If the order of accuracy of the integrator is k, then, unless the problem is degenerate, the power of the step-size h^k acts like the parameter μ_1 in Figure 9.20. We say the pitchfork is *broken up to the order of accuracy of the integrator*. This means, in a general setting symplecticity of an integrator cannot be expected to improve the numerical capturing of the periodic pitchfork bifurcation because the bifurcation is due to the integrable structure rather than to symplecticity. However, in many important cases, symplecticity does help because symplectic integrators preserve a modified Hamiltonian exponentially well Hairer, Lubich, and Wanner, 2013, Ch. IX and are, therefore, guaranteed to capture at least this part of the integrable structure very well. In the planar case, e.g. this means the whole integrable structure is captured exponentially well by symplectic integrators. Here, the discretisation parameter does not enter generically but unfolds the pitchfork bifurcation to a family of nearly perfect pitchforks. These pitchforks are broken only up to exponential order in $-h^{-1}$. The same is true in higher dimensions if the $n-1$ additional integrals/symmetries are captured at least exponentially well. □

9.5 Further remarks

Remark 9.5.1 (non-uniform meshes). The bifurcations considered in Section 9.2 are connected to the symplecticity of the Hamiltonian flow but not to the preservation of the Hamiltonian. We can, therefore, use a symplectic integrator together with a fixed but not necessarily uniform grid for the integration of Hamiltonian ODEs to preserve the bifurcations. In contrast, the periodic pitchfork bifurcation analysed in Section 9.4 is related to the energy preservation of the Hamiltonian flow. To make

use of the excellent energy behaviour of symplectic integrators using a uniform mesh is essential. △

Remark 9.5.2 (Conjugate symplectic methods). Numerical methods are called *conjugate* if their numerical flows Φ_h and Ψ_h are related by a change of coordinates χ_h such that $\Phi_h = \chi_h \circ \Psi_h \circ \chi_h$. An example is the trapezoidal rule, which is conjugate to the implicit midpoint rule Hairer, Lubich, and Wanner, 2013, Ch. VI.8. Numerical flows obtained using a conjugate symplectic method preserve a nearby symplectic form and share the excellent energy behaviour with flows obtained by a symplectic method because the flows are conjugate. To capture periodic pitchfork bifurcations, they are just as good as symplectic methods. In contrast, this is *not* true for the higher gradient-zero bifurcations considered in Section 9.2 because (unless in a degenerate situation) the boundary condition will not be Lagrangian with respect to the modified symplectic form such that the bifurcations in the numerical systems are broken up to the order of accuracy.

Some methods are conjugate to a symplectic method up to some (high) order. An example is Lobatto IIIA, which is conjugate symplectic up to order 6 (Hairer and Zbinden, 2012). If a k-order method is conjugate symplectic up to a high order $r > k$, then it will behave as good as an r-order scheme in resolving the periodic pitchfork bifurcation but will show order k broken D-series bifurcations in generic Hamiltonian boundary value problems. △

Chapter 10

Local intersections of Lagrangian manifolds correspond to catastrophe theory

Chapter 10 is an adaption of Offen, 2020a.

In this chapter we provide rigorous justification of our claimed equivalence of local Lagrangian intersection problems with catastrophe theory. While the process to associate function families to local Lagrangian intersection problems has been established early on in this work, a proof that the associate function families are well-defined up to stably right equivalence in the sense of catastrophe theory has been postponed. Moreover, given well-definedness, we need to make sure that stably right equivalence actually can distinguish local Lagrangian intersection problems up to symplectomorphisms acting on the ambient manifold such that we obtain a meaningful correspondence between the two problem classes.

The Lagrangian intersection problems in this work are motivated by a consideration of boundary value problems for symplectic maps where in contrast to classical results neither (a) all intersections are tangential nor (b) a natural cotangent bundle structure or Lagrangian fibration is present. Even if the considered manifolds are cotangent bundles, a classification relying on this structure is not suitable in our context as we would like to admit general symplectic perturbations to Hamiltonian diffeomorphisms by symplectic integrators. This encourages us to generalise classical results relying on assumption (a) or (b).

10.1 Introduction

Let us recall some definitions from catastrophe theory as needed in this chapter. Of fundamental importance for the classification results is the notion of right equivalence of map germs.

Definition 10.1.1 (right equivalence of map germs)**.** Two germs of smooth maps $f, g\colon (\mathbb{R}^k, 0) \to (\mathbb{R}, 0)$ are *right equivalent* if there exists a germ of a diffeomorphism $h\colon (\mathbb{R}^k, 0) \to (\mathbb{R}^k, 0)$ such that $f = g \circ h$. △

Golubitsky and Guillemin (1975) show that the question whether two map germs are right equivalent has a geometric analogue, namely whether two Lagrangian submanifolds in a cotangent bundle have the same contact with the zero-section.

Definition 10.1.2 (tangential contact of Lagrangian intersections (in cotangent bundles))**.** Let Λ, Λ' be two Lagrangian submanifolds in the cotangent bundle T^*X intersecting a point $z \in X \subset T^*X$ tangentially. The submanifolds Λ, Λ' have the *same contact with X at z* if and only if there exists a symplectomorphism Φ defined on an open neighbourhood U of $z \in T^*X$ such that

$$\Phi(\Lambda \cap U) = \Lambda' \cap U, \quad \Phi(z) = z, \quad \Phi(X \cap U) = X \cap U. \qquad \triangle$$

They prove the following theorem.

Theorem 10.1.1 (Golubitsky and Guillemin, 1975)**.** *Let U be an open neighbourhood of 0 in $\mathbb{R}^k$. The germs at 0 of two smooth maps $f, g\colon U \to \mathbb{R}$ with $f(0) = 0 = g(0)$, vanishing gradients at 0, i.e. $\mathrm{d}f|_0 = 0 = \mathrm{d}g|_0$, and vanishing Hessian matrices at 0 (in any local coordinate system) are right equivalent if and only if the Lagrangian manifolds $\Lambda = \mathrm{d}f(U)$ and $\Lambda' = \mathrm{d}g(U)$ have the same tangential contact with the zero-section at 0 in T^*U.*

In the above theorem $\mathrm{d}f(U)$ and $\mathrm{d}g(U)$ denote the image of $U \subset \mathbb{R}^k$ under the 1-form $\mathrm{d}f$ or $\mathrm{d}g$, respectively, where 1-forms are interpreted as maps $U \to T^*U$, i.e. as sections of the cotangent bundle $T^*U \to U$.

The strength of Theorem 10.1.1 is related to the *parametric Morse lemma*, which says that up to a local change of coordinates any function germ $F\colon (\mathbb{R}^K, 0) \to (\mathbb{R}, 0)$ with critical point at 0 can be split into a nondegenerate quadratic map Q_F and a fully degenerate part f, i.e. a representative of the germ F can be brought into the form $f(x^1, \ldots, x^{k(F)}) + Q_F(x^{k(F)+1}, \ldots, x^K)$, where $K - k(F)$ is the rank of the Hessian matrix of F at 0 (Bröcker, 1975, §14.12). Therefore, $F, G\colon (\mathbb{R}^K, 0) \to (\mathbb{R}, 0)$ are right equivalent if and only if the signatures of Q_F and Q_G coincide and their fully reduced parts f and g fulfil the geometric condition in Theorem 10.1.1.

Thus, Theorem 10.1.1 is very appealing because it allows us to turn an analysis problem into a geometric problem. The geometric problem itself, i.e. the description of intersecting Lagrangian manifolds, is, however, important in its own right. It is not only a main ingredient in our classification of Hamiltonian boundary value problems but also occurs, for instance, in dynamical systems, where intersections of Lagrangian invariant manifolds in phase spaces encode important information about the dynamics (Haro, 2000; Lomelí, Meiss, and Ramírez-Ros, 2008a). For global aspects of Lagrangian intersections we refer to Fukaya, 2010 and references therein. It is, therefore, desirable, to obtain a reverse direction of Theorem 10.1.1, i.e. a statement which allows one to turn the description of (possibly non-tangentially) intersecting Lagrangian manifolds in arbitrary symplectic manifolds into a problem in classical singularity theory or catastrophe theory.

In this chapter we will show that we can assign smooth function germs to local Lagrangian intersection problems such that the following theorem holds.

Theorem 10.1.2. *Let X, Λ and X', Λ' be Lagrangian submanifolds of a symplectic manifold Z such that Λ intersects X in an isolated point z and Λ' intersects X' in an isolated point z. Let f be the function germ assigned to the problem $z \in X \cap \Lambda$ and f' be the function germ assigned to the problem $z' \in X' \cap \Lambda'$. The germs f and f' are stably right equivalent*[1] *if and only if there exists a local symplectomorphism Φ mapping an open neighbourhood U of z to an open neighbourhood U' of z' with*

$$\Phi(z) = z', \quad \Phi(X \cap U) = X' \cap U', \quad \Phi(\Lambda \cap U) = \Lambda' \cap U'.$$

In other words (notions will be made precise later):

Theorem 10.1.3. *There exists a 1-1 correspondence between Lagrangian contact problems modulo stably contact equivalence and smooth real-valued function germs up to stably right equivalence.*

The theorems overcome the following issues which occur when trying to reverse Theorem 10.1.1.

- Let X, Λ be Lagrangian submanifolds of a symplectic manifold Z such that Λ intersects X in an isolated point z. After shrinking all manifolds around z, if necessary, there are many ways of mapping Z symplectically to a neighbourhood of the zero-section $X \subset T^*X$. We will refer to a particular choice of such an identification as a *choice of a cotangent bundle structure*. For most structures, Λ is the image of a section $\mathrm{d}f$ in the bundle $T^*X \to X$. The map f is not defined

[1] Two function germs are stably right equivalent if they become right equivalent after adding non-degenerate quadratic forms in new variables (see Definition 10.2.3).

independently of the auxiliary cotangent bundle structure but we will show that its stably right equivalence class is well-defined.

- The Lagrangian manifold $\mathrm{d}f(U)$ from Theorem 10.1.1 intersects the zero-section of $U \subset T^*U$ tangentially at 0. Golubitsky and Guillemin's proof of the *only if* direction fails when the intersection of U with $\mathrm{d}f(U)$ is not tangential. Indeed, the equivalence relation right equivalence considered by Golubitsky and Guillemin (1975) needs to be relaxed to stably right equivalence when non-tangential intersections are allowed.

The results may be compared with the correspondence of embeddings of a Lagrangian submanifold into a cotangent bundle with catastrophe theory (Bates and Weinstein, 1997). There, singularities occur because Lagrangian submanifolds fail to be projectable and intersect non-transversally with fibres. In contrast, in this chapter cotangent bundle structures are just of an auxiliary nature.

Furthermore, we provide a parameter-dependent version of the results and relate families of intersecting Lagrangian manifolds to unfoldings of singular map germs.

Theorem 10.1.4. *There exists a 1-1 correspondence between parameter-dependent Lagrangian contact problems up to stably right equivalence and unfoldings of smooth, real-valued function germs up to stably right equivalence as unfoldings.*

This allows transporting the highly developed notions and algebraic framework of catastrophe theory to Lagrangian contact problems and bifurcations of Lagrangian intersection problems. As a corollary, classification results for singularities apply to Lagrangian contact problems.

Moreover, intersection problems of Lagrangian manifolds are often subject to symmetry constraints which have an effect on which singularities occur generically and how the intersections unfold when parameters are present. Such symmetry constraints appear, for instance, in Hamiltonian boundary value problems as seen in Chapters 7 and 8. We will revisit our symmetry considerations within a purely geometric picture and show under which conditions symmetries in Lagrangian contact problems and in boundary value problems for symplectic maps, in particular, yield invariances of the assigned function germs.

The remainder of the chapter is structured as follows. In Section 10.2 we first review some of Golubitsky and Guillemin's results, and then prove that not necessarily tangential Lagrangian contact problems in arbitrary symplectic manifolds up to contact equivalence correspond to map germs up to stably right equivalence. In Section 10.3 we consider a symmetric setting and prove that invariances of generating functions of Lagrangian contact problems correspond to cotangent lifted maps leaving the manifolds of the contact problem invariant. In Section 10.4 we extend the identification results of

Section 10.2 to families of Lagrangian contact problems. In Section 10.5 we conclude the Theorems 10.1.3 and 10.1.4 and fit our application to boundary value problems for symplectic maps into this framework.

10.2 Lagrangian contact problems and catastrophe theory

Let us introduce the notion of *Lagrangian contact problems* and review some definitions based on Golubitsky and Guillemin, 1975; Mather, 1968.

Definition 10.2.1 (Lagrangian contact problem)**.** Let X, Λ be two Lagrangian submanifolds of a symplectic manifold Z intersecting in an isolated point $z \in \Lambda \cap X$. Then (X, Λ, z) is called a *Lagrangian contact problem (in Z)*. We say Λ *has contact with X in z*. In the special case where X and Λ are tangential at z the problem (X, Λ, z) is called a *tangential Lagrangian contact problem*. △

Definition 10.2.2 (contact equivalence of Lagrangian contact problems)**.** Let (X, Λ, z) and (X', Λ', z') be two Lagrangian contact problems in Z and Z', respectively. We say that (X, Λ, z) and (X', Λ', z') are *contact equivalent* or Λ *has the same contact* with X at z as Λ' has contact with X' at z' if there exist open neighbourhoods $U \subset Z$ of z and $U' \subset Z'$ of z' and a symplectic diffeomorphism $\Phi\colon U \to U'$ such that

$$\Phi(z) = z', \quad \Phi(X \cap U) = X' \cap U', \quad \Phi(\Lambda \cap U) = \Lambda' \cap U'. \qquad \triangle$$

Definition 10.2.3 (stably right equivalence of function germs)**.** Two germs of smooth maps $f\colon (\mathbb{R}^k, 0) \to (\mathbb{R}, 0)$, $x \mapsto f(x)$ and $g\colon (\mathbb{R}^l, 0) \to (\mathbb{R}, 0)$, $y \mapsto g(y)$ are *stably right equivalent* if there exist nondegenerate quadratic forms $Q_F(u)$ and $Q_G(v)$ such that the germs at 0 of $F(x, u) := f(x) + Q_F(u)$ and $G(y, v) := g(y) + Q_G(v)$ are right equivalent. △

Theorem 10.2.1. *Two germs of smooth maps $f, g\colon (\mathbb{R}^k, 0) \to (\mathbb{R}, 0)$, $x \mapsto f(x)$ in the same number of variables are stably right equivalent if and only if they are right equivalent.*

Proof. The statement follows from Weinstein's (1971a) strong form of the splitting lemma that we have recalled as Theorem 5.3.2. See Corollary 5.3.4. □

Remark 10.2.1 (Warning). Contact equivalence for Lagrangian contact problems is not to be confused with Mather's (1968) notion of contact equivalence for map germs which is related to the contact of a smooth manifold with a zero section of a smooth bundle (i.e. without symplectic structure). △

Definition 10.2.4 (cotangent bundle structure and projection)**.** Let X be a Lagrangian submanifold of a symplectic manifold Z. A symplectomorphism Φ from an open neighbourhood $U \subset Z$ with $X \subset U$ to a tubular neighbourhood of the zero section of $\pi\colon T^*X \to X$ is called a *cotangent bundle structure for Z (with respect to X)*. The map $\pi \circ \Phi$ is called the *(cotangent bundle) projection with respect to the structure Φ*. △

Remark 10.2.2. The existence of cotangent bundle structures (for a sufficiently small neighbourhood U of X) is guaranteed by Weinstein's generalisation of Darboux's theorem, see, for instance, Libermann and Marle, 1987, Thm. 15.3. Notice that, in comparison to the existence of local Darboux coordinates, Weinstein's generalisation has a global character since X does not need to be shrunk for symplectomorphisms to exist. As all considerations in this chapter are local, the globality is only exploited for notational convenience in this context. Moreover, we may refer to a function germ and a representative with the same symbol where a differentiation is not essential. △

Remark 10.2.3. Cotangent bundle structures for a symplectic manifold Z with respect to a Lagrangian submanifold X correspond to completely integrable Lagrangian subbundles of the tangent bundle TZ transverse to X. (See Libermann and Marle, 1987 for details.) Moreover, cotangent bundle structures are in 1 to 1 correspondence with 1-forms whose zero-set is X and whose exterior derivative is the symplectic structure. The cotangent bundle structure $\Phi\colon U \to V$, where U is an open neighbourhood of X and V is an open neighbourhood of the zero section of T^*X, associated to such a 1-form α is such that $\Phi^*\lambda = \alpha$ (Libermann and Marle, 1987; Golubitsky and Guillemin, 1975). △

For reference, let us recall some of Golubitsky and Guillemin's results and provide proofs for the cases where we would like to use the statement in a more general setting than in the original paper.

Lemma 10.2.2 (Golubitsky and Guillemin, 1975, Lemma 3.1)**.** *Let X be a Lagrangian submanifold of a symplectic manifold Z. Let $x_1, \dots, x_n$ be local coordinates on X centred at z. Consider two cotangent bundle structures Φ^α and Φ^β on Z with respect to X around z. Let $\xi_1, \dots, \xi_n$ be the conjugate momenta to $x_1, \dots, x_n$ with respect to the first structure. Let λ denote the canonical 1-form on T^*X, $\alpha \coloneqq (\Phi^\alpha)^*\lambda$, $\beta \coloneqq (\Phi^\beta)^*\lambda$. The closed 1-form $\alpha - \beta$ can locally be written as $\mathrm{d}H$ with*

$$H(x,\xi) = \sum_{i,j=1}^{n} h_{ij}(x,\xi)\xi_i\xi_j. \tag{10.2.1}$$

If the Lagrangian submanifold $\Lambda \subset Z$ is the image of the section $\mathrm{d}\phi^\alpha$ with respect to the Φ^α-structure as well as the image of the section $\mathrm{d}\phi^\beta$ with respect to the Φ^β-structure,

then

$$(\phi^\beta \circ k_{\alpha\beta})(x) = \phi^\alpha(x) + H(x, \nabla\phi^\alpha(x)) + \text{const.}, \tag{10.2.2}$$

where $k_{\alpha\beta}$ is the diffeomorphism $k_{\alpha\beta} = \pi^\beta \circ (\pi^\alpha|_\Lambda)^{-1}$. Here π^α and π^β are the projections corresponding to Φ^α and Φ^β, respectively.

Proof. The 1-forms α and β are primitives of the symplectic form on Z. Moreover, $\alpha|_z = 0$ if and only if $z \in X$. Analogously for β. Therefore, $\alpha - \beta$ is closed and has a local primitive H. The primitive must be of the form (10.2.1): in local coordinates we have

$$\alpha = \sum_j \xi_j \mathrm{d}x_j, \quad \beta = \sum_j (b_j \mathrm{d}x_j + c_j \mathrm{d}\xi_j), \quad \mathrm{d}H = \sum_j \left(\frac{\partial H}{\partial x_j} \mathrm{d}x_j + \frac{\partial H}{\partial \xi_j} \mathrm{d}\xi_j \right).$$

Now

$$\sum_j ((\xi_j - b_j)\mathrm{d}x_j + c_j \mathrm{d}\xi_j) = \alpha - \beta = \mathrm{d}H = \sum_j \left(\frac{\partial H}{\partial x_j} \mathrm{d}x_j + \frac{\partial H}{\partial \xi_j} \mathrm{d}\xi_j \right). \tag{10.2.3}$$

Setting $\xi = 0$ in (10.2.3) and using $c_j(x, 0) \equiv 0$ (which follows from $\beta|_{(x,\xi)=(x,0)} = 0$) we deduce that $\frac{\partial H}{\partial \xi_j}(x, 0) \equiv 0$. By Taylor's theorem there exists a primitive of the form (10.2.1).

Let $\iota \colon \Lambda \hookrightarrow Z$ denote the embedding of Λ into Z. The 1-forms $\iota^*\alpha$ and $\iota^*\beta$ are closed since Λ is Lagrangian. Locally around a point of interest $\iota^*\alpha$ and $\iota^*\beta$ have primitives which we denote by ϕ^α and ϕ^β, respectively. Due to $\iota^*\alpha - \iota^*\beta = \mathrm{d}(H \circ \iota)$ we have

$$\phi^\beta = \phi^\alpha + H \circ \iota + \text{const.} \tag{10.2.4}$$

on Λ. Expressing relation (10.2.4) in the canonical coordinates (x, ξ) of the α-cotangent bundle structure yields (10.2.2). □

Remark 10.2.4. If the manifolds X and Λ intersect nontrivially and $x_1, \ldots, x_n$ are centred coordinates at an intersection point of Λ and X, then the constant in (10.2.2) vanishes if we choose $\phi^\alpha(0) = \phi^\beta(0)$. △

The following lemma corresponds to Golubitsky and Guillemin, 1975, Prop.4.2 which is a result by Tougeron, 1968, p. 209 and is also contained in Weinstein, 1972, Appendix.

Lemma 10.2.3. *Let*

$$H(x, \xi) = \sum_{i,j=1}^{n} h_{ij}(x, \xi)\xi_i\xi_j$$

be defined on an open neighbourhood of the origin in $\mathbb{R}^n \times \mathbb{R}^n$. Consider a real valued map ϕ defined on an open neighbourhood of 0 in $\mathbb{R}^n$ such that $\phi(0) = 0$, $\nabla\phi(0) = 0$,

Hess $\phi(0) = 0$. *The map*

$$\psi(x) = \phi(x) + H(x, \nabla\phi(x)) \tag{10.2.5}$$

is right equivalent to ϕ on a neighbourhood of the origin in $\mathbb{R}^n$ and the right equivalence fixes the origin.

Proof. To simplify notation, we set

$$\overline{H}(x) = H(x, \nabla\phi(x)), \quad \overline{h}_{ij}(x) = h_{ij}(x, \nabla\phi(x)).$$

We prove the assertion using the homotopy method: define

$$\psi_t(x) = \phi(x) + t\overline{H}(x). \tag{10.2.6}$$

We seek a family of local diffeomorphisms f_t fixing 0 such that

$$\psi_t \circ f_t = \phi. \tag{10.2.7}$$

Differentiating (10.2.7) with respect to t we find

$$\frac{\mathrm{d}}{\mathrm{d}t}(\psi_t) \circ f_t + \left\langle \nabla\psi_t \circ f_t, \frac{\mathrm{d}}{\mathrm{d}t} f_t \right\rangle = 0.$$

Here, $\langle \cdot, \cdot \rangle$ denotes the scalar product in $\mathbb{R}^n$. An evaluation at $f_t^{-1}(x)$ yields

$$\frac{\mathrm{d}}{\mathrm{d}t}\psi_t + \langle \nabla\psi_t, w(x,t) \rangle = 0 \tag{10.2.8}$$

with

$$w(x,t) = \frac{\mathrm{d}}{\mathrm{d}t}(f_t)(f_t^{-1}(x)). \tag{10.2.9}$$

We will show that the ODE (10.2.8) is solvable for w around $x = 0$ with $w(0,t) = 0$. Then there exists an open neighbourhood $U \subset \mathbb{R}^n$ of 0 such that the initial value problem

$$\frac{\mathrm{d}}{\mathrm{d}t} f_t(x) = w(f_t(x), t), \quad f_0(x) = x \tag{10.2.10}$$

can be solved for all $x \in U$ on the interval $t \in [0,1]$. The obtained family of functions f_t fulfils $\frac{\mathrm{d}}{\mathrm{d}t}(\psi_t \circ f_t) = 0$ with $f_0 = \mathrm{id}$ and, therefore, (10.2.7). Moreover, $f_t(0) \equiv 0$ such that f_1 is the required right equivalence.

We now show that near $x = 0$ the ODE (10.2.8) is solvable for w with $w(0,t) = 0$.

Differentiating (10.2.6) with respect to x yields

$$\begin{aligned}\frac{\partial \psi_t}{\partial x_l} &= \frac{\partial \phi}{\partial x_l} + t\sum_{i,j}\left(\frac{\partial \overline{h}_{ij}}{\partial x_l}\frac{\partial \phi}{\partial x_i}\frac{\partial \phi}{\partial x_j} + 2\overline{h}_{ij}\frac{\partial^2 \phi}{\partial x_i \partial x_l}\frac{\partial \phi}{\partial x_j}\right)\\ &= \sum_j \underbrace{\left(\delta_{lj} + t\sum_i\left(\frac{\partial \overline{h}_{ij}}{\partial x_l}\frac{\partial \phi}{\partial x_i} + 2\overline{h}_{ij}\frac{\partial^2 \phi}{\partial x_i \partial x_l}\right)\right)}_{=:B_{lj}(t,x)}\frac{\partial \phi}{\partial x_j}\end{aligned} \tag{10.2.11}$$

The maps $B_{lj}(t,x)$ form a matrix B with $B(t,0) = \mathrm{Id}$. Therefore, there exists a neighbourhood of $x = 0$ such that B is invertible for all $t \in [0,1]$. We have

$$\nabla \phi = B^{-1}\nabla \psi_t. \tag{10.2.12}$$

The functions $\overline{h}_{ij}$ constitute a matrix which we denote by $\mathcal{H}$. Differentiating (10.2.6) with respect to t and using (10.2.12) we get

$$\frac{\mathrm{d}}{\mathrm{d}t}\psi_t = \nabla\phi^\top \mathcal{H}\nabla\phi \overset{(10.2.12)}{=} \nabla\psi_t^\top \underbrace{B^{-T}\mathcal{H}\nabla\phi}_{=:-w}.$$

Now $w(0,t) = 0$ and w solves (10.2.8). This completes the proof. □

The Lemmas 10.2.2 and 10.2.3 imply the following proposition.

Proposition 10.2.4. *Let (X,Λ,z) be a tangential Lagrangian contact problem in Z. Consider two cotangent bundle structures over X near z such that Λ is the image of the section $\mathrm{d}\phi^\alpha$ and $\mathrm{d}\phi^\beta$ with $\phi^\alpha(z) = 0 = \phi^\beta(z)$. Then ϕ^α and ϕ^β are right equivalent.*

Remark 10.2.5. As X and Λ are tangential at z, for any cotangent bundle structure the submanifold Λ is the image of a section of the cotangent bundle locally around the point of contact. This is not true for general Lagrangian contact problems. △

Theorem 10.2.5. *Let (X,Λ,z) and (X,Λ',z) be two tangential Lagrangian contact problems in Z. For any cotangent bundle structure over X near z such that Λ is the image of the section $\mathrm{d}\phi$ and Λ' the image of $\mathrm{d}\phi'$ with $\phi(z) = 0 = \phi'(z)$, the map germs ϕ and ϕ' are right equivalent if and only if the tangential Lagrangian intersection problems are contact equivalent.*

Proof. In the following, we may shrink Z, X, Λ, Λ' repeatedly to intersections with open neighbourhoods of z without mentioning. Assume $\phi = \phi' \circ r$ for a right equivalence r such that r fixes z. Its cotangent lifted map R (see Marsden and Ratiu, 1999a, §6.3 for definitions) fixes X and

$$R(\mathrm{d}\phi'|_x) = \mathrm{d}\phi'|_x \circ \mathrm{d}r|_{r^{-1}(x)} = \mathrm{d}(\phi' \circ r)|_{r^{-1}(x)} = \mathrm{d}\phi|_{r^{-1}(x)}, \qquad x \in X.$$

Therefore, the symplectic diffeomorphism R maps Λ' to Λ and, thus, provides a contact equivalence between (X, Λ, z) and (X, Λ', z).

Now assume there exists a symplectic diffeomorphism with $\Phi(X) = X$, $\Phi(z) = z$ and $\Phi(\Lambda) = \Lambda'$. Choose a cotangent bundle structure with projection denoted by $\pi\colon Z \to X$ such that Λ is the image of the section $\mathrm{d}\phi$ and Λ' the image of the section $\mathrm{d}\phi'$ around z with $\phi(z) = 0 = \phi'(z)$. Using Φ we can obtain a new cotangent bundle structure with bundle projection $\pi'\colon Z \to X$ such that $\pi' = \pi \circ \Phi^{-1}$. The map $\Phi \circ \mathrm{d}\phi$ maps X onto Λ' and is a section of $\pi'\colon Z \to X$. This means Λ' can be represented by $\mathrm{d}\phi$ in the new structure. Therefore, by Proposition 10.2.4, the map germs ϕ and ϕ' must be right equivalent. □

We recall the well-known *parametric Morse Lemma* or *Splitting Lemma* and establish some notation.

Lemma 10.2.6 (parametric Morse lemma)**.** *Let $\phi\colon (\mathbb{R}^n, 0) \to (\mathbb{R}, 0)$ be a function germ with critical point at the origin 0. Consider the decomposition $\mathbb{R}^n = \overline{X} \oplus \underline{X}$ for two linear subspaces $\overline{X}$ and $\underline{X}$ such that the Hessian matrix B of the restriction $\phi|_{\underline{X}}\colon (\underline{X}, 0) \to (\mathbb{R}, 0)$ is invertible. There exists a change of coordinates K on a neighbourhood of $0 \in \mathbb{R}^n$ of the form $K(\overline{x}, \underline{x}) = (\overline{x}, \kappa(\overline{x}, \underline{x}))$ with $K(0, 0) = (0, 0)$ such that*

$$(\phi \circ K)(\overline{x}, \underline{x}) = f(\overline{x}) + \underline{x}^\top B \underline{x}.$$

If we choose the dimension of $\underline{X}$ to be maximal,[2] then the 2-jet of f vanishes.

A proof is given in Bröcker, 1975, §14.12 or in Wassermann, 1974, Lemma 5.12. A fibred version including uniqueness results can be found in Weinstein, 1971a and is recalled as Theorem 5.3.2 in Section 5.3.

We leave the setting of tangential Lagrangian contact problems and extend Proposition 10.2.4: a function germ assigned to a (not necessarily tangential) Lagrangian intersection problem using any cotangent bundle structure for which the intersection problem is graphical is well-defined up to stably right equivalence. For this we first prove the following lemma.

Lemma 10.2.7. *On $\mathbb{R}^n = \overline{X} \oplus \underline{X}$ consider*

- *coordinates $x = (\overline{x}, \underline{x}) = ((x^1, \ldots, x^k), (x^{k+1}, \ldots, x^n))$,*
- *a nondegenerate symmetric matrix $Q \in \mathbb{R}^{(n-k)\times(n-k)}$,*
- *a map $g\colon \mathbb{R}^k \to \mathbb{R}^k$ whose 2-jet vanishes at 0,*

[2] We can choose $\dim \underline{X}$ to be the rank of the Hessian matrix of ϕ at 0

- *and a matrix valued function* $\mathcal{H}\colon \mathbb{R}^n \to \mathrm{Sym}(n)$ *with*

$$\mathcal{H}(x) = (h_{ij}(x))_{i,j=1,\dots,n} = \begin{pmatrix} H^{11}(x) & H^{12}(x) \\ H^{12}(x)^\top & 0 \end{pmatrix} \in \mathrm{Sym}(n) \subset \mathbb{R}^{n\times n}$$

for $H^{11}(x) \in \mathrm{Sym}(k)$ *and* $H^{12}(x) \in \mathbb{R}^{k\times(n-k)}$.

For $t \in \mathbb{R}$ *let*

$$\begin{aligned} \psi(x) &= g(\overline{x}) + \underline{x}^\top Q \underline{x} \\ \psi_t(x) &= g(\overline{x}) + \underline{x}^\top Q \underline{x} + t(\nabla\psi(x)^\top \mathcal{H}(x) \nabla\psi(x)). \end{aligned}$$

Then ψ_t *is right equivalent to* $\psi = \psi_0$ *around* $x = 0$ *and the right equivalence fixes 0.*

Proof. Motivated by the proof of Lemma 10.2.3 we define the components $B_{lj}(t,x)$ of a matrix $B(t,x) \in \mathbb{R}^{n\times n}$ as

$$B_{lj} = \delta_{lj} + t \sum_i \left(\frac{\partial h_{ij}}{\partial x_l} \frac{\partial \psi}{\partial x_i} + 2h_{ij} \frac{\partial^2 \psi}{\partial x_i \partial x_l} \right).$$

We have

$$B(t,0) = \mathrm{Id}_n + 2t\mathrm{Hess}\,\psi(0)\mathcal{H}(0) = \begin{pmatrix} \mathrm{Id}_k & 0 \\ 4tQH^{12}(0)^\top & \mathrm{Id}_{n-k}, \end{pmatrix} \tag{10.2.13}$$

which is invertible for all t. Using the same calculation as in (10.2.11) we obtain

$$\nabla\psi_t(x) = B(t,x)\nabla\psi(x).$$

Therefore,

$$\frac{\mathrm{d}}{\mathrm{d}t}\psi_t = \nabla\psi^\top \mathcal{H} \nabla\psi = \nabla\psi_t^\top \underbrace{B^{-T}\mathcal{H}\nabla\psi}_{=:-\omega} = -\langle \nabla\psi_t, \omega\rangle. \tag{10.2.14}$$

There exists a neighbourhood U of $0 \in \mathbb{R}^n$ such that the initial value problem

$$\frac{\mathrm{d}}{\mathrm{d}t} f_t(x) = \omega(f_t(x), t), \quad f_0(x) = x$$

is solvable for all $x \in U$ and all $t \in [0,1]$. Since $\omega(0,t) = 0$ we have $f_t(0) = 0$ and

$$\begin{aligned} \frac{\mathrm{d}}{\mathrm{d}t}(\psi_t \circ f_t) &= \frac{\mathrm{d}}{\mathrm{d}t}(\psi_t) \circ f_t + \left\langle \nabla\psi_t \circ f_t, \frac{\mathrm{d}}{\mathrm{d}t} f_t \right\rangle \\ &= \frac{\mathrm{d}}{\mathrm{d}t}(\psi_t) \circ f_t + \langle \nabla\psi_t, \omega\rangle \circ f_t \\ &\overset{(10.2.14)}{=} 0. \end{aligned}$$

Since $f_0 = \mathrm{id}_U$ we have

$$\psi_t \circ f_t = \psi_0 \circ f_0 = \psi$$

and f_t is the required right equivalence. □

Proposition 10.2.8. *Let (X, Λ, z) be a Lagrangian contact problem in Z. After shrinking Z to a sufficiently small neighbourhood of z, consider two cotangent bundle structures over X with projections $\pi^\alpha \colon Z \to X$, $\pi^\beta \colon Z \to X$ such that Λ is given as the image of the section $\mathrm{d}\phi^\alpha$ and $\mathrm{d}\phi^\beta$, respectively, whereas $\phi^\alpha(z) = 0 = \phi^\beta(z)$. Then the germs of ϕ^α and ϕ^β at z are stably right equivalent.*

Proof. By the parametric Morse Lemma (Lemma 10.2.6) there exist coordinates $x = (\overline{x}, \underline{x}) = ((x^1, \dots, x^k), (x^{k+1}, \dots, x^n))$ on X centred at z such that

$$\phi^\alpha(x) = f(\overline{x}) + \underline{x}^\top B \underline{x}$$

for a smooth function germ f with vanishing 2-jet at $\overline{x} = 0$ and an invertible symmetric matrix B. The map ϕ^α is stably right equivalent to f. By Lemma 10.2.2 we have

$$\phi^\beta \circ k_{\alpha\beta} = \phi^\alpha + H(x, \nabla\phi^\alpha), \tag{10.2.15}$$

for a map

$$H(x,\xi) = \sum_{i,j=1}^{n} h_{ij}(x,\xi)\xi_i\xi_j = \xi^\top \begin{pmatrix} H^{11}(x,\xi) & H^{12}(x,\xi) \\ H^{12}(x,\xi)^\top & H^{22}(x,\xi) \end{pmatrix} \xi$$

with matrices $H^{11}(x,\xi) \in \mathrm{Sym}(k)$, $H^{22}(x,\xi) \in \mathrm{Sym}(n-k)$, and $H^{12}(x,\xi) \in \mathbb{R}^{k\times(n-k)}$ and with $k_{\alpha\beta} = \pi^\beta \circ (\pi^\alpha|_\Lambda)^{-1}$. For $i, j \in \{1, 2\}$ define

$$\mathcal{H}(x) \coloneqq \mathcal{H}(\overline{x}, \underline{x}) \coloneqq H(x, \nabla\phi^\alpha(x)), \quad \mathcal{H}^{ij}(x) \coloneqq \mathcal{H}^{ij}(\overline{x}, \underline{x}) \coloneqq H^{ij}(x, \nabla\phi^\alpha(x)).$$

Therefore,

$$\mathcal{H}(x) = \nabla_{\overline{x}} f(\overline{x})^\top \mathcal{H}^{11}(x) \nabla_{\overline{x}} f(\overline{x}) + 4\underline{x}^\top B \mathcal{H}^{12}(x)^\top \nabla_{\overline{x}} f(\overline{x}) + 4\underline{x}^\top B \mathcal{H}^{22}(x) B \underline{x}.$$

We calculate

$$\begin{aligned} \phi^\beta(k_{\alpha\beta}(\overline{x}, \underline{x})) &\overset{(10.2.15)}{=} \phi^\alpha(\overline{x}, \underline{x}) + \mathcal{H}(x) \\ &= f(\overline{x}) + \underline{x}^\top (B + 4B\mathcal{H}^{22}(x)B)\underline{x} \\ &\quad + \nabla_{\overline{x}} f(\overline{x})^\top \mathcal{H}^{11}(x) \nabla_{\overline{x}} f(\overline{x}) + 4\underline{x}^\top B \mathcal{H}^{12}(x)^\top \nabla_{\overline{x}} f(\overline{x}). \end{aligned} \tag{10.2.16}$$

Let us define

$$B'(x) = B + 4B\mathcal{H}^{22}(x)B.$$

The kernel of Hess (ϕ^α) and the kernel of Hess (ϕ^β) at $(\overline{x}, \underline{x}) = (0,0)$ both describe the intersection $T_zX \cap T_z\Lambda$ (but in different coordinates). Indeed, the kernel of Hess $(\phi^\beta \circ k_{\alpha\beta})$ must coincide with the kernel of Hess (ϕ^α) which is $\overline{X} = \{\underline{x} = 0\}$. We calculate the Hessian matrix of $\phi^\beta \circ k_{\alpha\beta}$ at $(\overline{x}, \underline{x}) = (0,0)$ using (10.2.16) and obtain

$$\text{Hess}\,(\phi^\beta \circ k_{\alpha\beta})(0,0) = \begin{pmatrix} 0 & 0 \\ 0 & 2B'(0) \end{pmatrix}.$$

Since Λ is graphical in both cotangent bundle structures, $B'(0)$ must be invertible by a dimension argument. The function ϕ^α is stably right equivalent to

$$\phi_1^\alpha(x) := f(\overline{x}) + \underline{x}^\top B'(0)\underline{x}.$$

For x in a sufficiently small neighbourhood of 0 the signature of $B'(x)$ is constant. By Sylvester's law of inertia, there exists a smooth family of invertible matrices $A(x)$ such that

$$A(x)^{-T}B'(x)A^{-1}(x) = B'(0) \tag{10.2.17}$$

for all x near 0. Consider

$$r(\overline{x}, \underline{x}) = (\overline{x}, A(x)\underline{x}).$$

The map r fixes $x = 0$ and is a diffeomorphism on a neighbourhood of $x = 0$: the Jacobian matrix of r is given by the block matrix

$$\mathrm{D}r(x) = \begin{pmatrix} \mathrm{Id}_k & 0 \\ (\partial A(x))_{l=1,\dots,k} & (\partial A(x))_{l=k+1,\dots,n} + A(x) \end{pmatrix},$$

where $(\partial A(x))_{l=1,\dots,k}$ denotes the first k columns and $(\partial A(x))_{l=k+1,\dots,n}$ the remaining $n-k$ columns of an $(n-k) \times n$ matrix $\partial A(x)$ whose l-th column is given as

$$(\partial A(x))_l = \frac{\partial A}{\partial x^l}(x)\underline{x},$$

where the derivative $\frac{\partial A}{\partial x^l}$ is taken component-wise. Now the determinant of $\mathrm{D}r(0)$ coincides with the determinant of $A(0)$ which is non-zero, so r is indeed a right equivalence.

Let us define

$$\begin{aligned} \tilde{\mathcal{H}}^{11}(x) &= \mathcal{H}^{11}(r^{-1}(x)) \\ \tilde{\mathcal{H}}^{12}(x) &= \mathcal{H}^{12}(r^{-1}(x))BA(r^{-1}(x))^{-1}B'(0)^{-1} \end{aligned} \tag{10.2.18}$$

By Lemma 10.2.7 the map ϕ_1^α is right equivalent to

$$\begin{aligned}\phi_2^\alpha(x) :&= f(\overline{x}) + \underline{x}^\top B'(0)\underline{x} \\ &\quad + \nabla_{\overline{x}} f(\overline{x})^\top \tilde{\mathcal{H}}^{11}(x)\nabla_{\overline{x}} f(\overline{x}) + 4\underline{x}^\top B'(0)\tilde{\mathcal{H}}^{12}(x)^\top \nabla_{\overline{x}} f(\overline{x}).\end{aligned}$$

We have

$$\begin{aligned}(\phi_2^\alpha \circ r)(x) = f(\overline{x}) &+ \underline{x}^\top A(x)^\top B'(0)A(x)\underline{x} + \nabla_{\overline{x}} f(\overline{x})^\top \tilde{\mathcal{H}}^{11}(r(x))\nabla_{\overline{x}} f(\overline{x}) \\ &+ 4\underline{x}^\top A(x)^\top B'(0)\tilde{\mathcal{H}}^{12}(r(x))^\top \nabla_{\overline{x}} f(\overline{x}).\end{aligned} \tag{10.2.19}$$

Comparing (10.2.19) with (10.2.16) shows that the function $\phi_2^\alpha \circ r$ coincides with $\phi^\beta \circ k_{\alpha\beta}$. Thus, the maps ϕ^α and ϕ^β are stably right equivalent. □

Remark 10.2.6. We see from the proof of Proposition 10.2.8 that if the intersection of Λ and X is not tangential, then the dimension of $\underline{X}$ is greater than 0 and there exist two cotangent bundle structures such that ϕ^α and ϕ^β are stably right equivalent but *not* right equivalent: to a cotangent bundle structure over X defined[3] by a canonical 1-form α for which Λ is graphical choose another cotangent bundle structure $\beta = \alpha + \mathrm{d}H$ with

$$H(x,\xi) = \xi^\top \begin{pmatrix} 0 & 0 \\ 0 & \frac{1}{4}(B^{-1}DB^{-1} - B^{-1}) \end{pmatrix} \xi,$$

where D is an invertible symmetric matrix which has a different signature than B. As in the proof of Proposition 10.2.8, the coordinates (x,ξ) refer to Darboux coordinates with respect to the α-structure. We get $B' = D$ which is invertible such that Λ is graphical for the cotangent bundle structure defined by β. However, the signatures of $\operatorname{Hess}\phi^\alpha(0)$ and $\operatorname{Hess}\phi^\beta(0)$ do not coincide. △

Remark 10.2.7 (existence of cotangent bundle structures). Let (X,Λ,z) be a Lagrangian contact problem in a symplectic manifold Z. It is easy to see from a perturbation argument or from the classification of intersections of Lagrangian linear subspaces of finite dimensional symplectic vector spaces (Lorand and Weinstein, 2015) that there is always a cotangent bundle structure $\pi\colon Z \to X$ such that Λ is graphical, i.e. the image of a smooth section of $\pi\colon Z \to X$ locally around z or, equivalently, s.t. $\pi|_\Lambda\colon \Lambda \to X$ is an immersion around z. Indeed, we provide a proof in Lemma 6.3.3. △

Definition 10.2.5 ((fully reduced) generating function)**.** Let (X,Λ,z) be a Lagrangian contact problem in Z. Consider a cotangent bundle structure such that Λ is given as the image of the section $\mathrm{d}\phi$ locally around $z \in Z$ with $\phi(z) = 0$. We refer to ϕ, to the germ of ϕ at z, and to (the germ at 0 of) a coordinate expression of ϕ with centred coordinates at z as a *generating function of* (X,Λ,z). By the parametric Morse Lemma

[3]Recall from Remark 10.2.3 that suitable 1-forms define cotangent bundle structures.

(Lemma 10.2.6) there exist coordinates $x = (\overline{x}, \underline{x}) = ((x^1, \dots, x^k), (x^{k+1}, \dots, x^n))$ on X centred at z such that

$$\phi(x) = f(\overline{x}) + \underline{x}^\top B \underline{x}$$

for a smooth function germ f with vanishing 2-jet and an invertible matrix B. The map germ f is called a *fully reduced generating function of* (X, Λ, z). △

Now Proposition 10.2.8 can be phrased as follows.

Corollary 10.2.9. *Generating functions of Lagrangian contact problems are defined up to stably right equivalence.*

Using Theorem 10.2.1 we obtain the following corollary.

Corollary 10.2.10. *Fully reduced generating functions of Lagrangian contact problems are defined up to right equivalence.*

Lemma 10.2.11. *Consider a symplectic diffeomorphism $\Phi\colon Z \to Z'$. Any generating function of a Lagrangian contact problem (X, Λ, z) in Z is right equivalent to any generating function of the Lagrangian contact problem $(\Phi(X), \Phi(\Lambda), \Phi(z))$ in Z' when shrinking all involved manifolds to intersections with open neighbourhoods of $z \in Z$ or $\Phi(z) \in Z'$, if necessary.*

Proof. Cotangent bundle structures on Z over X correspond to cotangent bundle structures on Z' over $\Phi(X)$, whereas the corresponding canonical 1-forms λ and λ' relate by $\lambda = \Phi^*\lambda'$. Therefore, if $\iota\colon \Lambda \hookrightarrow Z$ is the embedding of Λ into Z and $\iota' = \Phi \circ \iota \circ (\Phi^{-1})|_{\Phi(\Lambda)}$ the embedding of $\Phi(\Lambda)$ into Z', then

$$\iota'^*\lambda' = (\Phi^{-1})|^*_{\Phi(\Lambda)} \iota^*\lambda.$$

Thus, the primitive of $\iota'^*\lambda'$ around $\Phi(z)$ which vanishes at $\Phi(z)$ and the primitive of $\iota^*\lambda$ around z which vanishes at z relate by $(\Phi^{-1})|_{\Phi(\Lambda)}$. Expressing the primitives in coordinates on X or $\Phi(X)$, we obtain generating functions which are right equivalent. □

We can now extend Theorem 10.2.5 to non-tangential Lagrangian contact problems.

Theorem 10.2.12. *Two Lagrangian contact problems (X, Λ, z) in Z and (X', Λ', z') in Z' with $\dim Z = \dim Z'$ are contact equivalent if and only if their generating functions are stably right equivalent.*

Proof. By Lemma 10.2.11 and the local nature of the problem it is sufficient to consider $Z' = Z$, $X' = X$ and $z' = z$. In the following we may shrink Z and all embedded manifolds to their intersections with open neighbourhoods of z repeatedly without

mentioning. Assume there exists a symplectic diffeomorphism with $\Phi(X) = X$, $\Phi(z) = z$ and $\Phi(\Lambda) = \Lambda'$. As justified in Remark 10.2.7, there exists a cotangent bundle structure over X with projection $\pi\colon Z \to X$ such that Λ is the image of the section $\mathrm{d}\phi$ and Λ' the image of the section $\mathrm{d}\phi'$ around z with $\phi(z) = 0 = \phi'(z)$. Consider the cotangent bundle structure $\pi'\colon Z \to X$ with $\pi' = \pi \circ \Phi^{-1}$. The map $\Phi \circ \mathrm{d}\phi$ maps X onto Λ' and is a section of $\pi'\colon Z \to X$. This means that Λ' is the image of the section $\mathrm{d}\phi$ with respect to the new structure. Therefore, ϕ and ϕ' are both generating functions of Λ'. By Corollary 10.2.9, the map germs ϕ and ϕ' are stably right equivalent.

Now let ϕ be a generating function of (X, Λ, z) and ϕ' of (X, Λ', z) and assume that the function germs ϕ and ϕ' are stably right equivalent. By Proposition 10.2.8, without loss of generality we may assume that ϕ, ϕ' refer to the same cotangent bundle structure $\pi\colon Z \to X$.

By the parametric Morse Lemma (Lemma 10.2.6) there exist coordinates $(\overline{x}, \underline{x}) = ((x^1, \ldots, x^k), (x^{k+1}, \ldots, x^n))$ and $(\overline{x'}, \underline{x'}) = ((x'^1, \ldots, x'^k), (x'^{k+1}, \ldots, x'^n))$ on X centred at z, function germs f, f' with vanishing 2-jets at 0 and invertible, symmetric matrices B and B' such that

$$\begin{aligned}\phi(\overline{x}, \underline{x}) &= f(\overline{x}) + \underline{x}^\top B \underline{x} \\ \phi'(\overline{x'}, \underline{x'}) &= f'(\overline{x'}) + \underline{x'}^\top B' \underline{x'}.\end{aligned}$$

Let D be an invertible, symmetric, $n-k$-dimensional matrix such that the matrix $-B^{-1} + DB'D$ is invertible. Define the maps

$$\begin{aligned}\phi^{(0)}(\overline{x}, \underline{x}) &= f'(\overline{x}) + \underline{x}^\top B' \underline{x} \\ \phi^{(1)}(\overline{x}, \underline{x}) &= f(\overline{x}) + \underline{x}^\top B' \underline{x} \\ \phi^{(2)}(\overline{x}, \underline{x}) &= f(\overline{x}) + \underline{x}^\top BDB'DB \underline{x}.\end{aligned}$$

We now show that we can map $\Lambda' = \mathrm{d}\phi'(X)$ to $\mathrm{d}\phi^{(0)}(X)$, then to $\mathrm{d}\phi^{(1)}(X)$, then to $\mathrm{d}\phi^{(2)}(X)$, and finally to $\Lambda = \mathrm{d}\phi(X)$ with symplectic diffeomorphisms which fix X and z.

- The change of coordinates between $(\overline{x}, \underline{x})$ and $(\overline{x'}, \underline{x'})$ induces a diffeomorphism χ locally defined around $z \in X$ with $\chi(z) = z$. The cotangent lift of χ fixes z and provides a symplectomorphism $\Phi^{(0)}$ between Λ' and $\mathrm{d}\phi^{(0)}(X)$ on an open neighbourhood of z in Z.

- Since ϕ and ϕ' are stably right equivalent, there exists a right equivalence r such that $f = f' \circ r$ (Theorem 10.2.1). Define $\tilde{r}(\overline{x}, \underline{x}) = (r(\overline{x}), \underline{x})$ and denote the cotangent lift of $\tilde{r}$ by $\Phi^{(1)}$. Now $\Phi^{(1)}$ maps $\mathrm{d}\phi^{(0)}(X)$ to a manifold which coincides with $\mathrm{d}\phi^{(1)}(X)$ on an open neighbourhood of z: indeed, denote $\overline{\pi}(x) = \overline{x}$, $\underline{\pi}(x) = \underline{x}$.

There exist appropriate choices of open neighbourhoods $V' \subset Z$ of z, $\tilde{V} \subset X$ of z, and $U, U' \subset \mathbb{R}^n$ of 0 such that

$$\begin{aligned}\Phi^{(1)}(\Lambda' \cap V') &= \Phi^{(1)}\left(\left\{\mathrm{d}(f' \circ \overline{\pi} + \underline{\pi}^\top B' \underline{\pi})|_{(\overline{x},\underline{x})} \mid (\overline{x},\underline{x}) \in U'\right\}\right) \\ &= \left(\left\{\mathrm{d}(f \circ \overline{\pi} + \underline{\pi}^\top B' \underline{\pi})|_{(r^{-1}(\overline{x}),\underline{x})} \mid (\overline{x},\underline{x}) \in U'\right\}\right) \\ &= \left(\left\{\mathrm{d}(f \circ \overline{\pi} + \underline{\pi}^\top B' \underline{\pi})|_{(\overline{x},\underline{x})} \mid (\overline{x},\underline{x}) \in U\right\}\right) \\ &= \mathrm{d}\phi^{(1)}(X \cap \tilde{V}).\end{aligned}$$

- Denote the cotangent lift of the map $(\overline{x},\underline{x}) \mapsto (\overline{x}, DB\underline{x})$ by $\Phi^{(2)}$. The symplectomorphism $\Phi^{(2)} \circ \Phi^{(1)}$ maps Λ' to a manifold which coincides with $\mathrm{d}\phi^{(2)}(X)$ on a neighbourhood of z.

- It remains to show that there exists a symplectomorphism mapping $\mathrm{d}\phi^{(2)}(X)$ to Λ which fixes X and z. Let λ denote the canonical 1-form of the cotangent bundle structure for which $\pi\colon Z \to X$ is the projection. We define another cotangent bundle structure over X by setting its canonical 1-form to $\lambda' = \lambda + \mathrm{d}H$ with

$$H(x,\xi) = \xi^\top \begin{pmatrix} 0 & 0 \\ 0 & \frac{1}{4}(-B^{-1} + DB'D) \end{pmatrix} \xi.$$

The manifold Λ is graphical with respect to the cotangent bundle structure defined by λ' by the choice of D. Let $\phi^{\lambda'}$ denote the generating function of Λ with respect to the new structure λ'. Applying Lemma 10.2.2 we get

$$(\phi^{\lambda'} \circ k)(\overline{x},\underline{x}) = f(\overline{x}) + \underline{x}^\top BDB'DB\underline{x}$$

for a diffeomorphism k on X. The cotangent lifted map K of k via the λ-structure maps $\mathrm{d}\phi^{\lambda'}|_x$ to $\mathrm{d}(\phi^{\lambda'} \circ k)|_{k^{-1}(x)} = \mathrm{d}(\phi^{(2)})|_{k^{-1}(x)}$ for each $x \in X$. Therefore,

$$\mathrm{d}\phi^{\lambda'}(X) \quad \text{and} \quad (K^{-1} \circ \Phi^{(2)} \circ \Phi^{(1)})(\Lambda')$$

coincide near z. Locally around z the symplectomorphism relating the cotangent bundle structures λ and λ' maps $\mathrm{d}\phi^{\lambda'}(X)$ to Λ and fixes X and z.

It follows that (X, Λ, z) and (X, Λ', z) are contact-equivalent. □

Corollary 10.2.13. *The local algebras (see Definition 5.3.5 in Section 5.3) of generating functions of contact equivalent Lagrangian contact problems are isomorphic.*

Rather than using X as a zero section for a cotangent bundle structure to describe

the Lagrangian contact problem (X, Λ, z) in Z we can use any other Lagrangian submanifold $L \subset Z$ as a reference manifold as explained in the following proposition. This gives us some flexibility when computing generating functions which we will exploit in a parameter-dependent setting.

Proposition 10.2.14. *Let (X, Λ, z) be a Lagrangian contact problem in the symplectic manifold $Z = T^*L$. Assume that X and Λ are graphical and given as the images of $\mathrm{d}\phi^X$ and $\mathrm{d}\phi^\Lambda$, for $\phi^X, \phi^\Lambda \colon L \to \mathbb{R}$ with $\phi^X(\pi(z)) = \phi^\Lambda(\pi(z))$, where $\pi \colon Z \to L$ is the bundle projection. The map*

$$\phi = \phi^\Lambda - \phi^X \tag{10.2.20}$$

expressed in local coordinates on L centred at $\pi(z)$ is stably right equivalent to any generating function of (X, Λ, z).

Proof. Denote the canonical 1-form on $Z = T^*L$ by λ and the cotangent bundle projection by $\pi \colon Z \to L$. Consider the fibre preserving diffeomorphism

$$\chi \colon Z \to Z, \quad z \mapsto z - \mathrm{d}\phi^X|_{\pi(z)}.$$

We have

$$\lambda' \coloneqq \chi^*\lambda = \lambda - \mathrm{d}(\phi^X \circ \pi).$$

The 1-form λ' on Z is a primitive of the symplectic structure $\mathrm{d}\lambda$ and vanishes exactly at the points on X. By Remark 10.2.3, λ' corresponds to a cotangent bundle structure on Z over X with the same Lagrangian fibres as the original structure. Let $\pi' \colon Z \to X$ denote the cotangent bundle projection. In the following we may localise the problem by intersecting L with open neighbourhoods of $\pi(z)$ in L and shrink $Z = T^*L$ and all embedded submanifolds accordingly repeatedly without mentioning. A generating function for (X, Λ, z) with respect to the structure λ' can be obtained as follows: let $S' \colon \Lambda \to \mathbb{R}$ be a primitive of the closed 1-form $\iota_\Lambda^*\lambda'$ around z with $S'(z) = 0$, where $\iota_\Lambda \colon \Lambda \hookrightarrow Z$ is the inclusion. A generating function for (X, Λ, z) with respect to λ' is given as $\phi' = S' \circ (\pi' \circ \iota_\Lambda)^{-1} \colon X \to \mathbb{R}$. An expression of ϕ' in local coordinates on X centred at z is, therefore, right equivalent to an expression of S' in local coordinates on Λ centred at z.

To show that a coordinate expression of ϕ centred at $\pi(z) \in L$ and a coordinate expression of ϕ' centred at z are right equivalent, it suffices to verify that the pullback of $\mathrm{d}S'$ to L via $\mathrm{d}\phi^\Lambda \colon L \to \Lambda$ coincides with $\mathrm{d}\phi$. Here and in the following calculation we neglect to differentiate between $\mathrm{d}\phi^\Lambda \colon L \to \Lambda$ and $\mathrm{d}\phi^\Lambda \colon L \to Z$. Indeed,

$$\begin{aligned}(\mathrm{d}\phi^\Lambda)^*(\mathrm{d}S') &= (\mathrm{d}\phi^\Lambda)^*(\iota_\Lambda^*\lambda') = (\mathrm{d}\phi^\Lambda)^*(\chi^*\lambda) = (\chi \circ \mathrm{d}\phi^\Lambda)^*\lambda \\ &= (\mathrm{d}\phi^\Lambda - \mathrm{d}\phi^X|_{\pi \circ \mathrm{d}\phi^\Lambda})^*\lambda = (\mathrm{d}\phi^\Lambda - \mathrm{d}\phi^X)^*\lambda = \mathrm{d}\phi^*\lambda = \mathrm{d}\phi.\end{aligned}$$

Since generating functions are well-defined up to stably right equivalence by Corollary 10.2.9, this shows that ϕ expressed in local coordinates centred at $\pi(z)$ is stably right equivalent to any generating function of (X, Λ, z). □

10.3 Symmetries

If a fully reduced generating function f of a Lagrangian contact problem (X, Λ, z) is invariant under a diffeomorphism $\overline{h}$ defined on a neighbourhood of 0, i.e. $f \circ \overline{h} = f$, then any other fully reduced generating function is of the form $f \circ r$ for a right equivalence r (Corollary 10.2.10) and is, therefore, invariant under $r^{-1} \circ \overline{h} \circ r$. Invariance of fully reduced generating functions is, thus, a well-defined concept. The fully reduced generating function f arises as the restriction of a generating function

$$\phi(x) = f(\overline{x}) + \underline{x}^\top B \underline{x}$$

for (X, Λ, z) to some appropriate submanifold $\overline{X} = \{(\overline{x}, \underline{x}) \,|\, \underline{x} = 0\} \subset X$ (obtained by the parametric Morse lemma (Lemma 10.2.6), for instance). The map $h(\overline{x}, \underline{x}) = (\overline{h}(\overline{x}), \underline{x})$ extends $\overline{h}$ to a diffeomorphism on a neighbourhood of z in X. We have $\phi \circ h = \phi$.

Let us understand the geometric meaning of invariance of generating functions of Lagrangian contact problems.

Lemma 10.3.1. *Consider the cotangent bundle $\pi\colon T^*X \to X$, let $\phi\colon X \to \mathbb{R}$ be a smooth function, and denote $\Lambda = \mathrm{d}\phi(X)$. If $\phi \circ h = \phi$ for some $h\colon X \to X$, then the cotangent lifted action $H\colon T^*X \to T^*X$ of h fulfils $H(X) = X$ and $H(\Lambda) = \Lambda$.*

Proof. As H is a cotangent lifted map $H(X) = X$. Let $\mathrm{d}\phi|_x \in \Lambda$. We have

$$H(\mathrm{d}\phi|_x) = \mathrm{d}\phi|_x \circ \mathrm{d}h|_{h^{-1}(x)} = \mathrm{d}(\phi \circ h)|_{h^{-1}(x)} = \mathrm{d}\phi|_{h^{-1}(x)}.$$

Clearly $\mathrm{d}\phi|_{h^{-1}(x)} \in \Lambda$. Since H is a diffeomorphism it follows that $H(\Lambda) = \Lambda$. □

In the following, it is convenient to view a generating function of a Lagrangian contact problem (X, Λ, z) in Z as functions $S\colon \Lambda \to \mathbb{R}$ obtained as a primitive of the closed 1-form $\iota_\Lambda^* \lambda$, where $\iota_\Lambda\colon \Lambda \to Z$ is the inclusion of Λ and the 1-form λ on Z defines a cotangent bundle structure over X (Remark 10.2.3). Provided that Λ is graphical for the cotangent bundle structure, the function S can be related to a generating function ϕ defined locally on X by $\phi = S \circ \pi|_\Lambda^{-1}$, where π denotes the cotangent bundle projection and $\pi|_\Lambda\colon \Lambda \cap V \to \pi(\Lambda \cap V)$ the restriction of π for an open neighbourhood $V \subset \Lambda$ containing z.

Lemma 10.3.2. *Let Z be a symplectic manifold with cotangent bundle structure over a simply connected Lagrangian submanifold X defined by a 1-form λ. Let $\iota_\Lambda\colon \Lambda \hookrightarrow Z$ be another embedded, simply connected Lagrangian submanifold. Consider a symplectmorphism $F\colon Z \to Z$ with $F(X) = X$ and $F(\Lambda) = \Lambda$. The 1-form $\lambda' = F^*\lambda$ defines another cotangent bundle structure over X. If $\mathrm{d}S = \iota_\Lambda^*\lambda$ and $\mathrm{d}S' = \iota_\Lambda^*\lambda'$ for $S, S'\colon \Lambda \to \mathbb{R}$, then*

$$S' = S \circ F|_\Lambda + \textit{const.},$$

where $F|_\Lambda\colon \Lambda \to \Lambda$ is the restriction of F to Λ.

Proof. Indeed, the 1-form $\lambda' = F^*\lambda$ defines a cotangent bundle structure over X because F is symplectic and λ' vanishes exactly at points on X. Moreover, we have

$$\mathrm{d}S' = \iota_\Lambda^*\lambda' = \iota_\Lambda^* F^*\lambda = (F \circ \iota_\Lambda)^*\lambda = (\iota_\Lambda \circ F|_\Lambda)^*\lambda = F|_\Lambda^* \iota_\Lambda^*\lambda = F|_\Lambda^* \mathrm{d}S$$

such that S' and S relate as claimed. □

Lemma 10.3.3. *If in the setting of Lemma 10.3.2 we have*

$$S = S \circ F|_\Lambda,$$

then F coincides on Λ with the cotangent lifted action of

$$h\colon X \to X, \quad h \coloneqq \pi \circ F^{-1} \circ \pi|_\Lambda^{-1}.$$

provided that Λ is graphical in the cotangent bundle structure λ.

Proof. Notice that $\pi|_\Lambda^{-1} = \mathrm{d}\phi$ for a map $\phi\colon X \to \mathbb{R}$ with $\phi(X) = \Lambda$. Denote the cotangent lifted action of h by H. For $\mathrm{d}\phi|_x \in \Lambda$ we have

$$\pi(H(\mathrm{d}\phi|_x)) = h^{-1}(x) = (\pi \circ F \circ \mathrm{d}\phi)(x) = \pi(F(\mathrm{d}\phi|_x)), \tag{10.3.1}$$

i.e. the basepoints of $H(\mathrm{d}\phi|_x)$ and $F(\mathrm{d}\phi|_x)$ coincide. The function ϕ is invariant under h such that $H(\mathrm{d}\phi|_x) \in \Lambda$ by Lemma 10.3.1. Since $F(\mathrm{d}\phi|_x) \in \Lambda$ and since the restriction of π to $\pi|_\Lambda = \pi \circ \iota_\Lambda\colon \Lambda \to X$ is a diffeomorphism we can conclude from (10.3.1) that

$$H(\mathrm{d}\phi|_x) = F(\mathrm{d}\phi|_x).$$

Therefore, $H \circ \iota_\Lambda = F \circ \iota_\Lambda$. □

We conclude from Lemmas 10.3.1 to 10.3.3 the following theorem.

Theorem 10.3.4. *Consider a Lagrangian contact problem (X, Λ, z) in Z, where X, Λ are simply connected. Fix a cotangent bundle structure over X near z defined by the*

1-form λ such that Λ is graphical. We denote the bundle projection by π. Consider $\mathrm{d}S = \iota_\Lambda^*\lambda$. We have $S \circ F_\Lambda = S$ for a diffeomorphism $F_\Lambda \colon \Lambda \to \Lambda$ if and only if F_Λ coincides on Λ with the cotangent lifted map H of $h = \pi \circ F_\Lambda^{-1} \circ \pi|_\Lambda^{-1}$.

In other words, an invariance of a Lagrangian contact problem (X, Λ, z) under a symplectic map F yields an invariance of the generating function related to a cotangent bundle structure if and only if F coincides on Λ with the cotangent lifted action for the invariance.

Remark 10.3.1. The symmetries characterised in Theorem 10.3.4 yield symmetries of the reduced generating function if F_Λ leaves a submanifold of $\mathrm{d}\phi(\overline{X}) \subset \Lambda$ invariant, where $\overline{X}$ is such that ϕ is stably right equivalent to $\phi|_{\overline{X}}$. △

10.4 Parameter dependent Lagrangian contact problems

Let us extend our analysis of Lagrangian contact problems to parameter dependent problems. This will help us to deepen the relation to catastrophe theory. A parameter dependent version of Lemma 10.2.7 holds true.

Lemma 10.4.1. *On $\mathbb{R}^n = \overline{X} \oplus \underline{X}$ consider coordinates $x = (\overline{x}, \underline{x})$ with $\overline{x} = (x^1, \dots, x^k)$ and $\underline{x} = (x^{k+1}, \dots, x^n)$, a smooth family of nondegenerate symmetric matrices $Q_\mu \in \mathbb{R}^{(n-k)\times(n-k)}$, a smooth family of maps g_μ defined on an open neighbourhood of $0 \in \mathbb{R}^k$ such that the 2-jet of g_0 vanishes at 0. Here $\mu \in I$ is the family parameter and I is an open neighbourhood of $0 \in \mathbb{R}^l$. Moreover, consider a smooth family of matrix valued functions $\mathcal{H}_\mu \colon \mathbb{R}^n \to \mathrm{Sym}(n)$ with*

$$\mathcal{H}_\mu(x) = (h_\mu^{ij}(x))_{i,j=1,\dots,n} = \begin{pmatrix} H_\mu^{11}(x) & H_\mu^{12}(x) \\ H_\mu^{12\top}(x) & 0 \end{pmatrix} \in \mathrm{Sym}(n) \subset \mathbb{R}^{n\times n}.$$

for $H_\mu^{11}(x) \in \mathrm{Sym}(k)$ and $H_\mu^{12}(x) \in \mathbb{R}^{k\times(n-k)}$. For $t \in \mathbb{R}$ let

$$\begin{aligned} \psi(\mu, x) &= g_\mu(\overline{x}) + \underline{x}^\top Q_\mu \underline{x} \\ \psi_t(\mu, x) &= g_\mu(\overline{x}) + \underline{x}^\top Q_\mu \underline{x} + t\nabla\psi(\mu, x)^\top \mathcal{H}_\mu(x) \nabla\psi(\mu, x). \end{aligned}$$

Then ψ_t is right equivalent to ϕ around $(\mu, x) = (0, 0)$. The right equivalence is fibred, i.e. of the form $(\mu, x) \mapsto (\mu, r_\mu(x))$, and fixes $(\mu, x) = (0, 0)$.

Proof. The proof is almost analogous to the proof of Lemma 10.2.7 with parameter-dependent data. Rather than repeating the calculations and arguments, we point out the two minor modifications that need to be made for the parameter dependent setting. (1) The 2-jet of g_μ does not necessarily vanish at $\overline{x} = 0$ unless $\mu = 0$. However, this is not an issue: in (10.2.13) the invertibility of $B_\mu(t, 0)$ follows from the invertibility of

$B_0(t,0)$ for all μ close to 0 and $t \in [0,1]$, which is sufficient for the argument. (2) The other difference is that $\omega_\mu(0,t)$ from (10.2.14) does not necessarily vanish if $\mu \neq 0$ and, therefore, the values $f_{\mu,t}(0)$ are only guaranteed to vanish if $\mu = 0$. However, this is sufficient as the sought right equivalence needs to fix $x = 0$ only at $\mu = 0$. □

Definition 10.4.1 (smooth Lagrangian family)**.** Let $I \subset \mathbb{R}^l$ be an open neighbourhood of the origin. A family $(\Lambda_\mu)_{\mu\in I}$ of Lagrangian submanifolds of a symplectic manifold Z is *smooth* at $\mu = 0$ around $z \in \Lambda_0$ if there exists an open neighbourhood $\tilde{Z}$ of z, a cotangent bundle structure $\pi\colon \tilde{Z} \to \Lambda_0 \cap \tilde{Z}$, an open neighbourhood $\tilde{I} \subset I$ of 0 and a smooth family of maps $(\phi_\mu)_{\tilde{I}}$ such that $\Lambda_\mu \cap \tilde{Z}$ is the image of the section $\mathrm{d}\phi_\mu\colon \Lambda_0 \to \tilde{Z}$ for all $\mu \in \tilde{I}$. △

Definition 10.4.1 is independent of the cotangent bundle structure $\pi\colon \tilde{Z} \to \Lambda_0 \cap \tilde{Z}$ because two different structures relate by a smooth transition (Lemma 10.2.2).

Definition 10.4.2 (parameter-dependent Lagrangian contact problem)**.** Let $(X_\mu)_{\mu\in I}$ and $(\Lambda_\mu)_{\mu\in I}$ be two smooth Lagrangian families in a symplectic manifold Z such that $X_0 \cap \Lambda_0$ intersects in an isolated point z_0 and such that the set $X_\mu \cap \Lambda_\mu$ is discrete for all $\mu \in I$. Then $((X_\mu)_{\mu\in I}, (\Lambda_\mu)_{\mu\in I}, z_0)$ is called a *(parameter-dependent) Lagrangian contact problem in Z*. △

Definition 10.4.3 (constant unfolding)**.** Let $\mathcal{L} = ((X_\mu)_{\mu\in I}, (\Lambda_\mu)_{\mu\in I}, z_0)$ be a Lagrangian contact problem. Let $\tilde{I} \subset \mathbb{R}^{\tilde{l}}$ be an open neighbourhood of 0. The Lagrangian contact problem $((X_\mu)_{(\mu,\tilde{\mu})\in I\times\tilde{I}}, (\Lambda_\mu)_{(\mu,\tilde{\mu})\in I\times\tilde{I}}, z_0)$ is called a *constant unfolding of $\mathcal{L}$*. Similarly, if $\mathcal{F} = (\phi_\mu)_{\mu\in I}$ is a smooth family of scalar-valued maps, then $(\phi_\mu)_{(\mu,\tilde{\mu})\in I\times\tilde{I}}$ is called a *constant unfolding of $\mathcal{F}$*. △

Definition 10.4.4 (Morse-reduced form)**.** Consider an open neighbourhood I of $0 \in \mathbb{R}^l$ and a family of scalar-valued maps $(\phi_\mu)_{\mu\in I}$ defined around $z_0 \in X$ with $\phi_0(z_0) = 0$ and $\mathrm{d}\phi_0|_{z_0} = 0$, where X is an n-dimensional manifold. Consider coordinates $(\overline{x}, \underline{x}) = ((x^1, \ldots, x^k), (x^{k+1}, \ldots, x^n))$ centred at 0 such that ϕ_μ is of the form

$$\phi_\mu(x) = f_\mu(\overline{x}) + \underline{x}^\top B \underline{x}$$

for a symmetric, nondegenerate matrix B and a smooth family of maps $(f_\mu)_{\mu\in I}$ such that $\nabla_{\overline{x}} f_0(0) = 0$ and $\mathrm{Hess}\, f_0(0) = 0$. Then $(f_\mu)_{\mu\in I}$ is a *Morse-reduced form* of $(\phi_\mu)_{\mu\in I}$. △

Remark 10.4.1. A potential parameter-dependence of the coordinates $x = (\overline{x}, \underline{x})$ is suppressed in our notation. △

Lemma 10.4.2 (existence and uniqueness of Morse-reduced forms)**.** *A family $(\phi_\mu)_{\mu\in I}$ as in Definition 10.4.4 has a Morse-reduced form $(f_\mu)_{\mu\in I}$ and $(f_\mu)_{\mu\in I}$ is locally around*

$(\mu, x) = (0,0)$ determined up to a right-action with a diffeomorphism of the form $K(\mu, \overline{x}) = (\mu, r_\mu(\overline{x}))$ with $K(0,0) = 0$ and addition of a term $\chi(\mu)$, where χ is smooth and $\chi(0) = 0$.

Proof. The lemma follows from the splitting theorem as formulated in Weinstein, 1971a and recalled in Theorem 5.3.2. Compared with Lemma 10.2.6 it incorporates uniqueness properties. Let us indicate a way to obtain the claimed existence result from Lemma 10.2.6. Let the dimension of the kernel of the Hessian matrix of ϕ_0 at z_0 be k. We find an $n-k$-dimensional submanifold $\underline{X} \subset X$ containing z_0 such that the Hessian matrix of $\phi_0|_{\underline{X}}$ at z_0 is nondegenerate. Consider a submanifold $\overline{X}$ containing z_0 that is transversal to $\underline{X}$. We apply the parametric[4] Morse Lemma (Lemma 10.2.6) to

$$(\mu, x) \mapsto \phi_\mu(x) - \underbrace{\langle \nabla_\mu \phi_\mu(0)|_{\mu=0}, \mu \rangle}_{=:\chi(\mu)} - \phi_0(0)$$

with respect to the splitting $(I \oplus \overline{X}) \oplus \underline{X}$. Notice that the 1-jet of the above map with respect to the coordinates $((\mu, \overline{x}), \underline{x})$ vanishes. A fibred change of coordinates yields coordinates $((\mu, \overline{x}), \underline{x})$ with $x = (\overline{x}, \underline{x}) = ((x^1, \dots, x^k), (x^{k+1}, \dots, x^n))$ on X centred at z_0 such that $(\overline{x}, 0)$ are coordinates on $\overline{X}$ and $(0, \underline{x})$ are coordinates on $\underline{X}$ and

$$\phi_\mu(x) = \tilde{f}_\mu(\overline{x}) + \phi_0(0) + \chi(\mu) + \underline{x}^\top B \underline{x} =: f_\mu(\overline{x}) + \underline{x}^\top B \underline{x}$$

The function $\overline{x} \mapsto f_0(\overline{x}) - \phi_0(0)$ has a vanishing 2-jet at $\overline{x} = 0$ and $B = \operatorname{Hess} \phi_0|_{\underline{X}}$ is invertible. □

Proposition 10.4.3. *Let $(X, (\Lambda_\mu)_{\mu \in I}, z_0)$ be a parameter dependent Lagrangian contact problem in Z. Let $I \subset \mathbb{R}^k$ denote an open neighbourhood of 0. Consider smooth families of cotangent bundle structures such that Λ_μ is given as the image of the section $\mathrm{d}\phi^\alpha_\mu$ and $\mathrm{d}\phi^\beta_\mu$ locally around $z_0 \in Z$ with $\phi^\alpha_0(z_0) = 0 = \phi^\beta_0(z_0)$, respectively. Then $(\phi^\alpha_\mu)_\mu$ and $(\phi^\beta_\mu)_\mu$ admit the same Morse-reduced forms up to an addition of a smooth map $\chi(\mu)$ with $\chi(0) = 0$.*

Proof. The following proof is a parameter-dependent version of the proof of Proposition 10.2.8 using Lemma 10.4.1 instead of Lemma 10.2.7.

Let the dimension of the kernel of the Hessian matrix of ϕ^α_0 at z_0 be k and the dimension of X n. By Lemma 10.4.2 there exists a local coordinate system $x = (\overline{x}, \underline{x}) = ((x^1, \dots, x^k), (x^{k+1}, \dots, x^n))$ on X centred at z_0 such that

$$\phi^\alpha_\mu(x) = f_\mu(\overline{x}) + \underline{x}^\top B \underline{x},$$

[4] In this context the parameters are $(\mu, \overline{x})$

the function $\overline{x} \mapsto f_0(\overline{x})$ has a vanishing 2-jet at $\overline{x} = 0$, and $B = \operatorname{Hess} \phi_0^\alpha|_{\underline{X}}$ is invertible. A fibre-wise application of Lemma 10.2.2 yields

$$\phi_\mu^\beta \circ k_{\alpha\beta}^\mu = \phi_\mu^\alpha + H_\mu(x, \nabla\phi_\mu^\alpha) + \chi(\mu), \tag{10.4.1}$$

for a smooth map χ with $\chi(0) = 0$ and

$$H_\mu(x,\xi) = \sum_{i,j=1}^{n} h_{ij}^\mu(x,\xi)\xi_i\xi_j = \xi^\top \begin{pmatrix} H_\mu^{11}(x,\xi) & H_\mu^{12}(x,\xi) \\ H_\mu^{12}(x,\xi)^\top & H_\mu^{22}(x,\xi) \end{pmatrix} \xi$$

with $H_\mu^{11}(x,\xi) \in \operatorname{Sym}(k)$, $H_\mu^{12}(x,\xi) \in \mathbb{R}^{k\times(n-k)}$, $H_\mu^{22}(x,\xi) \in \operatorname{Sym}(n-k)$, and with $k_{\alpha\beta}^\mu = \pi^\beta \circ (\pi^\alpha|_{\Lambda_\mu})^{-1}$. For $i,j \in \{1,2\}$ define

$$\mathcal{H}_\mu(x) = \mathcal{H}_\mu(\overline{x},\underline{x}) = H_\mu(x, \nabla\phi_\mu^\alpha(x)), \quad \mathcal{H}_\mu^{ij}(x) = \mathcal{H}_\mu^{ij}(\overline{x},\underline{x}) = H_\mu^{ij}(x, \nabla\phi_\mu^\alpha(x)).$$

Define

$$B'_\mu(x) = B + 4B\mathcal{H}_\mu^{22}(x)B.$$

We calculate

$$\begin{aligned} \phi_\mu^\beta(k_{\alpha\beta}^\mu(\overline{x},\underline{x})) &\overset{(10.4.1)}{=} \phi_\mu^\alpha(\overline{x},\underline{x}) + \mathcal{H}_\mu(x) + \chi(\mu) \\ &= f_\mu(\overline{x}) + \underline{x}^\top B'_\mu(x)\underline{x} + \nabla_{\overline{x}} f_\mu(\overline{x})^\top \mathcal{H}_\mu^{11}(x)\nabla_{\overline{x}} f_\mu(\overline{x}) \\ &\quad + 4\underline{x}^\top B\mathcal{H}_\mu^{12}(x)^\top \nabla_{\overline{x}} f_\mu(\overline{x}) + \chi(\mu). \end{aligned} \tag{10.4.2}$$

We calculate the Hessian matrix of $\phi_0^\beta \circ k_{\alpha\beta}^0$ at $(\overline{x},\underline{x}) = (0,0)$ using (10.4.2) and obtain

$$\operatorname{Hess}(\phi_0^\beta \circ k_{\alpha\beta})(0,0) = \begin{pmatrix} 0 & 0 \\ 0 & 2B'_0(0) \end{pmatrix}.$$

Since Λ_0 is graphical in both cotangent bundle structures, $B'_0(0)$ must be invertible by a dimension argument. For (μ, x) in a sufficiently small neighbourhood of $(0,0)$ the matrices $B'_\mu(x)$ are invertible and have constant signature. By Sylvester's law of inertia, there exists a smooth family of invertible matrices $A_\mu(x)$ such that

$$A_\mu^{-T}(x)B'_\mu(x)A_\mu^{-1}(x) = B'_\mu(0) \tag{10.4.3}$$

for all (μ, x) near $(0,0)$. Consider

$$r_\mu(\overline{x},\underline{x}) = (\overline{x}, A_\mu(x)\underline{x}).$$

For all μ near 0 the map r_μ fixes $x = 0$ and is a diffeomorphism on a neighbourhood of

$x = 0$. Let us define

$$\begin{aligned}\tilde{\mathcal{H}}^{11}_\mu(x) &= \mathcal{H}^{11}_\mu(r_\mu^{-1}(x))\\ \tilde{\mathcal{H}}^{12}_\mu(x) &= \mathcal{H}^{12}_\mu(r_\mu^{-1}(x))BA_\mu^{-1}(r_\mu^{-1}(x))B'_\mu(0)^{-1}.\end{aligned} \tag{10.4.4}$$

By Lemma 10.4.1 the map

$$\phi_1^\alpha \coloneqq f_\mu(\overline{x}) + \underline{x}^\top B'_\mu(0)\underline{x}$$

is right equivalent to

$$\begin{aligned}\phi_2^\alpha(\mu, x) \coloneqq f_\mu(\overline{x}) &+ \underline{x}^\top B'_\mu(0)\underline{x}\\ &+ \nabla_{\overline{x}} f_\mu(\overline{x})^\top \tilde{\mathcal{H}}^{11}_\mu(x)\nabla_{\overline{x}} f_\mu(\overline{x})\\ &+ 4\underline{x}^\top B'_\mu(0)\tilde{\mathcal{H}}^{12}_\mu(x)^\top \nabla_{\overline{x}} f_\mu(\overline{x}).\end{aligned}$$

We have

$$\begin{aligned}(\phi_2^\alpha \circ r_\mu)(x) = f_\mu(\overline{x}) &+ \underline{x}^\top A_\mu(x)^\top B'_\mu(0)A_\mu(x)\underline{x}\\ &+ \nabla_{\overline{x}} f_\mu(\overline{x})^\top \tilde{\mathcal{H}}^{11}_\mu(r_\mu(x))\nabla_{\overline{x}} f_\mu(\overline{x})\\ &+ 4\underline{x}^\top A_\mu(x)^\top B'_\mu(0)\tilde{\mathcal{H}}^{12}_\mu(r_\mu(x))^\top \nabla_{\overline{x}} f_\mu(\overline{x}).\end{aligned}$$

Comparing the above with (10.4.2) shows that the map $\phi_2^\alpha \circ r_\mu$ coincides with $\phi_\mu^\beta \circ k^\mu_{\alpha\beta} - \chi(\mu)$. This proves the claim. □

Definition 10.4.5 (stably equivalent as unfoldings)**.** Consider open neighbourhoods I of $0 \in \mathbb{R}^l$ and I' of $0 \in \mathbb{R}^{l'}$ and two families of scalar-valued maps $(\phi_\mu)_{\mu\in I}$ and $(\phi'_{\mu'})_{\mu'\in I'}$ defined around $0 \in \mathbb{R}^n$ or $0 \in \mathbb{R}^{n'}$, respectively. Assume that $\phi_0(0) = 0$ and $\phi'_0(0) = 0$. If

- there exists an extension of the parameter spaces I to $I \times \mathbb{R}^{L-l}$ and I' to $I' \times \mathbb{R}^{L-l')}$ for some $L \in \mathbb{N}$, $L \geq \max(l, l')$ where the additional parameters enter trivially in the map families (constant unfolding),
- there exist reparametrisations of both parameter spaces fixing $0 \in I \times \mathbb{R}^{L-l}$ and $0 \in I' \times \mathbb{R}^{L-l'}$, respectively,
- and for an open neighbourhood $\hat{I} \subset (I \times \mathbb{R}^{L-l}) \cap (I' \times \mathbb{R}^{L-l'})$ of 0 there exists a smooth function $\chi\colon \hat{I} \to \mathbb{R}$

such that the families $(\phi_{\hat{\mu}} + \chi(\hat{\mu}))_{\hat{\mu}\in\hat{I}}$ and $(\phi_{\hat{\mu}})_{\hat{\mu}\in\hat{I}}$ admit the same Morse-reduced forms, then $(\phi_\mu)_{\mu\in I}$ and $(\phi'_{\mu'})_{\mu'\in I'}$ are *stably right equivalent as unfoldings.* △

Remark 10.4.2. Definition 10.4.5 corresponds to the equivalence relation *reduction* in definition 5.3 (p.124) of Wassermann's dissertation (1974). The necessary notions are developed in Wassermann, 1974, §4, §5. Here, however, we use right equivalence where the reference uses right-left equivalence. △

Proposition 10.4.4. *Let $((X_\mu)_{\mu\in I}, (\Lambda_\mu)_{\mu\in I}, z_0)$ be a parameter-dependent Lagrangian contact problem in Z. Consider two cotangent bundle structures on Z over X_0 locally around $z_0 \in X_0 \cap \Lambda_0$ such that for each $\mu \in I$ near 0 after shrinking all involved manifolds around z_0, if necessary, the submanifold Λ_μ is the image of the section $\mathrm{d}\phi_\mu$ and X_μ the image of the section $\mathrm{d}\psi_\mu$ with respect to the first cotangent bundle structure and Λ_μ is the image of the section $\mathrm{d}\phi'_\mu$ and X_μ is the image of the section $\mathrm{d}\psi'_\mu$ with respect to the second cotangent bundle structure such that $\phi_0, \psi_0, \phi'_0, \psi'_0$ vanish at z_0. Then the families $(\rho_\mu)_\mu = (\phi_\mu - \psi_\mu)_\mu$ and $(\rho'_\mu)_\mu = (\phi'_\mu - \psi'_\mu)_\mu$ are stably right equivalent as unfoldings.*

Proof. We modify the first cotangent bundle structure using the fibre-preserving symplectic diffeomorphism $\xi \mapsto \xi - \mathrm{d}\psi_\mu|_{\pi(\xi)}$ and the second cotangent bundle structure by $\xi \mapsto \xi - \mathrm{d}\psi'_\mu|_{\pi'(\xi)}$ fibre-wise. In the updated structures all X_μ are zero-sections and Λ_μ is given as the image of the section $\mathrm{d}(\phi_\mu - \psi_\mu) = \mathrm{d}\rho_\mu$ with respect to the first structure and as the image of the section $\mathrm{d}(\phi'_\mu - \psi'_\mu) = \mathrm{d}\rho'_\mu$ with respect to the second structure. Now the claim follows by Proposition 10.4.3. □

The smooth family $(\rho_\mu)_\mu$ of maps constructed in Proposition 10.4.4 is called a *generating family for* $((X_\mu)_{\mu\in I}, (\Lambda_\mu)_{\mu\in I}, z_0)$. More precisely, we can formulate the following definition.

Definition 10.4.6 (generating family)**.** Consider a parameter-dependent Lagrangian contact problem $((X_\mu)_{\mu\in I}, (\Lambda_\mu)_{\mu\in I}, z_0)$ and a cotangent bundle structure over X_0 such that for μ in a neighbourhood of 0 in I the manifolds X_μ, Λ_μ are locally around z_0 given as the images of $\mathrm{d}\psi_\mu$ and $\mathrm{d}\phi_\mu$, respectively, for smooth function families $(\psi_\mu)_{\mu\in I}$, $(\phi_\mu)_{\mu\in I}$ with $\psi_0(z_0) = 0 = \phi_0(z_0)$. The family $\rho_\mu = \phi_\mu - \psi_\mu$ is called *generating family for* $((X_\mu)_{\mu\in I}, (\Lambda_\mu)_{\mu\in I}, z_0)$. △

Definition 10.4.7 (contact equivalence of parameter-dependent Lagrangian contact problems)**.** Let $\hat{\mathcal{L}} = ((X_{\hat\mu})_{\hat\mu\in\hat I}, (\Lambda_{\hat\mu})_{\hat\mu\in\hat I}, z_0)$ and $\mathcal{L}' = ((X'_{\mu'})_{\mu'\in I'}, (\Lambda'_{\mu'})_{\mu'\in I'}, z'_0)$ be Lagrangian contact problems in Z and Z' where $\dim Z = \dim Z'$. The families are called *contact equivalent* if there exists a constant unfolding $((X_\mu)_{\mu\in I}, (\Lambda_\mu)_{\mu\in I}, z_0)$ of $\hat{\mathcal{L}}$ and a constant unfolding $((X'_\mu)_{\mu\in I}, (\Lambda'_\mu)_{\mu\in I}, z'_0)$ of $\mathcal{L}'$ such that after shrinking Z to an open neighbourhood of z_0 and Z' to an open neighbourhood of z'_0, there exists a smooth family of symplectomorphisms $\Phi_\mu \colon Z \to Z'$ such that for all μ in an open neighbourhood of $0 \in I$

$$\Phi_\mu(X_\mu) = X'_{\theta(\mu)}, \quad \Phi(\Lambda_\mu) = \Lambda'_{\theta(\mu)}, \quad \Phi_0(z_0) = z'_0,$$

where θ is a diffeomorphism defined around $0 \in I$ fixing $\mu = 0$. △

We can conclude the section with the following theorem which extends Theorem 10.2.12 to the parameter-dependent case.

Theorem 10.4.5. *Two parameter-dependent Lagrangian contact problems in a symplectic manifold are contact equivalent if and only if their generating families are stably right equivalent as unfoldings.*

Proof. Let $((X_\mu)_{\mu\in I}, (\Lambda_\mu)_{\mu\in I}, z_0)$ and $((X'_{\mu'})_{\mu'\in I'}, (\Lambda'_{\mu'})_{\mu'\in I'}, z'_0)$ be parameter dependent Lagrangian contact problems in Z. Since symplectic manifolds of the same dimension are locally symplectomorphic, we can assume $z_0 = z'_0$. (Also see Lemma 10.2.11.) Moreover, as the notion of contact equivalence of Lagrangian contact problems as well as the notion of stably equivalence as unfoldings admits the extensions of the parameter spaces via constant unfoldings, it is sufficient to prove the assertion for $I = I'$. In the following, we will shrink the manifold Z to neighbourhoods of z_0, and I to a neighbourhood of 0, repeatedly, without mentioning. As seen in the proof of Proposition 10.4.4 we can reduce the problem to a problem with a constant family $X_\mu \equiv X$.

For the forward direction, assume that $(X, (\Lambda_\mu)_{\mu\in I}, z_0)$ and $(X, (\Lambda'_\mu)_{\mu\in I}, z_0)$ are contact equivalent. There exists a family of symplectomorphisms $\Phi_\mu \colon Z \to Z$ with

$$\Phi_\mu(X) = X, \quad \Phi_\mu(\Lambda_\mu) = \Lambda'_{\theta(\mu)}, \quad \Phi_0(z_0) = z_0.$$

for a local diffeomorphism fixing $\mu = 0$. After a reparametrisation of the second family, we can assume $\theta = \mathrm{id}$. Now the proof proceeds similarly to the first part of the proof of Theorem 10.2.12: consider a cotangent bundle structure over X such that Λ_μ is given as the image of $\mathrm{d}\phi_\mu$ for a smooth family $(\phi_\mu)_{\mu\in I}$ with $\phi_\mu(0) = 0$. Denote the cotangent bundle projection by π. Using Φ_μ we can construct another cotangent bundle structure over X with cotangent bundle projection $\pi'_\mu = \pi \circ \Phi_\mu^{-1}$. The map $\Phi_\mu \circ \mathrm{d}\phi_\mu$ is a section of π'_μ and maps X to Λ'_μ. Therefore, in the new structure, the family $(\Lambda'_\mu)_{\mu\in I}$ can again be represented by the family $(\phi_\mu)_{\mu\in I}$.

For the reverse direction, assume that $(X, (\Lambda_\mu)_{\mu\in I}, z_0)$ and $(X, (\Lambda'_\mu)_{\mu\in I}, z_0)$ have equivalent generating families. Consider a cotangent bundle structure over X such that Λ_μ, Λ'_μ are graphical and given as

$$\phi_\mu(X) = \Lambda_\mu, \quad \phi'_\mu(X) = \Lambda'_\mu.$$

By Lemma 10.4.2 there exist coordinates $(\overline{x}, \underline{x})$ and $(\overline{x'}, \underline{x'})$ centred at z_0 such that

$$\phi_\mu(\overline{x}, \underline{x}) = f_\mu(\overline{x}, \underline{x}) + \underline{x}^\top B \underline{x}$$
$$\phi_\mu(\overline{x'}, \underline{x'}) = f_\mu(\overline{x'}, \underline{x'}) + \underline{x'}^\top B' \underline{x'},$$

where the 2-jets of f and f' vanish at $\mu = 0$ and B and B' are nondegenerate, symmetric matrices. We have $f_\mu(\overline{x}) = f'_{\theta(\mu)}(r_\mu(x))$ for a diffeomorphism θ fixing 0 and a fibred right equivalence r such that $r_0(0) = 0$. After a reparametrisation of the second family, we can assume $\theta = \mathrm{id}$. Now the proof proceeds analogously to the second part of the proof of Theorem 10.2.12. Let us sketch the four steps to construct a family of symplectic maps around z_0 identifying the two contact problems.

- Λ'_μ is mapped to a manifold that coincides with $\mathrm{d}\phi^{(0)}_\mu(X)$ on a neighbourhood of z_0 with
$$\phi^{(0)}_\mu(\overline{x}, \underline{x}) = f'_\mu(\overline{x}, \underline{x}) + \underline{x}^\top B' \underline{x}$$
using the cotangent lift of the change of coordinates $(\overline{x}, \underline{x}) \mapsto (\overline{x'}, \underline{x'})$.

- On an open neighbourhood of z_0 the submanifold $\mathrm{d}\phi^{(0)}_\mu(X)$ is mapped to $\mathrm{d}\phi^{(1)}_\mu(X)$ with
$$\phi^{(1)}_\mu(\overline{x}, \underline{x}) = f_\mu(\overline{x}, \underline{x}) + \underline{x}^\top B' \underline{x}$$
using the cotangent lift of $(\overline{x}, \underline{x}) \mapsto (r_\mu(\overline{x}), \underline{x})$.

- On an open neighbourhood of z_0 the submanifold $\mathrm{d}\phi^{(1)}_\mu(X)$ is mapped to $\mathrm{d}\phi^{(2)}_\mu(X)$ with
$$\phi^{(2)}_\mu(\overline{x}, \underline{x}) = f_\mu(\overline{x}, \underline{x}) + \underline{x}^\top BDB'DB\underline{x}$$
for a suitable choice of a symmetric, invertible matrix D using the cotangent lift of $(\overline{x}, \underline{x}) \mapsto (\overline{x}, DB\underline{x})$.

- On an open neighbourhood of z_0 the submanifold $\mathrm{d}\phi^{(2)}_\mu(X)$ is mapped to $\tilde{\Lambda}_\mu$ using the cotangent lift of the fibred right equivalence defined by Lemma 10.4.1 for
$$\mathcal{H} = \begin{pmatrix} 0 & 0 \\ 0 & \frac{1}{4}(-B^{-1} + DB'D) \end{pmatrix} \in \mathbb{R}^{n \times n}.$$
Let the original cotangent bundle structure be defined by the 1-form λ. Λ_μ is mapped to $\tilde{\Lambda}_\mu$ using the symplectomorphism that identifies the cotangent bundle structure λ with $\lambda + \mathrm{d}H$, where $H(x, \xi) = \xi^\top \mathcal{H}(x, \xi)\xi$ in Darboux coordinates with respect to the original structure.

The procedure constructs the required family of symplectomorphisms. □

10.5 Concluding remarks and application to boundary value problems of symplectic maps

10.5.1 Stably contact equivalence

It is now justified to extend the notion of contact equivalence of Lagrangian contact problems to *stably contact equivalence*. This will allow us to compare Lagrangian contact problems in symplectic manifolds of *different dimensions*.

Definition 10.5.1. Two Lagrangian contact problems (in symplectic manifolds of possibly different dimensions) are *stably contact equivalent* if their generating functions are stably right equivalent. Moreover, two parameter-dependent Lagrangian contact problems (in symplectic manifolds of possibly different dimensions) are *stably contact equivalent* if their generating families are stably right equivalent as unfoldings. △

Proposition 10.5.1. *Two Lagrangian contact problems in symplectic manifolds of the same dimension are stably contact equivalent if and only if they are contact equivalent.*

Proof. The statement follows by Theorems 10.2.12 and 10.4.5. □

The following two theorems announced in Section 10.1 now follow trivially from Definition 10.5.1. Their geometric meaning is encoded in Theorems 10.2.12 and 10.4.5.

Theorem 10.1.3. *There exists a 1-1 correspondence between Lagrangian contact problems modulo stably contact equivalence and smooth real-valued function germs up to stably right equivalence.*

Theorem 10.1.4. *There exists a 1-1 correspondence between parameter-dependent Lagrangian contact problems up to stably right equivalence and unfoldings of smooth, real-valued function germs up to stably right equivalence as unfoldings.*

Remark 10.5.1. The notion of versality and stability can be translated to the setting of (parameter-dependent) Lagrangian contact problems such that classification results from catastrophe theory apply as reviewed in Section 5.4. A reference is, for instance, V. I. Arnold, Gusein-Zade, and Varchenko, 2012, Part II. △

10.5.2 Boundary value problems for symplectic maps

Let us summarise the implications of this chapter for our considerations of boundary value problems for symplectic maps: consider a smooth family of symplectic maps $\phi_\mu \colon Z \to Z'$ for $\mu \in I$, where $I \subset \mathbb{R}^l$ is an open neighbourhood of the origin. Let us denote the symplectic form of Z by ω and the symplectic form of Z' by ω'. Let $\mathrm{pr} \colon Z \times Z' \to Z$ and $\mathrm{pr} \colon Z \times Z' \to Z'$ denote projections to the first or second component

of the product. Define the symplectic form $\Omega = \mathrm{pr}^*\omega - \mathrm{pr}'^*\omega'$ on $Z \times Z'$. The graphs of $(\phi_\mu)_\mu$ define a smooth family $(\Lambda_\mu)_\mu$ of Lagrangian submanifolds in $Z \times Z'$.

The Lagrangian contact problems $((\Lambda_\mu)_\mu, (X_\mu)_\mu, z)$ for a smooth family $(X_\mu)_\mu$ of Lagrangian submanifolds of $Z \times Z'$ and a point $z \in Z \times Z'$ can be interpreted as a family of boundary value problems for the symplectic maps $(\phi_\mu)_\mu$, where $(X_\mu)_\mu$ represents the boundary conditions. The elements of the intersection $\Lambda_\mu \cap X_\mu$ correspond to solutions to the boundary value problem. Two parameter-dependent boundary value problems for symplectic maps are *equivalent* at a solution (see Definition 6.3.1 and Remark 6.3.1) if and only if their corresponding parameter-dependent Lagrangian contact problems in $Z \times Z'$ are contact equivalent. Therefore, Remark 10.5.1 applies to parameter-dependent boundary value problems for symplectic maps and relates the problem to classical catastrophe theory. For this also notice that small perturbations of the corresponding catastrophe theory problems relate to perturbations of the Lagrangian contact problems which can still be interpreted as boundary value problems for symplectic maps.

Part III

Structure preservation in numerical integration of PDEs

This part of the thesis considers how structure in partial differential equations can be exploited for numerical computations. The Hamiltonian structure of ordinary differential equations can be understood using concepts of finite dimensional symplectic geometry, which is the viewpoint taken in Part II of this work. However, the structure can also be understood as the existence of a variational principle. The latter viewpoint turns out to be useful when generalising ideas from Part II to the setting of partial differential equations.

In Chapter 11 we will approach a bifurcation analysis of partial differential equations with variational structure using the ideas of Part II: we reduce the classification of bifurcations in boundary value problems for a certain, common class of PDEs with parameters to the finite dimensional classification using the Infinite Dimensional Splitting Lemma. Exploiting the catastrophe theory setting, we develop detection equations for all bifurcations belonging to the A-series, including folds, cusps, swallowtails,.... Our approach allows a unified treatment of the continuous as well as the variationally discretised problem. In a numerical example we show how the derived formulas can be used to detect high codimensional bifurcations.

Another generalisation of Hamiltonian systems on symplectic manifolds are Hamiltonian systems which are defined on (possibly infinite dimensional) Poisson spaces. Many geometric features and conservation properties of the flow are related to the Poisson structure. A special class of such systems are *Lie–Poisson systems*, which cover many PDEs including Burgers' equation, KdV, Camassa-Holm and hydrodynamic equations. In Chapter 12 we use *Clebsch variables* to lift a Lie–Poisson formulation of Burgers' equations and related PDEs to a Hamiltonian system defined on a symplectic vector space, on which symplectic integration techniques can be applied. We show in numerical experiments that conservation properties of symplectic integration can outweigh disadvantages of the increased phase-space dimension.

A third generalisation of the concept of Hamiltonian systems on symplectic manifolds is *multi-symplecticity*. In Chapter 13 we show an approach to the question whether multisymplectic integrators preserve symmetric solutions such as travelling waves.

Chapter 11

Detection of high codimensional bifurcations in variational PDEs

Chapter 11 is an adaption of Kreusser, McLachlan, and Offen, 2020.

We derive bifurcation test equations for A-series singularities of nonlinear functionals and, based on these equations, we propose a numerical method for detecting high codimensional bifurcations in parameter-dependent PDEs such as parameter-dependent semilinear Poisson equations. As an example, we consider a Bratu-type problem and show how high codimensional bifurcations such as the swallowtail bifurcation can be found numerically. In particular, our original contributions are (1) the use of the Infinite-Dimensional Splitting Lemma, (2) the unified and simplified treatment of all A-series bifurcations, (3) the presentation in Banach spaces, i.e. our results apply both to the PDE and its (variational) discretization which allows a unified treatment of the continuous problem and its discretisation, (4) further simplifications for parameter-dependent semilinear Poisson equations (both continuous and discrete).

11.1 Introduction

In this chapter we deal with bifurcations of solutions of differential equations and in particular with those whose solutions are critical points of a functional. In comparison to ODEs, the detection of bifurcations of solutions of PDEs poses additional challenges including infinite dimensionality and, after discretisation, the need to solve large systems of equations. As a prototype of a PDE problem, we consider the semilinear Poisson equation

$$\begin{cases} \Delta u + f(u, \lambda) = 0 \\ u|_{\partial\Omega} = 0 \end{cases}$$

for u defined on $\Omega \subset \mathbb{R}^d, \lambda \in \mathbb{R}^k$. Its parameter-dependent solutions can be regarded as stationary solutions of an associated reaction–diffusion equation with many applications in the physical sciences.

More generally, we investigate singularities of functionals $S\colon E \to \mathbb{R}$ where the weak formulation of a PDE is recovered as $\mathrm{D}S(u) = 0$, where D denotes the Fréchet derivative. The existence of a variational structure has an effect on which singularities can occur generically as well as on their codimension. Using the Infinite-Dimensional Splitting lemma (Golubitsky and Marsden, 1983) will allow us to relate these singularities to classical catastrophe theory. Indeed, in the finite dimensional case, we have seen the effect of gradient structures in the review of singularity theory in Chapter 5: while the Whitney fold map $\mathbb{R}^2 \to \mathbb{R}^2$ is persistent even if no parameters are present, a catastrophe fold only occurs persistently in families of maps $\mathbb{R}^n \to \mathbb{R}$ with at least one parameter.

Singularities in correspondence to the Whitney singularities known from the finite dimensional setting were considered for a Banach space setting by Ambrosetti and Prodi (1972). Since then, fold and cusp maps have been studied extensively and many characterizations of fold and cusp maps have been given–see the papers by Church and Timourian and others (1985; 1988; 1987; 1992; 1993). Swallowtail and the butterfly maps were characterized in Ruf, 1995. Numerical approaches are discussed in Beyn, 1984; K. Böhmer, 1993; W. C. Böhmer and Sassmannshausen, 1999; Fink and Rheinboldt, 1987; Griewank and Reddien, 1989; Hermann, Middelmann, and Kunkel, 1998; Kunkel, 1988; Seydel, 2010.

Two approaches to bifurcation of solutions to PDEs are generalized Lyapunov-Schmidt reductions and topological methods in the calculus of variations which so far can only access relatively simple bifurcations (K. Böhmer, 1993; W. C. Böhmer and Sassmannshausen, 1999; Kunkel, 1988; Mei, 2000a). The Lyapunov-Schmidt reduction can be used to study solutions to nonlinear equations when the implicit function theorem cannot be applied and allows the reduction of infinite dimensional equations in Banach spaces to finite dimensional equations. However, Lyapunov-Schmidt reductions do not use the variational structure. This motivates the development of a method for detecting high codimensional catastrophe-type bifurcations in high-dimensional or even infinite dimensional phase spaces which makes use of the underlying variational structure.

The chapter is organised as follows. In Section 11.2 we recall an observation by Golubitsky and Marsden (1983) that catastrophe theory, i.e. the classification of the bifurcation behaviour of critical points of smooth, real-valued functions on (finite dimensional) spaces, applies to smooth, nonlinear functionals on Banach spaces. We use this result to derive explicit bifurcation test equations (also known as determining

equations or augmented systems) for all A-series singularities, expressed in terms of the derivatives of the original functional. Based on these derived augmented systems of equations, we propose a numerical method for finding high codimensional bifurcations in parameter-dependent PDEs. This numerical scheme is illustrated in Section 11.3 where we consider a Bratu-type boundary value problem as an example of a second order PDE and detect its high codimensional bifurcations numerically. Finally, we conclude in Section 11.4.

11.2 Augmented systems for nonlinear functionals

11.2.1 The Splitting Lemma in Banach spaces

The Splitting Lemma or Parametric Morse Lemma (see Theorem 5.3.2 or Lemma 10.2.6) can be extended to Banach spaces as follows.

Let E be a Banach space, let $U \subset E$ be an open neighbourhood of the origin and let $S\colon U \to \mathbb{R}$ be a smooth function with $S(0) = 0$. We define the following two assumptions.

Assumption 11.2.1. *There exists an inner product $\langle \cdot, \cdot \rangle_E$ on E and a Fredholm operator $T\colon E \to E$ of index 0 such that*

$$\mathrm{D}^2 S(0)(u, v) = \langle Tu, v \rangle_E \quad \textit{for all } u, v \in E.$$

In assumption 11.2.1 the symbol D denotes the Fréchet derivative. The second order derivative $D^2S(0)$ of S at 0 is a symmetric bilinear form on $E \times E$. The index-0 Fredholm operator T is symmetric such that $E = \ker T \oplus \operatorname{rg} T$, where $\ker T$ denotes the kernel of T and $\operatorname{rg} T$ the range of T. We denote elements $u \in E$ by its components $u = (x, y)$ with respect to the splitting, i.e. $x \in \ker T$ and $y \in \operatorname{rg} T$.

Assumption 11.2.2. *There exists a* partial gradient $\nabla_y S\colon U \to \operatorname{rg} T$ *with* $\nabla_y S(0) = 0$ *such that*

$$\forall u \in U, \quad \forall v \in \operatorname{rg} T : \quad \langle \nabla_y S(u), v \rangle_E = \mathrm{D}S(u)v.$$

Theorem 11.2.1 (Infinite-Dimensional Splitting Lemma (Golubitsky and Marsden, 1983))**.** *If assumptions 11.2.1 and 11.2.2 hold, then there exists a fibred change of coordinates $(\bar{x}, \bar{y}) = (x, \eta(x, y))$ on U fixing $(0, 0) \in E$ with $\eta\colon U \to \operatorname{rg} T$ such that $\mathrm{D}_y \eta(0, 0) = \mathrm{Id}$ and such that S takes the form*

$$S(\bar{x}, \bar{y}) = \frac{1}{2} \langle T\bar{y}, \bar{y} \rangle_E + r(\bar{x})$$

for a smooth function $r\colon \mathcal{O} \to \mathbb{R}$, where $\mathcal{O}$ is an open neighbourhood of $0 \in \ker T$ and $r(0) = 0$, $\mathrm{D}r(0) = 0$ and $\mathrm{D}^2 r(0) = 0$.

In Theorem 11.2.1 $\mathrm{D}_y\eta$ denotes the Fréchet derivative of η in the direction of $\operatorname{rg} T$. For a discussion of the setting and examples refer to Buchner, Marsden, and Schecter, 1983. The function r is defined as follows: by the implicit function theorem, there exists a unique, smooth function $F\colon U_{\ker T} \to U_{\operatorname{rg} T}$ for open neighbourhoods $U_{\ker T} \subset \ker T$ and $U_{\operatorname{rg} T} \subset \operatorname{rg} T$ of the origin in $\ker T$ and $\operatorname{rg} T$, respectively, such that

$$\begin{aligned} F(0) = 0, \quad \mathrm{D}F(0) = 0, \\ \forall x \in U_{\ker T} : \nabla_y S(x, F(x)) = 0. \end{aligned} \tag{11.2.1}$$

The map $r\colon U_{\ker T} \to \mathbb{R}$ is given by

$$r(x) = S(x, F(x)). \tag{11.2.2}$$

We see that critical points of S correspond to critical points of r which is defined on a finite dimensional space. Singularity theory for S thus reduces to ordinary, finite dimensional catastrophe theory (see Chapter 5 or V. I. Arnold, Gusein-Zade, and Varchenko, 2012; Wassermann, 1974). More precisely, to determine the singularities of S it suffices to determine the singularities of r.

11.2.2 Augmented systems for A-series singularities

A-series singularities for a given functional S are defined as follows.

Definition 11.2.1 (A-series singularity)**.** Let E be a Banach space, let $U \subset E$ be a neighbourhood of the origin and let $S\colon U \to \mathbb{R}$ be a smooth function with $S(0) = 0$. Assume that assumptions 11.2.1 and 11.2.2 hold and consider the function r from (11.2.2). The function S has a singularity of type A_n at 0 if $\ker T$ (with T as in assumption 11.2.1) is one-dimensional and

$$\left.\frac{\mathrm{d}^k}{\mathrm{d}x^k}\right|_{x=0} r(x) = 0, \quad k = 3, \dots, n, \qquad \left.\frac{\mathrm{d}^{n+1}}{\mathrm{d}x^{n+1}}\right|_{x=0} r(x) \neq 0.$$

△

Remark 11.2.1. The singularity A_2 is referred to as *fold*, A_3 as *cusp*, A_4 as *swallowtail* and A_5 as *butterfly singularity*. △

Remark 11.2.2. The Infinite-Dimensional Splitting Lemma (Theorem 11.2.1) allows us to borrow the notions of catastrophe theory and to define singularities of real-valued functionals $S\colon E \to \mathbb{R}$ fulfilling assumptions 11.2.1 and 11.2.2. In applications, $\mathrm{D}S(u)(v) = 0\ \forall v \in E$ is the weak formulation of a PDE. In the literature the gradient structure is typically not exploited for this purpose. Instead the more general class of

singularities of functionals $\tilde{S}\colon E \to \tilde{E}$ between two Banach spaces E and $\tilde{E}$ is considered as in Ambrosetti and Prodi, 1972; Berger, Church, and Timourian, 1985; Berger, Church, and Timourian, 1988; Lazzeri and Micheletti, 1987; Church and Timourian, 1992; Church and Timourian, 1993; Ruf, 1995; Ruf, 1990; Ruf, 1992; Church, Dancer, and Timourian, 1993. The general problem class $\tilde{S}(u) = 0$ contains the class of catastrophe problems $\mathrm{D}S(u) = 0$. However, since the class of functions $E \to \tilde{E}$ is richer, this leads to a different notion of A-series singularities since stability properties do not coincide. To illustrate this point, let $\tilde{E} = E$. A map $\tilde{S}\colon E \to E$ with a singularity that is persistent under small perturbations $\tilde{S} + \epsilon\tilde{P}$ with functions $\tilde{P}\colon E \to E$ is not necessarily of the form $\tilde{S} = \mathrm{D}S$. On the other hand a map $S\colon E \to \mathbb{R}$ with a singularity that is persistent under small perturbations $S + \epsilon P$ with functions $P\colon E \to \mathbb{R}$ does not necessarily yield a map $\tilde{S} = \mathrm{D}S\colon E \to E$ with a singularity that is persistent under small perturbations with functions of the bigger problem class $\tilde{P}\colon E \to E$ since perturbations with $\tilde{P} \neq \mathrm{D}P$ are allowed. Let us illustrate the different notions of singularities on the cusp singularity. As proved by Whitney, the cusp map $f\colon \mathbb{R}^2 \to \mathbb{R}^2$ with $f(z,w) = (z^3+zw, w)$ is stable. If we plot the z-component of solutions (z,w) to the system $f(z,w) = (\mu_1,\mu_2)$ over the (μ_1,μ_2)-plane, then we obtain the plot in the centre of Figure 5.1. On the other hand, consider the map $h\colon \mathbb{R}^2 \to \mathbb{R}$ with $h(z,w) = \frac{1}{4}z^4 + \frac{1}{2}w^2$. The map h has a cusp singularity at $(0,0)$. Its miniversal unfolding in catastrophe theory is given by $h_\mu(z,w) = \frac{1}{4}z^4 + \frac{1}{2}\mu_2 z^2 + \mu_1 z + \frac{1}{2}w^2$. If we plot the z-component of solutions (z,w) to the system $\nabla h_\mu(z,w) = (0,0)$ over the (μ_1,μ_2)-plane, then we also obtain the plot in the centre of Figure 5.1. Despite the same visualisation, the cusp map f is not to be confused with the map ∇h. The map f does not have a primitive $g\colon \mathbb{R}^2 \to \mathbb{R}$ with $\nabla g = f$. Moreover, the map f is stable in the class of smooth functions $\mathbb{R}^2 \to \mathbb{R}^2$ while the cusp catastrophe $h\colon \mathbb{R}^2 \to \mathbb{R}$ needs to be unfolded to be stable in the class of smooth functions $\mathbb{R}^2 \to \mathbb{R}$. Also see Chapter 5 where we contrast Whitney singularities and catastrophe singularities. In this chapter we will investigate the catastrophe setting and exploit the gradient structure for numerical continuation methods. △

The k^{th} derivative of S at a point $z \in U$ is a symmetric multi-linear form which we denote by $\mathrm{D}^{(k)}S(z)$. We can interpret the multi-linear form $\mathrm{D}^{(k)}S(z)$ as a linear form on $E^{\otimes k} = \bigotimes_{j=1}^{k} E$ where $\otimes$ denotes the tensor product. As a shorthand we define $S^{(k)} := \mathrm{D}^{(k)}S$ and $S_0^{(k)} := \mathrm{D}^{(k)}S(0)$.

We can express the condition for a function S to have an A-series singularity in terms of (Fréchet)-derivatives of S. For this we define the multi-index set $\mathcal{J}_k^n$ for $n, k \in \mathbb{N}$ with $k \leq n$ as

$$\left\{ j = (j_1, \dots, j_{n-k+1}) \colon \quad j_l \in \mathbb{N} \cup \{0\}, \quad \sum_{l=1}^{n-k+1} j_l = k, \quad \sum_{l=1}^{n-k+1} l \cdot j_l = n \right\}. \tag{11.2.3}$$

Moreover, for a multi-index $j \in \mathcal{J}_k^n$ we define $j! := j_1! j_2! \cdots j_{n-k+1}!$.

Theorem 11.2.2. *Let E be a Banach space and consider an inner product $\langle \cdot, \cdot \rangle_E$ on E. Let $U \subset E$ be a neighbourhood of the origin and let $S \colon U \to \mathbb{R}$ be a smooth function with $S(0) = 0$. Consider the following algorithm consisting of a sequence of tests. The algorithm terminates and returns the current value of the integer n if a test fails. In the algorithm F is considered as a function symbol of an unknown smooth map $I \to E$, where I is a small open interval in $\mathbb{R}$ containing 0 and with $F(0) = F^{(0)}(0) = 0$, $F^{(1)}(0) = 0$.*

- *Set $n = 1$. Test $S_0^{(1)} = 0$.*
- *Set $n = 2$. Test whether the kernel of $a \mapsto S_0^{(2)}(a, \cdot) \in E^*$ is 1-dimensional.*
- *Set $n = 3$. Select an element $\alpha \in E \setminus \{0\}$. Test $S^{(3)}(\alpha^{\otimes 3}) = 0$.*
- *Loop through the following two steps.*
  1. *Set $n := n + 1$. Determine $F^{(n-2)}(0) \in \{s\alpha \,|\, s \in \mathbb{R}\}^{\perp_E}$ using*

$$\forall \xi \in \{s\alpha \,|\, s \in \mathbb{R}\}^{\perp_E} :$$

$$\sum_{k=1}^{n-2} \sum_{j \in \mathcal{J}_k^{n-2}} \frac{(n-2)!}{j!} S_0^{(k+1)} \left(\xi \otimes \bigotimes_{l=1}^{n-k-1} \frac{\left(\frac{\mathrm{d}^l}{\mathrm{d}s^l}\Big|_{s=0} (s\alpha + F(s)) \right)^{\otimes j_l}}{(l!)^{j_l}} \right) = 0.$$

  2. *Test*

$$\sum_{k=1}^{n} \sum_{j \in \mathcal{J}_k^n} \frac{n!}{j!} S_0^{(k)} \left(\bigotimes_{l=1}^{n-k+1} \frac{\left(\frac{\mathrm{d}^l}{\mathrm{d}s^l}\Big|_{s=0} (s\alpha + F(s)) \right)^{\otimes j_l}}{(l!)^{j_l}} \right) = 0.$$

The following statements hold true.

- *The algorithm returns $n = 1$ if and only if 0 is not a critical point of S.*
- *The algorithm returns $n = 2$ or does not terminate if and only if 0 is a critical point of S but S does not have an A-series singularity at 0.*
- *If assumptions 11.2.1 and 11.2.2 are satisfied with respect to $\langle \cdot, \cdot \rangle_E$, then the algorithm returns $n \geq 3$ if and only if S has a singularity of type A_{n-1}.*

Before proving the theorem, let us formulate some corollaries which illustrate how the conditions in Theorem 11.2.2 simplify for small values of n.

Definition 11.2.2. We say that a functional S fulfilling assumptions 11.2.1 and 11.2.2 has a singularity *of type at least* A_n if

- it has a singularity of type A_N with $N \geq n$ or
- the algorithm in Theorem 11.2.2 does not terminate.

△

Corollary 11.2.3 (Fold (A_2))**.** *Let E be a Banach space and S be a (nonlinear) smooth functional defined on an open neighbourhood of $0 \in E$. Assume that assumptions 11.2.1 and 11.2.2 hold for a Fredholm operator T such that*

$$\ker T = \operatorname{span}_{\mathbb{R}}\{\alpha\} \tag{11.2.4}$$

is satisfied for a nontrivial element $\alpha \in E$. Then S has a singularity of type at least A_2 (fold singularity).

Corollary 11.2.4 (Cusp (A_3))**.** *Let E be a Banach space and S be a smooth functional defined on an open neighbourhood of $0 \in E$. Assume that assumptions 11.2.1 and 11.2.2 hold for a Fredholm operator T and $\alpha \in E \setminus \{0\}$ such that (11.2.4) holds, i.e. S has a singularity of type at least A_2. The functional S has a singularity of type at least A_3 if and only if*

$$S_0^{(3)}(\alpha, \alpha, \alpha) = 0. \tag{11.2.5}$$

Corollary 11.2.5 (Swallowtail (A_4))**.** *Let E be a Banach space and S be a smooth functional defined on an open neighbourhood of $0 \in E$. Assume that assumptions 11.2.1 and 11.2.2 hold for a Fredholm operator T and $\alpha \in E \setminus \{0\}$ such that (11.2.4) and (11.2.5) are satisfied, i.e. S has a singularity of type at least A_3. The functional S has a singularity of type at least A_4 if and only if*

$$S_0^{(2)}(v, \xi) = -S_0^{(3)}(\alpha, \alpha, \xi) \quad \forall \xi \in E \tag{11.2.6}$$

is solvable for $v \in E$ and

$$S_0^{(4)}(\alpha, \alpha, \alpha, \alpha) - 3S_0^{(2)}(v, v) = 0. \tag{11.2.7}$$

Corollary 11.2.6 (Butterfly (A_5))**.** *Let E be a Banach space and S be a smooth functional defined on an open neighbourhood of $0 \in E$. Assume that assumptions 11.2.1 and 11.2.2 hold for a Fredholm operator T and $\alpha \in E \setminus \{0\}$ such that (11.2.4) and*

(11.2.5) *are satisfied. Furthermore, assume that* (11.2.6) *holds for some* $v \in E$ *and* (11.2.7) *is satisfied, i.e. the functional* S *has a singularity of type at least* A_4*. The functional* S *has a singularity of type at least* A_5 *if and only if*

$$S_0^{(2)}(w,\xi) = -S_0^{(4)}(\alpha,\alpha,\alpha,\xi) - 3S_0^{(3)}(\alpha,v,\xi) \quad \forall \xi \in E \tag{11.2.8}$$

is solvable for $w \in E$ *and*

$$S_0^{(5)}(\alpha^{\otimes 5}) - 15S_0^{(3)}(\alpha,v,v) + 10S_0^{(3)}(\alpha,\alpha,w) = 0.$$

Remark 11.2.3. Notice that we do not need to require $v \in \operatorname{rg} T$ in (11.2.6) or $w \in \operatorname{rg} T$ in (11.2.8) since $S_0^{(2)}(w + t_1\alpha, v + t_2\alpha) = S_0^{(2)}(w,v)$ and $S_0^{(3)}(\alpha, v + t_1\alpha, \xi + t_2\alpha) = S_0^{(3)}(\alpha,v,\xi)$ for $\alpha \in E$ satisfying (11.2.4) and (11.2.5) such that the test equations are defined invariantly. △

The equations in the loop section of the algorithm presented in Theorem 11.2.2 can be obtained from the $(n-2)^{\text{th}}$ and n^{th} *complete exponential Bell polynomials* as we will see from Lemmas 11.2.7 and 11.2.10 and Remark 11.2.5.

Definition 11.2.3 (Complete exponential Bell polynomial)**.** The n^{th} *complete exponential Bell polynomial* is given as

$$B_n(x_1,\dots,x_n) = \sum_{k=1}^{n} \sum_{j \in \mathcal{J}_k^n} \frac{n!}{j!} \prod_{l=1}^{n-k+1} \left(\frac{x_l}{l!}\right)^{j_l}, \tag{11.2.9}$$

with the multi-index set $\mathcal{J}_k^n$ as in (11.2.3) and $j! = j_1!j_2!\dots j_{n-k+1}!$ for $j \in \mathcal{J}_k^n$. △

The first five complete exponential Bell polynomials are given by

$$\begin{aligned}
B_0 &= 1,\\
B_1(x_1) &= x_1,\\
B_2(x_1,x_2) &= x_1^2 + x_2,\\
B_3(x_1,x_2,x_3) &= x_1^3 + 3x_1x_2 + x_3,\\
B_4(x_1,x_2,x_3,x_4) &= x_1^4 + 6x_1^2x_2 + 4x_1x_3 + 3x_2^2 + x_4,\\
B_5(x_1,x_2,x_3,x_4,x_5) &= x_1^5 + 10x_2x_1^3 + 15x_2^2x_1 + 10x_3x_1^2 + 10x_3x_2 + 5x_4x_1 + x_5.
\end{aligned} \tag{11.2.10}$$

Remark 11.2.4. Complete exponential Bell polynomials appear as coefficients in the following formal power series.

$$\exp\left(\sum_{k=1}^{\infty} \frac{x_k}{k!} y^k\right) = \sum_{n=0}^{\infty} \frac{1}{n!} B_n(x_1,\dots,x_n) y^n.$$

Moreover, the n^{th} complete exponential Bell polynomial encodes information on the number of ways a set containing n elements can be partitioned into non-empty, disjoint subsets. For example, we can read off from

$$B_4(x_1, x_2, x_3, x_4) = x_1^4 + 6x_1^2 x_2 + 4x_1 x_3 + 3x_2^2 + x_4$$

that there is

- 1 partition consisting of 4 sets of cardinality 1,
- 6 partitions into 3 sets of which 2 have cardinality 1 and the other one has cardinality 2,
- 4 partitions into 2 sets of which 1 has cardinality 1 and the other one has cardinality 3,
- 3 partitions into 2 sets of cardinality 2,
- and 1 partition consisting of 1 set of cardinality 4.

(See Bell, 1927; Brualdi, 2004, for instance). △

Let us prepare the proof of Theorem 11.2.2 with two lemmas.

Lemma 11.2.7. *Let E be a Banach space, $U \subset E$ an open subset and $\alpha \in E$. Consider smooth functions $S\colon U \to \mathbb{R}$ and $F\colon I \to E$, where I is an open interval $I \subset \mathbb{R}$ such that $r(s) := S(s\alpha + F(s))$ is defined on I. For $n \in \mathbb{N}$ we have*

$$r^{(n)}(s) = B_n(\alpha + F'(s), F''(s), \dots, F^{(n)}(s)).$$

On the right-hand side of the equation multiplications are interpreted as tensor products. Moreover, the symbol "$+$" is replaced by "$+S^{(\text{degree})}(s\alpha + F(s))$", where degree *is the count of factors in the tensor product to which $S^{(\text{degree})}(s\alpha + F(s))$ is applied. In other words,*

$$r^{(n)}(s) = \sum_{k=1}^{n} \sum_{j \in \mathcal{J}_k^n} \frac{n!}{j!} S^{(k)}(s\alpha + F(s)) \left(\bigotimes_{l=1}^{n-k+1} \frac{\left(\frac{\mathrm{d}^l}{\mathrm{d}s^l}(s\alpha + F(s))\right)^{\otimes j_l}}{(l!)^{j_l}} \right),$$

where $j = (j_1, \dots, j_{n-k+1}) \in \mathcal{J}_k^n$ is defined in (11.2.3) and $j! = j_1! j_2! \dots j_{n-k+1}!$ for a multi-index $j \in \mathcal{J}_k^n$.

Corollary 11.2.8. *In the setting of Lemma 11.2.7, if $0 \in U$ and $S_0 = 0$, $S_0^{(1)} = 0$, $S_0^{(2)}(\alpha, \xi) = 0$ for all $\xi \in E$ and $F(0) = F'(0) = 0$, then the first five derivatives of r*

evaluated at 0 are given by

$$\begin{aligned}
r(0) &= 0\\
r'(0) &= 0\\
r''(0) &= 0\\
r'''(0) &= S_0^{(3)}(\alpha^{\otimes 3})\\
r''''(0) &= S_0^{(4)}(\alpha^{\otimes 4}) + 6S_0^{(3)}(\alpha^{\otimes 2}\otimes F''(0)) + 3S_0^{(2)}(F''(0)^{\otimes 2})\\
r'''''(0) &= S_0^{(5)}(\alpha^{\otimes 5}) + 10S_0^{(4)}(\alpha^{\otimes 3}\otimes F''(0)) + 10S_0^{(3)}(\alpha^{\otimes 2}\otimes F'''(0))\\
&\quad + 15S_0^{(3)}(\alpha\otimes (F''(0))^{\otimes 2}) + 10S_0^{(2)}(F''(0)\otimes F'''(0)).
\end{aligned}$$

Proof of Lemma 11.2.7. The statement is an extension of Faà di Bruno's formula (Andrews, 1984, §12.3) from $E = \mathbb{R}$ to arbitrary Banach spaces E. Since the chain rule for differentiation is valid for Fréchet derivatives (Penot, 2013, Thm. 2.47), the proof is analogous. □

As we see explicitly for $i \leq 5$ in Corollary 11.2.8, to determine $r^{(i)}(0)$ the $i-2$-jet of F is required at 0 in the setting of Corollary 11.2.8. This holds in general.

Corollary 11.2.9. *In the setting of Corollary 11.2.8 the value $r^{(i)}(0)$ can be calculated from the $i-2$-jet of F where $i \in \mathbb{N}$ with $i \geq 2$. We can write*

$$r^{(i)}(0) = B_i(\alpha, F''(0), \ldots, F^{(i-2)}(0), c_2, c_1),$$

where c_1, c_2 are any constants. On the right-hand side of the equation multiplications are interpreted as tensor products. Moreover, the symbol "+" is replaced by "$+S_0^{(\text{degree})}$", where degree *is the count of factors in the tensor product to which $S_0^{(\text{degree})}$ is applied.*

Proof. We use the combinatorial interpretation of Bell polynomials and Lemma 11.2.7. If a partition of an i-set contains a subset with $i-1$ elements, then there must be exactly one more non-empty subset containing one element to form a valid partition. Therefore, $F^{(i-1)}(0) = \frac{\mathrm{d}^{i-1}}{\mathrm{d}s^{i-1}}\Big|_0 (s\alpha + F(s))$ only occurs together with $\alpha = \frac{\mathrm{d}^1}{\mathrm{d}s^1}\Big|_0 (s\alpha + F(s))$ as $iF^{(i-1)}(0)\otimes\alpha$. This terms becomes an input argument of $S_0^{(2)}$ and, therefore, vanishes by the choice of α. If a partition of an i-set contains a subset with i elements, then there cannot be another non-empty subset in the partition. Therefore, $F^{(i)}(0) = \frac{\mathrm{d}^i}{\mathrm{d}s^i}\Big|_0 (s\alpha + F(s))$ becomes an input argument of $S_0^{(1)}$ which is zero. □

Lemma 11.2.10. *Let E be a Banach space and let U be an open neighbourhood of $0 \in E$. Consider a smooth function $S\colon U \to \mathbb{R}$ with $S(0) = 0$ such that assumptions 11.2.1 and 11.2.2 hold for a Fredholm operator T with $\ker T = \operatorname{span}_{\mathbb{R}}\{\alpha\}$ for a nontrivial*

element $\alpha \in E$. There exists an open interval I containing 0 and a unique function $F\colon I \to \operatorname{rg} T$ with $F(0) = 0$, $F'(0) = 0$ s.t.

$$\forall s \in I, \quad \forall \xi \in \operatorname{rg} T : \quad S^{(1)}(s\alpha + F(s))(\xi) = 0. \tag{11.2.11}$$

Moreover, all derivatives $F^{(n)}(0)$ with $n \geq 2$ can be obtained successively from

$$\forall \xi \in \operatorname{rg} T : 0 = \sum_{k=1}^{n} \sum_{j \in \mathcal{J}_k^n} \frac{n!}{j!} S_0^{(k+1)} \left(\xi \otimes \bigotimes_{l=1}^{n-k+1} \frac{\left(\frac{\mathrm{d}^l}{\mathrm{d}s^l}\Big|_{s=0} (s\alpha + F(s)) \right)^{\otimes j_l}}{(l!)^{j_l}} \right), \tag{11.2.12}$$

where $j = (j_1, \ldots, j_{n-k+1}) \in \mathcal{J}_k^n$ as defined in (11.2.3) and $j! = j_1! j_2! \ldots j_{n-k+1}!$.

Remark 11.2.5. Relation (11.2.12) can be expressed as

$$0 = B_n(\alpha, F''(0), \ldots, F^{(n)}(0)),$$

where multiplications in the definition of the Bell polynomial (11.2.9) are interpreted as tensor products. Furthermore, the symbol "+" is replaced by "$+S^{(\text{degree})}(s\alpha+F(s))\xi\otimes$" and parenthesis may be added around the input arguments of the form $S^{(\text{degree})}(s\alpha + F(s))$. △

Corollary 11.2.11. *The relations for $n = 2, 3, 4, 5$ of Lemma 11.2.10 read*

$$\begin{aligned}
0 &= S_0^{(3)}(\xi \otimes \alpha^{\otimes 2}) + S_0^{(2)}(\xi \otimes F''(0)) \\
0 &= S_0^{(4)}(\xi \otimes \alpha^{\otimes 3}) + 3S_0^{(3)}(\xi \otimes \alpha \otimes F''(0)) + S_0^{(2)}(\xi \otimes F'''(0)) \\
0 &= S_0^{(5)}(\xi \otimes \alpha^{\otimes 4}) + 6S_0^{(4)}(\xi \otimes \alpha^{\otimes 2} \otimes F''(0)) + 3S_0^{(3)}(\xi \otimes F''(0)^{\otimes 2}) \\
&\quad + 4S_0^{(3)}(\xi \otimes \alpha \otimes F'''(0)) + S_0^{(2)}(\xi \otimes F''''(0)) \\
0 &= S_0^{(6)}(\xi \otimes \alpha^{\otimes 5}) + 10S_0^{(5)}(\xi \otimes \alpha^{\otimes 3} \otimes F''(0)) \\
&\quad + 10S_0^{(4)}(\xi \otimes \alpha^{\otimes 2} \otimes F'''(0)) + 15S_0^{(4)}(\xi \otimes \alpha \otimes F''(0)^{\otimes 2}) \\
&\quad + 10S_0^{(3)}(\xi \otimes F''(0) \otimes F'''(0)) + 5S_0^{(3)}(\xi \otimes \alpha \otimes F''''(0)) \\
&\quad + S_0^{2}(\xi \otimes F'''''(0)).
\end{aligned}$$

Proof of Lemma 11.2.10. The operator T defines an isomorphism on $\operatorname{rg} T$. Thus, the implicit function theorem applies to $\nabla_y S$ and together with (11.2.11) provides the existence and uniqueness of F with $F(0) = 0$ and $F'(0) = 0$ in analogy to the proof of Theorem 11.2.1 which can be found in Golubitsky and Marsden, 1983. Let $\xi \in \operatorname{rg} T$. Differentiating

$$S^{(1)}(s\alpha + F(s))(\xi) = 0 \tag{11.2.13}$$

repeatedly with respect to s we obtain the following relations.

$$
\begin{aligned}
0 &= S^{(1)}(s\alpha + F(s))(\xi)\\
0 &= S^{(2)}(s\alpha + F(s))(\xi \otimes (\alpha + F'(s)))\\
0 &= S^{(3)}(s\alpha + F(s))(\xi \otimes (\alpha + F'(s))^{\otimes 2}) + S^{(2)}(s\alpha + F(s))(\xi \otimes F''(s))\\
0 &= S^{(4)}(x\alpha + F(x))(\xi \otimes (\alpha + F'(x))^{\otimes 3})\\
&\quad + 3S^{(3)}(x\alpha + F(x))(\xi \otimes (\alpha + F'(x)) \otimes F''(x))\\
&\quad + S^{(2)}(x\alpha + F(x))(\xi \otimes F'''(x))\\
0 &= \dots
\end{aligned}
$$

We encounter the same combinatorial relations as in Lemma 11.2.7 such that differentiating (11.2.13) n times gives

$$0 = B_n(\alpha + F'(s), F''(s), \dots, F^{(n)}(s)),$$

where multiplications in the equation above are interpreted as tensor products and "+" is replaced by "$+S^{(\text{degree})}(s\alpha + F(s))\xi\otimes$. One may add parenthesis around the input arguments of the form $S^{(\text{degree})}(s\alpha + F(s))$. In other words, the relations are given by

$$0 = \sum_{k=1}^{n} \sum_{j \in \mathcal{J}_n^k} \frac{n!}{j!} S^{(k+1)}(s\alpha + F(s)) \left(\xi \otimes \bigotimes_{l=1}^{n-k+1} \frac{\left(\frac{\mathrm{d}^l}{\mathrm{d}s^l}(s\alpha + F(s))\right)^{\otimes j_l}}{(l!)^{j_l}} \right).$$

An evaluation at $s = 0$ yields the claimed formula. In the n^{th} step of differentiation the term $F^{(n)}(0)$ only occurs as an input argument of S_0^2 and not elsewhere. Since the symmetric operator T restricted to $\operatorname{rg} T$ is an isomorphism on $\operatorname{rg} T$ this successively determines all derivatives of F at 0. □

Proof of Theorem 11.2.2 and its corollaries. The first two statements of the theorem follow immediately from the definitions. Assume that assumptions 11.2.1 and 11.2.2 hold for an operator T with 1-dimensional kernel. Let $\alpha \in \ker T \setminus \{0\}$. To analyse the singularities of S it suffices to analyse the singularities of the function $r\colon U_{\ker} \to \mathbb{R}$ provided by Theorem 11.2.1. Using the identification $\mathbb{R} \xrightarrow{\sim} \ker T$, $s \mapsto s\alpha$, we identify $U_{\ker}$ with an open interval I containing 0 and obtain $r\colon I \to \mathbb{R}$. The function r has the form $r(s) = S(s\alpha + F(s))$ for a smooth function $F\colon I \to \mathbb{R}$. The functional S has a singularity of type A_m at 0 if and only if $r^{(k)}(0) = 0$ for all $k \leq m$ and $r^{(m+1)}(0) \neq 0$.

The algorithm presented in the statement of Theorem 11.2.2 consists of a sequence of tests and a variable n acts as a counter. If the state of the variable n is k, then the test in the algorithm corresponds to testing $r^{(k)}(0) = 0$. This can be seen from Lemma 11.2.7.

(The formula for $r^{(k)}(0)$ is related to the k^{th} complete exponential Bell polynomial.) To evaluate $r^{(k)}(0)$ the $k-2$-jet of F is required as observed in Corollary 11.2.9. If the state of the variable n is $k \geq 4$, then $F^{(k-2)}(0)$ gets determined in the algorithm just before $r^{(k)}(0) = 0$ is tested. Lemma 11.2.10 justifies that the algorithm can determine $F^{(k-2)}(0)$ via the given formula (which is related to the $(k-2)^{\text{th}}$ complete exponential Bell polynomial) if all values $F^{(i)}(0)$ are defined for $i \leq k-3$. The values $F(0)$ and $F'(0)$ are set to be 0. The theorem follows by induction.

Corollaries 11.2.3 to 11.2.6 follow from Corollaries 11.2.8 and 11.2.11. In Corollaries 11.2.5 and 11.2.6 the bifurcation test equations $r^{(4)}(0) = 0$ and $r^{(5)}(0) = 0$ have been simplified using (11.2.6) and (11.2.8). □

Proposition 11.2.12. *Let E be a Banach space and S be a real-valued functional defined on an open neighbourhood of $0 \in E$ such that assumptions 11.2.1 and 11.2.2 hold. Consider the function r of the proof of Theorem 11.2.2, whose derivatives are bifurcation test equations. If S has a singularity of type A_{2k+1} with $k \in \mathbb{N}$ at 0, then the sign of $r^{(2n+2)}(0)$ is well-defined.*

Proof. The statement follows from the right-equivalence classification of singularities in catastrophe theory (Section 5.4) or can be deduced from our considerations as follows. The map $r(s) = S(s\alpha + F(s))$ considered in the proof of Theorem 11.2.2 is defined uniquely up to the choice of α, where α is as in assumption 11.2.1. The determining equations for the jet of F at 0 and the bifurcation test equations $r^{(j)}(0)$ ($j \in \mathbb{N}$) are related to Bell polynomials by Lemmas 11.2.7 and 11.2.10 and Remark 11.2.5.

- In any partition of an even number of elements there must be an even number of subsets (or none) with odd cardinality.
- In any partition of an odd number of elements there must be an odd number of subsets with odd cardinality.

Using the two combinatorial observations above we see inductively that the signs of the derivatives $F^{(2j)}(0)$ are defined invariantly of α because all derivatives $F^{(2j+1)}(0)$ change to $-F^{(2j+1)}(0)$ ($j \in \mathbb{N}$) as $\alpha \mapsto -\alpha$. We can conclude that the sign of $r^{(2k+2)}(0)$ is well-defined. □

Remark 11.2.6. The sign considered in Proposition 11.2.12 occurs in catastrophe theory if a classification of singularities up to *right-equivalence* is considered (Section 5.4). The singularities A_{2k+1} have a positive or negative signature defined by the sign of r^{n+2} at the singular point, while the singularities A_{2k} do not have signatures. If the algorithm in Theorem 11.2.2 returns $n = 2k+2$ with $k \in \mathbb{N}$ and assumptions 11.2.1 and 11.2.2 are satisfied, then the singularity A_{2k+1} is of the positive type if and only if the last

test equation (which corresponds to the n^{th} complete exponential Bell polynomial) is positive. Otherwise the singularity is of the negative type. △

Remark 11.2.7. If the functional S has $2k+1$ parameters ($k \in \mathbb{N}$), then, under non-degeneracy conditions, A_{2k+1} singularities occur as 1-parameter families (by the implicit function theorem). If two branches of A_{2k+1} singularities merge in a A_{2k+2} singularity, then one consists of singularities of the positive type and the other one of singularities of the negative type. This is because the bifurcation test equation $r^{(2k+2)}$, which determines the signs of the A_{2k+1} singularities, must have a nondegenerate zero at the A_{2k+2} singularity, i.e. its graph intersects the axis of abscissas transversally. △

Remark 11.2.8. Remark 11.2.7 applies to the fold bifurcation A_2 as well. In the finite dimensional case the signature of a solution z can be obtained as the sign of the determinant[1] of the Hessian matrix $S_z^{(2)}$ of S at z. In a numerical computation the sign can be determined by performing an LU-decomposition of $S_z^{(2)}$ without pivoting and counting whether the number of positive signs on the diagonal of U is even or odd. Keeping track of the signatures of solutions, cusps,..., provides information on which ones may be able to meet in a bifurcation. △

11.3 Example: semilinear Poisson equation

We will exemplify how the augmented systems derived in Section 11.2.2 can be applied to PDEs. For this, we consider a second order, semilinear PDE describing the steady state solutions in a reaction–diffusion process (Mei, 2000b). First, we will justify that the theory presented in Section 11.2.1 applies and write down the continuous recognition equations. By a concrete numerical example we will show how augmented systems can be employed in continuation methods to find high codimensional singularities.

11.3.1 Setup

For a smooth function $f\colon \mathbb{R}\times\mathbb{R}^s \to \mathbb{R}$ we consider the homogeneous Dirichlet problem

$$\begin{cases} \Delta u + f(u,\lambda) = 0 \\ u|_{\partial\Omega} = 0 \end{cases} \tag{11.3.1}$$

on an open and bounded domain $\Omega \subset \mathbb{R}^d$ with boundary $\partial\Omega$ of class $\mathcal{C}^k$, where $k > \frac{d}{2}+1$. We denote the standard volume form on Ω by $\mathrm{d}\mathbf{x}$. We consider the following setting which will allow us to employ the Infinite-Dimensional Splitting Lemma. A similar setting can be found in Buchner, Marsden, and Schecter, 1983, Example 7 for a more restricted class of functions f. An alternative treatment can be found in Ruf, 1995.

[1] which does not depend on the choice of basis since $\mathrm{D}S(z) = 0$

The Sobolev space $H^k(\Omega)$ is compactly embedded into $\mathcal{C}^1(\overline{\Omega})$ (Adams, 1975, Thm 6.2). Consider the Hilbert space $E = H_0^1(\Omega) \cap H^k(\Omega)$ with the structure inherited from $H^k(\Omega)$ (Adams, 1975; Lax, 2002). Let $\bar{f}$ be s.t. $\frac{\partial}{\partial t}\bar{f}(t,\lambda) = f(t,\lambda)$ and consider the non-linear functional $S\colon E \times \mathbb{R}^s \to \mathbb{R}$ defined as

$$S(u,\lambda) = \int_\Omega \left(-\frac{1}{2}\langle \nabla u, \nabla u\rangle + \bar{f}(u,\lambda)\right) \mathrm{d}\mathbf{x}.$$

The Fréchet derivatives of S in the directions $v_1, v_2, \ldots \in E$ exists and are given as

$$\begin{aligned} S^{(1)}(u,\lambda)(v_1) &= \int_\Omega \left(-\langle \nabla u, \nabla v_1\rangle + f(u,\lambda)v_1\right) \mathrm{d}\mathbf{x} \\ S^{(2)}(u,\lambda)(v_1,v_2) &= \int_\Omega \left(-\langle \nabla v_1, \nabla v_2\rangle + f'(u,\lambda)v_1v_2\right) \mathrm{d}\mathbf{x} \\ S^{(l)}(u,\lambda)(v_1,v_2,\ldots,v_l) &= \int_\Omega f^{(l)}(u,\lambda)v_1v_2\ldots v_l \,\mathrm{d}\mathbf{x}. \end{aligned}$$

Here $f^{(l)}(t,\lambda) = \frac{\partial^l}{\partial t^l} f(t,\lambda)$. The equation $S^{(1)}(u,\lambda)(v) = 0$ for all $v \in E$ is a weak formulation of (11.3.1). We consider the bilinear form $\langle \cdot,\cdot\rangle_E\colon E \times E \to \mathbb{R}$ with

$$\langle v, w\rangle_E = \int_\Omega \langle \nabla v, \nabla w\rangle \mathrm{d}\mathbf{x}, \qquad v, w \in E \tag{11.3.2}$$

where ∇v and ∇w denote weak derivatives of $v, w \in E$ and $\langle \cdot,\cdot\rangle$ the scalar product in $\mathbb{R}^d$. The bilinear form $\langle \cdot,\cdot\rangle_E$ is symmetric, positive definite by Poincaré's inequality and bounded using the Cauchy-Schwarz inequality. The embedding $E = H_0^1(\Omega) \cap H^k(\Omega) \hookrightarrow H^{k-2}(\Omega)$ is compact (Adams, 1975, Thm 6.2). Moreover, the Dirichlet Laplacian L is an isomorphism $H_0^1(\Omega) \cap H^k(\Omega) \to H^{k-2}(\Omega)$ (Friedman, 1969). Therefore, the operator $\Delta^{-1}\colon E \to E$ defined as the composition

$$H_0^1(\Omega) \cap H^k(\Omega) \hookrightarrow H^{k-2}(\Omega) \overset{L^{-1}}{\to} H_0^1(\Omega) \cap H^k(\Omega)$$

is compact. For each $(u,\lambda) \in E \times \mathbb{R}^s$ define the operator $T(u,\lambda)\colon E \to E$ by

$$T(u,\lambda)v = -v - \Delta^{-1}(f'(u,\lambda)v).$$

For each $(u,\lambda) \in E \times \mathbb{R}^s$ the operator $T(u,\lambda)\colon E \to E$ is a Fredholm operator: since $v \mapsto f'(u,\lambda)v$ is continuous from E into E and $\Delta^{-1}\colon E \to E$ is compact, it follows that the composition is compact and $T(u,\lambda)\colon E \to E$ is a Fredholm operator of index 0 (Fredholm alternative). We have

$$S^{(2)}(u,\lambda)(v_1,v_2) = \langle T(u,\lambda)v_1, v_2\rangle_E.$$

The operator $T(u,\lambda)$ is symmetric with respect to $\langle\cdot,\cdot\rangle_E$ such that we obtain the $\langle\cdot,\cdot\rangle_E$-orthogonality of $\ker(T(u,\lambda))$ and $\operatorname{rg}(T(u,\lambda))$. Since $T(u,\lambda)$ is a Fredholm operator, both spaces are closed in E. Moreover, $\operatorname{rg}(T(u,\lambda))$ has finite codimension. Since $T(u,\lambda)$ is symmetric, it is an elementary exercise to deduce that $E = \ker(T(u,\lambda)) \oplus \operatorname{rg}(T(u,\lambda))$. The projection $\operatorname{pr}\colon E \to \operatorname{rg}(T(u,\lambda))$ induced by the splitting is continuous. For each $\lambda \in \mathbb{R}^s$ we define the operator $\nabla_y S(\lambda)\colon E \to \operatorname{rg} T(u,\lambda)$ as

$$u \mapsto \operatorname{pr}(-u - \Delta^{-1}(f(u,\lambda)))$$

to $\operatorname{rg} T(u,\lambda)$. We have

$$S^{(1)}(u,\lambda)(v) = \left\langle -u - \Delta^{-1}(f(u,\lambda)), v\right\rangle_E = \langle \nabla_y S(\lambda)(u), v\rangle_E$$

for all $v \in \operatorname{rg}(T(u,\lambda))$. The observations imply the following proposition.

Proposition 11.3.1. *The equation*

$$\forall v \in E: \quad S^{(1)}(u,\lambda)(v) = \int_\Omega \big(-\langle\nabla u, \nabla v\rangle + f(u,\lambda)v\big)\mathrm{d}\mathbf{x} = 0$$

is a weak formulation of (11.3.1)*. Furthermore, assuming that* $S^{(1)}(u,\lambda) = 0$*, assumptions 11.2.1 and 11.2.2 hold with* $\langle\cdot,\cdot\rangle_E$ (11.3.2)*, the operator* $T(u,\lambda)\colon E \to E$ *and* $\nabla_y S(\lambda)\colon E \to \operatorname{rg} T(u,\lambda)$ *defined above for each* $(u,\lambda) \in E \times \mathbb{R}^s$*.*

We conclude that Theorem 11.2.1 applies to S such that the bifurcation behaviour of (11.3.1) reduces to finite dimensional catastrophe theory.

11.3.2 Augmented systems for the example problem

Let us write down the augmented systems for (11.3.1) provided by Corollaries 11.2.3 to 11.2.6.

Solution

$$\begin{cases} \Delta u + f(u,\lambda) = 0 \\ u|_{\partial\Omega} = 0 \end{cases} \tag{11.3.3}$$

Fold (A_2)

$$\begin{cases} \Delta\alpha + f'(u,\lambda)\alpha = 0 \\ \alpha|_{\partial\Omega} = 0 \\ \|\alpha\|_{L^2} = 1 \end{cases} \tag{11.3.4}$$

Cusp (A_3)

$$\int_\Omega f''(u,\lambda)\alpha^3 \mathrm{d}\mathbf{x} = 0 \tag{11.3.5}$$

Swallowtail (A_4)

$$\begin{cases} \Delta v + f'(u,\lambda)v + f''(u,\lambda)\alpha^2 = 0 \\ v|_{\partial\Omega} = 0 \end{cases} \tag{11.3.6}$$

$$\int_\Omega \left(f'''(u,\lambda)\alpha^4 - 3f'(u,\lambda)v^2\right)\ \mathrm{d}\mathbf{x} = 0$$

Butterfly (A_5)

$$\begin{cases} \Delta w + f'(u,\lambda)w + 3f''(u,\lambda)\alpha v + f'''(u,\lambda)\alpha^3 = 0 \\ w|_{\partial\Omega} = 0 \end{cases} \tag{11.3.7}$$

$$\int_\Omega \left(f''''(u,\lambda)\alpha^5 - 15f''(u,\lambda)\alpha v^2 + 10f''(u,\lambda)\alpha^2 w\right) \mathrm{d}\mathbf{x} = 0.$$

Remark 11.3.1. We can impose

$$\langle v, \alpha\rangle_E = \int_\Omega \langle \nabla v, \nabla\alpha\rangle \mathrm{d}\mathbf{x} = 0$$

in (11.3.6) or $\langle v, w\rangle_E = 0$ in (11.3.7) as discussed in Remark 11.2.3. The uniqueness condition allows us to interpret v as $F''(0)$ and w as $F'''(0)$ in the following general formula (11.3.8). △

Singularity A_n**,** $n \geq 4$ The equation to determine $F^{(n-2)}(0)\colon \Omega \to \mathbb{R}$ reads

$$\begin{cases} \Delta F^{(n-2)}(0) + B_{n-2}(\alpha, F''(0), \ldots, F^{(n-2)}(0)) = 0 \\ \int_\Omega \langle \nabla F^{(n-2)}(0), \nabla\alpha\rangle \mathrm{d}\mathbf{x} = 0 \\ F^{(n-2)}(0)|_{\partial\Omega} = 0. \end{cases} \tag{11.3.8}$$

To obtain the correct expression for the term $B_{n-2}(\alpha, F''(0), \ldots, F^{(n-2)}(0))$ in (11.3.8), the Bell polynomial B_{n-2} is first presented in its monomial form as in (11.2.10), then the summation sign $+$ is replaced by $+f^{(\text{degree})}(u,\lambda)$, where degree denotes the degree of the monomial it is multiplied with. Finally, the arguments $\alpha, F''(0), \ldots, F^{(n-2)}(0)$ are substituted into the expression. The bifurcation test equation is given as

$$\int_\Omega B_n(\alpha, F''(0), \ldots, F^{(n-2)}(0), 0, 0)\mathrm{d}\mathbf{x} = 0. \tag{11.3.9}$$

(Cf. Corollary 11.2.9.)

To obtain the correct expression for the term $B_n(\alpha, F''(0), \dots, F^{(n-2)}(0), 0, 0)$ in (11.3.9) the Bell polynomial B_n is first presented in its monomial form. Summands, which consist of a degree 2 monomial cx_ix_j are replaced by

$$c\left(-\langle \nabla F^{(i)}(0), \nabla F^{(j)}(0)\rangle + f'(u,\lambda)F^{(i)}(0)F^{(j)}(0)\right).$$

In the other summands we add $f^{(\text{degree}-1)}(u,\lambda)$ as a factor, whereas degree is the degree of the monomial making up the summand.

Remark 11.3.2. That S depends only quadratically on u has led to a significant simplification compared to the formulas for general functionals. Indeed, the first equation in (11.3.8) is of the form

$$\Delta F^{(n-2)}(0)(x) + \kappa(x)F^{(n-2)}(0)(x) = g(x), \qquad x \in \Omega$$

for a smooth map $g\colon \Omega \to \mathbb{R}$ and with $\kappa(x) = f'(u,\lambda)$. The map $F^{(n-2)}(0)\colon \Omega \to \mathbb{R}$ is sought. While the initial PDE (11.3.1) is a semilinear Poisson equation (Hsiao, 2006; Konishi, 1973), the equations which are added in the augmented system are linear PDEs. If $\kappa(x) \geq 0$ or $\kappa(x) \leq 0$ for all $x \in \Omega$, then this is the generalised Poisson equation considered in Grimm-Strele, 2010. △

Example 11.3.1. Let $f(u,\lambda) = \sum_{l=1}^{n} \frac{1}{l!}\lambda_l u^l$. For any choice of λ the constant function $u = 0$ is a solution to the problem (11.3.1). The condition for a singularity of type A_n at $(\lambda, u) = (\lambda, 0)$ is fulfilled if and only if $-\lambda_1$ is a simple eigenvalue of the Dirichlet Laplacian $\Delta\colon H_0^1(\Omega) \cap H^k(\Omega) \to H^{k-2}(\Omega)$ and

$$\lambda_i \begin{cases} = 0, & 2 \leq i \leq n-1 \\ \neq 0, & i = n \end{cases}$$

provided that $\int_\Omega \alpha^i \mathrm{d}\mathbf{x} \neq 0$ for $3 \leq i \leq n+1$, where α is the eigenfunction to the eigenvalue $-\lambda_1$. △

Proof. The function $u = 0$ solves (11.3.3). We have $f^{(l)}(0,\lambda) = \lambda_l$. The system (11.3.4) reads

$$\begin{cases} \Delta\alpha + \lambda_1\alpha = 0 \\ \alpha|_{\partial\Omega} = 0 \\ \|\alpha\|_{L^2} = 1 \end{cases}$$

It has a unique solution if and only if $-\lambda_1$ is a simple eigenvalue of the Dirichlet Laplacian. The cusp condition simplifies to $\lambda_2 = 0$. Assuming (11.3.3), (11.3.4), (11.3.5) we see that $F''(0) = 0$ solves (11.3.8) with $n = 4$. The swallowtail condition is fulfilled if and only if $\lambda_3 = 0$. Assuming that $F''(0) = \ldots = F^{(t-2)}(0) = 0$ and

$\lambda_3 = \lambda_4 = \ldots = \lambda_{t-1} = 0$ we see that $F^{(t-1)}(0) = 0$ solves (11.3.8) with $n = t+1$. The bifurcation test equation (11.3.9) for A_{t+1} is fulfilled if and only if $\lambda_t = 0$. The claim follows by induction. □

11.3.3 Numerical experiment

Let us return to the example of the Bratu problem which we considered in Sections 4.3 and 6.1. The classical Bratu problem considers the PDE

$$\Delta u + \lambda_1 \exp\left(\frac{u}{1+\lambda_2 u}\right) = 0$$

on a d-dimensional cube with zero Dirichlet boundary values. The boundary value problem is popular to study fold and cusp bifurcations (Mohsen, 2014). In the following we consider the domain $\Omega = (0,1) \times (0,1)$ and set

$$f(t,\lambda) = \lambda_1 \exp\left(\frac{t}{\lambda_2 t + 1}\right) + \lambda_3 \sin(\lambda_1 t)$$

in the Dirichlet problem (11.3.1) given as

$$\begin{cases} \Delta u + f(u,\lambda) = 0 \\ u|_{\partial\Omega} = 0. \end{cases}$$

The considered problem coincides with the Bratu problem for $\lambda_3 = 0$. Numerical experiments have been performed in Bolstad and Keller, 1986. The third parameter has been added to create a swallowtail bifurcation, which we will find numerically. As the topological boundary $\partial\Omega$ of the domain is not regular, the assumptions in Section 11.3.1 do not hold. However, the following numerical experiment illustrates on a classical example how the derived augmented systems can be used to locate bifurcations. As before, the primitive with respect to the first argument is denoted by $\bar{f}$, i.e. $\frac{\partial}{\partial t}\bar{f}(t,\lambda) = f(t,\lambda)$.

Discretisation via a discrete Lagrangian method

In view of Sections 11.2 and 11.3.1 it appears natural to use a variational method (see Section 3.6, Hairer, Lubich, and Wanner, 2013, Ch. VI.6 or Marsden and West, 2001a, for instance) to discretise (11.3.1). We obtain a mesh on Ω as the cross product of a uniform mesh in the x direction with N interior mesh points and spacing $\Delta x = \frac{1}{N+1}$ and a uniform mesh in the y direction with M interior mesh points and spacing$\Delta y = \frac{1}{M+1}$. Real-valued, continuous functions $u\colon \Omega \to \mathbb{R}$ are represented as matrices $U \in \mathbb{R}^{N\times M}$ where the component $U_{i,j}$ corresponds to the value $u(i\Delta x, j\Delta y)$ on the interior grid.

Alternatively, we can flatten the matrix U to a vector $\bar{u} \in \mathbb{R}^{N \cdot M}$ such that $U_{i,j} = \bar{u}_{(j-1)N+i}$. For the functional

$$S(u, \lambda) = \int_\Omega \left(-\frac{1}{2}(u_x^2 + u_y^2) + \bar{f}(u, \lambda) \right) \mathrm{d}x\mathrm{d}y$$

from Section 11.3.1 we consider the discrete functional

$$S_\Delta(U, \lambda) = \sum_{i=0}^{N} \sum_{j=0}^{M} \left(-\frac{1}{2} \left(\frac{(U_{i,j} - U_{i+1,j})^2}{\Delta x^2} + \frac{(U_{i,j} - U_{i,j+1})^2}{\Delta y^2} \right) + \bar{f}(U_{i,j}, \lambda) \right)$$

with $U_{0,j} = U_{i,0} = U_{N+1,j} = U_{i,M+1} = 0$. For $k \in \mathbb{N}$ define

$$\overline{D}(k) := \begin{pmatrix} -2 & 1 & & & \\ 1 & -2 & 1 & & \\ & \ddots & \ddots & \ddots & \\ & & 1 & -2 & 1 \\ & & & 1 & -2 \end{pmatrix} \in \mathbb{R}^{k \times k}.$$

The matrices

$$D_{xx} = \frac{1}{\Delta x^2} \overline{D}(N) \in \mathbb{R}^{N \times N}, \quad D_{yy} = \frac{1}{\Delta y^2} \overline{D}(M) \in \mathbb{R}^{M \times M}$$

are the standard central finite-difference discretisations of the operators $\frac{\partial^2}{\partial x^2}$ and $\frac{\partial^2}{\partial y^2}$. Define

$$L := \mathrm{Id}_M \otimes D_{xx} + D_{yy} \otimes \mathrm{Id}_N$$

where $\otimes$ denotes the Kronecker tensor product. Notice that

$$S_\Delta(\bar{u}, \lambda) = \frac{1}{2} \bar{u}^\top L \bar{u} + \bar{f}(\bar{u}, \lambda).$$

In the expression above the function $\bar{f}$ is evaluated component-wise, i.e the k^{th} component of $\bar{f}(u, \lambda)$ is given by $\bar{f}(u_k, \lambda)$. We have

$$\mathrm{D}_u S_\Delta(\bar{u}, \lambda) = L\bar{u} + f(\bar{u}, \lambda). \tag{11.3.10}$$

Remark 11.3.3. The expression (11.3.10) is the flattening of the matrix-valued function

$$(U, \lambda) \mapsto UD_{yy} + D_{xx}U + f(U, \lambda),$$

which can be obtained by a direct discretisation of the PDE (11.3.1) using standard central difference approximations for second derivatives (see Section 4.3). We see that

the equation $\mathrm{D}_u S_\Delta(\bar{u}, \lambda) = 0$ obtained from an application of the discrete Lagrangian principal to S leads to the same equations as a discretisation of the Laplacian operator using central finite-differences. △

Application of pseudo-arclength continuation to augmented discrete systems

To locate a singularity of a given type one can write down the augmented system of the singularity and solve the system using an iterative solver. This is called a *direct method*. For the convergence of the solver a good initial guess is required which is usually not available a priori. Instead, one may employ a continuation method and first continue a known solution along one parameter until a fold singularity is detected, then augment the system using the fold bifurcation test equation and continue a line of folds until a cusp is detected and so on. In the following numerical experiment we will use pseudo-arclength continuation (see Section 4.5 or Doedel, 2007). Our strategy of performing conceptually simple one-dimensional continuations of singularities of high codimension can be contrasted to higher-dimensional continuation of solutions (Henderson, 2007). More information on continuation methods can be found in Allgower and Georg, 2003; Bolstad and Keller, 1986; Deuflhard, 2011; Krauskopf, Osinga, and Galán-Vioque, 2007.

Whenever a bifurcation is detected one has the option to locate the singularity of the discrete system exactly using a direct method. Generally speaking, unless one has prior knowledge about the bifurcation diagram or is interested only in a specific parameter region one needs to search in different directions for bifurcations. Once arrived at a high codimensional bifurcation, the discretisation parameter is decreased, and a direct method is applied to approximate the location of the singularity in the continuous system. As starting values interpolated data from the coarser systems can be utilised.

To simplify notation in the following we will write u instead of $\bar{u}$, G for $\mathrm{D}S_\Delta$ and G_u for the Jacobian matrix $\mathrm{D}_u G$.

Fold Fixing $(\lambda_2, \lambda_3) = (0, 0)$ and starting at $\lambda_1 = 0$ we continue the solution $u = 0 \in \mathbb{R}^{N \cdot M}$ by applying pseudo-arclength continuation to

$$G(u(s), \lambda_1(s), \lambda_2, \lambda_3) = 0$$

until we find a fold. The singularity is detected when $\lambda_1(s)$ changes from being increasing to decreasing in s. (See the left plot in Figure 11.1.)

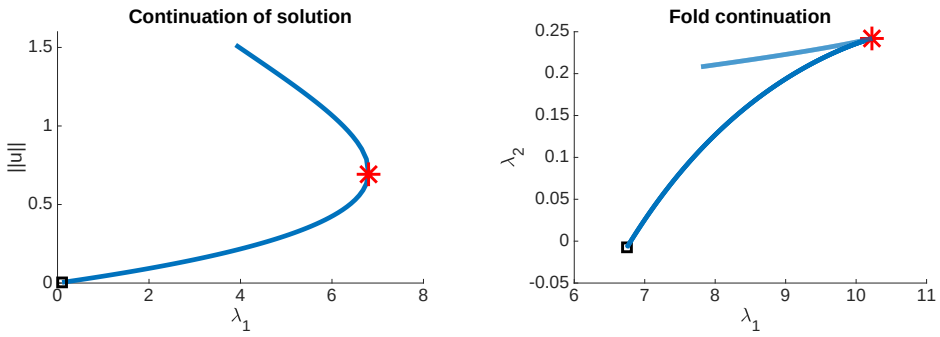

Figure 11.1: Numerical experiment with $(N, M) = (15, 15)$. The left figure shows a continuation of the solution $(u, \lambda) = (0, 0)$ of $G(u, \lambda_1, \lambda_2, \lambda_3) = 0$ along λ_1 while keeping $\lambda_2 = 0 = \lambda_3$ fixed. A fold point is marked by $*$. The right figure shows a continuation of the fold singularity by varying λ_1 and λ_2 while keeping $\lambda_3 = 0$ fixed. A cusp point is marked by $*$. In each plot the square marker shows where the continuation was initiated.

Cusp We allow λ_2 to be parameter dependent as well and apply pseudo-arclength continuation to

$$F^{(1)}(u(s), \alpha(s), \lambda_1(s), \lambda_2(s)) = \begin{pmatrix} G(u(s), \lambda_1(s), \lambda_2(s), \lambda_3) \\ G_u(u(s), \lambda_1(s), \lambda_2(s), \lambda_3)\alpha(s) \\ \alpha(s)^\top \alpha(s) - \Delta x \Delta y \end{pmatrix} = 0$$

starting with the approximated fold data and a random, normalised guess for α. (See the right plot in Figure 11.1.) During the continuation process we monitor the cusp condition

$$f_{uu}(u, \lambda_1(s), \lambda_2(s), \lambda_3)^\top \alpha^3 = 0, \tag{11.3.11}$$

where raising α to the third power is to be understood component-wise. After detecting a change of sign in the left-hand side of (11.3.11), we improve the accuracy of the location of the singular point by solving

$$\begin{pmatrix} G(u(s), \lambda_1(s), \lambda_2(s), \lambda_3) \\ G_u(u(s), \lambda_1(s), \lambda_2(s), \lambda_3)\alpha(s) \\ \alpha(s)^\top \alpha(s) - \Delta x \Delta y \\ f_{uu}(u, \lambda_1(s), \lambda_2(s), \lambda_3)^\top \alpha^3 \end{pmatrix} = 0$$

using Newton iterations.

Swallowtail We allow an s-dependence of λ_3 and apply pseudo-arclength continuation to the system

$$F^{(2)}(u(s),\alpha(s),\lambda_1(s),\lambda_2(s),\lambda_3(s)) = \begin{pmatrix} G(u(s),\lambda_1(s),\lambda_2(s),\lambda_3(s)) \\ G_u(u(s),\lambda_1(s),\lambda_2(s),\lambda_3(s))\alpha(s) \\ \alpha(s)^\top\alpha(s) - \Delta x\Delta y \\ f_{uu}(u,\lambda_1(s),\lambda_2(s),\lambda_3(s))^\top\alpha^3 \end{pmatrix} = 0$$

starting from the calculated cusp position. During this process, we monitor the swallowtail condition

$$f_{uuu}(u,\lambda_1,\lambda_2,\lambda_3)^\top\alpha^4 + 6(f_{uu}(u,\lambda).\alpha^2)^\top v + 3v^\top G_u(u,\lambda_1,\lambda_2,\lambda_3)v = 0, \qquad (11.3.12)$$

where $f_{uu}(u,\lambda).\alpha^2$ denotes the component-wise product of the vectors $f_{uu}(u,\lambda)$ and α^2. In each continuation step the vector v is obtained as follows: we calculate the vector $(v^\top,t)^\top \in \mathbb{R}^{N\cdot M+1}$ which minimises the Euclidean norm of

$$\begin{pmatrix} G_u(u,\lambda_1,\lambda_2,\lambda_3) & \alpha \end{pmatrix}\begin{pmatrix} v \\ t \end{pmatrix} - f_{uu}(u,\lambda).\alpha^2.$$

For this we calculate the (under non-degeneracy conditions unique) solution to

$$\left(G_u(u,\lambda_1,\lambda_2,\lambda_3)\cdot G_u(u,\lambda_1,\lambda_2,\lambda_3)^\top + \alpha\alpha^\top\right)\bar{v} = -f_{uu}(u,\lambda)$$

and obtain v as $v = G_u(u,\lambda_1,\lambda_2,\lambda_3)^\top\bar{v}$. (Notice that transposition can be omitted since $G_u(u,\lambda_1,\lambda_2,\lambda_3)$ is symmetric.)

As the left-hand side of (11.3.12) changes sign, we detect a candidate for a swallowtail point at $(u_{\mathrm{SW}},\lambda^{\mathrm{SW}}) = (u_{\mathrm{SW}},\lambda_1^{\mathrm{SW}},\lambda_2^{\mathrm{SW}},\lambda_3^{\mathrm{SW}})$. (See Figure 11.4.) Indeed, the swallowtail condition (11.3.12) has a regular root at the swallowtail point which implies that the singularity is not further degenerate.

In Figure 11.5 we do a fold continuation using pseudo-arclength continuation applied to $F^{(1)}$ starting at a cusp point near $(u_{\mathrm{SW}},\lambda^{\mathrm{SW}})$ while fixing λ_3. The fold line is continued in both directions and shows the characteristics of a swallowtail bifurcation. This verifies that $(u_{\mathrm{SW}},\lambda^{\mathrm{SW}})$ is indeed a swallowtail point of the discretised system.

Remark 11.3.4. As is known from catastrophe theory (see Section 5.4 or V. I. Arnold, Goryunov, et al., 1998; Lu, 1976), the only persistent bifurcations of codimension smaller or equal to 3 which critical points of a function $R\colon \mathbb{R}^n \to \mathbb{R}$ can undergo are A_2, A_3, A_4, D_4^+ and D_4^-. Other phenomena are removable under arbitrarily small perturbations of R. However, if a singularity D_4^+ or D_4^- occurs along a line of cusp bifurcations, then the swallowtail condition tends to $+\infty$ or $-\infty$ as one approaches the

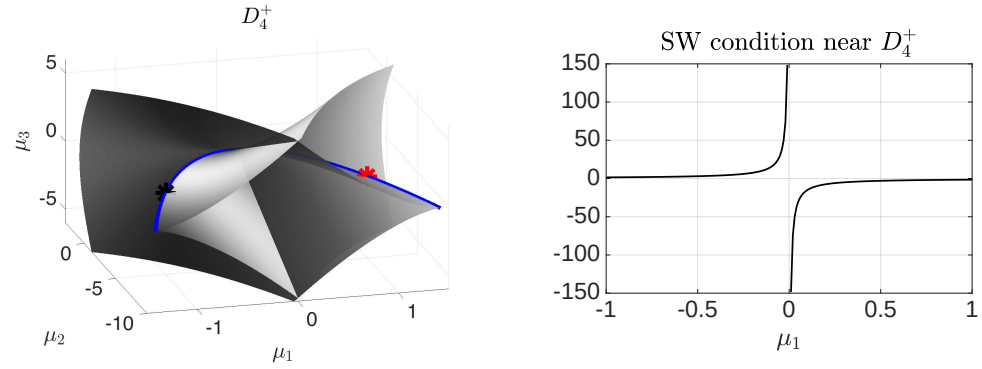

Figure 11.2: The left figure shows a singularity of type D_4^+, called *hyperbolic umbilic singularity*. It is a generic codimension 3 singularity in catastrophe theory. Here $\mu = (\mu_1, \mu_2, \mu_3)$ are parameters. Each point on the blue line (the edge) corresponds to a cusp singularity with an exception at $\mu = (0, 0, 0)$ where the D_4^+ singularity is located. The two points marked with asterisks are cusp points with different signatures. The figure to the right shows the value of the bifurcation test equation for A_4 along the line of cusps parametrised by μ_1. We see that the bifurcation test equation has a singularity at $\mu_1 = 0$, where the hyperbolic umbilic singularity is located, and that it changes sign at the singularity.

singularity. (See Figures 11.2 and 11.3.) Moreover, at the singularity, $\mathrm{Hess}(R)(z)$ has a 2-dimensional kernel and the value of the swallowtail condition is not defined. △

Remark 11.3.5. Forming augmented systems for the discrete functional S_Δ (recall $\mathrm{D}_u S_\Delta = G$) gives rise to the same system of equations as discretising the continuous augmented systems from Section 11.3.2. In other words, forming the augmented system commutes with discretisation. This extends Remark 11.3.3. △

Determination of the position and convergence of the swallowtail point

To calculate the position of the bifurcation point more accurately we apply Newton iterations to $F^{(3)}(u, \alpha, \bar{v}, \lambda)$ given as

$$F^{(3)}(u, \alpha, \bar{v}, \lambda) = \begin{pmatrix} G(u, \lambda) \\ G_u(u, \lambda)\alpha \\ \Delta x \Delta y \alpha^\top \alpha - 1 \\ f_{uu}(u, \lambda)^\top \alpha^3 \\ \left(G_u^2(u, \lambda) + \alpha\alpha^\top\right)\bar{v} + f_{uu}(u, \lambda) \\ f_{uuu}(u, \lambda)^\top \alpha^4 + 6(f_{uu}(u, \lambda).\alpha^2)^\top G_u(u, \lambda)\bar{v} + 3\bar{v}G_u^3(u, \lambda)\bar{v} \end{pmatrix}$$

until convergence using $(u_{\mathrm{SW}}, \alpha_{\mathrm{SW}}, 0_{NM\times 1}, \lambda^{\mathrm{SW}})$ as initial guess. We obtain a root $(u_{\mathrm{SW}}^1, \alpha_{\mathrm{SW}}^1, v_{\mathrm{SW}}^1, \lambda_{\mathrm{SW}}^1)$ with $(u_{\mathrm{SW}}^1, \alpha_{\mathrm{SW}}^1, \lambda_{\mathrm{SW}}^1)$ near $(u_{\mathrm{SW}}, \alpha_{\mathrm{SW}}, \lambda^{\mathrm{SW}})$. We successively

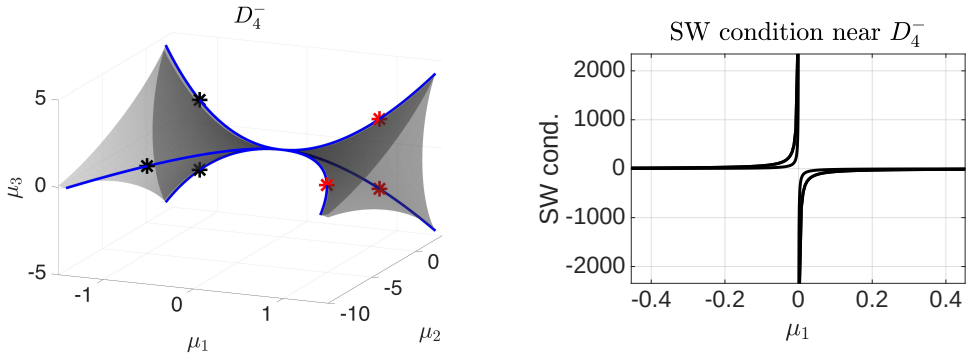

Figure 11.3: The left figure shows a singularity of type D_4^-, called *elliptic umbilic*. It is a generic codimension 3 singularity in catastrophe theory. Here $\mu = (\mu_1, \mu_2, \mu_3)$ are parameters. Each point on the blue lines (the edges) corresponds to a cusp singularity with an exception at $\mu = (0, 0, 0)$ where the D_4^- singularity is located. The three points on the line of cusps marked with asterisks with negative μ_1 values are of the positive type. The other three marked points are of the negative type. The figure to the right shows the value of the bifurcation test equation for A_4 (swallowtail condition) along the line of cusps parametrised by μ_1. Due to symmetries in this example, two lines are plotted above each other in the $\mu_1 < 0$ regime as well as in the $\mu_1 > 0$ regime. When the elliptic singularity is approached along a line of negative cusps, then the swallowtail condition tends to $-\infty$. Analogously, it tends to $+\infty$ if the singularity is approached through positive cusp points.

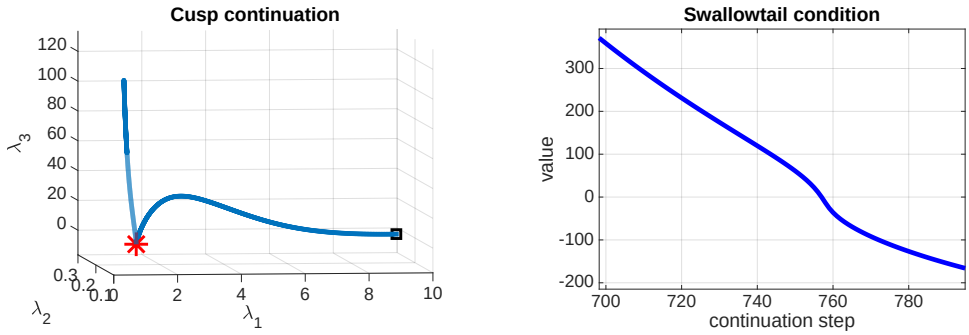

Figure 11.4: The left figure shows a continuation of the cusp singularity detected in Figure 11.1 by varying λ_1, λ_2 and λ_3. A swallowtail point is marked by $*$. The square marker shows where the continuation was initiated. As the line of cusps is numerically continued the swallowtail condition is monitored. To the right we see the value of the swallowtail condition versus the number of continuation steps. The root corresponds to the swallowtail point. Since the root is nondegenerate, we know that the butterfly condition is not fulfilled such that the singularity is indeed a swallowtail point and not further degenerate.

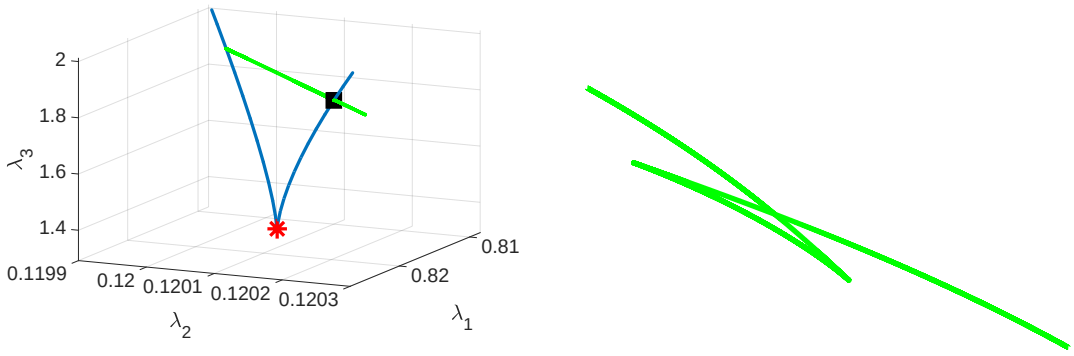

Figure 11.5: Numerical experiment with $(N, M) = (10, 10)$ showing a line of cusp points in the figure to the left. At the point marked with an asterisk the swallowtail condition (11.3.12) is fulfilled. From the point marked with a square we continue a branch of folds fixing the parameter λ_3. The figure to the right shows a projection of the line of folds along the λ_3-direction to the λ_1, λ_2 plane after rotation and rescaling. This is done to to make the structure of the branch visible as it is very flat in the original coordinates $(\lambda_1, \lambda_2, \lambda_3)$. The plot is characteristic for swallowtail bifurcations (compare with Figure 5.1 in Section 5.4).

increase $(N, M) = (N, N)$ and repeat the process of finding a root of $F^{(3)}$. As initial guesses for Newton's method in the j^{th}-step we use λ^j_{SW} from the previous calculation and linear interpolations of u^j_{SW}, α^j_{SW} and v^j_{SW} on the new grid with Dirichlet boundary conditions. The Jacobian matrix of $F^{(3)}$ required for the Newton iterations is given as

$$\mathrm{D}F^{(3)} = \begin{pmatrix} G_u & 0_{NM\times NM} & 0_{NM\times NM} & \mathrm{D}_\lambda f \\ \operatorname{diag}(f_{uu}.\alpha) & G_u & 0_{NM\times NM} & \mathrm{D}_\lambda f_u.\alpha \\ 0_{1\times NM} & 2\Delta x\Delta y\alpha^\top & 0_{1\times NM} & 0_{1\times 3} \\ (f_{uuu}.\alpha^3)^\top & 3(f_{uu}.\alpha^2)^\top & 0_{1\times NM} & (\mathrm{D}_\lambda f_{uu}^\top \alpha^3)^\top \\ \mathrm{D}_u F_5^{(3)} & \alpha\bar{v}^\top + \alpha^\top \bar{v}\mathrm{Id}_{NM} & G_u^2 + \alpha\alpha^\top & \mathrm{D}_\lambda F_5^{(3)} \\ \mathrm{D}_u F_6^{(3)} & \mathrm{D}_\alpha F_6^{(3)} & \mathrm{D}_v F_6^{(3)} & \mathrm{D}_\lambda F_6^{(3)} \end{pmatrix}$$

with

$$
\begin{aligned}
L &= \mathrm{Id}_M \otimes D_{xx} + D_{yy} \otimes \mathrm{Id}_N \\
\mathrm{D}_u F_5^{(3)} &= L.(f_{uu}.\bar{v}) + \mathrm{diag}\,(f_{uu}.L\bar{v} + 2f_u.f_{uu}.\bar{v} + f_{uuu}) \\
\mathrm{D}_\lambda F_5^{(3)} &= L((\mathrm{D}_\lambda f_u).\bar{v}) + (\mathrm{D}_\lambda f_u).(L\bar{v}) + 2(\mathrm{D}_\lambda f_u).f_u.\bar{v} + \mathrm{D}_\lambda f_{uu} \\
DQ^{(u)} &= 2(f_{uu}.\bar{v})^\top.(\bar{v}^\top L^2) + (f_{uu}.(L\bar{v}))^\top.(\bar{v}^\top L) + 4(f_u.f_{uu}.\bar{v})^\top.(\bar{v}^\top L) \\
&\quad + (f_{uu}.\bar{v})^\top.((f_u.\bar{v})^\top L) + ((f_{uu}.\bar{v}).(L(f_u.\bar{v})))^\top + 3(f_u^2.f_{uu}.\bar{v})^\top.\bar{v}^\top \\
\mathrm{D}_u F_6^{(3)} &= (f_{uuuu}.\alpha^4)^\top + 6((f_{uuu}.\alpha^2).(G_u\bar{v}))^\top + 6(f_{uu}^2.\bar{v}.\alpha^2)^\top + 3DQ^{(u)} \\
\mathrm{D}_\alpha F_6^{(3)} &= 4(f_{uuu}.\alpha^3)^\top + 12(f_{uu}.\alpha.(G_u\bar{v}))^\top \\
\mathrm{D}_{\bar{v}} F_6^{(3)} &= 6(f_{uu}.\alpha^2)^\top G_u + 6(G_u^3\bar{v})^\top \\
DQ^{(\lambda)} &= 2\bar{v}^\top L^2((\mathrm{D}_\lambda f_u).\bar{v}) + \bar{v}^\top L((\mathrm{D}_\lambda f_u).(L\bar{v})) + 4\bar{v}^\top L((\mathrm{D}_\lambda f_u).f_u.\bar{v}) \\
&\quad + 2(f_u.\bar{v})^\top L((\mathrm{D}_\lambda f_u).\bar{v}) + 3\bar{v}^\top((\mathrm{D}_\lambda f_u).f_u^2.\bar{v}) \\
\mathrm{D}_\lambda F_6^{(3)} &= ((\mathrm{D}_\lambda f_{uuu})^\top\alpha^4)^\top + 6(((\mathrm{D}_\lambda f_{uu}).\alpha^2)^\top G_u\bar{v})^\top \\
&\quad + 6(f_{uu}.\alpha^2)^\top((\mathrm{D}_\lambda f_u).\bar{v}) + 3DQ^{(\lambda)}
\end{aligned}
$$

Here we use the convention that "." denotes pointwise multiplication. Pointwise multiplication of a column vector with a matrix means that the vector is multiplied pointwise with each column of the matrix. Analogously for row vectors. Moreover, the power of a vector is to be understood pointwise. Zero matrices of dimension $s \times t$ are denoted by $0_{s\times t}$ and identity matrices by $\mathrm{Id}_{s\times t}$.

Remark 11.3.6. Appropriate sub-matrices of $\mathrm{D}F^{(3)}$ correspond to $\mathrm{D}F^{(1)}$ and $\mathrm{D}F^{(2)}$. These have been used for the pseudo-arclength continuation described in Section 11.3.3. The Jacobian matrices $\mathrm{D}F^{(1)}$, $\mathrm{D}F^{(2)}$ and $\mathrm{D}F^{(3)}$ and the matrices L, G_u involved in the function evaluations $F^{(1)}$, $F^{(2)}$ and $F^{(3)}$ are sparse and represented using an appropriate datatype in the numerical calculations. Moreover, compared to equations for a general functional S, the structure of the semilinear Poisson equation dramatically simplifies the augmented systems and numerical complexity because the multilinear operators G_{uu}, G_{uuu}, ... are diagonal and their diagonal is given by an evaluation of an appropriate derivative of f at u. The simplicity of the structure has been observed in the continuous setting in Remark 11.3.2. △

Figures 11.6 and 11.7 show that as $N = M$ increases, the position of the swallowtail point converges in the parameter space. We also observe that the data (u, α, v) converges to a fixed shape. Figure 11.8 shows the shape of (u, α, v) at the approximated swallowtail point for $(N, M) = (85, 85)$.

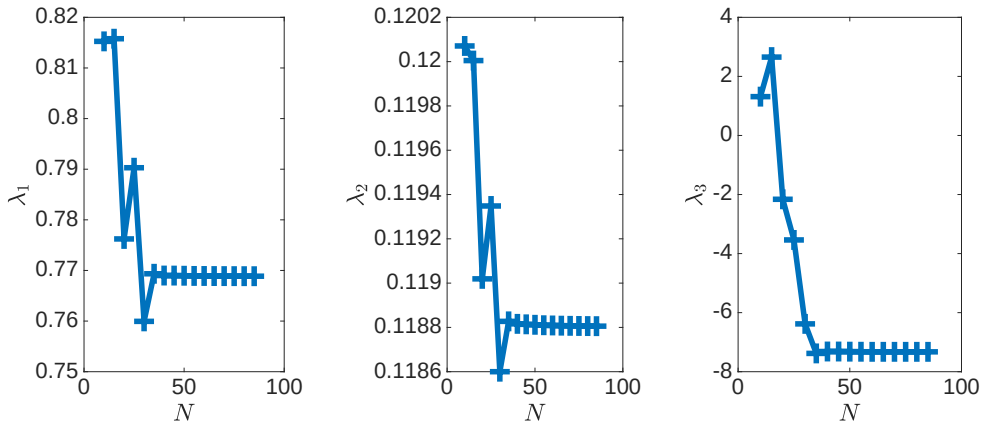

Figure 11.6: Position of the parameters λ_1, λ_2 and λ_3 as a function of the number of inner grid points per dimension N with $N = 10, 15, \ldots, 80, 85$. The position of λ is obtained by calculating a root of $F^{(3)}(u, \alpha, \bar{v}, \lambda)$ using Newton iterations until convergence (∞-norm smaller 10^{-9}). We see that the values converge as N increases.

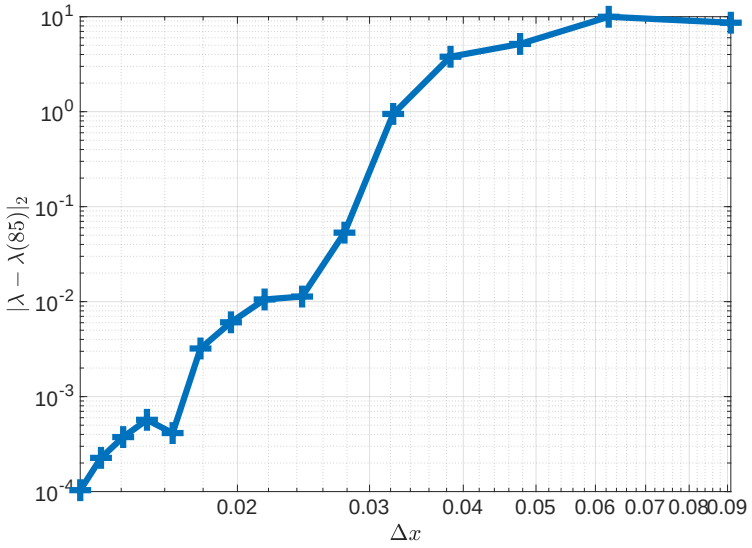

Figure 11.7: Euclidean distance of the parameter $(\lambda_1, \lambda_2, \lambda_3)$ to the calculated value at $N = 85$ as a function of the inner grid spacing $\Delta x = \frac{1}{N+1}$. Here N is the number of inner grid points per dimension N with $N = 10, 15, \ldots, 80, 85$. In each step the position of λ is obtained by calculating a root of $F^{(3)}(u, \alpha, \bar{v}, \lambda)$ using Newton iterations until convergence (∞-norm smaller 10^{-9}). We see that the values converge as Δx decreases.

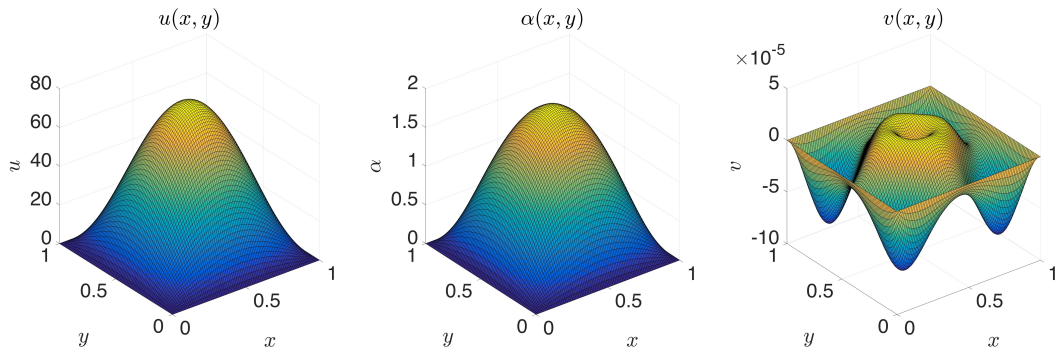

Figure 11.8: Plot of the data $u(x, y)$, $\alpha(x, y)$ and $v(x, y)$ at the approximated swallowtail point for $(N, M) = (85, 85)$.

11.4 Conclusion

In conclusion, we derived bifurcation test equations for A-series singularities of nonlinear functionals and, based on these equations, we developed numerical methods for the detection of high codimensional branching bifurcations in parameter-dependent PDEs where a variational integrator is used for the discretisation of the problem. This numerical computation is illustrated by detecting a swallowtail bifurcation in a Bratu-type problem. As part of future research, numerical experiments for finding high codimensional bifurcations for other PDE types can be performed. Another interesting question is the rigorous proof of the convergence rate to the singularity of the numerical method. Besides, bifurcation test equations for D-series singularities can be derived and the bifurcations can be numerically detected for different PDE types by considering either variational or non-variational integrators.

Chapter 12

Symplectic integration of PDEs using Clebsch variables

Chapter 12 is an adaption of McLachlan, Offen, and Tapley, 2019.

While in Chapter 11 we exploit variational structure of partial differential equations, in this chapter we make use of a different generalisation of Hamiltonian ODEs to the PDE setting. Many PDEs (Burgers' equation, KdV, Camassa-Holm, Euler's fluid equations,...) can be formulated as infinite dimensional Lie–Poisson systems. These are Hamiltonian systems on manifolds equipped with Poisson brackets. The Poisson structure is related to conservation properties and other geometric features of solutions to the PDE and is, therefore, of great interest for numerical integration. For the example of Burgers' equations and related PDEs we use Clebsch variables to lift the original system to a collective Hamiltonian system on a symplectic manifold whose structure is related to the original Lie–Poisson structure. On the collective Hamiltonian system a symplectic integrator can be applied. Our numerical examples show excellent conservation properties and indicate that the disadvantage of an increased phase-space dimension can be outweighed by the advantage of symplectic integration.

12.1 Motivation

Partial differential equations (PDEs) often exhibit interesting structure preserving properties, for example conserved quantities. In many examples, a deeper understanding of the structures can be achieved by viewing the PDE as the Lie–Poisson equation associated to an infinite dimensional Lie group. This means solutions to the PDE correspond to motions of a Hamiltonian system defined on the dual of the Lie-algebra of a Fréchet Lie-group.

Examples include Euler's equations for incompressible fluids, Burgers' equation,

equations in magnetohydrodynamics, the Korteweg-de Vries equation, the superconductivity equation, charged ideal fluid equations, the Camassa-Holm equation and the Hunter-Saxton equation (Vizman, 2008). Conserved quantities turn out to be related to the preservation of the Lie–Poisson bracket by the Hamiltonian flow.

This makes Lie–Poisson structures interesting for structure preserving integration. We will give a brief review of Hamiltonian systems on Poisson manifolds in Section 12.2.

An approach to construct Lie–Poisson integrators, which works universally in the finite dimensional setting, is to translate the Lie–Poisson system on a Lie-group G to a Hamiltonian system on the tangent bundle TG with a G-invariant Lagrangian. Using a variational integrator one obtains a Poisson-integrator for the original system (Marsden, Pekarsky, and Shkoller, 1999). These integrators, however, can be extremely complicated (McLachlan, Modin, and Verdier, 2014, p. 1526). Moreover, the fact that exponential maps do not constitute local diffeomorphisms for infinite dimensional manifolds restricts the approach to a finite dimensional setting. Other approaches for energy preserving integration of finite dimensional Poisson systems with good preservation properties, e.g. preservation of linear symmetries or (quadratic) Casimirs, include Brugnano, Calvo, et al., 2012; Cohen and Hairer, 2011; Dahlby, Owren, and Yaguchi, 2011. For a recent review article on Lie–Poisson integrators we refer to Diego, 2018.

Let us return to the infinite dimensional setting. For numerical computations a PDE needs to be discretised in space. In the Lie–Poisson setting this corresponds to an approximation of the dual of a Lie algebra $\mathfrak{g}^*$ by a finite dimensional space. The space $\mathfrak{g}^*$ typically corresponds to some space of $\mathbb{R}^k$-valued functions defined on a manifold. The most natural way of discretising $\mathfrak{g}^*$ is to introduce a grid on the manifold and identify a function with the values it takes over the grid. In this way we naturally obtain a finite dimensional approximation of $\mathfrak{g}^*$. However, the approximation does not inherit a Poisson structure in a natural way, as we will see in the example of the Burgers' equation (Remark 12.3.1). Therefore, finding a spatial discretisation with good structure preserving properties is a challenge.

Lie–Poisson systems $(\mathfrak{g}^*, \{,\}, H)$ can be realised as Hamiltonian systems of the form $(M, \Omega, \bar{H})$, where (M, Ω) is a symplectic manifold and the Hamiltonian is given as $\bar{H} = H \circ J$. The map $J\colon M \to \mathfrak{g}^*$ is required to be a Poisson map, i.e. the pullback of the Poisson structure on $\mathfrak{g}^*$ via J coincides with the Poisson structure on M induced by the symplectic form Ω (Vaisman, 1994). Hamiltonian systems of the form $(M, \Omega, H \circ J)$, where J is a Poisson map[1], are called *collective Hamiltonian systems* and the map J is called a *realisation of* $\mathfrak{g}^*$.

The flow of $(M, \Omega, H \circ J)$ maps fibres of J to fibres of J and is symplectic. Therefore, it descends to a Poisson map on the original system $(\mathfrak{g}^*, \{,\}, H)$. Since the Hamiltonian

[1] As in McLachlan, Modin, and Verdier, 2014 we do *not* require J to be surjective in contrast to Vaisman, 1994.

vector field to $H \circ J$ on (M, Ω) is J-related (Definition 2.3.1) to the Hamiltonian vector field to H on $(\mathfrak{g}^*, \{,\})$, motions of $(M, \Omega, H \circ J)$ descend to motions of $(\mathfrak{g}^*, \{,\}, H)$.

The reason to consider a collective system for numerical integrations rather than the Lie–Poisson system directly is that the symplectic structure can easily be preserved under spatial discretisations and widely applicable, efficient symplectic integrators are available (see Section 3.5 or Hairer, Lubich, and Wanner, 2013). The challenge of integrating $(\mathfrak{g}^*, \{,\}, H)$ in a structure preserving way thus shifts to finding a realisation, i.e. (M, Ω) and $J\colon M \to \mathfrak{g}^*$, such that all initial conditions of interest lie in the image of J and such that the system $(M, \Omega, H \circ J)$ is practical to work with.

A practical choice for a realisation is where J is a *Clebsch map* (Marsden and Weinstein, 1983): let X be a Riemannian manifold and let $M = T^*\mathcal{C}^\infty(X, \mathbb{R}^k) \cong C^\infty(X, \mathbb{R}^k) \times C^\infty(X, \mathbb{R}^k)^*$, where $C^\infty(X, \mathbb{R}^k)^*$ is identified with $C^\infty(X, \mathbb{R}^k)$ via the L^2 pairing. The vector space M is equipped with the symplectic form

$$\Omega((u_1, u_2), (v_1, v_2)) = \int_X (\langle u_1, v_2 \rangle_{\mathbb{R}^k} - \langle u_2, v_1 \rangle_{\mathbb{R}^k}) \operatorname{dvol}_X,$$

where $\langle ., . \rangle_{\mathbb{R}^k}$ denotes the scalar product in $\mathbb{R}^k$. For an element $(f, g) \in M$ we denote by $q^j(f)$ and $p_j(g)$ the post-composition of f and g with the projection map to the j^{th} component of $\mathbb{R}^k$. In other words, $q^1, \dots, q^k, p_1, \dots, p_k$ are maps $M \to \mathcal{C}^\infty(X, \mathbb{R})$ such that for $x \in X$

$$(f(x), g(x)) = \Big(\big(q^1(f)(x), \dots, q^k(f)(x)\big), \big(p_1(g)(x), \dots, p_k(g)(x)\big) \Big).$$

Identifying tangent spaces of the vector space M with M itself, we may write Ω as

$$\Omega = \int_X \left(\sum_{j=1}^k \mathrm{d}q^j \wedge \mathrm{d}p_j \right) \operatorname{dvol}_X = \int_X \langle \mathrm{d}q \wedge \mathrm{d}p \rangle_{\mathbb{R}^k} \operatorname{dvol}_X,$$

where $q = (q^1, \dots, q^k)$ and $p = (p_1, \dots, p_k)$. Indeed, the vector space M can be considered as a Fréchet manifold over $C^\infty(X, \mathbb{R})$ or $C^\infty(X, \mathbb{R}^k)$. It carries the coordinates $(q^1, \dots, q^k, p_1, \dots, p_k)$ or (q, p), respectively. If $J\colon M \to \mathfrak{g}^*$ is a realisation of a Lie Poisson system $(\mathfrak{g}^*, \{,\})$, then J is called a *Clebsch map* and (q, p) are called *Clebsch variables* (Marsden and Weinstein, 1983). In Clebsch variables Hamilton's equations for $\bar{H} = H \circ J\colon M \to \mathbb{R}$ are in canonical form, i.e.

$$q_t = \frac{\delta \bar{H}}{\delta p}, \qquad p_t = -\frac{\delta \bar{H}}{\delta q},$$

where $\frac{\delta \bar{H}}{\delta q}$ and $\frac{\delta \bar{H}}{\delta p}$ are variational derivatives. The reason why Clebsch variables are a natural choice of coordinates for a structure preserving setting is that if X is discretised

Continuous system	Spatially discretised system
Collective Hamiltonian system on an infinite-dimensional symplectic vector space in Clebsch variables $$q_t = \frac{\delta \bar{H}}{\delta p}, \quad p_t = -\frac{\delta \bar{H}}{\delta q}.$$ Exact solutions preserve the symplectic structure, the Hamiltonian $\bar{H} = H \circ J$, all conservation laws related to the Casimirs of the original PDE and the fibres of the Clebsch map $J(q,p) = u$.	Canonical Hamiltonian ODEs in $2N$ variables $$\hat{q}_t = \nabla_{\hat{p}} \hat{\bar{H}}, \quad \hat{p}_t = -\nabla_{\hat{q}} \hat{\bar{H}}.$$ The exact flow preserves the symplectic structure and the Hamiltonian $\hat{\bar{H}}$. Time-integration with the midpoint rule is symplectic.
Original PDE, interpreted as a Lie-Poisson equation $$u_t = \mathrm{ad}^*_{\frac{\delta H}{\delta u}} u.$$ Exact solutions preserve the Poisson structure, the Hamiltonian H and all Casimirs.	Non-Hamiltonian ODEs in N variables $$\hat{u}_t = K(\hat{u}) \nabla_{\hat{u}} \hat{H}, \qquad K^T = -K.$$ Exact solutions conserve $\hat{H}$. Time-integration with the midpoint rule is *not* symplectic.

Table 12.1: Overview of the collective Hamiltonian setting

using a mesh, then the integral in the expression for Ω naturally becomes a (weighted) sum over all mesh points and Hamilton's equations for the discretisation of the collective system $(M, \Omega, H \circ J)$ are in (a scaled version of the) canonical form. This means the system can be integrated using a symplectic integrator like, for instance, the implicit midpoint rule (Section 3.2.2). The setting is summarised in Table 12.1.

The symplectic system in Clebsch variables has, after spatial discretisation, twice as many variables as the discretisation of the PDE in the original variables. An increase in the number of variables needs some justification because it does not only lead to more work per integration step but, thinking of multi-step methods versus one-step methods, can also lead to worse stability behaviour (Hairer, Lubich, and Wanner, 2013, p. XV). Moreover, integrating a lifted, symplectic system with a symplectic integrator instead of the original system with a non-symplectic integrator is not necessarily of any advantage. If, for instance, we integrate the Hamiltonian system

$$\begin{aligned} \dot{u} &= F(u) &&= \nabla_p \langle F(u), p \rangle \\ \dot{p} &= -\mathrm{D}F(u)^\top p &&= -\nabla_u \langle F(u), p \rangle \end{aligned}$$

rather than the system $\dot{u} = F(u)$ directly, then preserving the symplectic structure in a

numerical computation does not have any effect: in this example the symplectic structure is artificially introduced and not related to the original system. This illustrates that using symplectic integrators is not an end in itself. It is the presence of a Poisson structure and its interplay with the symplecticity of the collective system which can justify doubling the number of variables as our numerical examples will indicate.

Let us provide examples for the application of Clebsch variables. Euler's equation in hydrodynamics for an ideal incompressible fluid with velocity u and pressure ρ on a 3-dimensional compact, Riemannian manifold X with boundary ∂X or a region $X \subset \mathbb{R}^3$ are given as

$$u_t + u \cdot \nabla u = -\nabla \rho, \qquad \operatorname{div} u = 0, \qquad u|_{\partial X} \text{ is parallel to } \partial X.$$

Elements in the dual of the Lie-algebra χ^*_{vol} to the Fréchet Lie-group of volume preserving diffeomorphisms $\mathcal{D}_{\mathrm{vol}}$ can be considered as 2-forms on X. The vector field $\nabla \times u$ is replaced by the 2-form $\mathrm{d}u^\flat$, where $u^\flat$ denotes the flattening of the vector field u. Euler's equations correspond to motions on the Lie–Poisson system to $\mathcal{D}_{\mathrm{vol}}$ with Hamiltonian $H(\sigma) = \frac{1}{2}\int_X \langle \Delta^{-1}\sigma, \sigma\rangle \operatorname{dvol}_X$, where Δ is the Laplace-DeRham operator and $\langle , \rangle$ the metric pairing of 2-forms (Marsden and Weinstein, 1983).

A Clebsch map $J\colon M \to \chi^*_{\mathrm{vol}}$ can be obtained as the momentum map of the cotangent lifted action of the action $(\eta, f) \mapsto f \circ \eta^{-1}$ of $\mathcal{D}_{\mathrm{vol}}$ on $\mathcal{C}^\infty(X, \mathbb{R})$. However, J is not surjective and flows with non-zero hydrodynamical helicity cannot be modelled. To overcome this issue one can consider $M = \mathcal{C}^\infty(X, S^2)$, where S^2 is the 2-sphere. The symplectic form σ_{S^2} on the sphere induces the symplectic form $\Omega = \int_X \sigma_{S^2} \operatorname{dvol}_X$ on M. We can define $J\colon M \to \chi^*_{\mathrm{vol}}$ as $J(s) = s^*\sigma_{S^2}$, where $s^*\sigma_{S^2}$ denotes the pull-back of σ_{S^2} to a 2-form on X which can be interpreted as an element in χ^*_{vol}. The map J is called a *spherical Clebsch map* and initial conditions with non-zero helicity are admissible. However, the helicity remains quantised (E. A. Kuznetsov and Mikhailov, 1980). Spherical Clebsch maps have been used for computational purposes in Chern et al., 2016: after a discretisation of the domain X, solutions to (regularised) hydrodynamical equations are approximated by integrating the corresponding set of ODEs on the product $\Pi_{\mathrm{mesh}(X)} S^2$ while preserving the spheres using a projection method (not preserving the symplectic form $\sum_{\mathrm{mesh}(X)} \sigma_{S^2}$, though).

In the case of Hamiltonian ODEs on (finite dimensional) Poisson spaces $(\mathfrak{g}^*, \{,\})$, no spatial discretisation is necessary. This setting applies to the rigid-body equations, for instance Marsden and Abraham, 1978. In the ODE setting, McLachlan, Modin, and Verdier (2014) apply symplectic integrators to the collective systems $(M, \Omega, H \circ J)$ with the property that the discrete flow preserves the fibres of J. Such integrators are called *collective integrators*. Their flow descends to a Poisson map on the original system $(\mathfrak{g}^*, \{,\}, H)$ such that one obtains a Poisson integrator for $(\mathfrak{g}^*, \{,\}, H)$. In this chapter,

we show how the collective integrator idea can be used in the infinite dimensional setting, i.e. for Lie–Poisson systems to infinite dimensional Lie-groups. In particular, we will consider the inviscid Burgers' equation

$$u_t + uu_x = 0$$

with $u(t,.) \in \mathcal{C}^\infty(S^1, \mathbb{R})$. The L^2-norm of $u(t,.)$ as well as the quantity

$$\int_{S^1} \sqrt{|u(t,.)|}\,\mathrm{d}x$$

are conserved quantities. They constitute the Hamiltonian and Casimirs of the Lie–Poisson formulation of the problem. Setting $u = q_x p$ we obtain the following system of PDEs

$$q_t = -\frac{1}{3}q_x^2 p, \qquad p_t = -\frac{1}{3}(q_x p^2)_x$$

with $q(t,\cdot) \in \mathcal{C}^\infty(S^1, S^1)$ and $p(t,\cdot) \in \mathcal{C}^\infty(S^1, \mathbb{R})$ which is the collective system. The variables q, p may be regarded as Clebsch variables (right in the middle between classical and spherical Clebsch variables).

We will also experiment with the following more complicated PDE which fits into the same setting as the inviscid Burgers' equation.

$$u_t = 3uu_x - \frac{9}{4}u^2u_x - u_xu_{xx} - 3u_x^2u_{xx} - 2uu_{xxx} - 2uu_xu_{xxx} - 6uu_{xx}^2$$

It has the conserved quantity $H(u) = \int_{S^1}(u^2 + u_x^2 - 1/2u^3 + u_x^3)\,\mathrm{d}x$ as well as $\int_{S^1}\sqrt{|u|}\,\mathrm{d}x$ in time. In Clebsch variables we have

$$\begin{aligned} q_t = \frac{\delta \bar{H}}{\delta p} &= q_x\Big(q_x p - \frac{3}{4}(q_x p)^2 - ((q_x p)_x + \frac{3}{2}(q_x p)_x^2)_x\Big) \\ p_t = -\frac{\delta \bar{H}}{\delta q} &= p\Big(\frac{3}{2}(q_x p)^2 - q_x p + \big((q_x p)_x + \frac{3}{2}(q_x p)_x^2\big)_x\Big)_x. \end{aligned}$$

The PDEs are discretised in space by introducing a periodic grid on S^1 and replacing the integral in $\bar{H}$ by a sum. Spatial derivatives are computed using a finite-difference method or a spectral method. In this way we obtain a system of Hamiltonian ODEs in canonical form.

In Section 12.6 we will see that integration using the symplectic midpoint rule yields an integrator with excellent structure preserving properties like bounded energy and Casimir errors, despite not preserving the fibres of J and, therefore, not descending to a Poisson integrator. The good behaviour is linked to the symplecticity of the collective system which is preserved exactly by the midpoint rule. Therefore, the conservation properties survive even when the equation is perturbed within the class of Hamiltonian

PDEs. This robustness can be an advantage over more traditional ways of discretising the PDE directly since these make use of structurally simple symmetries of the equation that are immediately destroyed when higher order terms are introduced. Our numerical experiments indicate that the advantage of symplectic integration can outweigh the disadvantage of doubling the variables from u to (q, p).

12.2 Introduction

Let us briefly review the setting of Hamiltonian systems on Poisson manifolds. For details we refer to Marsden and Ratiu, 1999b.

Definition 12.2.1 (Poisson manifold and Poisson bracket)**.** A *Poisson manifold* P is a smooth manifold together with an $\mathbb{R}$-bilinear map

$$\{\cdot,\cdot\}\colon \mathcal{C}^\infty(P)\times\mathcal{C}^\infty(P)\to\mathcal{C}^\infty(P)$$

satisfying

- $\{f,g\}=-\{g,f\}$ (skew-symmetry),
- $\{f,\{g,h\}\}+\{g,\{h,f\}\}+\{h,\{f,g\}\}=0$ (Jacobi identity),
- $\{fg,h\}=f\{g,h\}+g\{f,h\}$ (Leibniz's rule).

The map $\{\cdot,\cdot\}$ is called the *Poisson bracket*. △

Example 12.2.1. If G is a (Fréchet-) Lie-group with Lie-algebra $\mathfrak{g}$ and dual $\mathfrak{g}^*$, then

$$\{f,g\}(w)=\left\langle w,\left[\frac{\delta f}{\delta w},\frac{\delta g}{\delta w}\right]\right\rangle,\qquad w\in\mathfrak{g}^*,\ f,g\in\mathcal{C}^\infty(\mathfrak{g}^*) \tag{12.2.1}$$

is a (Lie-) Poisson bracket on $\mathfrak{g}^*$, where $\langle\cdot,\cdot\rangle$ denotes the duality pairing of $\mathfrak{g}^*$ and $\mathfrak{g}$, $[\cdot,\cdot]$ denotes the Lie bracket on $\mathfrak{g}$ and $\frac{\delta f}{\delta w}\in\mathfrak{g}$ is defined by

$$\forall v\in\mathfrak{g}^*:\quad \mathrm{D}f|_w(v)=\left\langle v,\frac{\delta f}{\delta w}\right\rangle$$

with Fréchet derivative D. △

Definition 12.2.2 (Hamiltonian system and Hamiltonian motion)**.** A *Hamiltonian system* $(P,\{\cdot,\cdot\},H)$ is a Poisson manifold $(P,\{\cdot,\cdot\})$ together with a smooth map $H\colon P\to\mathbb{R}$. The *Hamiltonian vectorfield* X_H to the system $(P,\{\cdot,\cdot\},H)$ is defined as the derivation $X_H=\{\cdot,H\}$. If $f\colon P\to\mathbb{R}$ is a smooth function, then the *motion of the system* $(P,\{\cdot,\cdot\},H)$ in the coordinate f is given by the differential equation $\dot f=\{f,H\}$, where the dot denotes a time-derivative. △

Example 12.2.2. A Hamiltonian system (M, ω, H) on a symplectic manifold (M, ω) constitutes a Hamiltonian system on the Poisson manifold $(M, \{\cdot, \cdot\})$. The Poisson bracket $\{\cdot, \cdot\}$ is defined by $\{f, g\} = \omega(X_f, X_g)$ where the vector fields X_f and X_g are defined by $\mathrm{d}f = \omega(X_f, \cdot)$ and $\mathrm{d}g = \omega(X_g, \cdot)$. If M is $2n$-dimensional with local coordinates $q^1, \ldots, q^n, p_1, \ldots, p_n$ and $\omega = \sum_{j=1}^n \mathrm{d}q^j \wedge \mathrm{d}p_j$, then

$$X_H = \sum_{j=1}^{n} \frac{\partial H}{\partial p_j}\frac{\partial}{\partial q^j} - \frac{\partial H}{\partial q^j}\frac{\partial}{\partial p_j}.$$

The motions of the system are given by

$$\begin{aligned}\dot{q}^j &= \{q^j, H\} = X_H(q^j) = \frac{\partial H}{\partial p_j},\\ \dot{p}_j &= \{p_j, H\} = X_H(p_j) = -\frac{\partial H}{\partial q^j}.\end{aligned}$$

with $j = 1, \ldots, n$. △

Remark 12.2.1. For Hamiltonian systems on a finite dimensional, symplectic manifold, there exist local coordinates such that the motions are given by

$$\dot{z} = S\nabla H(z),$$

for a constant, skew-symmetric, nondegenerate matrix S. The analogue for finite dimensional Poisson systems is that S is allowed to be z dependent and degenerate (but still skew-symmetric). △

Remark 12.2.2. Like in the symplectic case, the Hamiltonian is a conserved quantity under motions of the corresponding Hamiltonian system on a Poisson manifold. Additionally, the Poisson structure encodes interesting geometric features of Hamiltonian motions. Casimir functions, which are real valued functions f with $\{f, \cdot\} = 0$ are conserved quantities (with no dependence on the Hamiltonian). While the only Casimirs are constants if the Poisson structure is induced by a symplectic structure (as in Example 12.2.2), nontrivial Casimir functions are admissible in the Poisson case. Moreover, in a Poisson system a motion never leaves the coadjoint orbit in which it was initialised. We refer to Marsden and Ratiu, 1999b, Ch.10 for proofs and more properties of Poisson manifolds. △

In what follows we will present an integrator for Hamiltonian systems on the dual of the Lie-algebra of the group of diffeomorphisms on the circle $\mathrm{diff}(S^1)^*$. The setting covers, for example, Burgers' equation and perturbations. This shows how to apply the ideas of McLachlan, Modin, and Verdier, 2014 in the infinite dimensional setting of Hamiltonian PDEs.

12.3 Lie–Poisson structure on $\mathrm{diff}(S^1)^*$

Consider the Fréchet Lie-group $G = \mathrm{Diff}(S^1)$ of orientation preserving diffeomorphisms on the circle S^1. In the following we view S^1 as the quotient $\mathbb{R}/L\mathbb{Z}$ for $L > 0$ with coordinate x obtained from the universal covering $\mathbb{R} \to \mathbb{R}/L$. The Lie-algebra $\mathfrak{g}$ can be identified with the space of smooth vector fields on $\mathcal{S}^1$, where the Lie bracket is given as the negative of the usual Lie bracket of vector fields

$$\left[u\frac{\partial}{\partial x}, v\frac{\partial}{\partial x}\right] = (u_x v - v_x u)\frac{\partial}{\partial x}.$$

Here u_x and v_x denote the derivative of u and v with respect to the coordinate x on $S^1 = \mathbb{R}/L\mathbb{Z}$ (Kriegl and Michor, 1997, Thm. 43.1). The dual[2] $\mathfrak{g}^*$ of the Lie algebra can be identified with the quadratic differentials on the circle $\Omega^{\otimes 2}(S^1) = \{u \cdot (\mathrm{d}x)^2 \,|\, u \in \mathcal{C}^\infty(S^1, \mathbb{R})\}$. The dual pairing is given by

$$\left\langle u(\mathrm{d}x)^2, v\frac{\partial}{\partial x} \right\rangle = \int_{S^1} u(x)v(x)\mathrm{d}x$$

(Khesin and Wendt, 2009, Prop. 2.5). The coadjoint action of an element $\phi \in G$ on an element $u(\mathrm{d}x)^2 \in \mathfrak{g}^*$ is given as

$$\mathrm{Ad}^*_{\phi^{-1}}\left(u(\mathrm{d}x)^2\right) = (u \circ \phi) \cdot \phi_x^2 \cdot (\mathrm{d}x)^2 = \phi^*\left(u(\mathrm{d}x)^2\right).$$

We see that the coadjoint action on $u(\mathrm{d}x)^2$ preserves the zeros of u. The map $u \in \mathcal{C}^\infty(S^1, \mathbb{R})$ must have an even number of zeros. Consider two consecutive zeros $a, b \in S^1$. The integral

$$\int_a^b \sqrt{|u(x)|}\,\mathrm{d}x$$

is constant on the coadjoint orbit through $u(\mathrm{d}x)^2$ since the action corresponds to a diffeomorphic change of the integration variable in the above expression. It follows that the map $\Phi\colon \mathfrak{g}^* \to \mathbb{R}$ with

$$\Phi(u(\mathrm{d}x)^2) = \int_{S^1} \sqrt{|u(x)|}\,\mathrm{d}x$$

is a Casimir for the Poisson structure on $\mathfrak{g}^*$ (Khesin and Wendt, 2009). For $H \in \mathcal{C}^\infty(\mathfrak{g}^*, \mathbb{R})$ Hamilton's equations are given as

$$\frac{\mathrm{d}}{\mathrm{d}t}u(t,x)(\mathrm{d}x)^2 = \mathrm{ad}^*_{\frac{\delta H}{\delta u(t,\cdot)(\mathrm{d}x)^2}}\left(u(t,x)(\mathrm{d}x)^2\right)$$

[2] which does *not* coincide with the functional analytic dual to $\mathfrak{g}$

or, identifying $\mathfrak{g}$ and $\mathfrak{g}^*$ with $\mathcal{C}^\infty(S^1, \mathbb{R})$, as

$$u_t = \mathrm{ad}^*_{\frac{\delta H}{\delta u}} u.$$

Here $\frac{\delta H}{\delta u}$ denotes the functional or variational derivative of H and $\mathrm{ad}^*_\eta \colon \mathfrak{g}^* \to \mathfrak{g}^*$ the dual map to $\mathrm{ad}_\eta \colon \mathfrak{g} \to \mathfrak{g}$ given by

$$\mathrm{ad}_\eta(\mu) = [\eta, \mu]$$

(Marsden and Ratiu, 1999b, Prop. 10.7.1.).

Lemma 12.3.1. *Hamilton's equations can be rewritten as*

$$u_t = \left(\frac{\partial}{\partial x} u + u \frac{\partial}{\partial x} \right) \frac{\delta H}{\delta u}. \tag{12.3.1}$$

Proof. Let $v \in \mathfrak{g}$, $u \in \mathfrak{g}^*$ (both identified with $\mathcal{C}^\infty(S^1, \mathbb{R})$). Denoting the dual pairing between $\mathfrak{g}$ and $\mathfrak{g}^*$ by $\langle \cdot, \cdot \rangle$, we obtain

$$\begin{aligned}
\left\langle \mathrm{ad}^*_{\frac{\delta H}{\delta u}} u, v \right\rangle &= \left\langle u, \mathrm{ad}_{\frac{\delta H}{\delta u}} v \right\rangle = \left\langle u, \left[\frac{\delta H}{\delta u}, v \right] \right\rangle = \left\langle u, \left(\frac{\delta H}{\delta u} \right)_x \cdot v - \left(\frac{\delta H}{\delta u} \right) \cdot v_x \right\rangle \\
&= \left\langle u \cdot \left(\frac{\delta H}{\delta u} \right)_x, v \right\rangle - \left\langle u \cdot \left(\frac{\delta H}{\delta u} \right), v_x \right\rangle \\
&= \left\langle u \cdot \left(\frac{\delta H}{\delta u} \right)_x, v \right\rangle + \left\langle \left(u \cdot \left(\frac{\delta H}{\delta u} \right) \right)_x, v \right\rangle,
\end{aligned}$$

whereas the last equation follows using integration by parts. □

Example 12.3.1. On $\mathfrak{g}^*$ consider the Hamiltonian

$$H(u) = \int_{S^1} \mathcal{H}(u^{\mathrm{jet}}(x)) \mathrm{d}x$$

with $\mathcal{H} \colon \mathbb{R}^{K+1} \to \mathbb{R}$ and the K-jet of the map u

$$\begin{aligned}
u^{\mathrm{jet}}(x) &:= (u(x), u_x(x), u_{x^2}(x), \ldots, u_{x^K}(x)) \\
&:= \left(u(x), \left. \frac{\partial u}{\partial x} \right|_x, \left. \frac{\partial^2 u}{\partial x^2} \right|_x, \ldots, \left. \frac{\partial^K u}{\partial x^K} \right|_x \right).
\end{aligned}$$

By Lemma 12.3.1, Hamilton's equations are given as

$$u_t = \left(\frac{\partial}{\partial x} u + u \frac{\partial}{\partial x} \right) \sum_{j=0}^{K} (-1)^j \frac{\partial^j}{\partial x^j} \left(\frac{\partial \mathcal{H}}{\partial u_{x^j}} (u^{\mathrm{jet}}) \right).$$

For $\mathcal{H}(u) = -\frac{1}{6} u^2$ we obtain the inviscid Burgers' equation $u_t + u u_x = 0$. △

Remark 12.3.1. Using formula (12.2.1) from Example 12.2.1 identifying $\mathfrak{g} \cong \mathcal{C}^\infty(S^1, \mathbb{R})$ and $\mathfrak{g}^* \cong \mathcal{C}^\infty(S^1, \mathbb{R})$, the Lie–Poisson bracket is given by

$$\{F, G\}(u) = \int_{S^1} \left(\frac{\mathrm{d}}{\mathrm{d}x} \left(\frac{\delta F}{\delta u} \right) \frac{\delta G}{\delta u} - \frac{\delta F}{\delta u} \frac{\mathrm{d}}{\mathrm{d}x} \left(\frac{\delta G}{\delta u} \right) \right) f \, \mathrm{d}x,$$

where $\frac{\delta F}{\delta u}$ denotes the functional or variational derivative of F at u. Discretising $S^1 \cong \mathbb{R}/\mathbb{Z}$ using a (periodic) grid with N grid-points, we naturally obtain $\mathbb{R}^N$ as a discrete analogue of $\mathfrak{g}^*$. However, the above Poisson structure does not pass naturally to $\mathbb{R}^N$. △

12.4 The collective system

Let us construct a realisation $J \colon M \to \mathfrak{g}^*$ where M is a symplectic vector space. Consider the left-action of $g \in G = \mathrm{Diff}(S^1)$ on $q \in Q = \mathcal{C}^\infty(S^1, S^1)$ defined by $g.q = q \circ g^{-1}$.

Lemma 12.4.1. *The vector field $\hat{v}$ generated by the infinitesimal action of an element $v \in \mathfrak{g} \cong \mathfrak{X}(S^1)$ on Q is given by the Lie-derivative $-\mathcal{L}_v$. Interpreting v as an element in $\mathcal{C}^\infty(S^1, \mathbb{R})$, this becomes $\hat{v}_q = -v \cdot q_x \in \mathcal{C}^\infty(S^1, \mathbb{R}) \cong T_q Q$.*

Proof. Let $g \colon (-\epsilon, \epsilon) \to \mathrm{Diff}(S^1)$ be a smooth curve with $g_0 = \mathrm{id}$ and $\frac{\mathrm{d}}{\mathrm{d}t}\big|_{t=0} g_t = v \in \mathfrak{g} \cong \mathcal{C}^\infty(S^1, \mathbb{R})$. Let $x \in S^1$. Differentiating $x = g_t(g_t^{-1}(x))$ with respect to t at $t = 0$ we obtain

$$\left. \frac{\mathrm{d}}{\mathrm{d}t} \right|_{t=0} g_t^{-1}(x) = -v(x).$$

Let $q \in Q$. We have

$$\hat{v}_q(x) = \left. \frac{\mathrm{d}}{\mathrm{d}t} \right|_{t=0} (g_t.q)(x) = \left. \frac{\mathrm{d}}{\mathrm{d}t} \right|_{t=0} \left(q \circ g_t^{-1} \right)(x) = -v(x) q_x(x).$$

□

Let M denote the cotangent bundle over Q, which is viewed as $T^*Q \cong Q \times \mathcal{C}^\infty(S^1, \mathbb{R})$. The pairing of $(q, p) \in M$ with an element $v \in T_q Q \cong \mathcal{C}^\infty(S^1, \mathbb{R})$ is given by

$$\langle (q, p), v \rangle = \int_{S^1} p(x) v(x) \, \mathrm{d}x.$$

A symplectic structure on M is given by

$$\Omega((v^q, v^p), (w^q, w^p)) = \int_{S^1} (w^p v^q - v^p w^q) \, \mathrm{d}x.$$

For $(q,p) \in M$ and $\bar{H}\colon M \to \mathbb{R}$ the maps $\frac{\delta \bar{H}}{\delta q}$ and $\frac{\delta \bar{H}}{\delta p}$ can be defined by

$$\mathrm{D}\bar{H}|_{(q,p)}(w^q, 0) = \int_{S^1} \frac{\delta \bar{H}}{\delta q} w^q \mathrm{d}x, \quad \mathrm{D}\bar{H}|_{(q,p)}(0, w^p) = \int_{S^1} \frac{\delta \bar{H}}{\delta p} w^p \mathrm{d}x,$$

where D denotes the Gâteaux derivative. (Each map $\frac{\delta \bar{H}}{\delta q}$ and $\frac{\delta \bar{H}}{\delta p}$ can depend on both q and p although this is not incorporated in the notation.) Now

$$\mathrm{D}\bar{H}|_{(q,p)}(w^q, w^p) = \Omega\left(\left(\frac{\delta \bar{H}}{\delta p}, -\frac{\delta \bar{H}}{\delta q}\right), (w^q, w^p)\right)$$

and Hamilton's equations can be written in the familiar looking form

$$q_t = \frac{\delta \bar{H}}{\delta p}, \qquad p_t = -\frac{\delta \bar{H}}{\delta q}. \tag{12.4.1}$$

We consider the cotangent lifted action of the aforementioned action of G on Q to obtain a Hamiltonian group action of G on M given by

$$g.(q,p) = (q \circ g^{-1}, p \circ g^{-1} \cdot (g^{-1})_x).$$

Alternatively, interpreting the fibre component of elements in T^*Q as 1-forms the action is given by $g.(q, p\mathrm{d}x) = \big(q \circ g^{-1}, (g^{-1})^*(p\mathrm{d}x)\big)$.

Proposition 12.4.2. *The momentum map $J\colon M \to \mathfrak{g}^*$ of the cotangent lifted action of G on M is given as*

$$J(q,p) = -q_x \cdot p.$$

Proof. Using the formula for the momentum map of cotangent lifted action (see Marsden and Abraham, 1978, p. 283) we obtain

$$\langle v, J(q,p)\rangle = \langle (q,p), \hat{v}_q\rangle = \langle (q,p), -v \cdot q_x\rangle = -\int_{S^1} v(x)p(x)q_x(x)\mathrm{d}x = \langle v, -q_x \cdot p\rangle$$

for all $v \in \mathfrak{g}$, as claimed. In the above equations $\hat{v}_q$ denotes the vector field generated by the infinitesimal action of the element $v \in \mathfrak{g}$ as in Lemma 12.4.1. □

The manifold M is equipped with a Poisson structure defined by the symplectic structure Ω. By construction, the momentum map $J\colon M \to \mathfrak{g}^*$ is a Poisson map. It is surjective (take $q = \mathrm{id}$) and therefore called a *full realisation of* $\mathfrak{g}^*$. If H is a Hamiltonian on $\mathfrak{g}^*$, then the Hamiltonian flow of the *collective* system $(M, \Omega, H \circ J)$ maps fibres of J to fibres and descends to the Hamiltonian flow of the system $(\mathfrak{g}^*, \{\cdot,\cdot\}, H)$ because the Hamiltonian vector fields are J-related and J is a Poisson map. More generally, a symplectic map on M that maps fibres to fibres descends to a Poisson map on g^*.

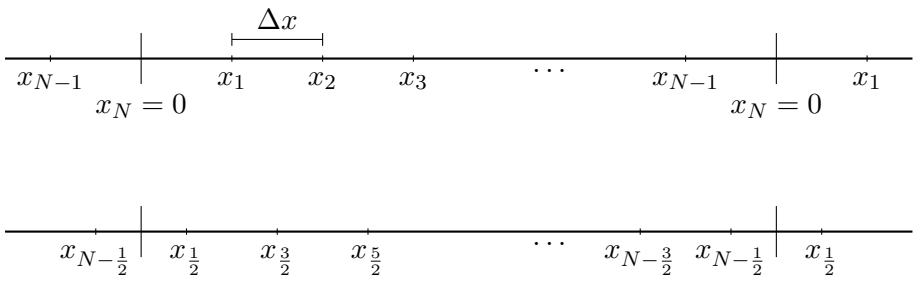

Figure 12.1: Uniform periodic grids on $S^1 \cong \mathbb{R}/L\mathbb{Z}$, $L > 0$.

Example 12.4.1. As in Example 12.3.1 we consider the Hamiltonian

$$H(u) = \int_{S^1} \mathcal{H}(u^{\text{jet}}(x))\mathrm{d}x$$

on $\mathfrak{g}^*$. Hamilton's equations of the collective system $(M, \Omega, \bar{H})$ with $\bar{H} = H \circ J$ can be calculated using (12.4.1) and are given as the following system of PDEs

$$\begin{aligned} q_t &= q_x \sum_{j=0}^{K} (-1)^j \frac{\partial^j}{\partial x^j} \left(\frac{\partial \mathcal{H}}{\partial u_{x^j}}(u^{\text{jet}}) \right), \\ p_t &= -\frac{\partial}{\partial x} \left(p \sum_{j=0}^{K} (-1)^j \frac{\partial^j}{\partial x^j} \left(\frac{\partial \mathcal{H}}{\partial u_{x^j}}(u^{\text{jet}}) \right) \right). \end{aligned}$$

Choosing $\mathcal{H}(u) = -\frac{1}{6}u^2$ (Burgers' equation) yields

$$q_t = -\frac{1}{3} q_x^2 p, \qquad p_t = -\frac{1}{3}(q_x p^2)_x.$$

△

12.5 Integrator of the collective system

12.5.1 Spatial discretisation

We use a second-order finite-difference method in space to discretise the realisation J and the Hamiltonian H to obtain a system of Hamiltonian ODEs in canonical form: as before, we consider S^1 as the quotient $\mathbb{R}/L\mathbb{Z}$. We introduce a uniform grid $(x_1, \ldots, x_N)$, $x_j = j \cdot \Delta x$, $\Delta x = 1/N$ with N points and periodic boundary conditions. Moreover, we consider the corresponding half-grid $(x_{1/2}, \ldots, x_{N-1/2})$. Both grids are illustrated in Figure 12.1.

In the discretised setting, elements in $Q = \mathcal{C}^\infty(S^1, S^1)$ and $\mathcal{C}^\infty(S^1, \mathbb{R})$ are approximated by their values on the considered grid. This leads to an approximation of $\mathfrak{g}^*$ and Q by the vector space $\mathbb{R}^N$ and an approximation of M by $T^*\mathbb{R}^N \cong \mathbb{R}^{2N}$, which we equip with coordinates $(\hat{q}, \hat{p}) = q^1, \dots, q^N, p_1, \dots, p_n$ in the usual way. Discretising the symplectic structure Ω we obtain

$$\omega = \Delta x \sum_{j=1}^{N} \mathrm{d}q^j \wedge \mathrm{d}p_j,$$

which is the standard symplectic structure up to the factor Δx.

For $q \in Q$ we obtain a second-order accurate approximation $D_{\Delta x}(\hat{q})$ of the spatial derivative q_x on the half-grid $(1/2\Delta x, 3/2\Delta x, \dots, (N-1/2)\Delta x)$ using compact central differences as follows:

$$\begin{aligned} &\left(q_x(\tfrac{1}{2}\Delta x), q_x(\tfrac{3}{2}\Delta x), \dots, q_x((N-\tfrac{3}{2})\Delta x), q_x((N-\tfrac{1}{2})\Delta x)\right)^\top \\ \approx \frac{1}{\Delta x} &\left[\underbrace{\begin{pmatrix} 1 & 0 & \dots & 0 & -1 \\ -1 & 1 & \dots & 0 & 0 \\ & \ddots & \ddots & & \\ & & \ddots & \ddots & \\ & & & -1 & 1 \end{pmatrix}}_{=:T} \begin{pmatrix} q(\Delta x) \\ q(2\Delta x) \\ \vdots \\ q((N-1)\Delta x) \\ q(N\Delta x) \end{pmatrix} + \begin{pmatrix} C(q) \\ 0 \\ \vdots \\ 0 \\ 0 \end{pmatrix} \right]. \end{aligned}$$

The quantity $C(q)/L$ is the winding number (degree)[3] of the map $q\colon S^1 \to S^1$. The values for q_x are now available on the half-grid. Notice that the quantity $C(q)$ is constant if q evolves smoothly subject to the PDE (12.4.1) because $C(q)$ can only take values in $L\mathbb{Z}$. A discrete version of the map $J\colon M \to g^*$ is given by $\hat{J}\colon \mathbb{R}^{2N} \to \mathbb{R}^N$ with $\hat{J}(\hat{q}, \hat{p}) = D_{\Delta x}\hat{q}.S\hat{p}$. Its values correspond to the half-grid. The matrix S is given as

$$S = \frac{1}{2} \begin{pmatrix} 1 & & & 1 \\ 1 & 1 & & \\ & \ddots & \ddots & \\ & & 1 & 1 \end{pmatrix}.$$

It averages the values of $\hat{p}$ to obtain second order accurate approximations of p on the half-grid. In this way, we obtain approximations to $u = q_x p$ on the half grid. Approximations for u_x and higher derivatives are obtained by successively applying

[3] Let $\pi\colon \mathbb{R} \to S^1$ denote the universal covering of $S^1 \cong \mathbb{R}/L\mathbb{Z}$ and let $\tilde{q}\colon \mathbb{R} \to \mathbb{R}$ be any lift of the map $\pi \circ q\colon \mathbb{R} \to S^1$ to the covering space. Now $C(q) = \tilde{q}(L) - \tilde{q}(0)$. If, for instance, q is the identity map on S^1, then $C(q) = L$.

$T_{\Delta x}$ and $T_{\Delta x}^{\top}$, i.e.

$$\frac{\partial^k u}{\partial x^k} \approx \frac{\partial^k_{\Delta x} u}{\partial_{\Delta x} x^k} := \begin{cases} D_{\Delta x}\hat{q}.S\hat{p} & \text{if } k = 0 \\ -T^{\top}\frac{\partial^{k-1}_{\Delta x} u}{\partial_{\Delta x} x^{k-1}}/\Delta x & \text{if } k \text{ is odd} \\ T\ \frac{\partial^{k-1}_{\Delta x} u}{\partial_{\Delta x} x^{k-1}}/\Delta x & \text{if } k \text{ is even.} \end{cases} \tag{12.5.1}$$

Here $T^{\top}$ denotes the transpose of the matrix T and . denotes component-wise multiplication. Now all approximations for even derivatives are available on the half-grid and all odd derivatives on the full-grid. A Hamiltonian of the form $\int_{S^1} \mathcal{H}(u, u_x, u_{xx}, \ldots)\mathrm{d}x$ is approximated by the sum

$$\int_{S^1} \mathcal{H}(u, u_x, u_{xx}, \ldots)\mathrm{d}x \approx \Delta x \sum_{j=1}^{N} \mathcal{H}(u(x_{j-1/2}), u_x(x_{j-1/2}), u_{xx}(x_{j-1/2}), \ldots). \tag{12.5.2}$$

To evaluate (12.5.2), all approximations of $\frac{\partial^k u}{\partial x^k}$ where k is odd are multiplied by S such that the approximation of the jet of u is available on the half-grid. The (second-order) averaging with S can be avoided if $\mathcal{H}$ is of the form

$$\begin{aligned} \mathcal{H}(u^{\text{jet}}(x)) = \mathcal{H}^{\text{even}}&(u(x), u_{xx}(x), u_{xxxx}(x), \ldots) \\ &+ \mathcal{H}^{\text{odd}}(u_x(x), u_{xxx}(x), u_{xxxxx}(x), \ldots). \end{aligned}$$

We can then approximate the Hamiltonian by

$$\begin{aligned} \int_{S^1} \mathcal{H}(u, u_x, u_{xx}, \ldots)\mathrm{d}x \approx \Delta x \sum_{j=1}^{N} &\mathcal{H}^{\text{even}}(u(x_{j-1/2}), u_{xx}(x_{j-1/2}), u_{xxxx}(x_{j-1/2}) \ldots) \\ &+ \Delta x \sum_{j=1}^{N} \mathcal{H}^{\text{odd}}(u_x(x_j), u_{xxx}(x_j), u_{xxxxx}(x_j), \ldots). \end{aligned} \tag{12.5.3}$$

Taking into account that the symplectic form ω is the canonical symplectic structure scaled by Δx, defining $\hat{H}$ as

$$\hat{H}(u) = \sum_{j=1}^{N} \mathcal{H}(u(x_{j-1/2}), u_x(x_{j-1/2}), u_{xx}(x_{j-1/2}), \ldots) \tag{12.5.4}$$

or as the corresponding term from (12.5.3) puts Hamilton's equations into the canonical form

$$\dot{\hat{q}} = \quad \nabla_{\hat{p}}\bar{\hat{H}}(\hat{q}, \hat{p}), \qquad \dot{\hat{p}} = -\nabla_{\hat{q}}\bar{\hat{H}}(\hat{q}, \hat{p}) \tag{12.5.5}$$

with collective Hamiltonian $\bar{\hat{H}} = \hat{H} \circ \hat{J} \colon \mathbb{R}^{2N} \to \mathbb{R}$. Here the dot denotes the time-derivative. Finally, (12.5.5) is a 2nd order accurate, spatial discretisation of (12.4.1).

Remark 12.5.1. An alternative to the described finite-difference discretisation are spectral methods. Notice that $q \in \mathcal{C}^\infty(S^1, S^1)$ can be split into the winding term $C(q)\mathrm{id}$ and the term $q - C(q)\mathrm{id}$ which has winding number zero. In a semi-spectral discretisation, the derivative of $q - C(q)\mathrm{id}$ is calculated in a Fourier basis and the winding term $C(q)\mathrm{id}$ is accounted for in the derivative q_x by adding the constant $C(q)/L$ component-wise. The derivatives of $u = q_x p$ can be calculated without complications.

A full spectral discretisation is also possible because embedding $\mathcal{C}^\infty(S^1, S^1)$ and $\mathcal{C}^\infty(S^1, \mathbb{R})$ into the Hilbert space L_2 and choosing any orthonormal basis will lead to a symplectic form ω which is in the standard form (splitting q as above to allow for a Fourier basis). Therefore, Hamilton's equations for the basis coefficients appear in canonical form. △

12.5.2 The integration scheme

A numerical solution to the original equation (12.3.1) can now be obtained as follows.

1. Lift an initial condition

$$\hat{u}^{(0)} = (u^{(0)}(x_1), \dots, (u^{(0)}(x_N))$$

to $(\hat{q}^{(0)}, \hat{p}^{(0)}) \in \hat{J}^{-1}(\hat{u}^{(0)})$, for example by setting

$$\begin{aligned} \hat{q}^{(0)} &= (\Delta x, 2\Delta x, \dots, N\Delta x), \\ \hat{p}^{(0)} &= \hat{u}^{(0)}, \end{aligned}$$

as we will do in our numerical experiments. Notice that $\hat{q}^{(0)}$ is a discretisation of the identity map on S^1. The exact and discrete derivative is the constant 1 function or vector.

2. The system of Hamiltonian ODEs (12.5.5) can be integrated subject to the initial conditions $(\hat{q}^{(0)}, \hat{p}^{(0)})$ using a symplectic numerical integrator.

3. Approximations to u can be calculated from $(\hat{q}, \hat{p})$ on the half-grid as $D_{\Delta x}\hat{q}.S\hat{p}$.

Remark 12.5.2. Conservation of $\bar{\hat{H}}$ in (12.5.5) exactly corresponds to conservation of the discretised Hamiltonian $\hat{H}$ (12.5.2) or (12.5.3) because we consistently relate u and (q, p) by (12.5.1). Therefore, using a symplectic integrator to solve the system (12.5.5) of Hamiltonian ODEs we expect excellent energy behaviour of the numerical solution.

In the following numerical experiments we will use the symplectic implicit midpoint rule (Section 3.2.2). The arising implicit equations will be solved using Newton iterations. △

Remark 12.5.3. In contrast to the case of Hamiltonian-ODEs on Poisson manifolds, it is hard for a symplectic integrator to maintain the fibration on the symplectic manifolds induced by the discretisation $\hat{J}$ of the realisation J. Indeed, the implicit midpoint rule used in our numerical examples fails to do so. This is why we do *not* obtain a (discretisation of a) Poisson integrator in this way. However, the described energy conservation properties of Remark 12.5.2 are independent of this drawback. Moreover, our numerical examples will show that we obtain excellent Casimir behaviour although this is not forced by this construction. △

12.6 Numerical experiments

For numerical experiments, we consider Hamiltonian systems $(\mathrm{diff}^*(S^1), \{\cdot,\cdot\}, H)$ with

$$H = \int_{S^1} \left(C_1 u^2 + C_2 u_x^2 + C_3 u^3 + C_4 u_x^3\right) \mathrm{d}x. \tag{12.6.1}$$

To gain a sense of the relative performance of the collective integration method from Section 12.5 we will now develop a conventional finite-difference approach for comparison that is based on McLachlan, 2003.

First, a finite dimensional discrete Hamiltonian approximation is obtained by

$$\hat{H} = \Delta x \sum_{j=1}^{N} (C_1 \hat{u}_j^2 + C_2 (\hat{u}_x)_j^2 + C_3 \hat{u}_j^3 + C_4 \, (\hat{u}_x)_j^3), \tag{12.6.2}$$

where $\hat{u}_x = T\hat{u}/\Delta x$ is a compact finite-difference approximation. The PDE is then written as a set of the Hamiltonian ODEs in skew-gradient form

$$\dot{\hat{u}} = K(\hat{u}) \nabla_{\hat{u}} \hat{H}_{\Delta x}. \tag{12.6.3}$$

Here, $K(\hat{u}) = (UD^{(1)} + D^{(1)}U)$ represents the discrete version of the coadjoint operator in equation (12.3.1), where $U = \mathrm{diag}(\hat{u})$ is a diagonal matrix with $\hat{u}_j$ on the jth diagonal and the matrix $D^{(1)}$ is a centred finite-difference matrix with the stencil $[-\frac{1}{2\Delta x}, 0, \frac{1}{2\Delta x}]$ on the main three diagonals and $-\frac{1}{2\Delta x}$ and $\frac{1}{2\Delta x}$ on the top right and bottom left corners,

respectively. This yields a skew-symmetric matrix $K(\hat{u})$ given as

$$\frac{1}{2\Delta x}\begin{pmatrix} 0 & u_1+u_2 & & & -u_n-u_1 \\ -u_1-u_2 & 0 & u_2+u_3 & & \\ & \ddots & \ddots & \ddots & \\ & & -u_{n-2}-u_{n-1} & 0 & u_{n-1}+u_n \\ u_1+u_n & & & -u_{n-1}-u_n & 0 \end{pmatrix},$$

where the diagonal dots denote the continuation of the stencil $[-u_{i-1}-u_i, 0, u_i+u_{i+1}]$ on the ith row. Note that

$$\frac{\mathrm{d}}{\mathrm{d}t}\hat{H} = (\nabla_{\hat{u}}\hat{H})^{\mathrm{T}}\dot{\hat{u}} = (\nabla_{\hat{u}}\hat{H})^{\mathrm{T}}K(\hat{u})\nabla_{\hat{u}}\hat{H} = 0, \tag{12.6.4}$$

hence, $\hat{H}$ is a first integral of this ODE. Finally, equation (12.6.3) is integrated using the implicit midpoint rule, which is solved using Newton iterations. This method will henceforth be referred to as the *conventional method*.

The conventional and collective methods are both order-two in space as shown by Figure 12.2, which show errors for travelling wave solutions of the cubic Hamiltonian system outlined in Section 12.6.2. The Hamiltonian error at time $t = t_n$ is calculated by $(\hat{H}(0) - \hat{H}(t_n))/\hat{H}(0)$ and similarly for the Casimir error. The solution error is

$$\frac{||\hat{u}_n - \hat{u}_e||_2}{||\hat{u}_e||_2},$$

where $\hat{u}_n$ is the numerical solution, $\hat{u}_e$ is the exact solution evaluated on the grid and $||\cdot||_2$ is the discrete L_2-norm. We see from Figure 12.2b that the collective method preserves the energy up to machine precision for this experiment. We remark that the solution error observed in Figure 12.2c is largely attributed to phase error and does not reflect the ability of the method to preserve the shape of the travelling wave.

12.6.1 Inviscid Burgers' equation

Setting $C_1 = 1$, $C_2 = 0$, $C_3 = 0$ and $C_4 = 0$ in equation (12.6.1) yields the well-known inviscid Burgers' equation

$$u_t = 6uu_x.$$

In the following example, the equation is modelled with the initial conditions $u(0, x) = 1 + \frac{1}{2}\cos(2\pi x/L)$, which develops a shock wave at about $t = 0.4$. Figure 12.3 shows three snapshots of the conventional and the collective solutions before and after the shock and Figure 12.4 shows the Casimir and Hamiltonian errors over time. Over the short simulation time, both methods yield qualitatively similar solutions. Due to the

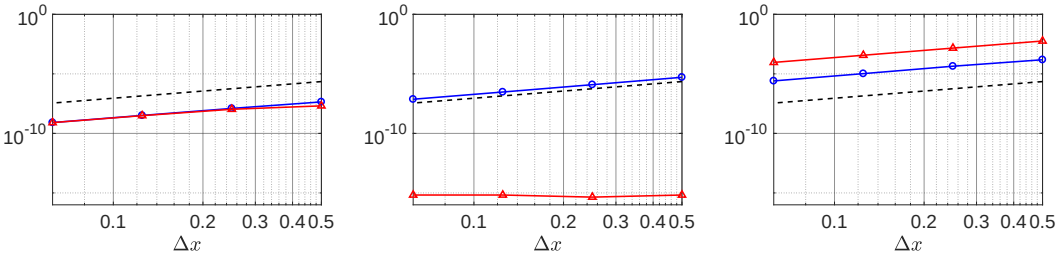

(a) Casimir error (b) Hamiltonian error (c) Solution error

Figure 12.2: Order-two convergence for the travelling wave solution of the extended Burgers' equation outlined in Section 12.6.2. The plots correspond to the conventional solution (○) and the collective solution (△) and an order-two reference line (– – –). The error is calculated after 512 timesteps, with $L = 8$, $\Delta t = 2^{-14}$ and $\Delta x = L/2^k$ for $k = 1, 2, 3$ and 4.

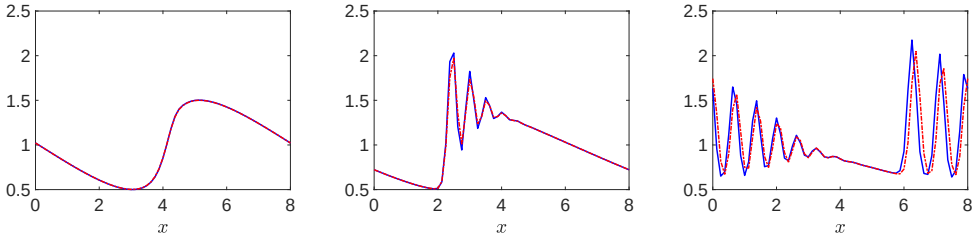

(a) $t = 0.317$ (b) $t = 0.635$ (c) $t = 1.37$

Figure 12.3: Inviscid Burgers' equation solutions of the conventional method (——) and collective method (– · – · –). The grid parameters are $n_x = 64$, $\Delta x = 0.125$, $L = 8$ and $\Delta t = 2^{-12}$. A shock forms at about $t = 0.4$.

presence of shock waves in the inviscid Burgers' equation, it is difficult to gain a sense of the long term behaviour of the methods as no solution exists after a finite time. From Figure 12.4b we see that the conventional method has exceptional Hamiltonian preservation properties and maintains the error at machine precision throughout the simulation. This can be explained by the fact that the implicit midpoint rule preserves quadratic invariants, that is, $\hat{H}$ is preserved exactly by the conventional method. Otherwise, the errors grow quadratically until the shock develops, after which, they appear bounded. The Hamiltonian error of the collective solution can also be reduced to machine precision by reducing the time step Δt.

12.6.2 Extended Burgers' equation

We now focus our attention to a cubic Hamiltonian problem that we have designed to admit non-symmetric travelling wave solutions. The PDE being modelled arises from setting $C_1 = 1/2$, $C_2 = 1/2$, $C_3 = -1/4$ and $C_4 = 1/2$ in equation (12.6.1), which

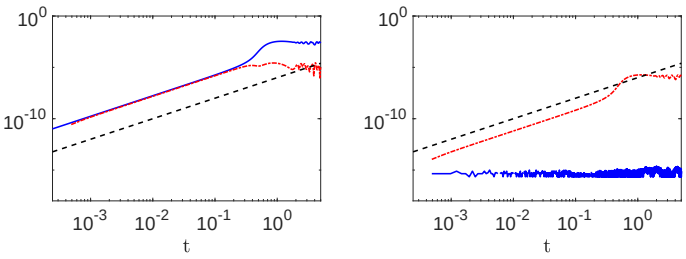

(a) Casimir error (b) Hamiltonian error

Figure 12.4: The errors corresponding to the conventional (——) and collective (–·–·–) methods for the inviscid Burgers' equation and $\mathcal{O}(t^2)$ reference lines (– – –).

yields

$$u_t = 3uu_x - \frac{9}{4}u^2u_x - u_xu_{xx} - 3u_x^2u_{xx} - 2uu_{xxx} - 2uu_xu_{xxx} - 6uu_{xx}^2$$

and is henceforth referred to as the *extended Burgers' equation*.

Travelling wave solutions

In this example, we look for solutions of the form $u(x,t) = f(s)$, where $s = x - ct$ for wave velocity c. This yields an ODE in s, which is solved to a high degree of accuracy on the grid using MATLAB's `ode45`. Figure 12.5 shows snapshots of travelling wave solutions to the extended inviscid Burgers' equation and their Fourier transforms and Figure 12.6 shows the corresponding errors. The errors of the collective solution are bounded whereas the conventional solution errors grow with time. In particular, the high frequency Fourier modes of the conventional solution erroneously drift away from that of the exact solution while the collective solution keeps these modes bounded. The effect of these erroneously large high frequency modes is that the solution appears less smooth as can be seen in Figure 12.5c. This is again highlighted by Figure 12.6c, which shows that the highest frequency mode (i.e., the mode whose wavelength is equal to the grid spacing Δx) grows exponentially in time. Figures 12.6a and 12.6b show the behaviour of the Casimir and Hamiltonian errors. This highlights the ability of the collective method to keep the errors bounded, while the errors of the conventional solution grow linearly with time. Towards the end of the simulation, the errors of the conventional solution become so large that the implicit equations arising from the midpoint rule become too difficult to solve numerically and the Newton iterations fail to converge. The simulation ends with the conventional method errors diverging to infinity.

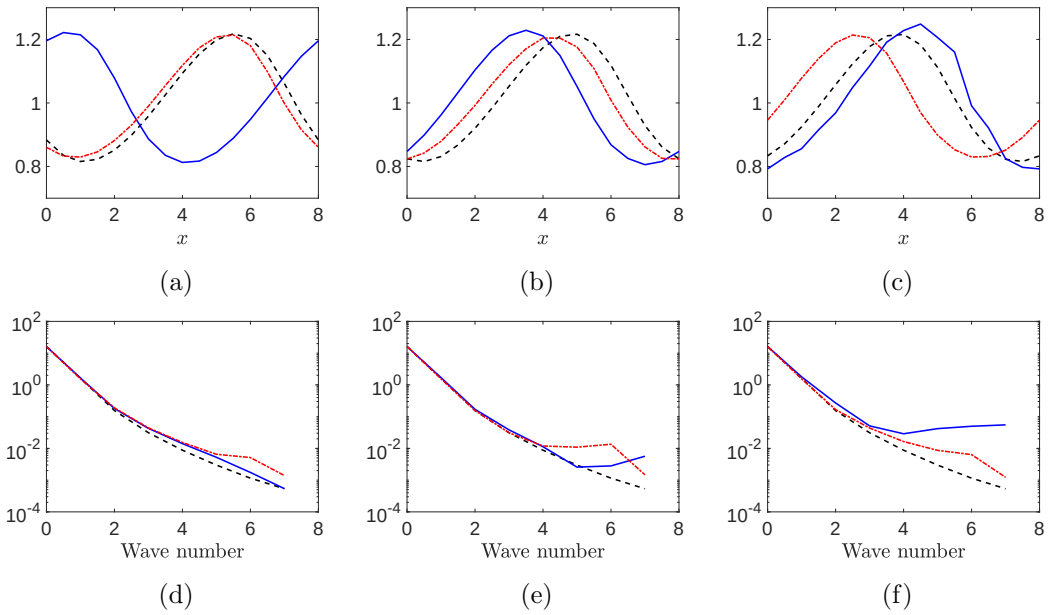

Figure 12.5: Travelling wave solutions of the extended Burgers' equation (top row) and the positive Fourier modes (bottom row) at $t = 109$ (left column), $t = 218$ (middle column) and $t = 437$ (right column). The plots correspond to the conventional method (——), collective method (– · –) and the exact travelling wave solution (– – –). The grid parameters are $n_x = 16$, $\Delta x = 0.5$, $L = 8$ and $\Delta t = 2^{-6}$.

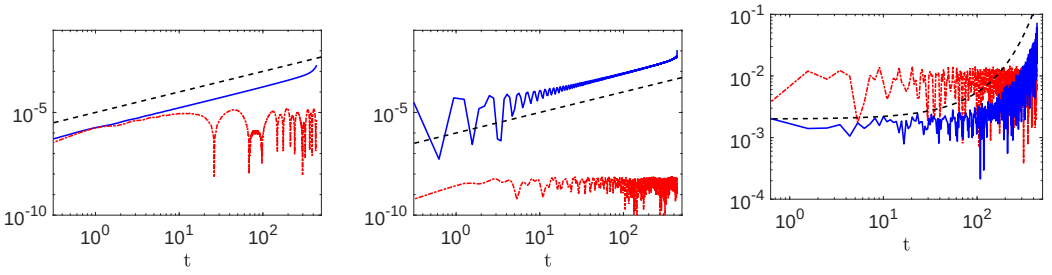

(a) Casimir error

(b) Hamiltonian error

(c) Highest frequency Fourier mode (increased vertical scale)

Figure 12.6: The errors corresponding to the conventional (——) and collective (– · –) methods for the travelling wave experiment. The reference lines (– – –) are $\mathcal{O}(t)$ in figures (a) and (b) and exponential in figure (c).

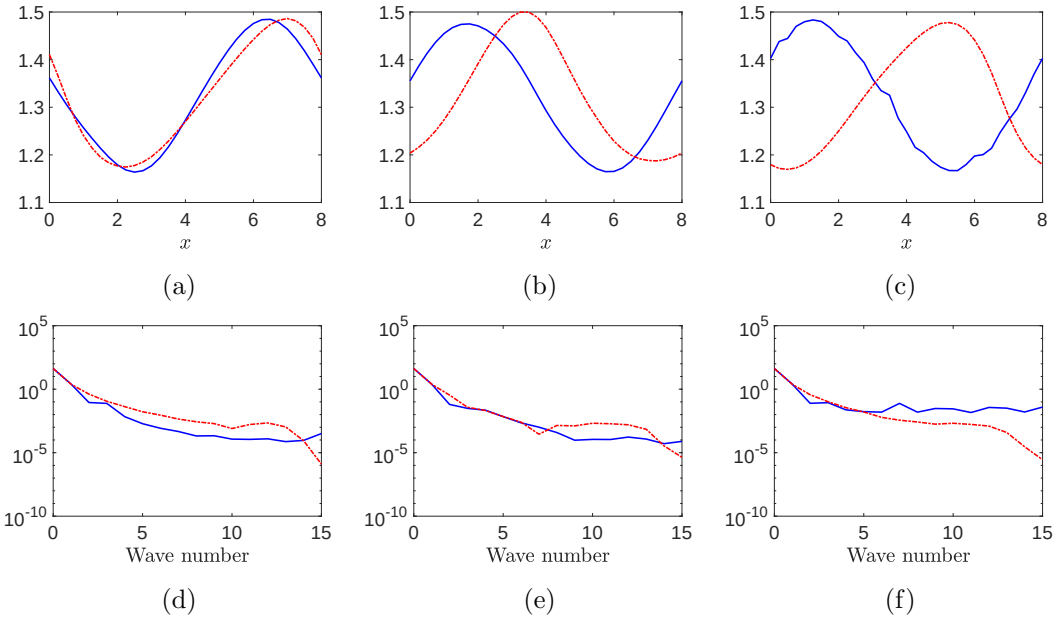

Figure 12.7: Periodic bump solutions of the extended Burgers' equation (top row) and the positive Fourier modes (bottom row) at $t = 10$ (left column), $t = 100$ (middle column) and $t = 1000$ (right column). The plots correspond to the conventional method (——) and the collective method (– – –). The grid parameters are $n_x = 32$, $\Delta x = 0.25$, $L = 8$ and $\Delta t = 2^{-8}$.

Periodic bump solutions

In this example, we model solutions to the extended Burgers' equation from the initial condition

$$u(x, 0) = 1 + \frac{1}{2}\exp(-\sin^2(\frac{\pi x}{L})).$$

Figure 12.7 shows snapshots of the solution and its positive Fourier modes and Figure 12.8 shows the behaviour of the Casimir and Hamiltonian errors over time. As in the travelling wave example, we see that the high frequency modes of the conventional solution grow with time causing rough wiggles in Figure 12.7c. The conventional solution has bounded Hamiltonian error, despite linear and exponential growth in the Casimir and highest frequency Fourier modes, respectively. In particular, the collective solution has excellent error behaviour, which appears to be bounded over the simulation period for all three plots of Figure 12.8.

12.7 Conclusion

We have demonstrated that Hamiltonian PDEs on Poisson manifolds can be integrated numerically while maintaining the structure preserving properties of Poisson systems

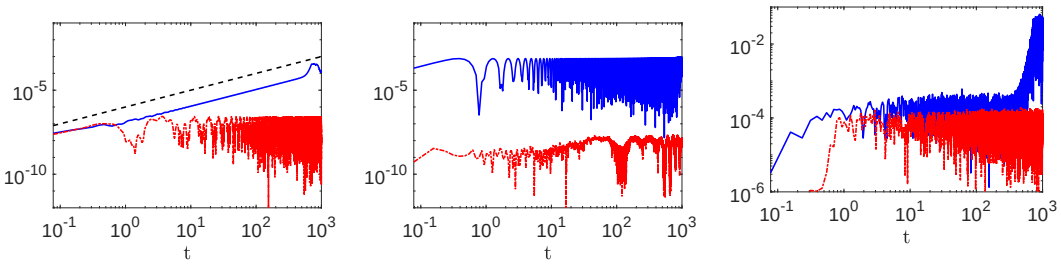

(a) Casimir error (b) Hamiltonian error (c) Highest Fourier frequency mode (increased vertical scale)

Figure 12.8: The errors corresponding to the conventional (——) and collective (—·—·—) methods for the periodic bump example. The reference line (– – –) in figure (a) is $\mathcal{O}(t)$.

very well. This is achieved by

1. realising the Poisson-Hamiltonian system as an infinite dimensional, collective Hamiltonian system on a symplectic manifold and lifting the initial condition from the Poisson system to the collective system,

2. discretising the collective system in space to obtain a system of Hamiltonian ODEs, and

3. using a symplectic integrator to solve the system.

The symplectic integrator will, in general, fail to preserve the fibration induced by the realisation. Therefore, the presented integrators for Hamiltonian PDEs cannot be expected to conserve the Poisson structure *exactly*. This is in contrast to the case of Hamiltonian ODEs on Poisson manifolds, where the fibres can be structurally simple for carefully chosen realisations and genuine Poisson integrators can be constructed. Regardless, in the ODE as well as in the PDE case the integrator is guaranteed to inherit the excellent energy behaviour from the symplectic integrator which is applied to the collective system. Moreover, our numerical examples for Hamiltonian PDEs show excellent Casimir behaviour as well. Indeed, energy as well as Casimir errors are bounded in long term simulations.

Structure preserving properties of conventional numerical schemes typically rely on the presence of structurally simple symmetries of the differential equation. If the discretisation is invariant under the same symmetry as the equation, then the numerical solution will share all geometric features of the exact solution which are due to the symmetry. The simple form of the symmetries, however, is immediately destroyed when higher order terms in the Hamiltonian are switched on. Although exact solutions still preserve the Hamiltonian, numerical solutions obtained using a traditional scheme fail to show a good energy behaviour. The advantage of the presented integration methods is that their excellent energy behaviour is guaranteed no matter how

complicated the Hamiltonian is. Our numerical examples for the extended Burgers' equation demonstrate the importance of structure preservation: while growing energy errors of the conventional solution cause a blow up, there are no signs of instabilities for the collective solution.

Chapter 13

Do multisymplectic integrators preserve Hamiltonian structures of symmetric solutions?

Work in this chapter has been concluded and submitted (McLachlan and Offen, 2020a).

An important feature of Hamiltonian ODEs is that their flow maps are symplectic. As discussed in the review section, preserving symplecticity under numerical discretisation is beneficial because other structure preserving properties come along with it automatically as, for instance, excellent energy conservation, preservation of topological properties of the phase portrait (e.g. absence of artificial attractors) or the preservation of bifurcations in boundary value problems. Symplectic structure generalises to the setting of partial differential equations in various ways. Variational structure (related to Hamiltonian structure via Legendre transformations) has been exploited in Chapter 11 to extend our techniques from the bifurcation analysis of boundary value problems for Hamiltonian ODEs to the PDE setting. Chapter 12 shows how classical symplectic integration techniques can be applied to PDEs that can be formulated as Hamiltonian systems on infinite dimensional Poisson manifolds to recover advantages of classical symplectic integration.

Another approach to generalise Hamiltonian systems on symplectic manifolds to the PDE setting is *multisymplecticity*. The conservation of a symplectic 2-form by the Hamiltonian flow in the ODE setting can be generalised to a multisymplectic conservation law which involves a 2-form for each spatial-temporal dimension. Roughly speaking, if the symplectic conservation law of Hamiltonian ODEs $Kz_t = \nabla H(z)$ is written as $\omega_t = 0$, then the multisymplectic conservation law for the PDE $Kz_t + Lz_x = \nabla H(z)$ has the form $\omega_t + \kappa_x = 0$ for $\omega = \mathrm{d}z \wedge K\mathrm{d}z$ and $\kappa = \mathrm{d}z \wedge L\mathrm{d}z$ with skew-symmetric

matrices K and L. An introduction is given, for instance, in Hydon, 2005. Many discretisation schemes have been shown to preserve discretised versions of multisymplectic conservation laws (McLachlan, Ryland, and Sun, 2014; McLachlan and Stern, 2019). One of them is the 5-point stencil. In the following chapter we will use a variational viewpoint to approach the question how multisymplectic integrators preserve structure that governs symmetric solutions of multisymplectic PDEs or Euler-Lagrange equations. In particular, we will show that after discretisation with the multisymplectic 5-point stencil travelling waves in the discretised non-linear wave equation are governed by a modified Hamiltonian principle, where the Hamiltonian is given as a formal power series defined on the original phase space or, equivalently, by a formal 1st order variational principle. The modified Lagrangian is obtained by backward error analysis and has the form of a formal P-series. This recovers the structure of the continuous system correctly which follows Palais' principle of symmetric criticality, reviewed below. Further research is proposed to clarify the role of multisymplecticity for the preservation of Palais' principle of symmetric criticality under discretisation by analysing an example of a rotating travelling wave.

13.1 Introduction

Many partial differential equations fulfil a variational principle, i.e. they occur as the Euler-Lagrange equations corresponding to an action functional $S\colon U \to \mathbb{R}$ of the form

$$S(u) = \int L(x_1, \ldots, x_n, u, u_{x_j}, u_{x_i x_j}, \ldots) \mathrm{d}x_1 \ldots \mathrm{d}x_n$$

defined on some function space U (typically a Banach space). Examples include the nonlinear wave equation, KdV (Whitham, 1967), the dispersionless Camassa-Holm equation (Cotter, Holm, and Hydon, 2007), the nonlinear Schrödinger equation, and many more. A variational formulation of a PDE can provide some interesting physical insights: for instance, a variational formulation allows for an application of Noether's theorem connecting continuous symmetries with conserved quantities.

Consider the action of a Lie group G on the function space U. Let us denote the set of elements $u \in U$ which are invariant under the action of the symmetry group G by U^{sym}, i.e. $U^{\mathrm{sym}} = \{u \in U \mid g \cdot u = u \; \forall g \in G\}$. Assume that U^{sym} is a submanifold of U. Critical points of the action $S\colon U \to \mathbb{R}$ which lie in U^{sym} are critical points of the restricted functional $S|_{U^{\mathrm{sym}}}$. If the converse holds true as well, i.e. if the critical points of $S|_{U^{\mathrm{sym}}}$ are critical points of S, then we say the *principle of symmetric critically* holds true. In other words, the principle of symmetric critically says that symmetric elements $u \in U^{\mathrm{sym}}$ which are stationary points of S with respect to symmetric variations are stationary with respect to all variations. Palais (1979) analyses when the principle of

symmetric critically applies. He proves in particular that the principle holds if the symmetry group is compact or the group action is isometric and U is a Banach space.

Variational principles are useful for constructing integration schemes too. These are highly practical and also allow for a theoretical analysis using discrete versions of tools known from the continuous setting such as, for example, the discrete Noether theorem (Marsden and West, 2001b).

The idea of backward error analysis is the following: the numerical solution of an ODE or PDE coincides with the exact solution of a modified equation at the grid points. The modified equation depends on the discretisation parameters and can be obtained as a series expansion of the discretised equation around the discretisation parameters. Finding the modified equation and analysing its structure is called *backward error analysis (BEA)* (see, for instance Hairer, Lubich, and Wanner, 2013, §IX). Recall from Section 3.7 that in case of Hamiltonian ODEs discretised by a symplectic integrator the modified equation has again Hamiltonian structure for a modified Hamiltonian with respect to the original symplectic structure on the same phase space. The Hamiltonian is given as a formal power series in the discretisation parameter which typically does not converge. However, optimal truncation results are available (Theorem 3.7.1). Vermeeren, 2017 observed that backward error analysis for variational integrators can be done purely on the Lagrangian side. When expanding discretised PDEs around discretisation parameters higher order derivatives occur which can, in contrast to the ODE case, *not* be eliminated. Therefore, the modified system is defined on a higher-dimensional phase space than the original PDE. Moreover, optimal truncation techniques have not yet been developed (see the open problems list in Marsden and West, 2001a, §5.3.2).

In the following we address the question whether the principle of symmetric criticality holds for variational integrators by analysing the non-linear wave equation

$$u_{tt} - u_{xx} - V'(u) = 0 \tag{13.1.1}$$

and the five-point stencil discretisation. The discretisation scheme is multisymplectic. In the continuous setting, the PDE (13.1.1) as well as its travelling waves are governed by a first-order variational principle. We will apply BEA techniques to derive a modified ODE which governs travelling waves of the discretised system. Our BEA lives in between the two worlds of BEA for ordinary and BEA for partial differential equations: the modified equation admits a reduction to a 2nd order ODE (which is the form of the ODE governing travelling waves in the exact system) but contains the two discretisation parameters Δt and Δx. We will analyse whether it is governed by a 1st order variational principle for a modified Lagrangian.

McDonald et al., 2016 consider (13.1.1) for scalar valued u discretised by the 5-point

stencil and show that the travelling waves in the modified equation are governed by a planar Hamiltonian system up to terms of order 6 in the discretisation parameters Δt and Δx. We extend this result and show that the result holds in higher dimensions and up to any order: there exists a first-order variational principle governing (higher-dimensional) travelling waves in the discretised PDE. The modified variational principle has the form of a formal P-series (see Hairer, Lubich, and Wanner, 2013, Ch. III.2.1). Moreover, this is true for all reduced functional equations which allow a formulation as a symmetric linear multi-step method.

Our proofs use the theory of symmetric linear multi-step methods and do not apply when considering phase-rotating travelling waves. This leaves the question whether the preservation of the principle of symmetric criticality is guaranteed by variational or multisymplectic integrators or rather related to compatibility of the symmetry of the sought solutions with the symmetries of the mesh to future research. An answer can shed some light on the role of multisymplecticity for discretisations.

13.2 Setting for example of rotating travelling waves

In the following, we will consider travelling waves with constant phase rotation in the nonlinear wave equation (13.1.1) and restrict later to the non-rotating case.

13.2.1 Continuous setting

Let $\Omega = \mathbb{R}^2$ and let $V\colon \mathbb{R} \to \mathbb{R}$ be an analytic potential. The Euler–Lagrange equations to the action functional

$$S(u) = \int \frac{1}{2} \left(\langle u_t, u_t \rangle - \langle u_x, u_x \rangle + V(\langle u, u \rangle) \right) \mathrm{d}(t, x), \tag{13.2.1}$$

with $u\colon \Omega \to \mathbb{R}^2$ recover the nonlinear wave equation (13.1.1), i.e.

$$u_{tt} - u_{xx} - V'(\langle u, u \rangle) u = 0. \tag{13.2.2}$$

Lemma 13.2.1. *Solutions of* (13.2.2) *of the form*

$$u(t, x) = R(t)\phi(x - ct) \tag{13.2.3}$$

with $\phi\colon \mathbb{R} \to \mathbb{R}^2$ *and*

$$J = \begin{pmatrix} 0 & 1 \\ -1 & 0 \end{pmatrix}, \qquad R(t) = \exp(t\alpha J) = \begin{pmatrix} \cos(\alpha t) & \sin(\alpha t) \\ -\sin(\alpha t) & \cos(\alpha t) \end{pmatrix} \tag{13.2.4}$$

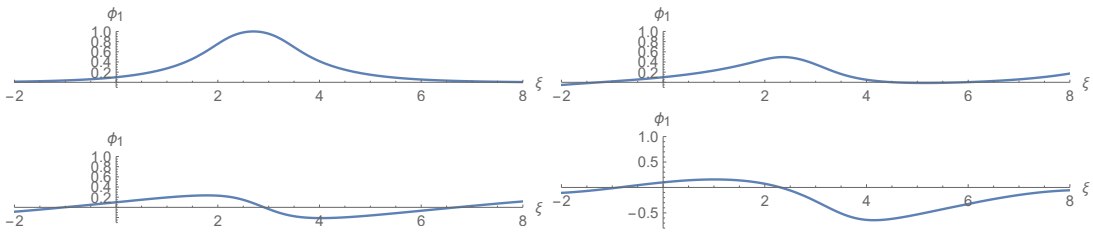

Figure 13.1: Dynamics of the amplitude variable $\phi_1(\xi)$ for $\alpha \in \{0, 0.3, 0.5, 0.7\}$ for the potential $V(a) = -\exp(-(a-1)^2)$ and the wave speed $c = 0.5$.

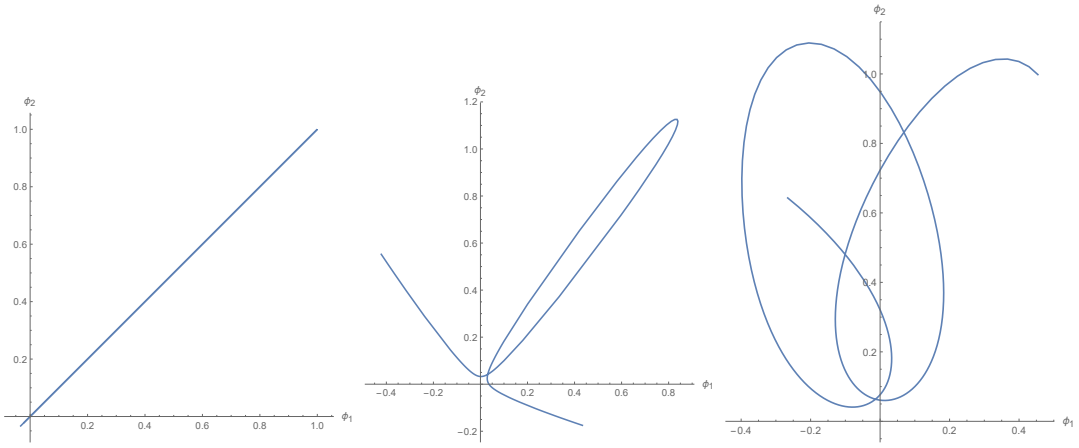

Figure 13.2: Phase portrait of the amplitude variables $\phi_1(\xi)$, $\phi_2(\xi)$ for $\alpha \in \{0, 0.1, 0.6\}$ for the potential $V(a) = -\exp(-(a-1)^2)$, the wave speed $c = 0.5$ and $\xi \in [-5, 10]$.

for $\alpha \in [0, 2\pi)$ *solve the ODE*

$$(\alpha^2 + V'(\langle\phi(\xi), \phi(\xi)\rangle))\phi(\xi) + 2c\alpha J\dot{\phi}(\xi) - (c^2 - 1)\ddot{\phi}(\xi) = 0. \tag{13.2.5}$$

On the other hand, solutions to (13.2.5) *give rise to solutions* $u(t, x) = R(t)\phi(x - ct)$ *of* (13.2.2).

The dynamics of $\phi_1(\xi)$ for different values of α and a sample potential V are displayed in Figure 13.1. Figure 13.2 shows phase plots of $\phi_1(\xi)$ and $\phi_2(\xi)$.

Lemma 13.2.2. *The system of ODEs* (13.2.5) *are the Euler-Lagrange equations to the action functional*

$$S^{\text{sym}}(\phi) = \int L(\phi, \dot{\phi}) \mathrm{d}\xi$$

with

$$L^0(\phi, \dot{\phi}) = \frac{1}{2}\left(\alpha^2\langle\phi, \phi\rangle - 2\alpha c\langle J\phi, \dot{\phi}\rangle + (c^2 - 1)\langle\dot{\phi}, \dot{\phi}\rangle + V(\langle\phi, \phi\rangle)\right). \tag{13.2.6}$$

Remark 13.2.1. Indeed, restricting S to symmetric functions of the form $(t, \xi) \mapsto R(t)\phi(\xi)$ yields the functional S^{sym} from Lemma 13.2.2. This shows that Palais' principle of symmetric criticality (Palais, 1979) is valid in this example, i.e. the critical points of S which are symmetric coincide with the points which are symmetric and critical with respect to symmetric variations. In other words, if u is symmetric and $\mathrm{D}S(u)(v) = 0$ for all symmetric test functions v, then $\mathrm{D}S(u)(v) = 0$ for all test functions v. Here, we assume that S can be defined on a Banach space and D is the Fréchet derivative. The validity of the principle of symmetric criticality also follows directly from Palais, 1979 in an appropriate functional analytic setting using the action of the compact Lie group $(\mathbb{Z}/\frac{2\pi}{\alpha}\mathbb{Z})$ on the domain of definition of S given by $s \cdot u = R(-s)u(t + s, \xi)$. △

Remark 13.2.2. The ODE (13.2.5) admits a Hamiltonian formulation on $\mathbb{R}^4$ equipped with the symplectic structure

$$\mathrm{d}q^1 \wedge \mathrm{d}p_1 + \mathrm{d}q^2 \wedge \mathrm{d}p_2.$$

The Hamiltonian is obtained as the Legendre transformation of the Lagrangian function L^0 defined in (13.2.6) and expressed in the canonical coordinates

$$q = \phi, \qquad p = \nabla_{\dot\phi} L^0 = (c^2 - 1)\dot\phi - c\alpha J\phi. \tag{13.2.7}$$

The Hamiltonian is given as

$$H(q, p) = \frac{1}{2(c^2 - 1)}(\|p\|^2 + 2c\alpha\langle p, Jq\rangle + \alpha^2\|q\|^2 - (c^2 - 1)V(\|q\|^2).$$

△

Remark 13.2.3. The 1-form $L^0(\phi, \dot\phi)\mathrm{d}\xi$ is invariant under the prolongation of the Lie group action of $S^1 \cong \mathbb{R}/(2\pi\mathbb{Z})$ on $\mathbb{R}^2$ defined by $\theta \cdot (\xi, \phi) = (\xi, \exp(\theta J^\top)\phi)$, where exp denotes the matrix exponential as in (13.2.4). By Noether's First Theorem (Mansfield, 2010, §7.2) the quantity

$$I^{\text{dyn}}_{\text{rot}}(\phi, \dot\phi) = \langle \nabla_{\dot\phi} L^0, J^\top\phi\rangle = \alpha c\|\phi\|^2 + (c^2 - 1)\langle J\dot\phi, \phi\rangle$$

is conserved along solutions of (13.2.5). In the canonical coordinates q, p from (13.2.7) the quantity is given as

$$I_{\text{rot}}(q, p) = \langle Jp, q\rangle.$$

Also see Figure 13.3. △

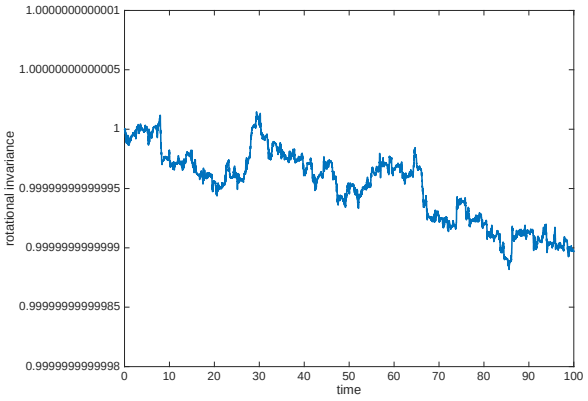

Figure 13.3: Evaluation of the conserved quantity I_{rot} (see Remark 13.2.3) along a numerically computed trajectory shows round-off errors only. Here $V(a) = -\frac{1}{2}a - a^2$, $\alpha = -1$, $c = 2$. The integrator is the symplectic midpoint rule. Implicit equations are solved using fixed point iterations.

13.2.2 5-Point stencil discretisation and modified equation

The 5-point stencil discretisation of (13.2.2) with respect to a mesh $\{(i\Delta t, j\Delta x)\}_{(i,j)\in\mathbb{Z}^2}$ and $u_{i,j}$ corresponding to the value of a function u at the mesh point $(i\Delta t, j\Delta x)$ is given as

$$0 = \frac{1}{\Delta t^2}\left(u_{i-1,j} - 2u_{i,j} + u_{i+1,j}\right) - \frac{1}{\Delta x^2}\left(u_{i,j-1} - 2u_{i,j} + u_{i,j+1}\right) - V'(\langle u_{i,j}, u_{i,j}\rangle)u_{i,j}. \tag{13.2.8}$$

The scheme is multisymplectic. It arises via a discretisation of the continuous action S as the following lemma shows.

Lemma 13.2.3. *A discrete solution $u_\Delta = (u_{i,j})_{i,j\in\mathbb{Z}}$ satisfies (13.2.8) if and only if for all $K \in \mathbb{N}$ it extremises*

$$S_\Delta^K(u) = \sum_{i,j=-K}^{K} \frac{\|u_{i-1,j} - u_{i,j}\|^2}{\Delta t^2} - \frac{\|u_{i,j-1} - u_{i,j}\|^2}{\Delta x^2} - V(\|u_{i,j}\|^2)$$

on all interior grid-point, i.e. $\nabla_{(u_{i,j})_{-K+1\le i,j\le K-1}} S_\Delta^K(u) = 0$.

For further analysis we consider the following functional equation arising from the stencil.

$$
\begin{aligned}
0 = & \frac{1}{\Delta t^2}\left(u(t-\Delta t,x) - 2u(t,x) + u(t+\Delta t,x)\right) \\
& - \frac{1}{\Delta x^2}\left(u(t,x-\Delta x) - 2u(t,x) + u(t,x+\Delta x)\right) \\
& - V'(\langle u(t,x), u(t,x)\rangle)u(t,x)
\end{aligned}
\tag{13.2.9}
$$

The ansatz for a symmetric solution from (13.2.3), i.e. $u(t,x) = R(t)\phi(x-ct)$ with $\xi = x - ct$ in (13.2.9) leads to the following functional equation for ϕ

$$
\begin{aligned}
0 = & \frac{1}{h^2\Delta t^2}\left(R(-\Delta t)\phi(\xi + c\Delta t) - 2\phi(\xi) + R(\Delta t)\phi(\xi - c\Delta t)\right) \\
& - \frac{1}{h^2\Delta x^2}\left(\phi(\xi+\Delta x) - 2\phi(\xi) + \phi(\xi - \Delta x)\right) \\
& - V'(\langle \phi(\xi), \phi(\xi)\rangle)\phi(\xi).
\end{aligned}
\tag{13.2.10}
$$

We have introduced the formal series variable h to the same power as the discretisation parameters. A series expansion of (13.2.10) around $h = 0$ followed by solving for $\ddot{\phi}$ in terms of ϕ, $\dot{\phi}$ and higher order terms yields a formal power series of the form

$$
\begin{aligned}
\ddot{\phi}(\xi) = & \frac{(\alpha^2 + V'(\langle\phi(\xi),\phi(\xi)\rangle))\phi(\xi) + 2c\alpha J\dot{\phi}(\xi)}{c^2-1} \\
& + h^2 g_2(\phi^{(4)}(\xi), \ldots, \dot{\phi}(\xi), \phi(\xi)) \\
& + h^4 g_4(\phi^{(6)}(\xi), \ldots, \dot{\phi(\xi)}, \phi(\xi)) \\
& + \ldots
\end{aligned}
\tag{13.2.11}
$$

Using this formula to replace $\ddot{\phi}$ and all higher derivatives on the right-hand side of (13.2.11) makes second order derivatives only occur in h^4 and higher order terms. Repeating this process iteratively we can push derivatives of order greater than 2 to $\mathcal{O}(h^r)$ terms for arbitrary r. We obtain a formal series of the form

$$
\ddot{\phi}(\xi) = \frac{(\alpha^2 + V'(\langle\phi(\xi),\phi(\xi)\rangle))\phi(\xi) + 2c\alpha J\dot{\phi}(\xi)}{c^2-1} + \sum_{j=2}^{\infty} h^{2j}\hat{g}_{2j}(\dot{\phi}(\xi),\phi(\xi)). \tag{13.2.12}
$$

The second order term is reported in Appendix B.1. Refer to Offen, 2020b for source code. The dependence of the dynamics of the amplitude variable $\phi_1(\xi)$ on Δx of a truncation of the modified equation is illustrated in Figure 13.4 for sample data.

13.3 Structure of modified equation

In this section, we will prove the following theorem.

Theorem 13.3.1. *For $\alpha = 0$ the series (13.2.12) arises as the Euler-Lagrange equation*

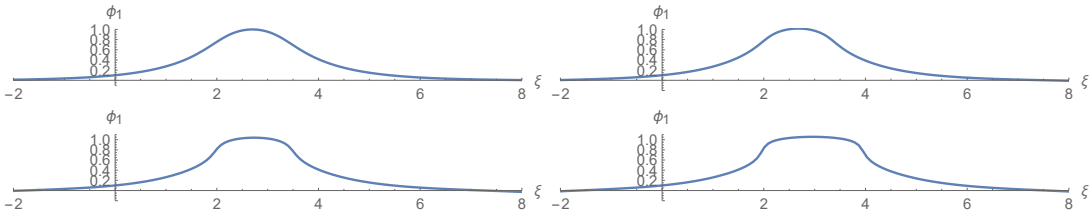

Figure 13.4: Dynamics of the amplitude variable $\phi_1(\xi)$ for $\alpha = 0$, $V(a) = -\exp(-(a-1)^2)$, $c = 0.5$ and $\Delta x \in \{0, 0.6, 1, 1.2\}$ for the modified equation truncated after $\mathcal{O}(h^3)$ terms.

of the formal series

$$L(\phi, \dot{\phi}) = L^0(\phi, \dot{\phi}) + h^2 L^2(\phi, \dot{\phi}) + h^4 L^2(\phi, \dot{\phi}) + \dots,$$

where $L^0(\phi, \dot{\phi})$ *is given as the Lagrangian of the action* S^{sym} *from Lemma 13.2.2.*

The theorem also holds if the potential $V(\|u\|^2)$ is consistently replaced in our derivation by a more general potential $W(u)$, where u is allowed to be $\mathbb{R}^k$-valued for $k \in \mathbb{N}$. However, we present the theory for $W(u) = \frac{1}{2}V(\|u\|^2)$ to compare the rotating case $\alpha \neq 0$ and the non-rotating case $\alpha = 0$.

13.3.1 Relation to linear multi-step methods

To prepare the proof of Theorem 13.3.1, let us recall some definitions for linear multi-step methods. For an introduction see Hairer, Wanner, and Lubich, 2006, for instance.

Definition 13.3.1 (linear multi-step formula for Newton's equation)**.** A *linear N-step formula for Newtons equation* $\ddot{y} = f(y)$ on $\mathbb{K}^n$ with $\mathbb{K} \in \{\mathbb{R}, \mathbb{C}\}$ is given by the formula

$$\sum_{i=0}^{N} a_i y_{i+j} = \Delta s^2 \sum_{i=0}^{N} b_i f(y_{i+j}), \tag{13.3.1}$$

where $a_j, b_j \in \mathbb{R}$, Δs is a discretisation parameter and $\{y_i\}_{i\in\mathbb{Z}}$ is a sequence in $\mathbb{K}^n$. △

Definition 13.3.2 (characteristic polynomials)**.** Given a linear multi-step formula (13.3.1) the polynomials

$$\rho(\tau) = \sum_{i=0}^{N} a_i \tau^i, \qquad \sigma(\tau) = \sum_{i=0}^{N} b_i \tau^i$$

are called *characteristic polynomials of the linear multi-step formula.* △

Remark 13.3.1. The formula (13.3.1) can be written as $\rho(e^D)\hat{y} = \Delta s^2 \sigma(e^D) f(\hat{y})$, where e^D is the shift operator and $\hat{y}$ is the sequence $\{y_i\}_{i\in\mathbb{Z}}$. △

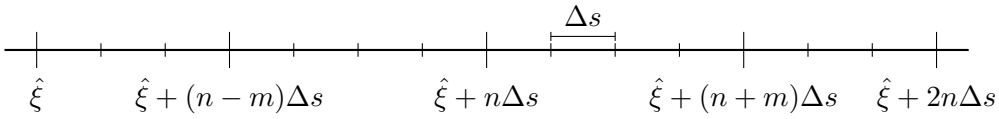

Figure 13.5: Illustration of the multi-step formula described in Lemma 13.3.2. The variable $\hat{\xi}$ corresponds to $\xi - c\Delta t$ when comparing with (13.2.10).

Definition 13.3.3 (order of a linear multi-step formula for Newton's equation)**.** A multi-step formula has order p if its characteristic polynomials ρ and σ satisfy

$$\rho(e^{\Delta s}) - \Delta s^2 \sigma(e^{\Delta s}) = \mathcal{O}(\Delta s^{p+2})$$

as Δs tends to 0. △

Definition 13.3.4 (symmetric linear multi-step formula for Newtons equation)**.** The multi-step formula (13.3.1) is *symmetric* if

$$a_{N-j} = a_j, \qquad b_{N-j} = b_j, \qquad 0 \leq j \leq N. \qquad \triangle$$

Definition 13.3.5 (linear multi-step method for Newton's equation)**.** A linear multi-step method for Newton's equation is a linear multi-step formula together with a starting procedure. More precisely, a linear multi-step method corresponding to a linear multi-step formula (13.3.1) of order p assigns ODEs $\ddot{y} = f(y)$ on $\mathbb{K}^n$ to maps

$$\Lambda \colon (0, \infty) \times \mathbb{K}^n \times \mathbb{K}^n \to (\mathbb{K}^n)^{\mathbb{N}}, \qquad \Lambda(\Delta s, y, y') = (y_j)_{j \in \mathbb{N}}.$$

The sequence $(y_j)_{j \in \mathbb{N}}$ is required to fulfil the multi-step formula (13.3.1). Moreover, $y_0 = y$ and for $0 < j < N$ the start values $y_1, \ldots, y_{N-1}$ approximates the exact flow[1]. △

Remark 13.3.2. To a sequence (y_n) computed using a linear multi-step method for Newton's equation of order p approximations of velocity values can be obtained using a finite difference approximation of the derivative $\frac{\mathrm{d}y}{\mathrm{d}t}$ of order p in terms of the values (y_n). These can be computed a posteriori. Provided $\tau = 1$ is a single root of ρ, the linear multi-step method together with the velocity approximation gives rise to an *underlying P-series method*, i.e. a (formal) P-series describing a map $\mathbb{K}^n \times \mathbb{K}^n \to \mathbb{K}^n \times \mathbb{K}^n$ such that the first component of its iteration fulfils the multi-step formula in the sense of formal power series (Hairer, Wanner, and Lubich, 2006). △

[1] See Hairer and Lubich, 2004, §1 for minimal requirements.

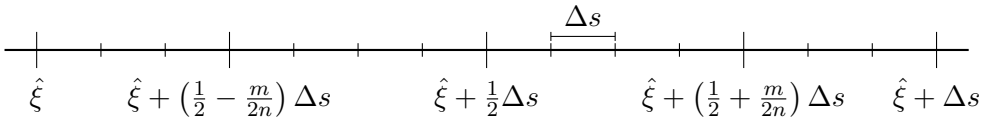

Figure 13.6: Illustration of the multi-step formula described in Lemma 13.3.2 with fractional steps as described in Remark 13.3.4. The variable $\hat{\xi}$ corresponds to $\xi - c\Delta t$ when comparing with (13.2.10). Moreover, notice that $\frac{m}{n} = \frac{\Delta x}{c\Delta t}$. In an appropriate form, we can extend the multi-step formulas to the case that $\frac{\Delta x}{c\Delta t}$ is irrational.

Lemma 13.3.2. *Assume that* $\frac{c\Delta t}{\Delta x} = \frac{n}{m}$ *with* $n, m \in \mathbb{N}$ *such that* n *and* m *do not have common divisors. Moreover, without loss of generality* $n \geq m$*. If* $\alpha = 0$ *in the definition of* R *from* (13.2.4)*, then the stencil* (13.2.10) *coincides with the multi-step formula defined by the characteristic polynomials*

$$\rho(\tau) = \frac{c^2}{n^2} - \frac{1}{m^2}\tau^{n-m} + 2\left(\frac{1}{m^2} - \frac{c^2}{n^2}\right)\tau^n - \frac{1}{m^2}\tau^{n+m} + \frac{c^2}{n^2}\tau^{2n}$$
$$\sigma(\tau) = \tau^n.$$

where $\Delta s = \frac{\Delta x}{m} = \frac{c\Delta t}{n}$*. The formula is symmetric, of order 2 and the multi-step formula involves* $2n$*-steps. See Figure 13.5 for an illustration.*

Proof. One can verify that $\rho(e^D)\phi = \Delta s^2 \sigma(e^D) V'(\|\phi\|^2)\phi$ is equivalent to (13.2.10). □

Remark 13.3.3. Even for the case $\alpha \neq 0$ we can formally recover (13.2.10) as $\rho(e^D)\phi = \Delta s^2 \sigma(e^D) V'(\|\phi\|^2)\phi$ if we allow the coefficients of ρ to be matrix valued (or, alternatively, complex valued if we identify $\mathbb{R}^2$ with $\mathbb{C}$). We obtain

$$\rho(\tau) = \frac{c^2}{n^2}R(\Delta t) - \frac{1}{m^2}\tau^{n-m} + 2\left(\frac{1}{m^2} - \frac{c^2}{n^2}\right)\tau^n - \frac{1}{m^2}\tau^{n+m} + \frac{c^2}{n^2}R(-\Delta t)\tau^{2n}$$

and $\sigma(\tau) = \tau^n$. In comparison to Lemma 13.3.2 the symmetry is destroyed. △

Remark 13.3.4. The characteristic functions ρ and σ correspond to a stencil with $2n$ steps as illustrated in Figure 13.5. We can reinterpret the formula as consisting of only 1 step which is made up of several fractional steps (see Figure 13.6). This guides us to considering the non-polynomial characteristic functions

$$\begin{aligned}\rho(\tau) = {} & 4c^2 R(\Delta t) - 4\frac{c^2\Delta t^2}{\Delta x^2}\tau^{\frac{1}{2} - \frac{\Delta x}{2c\Delta t}} + 8\left(\frac{c^2\Delta t^2}{\Delta x^2} - c^2\right)\tau^{\frac{1}{2}} \\ & - 4\frac{c^2\Delta t^2}{\Delta x^2}\tau^{\frac{1}{2} + \frac{\Delta x}{2c\Delta t}} + 4c^2 R(-\Delta t)\tau \\ \sigma(\tau) = {} & \tau^{\frac{1}{2}}\end{aligned}$$

where the stencil (13.2.10) can be recovered as $\rho(e^D)\phi = \Delta s^2\sigma(e^D)V'(\|\phi\|^2)\phi$. Here the step size Δs is given as $\Delta s = 2c\Delta t$. This formula does not depend on n or m and is also valid for irrational quotients $\frac{c\Delta t}{\Delta x}$. Moreover, the coefficients are symmetric if $\alpha = 0$. △

13.3.2 Proof of Theorem 13.3.1 and further remarks

Proof of Theorem 13.3.1. By Lemma 13.3.2 the functional equation (13.2.10) is given as $\rho(e^D)\phi = \Delta s^2\sigma(e^D)\phi$, where ρ and σ are characteristic polynomials of a symmetric linear multi-step method if $\alpha = 0$ in the definition of R from (13.2.4). As seen in Remark 13.3.4 the characteristic functions ρ and ϕ can also be well defined for irrational quotients $\frac{c\Delta t}{\Delta x}$. They are symmetric and vary smoothly in $\frac{c\Delta t}{\Delta x}$. By Chartier, Faou, and Murua, 2006 (see especially corollary 3 in §5) the underlying P-series method is formally conjugate to a P-series method which is symplectic for all equations of the form $\ddot{\phi} = \nabla W(\phi)$. Chosing $W(\phi) = V(\langle\phi,\phi\rangle)$ this means that the flow map of (13.2.12) is locally Hamiltonian with respect to a modified symplectic structure. Therefore, (13.2.12) is variational. □

Remark 13.3.5. It is clear from the proof of Theorem 13.3.1 that the Lagrangian L is itself a P-series in W with the potential $W(\phi) = \frac{1}{2}V(\langle\phi,\phi\rangle)$. For more information on P-series see Hairer, Lubich, and Wanner, 2013, Ch. III.2.1, for instance. △

Remark 13.3.6. Theorem 13.3.1 and related Lemmas have been stated for rotational-symmetric potentials to allow an easy comparison of rotating and non-rotating travelling waves. Indeed, Theorem 13.3.1 also holds for a general non-rotational symmetric potentials W and higher dimensions, i.e. travelling waves of the modified equation for $u_{tt} - u_{xx} - \nabla W(u)$ for $\mathbb{R}^k$ valued maps u with respect to the 5-point stencil are governed by a first-order variational principle. They arise as Euler-Lagrange equations and the Lagrangian is given as a formal P-series in W. △

The proof of Theorem 13.3.1 works because the mesh and the travelling waves (with $\alpha = 0$) are both invariant under translation symmetries. This allows us to formulate the following corollary of Theorem 13.3.1.

Corollary 13.3.3. *If we consider the following amended 5-point stencil*

$$\begin{aligned} 0 = &\frac{1}{\Delta t^2}\left(R(\Delta t)u_{i-1,j} - 2u_{i,j} + R(-\Delta t)u_{i+1,j}\right) \\ &- \frac{1}{\Delta x^2}\left(u_{i,j-1} - 2u_{i,j} + u_{i,j+1}\right) - V'(\langle u_{i,j}, u_{i,j}\rangle)u_{i,j}. \end{aligned} \tag{13.3.2}$$

for a fixed $\alpha \in [0, 2\pi)$, then rotating travelling waves of the form (13.2.3), i.e. $u(t,x) = R(t)\phi(x - ct)$, are governed by a 1st order variational principle, where the Lagrangian is a formal P-series.

13.4 Computational example

We make the following ansatz for L

$$L(\phi, \dot{\phi}) = L^0(\phi, \dot{\phi}) + h^2 L^2(\phi, \dot{\phi}) + h^4 L^4(\phi, \dot{\phi}) + h^6 L^6(\phi, \dot{\phi}) + \mathcal{O}(h^8) \tag{13.4.1}$$

with

$$L^0 = \frac{1}{2}\left(\alpha^2\langle\phi,\phi\rangle - 2\alpha c\langle J\phi, \dot{\phi}\rangle + (c^2-1)\langle\dot{\phi},\dot{\phi}\rangle + V(\langle\phi,\phi\rangle)\right).$$

and L given as a P-series in $W(\phi) = \frac{1}{2}V(\langle\phi,\phi\rangle)$ (Remark 13.3.5). Since P-series are related to bicoloured trees (see Hairer, Lubich, and Wanner, 2013, Ch. III.2.1), we can obtain an ansatz for L^j by constructing all trees with black and white nodes such that the sum of the degrees of all black nodes is j. White nodes are required to be of degree 1. The trees can then be translated into expression involving the derivatives of W (black nodes) and the terms ϕ_i with $i \in \{1, 2\}$ (white nodes). The second order trees are given as

The first tree corresponds to

$$\sum_{i=1}^{2} \frac{\partial^i W}{\partial \phi_i} \frac{\partial^i W}{\partial \phi_i} = \left(W^{(0,1)}\right)^2 + \left(W^{(1,0)}\right)^2.$$

Here and in the following $W^{(s,t)} = \frac{\partial^{s+t} W}{\partial \phi_1^s \partial \phi_2^t}$. The second tree corresponds to the term

$$\sum_{i,j=1}^{2} \frac{\partial^2 W}{\partial \phi_i \partial \phi_j} \dot{\phi}_i \dot{\phi}_j = 2W^{(1,1)}\dot{\phi}_1\dot{\phi}_2 + W^{(2,0)}\left(\dot{\phi}_1\right)^2 + W^{(0,2)}\left(\dot{\phi}_2\right)^2.$$

We obtain the ansatz

$$\begin{aligned} L^2 = a(2,1)&\left(\left(W^{(0,1)}\right)^2 + \left(W^{(1,0)}\right)^2\right) \\ &+ a(2,2)\left(2W^{(1,1)}\dot{\phi}_1\dot{\phi}_2 + W^{(2,0)}\left(\dot{\phi}_1\right)^2 + W^{(0,2)}\left(\dot{\phi}_2\right)^2\right). \end{aligned}$$

There are four order 4 trees given as

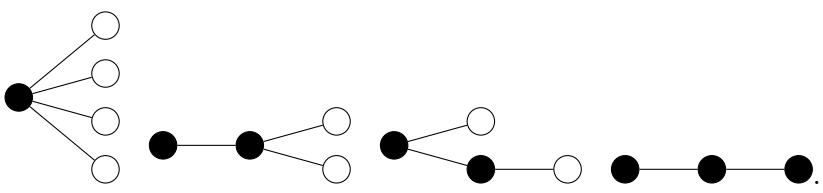

They correspond to the following terms

$$\sum_{i,j=1}^{2} \frac{\partial^4 W}{\partial\phi_i\partial\phi_j\partial\phi_k\partial\phi_l}\dot\phi_i\dot\phi_j\dot\phi_k\dot\phi_l, \quad \sum_{i,j=1}^{2} \frac{\partial W}{\partial\phi_i}\frac{\partial^3 W}{\partial\phi_i\partial\phi_j\partial\phi_k}\dot\phi_j\dot\phi_k,$$

$$\sum_{i,j=1}^{2} \frac{\partial^2 W}{\partial\phi_i\partial\phi_j}\dot\phi_i\frac{\partial^2 W}{\partial\phi_j\phi_k}\dot\phi_k, \quad \sum_{i,j=1}^{2} \frac{\partial W}{\partial\phi_i}\frac{\partial^2 W}{\partial\phi_i\partial\phi_j}\frac{\partial W}{\partial\phi_j}.$$

This leads to the following ansatz.

$$\begin{aligned}
L^4 = a(4,1)\Big(&4W^{(3,1)}\left(\dot\phi_1\right)^3\dot\phi_2 + 6W^{(2,2)}\left(\dot\phi_1\right)^2\left(\dot\phi_2\right)^2 \\
+ \quad &4W^{(1,3)}\dot\phi_1\left(\dot\phi_2\right)^3 + W^{(4,0)}\left(\dot\phi_1\right)^4 + W^{(0,4)}\left(\dot\phi_2\right)^4\Big) \\
+ a(4,2)\Big(&2W^{(0,1)}W^{(1,2)}\dot\phi_1\dot\phi_2 + 2W^{(1,0)}W^{(2,1)}\dot\phi_1\dot\phi_2 + W^{(0,1)}W^{(2,1)}\left(\dot\phi_1\right)^2 \\
+ \quad &W^{(1,0)}W^{(3,0)}\left(\dot\phi_1\right)^2 + W^{(0,1)}W^{(0,3)}\left(\dot\phi_2\right)^2 + W^{(1,0)}W^{(1,2)}\left(\dot\phi_2\right)^2\Big) \\
+ a(4,3)\Big(&2W^{(1,1)}W^{(0,2)}\dot\phi_1\dot\phi_2 + 2W^{(1,1)}W^{(2,0)}\dot\phi_1\dot\phi_2 + \left(W^{(1,1)}\right)^2\left(\dot\phi_1\right)^2 \\
+ \quad &\left(W^{(2,0)}\right)^2\left(\dot\phi_1\right)^2 + \left(W^{(0,2)}\right)^2\left(\dot\phi_2\right)^2 + \left(W^{(1,1)}\right)^2\left(\dot\phi_2\right)^2\Big) \\
+ a(4,4)\Big(&W^{(0,2)}\left(W^{(0,1)}\right)^2 + 2W^{(1,0)}W^{(1,1)}W^{(0,1)} + \left(W^{(1,0)}\right)^2 W^{(2,0)}\Big)
\end{aligned}$$

There are 10 order 6 trees which we list below.

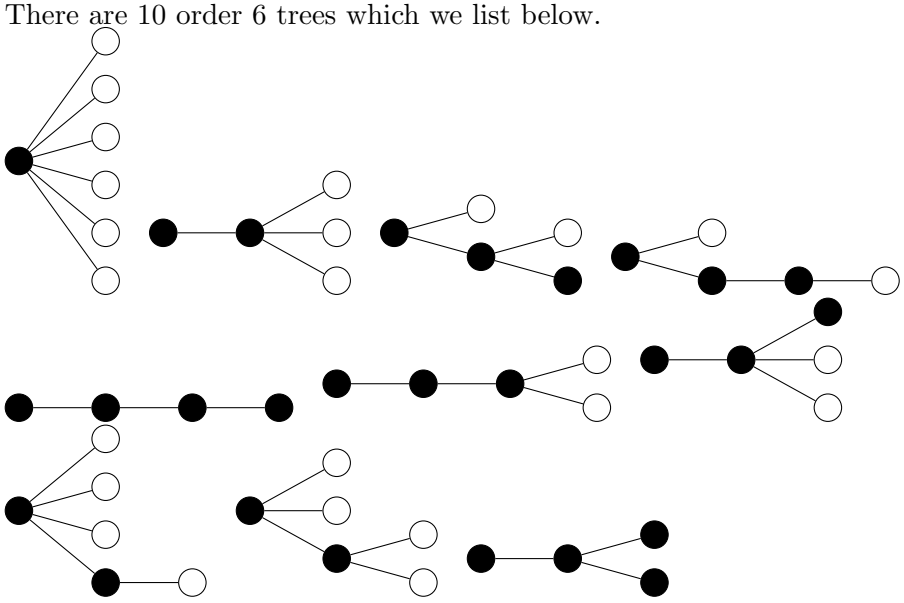

The corresponding expression for L^6 can be found in Appendix B.2. We compute the Euler-Lagrange equations for the ansatz and solve for $\ddot\phi(\xi)$ using a series ansatz.

Comparing coefficients with (13.2.12) yields $\alpha = 0$ and

$$
\begin{aligned}
a(2,1) &= \frac{c^4\Delta t^2 - \Delta x^2}{24\left(c^2-1\right)^2} \\
a(2,2) &= \frac{c^4\Delta t^2 - \Delta x^2}{12\left(c^2-1\right)} \\
a(4,1) &= \frac{-3\Delta t^4c^8 - 2\Delta t^4c^6 + 10\Delta t^2\Delta x^2c^4 - 2\Delta x^4c^2 - 3\Delta x^4}{2160\left(c^2-1\right)^2} \\
a(4,2) &= \frac{-3\Delta t^4c^8 - 2\Delta t^4c^6 + 10\Delta t^2\Delta x^2c^4 - 2\Delta x^4c^2 - 3\Delta x^4}{360\left(c^2-1\right)^3} \\
a(4,3) &= \frac{-2\Delta t^4c^8 - 3\Delta t^4c^6 + 10\Delta t^2\Delta x^2c^4 - 3\Delta x^4c^2 - 2\Delta x^4}{720\left(c^2-1\right)^3} \\
a(4,4) &= \frac{-3\Delta t^4c^8 - 2\Delta t^4c^6 + 10\Delta t^2\Delta x^2c^4 - 2\Delta x^4c^2 - 3\Delta x^4}{720\left(c^2-1\right)^4}
\end{aligned}
$$

$$
\begin{aligned}
a(6,1) &= \frac{10\Delta t^6c^{12} + 22\Delta t^6c^{10} + 3\Delta t^6c^8 - 77\Delta t^4\Delta x^2c^8 + 28\Delta t^2\Delta x^4c^6 - 28\Delta t^4\Delta x^2c^6 - 3\Delta x^6c^4 + 77\Delta t^2\Delta x^4c^4 - 22\Delta x^6c^2 - 10\Delta x^6}{302400\left(c^2-1\right)^3} \\
a(6,2) &= \frac{10\Delta t^6c^{12} + 22\Delta t^6c^{10} + 3\Delta t^6c^8 - 77\Delta t^4\Delta x^2c^8 + 28\Delta t^2\Delta x^4c^6 - 28\Delta t^4\Delta x^2c^6 - 3\Delta x^6c^4 + 77\Delta t^2\Delta x^4c^4 - 22\Delta x^6c^2 - 10\Delta x^6}{5040\left(c^2-1\right)^5} \\
a(6,3) &= \frac{10\Delta t^6c^{12} + 22\Delta t^6c^{10} + 3\Delta t^6c^8 - 77\Delta t^4\Delta x^2c^8 + 28\Delta t^2\Delta x^4c^6 - 28\Delta t^4\Delta x^2c^6 - 3\Delta x^6c^4 + 77\Delta t^2\Delta x^4c^4 - 22\Delta x^6c^2 - 10\Delta x^6}{30240\left(c^2-1\right)^5} \\
a(6,4) &= \frac{72\Delta t^6c^{12} + 94\Delta t^6c^{10} + 9\Delta t^6c^8 - 413\Delta t^4\Delta x^2c^8 + 112\Delta t^2\Delta x^4c^6 - 112\Delta t^4\Delta x^2c^6 - 9\Delta x^6c^4 + 413\Delta t^2\Delta x^4c^4 - 94\Delta x^6c^2 - 72\Delta x^6}{120960\left(c^2-1\right)^6} \\
a(6,5) &= \frac{72\Delta t^6c^{12} + 94\Delta t^6c^{10} + 9\Delta t^6c^8 - 413\Delta t^4\Delta x^2c^8 + 112\Delta t^2\Delta x^4c^6 - 112\Delta t^4\Delta x^2c^6 - 9\Delta x^6c^4 + 413\Delta t^2\Delta x^4c^4 - 94\Delta x^6c^2 - 72\Delta x^6}{60480\left(c^2-1\right)^5} \\
a(6,6) &= \frac{10\Delta t^6c^{12} + 22\Delta t^6c^{10} + 3\Delta t^6c^8 - 77\Delta t^4\Delta x^2c^8 + 28\Delta t^2\Delta x^4c^6 - 28\Delta t^4\Delta x^2c^6 - 3\Delta x^6c^4 + 77\Delta t^2\Delta x^4c^4 - 22\Delta x^6c^2 - 10\Delta x^6}{6720\left(c^2-1\right)^5} \\
a(6,7) &= \frac{10\Delta t^6c^{12} + 22\Delta t^6c^{10} + 3\Delta t^6c^8 - 77\Delta t^4\Delta x^2c^8 + 28\Delta t^2\Delta x^4c^6 - 28\Delta t^4\Delta x^2c^6 - 3\Delta x^6c^4 + 77\Delta t^2\Delta x^4c^4 - 22\Delta x^6c^2 - 10\Delta x^6}{15120\left(c^2-1\right)^4} \\
a(6,8) &= \frac{72\Delta t^6c^{12} + 94\Delta t^6c^{10} + 9\Delta t^6c^8 - 413\Delta t^4\Delta x^2c^8 + 112\Delta t^2\Delta x^4c^6 - 112\Delta t^4\Delta x^2c^6 - 9\Delta x^6c^4 + 413\Delta t^2\Delta x^4c^4 - 94\Delta x^6c^2 - 72\Delta x^6}{120960\left(c^2-1\right)^4} \\
a(6,9) &= \frac{10\Delta t^6c^{12} + 22\Delta t^6c^{10} + 3\Delta t^6c^8 - 77\Delta t^4\Delta x^2c^8 + 28\Delta t^2\Delta x^4c^6 - 28\Delta t^4\Delta x^2c^6 - 3\Delta x^6c^4 + 77\Delta t^2\Delta x^4c^4 - 22\Delta x^6c^2 - 10\Delta x^6}{20160\left(c^2-1\right)^4} \\
a(6,10) &= \frac{10\Delta t^6c^{12} + 22\Delta t^6c^{10} + 3\Delta t^6c^8 - 77\Delta t^4\Delta x^2c^8 + 28\Delta t^2\Delta x^4c^6 - 28\Delta t^4\Delta x^2c^6 - 3\Delta x^6c^4 + 77\Delta t^2\Delta x^4c^4 - 22\Delta x^6c^2 - 10\Delta x^6}{20160\left(c^2-1\right)^6}
\end{aligned}
$$

A P-series ansatz allows an (up to moderate orders of h) efficient calculation of the formal series L. Refer to Offen, 2020b for source code.

13.5 Numerical experiments in the rotating case $\alpha \neq 0$

It is not clear whether there exists a variational principle governing (13.2.12) if $\alpha \neq 0$. The assumption that L is a P-series, forces $\alpha = 0$ in the computational example above. Therefore, in any 1st order Lagrangian principle governing (13.2.12) the Lagrangian cannot possibly be given as a P-series if $\alpha \neq 0$. The derivation of L in the case $\alpha = 0$ via symmetric multi-step methods suggests that P-series exhibit symmetries which are broken when $\alpha \neq 0$. Also see Remark 13.3.3.

Figure 13.7 shows a numerical experiment with the modified system truncated after the $O(h^3)$ term with $\alpha = -1$. The experiment suggests that the the Liouville torus of the exact system survives when switching on the discretisation parameters Δx and Δt. Moreover, the quantities H and I_{rot} show oscillatory behaviour rather than linear error growth. This suggests that there are modified quantities which the truncated modified system preserves up to $\mathcal{O}(h^4)$-terms. Indeed, using a polynomial ansatz we can find corrected conserved quantities for general quadratic potentials as well.

The corrected quantity $H_{\text{corrected}}$ of H for a quadratic potential $V(a) = v_1 a + \frac{1}{2} v_2 a^2$ can be found in Appendix B.3. We have also computed the modified quantity for some cubic potentials (rather than for general cubic potentials due to computational complexity). Refer to Offen, 2020b for source code.

The existence of a Hamiltonian system that recovers the modified ODE (13.2.12) up to higher order and for which $H_{\text{mod}} = H_{\text{corrected}} + O(h^4)$ is the Hamiltonian with respect to a modified symplectic structure would explain the good conservation of $H_{\text{corrected}}$ along trajectories of the modified system. Notice that the modified ODE inherits the rotational invariance of the reduced stencil (13.2.10). The conservation of a modification of I_{rot} would follow from Noether's theorem.

Moreover, we are reporting second order terms of modified Lagrangians for general cubic potentials for some special choices of the parameters such as $c = 0$ and $\Delta x = c\Delta t$ in Appendix B.4. These have been computed using a polynomial ansatz for L in h, ϕ and $\dot{\phi}$.

Whether or not the modified ODE (13.2.12) for general α is governed by a variational principle or which other mechanism is causing the structure-preserving behaviour is left to future research.

Remark 13.5.1. The work presented in this chapter has been concluded, see McLachlan and Offen, 2020a. △

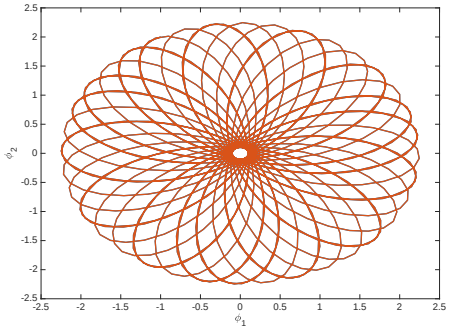

(a) Phaseplot motion in modified system

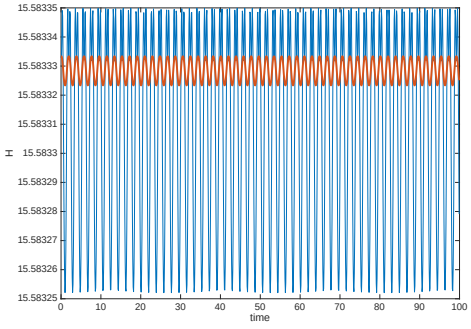

(b) H along motion in exact/modified system

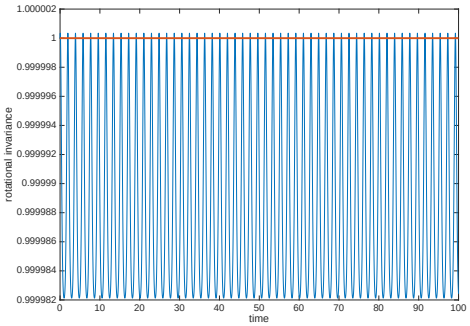

(c) I_{rot} along motion in exact/modified system

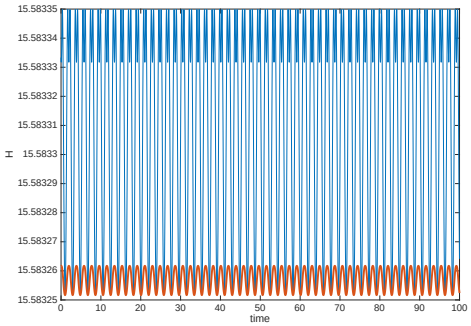

(d) H and $H_{\text{corrected}}$ modified system

Figure 13.7: Numerical integration of the truncated modified ODE (13.2.12) at $\mathcal{O}(h^3)$ with $V(a) = -\frac{1}{2}s - s^2$, $\Delta x = 0.001$, $\Delta t = 0.0012$, $\alpha = -1$, $c = 2$. The phase plot (a) of $(\phi^1(\xi), \phi^2(\xi))$ for $\xi \in [0, 100]$ looks like a Liouville torus in a completely integrable system. This observation persists also if V is of higher degree. (b) While the Hamiltonian H is conserved up to numerical errors on a trajectory of the exact system ($\Delta x = 0 = \Delta t$) it oscillates when evaluated on a trajectory of the truncated modified system. The quantity I_{rot} shows a similar behaviour displayed in (c). The oscillations of H and I_{rot} on trajectories of the modified system in (b) and (c) suggest that H and I_{rot} can be corrected with second order terms to reduce the oscillations. A corrected version of the Hamiltonian is compared to the original Hamiltonian on a trajectory of the modified system in (d).

Chapter 14

Conclusions and open problems

14.1 Catastrophe theory and Hamiltonian boundary value problems

Classical catastrophe theory considers the bifurcation behaviour of critical points of families of scalar valued maps. The central idea is to restrict to phenomena that are stable, i.e. persistent under small perturbations because only persistent phenomena will occur in systems arising from real-world applications. This gives the theory some universal character and the restriction to stable phenomena greatly reduces complexity and allows for meaningful, practical classification results.

In this work we developed a framework which allows us to apply the highly developed techniques and classification results of classical catastrophe theory to boundary value problems which exhibit a Hamiltonian structure and to relate notions of stability. Hamiltonian boundary value problems cover a wide range of problems classes, including boundary value problems in classical mechanics, conjugate loci, and optimal control problems. Moreover, the notion is easily generalised to boundary value problems for symplectic maps or to PDEs with variational structure.

More specifically, in Chapter 6 we introduced the notion of Lagrangian boundary conditions, which cover typical cases such as periodic boundary conditions or boundary conditions that arise from Dirichlet or Neumann problems. The boundary value problems are systematically translated into local intersection problems of Lagrangian submanifolds. This allows the use of techniques from Symplectic Geometry. We showed that Lagrangian boundary value problems modulo local symplectomorphisms correspond to smooth function germs modulo stably right equivalence (Chapters 6 and 10). Thus, classification results of catastrophe theory apply to Lagrangian boundary value problems. We also proved a parameter-dependent version, which is important to analyse bifurcation problems: families of Lagrangian boundary value problems modulo local

symplectomorphisms correspond to unfoldings of smooth function germs modulo stably right equivalence in the sense of catastrophe theory (Theorem 6.3.1). This puts Hamiltonian boundary value problems rigorously into the catastrophe theory setting. Comparing our framework to analysing bifurcations of critical points of action functionals which govern Hamiltonian systems, our geometrical approach is purely finite-dimensional and provides a high degree of flexibility to introduce and analyse different boundary conditions.

While the relation of Lagrangian boundary value problems for symplectic maps with catastrophe theory via Lagrangian intersection problems is well founded and the classification results from classical catastrophe theory are handy to work with, the induced classification of boundary value problems may not be the finest one: local Lagrangian intersection problems are classified up to symplectomorphisms and the classification exactly corresponds to catastrophe theory (Theorems 10.1.3 and 10.1.4). However, Lagrangian intersection problems arising from Lagrangian boundary value problems carry some extra structure. Structure that is ignored in the presented classification is, for instance, the product structure of the ambient manifold and its symplectic form as well as that one of the manifolds is a graph. We believe that there is no essential difference between the two classifications unless, possibly, in very high-codimensional examples or in non-generic systems such as systems with symmetries, fixed boundary conditions, or other restrictions, as there has not been any indication of this in our numerical experiments. Moreover, small perturbations of Lagrangian intersection problems that arise from Lagrangian boundary value problems yield new Lagrangian intersection problems that arise from Lagrangian boundary value problems. Therefore, the notions of topological stability, versality, unfoldings, etc. in the catastrophe theory framework provide reasonable notions for Lagrangian boundary value problems. However, a more detailed analysis would be even more satisfying.

Furthermore, it is of interest to investigate whether the classification of Lagrangian intersection problems can be extended to local isotropic and coisotropic intersection problems. Results in this context could be applied to under- and overdetermined boundary value problems.

Our initial notion of stability for bifurcation phenomena of Hamiltonian boundary value problems allows symmetry destroying perturbations as well as small but arbitrary perturbations of the Lagrangian boundary conditions. In practice, however, families of Hamiltonian boundary value problems might not be in general position in this sense. Therefore, next to a classification of the generic case, in Chapters 7 and 8 we considered the effects of geometric obstructions for the occurrence of singularities of certain important boundary conditions such as separated Lagrangian boundary conditions, which

include those arising from Dirichlet or Neumann problems. We proved that depending on the dimension of the phase space not all catastrophe singularities can occur, in contrast to the case of more general boundary conditions (Propositions 7.1.1 and 7.1.2).

Moreover, we analysed the effect of extra structure on the bifurcation behaviour. In Hamiltonian boundary value problems in completely integrable systems with symmetrically separated Lagrangian boundary conditions we showed that a novel periodic pitchfork bifurcation occurs persistently (Theorem 7.2.1). The bifurcation is related to the generic occurrence of families of Liouville tori in completely integrable Hamiltonian systems rather than a $\mathbb{Z}/2\mathbb{Z}$-symmetry of the Hamiltonian. We also analysed the case of symmetries and time-reversal symmetries as well as conformal symplectic symmetries (Theorem 8.3.2). For instance, we explained within our framework obstructions of the degeneracy of bifurcations in conjugate loci (Proposition 8.3.6) and how certain structurally simple symmetries induce symmetries of the generating function of Lagrangian boundary value problems (Corollaries 7.3.4 and 7.3.8).

In future research it would be interesting to develop a more general framework to analyse the effects of symmetries on the bifurcation behaviour of Hamiltonian boundary value problems as well as to study more examples. Besides, the symplectic structure of the steady states of initial-value problems like in our running example, the Bratu problem (6.1.1), may also be relevant to their stability.

14.2 Preservation of bifurcations under discretisations

In Chapter 9 we investigated implications of the theoretical framework for Hamiltonian boundary value problems for numerical computations of bifurcation diagrams. We proved and demonstrated in numerical examples that symplectic integrators preserve all generic bifurcations of this problem class while non-symplectic integrators break certain generic bifurcations (Propositions 9.2.1 and 9.2.2).

In the singularity theory framework, a Hamiltonian boundary value problem corresponds to a problem of the form $\nabla S_\mu(x) = 0$, where a critical point x of S_μ is sought and μ denotes parameters. The application of a symplectic integrator corresponds to a perturbation of the form $\nabla(S_\mu(x) + \epsilon F_\mu(x)) = 0$ for smooth F_μ and sufficiently small ϵ. This is a perturbation within the class of catastrophe problems. However, a non-symplectic integrator destroys the gradient structure of the problem and corresponds to a perturbation of the form $\nabla(S_\mu(x)) + \epsilon G_\mu(x) = 0$, where G_μ does *not* arise as the gradient of a scalar valued function family. The perturbation does, therefore, not respect the problem structure and some bifurcations become unstable such as D-series bifurcations. Indeed, non-symplectic integrators remove the problem from the catastrophe theory setting and pose them in the setting of general singularity theory for local equidimensional maps, i.e. maps between spaces of the same dimension. Therefore,

only those bifurcations are preserved by non-symplectic integrators which are stable in the problem class of equidimensional maps as well, such as A-series singularities. Intuitively, these singularities do not need the gradient structure to be stable. In contrast, symplectic integrators perturb the problem within the catastrophe theory setting and, therefore, all generic bifurcations are preserved.

While the usefulness of symplectic integration for long-term simulations is well studied and analysed in classical literature, the importance of structure preservation in numerical computations of solutions to boundary value problems had previously not been recognised because boundary value problems are typically posed on intervals of short or moderate length such that the classically known advantages of symplectic integration do not seem to be relevant in this context (Chyba, Hairer, and Vilmart, 2009, §7). Our research highlights that for bifurcation problems of solutions to boundary value problems preservation of symplectic structure can be crucial. Indeed, in contrast to long-term behaviour of numerical solutions the bifurcation behaviour is related to the preservation of symplecticity of the problem itself rather its by-products, namely excellent energy conservation properties and almost conservation of Hamiltonian structure.

14.3 Locating bifurcations

After the classification of persistent bifurcations and investigations into strategies to preserve the bifurcation behaviour under discretisation, we turned to the question how to find the most degenerate, high-codimensional bifurcation points in given parameter-dependent problems. Since high-codimensional bifurcations act as organising centres in bifurcation diagrams, knowing their location is valuable information when investigating mathematical models. However, even if bifurcations are preserved under discretisation it can be computationally challenging to find them, especially in high-dimensional systems arising, for instance, from discretisations of PDEs. Indeed, it is natural to develop strategies that apply to the continuous system and its discretisation alike.

We considered three generalisations of symplectic structure to the setting of PDEs. One of them is differential equations with variational structure (Chapter 11). We showed for this problem class how catastrophe theory can be used to locate high-codimensional bifurcation points. In particular, we derived augmented systems for all A-series bifurcations (Theorem 11.2.2) and employed these in numerical examples to locate a swallowtail bifurcation (codimension 3) in a parameter-dependent variational PDE. The derivations make use of the Infinite-Dimensional Splitting Lemma exploiting the variational structure of the problem. This is to be contrasted with approaches in the existing literature where mostly Lyapunov–Schmidt reduction techniques are used which do not make use of variational structures. The existing literature mostly

considers bifurcations or singularities which are persistent in a wider class of PDEs or nonlinear operators. Within the restricted class of variational problems, however, types of singularities or codimensions of singularities can be different and techniques to derive augmented systems or bifurcation test equations are adapted to the variational setting.

In future research, it would be interesting to develop strategies to locate D-series bifurcations numerically by exploiting the variational structure and to explore relationships to existing results about bifurcations of solutions to PDEs and critical points of operators. Our analysis relies on the validity of the assumptions of the Infinite-Dimensional Splitting Lemma. It would be interesting to understand the cases where these assumptions fail as well as to extend existing highly developed bifurcation continuation software packages like AUTO (Doedel, Champneys, Dercole, et al., 2007) or pde2path (Uecker, Wetzel, and Rademacher, 2014) to the high-codimensional bifurcation analysis considered in this work and to compute higher-dimensional manifolds of solutions or singularities using manifold continuation (Henderson, 2002).

We would like to remark that our example problems, the Hénon-Heiles-type example (Figure 9.3) and the conjugate locus (Figure 9.8), have been set up such that they are easy to compute. Also, the swallowtail bifurcation in Figure 11.5 occurs along a line of lower codimensional bifurcations and could therefore be found by continuing a line of cusps. However, it is not always the case that a curve of lower codimensional singularities connects to a curve of singularities of the next codimension which, itself, connects to a curve of singularities of the next codimension, et cetera, and the highest singular points can be found in this way. This is illustrated in Figure 14.1 for the cusp but applies to the other elementary bifurcations as well. On the other hand, trying to solve the augmented system of high-codimensional singularities directly without having a good initial guess obtained, possibly, from a continuation method, is typically not feasible with standard numerical methods. It would be nice to have a more general technique to locate high-codimensional bifurcations, e.g. using manifold continuation techniques or using more data and hints to guide the continuation method to the most singular points.

14.4 Preservation of Hamiltonian structures in PDEs

While PDEs with variational structure can be understood as generalising ODEs with Hamiltonian structure, another generalisation is to pose Hamiltonian systems on (possibly infinite-dimensional) Poisson manifolds, for instance Lie–Poisson systems. Many differential equations of practical relevance (Euler's incompressible fluid equations, Burgers' equations, rigid body dynamics) can be formulated as Lie–Poisson systems and many of the structure preserving properties of the motions can be understood

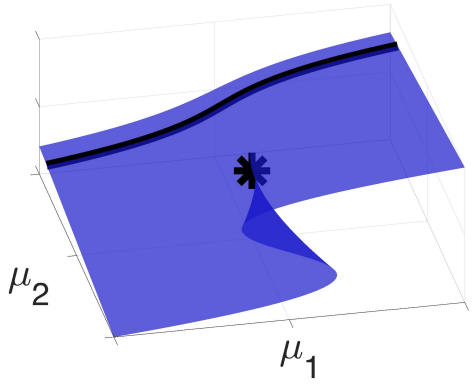

Figure 14.1: Many curves of solutions do not intersect with the curve of fold bifurcations along which a cusp bifurcation occurs. One example is the black, solid curve of solutions which does not come close to fold points or the cusp point marked by an asterisk. This illustrates the problem of finding bifurcations by continuing branches of solutions or lower dimensional bifurcations along just one parameter. The problem occurs for other generic bifurcations in an analogous way because of their geometric structure (see Figures 5.1 and 5.2): near a hyperbolic umbilic singularity, for instance, there are many curves of fold bifurcations which do not connect to higher order bifurcations such as cusps or the hyperbolic umbilic point.

through the preservation of the Poisson structure of the system. This includes, for instance, the conservation of conserved quantities which arise as Casimir functions, i.e. annihilators of the Poisson bracket. Therefore, Poisson structures are of interest for structure preserving numerical integration.

The idea of collective integration is to lift the original system to a Hamiltonian system on a symplectic space on which standard symplectic integration techniques can be applied. In the lifted system, the symplectic structure is closely related to the original Poisson structure via a realisation, which is a map from the lifted system to the original system. In contrast to general methods for constructing integrators for Poisson systems, a carefully chosen realisation can lead to better and simpler integration schemes.[1]

While collective integration techniques have been studied for finite-dimensional Lie–Poisson systems, we demonstrate their potential for infinite-dimensional systems. In Chapter 12 we used Clebsch variables to lift the Lie–Poisson system corresponding to an extended Burgers' equation to a collective Hamiltonian system where we apply symplectic integration techniques and observe excellent energy as well as Casimir conservation properties.

For future research, it is of interest to obtain theoretical results that rigorously explain the excellent preservation of the Casimir as well as to apply the technique to

[1]This is exemplified in McLachlan, Modin, and Verdier, 2014.

other PDEs which admit formulations as Lie–Poisson systems such as the incompressible Euler equations. Moreover, it would be helpful to make the process of realising Hamiltonian Poisson systems as symplectic Hamiltonian systems that are suitable with respect to numerical aspects more automatic and less problem specific.

Another generalisation of Hamiltonian systems on symplectic manifolds, that is relevant for the numerical treatment of PDEs, are multisymplectic systems. While the flow of Hamiltonian ODEs preserves the symplectic structure of the system, in the PDE analogue a conservation law is fulfilled involving a differential 2-form for each spatial-temporal dimension. While the relevance of preserving symplecticity of Hamiltonian ODEs is well understood, we have presented some investigations into the role of preserving multisymplectic conservation laws when discretising multisymplectic PDEs.

An important tool to explain the excellent behaviour of symplectic integrators in long-term simulations is backward error analysis, i.e. the description of the continuous system whose exact solution evaluated at discrete points coincides with the numerical solution. Such a system is called a modified equation. While PDEs do not appear to be accessible to backward error analysis in the way that Hamiltonian ODEs are because the modified equations are defined on larger phase spaces than the original equation, in Chapter 13 we considered symmetric solutions for 1-dimensional symmetry groups of the discretised equations in order to keep using the tools for the ODE setting. For our analysis, we used a variational formulation of multisymplectic PDEs such that solutions are stationary points of action functionals.

Consider the action of a symmetry group. Clearly, if a point is stationary for all variations and is also symmetric then it is also stationary with respect to symmetric variations only. Under certain conditions on the symmetry action the following reverse statement is true: if a symmetric point is stationary for all symmetric variations then it is a solution of the original system, i.e. it is a stationary point of the action functional for all variations. Therefore, the equations obtained by a reduction by the symmetry group are governed by a variational principle as well. This is called Palais' principle of symmetric criticality.

In Chapter 13 we analysed whether multisymplectic integrators preserve a discrete form of Palais' principle. We extended a result by McDonald et al., 2016 and proved that in the multidimensional nonlinear wave equation travelling waves are governed by a first order variational principle in the backward error analysis sense, i.e. the variational structure of the continuous system is preserved (Theorem 13.3.1). More general results in this direction have the potential to shine some light on the role of multisymplecticity for numerical computations as well as to clarify which effects are related to symmetries of the system and which effects are related to the multisymplectic structure itself.

Bibliography

Abbott, J. P. (1978). "An efficient algorithm for the determination of certain bifurcation points". In: *Journal of Computational and Applied Mathematics* 4.1, pp. 19–27.

Adams, R. (1975). *Sobolev spaces*. Pure and applied mathematics; a series of monographs and textbooks; v.65. Academic Press.

Allgower, E. L. and K. Georg (Jan. 2003). *Introduction to Numerical Continuation Methods*. Society for Industrial and Applied Mathematics. DOI: 10.1137/1.9780898719154.

Alnaes, M. S. et al. (Dec. 2015). "The FEniCS Project Version 1.5". In: *Archive of Numerical Software* 3.100, pp. 9–23. DOI: 10.11588/ans.2015.100.20553.

Ambrosetti, A. and G. Prodi (1972). "On the inversion of some differentiable mappings with singularities between Banach spaces". In: *Annali di Matematica Pura ed Applicata* 93.1, pp. 231–246. ISSN: 1618-1891. DOI: 10.1007/BF02412022.

Amodio, P., L. Brugnano, and F. Iavernaro (Aug. 2015). "Energy-conserving methods for Hamiltonian boundary value problems and applications in astrodynamics". In: *Advances in Computational Mathematics* 41.4, pp. 881–905. ISSN: 1572-9044. DOI: 10.1007/s10444-014-9390-z.

Andrews, G. E. (1984). *The Theory of Partitions*. Encyclopedia of Mathematics and its Applications. Cambridge University Press. DOI: 10.1017/CBO9780511608650.

Arnold, D. N. and A. Logg (Nov. 2014). "Periodic Table of the Finite Elements". In: *Archive of Numerical Software* 47.9. URL: http://femtable.org.

Arnold, V. I. (1978). "Critical points of functions on a manifold with boundary, the simple Lie groups B_k, C_k, and F_4 and singularities of evolutes". In: *Russian Mathematical Surveys* 33.5, p. 99. URL: http://stacks.iop.org/0036-0279/33/i=5/a=R04.

— (1989). "Introduction to perturbation theory". In: *Mathematical Methods of Classical Mechanics*. New York, NY: Springer New York, pp. 271–300. ISBN: 978-1-4757-2063-1. DOI: 10.1007/978-1-4757-2063-1_10.

Arnold, V. I., V. V. Goryunov, et al. (1993). "Singularity Theory II Classification and Applications". In: *Dynamical Systems VIII: Singularity Theory II. Applications*. Berlin, Heidelberg: Springer Berlin Heidelberg, pp. 1–235. ISBN: 978-3-662-06798-7. DOI: 10.1007/978-3-662-06798-7_1.

— (1998). "Critical Points of Functions". In: *Singularity Theory I*. Berlin, Heidelberg: Springer Berlin Heidelberg, pp. 10–50. ISBN: 978-3-642-58009-3. DOI: 10.1007/978-3-642-58009-3_1.

Arnold, V. I., S. M. Gusein-Zade, and A. N. Varchenko (1985). *Singularities of Differentiable Maps*. Birkhäuser Boston. DOI: 10.1007/978-1-4612-5154-5.

— (2012). *Singularities of Differentiable Maps, Volume 1*. Birkhäuser Boston. DOI: 10.1007/978-0-8176-8340-5.

Arnold, V. I., E. Khukhro, et al. (2007). *Mathematical Aspects of Classical and Celestial Mechanics*. Encyclopaedia of Mathematical Sciences. Springer Berlin Heidelberg. ISBN: 9783540489269. DOI: 10.1007/978-3-540-48926-9.

Atkinson, K., W. Han, and D. E. Stewart (2011). *Numerical Solution of Ordinary Differential Equations*. Pure and Applied Mathematics: A Wiley Series of Texts, Monographs and Tracts. Wiley. ISBN: 9781118164525.

Baek, J., A. Deopurkar, and K. Redfield (2007). *Finding geodesics on surfaces*. [online]. URL: `http://cs.stanford.edu/people/jbaek/18.821.paper2.pdf`.

Bailey, P. (1968). *Nonlinear Two Point Boundary Value Problems*. Mathematics in Science and Engineering. Elsevier Science. ISBN: 9780080955520.

Bashir-Ali, Z., J. R. Cash, and H. H. M. Silva (Nov. 1998). "Lobatto deferred correction for stiff two-point boundary value problems". In: *Computers and Mathematics with Applications* 36.10-12, pp. 59–69. DOI: `10.1016/s0898-1221(98)80009-6`.

Bates, S. and A. Weinstein (1997). *Lectures on the Geometry of Quantization*. Vol. 8. American Mathematical Society. ISBN: 978-0-8218-0798-9.

Bathe, K.-J. and E. N. Dvorkin (1983). "On the automatic solution of nonlinear finite element equations". In: *Nonlinear Finite Element Analysis and Adina*. Elsevier, pp. 871–879.

Bell, E. T. (1927). "Partition Polynomials". In: *Annals of Mathematics* 29.1/4, pp. 38–46. ISSN: 0003486X. URL: `http://www.jstor.org/stable/1967979`.

Berger, M. S., P. T. Church, and J. G. Timourian (1985). "Folds and Cusps in Banach Spaces, with Applications to Nonlinear Partial Differential Equations. I". In: *Indiana University Mathematics Journal* 34.1, pp. 1–19. ISSN: 00222518, 19435258. URL: `http://www.jstor.org/stable/24893888`.

— (1988). "Folds and Cusps in Banach Spaces with Applications to Nonlinear Partial Differential Equations. II". In: *Transactions of the American Mathematical Society* 307.1, pp. 225–244. ISSN: 00029947. URL: `http://www.jstor.org/stable/2000760`.

Bernfeld, R. and V. Lakshmikantham (1974). *An Introduction to Nonlinear Boundary Value Problems*. Mathematics in Science and Engineering. Elsevier Science. ISBN: 9780080956183.

Beyn, W.-J. (1984). "Defining Equations for Singular Solutions and Numerical Applications". In: *Numerical Methods for Bifurcation Problems*. Birkhäuser Basel, pp. 42–56. DOI: `10.1007/978-3-0348-6256-1_3`.

Beyn, W.-J. and V. Thümmler (2007). "Phase Conditions, Symmetries and PDE Continuation". In: *Numerical Continuation Methods for Dynamical Systems: Path following and boundary value problems*. Dordrecht: Springer Netherlands, pp. 301–330. ISBN: 978-1-4020-6356-5. DOI: `10.1007/978-1-4020-6356-5_10`.

Bhatia, R. and P. Rosenthal (1997). "How and Why to Solve the Operator Equation AX-XB = Y". In: *Bulletin of the London Mathematical Society* 29.1, pp. 1–21. DOI: `10.1112/S0024609396001828`.

Böhmer, K. (1993). "On a numerical Liapunov-Schmidt method for operator equations". In: *Computing* 51, pp. 237–269. DOI: `10.1007/BF02238535`.

Böhmer, W. C. and N. Sassmannshausen (1999). "Numerical Liapunov-Schmidt spectral methods for k-determined problems". In: *Computer Methods in Applied Mechanics and Engineering* 170.3, pp. 277–312. ISSN: 0045-7825. DOI: `https://doi.org/10.1016/S0045-7825(98)00199-6`.

Bolstad, J. H. and H. B. Keller (1986). "A multigrid continuation method for elliptic problems with folds". In: *SIAM J. Sci. and Stat. Comput.* 7.4, pp. 1081–1104. DOI: `10.1137/0907074`.

Brandt, A. (1977). "Multi-Level Adaptive Solutions to Boundary-Value Problems". In: *Mathematics of Computation* 31.138, pp. 333–390. DOI: `10.2307/2006422`.

Brenner, S. C. and L. R. Scott (2008). *The Mathematical Theory of Finite Element Methods*. Springer New York. ISBN: 978-0-387-75934-0. DOI: `10.1007/978-0-387-75934-0`.

Bröcker, T. (1975). *Differentiable Germs and Catastrophes*. London Mathematical Society Lecture Note Series. Cambridge University Press. DOI: `10.1017/CBO9781107325418`.

Brualdi, R. (2004). *Introductory Combinatorics*. Pearson/Prentice Hall. ISBN: 9780131001190.

Brugnano, L., M. Calvo, et al. (2012). "Energy-preserving methods for Poisson systems". In: *Journal of Computational and Applied Mathematics* 236.16, pp. 3890–3904. ISSN: 0377-0427. DOI: 10.1016/j.cam.2012.02.033.

Brugnano, L., F. Iavernaro, and D. Trigiante (2012). "Energy- and quadratic invariants-preserving integrators based upon Gauss collocation formulae". In: *SIAM Journal on Numerical Analysis* 50.6, pp. 2897–2916. ISSN: 00361429. URL: http://www.jstor.org/stable/41820088.

— (2015). "Analysis of Hamiltonian Boundary Value Methods (HBVMs): A class of energy-preserving Runge–Kutta methods for the numerical solution of polynomial Hamiltonian systems". In: *Communications in Nonlinear Science and Numerical Simulation* 20.3, pp. 650–667. ISSN: 1007-5704. DOI: https://doi.org/10.1016/j.cnsns.2014.05.030.

Buchner, M., J. E. Marsden, and S. Schecter (Nov. 1983). "Examples for the Infinite Dimensional Morse Lemma". In: *SIAM Journal on Mathematical Analysis* 14.6, pp. 1045–1055. DOI: 10.1137/0514084.

Butcher, J. C. (2009). "On fifth and sixth order explicit Runge–Kutta methods: order conditions and order barriers". In: *Canadian Applied Mathematics Quarterly* 17.3, pp. 433–445. URL: http://www.math.ualberta.ca/ami/CAMQ/pdf_files/vol_17/17_3/17_3b.pdf.

— (2010). "Trees and numerical methods for ordinary differential equations". In: *Numerical Algorithms* 53.2, pp. 153–170. ISSN: 1572-9265. DOI: 10.1007/s11075-009-9285-0.

Cash, J. R., D. Hollevoet, et al. (Feb. 2013). "Algorithm 927: the Matlab code bvptwp.m for the numerical solution of two point boundary value problems". In: *ACM Transactions on Mathematical Software* 39.2, pp. 1–12. DOI: 10.1145/2427023.2427032.

Cash, J. R. and F. Mazziay (2006). "Hybrid mesh selection algorithms based on conditioning for two-point boundary value problems". In: *Journal of Numerical Analysis, Industrial and Applied Mathematics* 1.1, pp. 81–90. URL: https://www.scopus.com/inward/record.uri?eid=2-s2.0-48349113977&partnerID=40&md5=8b906151d0c2e400de328718f09454ef.

Chang, S.-L., C.-S. Chien, and B.-W. Jeng (2005). "Tracing the solution surface with folds of a two-parameter system". In: *International Journal of Bifurcation and Chaos* 15.08, pp. 2689–2700. DOI: 10.1142/S0218127405013630.

Chartier, P., E. Faou, and A. Murua (June 2006). "An Algebraic Approach to Invariant Preserving Integators: The Case of Quadratic and Hamiltonian Invariants". In: *Numerische Mathematik* 103.4, pp. 575–590. ISSN: 0945-3245. DOI: 10.1007/s00211-006-0003-8.

Chern, A. et al. (2016). "Schrödinger's smoke". In: *ACM Transactions on Graphics (TOG)* 35.4, p. 77. DOI: 10.1145/2897824.2925868.

Church, P. T., E. N. Dancer, and J. G. Timourian (1993). "The Structure of a Nonlinear Elliptic Operator". In: *Transactions of the American Mathematical Society* 338.1, pp. 1–42. ISSN: 00029947. URL: http://www.jstor.org/stable/2154442.

Church, P. T. and J. G. Timourian (1992). "Global fold maps in differential and integral equations". In: *Nonlinear Analysis: Theory, Methods & Applications* 18.8, pp. 743–758. ISSN: 0362-546X. DOI: 10.1016/0362-546X(92)90169-F.

— (1993). "Global cusp maps in differential and integral equations". In: *Nonlinear Analysis: Theory, Methods & Applications* 20.11, pp. 1319–1343. ISSN: 0362-546X. DOI: 10.1016/0362-546X(93)90134-E.

Chyba, M., E. Hairer, and G. Vilmart (2009). "The role of symplectic integrators in optimal control". In: *Optimal Control Applications and Methods* 30.4, pp. 367–382. DOI: 10.1002/oca.855. eprint: https://onlinelibrary.wiley.com/doi/pdf/10.1002/oca.855.

Ciriza, E. and J. Pejsachowicz (2000). "A Bifurcation Theorem for Lagrangian Intersections". In: *Recent Trends in Nonlinear Analysis: Festschrift Dedicated to Alfonso Vignoli on the Occasion of His*

Sixtieth Birthday. Basel: Birkhäuser Basel, pp. 105–115. ISBN: 978-3-0348-8411-2. DOI: 10.1007/978-3-0348-8411-2_12.

Cohen, D. and E. Hairer (Mar. 2011). "Linear energy-preserving integrators for Poisson systems". In: *BIT Numerical Mathematics* 51.1, pp. 91–101. ISSN: 1572-9125. DOI: 10.1007/s10543-011-0310-z.

Cotter, C. J., D. D. Holm, and P. E. Hydon (2007). "Multisymplectic formulation of fluid dynamics using the inverse map". In: *Proceedings of the Royal Society A: Mathematical, Physical and Engineering Sciences* 463.2086, pp. 2671–2687. DOI: 10.1098/rspa.2007.1892.

Crisfield, M. (1981). "A fast incremental/iterative solution procedure that handles "snap-through"". In: *Computational Methods in Nonlinear Structural and Solid Mechanics*. Elsevier, pp. 55–62. DOI: 10.1016/b978-0-08-027299-3.50009-1.

Dahlby, M., B. Owren, and T. Yaguchi (2011). "Preserving multiple first integrals by discrete gradients". In: *Journal of Physics A: Mathematical and Theoretical* 44.30, p. 305205. URL: http://stacks.iop.org/1751-8121/44/i=30/a=305205.

Demazure, M. (2000). *Bifurcations and Catastrophes*. Springer Berlin Heidelberg. DOI: 10.1007/978-3-642-57134-3.

Deuflhard, P. (2011). "Parameter Dependent Systems: Continuation Methods". In: *Newton Methods for Nonlinear Problems: Affine Invariance and Adaptive Algorithms*. Berlin, Heidelberg: Springer Berlin Heidelberg, pp. 233–282. ISBN: 978-3-642-23899-4. DOI: 10.1007/978-3-642-23899-4_5.

Dhooge, A., W. Govaerts, and Y. A. Kuznetsov (June 2003). "MATCONT: A Matlab Package for Numerical Bifurcation Analysis of ODEs". In: *ACM Trans. Math. Softw.* 29.2, pp. 141–164. ISSN: 0098-3500. DOI: 10.1145/779359.779362.

Dhooge, A., W. Govaerts, Y. A. Kuznetsov, et al. (2003). "CL_MATCONT: A Continuation Toolbox in Matlab". In: *Proceedings of the 2003 ACM Symposium on Applied Computing*. SAC '03. Melbourne, Florida: ACM, pp. 161–166. ISBN: 1-58113-624-2. DOI: 10.1145/952532.952567.

Diego, D. M. de (2018). "Lie-Poisson integrators". In: *arXiv:1803.01427*. eprint: arXiv:1803.01427.

Doedel, E. J., A. R. Champneys, T. F. Fairgrieve, et al. (2000). *auto97-auto2000: Continuation and Bifurcation Software for Ordinary Differential Equations (with HomCont)*. Tech. rep. Concordia University, Montreal, Canada. URL: http://cmvl.cs.concordia.ca/auto/#documentation.

Doedel, E. J., W. Govaerts, and Y. A. Kuznetsov (Feb. 2003). "Computation of Periodic Solution Bifurcations in ODEs Using Bordered Systems". In: *SIAM J. Numer. Anal.* 41.2, pp. 401–435. ISSN: 0036-1429. DOI: 10.1137/S0036142902400779.

Doedel, E. J. (2007). "Lecture Notes on Numerical Analysis of Nonlinear Equations". In: *Numerical Continuation Methods for Dynamical Systems*. Springer Netherlands, pp. 1–49. DOI: 10.1007/978-1-4020-6356-5_1.

Doedel, E. J., A. R. Champneys, F. Dercole, et al. (2007). *AUTO-07P: Continuation and bifurcation software for ordinary differential equations*.

Du Plessis, A. and C. T. C. Wall (1995). *The geometry of topological stability*. London Mathematical Society Monographs. Clarendon Press. ISBN: 9780198535881.

Eliashberg, Y. and M. Gromov (1998). "Lagrangian intersection theory: finite-dimensional approach". In: *Geometry of Differential Equations*. AMS Translations Series. American Mathematical Society, pp. 27–118. ISBN: 9780821810941.

Enright, W. H. and P. H. Muir (1996). "Runge–Kutta Software with Defect Control for Boundary Value ODEs". In: *SIAM Journal on Scientific Computing* 17.2, pp. 479–497. DOI: 10.1137/S1064827593251496. eprint: https://doi.org/10.1137/S1064827593251496.

Fink, J. P. and W. C. Rheinboldt (1987). "A Geometric Framework for the Numerical Study of Singular Points". In: *SIAM Journal on Numerical Analysis* 24.3, pp. 618–633. ISSN: 00361429. DOI: 10.1137/0724042.

Flaherty, F. and M. do Carmo (1992). *Riemannian Geometry*. Mathematics: Theory & Applications. Birkhäuser Boston. ISBN: 978-0-8176-3490-2. DOI: 10.1007/978-1-4757-2201-7.

Friedman, A. (1969). *Partial Differential Equations*. Holt, Rinehart and Winston Inc., New York. ISBN: 0030774551.

Fukaya, K. (2010). *Lagrangian Intersection Floer Theory: Anomaly and Obstruction, Part I*. AMS/IP studies in advanced mathematics. American Mathematical Society. ISBN: 9780821852491.

Galan-Vioque, J., F. J. M. Almaraz, and E. F. Macías (Dec. 2014). "Continuation of periodic orbits in symmetric Hamiltonian and conservative systems". In: *The European Physical Journal Special Topics* 223.13, pp. 2705–2722. ISSN: 1951-6401. DOI: 10.1140/epjst/e2014-02287-6.

Gander, M. and S. Vandewalle (2007). "Analysis of the Parareal Time-Parallel Time-Integration Method". In: *SIAM J. Sci. Comput.* 29.2, pp. 556–578. ISSN: 0167-8191. DOI: 10.1137/05064607X.

Geiser, J., K. F. Lüskow, and R. Schneider (2015). "Iterative Implicit Methods for Solving Nonlinear Dynamical Systems: Application of the Levitron". In: *Finite Difference Methods,Theory and Applications: 6th International Conference, FDM 2014, Lozenetz, Bulgaria, June 18-23, 2014, Revised Selected Papers*. Cham: Springer International Publishing, pp. 193–200. ISBN: 978-3-319-20239-6. DOI: 10.1007/978-3-319-20239-6_19.

Gilmore, R. (1993). *Catastrophe Theory for Scientists and Engineers*. Dover Books on Advanced Mathematics. Dover Publications. ISBN: 9780486675398.

Golubitsky, M. and V. Guillemin (1975). "Contact equivalence for Lagrangian manifolds". In: *Advances in Mathematics* 15.3, pp. 375–387. DOI: 10.1016/0001-8708(75)90143-7.

Golubitsky, M., I. Stewart, and J. E. Marsden (1987). "Generic bifurcation of Hamiltonian systems with symmetry". In: *Physica D: Nonlinear Phenomena* 24.1, pp. 391–405. ISSN: 0167-2789. DOI: 10.1016/0167-2789(87)90087-X.

Golubitsky, M. and V. Guillemin (1973). "Transversality". In: *Stable Mappings and Their Singularities*. New York, NY: Springer US, pp. 30–71. ISBN: 978-1-4615-7904-5. DOI: 10.1007/978-1-4615-7904-5_2.

Golubitsky, M. and J. E. Marsden (Nov. 1983). "The Morse Lemma in Infinite Dimensions via Singularity Theory". In: *SIAM Journal on Mathematical Analysis* 14.6, pp. 1037–1044. DOI: 10.1137/0514083.

Govaerts, W., Y. A. Kuznetsov, and B. Sijnave (Dec. 1998). "Implementation of Hopf and double-Hopf Continuation Using Bordering Methods". In: *ACM Trans. Math. Softw.* 24.4, pp. 418–436. ISSN: 0098-3500. DOI: 10.1145/293686.293693.

Grass, D. and H. Uecker (2017). "Optimal management and spatial patterns in a distributed shallow lake model". In: *Electronic Journal of Differential Equations* 01, pp. 1–21.

Griewank, A. and G. W. Reddien (1989). "Computation of cusp singularities for operator equations and their discretizations". In: *Journal of Computational and Applied Mathematics* 26, pp. 133–153.

Grimm-Strele, H. (Mar. 2010). "Numerical solution of the generalised Poisson equation on parallel computers". diploma thesis. Universität Wien. URL: https://core.ac.uk/display/11589985.

Hairer, E. and C. Lubich (June 2004). "Symmetric multistep methods over long times". In: *Numerische Mathematik* 97.4, pp. 699–723. ISSN: 0945-3245. DOI: 10.1007/s00211-004-0520-2.

Hairer, E., C. Lubich, and G. Wanner (2003). "Geometric numerical integration illustrated by the Störmer-Verlet method". In: *Acta Numerica* 12, pp. 399–450.

— (2013). *Geometric Numerical Integration: Structure-Preserving Algorithms for Ordinary Differential Equations*. Springer Series in Computational Mathematics. Springer Berlin Heidelberg. ISBN: 9783662050187. DOI: 10.1007/3-540-30666-8.

Hairer, E., G. Wanner, and C. Lubich (2006). "Dynamics of Multistep Methods". In: *Geometric Numerical Integration: Structure-Preserving Algorithms for Ordinary Differential Equations*. Berlin,

Heidelberg: Springer Berlin Heidelberg, pp. 567–616. ISBN: 978-3-540-30666-5. DOI: 10.1007/3-540-30666-8_15.

Hairer, E. and C. J. Zbinden (2012). "Conjugate symplectic B-series". In: *AIP Conference Proceedings* 1479.3. DOI: 10.1063/1.4756053.

Hall, B. (2013). *Quantum Theory for Mathematicians*. Graduate Texts in Mathematics. Springer New York. ISBN: 9781461471165. DOI: 10.1007/978-1-4614-7116-5.

Haro, À. (July 1998). "The primitive function of an exact symplectomorphism". PhD thesis. Universitat de Barcelona. URL: http://www.maia.ub.es/~alex/thesis.pdf.

— (June 2000). "The primitive function of an exact symplectomorphism". In: *Nonlinearity* 13.5, pp. 1483–1500. DOI: 10.1088/0951-7715/13/5/304.

Henderson, M. E. (2002). "Multiple parameter continuation: computing implicitly defined k-manifolds". In: *International Journal of Bifurcation and Chaos* 12.03, pp. 451–476. DOI: 10.1142/S0218127402004498.

— (2007). "Higher-Dimensional Continuation". In: *Numerical Continuation Methods for Dynamical Systems: Path following and boundary value problems*. Dordrecht: Springer Netherlands, pp. 77–115. ISBN: 978-1-4020-6356-5. DOI: 10.1007/978-1-4020-6356-5_3.

Hénon, M. (1983). "Numerical exploration of Hamiltonian Systems". In: *Chaotic Behaviour of Deterministic Systems, Les Houches, XXXVI*. Ed. by G. Iooss, R. Helleman, and R. Stora. Elsevier, pp. 53–170.

Hermann, M., W. Middelmann, and P. Kunkel (1998). "Augmented Systems for the Computation of Singular Points in Banach Space Problems". In: *ZAMM - Journal of Applied Mathematics and Mechanics / Zeitschrift für Angewandte Mathematik und Mechanik* 78.1, pp. 39–50. DOI: 10.1002/(SICI)1521-4001(199801)78:1<39::AID-ZAMM39>3.0.CO;2-J.

Hsiao, G. C. (2006). "A Newton-imbedding procedure for solutions of semilinear boundary value problems in Sobolev spaces". In: *Complex Variables and Elliptic Equations* 51.8-11, pp. 1021–1032. DOI: 10.1080/17476930600738543.

Hydon, P. E. (Apr. 2005). "Multisymplectic conservation laws for differential and differential-difference equations". In: *Proceedings of the Royal Society A: Mathematical, Physical and Engineering Sciences* 461.2058, pp. 1627–1637. DOI: 10.1098/rspa.2004.1444.

Ilie, S., G. Söderlind, and R. Corless (2008). "Adaptivity and computational complexity in the numerical solution of ODEs". In: *Journal of Complexity* 24.3, pp. 341–361. ISSN: 0885-064X. DOI: 10.1016/j.jco.2007.11.004.

Itoh, J. and K. Kiyohara (June 2004). "The cut loci and the conjugate loci on ellipsoids". In: *manuscripta mathematica* 114.2, pp. 247–264. ISSN: 1432-1785. DOI: 10.1007/s00229-004-0455-z.

Janeczko, S. and T. Mostowski (1995). "Relative generic singularities of the exponential map". In: *Compositio Mathematica* 96.3, pp. 345–370. URL: http://www.numdam.org/item?id=CM_1995__96_3_345_0.

Keller, H. B. (1976). "Numerical Solution of Bifurcation and Nonlinear Eigenvalue Problems". In: *Applications of Bifurcation Theory. Proceedings of an Advanced Seminar Conducted by the Mathematics Research Center the University of Wisconsin at Madison October 27-29 1976*. New York: Academic Press, pp. 359–383. ISBN: 0125742509. URL: https://apps.dtic.mil/docs/citations/ADA068109.

Khesin, B. and R. Wendt (2009). "Infinite-Dimensional Lie Groups: Their Geometry, Orbits, and Dynamical Systems". In: *The Geometry of Infinite-Dimensional Groups*. Berlin, Heidelberg: Springer Berlin Heidelberg, pp. 47–153. ISBN: 978-3-540-77263-7. DOI: 10.1007/978-3-540-77263-7_2.

Kielhöfer, H. (2012). "Local Theory". In: *Bifurcation Theory: An Introduction with Applications to Partial Differential Equations*. New York, NY: Springer New York, pp. 7–193. ISBN: 978-1-4614-0502-3. DOI: 10.1007/978-1-4614-0502-3_2.

Kierzenka, J. and L. F. Shampine (Sept. 2001). "A BVP Solver Based on Residual Control and the Maltab PSE". In: *ACM Trans. Math. Softw.* 27.3, pp. 299–316. ISSN: 0098-3500. DOI: 10.1145/502800.502801.

Kobayashi, S. (1972). *Transformation Groups in Differential Geometry*. Springer, Berlin, Heidelberg. ISBN: 978-3-642-61981-6. DOI: 10.1007/978-3-642-61981-6.

Konishi, Y. (1973). "Semi-linear Poisson's equations". In: *Proc. Japan Acad.* 49.2, pp. 100–105. DOI: 10.3792/pja/1195519431.

Krauskopf, B., H. M. Osinga, and J. Galán-Vioque, eds. (2007). *Numerical Continuation Methods for Dynamical Systems*. Springer Netherlands. ISBN: 978-1-4020-6356-5. DOI: 10.1007/978-1-4020-6356-5.

Kreusser, L. M., R. I. McLachlan, and C. Offen (2020). "Detection of high codimensional bifurcations in variational PDEs". In: *Nonlinearity* 33, pp. 2335–2363. DOI: 10.1088/1361-6544/ab7293. arXiv: 1903.02659.

Kriegl, A. and P. W. Michor (1997). *The Convenient Setting of Global Analysis*. Vol. 53. AMS. ISBN: 978-0-8218-3396-4. DOI: 10.1090/surv/053.

Kunkel, P. (1988). "Quadratically Convergent Methods for the Computation of Unfolded Singularities". In: *SIAM Journal on Numerical Analysis* 25.6, pp. 1392–1408. DOI: 10.1137/0725081.

Kuznetsov, E. A. and A. Mikhailov (1980). "On the topological meaning of canonical Clebsch variables". In: *Physics Letters A* 77.1, pp. 37–38. ISSN: 0375-9601. DOI: 10.1016/0375-9601(80)90627-1.

Larsson, S. and V. Thomée (2003). "Introduction". In: *Partial Differential Equations with Numerical Methods*. Berlin, Heidelberg: Springer Berlin Heidelberg, pp. 1–14. ISBN: 978-3-540-88706-5. DOI: 10.1007/978-3-540-88706-5_1.

Lax, P. D. (2002). *Functional analysis*. John Wiley & Sons. ISBN: 0-471-55604-1.

Lazzeri, F. and A. Micheletti (1987). "An application of singularity theory to nonlinear differentiable mappings between Banach spaces". In: *Nonlinear Analysis: Theory, Methods & Applications* 11.7, pp. 795–808. ISSN: 0362-546X. DOI: https://doi.org/10.1016/0362-546X(87)90108-8.

Leimkuhler, B. J. and R. D. Skeel (1994). "Symplectic Numerical Integrators in Constrained Hamiltonian Systems". In: *Journal of Computational Physics* 112.1, pp. 117–125. ISSN: 0021-9991. DOI: 10.1006/jcph.1994.1085.

Libermann, P. and C. M. Marle (1987). "Symplectic manifolds and Poisson manifolds". In: *Symplectic Geometry and Analytical Mechanics*. Dordrecht: Springer Netherlands, pp. 89–184. ISBN: 978-94-009-3807-6. DOI: 10.1007/978-94-009-3807-6_3.

Lochak, P., J.-P. Marco, and D. Sauzin (2003). "On the splitting of invariant manifolds in multidimensional near-integrable Hamiltonian systems". In: *Mem. Amer. Math. Soc.* 163.775, pp. viii+145. ISSN: 0065-9266.

Logg, A. and G. N. Wells (Apr. 2010). "Dolfin". In: *ACM Transactions on Mathematical Software* 37.2, pp. 1–28. ISSN: 0098-3500. DOI: 10.1145/1731022.1731030.

Lomelí, H. E., J. D. Meiss, and R. Ramírez-Ros (Feb. 2008a). "Canonical Melnikov theory for diffeomorphisms". In: *Nonlinearity* 21.3, pp. 485–508. DOI: 10.1088/0951-7715/21/3/007.

— (2008b). "Canonical Melnikov theory for diffeomorphisms". In: *Nonlinearity* 21.3, pp. 485–508. ISSN: 0951-7715.

Lorand, J. and A. Weinstein (2015). "(Co)isotropic Pairs in Poisson and Presymplectic Vector Spaces". In: *SIGMA 11* 11. DOI: 10.3842/SIGMA.2015.072. eprint: 1503.00169.

Lu, Y. (1976). *Singularity theory and an introduction to catastrophe theory*. Universitext (1979). Springer-Verlag. ISBN: 9783540902218. DOI: 10.1007/978-1-4612-9909-7.

Mansfield, E. L. (2010). "Variational problems with symmetry". In: *A Practical Guide to the Invariant Calculus*. Cambridge Monographs on Applied and Computational Mathematics. Cambridge University Press, pp. 206–240. DOI: 10.1017/CBO9780511844621.009.

Marsden, J. E. and M. West (2001a). "Discrete mechanics and variational integrators". In: *Acta Numerica* 10, pp. 357–514. DOI: 10.1017/S096249290100006X.

— (2001b). "Discrete mechanics and variational integrators". In: *Acta Numerica* 10, pp. 357–514. DOI: 10.1017/S096249290100006X.

Marsden, J. E. and R. Abraham (1978). *Foundations of Mechanics*. 2nd ed. Redwood City, CA.: Addison-Wesley Publishing Co. ISBN: 080530102X. URL: http://resolver.caltech.edu/CaltechBOOK:1987.001.

Marsden, J. E., G. Misiolek, et al. (2007). *Hamiltonian Reduction by Stages*. Springer Berlin Heidelberg. DOI: 10.1007/978-3-540-72470-4.

Marsden, J. E., S. Pekarsky, and S. Shkoller (1999). "Discrete Euler-Poincaré and Lie-Poisson equations". In: *Nonlinearity* 12.6, p. 1647. URL: http://stacks.iop.org/0951-7715/12/i=6/a=314.

Marsden, J. E. and T. S. Ratiu (1999a). "Cotangent Bundles". In: *Introduction to Mechanics and Symmetry: A Basic Exposition of Classical Mechanical Systems*. New York, NY: Springer New York, pp. 165–180. ISBN: 978-0-387-21792-5. DOI: 10.1007/978-0-387-21792-5_6.

— (1999b). *Introduction to Mechanics and Symmetry: A Basic Exposition of Classical Mechanical Systems*. New York, NY: Springer New York. ISBN: 978-0-387-21792-5. DOI: 10.1007/978-0-387-21792-5.

Marsden, J. E. and A. Weinstein (1983). "Coadjoint orbits, vortices, and Clebsch variables for incompressible fluids". In: *Physica D: Nonlinear Phenomena* 7.1, pp. 305–323. ISSN: 0167-2789. DOI: 10.1016/0167-2789(83)90134-3.

Mather, J. N. (Dec. 1968). "Stability of C^∞ mappings: III. Finitely determined map-germs". In: *Publications Mathématiques de l'Institut des Hautes Études Scientifiques* 35.1, pp. 127–156. ISSN: 1618-1913. DOI: 10.1007/BF02698926.

Mazzia, F., A. Sestini, and D. Trigiante (Jan. 2006). "B-Spline Linear Multistep Methods and their Continuous Extensions". In: *SIAM Journal on Numerical Analysis* 44.5, pp. 1954–1973. DOI: 10.1137/040614748.

— (2009). "The continuous extension of the B-spline linear multistep methods for BVPs on non-uniform meshes". In: *Applied Numerical Mathematics* 59.3, pp. 723–738. ISSN: 0168-9274. DOI: 10.1016/j.apnum.2008.03.036.

Mazzia, F. and D. Trigiante (June 2004). "A Hybrid Mesh Selection Strategy Based on Conditioning for Boundary Value ODE Problems". In: *Numerical Algorithms* 36.2, pp. 169–187. DOI: 10.1023/b:numa.0000033132.99233.c8.

McDonald, F. et al. (2016). "Travelling wave solutions of multisymplectic discretizations of semi-linear wave equations". In: *Journal of Difference Equations and Applications* 22.7, pp. 913–940. DOI: 10.1080/10236198.2016.1162161.

McDuff, D. and D. Salamon (2017). *Introduction to Symplectic Topology*. Oxford Graduate Texts in Mathematics Series. Oxford University Press. ISBN: 9780198794899.

McLachlan, R. I. (2003). "Spatial discretization of partial differential equations with integrals". In: *IMA Journal of Numerical Analysis* 23.4, pp. 645–664. DOI: 10.1093/imanum/23.4.645.

McLachlan, R. I., K. Modin, H. Munthe-Kaas, et al. (2017). "Butcher series: A story of rooted trees and numerical methods for evolution equations". In: *Asia Pacific Mathematics Newsletter* 7.1, pp. 1–11. arXiv: 1512.00906.

McLachlan, R. I., K. Modin, and O. Verdier (2014). "Collective symplectic integrators". In: *Nonlinearity* 27.6, p. 1525. DOI: 10.1088/0951-7715/27/6/1525.

McLachlan, R. I. and C. Offen (2018a). "Bifurcation of solutions to Hamiltonian boundary value problems". In: *Nonlinearity* 31.6, pp. 2895–2927. DOI: 10.1088/1361-6544/aab630. arXiv: 1710.09991.

— (2018b). "Hamiltonian boundary value problems, conformal symplectic symmetries, and conjugate loci". In: *New Zealand Journal of Mathematics (NZJM)* 48, pp. 83–99. arXiv: 1804.07479.

— (Aug. 2019). "Symplectic integration of boundary value problems". In: *Numerical Algorithms* 81.4, pp. 1219–1233. ISSN: 1572-9265. DOI: 10.1007/s11075-018-0599-7. arXiv: 1804.09042.

— (June 2020a). "Backward error analysis for variational discretisations of partial differential equations". In: *Nonlinearity (submitted)*. arXiv: 2006.14172.

— (2020b). "Preservation of bifurcations of Hamiltonian boundary value problems under discretisation". In: *Foundations of Computational Mathematics (FoCM)*. DOI: 10.1007/s10208-020-09454-z. arXiv: 1804.07468.

McLachlan, R. I., C. Offen, and B. K. Tapley (July 2019). "Symplectic integration of PDEs using Clebsch variables". In: *Journal of Computational Dynamics* 6.1, pp. 111–130. ISSN: 2158-2505. DOI: 10.3934/jcd.2019005. arXiv: 1810.01627.

McLachlan, R. I. and M. Perlmutter (2001). "Conformal Hamiltonian systems". In: *Journal of Geometry and Physics* 39.4, pp. 276–300. ISSN: 0393-0440. DOI: 10.1016/S0393-0440(01)00020-1.

McLachlan, R. I., B. N. Ryland, and Y. Sun (2014). "High Order Multisymplectic Runge–Kutta Methods". In: *SIAM Journal on Scientific Computing* 36.5, A2199–A2226. DOI: 10.1137/140958050.

McLachlan, R. I. and A. Stern (Apr. 2019). "Multisymplecticity of Hybridizable Discontinuous Galerkin Methods". In: *Foundations of Computational Mathematics (FoCM)* 20.1, pp. 35–69. DOI: 10.1007/s10208-019-09415-1.

Mei, Z. (2000a). "Liapunov-Schmidt Method". In: *Numerical Bifurcation Analysis for Reaction-Diffusion Equations*. Berlin, Heidelberg: Springer Berlin Heidelberg, pp. 101–127. ISBN: 978-3-662-04177-2. DOI: 10.1007/978-3-662-04177-2_6.

— (2000b). "Reaction-Diffusion Equations". In: *Numerical Bifurcation Analysis for Reaction-Diffusion Equations*. Berlin, Heidelberg: Springer Berlin Heidelberg, pp. 1–6. ISBN: 978-3-662-04177-2. DOI: 10.1007/978-3-662-04177-2_1.

Milnor, J. (1969). *Morse Theory*. Vol. 51. Annals of Mathematics Studies. Princeton University Press. ISBN: 9781400881802.

Mohsen, A. (2014). "A simple solution of the Bratu problem". In: *Computers & Mathematics with Applications* 67.1, pp. 26–33. ISSN: 0898-1221. DOI: 10.1016/j.camwa.2013.10.003.

Oberman, A. M. and I. Zwiers (2016). "Adaptive Finite Difference Methods for Nonlinear Elliptic and Parabolic Partial Differential Equations with Free Boundaries". In: *Journal of Scientific Computing* 68.1, pp. 231–251. ISSN: 1573-7691. DOI: 10.1007/s10915-015-0137-x.

Offen, C. (2019a). *Singularities Illustrations Cusp and Swallowtail*. https://www.youtube.com/playlist?list=PLIp-UrijLTJ5m-3ZASHPurIkehiBuW_s0. Accessed 13/01/20. Youtube.

— (2019b). *Singularities Illustrations Elliptic Umbilic*. https://www.youtube.com/playlist?list=PLIp-UrijLTJ7NUg6Vb3J_dV-mmdXFNPfN. Accessed 03/11/19. Youtube.

— (2019c). *Singularities Illustrations Hyperbolic Umbilic*. https://www.youtube.com/watch?v=RU5DBPZTEG8&list=PLIp-UrijLTJ5C1dMN5vBaN63fWUiPg98e. Accessed 03/11/19. Youtube.

— (Mar. 2020a). "Local intersections of Lagrangian manifolds correspond to catastrophe theory". In: *Annales Henri Lebesgue (submitted)*. arXiv: 1811.10165.

— (Mar. 2020b). *Release v1.2 of GitHub repository Christian-Offen/multisymplectic*. Version v1.2. DOI: 10.5281/zenodo.3726256.

Oh, Y.-G. (1995). "Floer cohomology of Lagrangian intersections and pseudo-holomorphic disks, III: Arnold-Givental Conjecture". In: *The Floer Memorial Volume*. Basel: Birkhäuser Basel, pp. 555–573. ISBN: 978-3-0348-9217-9. DOI: 10.1007/978-3-0348-9217-9_23.

Palais, R. S. (1979). "The principle of symmetric criticality". In: *Comm. Math. Phys.* 69.1, pp. 19–30. URL: https://projecteuclid.org:443/euclid.cmp/1103905401.

Penot, J.-P. (2013). "Elements of Differential Calculus". In: *Calculus Without Derivatives*. New York, NY: Springer New York, pp. 117–186. ISBN: 978-1-4614-4538-8. DOI: 10.1007/978-1-4614-4538-8_2.

Piccione, P., A. Portaluri, and D. V. Tausk (Apr. 2004). "Spectral Flow, Maslov Index and Bifurcation of Semi-Riemannian Geodesics". In: *Annals of Global Analysis and Geometry* 25.2, pp. 121–149. ISSN: 1572-9060. DOI: 10.1023/B:AGAG.0000018558.65790.db.

Polterovich, L. (2001). "Lagrangian Intersections". In: *The Geometry of the Group of Symplectic Diffeomorphism*. Basel: Birkhäuser Basel, pp. 43–49. ISBN: 978-3-0348-8299-6. DOI: 10.1007/978-3-0348-8299-6_6.

Portaluri, A. and N. Waterstraat (2014). "Bifurcation results for critical points of families of functionals". In: *Differential Integral Equations* 27.3-4, pp. 369–386. ISSN: 0893-4983. URL: http://projecteuclid.org/euclid.die/1391091370.

Poston, T. and I. Stewart (1978). *Catastrophe Theory and Its Applications*. Dover Books on Mathematics. Dover Publications. ISBN: 9780486692715.

Rathgeber, F. et al. (Dec. 2016). "Firedrake: Automating the Finite Element Method by Composing Abstractions". In: *ACM Trans. Math. Softw.* 43.3. ISSN: 0098-3500. DOI: 10.1145/2998441.

Renardy, M. and R. C. Rogers (2004a). *An Introduction to Partial Differential Equations*. Springer-Verlag. ISBN: 978-1-4419-1820-8. DOI: 10.1007/b97427.

— (2004b). *An Introduction to Partial Differential Equations*. New York, NY: Springer New York. ISBN: 978-0-387-21687-4. DOI: 10.1007/b97427.

Rheinboldt, W. C. (1981). "Numerical analysis of continuation methods for nonlinear structural problems". In: *Computational Methods in Nonlinear Structural and Solid Mechanics*. Elsevier, pp. 103–113.

Riks, E. (1972). "The application of Newton's method to the problem of elastic stability". In: *Journal of Applied Mechanics* 39.4, pp. 1060–1065.

Ruf, B. (1992). "Forced secondary bifurcation in an elliptic boundary value problem". In: *Differential Integral Equations* 5.4, pp. 793–804. URL: https://projecteuclid.org:443/euclid.die/1370955419.

— (1990). "Singularity theory and the geometry of a nonlinear elliptic equation". en. In: *Annali della Scuola Normale Superiore di Pisa, Classe di Scienze* 17.4, pp. 1–33. URL: http://www.numdam.org/item/ASNSP_1990_4_17_1_1_0.

— (1995). "Higher Singularities and Forced Secondary Bifurcation". In: *SIAM Journal on Mathematical Analysis* 26.5, pp. 1342–1360. DOI: 10.1137/S0036141093243848.

Seydel, R. (2010). *Practical Bifurcation and Stability Analysis*. Springer New York. DOI: 10.1007/978-1-4419-1740-9.

Silva, A. C. da (2008). "Generating Functions". In: *Lectures on Symplectic Geometry*. Berlin, Heidelberg: Springer Berlin Heidelberg, pp. 25–31. ISBN: 978-3-540-45330-7. DOI: 10.1007/978-3-540-45330-7_4.

Tabor, M. (1989). *Chaos and integrability in nonlinear dynamics: an introduction*. Wiley-Interscience publication. Wiley. ISBN: 9780471827283.

Tan, X. (2005). "Almost symplectic Runge–Kutta schemes for Hamiltonian systems". In: *Journal of Computational Physics* 203.1, pp. 250–273. ISSN: 0021-9991. DOI: 10.1016/j.jcp.2004.08.012.

Teschl, G. (Aug. 2012). *Ordinary Differential Equations and Dynamical Systems*. American Mathematical Society. DOI: 10.1090/gsm/140.

The MathWorks, I. (2019). *Partial Differential Equation Toolbox*. Natick, Massachusetts, United State. URL: https://www.mathworks.com/help/pde/.

Thielhelm, H., A. Vais, and F.-E. Wolter (Feb. 2015). "Geodesic bifurcation on smooth surfaces". In: *The Visual Computer* 31.2, pp. 187–204. ISSN: 1432-2315. DOI: 10.1007/s00371-014-1041-3.

Thom, R. (1973). *Stabilité structurelle et morphogénèse:* Mathematical physics monograph series. W. A. Benjamin.

Tougeron, J.-C. (1968). "Idéaux et fonctions différentiables. I". fr. In: *Annales de l'Institut Fourier* 18.1, pp. 177–240. DOI: 10.5802/aif.281.

Uecker, H., D. Wetzel, and J. Rademacher (June 2014). "pde2path - A Matlab Package for Continuation and Bifurcation in 2D Elliptic Systems". In: *Numerical Mathematics: Theory, Methods and Applications* 7.1, pp. 58–106. DOI: 10.4208/nmtma.2014.1231nm.

Uecker, H. (Mar. 2016). "Optimal harvesting and spatial patterns in a semiarid vegetation system". In: *Natural Resource Modeling* 29.2, pp. 229–258. DOI: 10.1111/nrm.12089.

Vaisman, I. (1994). "Symplectic Realizations of Poisson Manifolds". In: *Lectures on the Geometry of Poisson Manifolds*. Basel: Birkhäuser Basel, pp. 115–133. ISBN: 978-3-0348-8495-2. DOI: 10.1007/978-3-0348-8495-2_9.

Vermeeren, M. (June 2017). "Modified equations for variational integrators". In: *Numerische Mathematik* 137.4, pp. 1001–1037. DOI: 10.1007/s00211-017-0896-4.

Vizman, C. (2008). "Geodesic Equations on Diffeomorphism Groups". In: *SIGMA* 4.030, pp. 1–22. DOI: 10.3842/SIGMA.2008.030. eprint: arXiv:0803.1678.

Wagner, W. and P. Wriggers (1988). "A simple method for the calculation of postcritical branches". In: *Engineering computations* 5.2, pp. 103–109.

Wall, C. T. C. (1971). "Lectures on C^∞ stability and classification". In: *Proceedings of Liverpool Singularities — Symposium I*. Ed. by C. T. C. Wall. Berlin, Heidelberg: Springer Berlin Heidelberg, pp. 178–206. ISBN: 978-3-540-36531-0. DOI: 10.1007/BFb0066823.

— (1977). "Geometric properties of generic differentiable manifolds". In: *Geometry and Topology*. Ed. by J. Palis and M. do Carmo. Berlin, Heidelberg: Springer Berlin Heidelberg, pp. 707–774. ISBN: 978-3-540-37301-8.

— (Nov. 1981). "Finite Determinacy of Smooth Map-Germs". In: *Bulletin of the London Mathematical Society* 13.6, pp. 481–539. DOI: 10.1112/blms/13.6.481.

Warner, F. (1983). *Foundations of Differentiable Manifolds and Lie Groups*. Springer New York. ISBN: 978-1-4757-1799-0. DOI: 10.1007/978-1-4757-1799-0.

Wassermann, G. (1974). *Stability of Unfoldings*. Springer Berlin Heidelberg. ISBN: 978-3-540-38423-6. DOI: 10.1007/bfb0061658.

— (1988). "Classification of singularities with compact Abelian symmetry". In: *Banach Center Publications* 20.1, pp. 475–498.

Waters, T. (2017). "Bifurcations of the conjugate locus". In: *Journal of Geometry and Physics* 119, pp. 1–8. ISSN: 0393-0440. DOI: 10.1016/j.geomphys.2017.04.003.

Weinstein, A. (1970). "The generic conjugate locus". In: *Global Analysis - Proceedings of Symposia in Pure Mathematics*. Ed. by S.-S. Chern and S. Smale. Vol. 15. Providence, Rhode Island: American Mathematical Society, pp. 299–301. DOI: 10.1090/pspum/015/0271993.

— (1971a). "Singularities of families of functions". In: *Differentialgeometrie im Grossen (Ber. Tagung, Math. Forschungsinst., Oberwolfach, 1969)* 4, pp. 323–330.

— (1971b). "Symplectic manifolds and their Lagrangian submanifolds". In: *Advances in Mathematics* 6.3, pp. 329–346. ISSN: 0001-8708. DOI: 10.1016/0001-8708(71)90020-X.

— (1972). "The invariance of Poincaré's generating function for canonical transformations". In: *Inventiones mathematicae* 16.3, pp. 202–213. DOI: 10.1007/BF01425493.

Weinstein, A. (1973). "Lagrangian Submanifolds and Hamiltonian Systems". In: *Annals of Mathematics* 98.3, pp. 377–410. ISSN: 0003486X. DOI: 10.2307/1970911.

Whitham, G. B. (1967). "Variational methods and applications to water waves". In: *Proceedings of the Royal Society of London. Series A. Mathematical and Physical Sciences* 299.1456, pp. 6–25. DOI: 10.1098/rspa.1967.0119.

Wriggers, P. and J. C. Simo (1990). "A general procedure for the direct computation of turning and bifurcation points". In: *International journal for numerical methods in engineering* 30.1, pp. 155–176.

Appendix A

Simplified calculation for the hyperbolic umbilic

The hyperbolic umbilic singularity D_4^+ admits a representation by the germ $x^3 + y^3$. This is being used in the following argumentation which provides an alternative, simpler argumentation compared to Lemmas 9.2.3 and 9.2.5 and Proposition 9.2.6 in Section 9.2 *for this case*. However, for a general treatment we prefer a Lemma 9.2.3-type calculation as it applies to all D-series bifurcations.

Lemma A.0.1 (Break of hyperbolic umbilic)**.** *Let $g_\mu \colon \mathbb{R}^2 \to \mathbb{R}$ be a versal unfolding of the D_4^+ singularity $x^3 + y^3$. A miniversal unfolding of ∇g_μ in $\mathbb{R}[[x, y]]^2$ considered as the free module of rank 2 over the ring $\mathbb{R}[[x, y]]$ is given as*

$$\begin{pmatrix} x \\ y \end{pmatrix} \mapsto \begin{pmatrix} x^2 \\ y^2 \end{pmatrix} + \mu_1 \begin{pmatrix} 1 \\ 0 \end{pmatrix} + \mu_2 \begin{pmatrix} 0 \\ 1 \end{pmatrix} + \mu_3 \begin{pmatrix} y \\ x \end{pmatrix} + \mu_4 \begin{pmatrix} y \\ 0 \end{pmatrix}.$$

Proof. An unfolding of the D_4^+ singularity is given by

$$g_\mu(x, y) = x^3 + y^3 + \mu_1 x + \mu_2 y + \mu_3 xy$$

(see Wall, 1971, p.188, for instance). The gradient ∇g_μ constitutes a (non-versal) unfolding of the roots-of-a-function problem

$$f \colon \begin{pmatrix} x \\ y \end{pmatrix} \mapsto 3 \begin{pmatrix} x^2 \\ y^2 \end{pmatrix}$$

in $\mathbb{R}[[x, y]]^2$, which is the free module of rank 2 over the ring of formal power series $\mathbb{R}[[x, y]]$. Let us imitate the procedure presented in Wall, 1971, p.187 in the module $\mathbb{R}[[x, y]]^2$ to unfold f versally. We obtain relations r_1 and r_2 as (rescaled) components

of f. Let I be the ideal in $\mathbb{R}[[x,y]]$ generated by r_1, r_2 with $r_1 = x^2$, $r_2 = y^2$. Consider

$$\partial_1 r = \begin{pmatrix} \frac{\partial r_1}{\partial x} \\ \frac{\partial r_2}{\partial x} \end{pmatrix} = \begin{pmatrix} 2x \\ 0 \end{pmatrix}, \quad \partial_2 r = \begin{pmatrix} \frac{\partial r_1}{\partial y} \\ \frac{\partial r_2}{\partial y} \end{pmatrix} = \begin{pmatrix} 0 \\ 2y \end{pmatrix}.$$

Let L be the submodule generated by $I\mathbb{R}[[x,y]]^2$, $\partial_1 r$ and $\partial_2 r$ in $\mathbb{R}[[x,y]]^2$. The quotient Q of the modules $\mathbb{R}[[x,y]]^2$ and L is given as

$$\begin{aligned} Q &= \mathbb{R}[[x,y]]^2/L \\ &= \mathbb{R}[[x,y]]^2 / \left\langle \begin{pmatrix} x^2 \\ 0 \end{pmatrix}, \begin{pmatrix} 0 \\ x^2 \end{pmatrix}, \begin{pmatrix} y^2 \\ 0 \end{pmatrix}, \begin{pmatrix} 0 \\ y^2 \end{pmatrix}, \begin{pmatrix} x \\ 0 \end{pmatrix}, \begin{pmatrix} 0 \\ y \end{pmatrix} \right\rangle_{\mathbb{R}[[x,y]]} \\ &= \operatorname{span}_{\mathbb{R}} \left\{ \left[\begin{pmatrix} 1 \\ 0 \end{pmatrix} \right], \left[\begin{pmatrix} 0 \\ 1 \end{pmatrix} \right], \left[\begin{pmatrix} 0 \\ x \end{pmatrix} \right], \left[\begin{pmatrix} y \\ 0 \end{pmatrix} \right] \right\} \\ &= \operatorname{span}_{\mathbb{R}} \left\{ \left[\begin{pmatrix} 1 \\ 0 \end{pmatrix} \right], \left[\begin{pmatrix} 0 \\ 1 \end{pmatrix} \right], \left[\begin{pmatrix} y \\ x \end{pmatrix} \right], \left[\begin{pmatrix} y \\ 0 \end{pmatrix} \right] \right\}. \end{aligned}$$

Here $\langle ., \ldots, . \rangle_{\mathbb{R}[[x,y]]}$ denotes the submodule of the module $\mathbb{R}[[x,y]]^2$ over the ring $\mathbb{R}[[x,y]]$ spanned by the elements listed between the brackets. In the last equations $\operatorname{span}_{\mathbb{R}}\{., \ldots, .\}$ denotes the space of all linear combinations of the elements listed between the brackets using coefficients in $\mathbb{R}$. These elements form an $\mathbb{R}$-basis of Q such that we obtain the universal unfolding

$$f_\mu(x,y) = 3 \begin{pmatrix} x^2 \\ y^2 \end{pmatrix} + \mu_1 \begin{pmatrix} 1 \\ 0 \end{pmatrix} + \mu_2 \begin{pmatrix} 0 \\ 1 \end{pmatrix} + \mu_3 \begin{pmatrix} y \\ x \end{pmatrix} + \mu_4 \begin{pmatrix} y \\ 0 \end{pmatrix}. \tag{A.0.1}$$

of f. Comparing with the unfolding

$$\nabla g_\mu(x,y) = 3 \begin{pmatrix} x^2 \\ y^2 \end{pmatrix} + \mu_1 \begin{pmatrix} 1 \\ 0 \end{pmatrix} + \mu_2 \begin{pmatrix} 0 \\ 1 \end{pmatrix} + \mu_3 \begin{pmatrix} y \\ x \end{pmatrix}$$

yields that in $\nabla g_\mu(x,y)$ all parameters enter transversally, and it suffices to add the unfolding term $\mu_4 \begin{pmatrix} y \\ 0 \end{pmatrix}$ destroying the gradient structure to obtain a universal unfolding in the roots-of-a-function problem. □

We can quantify and verify our observations from Figure 9.1 in the model f_μ from (A.0.1).

Proposition A.0.2. *A hyperbolic umbilic singularity in the critical-points problem $\nabla g_\mu = 0$ for a smooth family of real valued maps g_μ breaks up into two swallowtail points if the problem $\nabla g_\mu = 0$ is perturbed to a problem $f_\mu = 0$, where the perturbation*

takes a general form.

Proof. It suffices to verify the assertion using the model f_μ from (A.0.1). The equations $f_\mu(x,y) = 0$ and $\det \mathrm{D}f_\mu(x,y) = 0$ are equivalent to

$$\begin{aligned} \mu_1 &= -3x^2 - (\mu_3 + \mu_4)y \\ \mu_2 &= -3y^2 - \mu_3 x \\ 36xy &= \mu_3(\mu_3 + \mu_4). \end{aligned} \tag{A.0.2}$$

Let $\mu_4 \neq 0$. Since the Jacobi matrix $\mathrm{D}f_\mu$ never vanishes, only A-series singularities are possible (see the classification Du Plessis and Wall, 1995, p.339). Since A-series bifurcations are determined by their codimension we can deduce the following: if $\mu_3 \notin \{0, -\mu_4\}$ then cusp bifurcations (codimension 2) occur along the hyperbola defined by (A.0.2) for specific values of (μ_1, μ_2). If, however, $\mu_3 \in \{0, -\mu_4\}$ then the cusp bifurcations merge to a swallowtail (codimension 3) at $(x,y) = (0,0)$. □

Appendix B

Additional computational results for Chapter 13

B.1 Computational result for reduced modified equation

Here we report the 2nd order term of the reduced modified ODE (13.2.12)

$$\ddot{\phi}(\xi) = \frac{(\alpha^2 + V'(\langle\phi(\xi), \phi(\xi)\rangle))\phi(\xi) + 2c\alpha J\dot{\phi}(\xi)}{c^2 - 1} + \sum_{j=2}^{\infty} h^{2j}\hat{g}_{2j}(\dot{\phi}(\xi), \phi(\xi)).$$

First component of $\hat{g}_2(\phi, \dot{\phi})$.

$$\begin{aligned}
&\frac{2\Delta t^2\alpha^3\dot{\phi_2}(\xi)c^7}{3(c^2-1)^4} + \frac{\Delta t^2\alpha^4\phi_1(\xi)c^6}{3(c^2-1)^4} + \frac{\Delta t^2\alpha^2\phi_1(\xi)V'(\phi_1(\xi)^2+\phi_2(\xi)^2)c^6}{3(c^2-1)^4} - \frac{5\Delta t^2\alpha^3\dot{\phi_2}(\xi)c^5}{3(c^2-1)^3} \\
&- \frac{\Delta t^2\alpha V'(\phi_1(\xi)^2+\phi_2(\xi)^2)\dot{\phi_2}(\xi)c^5}{3(c^2-1)^3} - \frac{\Delta t^2\alpha\phi_1(\xi)^2\dot{\phi_2}(\xi)V''(\phi_1(\xi)^2+\phi_2(\xi)^2)c^5}{3(c^2-1)^3} \\
&- \frac{\Delta t^2\alpha\phi_2(\xi)^2\dot{\phi_2}(\xi)V''(\phi_1(\xi)^2+\phi_2(\xi)^2)c^5}{3(c^2-1)^3} - \frac{\Delta t^2\phi_1(\xi)\dot{\phi_1}(\xi)^2V''(\phi_1(\xi)^2+\phi_2(\xi)^2)c^4}{2(c^2-1)^2} \\
&- \frac{\Delta t^2\phi_2(\xi)\dot{\phi_1}(\xi)\dot{\phi_2}(\xi)V''(\phi_1(\xi)^2+\phi_2(\xi)^2)c^4}{3(c^2-1)^2} - \frac{\Delta t^2\phi_1(\xi)^3\dot{\phi_1}(\xi)^2V^{(3)}(\phi_1(\xi)^2+\phi_2(\xi)^2)c^4}{3(c^2-1)^2} \\
&- \frac{\Delta t^2\phi_1(\xi)\phi_2(\xi)^2\dot{\phi_2}(\xi)^2V^{(3)}(\phi_1(\xi)^2+\phi_2(\xi)^2)c^4}{3(c^2-1)^2} - \frac{2\Delta t^2\phi_1(\xi)^2\phi_2(\xi)\dot{\phi_1}(\xi)\dot{\phi_2}(\xi)V^{(3)}(\phi_1(\xi)^2+\phi_2(\xi)^2)c^4}{3(c^2-1)^2} \\
&- \frac{\Delta t^2\phi_1(\xi)\dot{\phi_2}(\xi)^2V''(\phi_1(\xi)^2+\phi_2(\xi)^2)c^4}{6(c^2-1)^2} - \frac{3\Delta t^2\alpha^4\phi_1(\xi)c^4}{4(c^2-1)^3} - \frac{5\Delta t^2\alpha^2\phi_1(\xi)V'(\phi_1(\xi)^2+\phi_2(\xi)^2)c^4}{6(c^2-1)^3} \\
&- \frac{\Delta t^2\alpha^2\phi_1(\xi)^3V''(\phi_1(\xi)^2+\phi_2(\xi)^2)c^4}{6(c^2-1)^3} - \frac{\Delta t^2\alpha^2\phi_1(\xi)\phi_2(\xi)^2V''(\phi_1(\xi)^2+\phi_2(\xi)^2)c^4}{6(c^2-1)^3} \\
&- \frac{\Delta t^2\phi_1(\xi)^3V'(\phi_1(\xi)^2+\phi_2(\xi)^2)V''(\phi_1(\xi)^2+\phi_2(\xi)^2)c^4}{6(c^2-1)^3} \\
&- \frac{\Delta t^2\phi_1(\xi)\phi_2(\xi)^2V'(\phi_1(\xi)^2+\phi_2(\xi)^2)V''(\phi_1(\xi)^2+\phi_2(\xi)^2)c^4}{6(c^2-1)^3} - \frac{\Delta t^2\phi_1(\xi)V'(\phi_1(\xi)^2+\phi_2(\xi)^2)^2c^4}{12(c^2-1)^3} \\
&+ \frac{\Delta t^2\alpha^3\dot{\phi_2}(\xi)c^3}{(c^2-1)^2} + \frac{\Delta t^2\alpha V'(\phi_1(\xi)^2+\phi_2(\xi)^2)\dot{\phi_2}(\xi)c^3}{3(c^2-1)^2} + \frac{2\Delta t^2\alpha\phi_1(\xi)\phi_2(\xi)\dot{\phi_1}(\xi)V''(\phi_1(\xi)^2+\phi_2(\xi)^2)c^3}{3(c^2-1)^2}
\end{aligned}$$

$$+\frac{2\Delta t^2\alpha\phi_2(\xi)^2\dot{\phi_2}(\xi)V''(\phi_1(\xi)^2+\phi_2(\xi)^2)c^3}{3(c^2-1)^2}-\frac{2\Delta x^2\alpha^3\dot{\phi_2}(\xi)c^3}{3(c^2-1)^4}+\frac{5\Delta t^2\alpha^4\phi_1(\xi)c^2}{12(c^2-1)^2}$$
$$+\frac{\Delta t^2\alpha^2\phi_1(\xi)V'(\phi_1(\xi)^2+\phi_2(\xi)^2)c^2}{2(c^2-1)^2}-\frac{\Delta x^2\alpha^4\phi_1(\xi)c^2}{3(c^2-1)^4}-\frac{\Delta x^2\alpha^2\phi_1(\xi)V'(\phi_1(\xi)^2+\phi_2(\xi)^2)c^2}{3(c^2-1)^4}$$
$$+\frac{\Delta t^2\alpha^3\dot{\phi_2}(\xi)c}{3(c^2-1)^2}+\frac{\Delta x^2\alpha^3\dot{\phi_2}(\xi)c}{3(c^2-1)^3}+\frac{\Delta x^2\alpha V'(\phi_1(\xi)^2+\phi_2(\xi)^2)\dot{\phi_2}(\xi)c}{3(c^2-1)^3}$$
$$+\frac{\Delta x^2\alpha\phi_1(\xi)^2\dot{\phi_2}(\xi)V''(\phi_1(\xi)^2+\phi_2(\xi)^2)c}{3(c^2-1)^3}+\frac{\Delta x^2\alpha\phi_2(\xi)^2\dot{\phi_2}(\xi)V''(\phi_1(\xi)^2+\phi_2(\xi)^2)c}{3(c^2-1)^3}$$
$$+\frac{\Delta x^2\phi_1(\xi)V'(\phi_1(\xi)^2+\phi_2(\xi)^2)^2}{12(c^2-1)^3}+\frac{\Delta t^2\alpha^4\phi_1(\xi)}{12(c^2-1)^2}+\frac{\Delta x^2\alpha^4\phi_1(\xi)}{12(c^2-1)^3}+\frac{\Delta x^2\alpha^2\phi_1(\xi)V'(\phi_1(\xi)^2+\phi_2(\xi)^2)}{6(c^2-1)^3}$$
$$+\frac{\Delta x^2\alpha^2\phi_1(\xi)^3V''(\phi_1(\xi)^2+\phi_2(\xi)^2)}{6(c^2-1)^3}+\frac{\Delta x^2\alpha^2\phi_1(\xi)\phi_2(\xi)^2V''(\phi_1(\xi)^2+\phi_2(\xi)^2)}{6(c^2-1)^3}$$
$$+\frac{\Delta x^2\phi_1(\xi)\dot{\phi_1}(\xi)^2V''(\phi_1(\xi)^2+\phi_2(\xi)^2)}{2(c^2-1)^2}+\frac{\Delta x^2\phi_1(\xi)\dot{\phi_2}(\xi)^2V''(\phi_1(\xi)^2+\phi_2(\xi)^2)}{6(c^2-1)^2}$$
$$+\frac{\Delta x^2\phi_1(\xi)^3V'(\phi_1(\xi)^2+\phi_2(\xi)^2)V''(\phi_1(\xi)^2+\phi_2(\xi)^2)}{6(c^2-1)^3}$$
$$+\frac{\Delta x^2\phi_1(\xi)\phi_2(\xi)^2V'(\phi_1(\xi)^2+\phi_2(\xi)^2)V''(\phi_1(\xi)^2+\phi_2(\xi)^2)}{6(c^2-1)^3}+\frac{\Delta x^2\phi_2(\xi)\dot{\phi_1}(\xi)\dot{\phi_2}(\xi)V''(\phi_1(\xi)^2+\phi_2(\xi)^2)}{3(c^2-1)^2}$$
$$+\frac{\Delta x^2\phi_1(\xi)^3\dot{\phi_1}(\xi)^2V^{(3)}(\phi_1(\xi)^2+\phi_2(\xi)^2)}{3(c^2-1)^2}+\frac{\Delta x^2\phi_1(\xi)\phi_2(\xi)^2\dot{\phi_2}(\xi)^2V^{(3)}(\phi_1(\xi)^2+\phi_2(\xi)^2)}{3(c^2-1)^2}$$
$$+\frac{2\Delta x^2\phi_1(\xi)^2\phi_2(\xi)\dot{\phi_1}(\xi)\dot{\phi_2}(\xi)V^{(3)}(\phi_1(\xi)^2+\phi_2(\xi)^2)}{3(c^2-1)^2}$$

Second component of $\hat{g}_2(\phi,\dot{\phi})$.

$$-\frac{2\Delta t^2\alpha^3\dot{\phi_1}(\xi)c^7}{3(c^2-1)^4}+\frac{\Delta t^2\alpha^4\phi_2(\xi)c^6}{3(c^2-1)^4}+\frac{\Delta t^2\alpha^2\phi_2(\xi)V'(\phi_1(\xi)^2+\phi_2(\xi)^2)c^6}{3(c^2-1)^4}+\frac{5\Delta t^2\alpha^3\dot{\phi_1}(\xi)c^5}{3(c^2-1)^3}$$
$$+\frac{\Delta t^2\alpha V'(\phi_1(\xi)^2+\phi_2(\xi)^2)\dot{\phi_1}(\xi)c^5}{3(c^2-1)^3}+\frac{\Delta t^2\alpha\phi_1(\xi)^2\dot{\phi_1}(\xi)V''(\phi_1(\xi)^2+\phi_2(\xi)^2)c^5}{3(c^2-1)^3}$$
$$+\frac{\Delta t^2\alpha\phi_2(\xi)^2\dot{\phi_1}(\xi)V''(\phi_1(\xi)^2+\phi_2(\xi)^2)c^5}{3(c^2-1)^3}-\frac{\Delta t^2\phi_2(\xi)\dot{\phi_2}(\xi)^2V''(\phi_1(\xi)^2+\phi_2(\xi)^2)c^4}{2(c^2-1)^2}$$
$$-\frac{\Delta t^2\phi_1(\xi)\dot{\phi_1}(\xi)\dot{\phi_2}(\xi)V''(\phi_1(\xi)^2+\phi_2(\xi)^2)c^4}{3(c^2-1)^2}-\frac{\Delta t^2\phi_1(\xi)^2\phi_2(\xi)\dot{\phi_1}(\xi)^2V^{(3)}(\phi_1(\xi)^2+\phi_2(\xi)^2)c^4}{3(c^2-1)^2}$$
$$-\frac{\Delta t^2\phi_2(\xi)^3\dot{\phi_2}(\xi)^2V^{(3)}(\phi_1(\xi)^2+\phi_2(\xi)^2)c^4}{3(c^2-1)^2}-\frac{2\Delta t^2\phi_1(\xi)\phi_2(\xi)^2\dot{\phi_1}(\xi)\dot{\phi_2}(\xi)V^{(3)}(\phi_1(\xi)^2+\phi_2(\xi)^2)c^4}{3(c^2-1)^2}$$
$$-\frac{\Delta t^2\phi_2(\xi)\dot{\phi_1}(\xi)^2V''(\phi_1(\xi)^2+\phi_2(\xi)^2)c^4}{6(c^2-1)^2}-\frac{3\Delta t^2\alpha^4\phi_2(\xi)c^4}{4(c^2-1)^3}-\frac{5\Delta t^2\alpha^2\phi_2(\xi)V'(\phi_1(\xi)^2+\phi_2(\xi)^2)c^4}{6(c^2-1)^3}$$
$$-\frac{\Delta t^2\alpha^2\phi_2(\xi)^3V''(\phi_1(\xi)^2+\phi_2(\xi)^2)c^4}{6(c^2-1)^3}-\frac{\Delta t^2\alpha^2\phi_1(\xi)^2\phi_2(\xi)V''(\phi_1(\xi)^2+\phi_2(\xi)^2)c^4}{6(c^2-1)^3}$$
$$-\frac{\Delta t^2\phi_2(\xi)^3V'(\phi_1(\xi)^2+\phi_2(\xi)^2)V''(\phi_1(\xi)^2+\phi_2(\xi)^2)c^4}{6(c^2-1)^3}$$
$$-\frac{\Delta t^2\phi_1(\xi)^2\phi_2(\xi)V'(\phi_1(\xi)^2+\phi_2(\xi)^2)V''(\phi_1(\xi)^2+\phi_2(\xi)^2)c^4}{6(c^2-1)^3}-\frac{\Delta t^2\phi_2(\xi)V'(\phi_1(\xi)^2+\phi_2(\xi)^2)^2c^4}{12(c^2-1)^3}$$
$$+\frac{2\Delta x^2\alpha^3\dot{\phi_1}(\xi)c^3}{3(c^2-1)^4}-\frac{4\Delta t^2\alpha^3\dot{\phi_1}(\xi)c^3}{3(c^2-1)^2}-\frac{\Delta t^2\alpha V'(\phi_1(\xi)^2+\phi_2(\xi)^2)\dot{\phi_1}(\xi)c^3}{3(c^2-1)^2}$$
$$-\frac{2\Delta t^2\alpha\phi_1(\xi)^2\dot{\phi_1}(\xi)V''(\phi_1(\xi)^2+\phi_2(\xi)^2)c^3}{3(c^2-1)^2}-\frac{2\Delta t^2\alpha\phi_1(\xi)\phi_2(\xi)\dot{\phi_2}(\xi)V''(\phi_1(\xi)^2+\phi_2(\xi)^2)c^3}{3(c^2-1)^2}$$
$$+\frac{\Delta t^2\alpha^4\phi_2(\xi)c^2}{2(c^2-1)^2}+\frac{\Delta t^2\alpha^2\phi_2(\xi)V'(\phi_1(\xi)^2+\phi_2(\xi)^2)c^2}{2(c^2-1)^2}-\frac{\Delta x^2\alpha^4\phi_2(\xi)c^2}{3(c^2-1)^4}$$
$$-\frac{\Delta x^2\alpha^2\phi_2(\xi)V'(\phi_1(\xi)^2+\phi_2(\xi)^2)c^2}{3(c^2-1)^4}+\frac{\Delta t^2\alpha^3\dot{\phi_1}(\xi)c}{3(c^2-1)}-\frac{\Delta x^2\alpha^3\dot{\phi_1}(\xi)c}{3(c^2-1)^3}-\frac{\Delta x^2\alpha V'(\phi_1(\xi)^2+\phi_2(\xi)^2)\dot{\phi_1}(\xi)c}{3(c^2-1)^3}$$

$$
\begin{aligned}
&- \frac{\Delta x^2 \alpha \phi_1(\xi)^2 \dot{\phi_1}(\xi) V''(\phi_1(\xi)^2 + \phi_2(\xi)^2) c}{3(c^2-1)^3} - \frac{\Delta x^2 \alpha \phi_2(\xi)^2 \dot{\phi_1}(\xi) V''(\phi_1(\xi)^2 + \phi_2(\xi)^2) c}{3(c^2-1)^3} \\
&+ \frac{\Delta x^2 \phi_2(\xi) V'(\phi_1(\xi)^2 + \phi_2(\xi)^2)^2}{12(c^2-1)^3} + \frac{\Delta x^2 \alpha^4 \phi_2(\xi)}{12(c^2-1)^3} + \frac{\Delta x^2 \alpha^2 \phi_2(\xi) V'(\phi_1(\xi)^2 + \phi_2(\xi)^2)}{6(c^2-1)^3} \\
&+ \frac{\Delta x^2 \alpha^2 \phi_2(\xi)^3 V''(\phi_1(\xi)^2 + \phi_2(\xi)^2)}{6(c^2-1)^3} + \frac{\Delta x^2 \phi_2(\xi) \dot{\phi_1}(\xi)^2 V''(\phi_1(\xi)^2 + \phi_2(\xi)^2)}{6(c^2-1)^2} \\
&+ \frac{\Delta x^2 \phi_2(\xi) \dot{\phi_2}(\xi)^2 V''(\phi_1(\xi)^2 + \phi_2(\xi)^2)}{2(c^2-1)^2} + \frac{\Delta x^2 \alpha^2 \phi_1(\xi)^2 \phi_2(\xi) V''(\phi_1(\xi)^2 + \phi_2(\xi)^2)}{6(c^2-1)^3} \\
&+ \frac{\Delta x^2 \phi_2(\xi)^3 V'(\phi_1(\xi)^2 + \phi_2(\xi)^2) V''(\phi_1(\xi)^2 + \phi_2(\xi)^2)}{6(c^2-1)^3} \\
&+ \frac{\Delta x^2 \phi_1(\xi)^2 \phi_2(\xi) V'(\phi_1(\xi)^2 + \phi_2(\xi)^2) V''(\phi_1(\xi)^2 + \phi_2(\xi)^2)}{6(c^2-1)^3} + \frac{\Delta x^2 \phi_1(\xi) \dot{\phi_1}(\xi) \dot{\phi_2}(\xi) V''(\phi_1(\xi)^2 + \phi_2(\xi)^2)}{3(c^2-1)^2} \\
&+ \frac{\Delta x^2 \phi_1(\xi)^2 \phi_2(\xi) \dot{\phi_1}(\xi)^2 V^{(3)}(\phi_1(\xi)^2 + \phi_2(\xi)^2)}{3(c^2-1)^2} + \frac{\Delta x^2 \phi_2(\xi)^3 \dot{\phi_2}(\xi)^2 V^{(3)}(\phi_1(\xi)^2 + \phi_2(\xi)^2)}{3(c^2-1)^2} \\
&+ \frac{2\Delta x^2 \phi_1(\xi) \phi_2(\xi)^2 \dot{\phi_1}(\xi) \dot{\phi_2}(\xi) V^{(3)}(\phi_1(\xi)^2 + \phi_2(\xi)^2)}{3(c^2-1)^2} - \frac{\Delta t^2 \alpha^4 \phi_2(\xi)}{12(c^2-1)}
\end{aligned}
$$

Refer to Offen, 2020b for source code.

B.2 Higher order terms in computation of Section 13.4

We report the order 6 terms of the ansatz in Section 13.4 for the variational structure of a travelling wave in the non-linear wave equation discretised with the multisymplectic 5-point stencil. Refer to Offen, 2020b for source code.

The trees displayed on page 277 yield the following ansatz for the Lagrangian L^6 in (13.4.1). In the following $W^{(i,j)} = \frac{\partial^{i+j} W}{\partial \phi_1^i \partial \phi_2^j}$.

$$
\begin{aligned}
L^6 = a(6,4)\Big(&(W^{(0,1)})^2 (W^{(0,2)})^2 + 2W^{(0,1)} W^{(1,0)} W^{(1,1)} W^{(0,2)} + (W^{(0,1)})^2 (W^{(1,1)})^2 + (W^{(1,0)})^2 (W^{(1,1)})^2 \\
&+ (W^{(1,0)})^2 (W^{(2,0)})^2 + 2W^{(0,1)} W^{(1,0)} W^{(1,1)} W^{(2,0)} \Big) + a(6,3)\Big(2W^{(1,1)} (W^{(0,2)})^2 \dot{\phi_1} \dot{\phi_2} \\
&+ 2W^{(1,1)} W^{(2,0)} W^{(0,2)} \dot{\phi_1} \dot{\phi_2} + 2(W^{(1,1)})^3 \dot{\phi_1} \dot{\phi_2} + 2W^{(1,1)} (W^{(2,0)})^2 \dot{\phi_1} \dot{\phi_2} + (W^{(1,1)})^2 W^{(0,2)} (\dot{\phi_1})^2 \\
&+ (W^{(2,0)})^3 (\dot{\phi_1})^2 + 2(W^{(1,1)})^2 W^{(2,0)} (\dot{\phi_1})^2 + (W^{(0,2)})^3 (\dot{\phi_2})^2 + 2(W^{(1,1)})^2 W^{(0,2)} (\dot{\phi_2})^2 + (W^{(1,1)})^2 W^{(2,0)} \\
&(\dot{\phi_2})^2 \Big) + a(6,10)\Big(W^{(0,3)} (W^{(0,1)})^3 + 3W^{(1,0)} W^{(1,2)} (W^{(0,1)})^2 + 3(W^{(1,0)})^2 W^{(2,1)} W^{(0,1)} \\
&+ (W^{(1,0)})^3 + W^{(3,0)} \Big) + a(6,5)\Big(2W^{(0,1)} W^{(0,2)} W^{(1,2)} \dot{\phi_1} \dot{\phi_2} + 2W^{(1,0)} W^{(1,1)} W^{(1,2)} \dot{\phi_1} \dot{\phi_2} \\
&+ 2W^{(0,1)} W^{(1,1)} W^{(2,1)} \dot{\phi_1} \dot{\phi_2} + 2W^{(1,0)} W^{(2,0)} W^{(2,1)} \dot{\phi_1} \dot{\phi_2} + W^{(0,1)} W^{(0,2)} W^{(2,1)} (\dot{\phi_1})^2 \\
&+ W^{(1,0)} W^{(1,1)} W^{(2,1)} (\dot{\phi_1})^2 + W^{(0,1)} W^{(1,1)} W^{(3,0)} (\dot{\phi_1})^2 + W^{(1,0)} W^{(2,0)} W^{(3,0)} (\dot{\phi_1})^2 \\
&+ W^{(0,1)} W^{(0,2)} W^{(0,3)} (\dot{\phi_2})^2 + W^{(0,3)} W^{(1,0)} W^{(1,1)} (\dot{\phi_2})^2 + W^{(0,1)} W^{(1,1)} W^{(1,2)} (\dot{\phi_2})^2 \\
&+ W^{(1,0)} W^{(1,2)} W^{(2,0)} (\dot{\phi_2})^2 \Big) + a(6,2)\Big(W^{(0,1)} W^{(0,3)} W^{(1,1)} \dot{\phi_1} \dot{\phi_2} + W^{(0,1)} W^{(0,2)} W^{(1,2)} \dot{\phi_1} \dot{\phi_2} \\
&+ W^{(1,0)} W^{(1,1)} W^{(1,2)} \dot{\phi_1} \dot{\phi_2} + W^{(0,1)} W^{(1,2)} W^{(2,0)} \dot{\phi_1} \dot{\phi_2} + W^{(0,2)} W^{(1,0)} W^{(2,1)} \dot{\phi_1} \dot{\phi_2} \\
&+ W^{(0,1)} W^{(1,1)} W^{(2,1)} \dot{\phi_1} \dot{\phi_2} + W^{(1,0)} W^{(2,0)} W^{(2,1)} \dot{\phi_1} \dot{\phi_2} + W^{(1,0)} W^{(1,1)} W^{(3,0)} \dot{\phi_1} \dot{\phi_2} \\
&+ W^{(0,1)} W^{(1,1)} W^{(1,2)} (\dot{\phi_1})^2 + W^{(1,0)} W^{(1,1)} W^{(2,1)} (\dot{\phi_1})^2 + W^{(0,1)} W^{(2,0)} W^{(2,1)} (\dot{\phi_1})^2 \\
&+ W^{(1,0)} W^{(2,0)} W^{(3,0)} (\dot{\phi_1})^2 + W^{(0,1)} W^{(0,2)} W^{(0,3)} (\dot{\phi_2})^2 + W^{(0,2)} W^{(1,0)} W^{(1,2)} (\dot{\phi_2})^2 \\
&+ W^{(0,1)} W^{(1,1)} W^{(1,2)} (\dot{\phi_2})^2 + W^{(1,0)} W^{(1,1)} W^{(2,1)} (\dot{\phi_2})^2 \Big) + a(6,8)\Big(4W^{(1,2)} W^{(2,1)} (\dot{\phi_1})^3 \dot{\phi_2}
\end{aligned}
$$

$$
\begin{aligned}
&+ 4W^{(2,1)}W^{(3,0)}(\dot{\phi_1})^3\dot{\phi_2} + 4(W^{(1,2)})^2(\dot{\phi_1})^2(\dot{\phi_2})^2 + 4(W^{(2,1)})^2(\dot{\phi_1})^2(\dot{\phi_2})^2 + 2W^{(0,3)}W^{(2,1)}(\dot{\phi_1})^2(\dot{\phi_2})^2 \\
&+ 2W^{(1,2)}W^{(3,0)}(\dot{\phi_1})^2(\dot{\phi_2})^2 + 4W^{(0,3)}W^{(1,2)}\dot{\phi_1}(\dot{\phi_2})^3 + 4W^{(1,2)}W^{(2,1)}\dot{\phi_1}(\dot{\phi_2})^3 + (W^{(2,1)})^2(\dot{\phi_1})^4 \\
&+ (W^{(3,0)})^2(\dot{\phi_1})^4 + (W^{(0,3)})^2(\dot{\phi_2})^4 + (W^{(1,2)})^2(\dot{\phi_2})^4\Big) + a(6,6)\Big(2(W^{(0,1)})^2W^{(1,3)}\dot{\phi_1}\dot{\phi_2} \\
&+ 4W^{(0,1)}W^{(1,0)}W^{(2,2)}\dot{\phi_1}\dot{\phi_2} + 2(W^{(1,0)})^2W^{(3,1)}\dot{\phi_1}\dot{\phi_2} + (W^{(0,1)})^2W^{(2,2)}(\dot{\phi_1})^2 \\
&+ 2W^{(0,1)}W^{(1,0)}W^{(3,1)}(\dot{\phi_1})^2 + (W^{(1,0)})^2W^{(4,0)}(\dot{\phi_1})^2 + (W^{(0,1)})^2W^{(0,4)}(\dot{\phi_2})^2 + 2W^{(0,1)}W^{(1,0)}W^{(1,3)}(\dot{\phi_2})^2 \\
&+ (W^{(1,0)})^2W^{(2,2)}(\dot{\phi_2})^2\Big) + a(6,7)\Big(3W^{(1,1)}W^{(2,2)}(\dot{\phi_1})^3\dot{\phi_2} + W^{(0,2)}W^{(3,1)}(\dot{\phi_1})^3\dot{\phi_2} \\
&+ 3W^{(2,0)}W^{(3,1)}(\dot{\phi_1})^3\dot{\phi_2} + W^{(1,1)}W^{(4,0)}(\dot{\phi_1})^3\dot{\phi_2} + 3W^{(1,1)}W^{(1,3)}(\dot{\phi_1})^2(\dot{\phi_2})^2 + 3W^{(0,2)}W^{(2,2)}(\dot{\phi_1})^2(\dot{\phi_2})^2 \\
&+ 3W^{(2,0)}W^{(2,2)}(\dot{\phi_1})^2(\dot{\phi_2})^2 + 3W^{(1,1)}W^{(3,1)}(\dot{\phi_1})^2(\dot{\phi_2})^2 + W^{(0,4)}W^{(1,1)}\dot{\phi_1}(\dot{\phi_2})^3 + 3W^{(0,2)}W^{(1,3)}\dot{\phi_1}(\dot{\phi_2})^3 \\
&+ W^{(1,3)}W^{(2,0)}\dot{\phi_1}(\dot{\phi_2})^3 + 3W^{(1,1)}W^{(2,2)}\dot{\phi_1}(\dot{\phi_2})^3 + W^{(1,1)}W^{(3,1)}(\dot{\phi_1})^4 + W^{(2,0)}W^{(4,0)}(\dot{\phi_1})^4 \\
&+ W^{(0,2)}W^{(0,4)}(\dot{\phi_2})^4 + W^{(1,1)}W^{(1,3)}(\dot{\phi_2})^4\Big) + a(6,9)\Big(4W^{(0,1)}W^{(3,2)}(\dot{\phi_1})^3\dot{\phi_2} + 4W^{(1,0)}W^{(4,1)}(\dot{\phi_1})^3\dot{\phi_2} \\
&+ 6W^{(0,1)}W^{(2,3)}(\dot{\phi_1})^2(\dot{\phi_2})^2 + 6W^{(1,0)}W^{(3,2)}(\dot{\phi_1})^2(\dot{\phi_2})^2 + 4W^{(0,1)}W^{(1,4)}\dot{\phi_1}(\dot{\phi_2})^3 + 4W^{(1,0)}W^{(2,3)}\dot{\phi_1}(\dot{\phi_2})^3 \\
&+ W^{(0,1)}W^{(4,1)}(\dot{\phi_1})^4 + W^{(1,0)}W^{(5,0)}(\dot{\phi_1})^4 + W^{(0,1)}W^{(0,5)}(\dot{\phi_2})^4 + W^{(1,0)}W^{(1,4)}(\dot{\phi_2})^4\Big) \\
&+ a(6,1)\Big(6W^{(5,1)}(\dot{\phi_1})^5\dot{\phi_2} + 15W^{(4,2)}(\dot{\phi_1})^4(\dot{\phi_2})^2 + 20W^{(3,3)}(\dot{\phi_1})^3(\dot{\phi_2})^3 + 15W^{(2,4)}(\dot{\phi_1})^2(\dot{\phi_2})^4 \\
&+ 6W^{(1,5)}\dot{\phi_1}(\dot{\phi_2})^5 + W^{(6,0)}(\dot{\phi_1})^6 + W^{(0,6)}(\dot{\phi_2})^6\Big)
\end{aligned}
$$

B.3 Corrected conserved quantity

In the modified system considered in Section 13.5 the quantity H is conserved up to order $O(h^2)$ along solutions. Using a polynomial ansatz we can compute a correction term such that the corrected quantity is conserved along solutions up to $O(h^4)$. See Figure 13.7 for a numerical experiment. The expression for the corrected quantity is given as

$$
\begin{aligned}
H_{\text{corrected}}(q,p) = H(q,p) - \frac{\|q\|^2}{24\left(c^2-1\right)^3}\Big(&c^6\Delta t^2 q_1^4 v_2^2 + c^6\Delta t^2 q_2^4 v_2^2 \\
&+ 2c^6\Delta t^2 q_1^2 q_2^2 v_2^2 + 4\alpha c^5\Delta t^2 p_2 q_1 v_2 + 6p_1^2 v_2\left(\Delta x^2 - c^4\Delta t^2\right) \\
&- 6c^4\Delta t^2 p_2^2 v_2 - 7\alpha^2 c^4\Delta t^2 q_1^2 v_2 - 7\alpha^2 c^4\Delta t^2 q_2^2 v_2 \\
&- c^4\Delta t^2 q_1^4 v_2^2 - c^4\Delta t^2 q_2^4 v_2^2 - 2c^4\Delta t^2 q_1^2 q_2^2 v_2^2 + 8\alpha c^3\Delta t^2 p_2 q_1 v_2 \\
&+ 3\alpha^4 c^2\Delta t^2 + 3\alpha^2 c^2\Delta t^2 q_1^2 v_2 + 3\alpha^2 c^2\Delta t^2 q_2^2 v_2 - 3\alpha^4 c^2\Delta x^2 \\
&+ 3\alpha^2 c^2\Delta x^2 q_1^2 v_2 + 3\alpha^2 c^2\Delta x^2 q_2^2 v_2 - c^2\Delta x^2 q_1^4 v_2^2 - c^2\Delta x^2 q_2^4 v_2^2 \\
&- 2c^2\Delta x^2 q_1^2 q_2^2 v_2^2 - 4\alpha c p_1 q_2 v_2\left(c^4\Delta t^2 + 2c^2\Delta t^2 - 3\Delta x^2\right) \\
&+ v_1\Big(-2\alpha^2\left(c^4\Delta t^2 + c^2\left(\Delta x^2 - 3\Delta t^2\right) + \Delta x^2\right) \\
&+ \left(c^2-1\right)q_1^2 v_2\left(c^4\Delta t^2 - \Delta x^2\right) + \left(c^2-1\right)q_2^2 v_2\left(c^4\Delta t^2 - \Delta x^2\right)\Big) \\
&- \left(c^2-1\right)v_1^2\left(c^4\Delta t^2 - \Delta x^2\right) - 12\alpha c\Delta x^2 p_2 q_1 v_2 \\
&+ \alpha^4\Delta t^2 - \alpha^4\Delta x^2 + 6\Delta x^2 p_2^2 v_2 + \alpha^2\Delta x^2 q_1^2 v_2 \\
&+ \alpha^2\Delta x^2 q_2^2 v_2 + \Delta x^2 q_1^4 v_2^2 + \Delta x^2 q_2^4 v_2^2 + 2\Delta x^2 q_1^2 q_2^2 v_2^2\Big).
\end{aligned}
$$

B.4 Modified Lagrangian in special cases

In the following we report results for a general cubic potential

$$V(a) = v_0 + v_1 a + \frac{1}{2} v_2 a^2 + \frac{1}{6} v_3 a^3. \tag{B.4.1}$$

We make the ansatz

$$L = L^0(\phi, \dot{\phi}) + h^2 L^2(\phi, \dot{\phi}) + \mathcal{O}(h^4),$$

where L^0 and L^2 are general order 10 polynomials in ϕ and $\dot{\phi}$. The modified equation for $\ddot{\phi}$ for the potential V from (B.4.1) is substituted into the Euler-Lagrange equations $\mathcal{E}(L) = 0$ for L (truncated after the h^2-term), where $\mathcal{E}$ is the Euler-Lagrange operator. Since the initial values $\phi(0), \dot{\phi}(0)$ can be chosen independently and $\mathcal{E}(L)$ truncated after $\mathcal{O}(h^2)$ is a multivariate polynomial in h, ϕ, $\dot{\phi}$, we can equate each coefficient with zero and obtain a linear system of equations. In the special cases $\alpha = 0$, $c = 0$ or $\Delta x = c\Delta t$ this system is solvable. In each case L^0 can be chosen as the exact Lagrangian (13.2.6). For each case we report one admissible choice for L^2 below.

B.4.1 Non-rotating wave, $\alpha = 0$.

In this case the wave is not rotating and the case is covered by Theorem 13.3.1. The term L^2 obtained using the mentioned ansatz is given as

$$\begin{aligned}
&\frac{(c^4\Delta t^2 - \Delta x^2)}{288(c^2-1)^2}\Big(3\Big(v_3(\phi_1(\xi)^2+\phi_2(\xi)^2)\Big(4(c^2-1)(\phi_1(\xi)^2(5\dot{\phi_1}(\xi)^2+\dot{\phi_2}(\xi)^2)\\
&+8\phi_2(\xi)\phi_1(\xi)\dot{\phi_1}(\xi)\dot{\phi_2}(\xi)+\phi_2(\xi)^2(\dot{\phi_1}(\xi)^2+5\dot{\phi_2}(\xi)^2))+v_3(\phi_1(\xi)^2+\phi_2(\xi)^2)^4\Big)\\
&+4v_2\Big(2(c^2-1)(\phi_1(\xi)^2(3\dot{\phi_1}(\xi)^2+\dot{\phi_2}(\xi)^2)+4\phi_2(\xi)\phi_1(\xi)\dot{\phi_1}(\xi)\dot{\phi_2}(\xi)\\
&+\phi_2(\xi)^2(\dot{\phi_1}(\xi)^2+3\dot{\phi_2}(\xi)^2))+v_3(\phi_1(\xi)^2+\phi_2(\xi)^2)^4\Big)+4v_2^2(\phi_1(\xi)^2+\phi_2(\xi)^2)^3\Big)\\
&-12v_1^2(\phi_1(\xi)^2+\phi_2(\xi)^2)+4v_1(\phi_1(\xi)^2+\phi_2(\xi)^2)^2(2v_3(\phi_1(\xi)^2+\phi_2(\xi)^2)+3v_2)\Big).
\end{aligned}$$

The expression for L^2 does not happen to coincide with the terms obtained using a P-series ansatz in Section 13.4. However, the Euler-Lagrange equations for both Lagrangians govern the modified, reduced ODE (13.2.12).

B.4.2 Standing wave speed, $c = 0$

If the wave speed is zero, the functional equation (13.2.10) simplifies to

$$0 = -\frac{1}{\Delta x^2}\phi(\xi+\Delta x) + \left(\frac{2}{\Delta x^2} + \frac{2}{\Delta t^2}(\cos(\alpha\Delta t)-1)\right)\phi(\xi) - \frac{1}{\Delta x^2}\phi(\xi-\Delta x) - V'(\|\phi\|^2)\phi.$$

As this corresponds to a linear 3-step method, the underlying 1-step map is conjugate symplectic, i.e. symplectic with respect to a modified symplectic structure. Therefore, the reduced series expansion (13.2.11) is variational. The Lagrangian is given as $L = L^0 + h^2L^2 + \mathcal{O}(h^4)$, where L^2 is given by the following expression.

$$\begin{aligned}
&\frac{1}{288}\Big(-3\phi_1(\xi)^2\Big(4\alpha^4\Delta t^2 - 4\alpha^4\Delta x^2 \\
&+ 8\Delta x^2 v_2\Big(\alpha^2\phi_2(\xi)^2 - 3\dot{\phi_1}(\xi)^2 - \dot{\phi_2}(\xi)^2 + 2v_3\phi_2(\xi)^6\Big) \\
&+ 8\alpha^2\Delta x^2 v_3\phi_2(\xi)^4 + 8\Delta x^2 v_1\Big(-\alpha^2 + v_3\phi_2(\xi)^4 + v_2\phi_2(\xi)^2\Big) - 24\Delta x^2 v_3\phi_2(\xi)^2\dot{\phi_1}(\xi)^2 \\
&- 24\Delta x^2 v_3\phi_2(\xi)^2\dot{\phi_2}(\xi)^2 + 5\Delta x^2 v_3^2\phi_2(\xi)^8 + 12\Delta x^2 v_2^2\phi_2(\xi)^4 - 4\Delta x^2 v_1^2\Big) \\
&+ \phi_2(\xi)^2\Big(-12\alpha^4\Delta t^2 + 12\alpha^4\Delta x^2 \\
&- 12\Delta x^2 v_2\Big(\alpha^2\phi_2(\xi)^2 - 2\dot{\phi_1}(\xi)^2 - 6\dot{\phi_2}(\xi)^2 + v_3\phi_2(\xi)^6\Big) \\
&- 8\alpha^2\Delta x^2 v_3\phi_2(\xi)^4 + 4\Delta x^2 v_1(6\alpha^2 - 2v_3\phi_2(\xi)^4 - 3v_2\phi_2(\xi)^2) + 12\Delta x^2 v_3\phi_2(\xi)^2\dot{\phi_1}(\xi)^2 \\
&+ 60\Delta x^2 v_3\phi_2(\xi)^2\dot{\phi_2}(\xi)^2 - 3\Delta x^2 v_3^2\phi_2(\xi)^8 - 12\Delta x^2 v_2^2\phi_2(\xi)^4 + 12\Delta x^2 v_1^2\Big) \\
&- 6\Delta x^2\phi_1(\xi)^4\Big(v_3(-2(5\dot{\phi_1}(\xi)^2 + \dot{\phi_2}(\xi)^2) + 4\phi_2(\xi)^2(\alpha^2 + v_1) + 5v_3\phi_2(\xi)^6) \\
&+ 2v_2(\alpha^2 + 6v_3\phi_2(\xi)^4 + v_1) + 6v_2^2\phi_2(\xi)^2\Big) - 2\Delta x^2\phi_1(\xi)^6\Big(v_3(4\alpha^2 + 15v_3\phi_2(\xi)^4 + 4v_1) \\
&+ 24v_3v_2\phi_2(\xi)^2 + 6v_2^2\Big) + 96\Delta x^2 v_3\phi_2(\xi)\phi_1(\xi)^3\dot{\phi_1}(\xi)\dot{\phi_2}(\xi) \\
&+ 96\Delta x^2\phi_2(\xi)\phi_1(\xi)\dot{\phi_1}(\xi)\dot{\phi_2}(\xi)(v_3\phi_2(\xi)^2 + v_2) - 3\Delta x^2 v_3^2\phi_1(\xi)^{10} \\
&- 3\Delta x^2 v_3\phi_1(\xi)^8(5v_3\phi_2(\xi)^2 + 4v_2)\Big)
\end{aligned}$$

B.4.3 Special discretisation values, $\Delta x = c\Delta t$

If the wave speed vanishes, the stencil (13.2.9) only relates the three points $\phi(\xi)$, $\phi(\xi+\Delta x)$, $\phi(\xi-\Delta x)$ rather than 5 points. The second order term of the Lagrangian is given as

$$\begin{aligned}
&\frac{\Delta t^2}{1440(c^2-1)^2}\Big(15c^2(c^2-1)v_3^2\phi_1(\xi)^{10} + 15c^2(c^2-1)v_3(5v_3\phi_2(\xi)^2 + 4v_2)\phi_1(\xi)^8 \\
&+ 10c^2\Big(6(c^2-1)v_2^2 + 24(c^2-1)v_3\phi_2(\xi)^2v_2 + v_3\Big(15(c^2-1)v_3\phi_2(\xi)^4 \\
&+ 2(3c^2-5)\alpha^2 + 4(c^2-1)v_1\Big)\Big)\phi_1(\xi)^6 + 30c^2\Big(6(c^2-1)v_2^2\phi_2(\xi)^2
\end{aligned}$$

$$
\begin{aligned}
&+ 2v_2\Big(6(c^2-1)v_3\phi_2(\xi)^4 + 2(c^2-2)\alpha^2 + (c^2-1)v_1\Big)\\
&+ v_3\Big(5(c^2-1)v_3\phi_2(\xi)^6 + 2((3c^2-5)\alpha^2 + 2(c^2-1)v_1)\phi_2(\xi)^2\\
&- 24c(c^2-1)\alpha\dot{\phi_1}(\xi)\phi_2(\xi) + 2(c^2-1)^2(5\dot{\phi_1}(\xi)^2 + \dot{\phi_2}(\xi)^2)\Big)\Big)\phi_1(\xi)^4\\
&+ 480c^2(c^2-1)^2v_3\phi_2(\xi)\dot{\phi_1}(\xi)\dot{\phi_2}(\xi)\phi_1(\xi)^3 - 15\Big(-5c^4v_3^2\phi_2(\xi)^8 + 5c^2v_3^2\phi_2(\xi)^8\\
&- 12c^2(c^2-1)v_2^2\phi_2(\xi)^4 - 12c^4\alpha^2v_3\phi_2(\xi)^4 + 20c^2\alpha^2v_3\phi_2(\xi)^4 + 32c^5\alpha v_3\dot{\phi_1}(\xi)\phi_2(\xi)^3\\
&- 32c^3\alpha v_3\dot{\phi_1}(\xi)\phi_2(\xi)^3 - 24c^6v_3\dot{\phi_1}(\xi)^2\phi_2(\xi)^2 + 48c^4v_3\dot{\phi_1}(\xi)^2\phi_2(\xi)^2\\
&- 24c^2v_3\dot{\phi_1}(\xi)^2\phi_2(\xi)^2 - 24c^6v_3\dot{\phi_2}(\xi)^2\phi_2(\xi)^2 + 48c^4v_3\dot{\phi_2}(\xi)^2\phi_2(\xi)^2\\
&- 24c^2v_3\dot{\phi_2}(\xi)^2\phi_2(\xi)^2 + 12c^2\alpha^4 + 4\alpha^4 + 4c^2(c^2-1)v_1^2\\
&- 8c^2v_1\Big((c^2-1)v_3\phi_2(\xi)^4 + (c^2-1)v_2\phi_2(\xi)^2 - 2\alpha^2\Big)\\
&- 8c^2v_2\Big(2(c^2-1)v_3\phi_2(\xi)^6 + 2(c^2-2)\alpha^2\phi_2(\xi)^2 - 8c(c^2-1)\alpha\dot{\phi_1}(\xi)\phi_2(\xi)\\
&+ (c^2-1)^2(3\dot{\phi_1}(\xi)^2 + \dot{\phi_2}(\xi)^2)\Big)\Big)\phi_1(\xi)^2\\
&+ 480c^2(c^2-1)^2\phi_2(\xi)(v_3\phi_2(\xi)^2 + v_2)\dot{\phi_1}(\xi)\dot{\phi_2}(\xi)\phi_1(\xi) + \phi_2(\xi)\Big(15c^2(c^2-1)v_3^2\phi_2(\xi)^9\\
&+ 60c^2(c^2-1)v_2v_3\phi_2(\xi)^7 + 20c^2\Big(3(c^2-1)v_2^2 + ((3c^2-5)\alpha^2 + 2(c^2-1)v_1)v_3\Big)\phi_2(\xi)^5\\
&- 144c^3(c^2-1)\alpha v_3\dot{\phi_1}(\xi)\phi_2(\xi)^4 + 60c^2\Big(v_3(\dot{\phi_1}(\xi)^2 + 5\dot{\phi_2}(\xi)^2)(c^2-1)^2\\
&+ (2(c^2-2)\alpha^2 + (c^2-1)v_1)v_2\Big)\phi_2(\xi)^3 - 320c^3(c^2-1)\alpha v_2\dot{\phi_1}(\xi)\phi_2(\xi)^2\\
&- 60\Big((3c^2+1)\alpha^4 + 4c^2v_1\alpha^2 + c^2(c^2-1)v_1^2 - 2c^2(c^2-1)^2v_2(\dot{\phi_1}(\xi)^2 + 3\dot{\phi_2}(\xi)^2)\Big)\phi_2(\xi)\\
&+ 480c(c^2+1)\alpha^3\dot{\phi_1}(\xi)\Big)\Big).
\end{aligned}
$$

Statements of contribution

Most of the work presented in Parts II and III thesis has been published or is submitted and under review at the time of writing.

- Chapters 6 and 7 mainly consist of the publication McLachlan and Offen, 2018a.
- Chapter 8 covers McLachlan and Offen, 2018b.
- Chapter 9 consists of McLachlan and Offen, 2020b; McLachlan and Offen, 2019.
- Chapter 11 consists of Kreusser, McLachlan, and Offen, 2020.
- A manuscript based on Chapter 10 has been submitted to *Annales Henri Lebesgue*, Offen, 2020.
- Chapter 12 is published as McLachlan, Offen, and Tapley, 2019.
- The work in Chapter 13 has been concluded and submitted to *Nonlinearity*, McLachlan and Offen, 2020a.

The author's contribution to the collaborative publications consists of the methodology, analysis, and writing as outlined in the following statements of contributions.

References

Kreusser, L. M., R. I. McLachlan, and C. Offen (2020). "Detection of high codimensional bifurcations in variational PDEs". In: *Nonlinearity* 33, pp. 2335–2363. DOI: 10.1088/1361-6544/ab7293. arXiv: 1903.02659.

McLachlan, R. I. and C. Offen (2018a). "Bifurcation of solutions to Hamiltonian boundary value problems". In: *Nonlinearity* 31.6, pp. 2895–2927. DOI: 10.1088/1361-6544/aab630. arXiv: 1710.09991.

— (2018b). "Hamiltonian boundary value problems, conformal symplectic symmetries, and conjugate loci". In: *New Zealand Journal of Mathematics (NZJM)* 48, pp. 83–99. arXiv: 1804.07479.

McLachlan, R. I. and C. Offen (Aug. 2019). "Symplectic integration of boundary value problems". In: *Numerical Algorithms* 81.4, pp. 1219–1233. ISSN: 1572-9265. DOI: 10.1007/s11075-018-0599-7. arXiv: 1804.09042.

— (June 2020a). "Backward error analysis for variational discretisations of partial differential equations". In: *Nonlinearity (submitted)*. arXiv: 2006.14172.

— (2020b). "Preservation of bifurcations of Hamiltonian boundary value problems under discretisation". In: *Foundations of Computational Mathematics (FoCM)*. DOI: 10.1007/s10208-020-09454-z. arXiv: 1804.07468.

McLachlan, R. I., C. Offen, and B. K. Tapley (July 2019). "Symplectic integration of PDEs using Clebsch variables". In: *Journal of Computational Dynamics* 6.1, pp. 111–130. ISSN: 2158-2505. DOI: 10.3934/jcd.2019005. arXiv: 1810.01627.

Offen, C. (Mar. 2020). "Local intersections of Lagrangian manifolds correspond to catastrophe theory". In: *Annales Henri Lebesgue (submitted)*. arXiv: 1811.10165.

MASSEY UNIVERSITY
GRADUATE RESEARCH SCHOOL

STATEMENT OF CONTRIBUTION
DOCTORATE WITH PUBLICATIONS/MANUSCRIPTS

We, the candidate and the candidate's Primary Supervisor, certify that all co-authors have consented to their work being included in the thesis and they have accepted the candidate's contribution as indicated below in the *Statement of Originality*.

Name of candidate:	Christian Offen
Name/title of Primary Supervisor:	Prof. Robert McLachlan
Name of Research Output and full reference:	
McLachlan, R.I. and Offen, C., 2018. Bifurcation of solutions to Hamiltonian boundary value problems. Nonlinearity, 31(6), 2895–2927	
In which Chapter is the Manuscript /Published work:	Chapter 6 and 7
Please indicate:	
• The percentage of the manuscript/Published Work that was contributed by the candidate:	70%
and	
• Describe the contribution that the candidate has made to the Manuscript/Published Work:	
methodology, analysis, writing	
For manuscripts intended for publication please indicate target journal:	
Candidate's Signature:	Christian Offen
Date:	23/07/2020
Primary Supervisor's Signature:	McLachlan, Robert Digitally signed by McLachlan, Robert Date: 2020.07.23 14:03:50 +12'00'
Date:	23/07/2020

(This form should appear at the end of each thesis chapter/section/appendix submitted as a manuscript/ publication or collected as an appendix at the end of the thesis)

MASSEY UNIVERSITY
GRADUATE RESEARCH SCHOOL

STATEMENT OF CONTRIBUTION
DOCTORATE WITH PUBLICATIONS/MANUSCRIPTS

We, the candidate and the candidate's Primary Supervisor, certify that all co-authors have consented to their work being included in the thesis and they have accepted the candidate's contribution as indicated below in the *Statement of Originality*.

Name of candidate:	Christian Offen
Name/title of Primary Supervisor:	Prof. Robert McLachlan
Name of Research Output and full reference:	
McLachlan, R.I. and Offen, C., 2018. New Zealand Journal of Mathematics, 48, p.83-99	
In which Chapter is the Manuscript /Published work:	Chapter 8
Please indicate:	
• The percentage of the manuscript/Published Work that was contributed by the candidate:	70%
and	
• Describe the contribution that the candidate has made to the Manuscript/Published Work:	
methodology, analysis, writing	
For manuscripts intended for publication please indicate target journal:	
Candidate's Signature:	Christian Offen
Date:	23/07/2020
Primary Supervisor's Signature:	McLachlan, Robert Digitally signed by McLachlan, Robert Date: 2020.07.23 14:03:50 +12'00'
Date:	23/07/2020

(This form should appear at the end of each thesis chapter/section/appendix submitted as a manuscript/ publication or collected as an appendix at the end of the thesis)

MASSEY UNIVERSITY
GRADUATE RESEARCH SCHOOL

STATEMENT OF CONTRIBUTION
DOCTORATE WITH PUBLICATIONS/MANUSCRIPTS

We, the candidate and the candidate's Primary Supervisor, certify that all co-authors have consented to their work being included in the thesis and they have accepted the candidate's contribution as indicated below in the *Statement of Originality*.

Name of candidate:	Christian Offen
Name/title of Primary Supervisor:	Prof. Robert McLachlan
Name of Research Output and full reference:	
McLachlan, R.I. and Offen, C., 2020. Preservation of bifurcations of Hamiltonian boundary value problems under discretisation, Foundations of Computational Mathematics (FoCM)	
In which Chapter is the Manuscript /Published work:	Chapter 9
Please indicate:	
• The percentage of the manuscript/Published Work that was contributed by the candidate:	70%
and	
• Describe the contribution that the candidate has made to the Manuscript/Published Work:	
methodology, analysis, writing	
For manuscripts intended for publication please indicate target journal:	
Candidate's Signature:	Christian Offen
Date:	23/07/2020
Primary Supervisor's Signature:	McLachlan, Robert Digitally signed by McLachlan, Robert Date: 2020.07.23 14:03:50 +12'00'
Date:	23/07/2020

(This form should appear at the end of each thesis chapter/section/appendix submitted as a manuscript/ publication or collected as an appendix at the end of the thesis)

MASSEY UNIVERSITY
GRADUATE RESEARCH SCHOOL

STATEMENT OF CONTRIBUTION
DOCTORATE WITH PUBLICATIONS/MANUSCRIPTS

We, the candidate and the candidate's Primary Supervisor, certify that all co-authors have consented to their work being included in the thesis and they have accepted the candidate's contribution as indicated below in the *Statement of Originality*.

Name of candidate:	Christian Offen
Name/title of Primary Supervisor:	Prof. Robert McLachlan
Name of Research Output and full reference:	
McLachlan, R.I. and Offen, C., 2018. Symplectic Integration of Boundary Value Problems. Numerical Algorithms, 81(4), p.1219-1233	
In which Chapter is the Manuscript /Published work:	Chapter 9
Please indicate:	
• The percentage of the manuscript/Published Work that was contributed by the candidate:	70%
and	
• Describe the contribution that the candidate has made to the Manuscript/Published Work:	
methodology, analysis, writing	
For manuscripts intended for publication please indicate target journal:	
Candidate's Signature:	Christian Offen
Date:	23/07/2020
Primary Supervisor's Signature:	McLachlan, Robert Digitally signed by McLachlan, Robert Date: 2020.07.23 14:03:50 +12'00'
Date:	23/07/2020

(This form should appear at the end of each thesis chapter/section/appendix submitted as a manuscript/ publication or collected as an appendix at the end of the thesis)

MASSEY UNIVERSITY
GRADUATE RESEARCH SCHOOL

STATEMENT OF CONTRIBUTION
DOCTORATE WITH PUBLICATIONS/MANUSCRIPTS

We, the candidate and the candidate's Primary Supervisor, certify that all co-authors have consented to their work being included in the thesis and they have accepted the candidate's contribution as indicated below in the *Statement of Originality*.

Name of candidate:	Christian Offen
Name/title of Primary Supervisor:	Prof. Robert McLachlan
Name of Research Output and full reference:	
Kreusser, L.M. and McLachlan, R.I. and Offen, C., 2020. Detection of high codimensional bifurcations in variational PDEs. Nonlinearity, 33(5), 2335–2363	
In which Chapter is the Manuscript /Published work:	Chapter 11
Please indicate:	
• The percentage of the manuscript/Published Work that was contributed by the candidate:	70%
and	
• Describe the contribution that the candidate has made to the Manuscript/Published Work:	
methodology, analysis, writing	
For manuscripts intended for publication please indicate target journal:	
Candidate's Signature:	Christian Offen
Date:	23/07/2020
Primary Supervisor's Signature:	McLachlan, Robert Digitally signed by McLachlan, Robert Date: 2020.07.23 14:03:50 +12'00'
Date:	23/07/2020

(This form should appear at the end of each thesis chapter/section/appendix submitted as a manuscript/ publication or collected as an appendix at the end of the thesis)

MASSEY UNIVERSITY
GRADUATE RESEARCH SCHOOL

STATEMENT OF CONTRIBUTION
DOCTORATE WITH PUBLICATIONS/MANUSCRIPTS

We, the candidate and the candidate's Primary Supervisor, certify that all co-authors have consented to their work being included in the thesis and they have accepted the candidate's contribution as indicated below in the *Statement of Originality*.

Name of candidate:	Christian Offen
Name/title of Primary Supervisor:	Prof. Robert McLachlan
Name of Research Output and full reference:	
McLachlan, R.I. and Tapley, B.K. and Offen, C., 2019. Symplectic Integration of PDEs Using Clebsch Variables. Journal of Computational Dynamics, 6(1), p.111-130	
In which Chapter is the Manuscript /Published work:	Chapter 12
Please indicate:	
• The percentage of the manuscript/Published Work that was contributed by the candidate:	70%
and	
• Describe the contribution that the candidate has made to the Manuscript/Published Work:	
methodology, analysis, writing	
For manuscripts intended for publication please indicate target journal:	
Candidate's Signature:	Christian Offen
Date:	23/07/2020
Primary Supervisor's Signature:	McLachlan, Robert Digitally signed by McLachlan, Robert Date: 2020.07.23 14:03:50 +12'00'
Date:	23/07/2020

(This form should appear at the end of each thesis chapter/section/appendix submitted as a manuscript/ publication or collected as an appendix at the end of the thesis)

MASSEY UNIVERSITY
GRADUATE RESEARCH SCHOOL

STATEMENT OF CONTRIBUTION
DOCTORATE WITH PUBLICATIONS/MANUSCRIPTS

We, the candidate and the candidate's Primary Supervisor, certify that all co-authors have consented to their work being included in the thesis and they have accepted the candidate's contribution as indicated below in the *Statement of Originality*.

Name of candidate:	Christian Offen
Name/title of Primary Supervisor:	Prof. Robert McLachlan
Name of Research Output and full reference:	
McLachlan, R.I. and Offen, C., 2020. Robert Backward error analysis for variational discretisations of partial differential equations, preprint arXiv:2006.14172	
In which Chapter is the Manuscript /Published work:	Chapter 13
Please indicate:	
• The percentage of the manuscript/Published Work that was contributed by the candidate:	70%
and	
• Describe the contribution that the candidate has made to the Manuscript/Published Work:	
methodology, analysis, writing	
For manuscripts intended for publication please indicate target journal:	
Nonlinearity - IOPscience	
Candidate's Signature:	Christian Offen
Date:	23/07/2020
Primary Supervisor's Signature:	McLachlan, Robert Digitally signed by McLachlan, Robert Date: 2020.07.23 14:03:50 +12'00'
Date:	23/07/2020

(This form should appear at the end of each thesis chapter/section/appendix submitted as a manuscript/ publication or collected as an appendix at the end of the thesis)